TESIS DOCTORAL

SUSPENSIONES GRANULARES. UN ENFOQUE CINÉTICO

RUBÉN GÓMEZ GONZÁLEZ

PROGRAMA DE DOCTORADO EN MODELIZACIÓN Y EXPERIMENTACIÓN EN CIENCIA Y TECNOLOGÍA (R007)

2022

TESIS DOCTORAL

SUSPENSIONES GRANULARES. UN ENFOQUE CINÉTICO

RUBÉN GÓMEZ GONZÁLEZ

PROGRAMA DE DOCTORADO EN MODELIZACIÓN Y EXPERIMENTACIÓN EN CIENCIA Y TECNOLOGÍA (R007)

Conformidad del director

Dr. D. Vicente Garzó Puertos

Esta tesis cuenta con la autorización del director de la misma y de la Comisión Académica del programa. Dichas autorizaciones constan en el Servicio de la Escuela Internacional de Doctorado de la Universidad de Extremadura.

2022

Resumen

La materia granular en condiciones de flujo rápido puede modelarse como un gas granular compuesto por esferas duras inelásticas. En su estado natural, la materia granular se encuentra generalmente sumergida en un fluido, como aire o agua, de tal manera que el flujo granular es un proceso multifásico. A pesar de que la influencia del fluido intersticial no se ha tenido en cuenta en numerosos trabajos, existen situaciones en las que el efecto de la fase fluida no puede ignorarse y, por tanto, en principio, uno tiene que empezar por una descripción teórica que tenga en cuenta ambas fases (fluida y sólida). En este trabajo, modelamos los granos como partículas inmersas en un gas viscoso a temperatura constante. Como suele ser habitual, la influencia de la fase gaseosa sobre los granos aparece modelada en las ecuaciones cinéticas de Enskog y Boltzmann como un término tipo Fokker–Planck (fuerza de arrastre más término tipo Langevin). En este caso, la energía adquirida por los granos debido a su contacto con el gas intersticial compensa la energía disipada por colisiones binarias inelásticas de modo que el sistema alcanza un estado estacionario de no equilibrio. El principal objetivo de la presente tesis es determinar los coeficientes de transporte de suspensiones mono y bidispersas a través de dos vías diferentes pero complementarias. La primera de ellas consiste en resolver las ecuaciones cinéticas mediante métodos analíticos (método de Chapman–Enskog, método de los momentos de Grad, modelo cinético tipo BGK y modelos de Maxwell inelásticos) y la segunda emplea resultados de simulación (simulaciones numéricas de Monte Carlo). Además, como complemento se realiza un análisis exhaustivo de los estados homogéneos estacionarios y dependientes del tiempo, así como de las propiedades no newtonianas de suspensiones granulares sometidas a la acción de un flujo tangencial uniforme.

University of Extremadura

Doctoral Thesis

Granular suspensions. A kinetic theory approach

Author:
Rubén GÓMEZ GONZÁLEZ

Supervisor:
Dr. Vicente GARZÓ PUERTOS

A thesis submitted in fulfilment of the requirements for the degree of Doctor of Philosophy

in the

Department of Physics

2022

Abstract

Granular matter under rapid flow conditions can be modeled as a granular gas composed of inelastic hard spheres. It is known that granular matter in nature is generally immersed in a fluid, like air or water, and so a granular flow is a multiphase process. Despite the fact that the influence of the interstitial fluid on the granular flow has been ignored in numerous works, there are situations where the effect of the fluid phase cannot be neglected, and hence, in principle, one has to start from a theoretical description that accounts for both phases (fluid and solid phases). In this work, we consider that the grains are immersed in a viscous gas at a fixed temperature (granular suspension). As usual, we model the influence of the gas phase on grains by means of a Fokker–Planck term (drag friction plus Langevin-like term) in the Enskog or Boltzmann kinetic equations. In this case, the energy gained by grains due to their thermal contact with the interstitial gas is compensated for by the collisional dissipation due to binary inelastic collisions and so, the system reaches a a non-equilibrium steady state. The main objective of the present thesis is to determine the transport properties of mono and bidisperse granular suspensions by two different but complementary routes: (i) analytical methods (Chapman–Enskog method, Grad's moments method, BGK-type kinetic model, and inelastic Maxwell models) and (ii) computational simulations (direct simulation Monte Carlo method). Moreover, we perform an exhaustive analysis of the time-dependent and steady homogeneous states as well as of the non-Newtonian properties under simple shear flow of granular suspensions.

A mi familia

Agradecimientos

Esta tesis ha sido posible gracias a todas las personas que me han ayudado a la consecución de mis objetivos académicos y personales.

Me gustaría agradecer en primer lugar a mi director de tesis, Vicente Garzó. Desde el primer momento en el que crucé la puerta de su despacho para decirle que sería mi tutor de TFG, Vicente se ha volcado para que mi futuro académico fuese lo más brillante posible. Siempre llevaré conmigo todos los consejos y aprendizajes de los que me he empapado en estos cuatro años. Gracias por hacerme esta etapa más fácil y guiarme a la hora de enfrentarme al mundo de la investigación.

Quiero agradecer también toda la ayuda que me ha prestado Nagi Khalil de la Universidad Rey Juan Carlos de Madrid. Recuerdo con especial cariño las estancias en Palma de Mallorca y Móstoles con Nagi como anfitrión. Fue la persona con la que aprendí a realizar las simulaciones de Monte Carlo que tan útiles me ha resultado para el desarrollo de mi tesis. Podría decirse que ha sido un director no oficial.

También me gustaría mencionar en estos agradecimientos a Andrea Puglisi por su hospitalidad durante mi estancia de investigación en la Universidad La Sapienza de Roma. Andrea me introdujo al mundo de la materia activa que probablemente sea fruto de futuras publicaciones.

Por supuesto, no puedo olvidarme de todos los miembros del grupo SPhinX con los que he trabajado estos últimos cuatro años. Los investigadores "seniors" Enrique Abad, Antonio Astillero, Santos Bravo, Antonio Gordillo, Juan José Meléndez, Álvaro Rodríguez, Juan Jesús Ruiz, Andrés Santos y Francisco Vega que me han dado consejo y me ofrecido ayuda siempre que la he necesitado. Me siento también orgulloso de haber conocido a mis "coffee breakers" Alberto, Beatriz, Felipe, Javier, Jesús, Juan, Juanfran, Miguel y Moisés. Me gustaría además valorar la labor de Francisco Naranjo como gestor del grupo.

Quiero extender mi profundo agradecimiento a los revisores externos de mi tesis, Mariano López de Haro y Rodrigo Soto, por su disposición a leer mi trabajo minuciosamente.

Fuera del ámbito académico, quiero agradecer a mi familia. Por hacer lo imposible porque tuviese la mejor educación posible. Por apoyarme en todos mis proyectos y darme la confianza para conseguirlos. Y sobre todo, por darme los valores para convertirme en la persona que hoy soy.

No me olvido de María, la persona que ha sido mi apoyo emocional desde que di mis primeros pasos en la Física y que es mi fuente constante de energía. Gracias a ti no solo estoy escribiendo estas líneas si no que no hubiesen sido posibles muchas otras cosas en mi vida.

Agradezco la financiación para la realización de esta tesis proveniente del Gobierno de España mediante la ayuda predoctoral con referencia BES-2017-079725.

Contents

Glossary

BBGKY: **B**ogoliubov–**B**orn–**G**reen–**K**irkwood–**Y**von (p. 17)[1]
BDS: **B**rey–**D**ufty–**S**antos (p. 36)
BGK: **B**hatnagar–**G**ross–**K**rook (p. 14)
CE: **C**hapman–**E**nskog (p. 10)
CST: **C**ontinuous **S**hear **T**hickening (p. 169)
DEM: **D**iscrete **E**lement **M**ethod (p. 9)
DNS: **D**irect **N**umerical **S**imulation (p. 8)
DSMC: **D**irect **S**imulation **M**onte **C**arlo (p. 9)
DST: **D**iscontinuous **S**hear **T**hickening (p. 14)
EDLSHS: **E**vent **D**riven **L**angevin **S**imulation for **H**ard **S**pheres (p. 14)
HCS: **H**omogeneous **C**ooling **S**tate (p. 6)
HSS: **H**omogeneous **S**teady **S**tate (p. 11)
IHS: **I**nelastic **H**ard **S**pheres (p. 14)
IMM: **I**nelastic **M**axwell **M**odels (p. 14)
MD: **M**olecular **D**ynamics (p. 9)
NS: **N**avier–**S**tokes (p. 6)
RET: **R**evised **E**nskog **T**heory (p. 19)
USF: **U**niform **S**hear **F**low (p. 14)

[1]The page number between parentheses is that where the acronym is introduced for the first time.

Chapter 1

Introduction to Granular Suspensions

1.1 Introduction

Granular matter can be defined as large conglomerations of discrete macroscopic particles (let us call them *grains*) of different sizes (typically larger than 1 μm), shapes, micromechanical, and chemical properties [1]. Grains are ubiquitous in many industrial and natural processes. They form an extremely vast family that ranges from sand to astronomical objects, so they span several orders of magnitude in size [2].

The macroscopic size of grains deals to a collective motion governed by dissipative dynamics. Namely, when two particles collide, part of their kinetic energy is lost due to processes of friction, fraction, internal vibration, or plastic deformation; in other words, thermodynamically they are in a non-equilibrium state [3, 4]. For this reason, granular media exhibit intermediate behaviors between solids and fluids. For example, a jar of rice at rest behaves like a solid; any small external perturbation is quickly dissipated. On the other hand, if they are noncohesive, then the forces between the grains are only repulsive so that the shape of the material is determined by external boundaries and gravity. Additionally, when submitted to a strong excitation, grains acquire a kind of random motion that suppresses in part the effects of inelasticity and gravity. This complex behavior (different from that found in solids, liquids, or gases) causes the granular media to be considered an additional state of matter in its own right [2, 3, 5, 6].

A primary motivation for the study of granular matter relies on their involvement in many industrial processes. In fact, it is estimated that granular matter is the second most used type of material in industry after water [1, 7]. The conveying and handling of grains play major roles in many industries [8], including chemical (e.g., thermal processing of fossil fuel [9]), pharmaceutical (e.g., pills segregation [10] or powders hoppers [11]), agriculture (e.g., storage, transport, and processing of grains [12, 13]), or mining (e.g., particle crushing or breakage [14]). Their comprehension is also of great importance for the understanding of geological processes such as earthquakes, snow avalanches, or landslides [15, 16].

As on Earth, granular media has strong implications on the morphology of extraterrestrial bodies [17–19]. Moreover, the wide variety of particle features makes the granular media to be present out of our planet in the form of small bodies and dust [20–22]. The origin, formation, and evolution of the Solar System can be better understood by analyzing the physics of granular media as asteroids, comets, or planetesimals [23]. Many physical phenomena of the Universe focus on the formation and evolution of planetary rings. The study of rings' dynamics would allow astronomers to understand important mechanisms which would explain the behavior of celestial objects far away from us, like spiral galaxies [24]. Even historically, Maxwell's advances on the kinetic theory of granular gases were motivated by the attempt to describe Saturn's rings [25].

Most studies have focused on "dry" granular media, for which interactions between grains are dominated by solid contact [2], such as dry sand or interplanetary dust. Nonetheless, grains are generally immersed in a fluid like water or air, so a granular flow is a multiphase process [4]. A rather large spectrum of societal concerns involves wet granular material. Examples are rain-induced and submarine landslides, food processing, or civil engineering [26–28]. In this kind of mixtures (called *suspensions*), the interstitial fluid perturbs the interactions between the grains (which are essentially noncohesive and short-range) to add new effects to the dynamics of grains, such as lubrication or cohesiveness. Suspensions of solid particles are commonly encountered in applications in a large number of industries [29–31]. The rheology of such particles in Newtonian suspending fluids shows rich non-linear phenomena as shear thickening [32] or normal stress differences [33] distinct from those found in ordinary fluids. Thus, it is clear the broad spectrum of potential applications entailing the presence of granular matter.

Despite their industrial, geophysical, and planetary applications, understanding the granular media from a fundamental point of view poses a great challenge. No theoretical framework is able to cover such complexity and provide a general description of the different phenomena observed in granular flows.

The main reasons of such lack of generality fall on the complex and dissipative character of collisions between grains. Granular media are composed of a large number of particles each of which varies in size and characteristics. Thus, the contact between two particles involves non-trivial and highly non-linear phenomena such as friction and inelastic shocks [2, 5, 34]. Moreover, although the number of grains is generally much smaller than Avogadro's number due to their macroscopic size, this number is large enough so that accounting for each individual collision is almost impossible [4]. This lack of generality would be even more accentuated in the case of suspensions, since in particular the different phases evolve over quite different spatial and temporal scales. An alternative approach to handle the study of granular media consists on a statistical description based on the representation of the macroscopic quantities as averaged "microscopic" variables. Namely, to express the macroscopic properties in terms of the fundamental microscopic features of the particles, such as mass, shape, coefficients of restitution, and collisional properties [3]. However, it is not clear that a theory derived from equilibrium thermodynamics can be a priori applied to granular substances. The reason is that unlike molecules, grains collide inelastically and therefore they are inherently out of equilibrium [35, 36].

In addition, some researchers have expressed doubts concerning the applicability of different theories to granular matter, specially those related to elasticity theory and simple hydrodynamics [37, 38]. These theories arise out of an averaging process over length and time scales that must be well separated from the relevant macroscopic scales. Since even in the largest system, the size of the container may be only a thousand grains diameters [6], the lack of scale separation questions the approaches based on a continuum description [39]. Despite their ranges of applicability, the successes of these theories are notable and speaks for themselves [40–42]. Therefore, further investigation regarding the theoretical modeling of granular matter is clearly worth pursuing.

1.2 Granular Gases

For the sake of a better theoretical description, granular matter may be classified into two different density regimes: dense and dilute. Although the density is a continuous variable and sometimes it is difficult to establish a criterion of whether a material is dense or dilute, this artificial dichotomy facilitates the description of granular media. For example, for hard repulsive potentials, the dense regime is characterized by collective static friction whereas a dilute gas evolves through binary collisions. Thus, the physics entailing each regime is completely different and so are the mathematical treatments. Besides that, the gravitational potential energy of a grain is much larger than its thermal energy scale k_BT (where k_B is the Boltzmann's constant). For example, at room temperature ($T = 300$ K), a common grain of sand would require an energy of the order of 10^5 k_BT to counteract the effect of gravity and rise a distance equal to its diameter [6]. Ordinary temperature therefore plays no role in the motion of grains, such that thermal fluctuations are negligible compared with the particles interaction (*athermal* systems). This nonergodicity causes that unless driven externally, grains stay in a single configuration. At the core of statistical description, we can establish an equivalence between density and the response to an external driving. Hence, solid or fluid-like behavior is completely controlled by the driving protocol [43].

In this sense, granular matter arises in two classes of states: compact and activated [3]. In the first case, the material remains at rest at the bottom of the container. It is able to resiliently withstand enormous loads and form into piles of jammed particles. The effect of gravity and the static friction either between grains and with the walls of the repository dissipate energy. Thus, grains seem to be inactive, although they do in fact have some kinetic energy due to the room temperature [4]. In this context, the unusual behaviors that compact granular matter exhibits raise important questions. For example, the understanding of the network of forces within the container and of the distribution of packing configurations that give rise to the Janssen effect (sand flows in an hourglass at nearly constant rate) [44], clogging and jamming (blockage via formation of particle bridges and arches) [45], or dilatancy (dense granular material expands in volume when sheared) [46]. These issues are of crucial practical interest for the prediction of earthquakes and to mitigate the collapse of storage silos [47, 48]. Conversely, when loads overcome particle bonds, the system will collapse and

begin to flow [5]. At this first stage of deformation, particles will come off forming aggregates that move along narrow shear bands [49]. Far beyond the initial spillover, when grains are submitted to a strong excitation (e.g., by vibration, shear, or other external thermalization), a fluidized phase arises [50]. In this case, the velocities of grains contain apparently random components that will result in nearly instantaneous collisions between grains in a similar way as atoms or molecules interact in an ordinary gas [4, 5, 51]. For this reason, strongly-activated granular materials are commonly referred to as "granular gases" and the inherent regime where such systems live to as "rapid granular flows" [52, 53]. The main aim of the present thesis is to provide new insights in the theoretical study of granular matter when it admits a gas-like description.

A rigorous theoretical treatment of granular gases is rather intricate. It involves a large number of parameters since the dominant particle interactions depend on the particles size, shape, magnetization, or electrical charge [54]. If real progress is to be achieved in the granular description, many of subtle effects have to be neglected. The core of the governing equations must therefore focus on the general features that capture the phenomenology of real systems. In that regard, we can screen the subtleties to summarize the particle interactions in two major concepts: excluded volume and dissipation [55].

Grains are solid so they cannot interpenetrate. Moreover, if the gas is noncohesive, the duration of a collision becomes irrelevant when compared with the hydrodynamic scale. Thus, collisions can be considered instantaneous and well-located; particles move freely almost all the time until they collide. When two particles touch, their velocities instantly change according to the mechanisms of the collision and the properties of the colliding particles (i.e., masses, sizes, or shapes). A concise approach that accounts for noncohesiveness and rigidity is the hard-sphere model. The hard repulsive forces sustain a general theory that provides a basically correct description of the structure and dynamics of simple fluids [56]. However, as said before, the macroscopic size of particles entails a consequent loss of energy in each collision [3]. Therefore, the mathematical description of the collision must consider, among other things, what processes, if any, dissipate energy. Progress in that regard has been significant by means of the extension of the hard-sphere models to inelastic collisions. The hard-sphere dynamics with inelastic collisions constitutes one of the most noteworthy models for granular media in rapid flow [4, 57].

For hard spheres, the kinetic theory, based on the Enskog and Boltzmann kinetic equations, is the broader field that contemplates the dynamics of particles without doing any initial assumption on the dissipative character of collisions [58, 59]. Since the kinetic theory is based on several approximations, it needs the aid of numerical simulations to test the reliability of the theoretical results. Therefore, kinetic theory together with computer simulation are likely the best tools to describe granular gases. On the other hand, the study of granular gases from a kinetic point of view supposes an interesting and important challenge since it involves the extension of the classical kinetic equations to dissipative dynamics. The application of such theories allows us to obtain the hydrodynamic equations of motion that encompass the microscopic properties into a coarse-grained macroscopic description. The resulting equations establish an analogy with the Navier–Stokes (NS) equations that describe the flow of ordinary fluids. Nonetheless, granular hydrodynamics include a new ingredient in the balance of energy: a "sink" or "cooling" term that measures the rate of energy dissipation due to the inelasticity of collisions. This term provides the basic precondition for the existence of the homogeneous cooling state (HCS) in absence of gradients. Namely, a homogeneous state where temperature monotonically decays in time [4, 60].

The homogeneous cooling situation conforms an idealized state where the loss of mechanical energy is uniform in the whole system. However, the absence of energy excitation leads the grains to collapse into zones of larger density [60, 61]. Within these regions, the collision rate is enhanced and, consequently, the loss of kinetic energy is also enhanced [62, 63]. If the cooling rate is great enough, the pressure cannot pull the particles apart and, density gradients appear associated with mass fluxes from dilute to dense domains. This way, cluster instabilities arise inducing bigger and denser clusters [64]. Thereby, an initially homogeneous granular gas is unstable to the formation of aggregates and the homogeneity is destroyed [53, 65]. The onset of the cluster instability has been widely studied at the NS hydrodynamic level [66–76].

Since non-homogeneous situations can prevent the investigations of granular matter in rapid flow, the study of granular gases necessitates the challenging condition that particles distribute homogeneously and isotropically under external excitations to maintain the gaseous state [60]. Several experimental investigations are performed by exciting the particles by means of mechanical-boundary shaking, air-fluidized bed, or

magnetic forces [77–82]. Nonetheless, this way of supplying energy can create instabilities and inhomogeneities [83–86], so research is mostly carried out via computer simulations that drive the granular agitation as a bulk *thermostat* [61, 87–94]. By now, simulation data of granular gases driven by thermostats is well accepted as it was reproduced using different theoretical approaches [95–100]. However, if real experiments of solid particles thermostated by external driving want to be reproduced by simulations, it will be desirable to build more realistic theoretical tools together with new simulation techniques, so that they can supplement each other by serving as a reference for comparison.

An interesting example of thermostated granular gases is the case of solid particles immersed in an interstitial fluid. Although granular matter surrounded by a fluid (like the air, for instance) is commonplace in nature and industry, most of theoretical and computational studies have neglected the impact of the gas phase on the dynamics of solid particles. The sort criterion to still consider a granular gas is established on the basis of the ratio of the stress due to the grains to that due to the fluid (Bagnold number). If the effect of the surrounding fluid on the dynamics of grains cannot be ignored, the system is to be considered a suspension [101]. It is known that in many practical applications (like for instance species segregation in granular mixtures [102–108]) the underlying gas-solid interaction can play significant roles. For this reason, the study of granular suspensions has generated growing interest in the scientific community [109].

The dynamics of gas-solid flows is rich and extraordinarily complex so their understanding is really challenging. The dynamics of this kind of multiphase flows evolves through nonhydrodynamic (example is the Brownian motion) and hydrodynamic forces [109]. The latter are hard to treat analytically since the determination of the many-body interactions among the particles (for instance, several friction mechanisms [110]) raises many difficulties: some of them often associated with the long-range character of the hydrodynamic interactions. On the other hand, short-range hydrodynamic interactions (such as lubrication forces) are also factors which substantially influence the collision dynamics of two approaching particles [111, 112]. The most widespread way to mimic the gas-solid interactions is by means of the Stokesian dynamics [113]. This kind of molecular-dynamics-like approach considers that large and discrete particles are dispersed in a continuum fluid. The capability of the method relies on the possibility to

describe the hydrodynamic interactions via the linear Stokes equation at low-Reynolds numbers.

Among the different types of gas-solid flows, an interesting problem is the so-called particle-laden suspensions [74, 114–119]. In this kind of suspensions, dilute and immiscible particles are immersed in a denser fluid so that the dispersion of particles causes that the hydrodynamics interactions become less relevant [120]. Hence, the dynamics of solid particles arises from the thermal fluctuations in the fluid, and therefore interparticle, external, and Brownian forces prevail [113]. Moreover, one can assume that the number density of the solid phase is much smaller than that of the surrounding fluid, so that the latter is not affected by the presence of the solid particles. In this situation, the external fluid may be treated as a thermostat (or bath) at a fixed temperature. In the case of dilute systems where interparticle (grain-grain) collisions are still relevant [121], the classical kinetic theory of gases [122–124] conveniently adapted to account for inelastic collisions and gas-solid effects can be considered an appropriate tool to model granular suspensions.

As said before, the fluid-like behavior can be understood as a response to an external driving. In this context, solid particles driven by means of the action of a surrounding fluid evolve through binary instantaneous collisions. Thus, the gas-solid interactions can be modeled in an effective way via a fluid-solid force that appears in the starting kinetic equation [114, 115, 125]. Some models for granular suspensions [126–135] only consider the isolated body resistance via a linear drag law. Other models [136, 137] include also an additional Langevin-type stochastic term.

In this thesis, based on the results obtained in direct numerical simulations (DNS), the impact of the viscous gas on solid particles in high-velocity—but low-Reynolds numbers— gas-solid flows is by means of a force constituted by three different terms: (i) a term proportional to the difference between the mean flow velocities of both phases, (ii) a drag force term proportional to the particle velocity, and (iii) a stochastic Langevin-like term taking into account the effects of neighboring particles [137]. While the second term mimics the dissipation of energy due to the friction of grains on the viscous gas, the third term models the energy gained by the solid particles due to their interaction with the particles of the interstitial gas.

In the case of homogeneous states, the loss of energy due both to inelastic collisions and viscous drag and the external injection of energy to grains are responsible for

the fluctuations and evolution of the *granular* temperature. Since granular materials are athermal, the granular temperature is defined in terms of the mean value of the fluctuations of the instantaneous velocities of the particles with respect of the mean flow velocity [138]. This description opens up new possibilities for definition under out-of-equilibrium conditions of a statistical temperature on which kinetic theories can be built [35]. Within the framework of the fluctuation approach, the action of the external driving and the collisions on the velocities of particles compete to govern the time evolution of temperature, so that a steady state is reached when both mechanisms compensate each other [139, 140]. The above steady condition significantly simplifies the description of granular gases since it eliminates the time dependence in the resulting equations for homogeneous states.

The previous Fokker–Planck model (drag force plus random stochastic term) assumes multiple approximations, so it is worth testing theoretical results against computer simulations. In particular, molecular dynamics (MD) simulations have been used to test the Fokker–Planck model [137] in several problems, including the onset of instabilities [141], rheological properties under shear [142–144], or binary suspensions in homogeneous situations [94]. Simulations using the discrete element model (DEM) method [145] and DNS data [146] have assessed kinetic-theory results for describing clustering instabilities. In addition, the direct simulation Monte Carlo (DSMC) method has been employed to validate different theoretical approaches used to solve the pertinent kinetic equations [98, 147]. In spite of the apparent simplicity of the suspension model, simulation results show in general good agreements.

This thesis is devoted to the study of the influence of the interstitial gas on the properties of granular particles. Kinetic theory tools will be used along the thesis. The theoretical results provided will be supplemented in most cases with Monte Carlo simulations. It is worth mentioning that both the study of monocomponent and binary suspensions will be addressed. In the former situation, the novelty of the results reported here with respect to previous works [148, 149] is based on the consideration of a new density dependence on the drag coefficient that may affect the dynamics properties of grains. On the other hand, since a real granular system is usually characterized by some degree of polydispersity in density and size, we will also study multicomponent suspensions. The importance of their study relies on the set of phenomena, such as particle segregation or demixing [150, 151], that has no monocomponent counterpart.

For the sake of simplicity, bidisperse suspensions composed of two species of solid particles immersed in a viscous fluid will be considered. Needless to say, the disparity of particles induces additional difficulties that prevents in some cases a clear theoretical description of such systems. Therefore, the lack of theoretical results regarding the influence of a fluid phase on the dynamic properties of a granular mixture is significant. For this reason, we will analyze first the impact of the interstitial fluid on the failure of the energy equipartition in granular mixtures (namely, that the granular temperature T could not be equally distributed among the species of the mixture). The nonequipartition is well-established in the case of granular mixtures since it has been studied by means of kinetic theory [152, 153], computer simulations [154–167] and real experiments [168, 169]. Hence, it is worthwhile to compare these results to those obtained when the Fokker–Planck model is accounted for. In addition, as happen in the monocomponent case [137, 148, 149] and for driven granular mixtures at low-densities [94], we want to see if the transport coefficients of moderately dense granular mixtures are perturbed by the presence of the external fluid and if so, quantify this influence. Note that this extension involves quite long and complex calculations since the number of transport coefficients are larger than for a single gas and additionally they depend on many parameters (masses and diameters, concentrations, and coefficients of restitution).

1.3 Structure of the Thesis

We have organized this thesis as follows.

In Chapter 2 we present the suspension model previously introduced in the context of dilute and low-Reynolds number gas-solid flows. Furthermore, we display the general theoretical and numerical tools employed throughout this work.

To begin with, we first consider an ensemble of identical *smooth* solid particles (hard disks or spheres) immersed in a viscous gas in Chapter 3 (**Article 1**). Collisions between grains are inelastic and are characterized by a (positive) constant coefficient of normal restitution $\alpha \leq 1$, where $\alpha = 1$ corresponds to elastic collisions (ordinary gases). The objective of **Article 1** is to consider the Enskog kinetic theory for moderately dense granular suspensions as a model to determine the NS transport coefficients. To do so, a Chapman–Enskog-like (CE) expansion [122] conveniently adapted to dissipative dynamics is applied to solve the Enskog kinetic equation. The first step is to characterize

the reference state in the perturbation scheme, namely the homogeneous steady state (HSS). In the HSS, the energy lost due to both inelastic collisions and the friction with the interstitial gas is exactly compensated for by the energy injected by the collisions with the more rapid particles of the molecular gas. This simple situation allows us to compute the steady granular temperature T and the kurtosis or fourth cumulant a_2 (measuring the deviation of the distribution function from its Maxwellian form). DSMC simulations compare very well with the theoretical predictions. Then, we assume that we slightly perturb the HSS by small spatial gradients. Explicit expressions for the NS transport coefficients under steady-state conditions are obtained. As an application, a linear stability analysis is performed showing that the HSS is always linearly stable with respect to long enough wavelength excitations. The new contributions of **Article 1** are two-fold. On the one side, the gas-solid interactions entail time-correlation forces; the response of the grains to an applied force is not simultaneous with the application of the force. Therefore, the collisions with the interstitial fluid and the cooling due to viscous friction and inelasticity cannot be locally compensated. This fact introduces the possibility of a local energy unbalance, and hence the zeroth-order distributions of the perturbation scheme are not in general stationary distributions. Nevertheless, previous articles [90, 170] are based on the simplifying assumption that the reference state is stationary at any point of the system. On the other side, this study extends previous works [148, 149] since, as usual in granular suspension models [125, 171], an additional density dependence is implemented on the reduced drag coefficient and, consequently, on the zeroth-order solution.

The extension of the monocomponent case to multicomponent granular suspensions is analyzed in Chapter 4 (**Articles 2** and **3**) and Chapter 5 (**Articles 4** and **5**). A subtle point of the model regards the drag coefficients of the mixture. One can chose that the body resistance is the same for both species, or distinguish the gas-solid interactions on the basis of the mechanical properties of each species. Here, for consistency with simulations of bidisperse gas-solid flows [172–174], we decided to pursue the second option. While Chapter 4 deals with homogeneous situations, Chapter 5 also considers an expansion in gradients of the HSS within the scope of the CE procedure to compute the transport coefficients.

Article 2 studies the homogeneous description of bidisperse granular suspension in the context of the Enskog equation. The lack of scale separation between microscopic

and macroscopic scales is one of the fundamental open question in granular gases [39, 175–177]. The reason is that collisional dissipation introduces a new time scale in the temperature evolution not present in elastic gases [4]. For this reason, we explore first the "aging to hydrodynamics". It is found that, regardless of the initial conditions, the system reaches a universal hydrodynamic regime where all the dependence of the system occurs through the (global) temperature. This fact simplifies further studies such as the determination of the transport coefficients of the mixture. After times longer than the mean-free time, the system is shown to reach a steady state. As a complement to the transient regime, a comprehensive study on the steady values of the properties is carried out. Moreover, theoretical results are confronted against DSMC simulations for both time-dependent and steady homogeneous states with an excellent agreement, excluding some discrepancies found in the steady values of the fourth cumulants.

Also in the transient regime, the discrimination on the way of interacting between the surrounding fluid and the individual species (encoded in the drag coefficients) provokes the emergence of memory effects. Memory effects are astonishingly common among nonequilibrium systems, including granular matter [178, 179]. Memory connotes the ability to encode, access, and erase signatures of past history in the state of a system [180]. A complete specification of the state of a macroscopic system requires knowledge of a very large number of variables. Thus, the evolution of granular suspensions is not uniquely determined by their current state (through the few macroscopic variables that one measures at an experiment), since it depends on the information contained in other "hidden" variables. Memories can have important practical consequences, such us jamming control, refrigeration times, or industrial handling and transport [179, 181]. In the case of bidisperse suspensions, the evolution of the (total) temperature is coupled with that of the partial temperatures of the species so unusual temperature relaxation towards the steady state turns up to be feasible. In this regard, the Mpemba effect (namely, when an initially hotter sample cools down sooner) [182, 183] is a memory effect frequently discussed in gas-solid literature [100, 184, 185]. On the other hand, given the complexity of the analytical expressions achieved for granular mixtures, it is preferable, at the outset, to analyze first ordinary mixtures (elastic collisions) to provide a straightforward explanation for the Mpemba-like effect. **Article 3** thoroughly analyzes the Mpemba effect in the context of molecular suspensions, for initial states

close to and far away from equilibrium. The extension to granular suspensions is accomplished in **Article 2**. DSMC and MD simulations concur with theoretical results in both molecular and granular systems.

The aim of Chapter 5 is to determine the NS transport coefficients of a binary granular suspension by means of the CE method. The starting point is the Enskog kinetic equations. Due to the inherent complexity of the kinetic equations, many of the pioneering papers [186–188] devoted to compute the NS transport coefficient of granular mixtures consider nearly elastic particles and equipartition of the total granular kinetic energy in the HCS. Although the failure of energy equipartition due to inelastic character of collisions is completely established and has been considered in more recent papers on granular mixtures [189–193], there is an additional contribution to the nonequipartition of energy not covered by the one appearing in the HCS. The origin of these inhomogeneous contributions comes from the fact that the partial temperatures of the species are non-hydrodynamic quantities. Thus, as stated in the CE method, they have to be perturbed in terms of gradients of the hydrodynamics fields (those that characterize the macroscopic state of the system). To the best of our knowledge, the first-order contributions to the partial temperature have only been calculated in elastic systems [194–196] and recently noticed in an Erratum for driven granular mixtures at low density [197]. Before considering binary granular suspensions, it would therefore seem appropriate to measure the influence of the first-order contributions to the partial temperatures on transport properties in polydisperse dense "dry" granular mixtures. These efforts are expected to further clarify the origin of violation of the equipartition theorem observed in real experiments of agitated granular mixtures [168, 169]. The goal of **Article 4** is to determine the first-order partial temperatures from the CE solution to the (inelastic) version of the Enskog kinetic equation [4]. In addition, we show the influence of these coefficients on the bulk viscosity and on the first-order contribution to the cooling rate, which cannot be neglected for disparate masses and/or strong dissipation. Once the basis of the CE procedure for binary granular mixtures is well consolidated, a systematic extension of previous theoretical results for dilute multicomponent granular suspensions [99] to moderate densities allows us to identify the NS transport coefficient. **Article 5** focuses on the evaluation of the mass and momentum fluxes for dense binary granular suspensions, together with the cooling rate up to first order in the spatial gradients.

In Chapter 6 (**Articles 6** and **7**) we study non-Newtonian rheological properties in dilute granular suspensions. **Article 6** addresses the study a set of smooth hard spheres immersed in a viscous fluid under simple or uniform shear flow (USF). Two simpler collision models that are often used to prevent the mathematical difficulties arising from the Boltzmann collision operator are considered to determine the velocity moments up to the fourth degree. These alternative models, that try to mimic the hard-sphere dynamics, are the so-called Inelastic Maxwell Models (IMM) [198] and a Bhatnagar-Gross-Krook (BGK)-type kinetic model [199]. The efforts of computing the second- and fourth-degree moments for IMM and BGK in the USF problem may be justified at least for two different reasons. The first one is to assess the reliability of the results derived for the IMM and BGK model when compared with those obtained for inelastic hard sphere (IHS) results obtained by Hayakawa *et al* [142, 143] by two alternative ways: (i) Grad's moment method to analytically solve the inelastic Boltzmann equation [200] and (ii) event-driven Langevin simulations for hard spheres (EDLSHS). As expected, a discontinuous shear thickening (DST) transition is observed when the viscosity abruptly increases above a critical value of the applied shear rate. On the other hand, the mathematical difficulties encountered in the form of the collision rate for hard spheres prevents the possibility of obtaining explicit results for higher velocity moments. To that effect, once the results derived from the IMM and BGK model show to qualitatively reproduce the rheological properties in the IHS model, we can go beyond to derive the first non-trivial higher-order velocity moments, namely the fourth-degree ones. The knowledge of the fourth-degree moments not only provides some indirect information of the distribution function, but also is required to analyze the stability of the USF state [201].

A more realistic approach in assessing the granular modeling is to consider inelastic rough spheres [51, 202]. In this model, apart from the normal coefficient of restitution α, a coefficient of tangential restitution $-1 \leq \beta \leq 1$ is introduced to measure the energy dissipation with respect to the angular velocity. While $\beta = -1$ refers to perfectly smooth spheres, $\beta = 1$ means perfectly rough spheres. Total energy is conserved in a collision in the cases $\alpha = 1$ and $\beta = \pm 1$. The purpose of **Article 7** is to assess the impact of roughness on the rheological properties of the suspensions. Following a model introduced years ago by Hess [203], we assume that the influence of the interstitial fluid in the rotational dynamics of grains is via a viscous drag force plus a stochastic

Langevin-like term, just as the translational part. This suspension model is solved by two different theoretical tools: (i) Grad's moment method and (ii) a BGK-type kinetic model for inelastic rough hard spheres [204]. As a complement of the previous results, we analyze the stability of the steady solution for non-Newtonian rheology. Surprisingly, the analysis shows that the steady solution is linearly unstable in some regions of the parameter space.

The work is ended with a brief discussion of the results reported in the thesis as well as the main conclusions.

Chapter 2

Kinetic Theory of Granular Suspensions

2.1 Introduction

In this Chapter we overview the theoretical tools together with the suspension model studied throughout this thesis and the alternative methods that will be used to solve the kinetic equations.

As discussed previously, one of the main aims in the context of rapid granular flows is the construction of pertinent hydrodynamics by means of kinetic theories for granular gases. The above theories have been developed to calculate collective properties of grains such as the granular temperature, distribution functions, or transport properties. Kinematics of grains are expressed in terms of the lower moments of the one-body distribution function $f(\mathbf{r}, \mathbf{v}; t)$. It is defined in such a way that $f(\mathbf{r}, \mathbf{v}; t)\mathrm{d}\mathbf{r}\mathrm{d}\mathbf{v}$ gives the average number of particles which at time t lie in the volume element $\mathrm{d}\mathbf{r}$ around the point $\mathbf{r}$ moving with instantaneous velocities in the range $\mathrm{d}\mathbf{v}$ about $\mathbf{v}$. Knowledge of the distribution function f permits us to establish a connection of macroscopic predictions with the underlying microscopic interactions.

The kinetic theory of inelastic hard spheres can be highly elaborated in close analogy with that for elastic collisions [4, 122, 205]. A rigorous derivation of the Boltzmann equation stems as a formulation in terms of a pseudo-Liouville equation for the N-particle distribution function, to obtain the Bogoliubov–Born–Green–Kirkwood–Yvon (BBGKY) hierarchy [206, 207]. Since the BBGKY hierarchy does not lead to a closed

set of equations for the distribution functions, a conjecture is assumed for the two-body distribution function $f_2(\mathbf{v_2}, \mathbf{r_2}, \mathbf{v_1}, \mathbf{r_1}; t)$ (it represents the probability of finding a particle at the point $\mathbf{r_1}$ and another at $\mathbf{r_2}$ at time t with velocities $\mathbf{v_1}$ and $\mathbf{v_2}$, respectively). For many-particle systems interacting via short-range potentials, the BBGKY hierarchy reduces to the so-called Boltzmann hierarchy in the Boltzmann-Grad limit [208–210]. In this case, the two-body distribution function f_2 factorizes into the product of the one-body distribution functions $f(\mathbf{r_1}, \mathbf{v_1}; t)$ and $f(\mathbf{r_2}, \mathbf{v_2}; t)$ for any pair of pre-collisional velocities $\mathbf{v_1}$ and $\mathbf{v_2}$. This is essentially the molecular chaos hypothesis (or *Stosszahlansatz*) used by Boltzmann to derive the governing equation for f [123, 206]. Note that the factorization of f_2 can be only applied to the velocities of the particles that are about to collide; after the collisions the velocities of the particles are strongly correlated. Nevertheless, it is very unlikely that two particles of a dilute gas recollide during a long period of time so the use of the molecular chaos hypothesis is justified. Apart from that, the Boltzmann equation has the property of preserving the initial chaos and therefore, it constitutes a closed equation for the one-body distribution function. A more intuitive and stepwise derivation of the Boltzmann equation for inelastic hard spheres by using a procedure similar to that made by Boltzmann himself in the case of elastic collisions can be found in Ref. [4].

For the sake of clarity, let us first consider a granular gas composed of inelastic hard disks ($d = 2$) or spheres ($d = 3$) of mass m and diameter σ. Here d indicates the dimension of the system. Particles are assumed to be completely smooth so that inelasticity of collisions is characterized only by the constant (positive) coefficient of restitution α ($\alpha \leq 1$). Multicomponent granular gases formed by particles with different mechanical properties are considered in Section 2.2.2. For low densities, the one-particle velocity distribution function $f(\mathbf{r}, \mathbf{v}; t)$ verifies the nonlinear Boltzmann kinetic equation:

$$\frac{\partial f}{\partial t} + \mathbf{v} \cdot \nabla f + \frac{1}{m} \frac{\partial}{\partial \mathbf{v}} \cdot (\mathbf{F} f) = J[\mathbf{v}|f, f], \tag{2.1}$$

where $\mathbf{F}(\mathbf{r}, \mathbf{v}; t)$ represents the action of an *external* force (for instance, the gravity) and the Boltzmann collision operator is

$$J[\mathbf{v}_1|f, f] = \sigma^{d-1} \int \mathrm{d}\mathbf{v}_2 \int \mathrm{d}\widehat{\boldsymbol{\sigma}}\, \Theta(\widehat{\boldsymbol{\sigma}} \cdot \mathbf{g}_{12})(\widehat{\boldsymbol{\sigma}} \cdot \mathbf{g}_{12}) \left[\alpha^{-2} f(\mathbf{v}_1'') f(\mathbf{v}_2'') - f(\mathbf{v}_1) f(\mathbf{v}_2)\right]. \tag{2.2}$$

Here, $\mathbf{g}_{12} = \mathbf{v}_1 - \mathbf{v}_2$ is the relative velocity, $\widehat{\boldsymbol{\sigma}}$ is a unit vector along the line of centers

of the two spheres at contact, and Θ is the Heaviside step function. The relationship between the pre-collisional velocities $(\mathbf{v}_1'', \mathbf{v}_2'')$ and the post-collisional velocities $(\mathbf{v}_1, \mathbf{v}_2)$ is

$$\mathbf{v}_1'' = \mathbf{v}_1 - \frac{1+\alpha}{2\alpha}(\widehat{\boldsymbol{\sigma}} \cdot \mathbf{g}_{12})\widehat{\boldsymbol{\sigma}}, \quad \mathbf{v}_2'' = \mathbf{v}_2 + \frac{1+\alpha}{2\alpha}(\widehat{\boldsymbol{\sigma}} \cdot \mathbf{g}_{12})\widehat{\boldsymbol{\sigma}}. \tag{2.3}$$

Equations (2.3) give the so-called inverse or *restituting* collisions. Inversion of these collision rules provides the form of the so-called *direct* collisions, namely, collisions where the pre-collisional velocities $(\mathbf{v}_1, \mathbf{v}_2)$ lead to the post-collisional velocities $(\mathbf{v}_1', \mathbf{v}_2')$ [60]:

$$\mathbf{v}_1' = \mathbf{v}_1 - \frac{1}{2}(1+\alpha)(\widehat{\boldsymbol{\sigma}} \cdot \mathbf{g}_{12})\widehat{\boldsymbol{\sigma}}, \quad \mathbf{v}_2' = \mathbf{v}_2 + \frac{1}{2}(1+\alpha)(\widehat{\boldsymbol{\sigma}} \cdot \mathbf{g}_{12})\widehat{\boldsymbol{\sigma}}. \tag{2.4}$$

A schematic representation of the inverse and direct collisions is illustrated in Fig. 2.1 for inelastic colliding spheres of diameters σ. From Eqs. (2.3) and (2.4), one gets the relations

$$\left(\widehat{\boldsymbol{\sigma}} \cdot \mathbf{g}_{12}''\right) = -\alpha^{-1}\left(\widehat{\boldsymbol{\sigma}} \cdot \mathbf{g}_{12}\right), \quad \left(\widehat{\boldsymbol{\sigma}} \cdot \mathbf{g}_{12}'\right) = -\alpha\left(\widehat{\boldsymbol{\sigma}} \cdot \mathbf{g}_{12}\right), \tag{2.5}$$

where $\mathbf{g}_{12}'' = \mathbf{v}_1'' - \mathbf{v}_2''$ and $\mathbf{g}_{12}' = \mathbf{v}_1' - \mathbf{v}_2'$. Since $\alpha \leq 1$, it is quite apparent from Eq. (2.5) that the magnitude of the normal component of the relative velocity decreases for inelastic collisions. In addition, the direct and inverse collisions are not equivalent when $\alpha < 1$ since there is no time reversal when the collisions are inelastic.

The change in kinetic energy of the colliding pair in a binary collision can be easily obtained from Eq. (2.4):

$$\Delta E \equiv E' - E = \frac{m}{2}\left[v_1'^2 + v_2'^2 - v_1^2 - v_2^2\right] = -\frac{m}{4}\left(\widehat{\boldsymbol{\sigma}} \cdot \mathbf{g}_{12}\right)^2\left(1-\alpha^2\right), \tag{2.6}$$

Therefore, for elastic collisions ($\alpha = 1$), $\Delta E = 0$ and then the energy is conserved in a collision. Otherwise, $\Delta E < 0$ and part of the kinetic energy of two colliding grains is lost.

Equation (2.1) is restricted to the case of a low density gas. At higher densities, the revised Enskog kinetic theory (RET) is known to be the most general theory that provide an accurate description of elastic gases [211–214]. Its generalization to inelastic collisions constitutes a unique basis for the description of granular gases at moderate densities [57, 77, 215]. The Enskog kinetic equation is given by

$$\frac{\partial f}{\partial t} + \mathbf{v} \cdot \nabla f + \frac{1}{m}\frac{\partial}{\partial \mathbf{v}} \cdot (\mathbf{F} f) = J_{\mathrm{E}}[\mathbf{r}, \mathbf{v}|f, f], \tag{2.7}$$

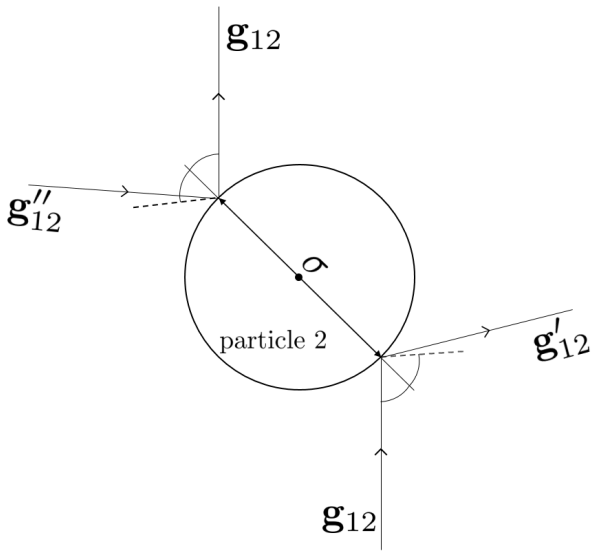

Figure 2.1: Direct and inverse inelastic binary collisions in the reference frame of particle 2. The spheres have a common diameter σ. The solid lines correspond to a given case where the coefficient of restitution satisfies $0 < \alpha < 1$. The dashed lines correspond to elastic collisions ($\alpha = 1$).

where the Enskog collision operator is

$$J_{\mathrm{E}}[\mathbf{r},\mathbf{v}_1|f,f] = \sigma^{d-1}\int \mathrm{d}\mathbf{v}_2 \int \mathrm{d}\widehat{\boldsymbol{\sigma}}\ \Theta(\widehat{\boldsymbol{\sigma}}\cdot\mathbf{g}_{12})(\widehat{\boldsymbol{\sigma}}\cdot\mathbf{g}_{12})\left[\alpha^{-2}\chi(\mathbf{r},\mathbf{r}-\boldsymbol{\sigma})f(\mathbf{r},\mathbf{v}_1'';t)\right.$$
$$\left.\times f(\mathbf{r}-\boldsymbol{\sigma},\mathbf{v}_2'';t) - \chi(\mathbf{r},\mathbf{r}+\boldsymbol{\sigma})f(\mathbf{r},\mathbf{v}_1;t)f(\mathbf{r}+\boldsymbol{\sigma},\mathbf{v}_2;t)\right]. \tag{2.8}$$

The notation here is the same as in Eqs. (2.1) and (2.2). In contrast to the Boltzmann equation, the Enskog theory accounts for the separation of the centers of the colliding spheres since the diameter of the sphere σ is not negligible when compared with the mean free path between particles ℓ (i.e., the average length that a particle travels between two successive collisions). As a consequence, the distribution function varies over distances equal to the diameter of the spheres (represented by $\pm\boldsymbol{\sigma} = \pm\sigma\widehat{\boldsymbol{\sigma}}$). Although the Enskog equation still maintains the molecular chaos hypothesis, it takes into account spatial correlations through the pair correlation distribution function at contact $\chi[\mathbf{r}_1,\mathbf{r}_2|n(t)]$. In the RET, the pair correlation function χ is the same as that of an equilibrium system with non-uniform density field

$$n(\mathbf{r};t) = \int \mathrm{d}\mathbf{v}\ f(\mathbf{r},\mathbf{v};t). \tag{2.9}$$

2.2 Suspension Model

2.2.1 Monocomponent case

We consider the same system of smooth spheres characterized in Section 2.1 at moderate densities. Nevertheless, the solid particles are immersed in an ordinary gas of viscosity η_{g}. Figure 2.2 shows a schematic diagram of the system considered in this section. For the sake of generality, let us assume that the whole system is in the presence of a gravitational field, so that each particle feels the action of the force $F_i = m_i g$, where g is the gravity acceleration. As usual, the action of the external fluid on the motion of particles is accounted for by the action of an effective external force [116, 137, 141–144]. This approach leads to the following Enskog equation [4]

$$\frac{\partial f}{\partial t} + \mathbf{v}\cdot\nabla f + \mathbf{g}\cdot\frac{\partial f}{\partial \mathbf{v}} + \mathcal{F} f = J_{\mathrm{E}}[\mathbf{r},\mathbf{v}|f,f]. \tag{2.10}$$

In Eq. (2.10) the operator $\mathcal{F}$ represents the fluid-solid interaction force that models the effect of the viscous gas on the solid particles. Although not explicitly stated, the form of the Enskog equation (2.10) has been obtained by writing the equation of motion for a particle of velocity $\mathbf{v}$ as [92, 136, 216–218]

$$m\dot{\mathbf{v}} = \mathbf{F}^{\mathrm{int}} + \mathbf{F}^{\mathrm{coll}}, \tag{2.11}$$

where $\mathbf{F}^{\mathrm{int}}$ tries to mimic the fluid-solid interaction while $\mathbf{F}^{\mathrm{coll}}$ is the force due to grain-grain collisions. A crucial assumption of this model is that the action of the external fluid is decoupled from that of the collisions. Namely, the Enskog collision operator is the same as for a granular gas where the presence of the interstitial gas is neglected. This hypothesis holds up when the mean free time between collisions τ is much smaller than the time needed by the gas to notably affect the dynamics of grains [116, 125, 127, 128]. In other words, the surrounding fluid must be dilute enough in such a manner that its influence on the collision process can be ignored.

For low-Reynolds numbers, the external fluid-solid force can be decomposed into two independent terms: (i) a viscous drag force $\mathbf{F}^{\mathrm{drag}}$ proportional to the instantaneous velocity $\mathbf{v}$ of the particle and (ii) an stochastic Langevin-like term $\mathbf{F}^{\mathrm{st}}$. While the first term models the viscous friction on grains, the second tries to mimic the random collisions with the particles of the bath. In addition, since the model tries to model

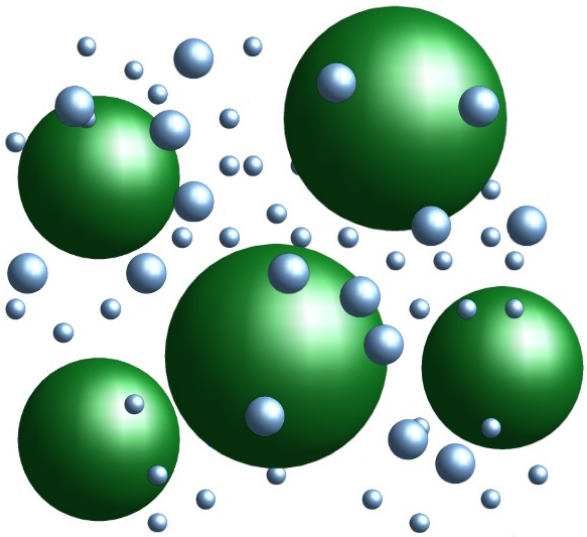

Figure 2.2: Schematic representation of a granular suspension. Solid particles are immersed in a carrier fluid of mass $m_g \ll m$.

gas-solid flows, the drag is referred to the known mean flow velocity of the gas phase $\mathbf{U}_g$. Thus, the drag force

$$\mathbf{F}^{\text{drag}} = -m\gamma(\mathbf{v} - \mathbf{U}_g) \tag{2.12}$$

is represented in the Enskog equation (2.10) by the operator

$$\mathbf{F}^{\text{drag}} f = -\gamma \frac{\partial}{\partial \mathbf{v}} \cdot (\mathbf{v} - \mathbf{U}_g) f, \tag{2.13}$$

being γ the drag or friction coefficient. The second term $\mathbf{F}^{\text{st}}$ is represented by a Gaussian white noise with the conditions [219]

$$\langle \mathbf{F}_i^{\text{st}}(t) \rangle = 0, \quad \langle \mathbf{F}_i^{\text{st}}(t) \mathbf{F}_j^{\text{st}}(t') \rangle = 2m^2 \gamma T_{\text{ex}} \mathrm{I} \delta_{ij} \delta(t - t'), \tag{2.14}$$

where I is a unit tensor and i and j refer to different particles. Since we want that the gas phase drives the granular gas acting as a bulk thermostat, the temperature of the bath T_{ex} is assumed to be constant. Note that in contrast to previous works in granular gases driven by thermostats [99], the strength of the correlation in Eq. (2.14) is chosen to be consistent with the fluctuation-dissipation theorem for elastic collisions [219]. The representation of the white-noise operator acting on the distribution f in

the Enskog equation is given by[1] [220]

$$\mathbf{F}^{\mathrm{st}} f = -\frac{\gamma T_{\mathrm{ex}}}{m}\frac{\partial^2}{\partial v^2} f. \tag{2.15}$$

Therefore, according to equations (2.13) and (2.15), the Enskog equation (2.10) reads

$$\frac{\partial f}{\partial t} + \mathbf{v}\cdot\nabla f + \mathbf{g}\cdot\frac{\partial f}{\partial \mathbf{v}} - \gamma\Delta\mathbf{U}\cdot\frac{\partial f}{\partial \mathbf{v}} - \gamma\frac{\partial}{\partial \mathbf{v}}\cdot(\mathbf{V}f) - \frac{\gamma T_{\mathrm{ex}}}{m}\frac{\partial^2 f}{\partial v^2} = J_{\mathrm{E}}[\mathbf{r},\mathbf{v}|f,f]. \tag{2.16}$$

Here, $\Delta\mathbf{U} = \mathbf{U} - \mathbf{U}_{\mathrm{g}}$, $\mathbf{V} = \mathbf{v} - \mathbf{U}$ is the peculiar velocity, and

$$\mathbf{U}(\mathbf{r};t) = \frac{1}{n(\mathbf{r};t)}\int \mathrm{d}\mathbf{v}\ \mathbf{v} f(\mathbf{r},\mathbf{v};t) \tag{2.17}$$

is the mean flow velocity of the solid particles. As discussed above, since granular gases are athermal, we define the *granular* temperature as the variance of the velocity of particles with respect to the mean flow velocity $\mathbf{U}$ of the granular gas. Namely,

$$T(\mathbf{r};t) = \frac{m}{dn(\mathbf{r};t)}\int \mathrm{d}\mathbf{v}\ \mathbf{V}(\mathbf{r};t)^2 f(\mathbf{r},\mathbf{v};t). \tag{2.18}$$

To completely define the suspension model, it still remains to explicitly write the drag coefficient γ. Although the drag coefficient is in general a tensor, for dilute suspensions one can assume that γ is a scalar proportional to the viscosity of the solvent $\eta_{\mathrm{g}} \propto T_{\mathrm{ex}}$ [116]. In addition, following the investigations of granular suspensions by Koch and Sangani [125, 171], γ depends on density through the solid volume fraction

$$\phi = \frac{\pi^{d/2}}{2^{d-1} d\Gamma\left(\frac{d}{2}\right)} n\sigma^d. \tag{2.19}$$

Therefore, we can write γ as

$$\gamma = \gamma_0 R(\phi), \quad \gamma_0 \propto \eta_{\mathrm{g}}. \tag{2.20}$$

[1] In what follows we will take temperature as units of energy so that $k_{\mathrm{B}} = 1$.

For hard spheres ($d = 3$), the function $R(\phi)$ is given by [125, 171]

$$R(\phi) = \begin{cases} 1 + 3\sqrt{\dfrac{\phi}{2}}, & \text{if } \phi \leq 0.1 \\ 1 + \dfrac{3}{\sqrt{2}}\phi^{1/2} + \dfrac{135}{64}\phi \ln \phi + 11.26 & \\ \times \phi\left(1 - 5.1\phi + 16.57\phi^2 - 21.77\phi^3\right) - \phi\chi(\phi)\ln\epsilon_m, & \text{if } \phi > 0.1 \end{cases} . \quad (2.21)$$

The parameter ϵ_m mimics lubrication forces between two approaching particles and its value lies in the range $[0.01, 0.05]$. Here, we set $\epsilon_m = 0.01$ for the sake of simplicity. Expression (2.21) has been derived by using an analytical closure for Stokes flow in the case of very dilute suspensions ($\phi \leq 0.1$) [125] and simulations based on multipole expansion at higher densities ($\phi > 0.1$) [171].

2.2.2 Binary mixtures

A real granular gas is composed of particles of disparate nature in the sense that its composition in terms of masses and sizes is quite varied. To account for the effect of dispersity, we consider here a binary mixture of hard disks or spheres of masses m_i and diameters σ_i (i=1,2) immersed in a viscous fluid. As above, collisions among particles are characterized by a constant normal coefficient of restitution $\alpha_{ij} \leq 1$. Indices i and j refer to collisions between particles of species i and j. An example of a binary suspension is illustrated in Fig. 2.3. The extension of the Enskog equation (2.7) to polydisperse mixtures is straightforward. In the case of a binary suspension subjected to the action of gravity, the one-body velocity distribution function $f_i(\mathbf{r}, \mathbf{v}; t)$ of the species or component i verifies the set of two coupled Enskog equations [4]

$$\frac{\partial f_i}{\partial t} + \mathbf{v}\cdot\nabla f_i + \mathbf{g}\cdot\frac{\partial f_i}{\partial \mathbf{v}} + \mathcal{F}_i f_i = \sum_{j=1}^{2} J_{\mathrm{E},ij}[\mathbf{r}, \mathbf{v}|f_i, f_j], \quad (2.22)$$

where the Enskog collision operator is

$$\begin{aligned} J_{\mathrm{E},ij}[\mathbf{r}, \mathbf{v}_1|f_i, f_j] \;=\; & \sigma_{ij}^{d-1}\int \mathrm{d}\mathbf{v}_2 \int \mathrm{d}\widehat{\boldsymbol{\sigma}}\; \Theta(\widehat{\boldsymbol{\sigma}}\cdot\mathbf{g}_{12})(\widehat{\boldsymbol{\sigma}}\cdot\mathbf{g}_{12})\Big[\alpha_{ij}^{-2}\chi_{ij}(\mathbf{r}, \mathbf{r}-\boldsymbol{\sigma}_{ij}) \\ & f_i(\mathbf{r}, \mathbf{v}_1''; t)\times f_j(\mathbf{r}-\boldsymbol{\sigma}_{ij}, \mathbf{v}_2''; t) - \chi_{ij}(\mathbf{r}, \mathbf{r}+\boldsymbol{\sigma}_{ij}) \\ & f(\mathbf{r}, \mathbf{v}_1; t) f(\mathbf{r}+\boldsymbol{\sigma}_{ij}, \mathbf{v}_2; t)\Big]. \end{aligned} \quad (2.23)$$

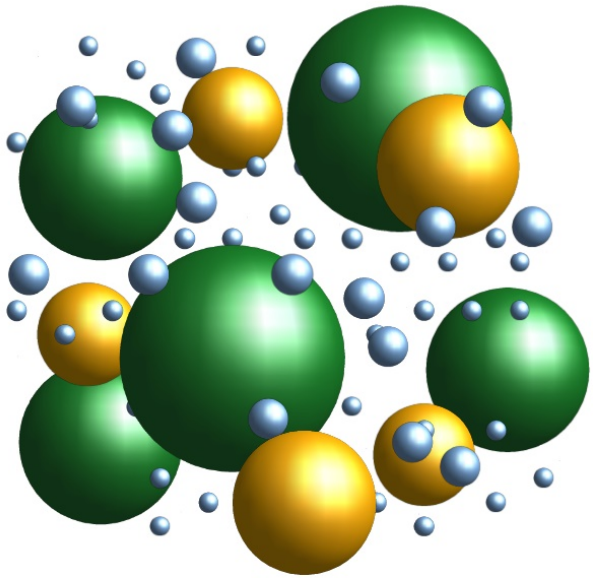

Figure 2.3: Schematic representation of a bidisperse suspension. Two kinds of particles of masses m_1 and m_2 are immersed in an interstitial gas of mass $m_g \ll m_{1,2}$.

In Eq. (2.22) the operator $\mathcal{F}_i$ models the effect of the surrounding gas on the solid particles of the species i. The notation is the same as in Eqs. (2.1) and (2.2), except that $\boldsymbol{\sigma}_{ij} = \sigma_{ij}\widehat{\boldsymbol{\sigma}}$, $\sigma_{ij} = (\sigma_i + \sigma_j)/2$ and $\chi_{ij}(\mathbf{r}, \mathbf{r} \pm \boldsymbol{\sigma}_{ij})$. The latter is the equilibrium pair correlation function of two hard spheres, one for the species i and the other for the species j at contact (namely, when the distance between their centers is σ_{ij}). In addition, the precollisional velocities $(\mathbf{v}_1'', \mathbf{v}_2'')$ are given by

$$\mathbf{v}_1'' = \mathbf{v}_1 - \mu_{ji}\left(1 + \alpha_{ij}^{-1}\right)(\widehat{\boldsymbol{\sigma}} \cdot \mathbf{g}_{12})\widehat{\boldsymbol{\sigma}}, \quad \mathbf{v}_2'' = \mathbf{v}_2 + \mu_{ij}\left(1 + \alpha_{ij}^{-1}\right)(\widehat{\boldsymbol{\sigma}} \cdot \mathbf{g}_{12})\widehat{\boldsymbol{\sigma}}, \tag{2.24}$$

where $\mu_{ij} = m_i/(m_i + m_j)$. The form of the corresponding Boltzmann collision operator $J_{ij}[f_i, f_j]$ can be derived from Eq. (2.22) by taking $\chi_{ij}(\mathbf{r}, \mathbf{r} \pm \boldsymbol{\sigma}_{ij}) \to 1$ and $f_j(\mathbf{r} \pm \boldsymbol{\sigma}_{ij}) \simeq f_j(\mathbf{r})$ in the operator $J_{\mathrm{E},ij}[\mathbf{r}, \mathbf{v}_1 | f_i, f_j]$ given in Eq. (2.23). Its explicit form is

$$\begin{aligned} J_{ij}[\mathbf{v}_1|f_i, f_j] &= \sigma_{ij}^{d-1} \int d\mathbf{v}_2 \int d\widehat{\boldsymbol{\sigma}}\, \Theta(\widehat{\boldsymbol{\sigma}} \cdot \mathbf{g}_{12})(\widehat{\boldsymbol{\sigma}} \cdot \mathbf{g}_{12}) \Big[\alpha_{ij}^{-2} f_i(\mathbf{v}_1'') f_j(\mathbf{v}_2'') \\ &\quad - f_i(\mathbf{v}_1) f_j(\mathbf{v}_2)\Big]. \end{aligned} \tag{2.25}$$

Turning now to the suspension model, the expression of $\mathcal{F}_i$ is discussed below. As in the monocomponent case, if the gas phase is dilute enough, $\mathcal{F}_i$ takes the form of a Fokker-Plank operator (drag plus stochastic terms). A crucial point of the model regards the selection of $\mathcal{F}_i$ with respect to the way of interchange of energy between the bath and each species. The simplest option would be to define $\mathcal{F}_i$ to be the same for both species. However, in accordance with simulations of bidisperse gas-solid flows [172–174], the drag coefficients γ_i of the species $i = 1, 2$ are chosen to be different. Thus, the extension of Eqs. (2.13) and (2.15) to binary mixtures yields the following expression for the operator $\mathcal{F}_i$

$$\mathcal{F}_i f_i = \mathcal{F}_i^{\text{drag}} f_i + \mathcal{F}_i^{\text{st}} f_i = -\gamma_i \Delta\mathbf{U} \cdot \frac{\partial f}{\partial \mathbf{v}} - \gamma_i \frac{\partial}{\partial \mathbf{v}} \cdot (\mathbf{V} f_i) - \frac{\gamma_i T_{\text{ex}}}{m_i} \frac{\partial^2 f_i}{\partial v^2}. \tag{2.26}$$

The set of Enskog equations (2.22) reads

$$\frac{\partial f_i}{\partial t} + \mathbf{v}\cdot\nabla f_i + \mathbf{g}\cdot\frac{\partial f_i}{\partial \mathbf{v}} - \gamma_i \Delta\mathbf{U}\cdot\frac{\partial f}{\partial \mathbf{v}} - \gamma_i \frac{\partial}{\partial \mathbf{v}}\cdot(\mathbf{V} f_i) - \frac{\gamma_i T_{\text{ex}}}{m_i}\frac{\partial^2 f_i}{\partial v^2} = \sum_{j=1}^{2} J_{\text{E},ij}[\mathbf{r}, \mathbf{v}|f_i, f_j], \tag{2.27}$$

where the local mean flow velocity of the mixture is

$$\mathbf{U}(\mathbf{r}; t) = \frac{1}{\rho(\mathbf{r}; t)} \sum_{i=1}^{2} \int \mathrm{d}\mathbf{v}\ m_i \mathbf{v} f_i(\mathbf{r}, \mathbf{v}; t). \tag{2.28}$$

Here, $\rho = \sum_i \rho_i$ is the total mass density and $\rho_i = n_i m_i$ is the mass density of the species i defined in terms of the local number density of the species i. Namely,

$$n_i(\mathbf{r}; t) = \int \mathrm{d}\mathbf{v}\ f_i(\mathbf{r}, \mathbf{v}; t). \tag{2.29}$$

Apart from the partial densities n_i and the flow velocity $\mathbf{U}$, the other important hydrodynamic field is the granular temperature T . It is defined as

$$nT = \sum_i n_i T_i, \tag{2.30}$$

where $n = n_1 + n_2$ is the total number density. Moreover,

$$T_i = \frac{m_i}{d n_i} \int \mathrm{d}\mathbf{v}\ V^2 f_i(\mathbf{v}) \tag{2.31}$$

is the partial temperature of the species i.

Consistent with the monocomponent case, we define γ_i as scalars that depend on density. In this case, the results obtained in lattice-Boltzmann simulations of low-Reynolds-number fluid flow in bidisperse suspensions [172–174] provide the expressions of γ_i. They are given by $\gamma_i = \gamma_0 R(\phi, \phi_i)$, where

$$\gamma_0 = \frac{18\eta_g}{\rho\sigma_{12}^2}, \quad R(\phi,\phi_i) = \frac{\rho\sigma_{12}^2}{\rho_i\sigma_i^2}\frac{(1-\phi)\phi_i\sigma_i}{\phi}\sum_{i=1}^{2}\frac{\phi_j}{\sigma_j}\left[\frac{10\phi}{(1-\phi)^2}+(1-\phi)^2(1+1.5)\sqrt{\phi}\right]. \tag{2.32}$$

Here, ϕ_i is the partial volume fraction of the species i and $\phi = \phi_i + \phi_2$ is the total volume fraction.

2.2.3 Rough spheres

Let us consider a dilute ensemble of inelastic rough hard spheres of diameter σ, mass m, and moment of inertia I immersed in a molecular gas. Inelasticity of collisions among particles is characterized by a coefficient of normal restitution ($\alpha \leq 1$) and a coefficient of tangential restitution ($-1 \leq \beta \leq 1$). For the sake of clarification, a schematic representation of the rough-spheres multiphase system can be found in Fig. 2.4. As in the case of binary mixtures, the Boltzmann equation (2.1) can be easily extended to the case of rough spheres. In these circumstances, the one-body distribution function $f(\mathbf{r}, \mathbf{v}, \boldsymbol{\omega}; t)$ gives the average number of particles which at instant t have linear velocities $\mathbf{v}$ and angular velocities $\boldsymbol{\omega}$. In addition, as before we assume that the influence of the interstitial gas on grains is via an effective instantaneous force characterized by the operator $\mathcal{F}f$. Contemplating the effects of the gravity field, the velocity distribution f obeys the Boltzmann kinetic equation [4, 60, 202, 221, 222]

$$\frac{\partial f}{\partial t} + \mathbf{v}\cdot\nabla f + \mathbf{g}\cdot\frac{\partial f}{\partial \mathbf{v}} + \mathcal{F}f = J\big[\mathbf{v},\boldsymbol{\omega}|f,f\big], \tag{2.33}$$

where $J[f,f]$ is the Boltzmann collision operator given by [4, 60]

$$\begin{aligned} J[\mathbf{v}_1,\boldsymbol{\omega}_1|f,f] &= \sigma^2\int \mathrm{d}\mathbf{v}_2\int \mathrm{d}\boldsymbol{\omega}_2\int \mathrm{d}\widehat{\boldsymbol{\sigma}}\;\Theta(\widehat{\boldsymbol{\sigma}}\cdot\mathbf{g})(\widehat{\boldsymbol{\sigma}}\cdot\mathbf{g})\Big[\frac{1}{\alpha^2\beta^2}f(\mathbf{r},\mathbf{v}_1'',\boldsymbol{\omega}_1'';t) \\ &\quad \times f(\mathbf{r},\mathbf{v}_2'',\boldsymbol{\omega}_2'';t) - f(\mathbf{r},\mathbf{v}_1,\boldsymbol{\omega}_1;t)f(\mathbf{r},\mathbf{v}_2,\boldsymbol{\omega}_2;t)\Big]. \end{aligned} \tag{2.34}$$

In Eq. (2.34), the collision rules that govern the change of the precollisional velocities

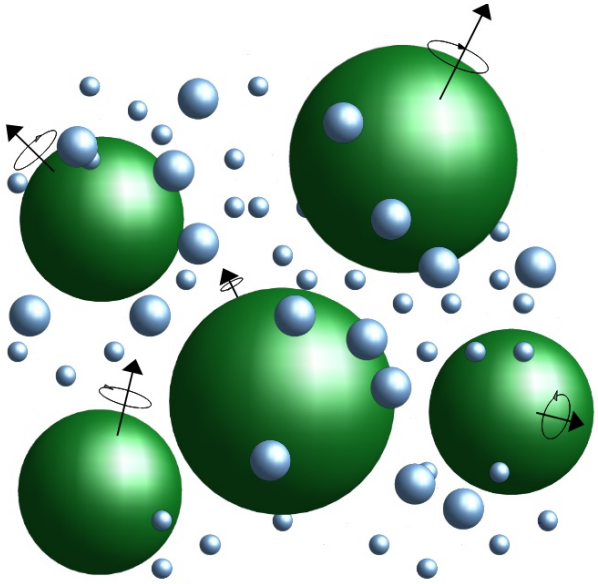

Figure 2.4: Schematic representation of a system of rough spheres immersed in a molecular gas of mass $m_g \ll m$.

$\{\mathbf{v}_1'', \boldsymbol{\omega}_1'', \mathbf{v}_2'', \boldsymbol{\omega}_2''\}$ into $\{\mathbf{v}_1, \boldsymbol{\omega}_1, \mathbf{v}_2, \boldsymbol{\omega}_2\}$ are [202, 221–224]

$$\mathbf{v}_1'' = \mathbf{v}_1 - \mathbf{Q}'', \quad \mathbf{v}_2'' = \mathbf{v}_2 + \mathbf{Q}'', \tag{2.35}$$

$$\boldsymbol{\omega}_1'' = \boldsymbol{\omega}_1 - \frac{2}{\sigma\kappa}\widehat{\boldsymbol{\sigma}} \times \mathbf{Q}'', \quad \boldsymbol{\omega}_2'' = \boldsymbol{\omega}_2 - \frac{2}{\sigma\kappa}\widehat{\boldsymbol{\sigma}} \times \mathbf{Q}'', \tag{2.36}$$

where the impulse $\mathbf{Q}''$ is given by

$$\mathbf{Q}'' = \frac{1+\alpha^{-1}}{2}\widehat{\boldsymbol{\sigma}}(\widehat{\boldsymbol{\sigma}} \cdot \mathbf{g}) - \frac{\kappa}{1+\kappa}\frac{1+\beta^{-1}}{2}\Big[\widehat{\boldsymbol{\sigma}}(\widehat{\boldsymbol{\sigma}} \cdot \mathbf{g}) - \mathbf{g} + \frac{\sigma}{2}\widehat{\boldsymbol{\sigma}} \times (\boldsymbol{\omega}_1 + \boldsymbol{\omega}_2)\Big]. \tag{2.37}$$

In Eqs. (2.36) and (2.37), $\kappa = 4I/m\sigma^2$ is a dimensionless parameter characterizing the mass distribution within a sphere. The parameter κ runs from the values $\kappa = 0$ (mass concentrated on the center) and $\kappa = \frac{2}{3}$ (mass concentrated on the surface). In the case of uniformly distributed mass, $\kappa = \frac{2}{5}$.

As in the previous models of granular suspensions described in 2.2.1 and 2.2.2, the operator $\mathcal{F}$ has the form of a Fokker–Plank equation when acting on the translational degrees of freedom of the spheres. On the other hand, although the effect of the

external fluid on the angular velocity of particles is not known a priori, we expect that the mathematical structure of this terms is similar to the translational case. In fact, following a generalized Fokker–Planck equation for rotating spheres proposed many years ago by Hess [203], we write the operator $\mathcal{F}f$ as

$$\mathcal{F}f = \mathcal{F}^{\text{tr}}f + \mathcal{F}^{\text{rot}}f, \tag{2.38}$$

where $\mathcal{F}^{\text{tr}}$ and $\mathcal{F}^{\text{rot}}$ denote the corresponding Fokker–Planck terms associated with the translational and rotational degrees of freedom of spheres. As usual, the translational part $\mathcal{F}^{\text{tr}}f$ can be written as in Eqs. (2.13) and (2.15). Namely,

$$\mathcal{F}^{\text{tr}}f = -\gamma_t \frac{\partial}{\partial \mathbf{v}} \cdot (\mathbf{v} - \mathbf{U}_g) f - \gamma_t \frac{T_{\text{ex}}}{m} \frac{\partial^2 f}{\partial v^2}, \tag{2.39}$$

where γ_t now refers to the drag coefficient associated with the translational degrees of freedom. In the case of very dilute suspensions, $\gamma_t = 3\pi\sigma\eta_g/m$. Similarly, the rotational part $\mathcal{F}^{\text{rot}}f$ has an analogous structure to Eq. (2.39) except that the linear velocity $\mathbf{v}$ is replaced by the angular velocity $\boldsymbol{\omega}$. It is given by [203]

$$\mathcal{F}^{\text{rot}}f = -\gamma_r \frac{\partial}{\partial \boldsymbol{\omega}} \cdot \boldsymbol{\omega} f - \gamma_r \frac{T_{\text{ex}}}{m} \frac{\partial^2 f}{\partial \omega^2}, \tag{2.40}$$

where $\gamma_r = \pi\sigma^3\eta_g/I$. Note that we are assuming for simplicity that the mean angular velocity of the surrounding gas is zero. Moreover, for the sake of consistency with Grad's solution in the USF (defined in terms of a *two-temperature* Maxwellian distribution (2.56) where the translational and rotational degrees of freedom are decorrelated) we are also neglecting in Eqs. (2.39) and (2.40) the coupling of translational and rotational velocities. Besides symmetry considerations, it must be remarked that this model has been recently considered to study the segregation dynamics in a binary mixture of microswimmers with good agreement between experiments and theory [225].

According to Eqs. (2.39) and (2.40), the Boltzmann kinetic equation (2.33) can be written as

$$\frac{\partial f}{\partial t} + \mathbf{v}\cdot\nabla f - \gamma_t \Delta\mathbf{U}\cdot\frac{\partial f}{\partial \mathbf{v}} - \gamma_t \frac{\partial}{\partial \mathbf{v}}\cdot\mathbf{V} f - \gamma_t \frac{T_{\text{ex}}}{m}\frac{\partial^2 f}{\partial v^2} - \gamma_r \frac{\partial}{\partial \boldsymbol{\omega}}\cdot\boldsymbol{\omega} f - \gamma_r \frac{T_{\text{ex}}}{I}\frac{\partial^2 f}{\partial \omega^2} = J[f,f], \tag{2.41}$$

where

$$\mathbf{U}(\mathbf{r};t)=\frac{1}{n(\mathbf{r};t)}\int \mathrm{d}\mathbf{v}\int \mathrm{d}\boldsymbol{\omega}\ \mathbf{v}f(\mathbf{r},\mathbf{v},\boldsymbol{\omega};t) \tag{2.42}$$

is the mean flow velocity of rough spheres and

$$n(\mathbf{r};t)=\int \mathrm{d}\mathbf{v}\int \mathrm{d}\boldsymbol{\omega}\ f(\mathbf{r},\mathbf{v},\boldsymbol{\omega};t) \tag{2.43}$$

is the number density. In the rough case, the temperature is defined as

$$T=\frac{1}{2}\left(T_t+T_r\right), \tag{2.44}$$

where the (partial) translational T_t and rotational T_r temperatures are defined as

$$T_t(\mathbf{r};t) = \frac{m}{3n(\mathbf{r};t)}\int \mathrm{d}\mathbf{v}\int \mathrm{d}\boldsymbol{\omega}\ V^2 f(\mathbf{r},\mathbf{v},\boldsymbol{\omega};t), \tag{2.45}$$

$$T_r(\mathbf{r};t) = \frac{I}{3n(\mathbf{r};t)}\int \mathrm{d}\mathbf{v}\int \mathrm{d}\boldsymbol{\omega}\ \omega^2 f(\mathbf{r},\mathbf{v},\boldsymbol{\omega};t). \tag{2.46}$$

It is worth noting that we have not referred the angular velocities ω to the mean value $\Omega=\langle\boldsymbol{\omega}\rangle$ in the definition of T_r because the total temperature $T=(T_t+T_r)/2$ would not then be a conserved quantity for $\alpha=\beta=1$.

2.3 The Chapman–Enskog Method

The Chapman–Enskog (CE) method conveniently adapted to inelastic collisions will be implemented to solve the Enskog equations of monocomponent suspensions, dry granular mixtures, and bidisperse suspensions in Articles 1, 4, and 5, respectively.

As we have already discussed, one of the main aims of kinetic theory is to express the macroscopic properties of the system in terms of microscopic quantities. In the case of granular suspensions, two new ingredients are added in the balance equations with respect to ordinary gases: (i) a cooling term characterizing the rate of energy dissipated due to the inelasticity of collisions and (ii) the influence of the external bath by means of the presence of the drag coefficients and the external temperature T_{ex}. Therefore, the macroscopic balance equations are not closed equations for the hydrodynamic fields $\{n,\mathbf{U},T\}$ ($\{n_1,n_2,\mathbf{U},T\}$ in a binary mixture) due to the presence, not only of the pressure tensor P, the heat flux $\mathbf{q}$, and the mass flux $\mathbf{j}_i$ for species i in the case of a

mixture [122], but also of the cooling rate ζ[1] [see for instance Eqs. (20-22) of Article 4]. To close these equations, one has to express the fluxes and the cooling rate in terms of the hydrodynamic fields and their spatial gradients. Explicit knowledge of f together with Eqs. (2.21) and (2.22) would yield a closed set of equations for the hydrodynamic fields. Although the exact form of f is not known, a good approximation of this distribution can be derived by looking for a *normal* (or hydrodynamic) solution to the kinetic equation. The existence of a normal solution implies that all space and time dependence of the velocity distribution function only occurs through the hydrodynamic fields:

$$f(\mathbf{v},\mathbf{r};t) = f\left[\mathbf{v}|n(\mathbf{r};t),T(\mathbf{r};t),U(\mathbf{r};t)\right]. \tag{2.47}$$

The notation on the right hand side indicates a functional dependence on the density, temperature and flow velocity.

The conjecture raised in Eq. (2.47) can be clearly justified when analyzing the time evolution of granular suspensions. In analogy to the molecular case [122, 123, 205], the evolution of granular suspensions towards a steady state goes through two different stages as follows [4, 60]. At a very early stage ($t \sim \tau$, τ being the mean free time), a kinetic regime drives the evolution of granular suspensions. The first collisions between neighboring particles take place and the main effect of collisions is to relax quickly the gas toward a local time-dependent non-equilibrium distribution function (the so-called local homogeneous cooling state in the case of dry granular gases). This kinetic stage has a high dependence on the initial conditions. Then, for times much longer than the mean free time ($t \gg \tau$), a hydrodynamics stage is identified. Since the hydrodynamic fields are collisional *invariants* in the case of molecular gases (namely, the density of mass, momentum, and energy are conserved in elastic collisions), the classical CE method considers that the hydrodynamic regime is characterized by a slower evolution of the hydrodynamic fields as they approach towards the global equilibrium. Therefore, at this second stage, the response of the system to any spatial deviation from the local equilibrium distribution will be characterized by the evolution of the fields n, $\mathbf{U}$, and T. Although the temperature is not conserved in granular systems, kinetic models as well as DSMC and MD simulations suggest that the granular temperature can still be considered as a *slow* variable (i.e., its time evolution is much slower than other velocity

[1]For the sake of clarity, we will consider henceforth a monocomponent gas. The application of the CE method to bidisperse granular gases is analogous and can be found in Chapter 4.

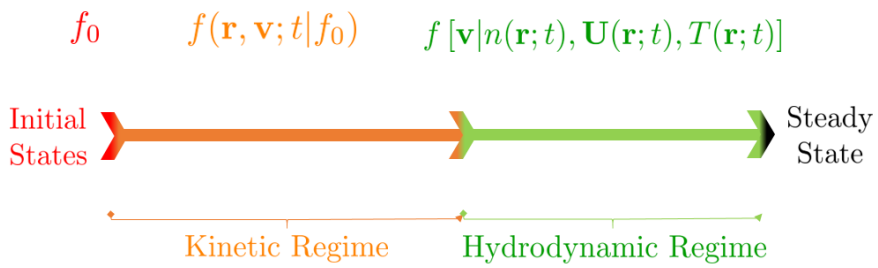

Figure 2.5: Schematic representation of the time evolution of the distribution function f for granular suspensions.

moments of f such as those related to the irreversible fluxes) [4, 226–230]. For the sake of illustration, a schematic representation of the evolution of the distribution function f via the kinetic and hydrodynamic regimes is displayed in Fig. 2.5.

The normal solution (2.47) means that in order to know f at the point $\mathbf{r}$, we need to know not only the hydrodynamic fields at this point, but also all their spatial derivatives evaluated at the same point $\mathbf{r}$. The simplest way of obtaining the explicit form of the normal solution (2.47) is to assume weak spatial gradients. In this case, f can be expanded in a series expansion in powers of the gradients of the hydrodynamic fields. The resulting series can then be truncated at a finite number of terms, thus yielding an approximation of the distribution function. Therefore, the CE procedure becomes more effective when the gradients of the hydrodynamic fields (or the inhomogeneities of the system) are small so that the series expansion converges [231]. Thus, we need to quantify somehow the inhomogeneity of the system such that the expansion is implemented rigorously.

A straightforward way to quantify the inhomogeneity of the granular system is by analyzing the order of magnitude of the different terms appearing in the Enskog equation (2.7). Let us define a typical *hydrodynamic* length h (over which the distribution function varies significantly) and a typical velocity of the thermal motion of particles v_{th}. Associated to them, we introduce a typical hydrodynamic time $\tau_h = h/v_{\text{th}}$. Hence,

$$\frac{\partial f}{\partial t} = \mathcal{O}\left(\tau_h^{-1} f\right), \quad \mathbf{v}\cdot\nabla f = \mathcal{O}\left(v_{\text{th}} h^{-1} f\right), \quad J_{\text{E}}[f,f] = \mathcal{O}\left(n\sigma^{d-1} v_{\text{th}}\right). \tag{2.48}$$

If we compare the magnitude of the left hand side of the Enskog equation (2.7) with the right hand side, we can therefore establish a relation between the gradients of the system

(or hydrodynamic scale) with respect to the microscopic length $n\sigma^{d-1}$ that measures the collision (or microscopic) stage. Thus, we can express the relative magnitude of both sides in terms of the ratio $(n\sigma^{d-1})^{-1}/h$. For hard spheres, $\ell = (n\sigma^{d-1})^{-1}$ is proportional to the mean free path between collisions. Since the ratio $\mathrm{K_n} = \ell/h$, known as the Knudsen number [232], relates the macroscopic and microscopic scales, it may be also useful to quantify the inhomogeneity of the system. The normal solution (2.47) holds up then if $\mathrm{K_n} \to 0$. As a consequence, $\tau/\tau_h \to 0$ and so, there is a separation between the microscopic (τ) and macroscopic (τ_h) times.

In addition, the boundary conditions can create correlations between inelasticity and spatial gradients (e.g., non-Newtonian flows under shear [51]) and both quantities cannot be chosen separately. This constraint prevents the application of the CE method for strong inelasticities since the strength of the gradients increases with increasing inelasticity. In order to avoid such difficulties, the normal solution is restricted to much longer times than the mean free time (hydrodynamic stage) and distances from the boundaries larger than the mean free path.

In accordance with Eq. (2.48), since $h \sim |\nabla \ln f|^{-1}$, small spatial variations imply low Knudsen numbers. On this basis, as said before, the functional dependence (2.47) can be made local in space through an expansion in the gradients of the hydrodynamic fields. To generate it, f is written as a series expansion in a formal book-keeping parameter ϵ measuring the non-uniformity of the system:

$$f = f^{(0)} + \epsilon f^{(1)} + \epsilon f^{(2)} + \cdots , \tag{2.49}$$

where each factor ϵ means an implicit gradient. Moreover, in ordering the different level of approximations in the kinetic equation, one has to characterize the magnitude of the friction coefficient γ, the gravity field $\mathbf{g}$, and the term $\Delta\mathbf{U}$ relative to the spatial gradients as well. As in the case of elastic collisions [215], the gravity field is considered to be at least of first order in the perturbation expansion since it induces a pressure gradient ∇p (the so-called barometric formula). In addition, with respect to the drag coefficient γ, it is considered to be to zeroth order in gradients since it does not induce any flux in the system. Finally, since $\mathbf{U}$ relaxes to $\mathbf{U}_\mathrm{g}$ in the absence of gradients, we expect that the term $\Delta\mathbf{U}$ is at least of first order in the gradients.

According to the expansion (2.49), the Enskog operator $J_{\mathrm{E}}[f,f]$ and the time derivative ∂_t are also expanded in terms of the parameter ϵ as

$$\partial_t = \partial_t^{(0)} + \epsilon\partial_t^{(1)} + \epsilon^2\partial_t^{(2)} + \cdots, \quad J_{\mathrm{E}} = J_{\mathrm{E}}^{(0)} + \epsilon J_{\mathrm{E}}^{(1)} + \epsilon^2 J_{\mathrm{E}}^{(2)} + \cdots \tag{2.50}$$

Moreover, the fluxes P and $\mathbf{q}$ and the cooling rate ζ are given by the representations

$$\begin{gathered} \mathrm{P} = \mathrm{P}^{(0)} + \epsilon\mathrm{P}^{(1)} + \epsilon^2\mathrm{P}^{(2)} + \cdots, \quad \mathbf{q} = \mathbf{q}^{(0)} + \epsilon\mathbf{q}^{(1)} + \epsilon^2\mathbf{q}^{(2)} + \cdots, \\ \zeta = \zeta^{(0)} + \epsilon\zeta^{(1)} + \epsilon^2\zeta^{(2)} + \cdots \end{gathered} \tag{2.51}$$

When the solution (2.47) is inserted in the Enskog equation (2.10), and the expansion (2.50) for the time derivative is implemented, the time derivative of f can be written as

$$\partial_t^{(k)} f = \left(\partial_t^{(k)} n\right) \frac{\partial f}{\partial n} + \left(\partial_t^{(k)} \mathbf{U}\right) \frac{\partial f}{\partial \mathbf{U}} + \left(\partial_t^{(k)} T\right) \frac{\partial f}{\partial T}, \tag{2.52}$$

where the time derivatives $\partial_t^{(k)} n$, $\partial_t^{(k)}\mathbf{U}$, and $\partial_t^{(k)} T$ are determined from the corresponding balance equations at this order.

The introduction of these expansions into the Enskog equation leads to a set of integro-differential equations for the approximation $f^{(k)}$. The zeroth-order equation involves only $f^{(0)}$; the second-order, $f^{(0)}$ and $f^{(1)}$; the third-order, $f^{(0)}$, $f^{(1)}$, and $f^{(2)}$; etc. The zeroth-order level gives the so-called Euler equations, the first-order approximation leads to the NS equations, while the second and third order are the Burnett and super-Burnett equations. Here, we will retain our calculation up to the first order in the gradients (NS hydrodynamic level).

In contrast to previous works on the CE method applied to granular gases [66, 148, 149, 215], two modifications are introduced with regard to the zeroth-order distribution $f^{(0)}$: (i) a time dependence caused by a local imbalance of energy between collisions and the action of the interstitial fluid and (ii) the influence of density on the reference distribution introduced by the parameters of the gas-solid force.

2.4 Grad's Moment Method

Grad's moment method will be employed in Article 7 to obtain the collisional moments of a dilute suspension composed of inelastic rough spheres under simple shear flow.

Grad's moment method is the best known alternative to the CE method. Just as the molecular case [200], the basis of this approach consists on an expansions of the distribution function in a complete set of orthogonal polynomials [generalized Hermite polynomials $H_k(\mathbf{v})$] with a Gaussian measure. The coefficients of the expansion give the corresponding velocity moments. The key factor of the method resides in the selection of the coefficients to be the same as those of the exact distribution function. Following Grad's paper [200], we assume that the state of the gas can be described accurately by an extended set of moments

$$\langle \psi \rangle = \frac{1}{n(\mathbf{r},t)} \int \mathrm{d}\mathbf{v} \int \mathrm{d}\boldsymbol{\omega}\, \psi(\mathbf{r},\mathbf{v},\boldsymbol{\omega};t) f(\mathbf{r},\mathbf{v},\boldsymbol{\omega};t), \tag{2.53}$$

where $\psi(\mathbf{r},\mathbf{v},\boldsymbol{\omega};t)$ is an arbitrary dynamic property of the velocities $\mathbf{v}$ and $\boldsymbol{\omega}$.

The resulting hierarchy of moment equations is infinite and must therefore be truncated at some given order k. This means that the moments of degree higher than k are neglected in the corresponding solution. In the case of a three-dimensional gas, the standard Grad's method retains the moments associated to the density n, the three components of the linear velocity field $\mathbf{U}$, the (partial) translational temperature T_t, the five components of the pressure tensor P $[T_t = (P_{xx} + P_{yy} + P_{zz})/(3n)]$, and the three components of heat flux $\mathbf{q}$ [200, 233]. This represents a total of thirteen moments and, as a consequence, the method is referred to as the 13-moment method. Here, we add a new velocity moment related to the so-called partial rotational temperature, which stems from the definition of the Maxwellian distribution.

At a microscopic level, the main advantage of the simple shear flow is that this state becomes spatially homogeneous when the velocities of the particles $\mathbf{v}$ are referred to the frame moving with the mean flow velocity $\mathbf{U}$. Moreover, since the heat flux vanishes by symmetry in the simple shear flow problem, the explicit form of the non-equilibrium distribution function $f(\mathbf{V},\boldsymbol{\omega})$ in this approximation is [223, 234]

$$f(\mathbf{V},\boldsymbol{\omega}) \to f_0(\mathbf{V},\boldsymbol{\omega})\Big[1 + \frac{m}{2nT_t^2}\left(V_iV_j - \frac{1}{3}V^2\delta_{ij}\right)\Pi_{ij}\Big], \tag{2.54}$$

where

$$\Pi_{ij} = P_{ij} - nT_t\delta_{ij} \tag{2.55}$$

is the traceless part of the pressure tensor $P_{ij} = \rho\langle V_iV_j\rangle$ and f_0 is the

two-temperature Maxwellian velocity distribution

$$f_0(\mathbf{V},\boldsymbol{\omega}) = n\Big(\frac{mI}{4\pi^2 T_t T_r}\Big)^{3/2} \exp\left(-\frac{mV^2}{2T_t}\right) \exp\left(-\frac{I\omega^2}{2T_r}\right). \tag{2.56}$$

Upon writing the distribution (2.54) we have ignored the possible contributions to f coming from a sum of projections along the three polar vectors $\mathbf{V}$, $(\mathbf{V}\cdot\boldsymbol{\omega})$, and $\mathbf{V}\times\boldsymbol{\omega}$ [235, 236]. This can be justified since the selection of the Maxwellian weight distribution f_0 entails that the orientational correlations between $\mathbf{V}$ and $\boldsymbol{\omega}$ are neglected [see Eq. (2.38)], and hence the distribution is isotropic in the velocity space. Moreover, theoretical results for the temperature ratio T_t/T_r assuming the approximation f_0 to f in homogeneous states have been shown to compare very well with both Monte Carlo and MD simulations [237].

2.5 BGK-type Kinetic Model

We consider a Bhatnagar–Gross-Krook (BGK)-type kinetic model of the Boltzmann equation to obtain the rheological properties of a granular suspension under simple shear flow in Articles 6 and 7.

We do know already that while the mass m and momentum $m\mathbf{v}$ are collisional invariants of the Boltzmann collision operator, the energy is not conserved in the case of inelastic collisions. Strictly speaking,

$$\int \mathrm{d}\mathbf{v} \left\{1, m\mathbf{v}, \frac{1}{2}m\mathbf{V}^{\mathbf{2}}\right\} J[\mathbf{v}|f,f] = \left\{0, \mathbf{0}, -\frac{d}{2}nT\zeta\right\}, \tag{2.57}$$

where

$$\zeta = -\frac{m}{dnT}\int \mathrm{d}\mathbf{v}\; V^2 J[\mathbf{v}|f,f] \tag{2.58}$$

is the cooling rate. Therefore, guided by the results provided by Brey, Dufty, and Santos (BDS) [199], the (inelastic) Boltzmann collision operator $J^{(\alpha)}[\mathbf{v}|f,f]$ can be written as

$$J^{(\alpha)}[\mathbf{v}|f,f] \to \upsilon(\alpha) J^{(1)}[\mathbf{v}|f,f] + \frac{\zeta}{2}\frac{\partial}{\partial\mathbf{v}}\cdot(\mathbf{V}f), \tag{2.59}$$

where $J^{(1)}[f,f]$ is the collision operator for elastic collisions ($\alpha = 1$). The frequency $\upsilon(\alpha)$ tries to mimic the granular trends that are observed in the collisional moments of granular gases. It can be selected for instance to agree with the IHS results. Given that

the cooling rate cannot be exactly evaluated, we take here the expression of ζ obtained from the definition (2.58) by replacing f by its Maxwellian form.

For ordinary gases, the simplest choice for $J^{(1)}[f,f]$ that retains its collisional invariants $\left\{1, \mathbf{v}, V^2\right\}$ is the well-known BGK approximation [238, 239]. Its explicit form is

$$J^{(1)}[\mathbf{v}|f,f] \to K[f] = -\nu(f - f_{\mathrm{L}}), \tag{2.60}$$

where ν is an effective collision frequency that stems from the Boltzmann collision operator and f_{L} is the local equilibrium distribution function. Behind this simple equation, the BGK model assumes that the non-equilibrium distribution function f relaxes towards the local equilibrium distribution function f_{L} in a time ν^{-1}. Inserting Eq. (2.60) into Eq. (2.59), the BGK-type kinetic model reads

$$J^{(\alpha)}[\mathbf{v}|f,f] \to -\upsilon(\alpha)\nu(f - f_{\mathrm{L}}) + \frac{\zeta}{2}\frac{\partial}{\partial \mathbf{v}} \cdot (\mathbf{V}f)\,. \tag{2.61}$$

In the context of inelastic rough spheres, the operator $J^{(\alpha,\beta)}[\mathbf{v},\boldsymbol{\omega}|f,f]$ becomes [204]

$$J^{(\alpha,\beta)}[\mathbf{v},\boldsymbol{\omega}|f,f] \to -\upsilon(\alpha,\beta)\nu_t\,(f - f_0) + \frac{\zeta_t}{2}\frac{\partial}{\partial \mathbf{V}} \cdot (\mathbf{V}f) + \frac{\zeta_r}{2}\frac{\partial}{\partial \boldsymbol{\omega}} \cdot (\boldsymbol{\omega}f)\,, \tag{2.62}$$

where f_0 is the two-temperature Maxwellian distribution defined in Eq. (2.56). The partial energy production rates associated with the translational (ζ_t) and rotational (ζ_r) degrees of freedom are

$$\zeta_t = -\frac{m}{3nT_t}\int \mathrm{d}\mathbf{v} \int \mathrm{d}\boldsymbol{\omega}\; v^2 J[f,f], \quad \zeta_r = -\frac{I}{3nT_r}\int \mathrm{d}\mathbf{v} \int \mathrm{d}\boldsymbol{\omega}\; \omega^2 J[f,f]. \tag{2.63}$$

They can be determined for instance by replacing f by Grad's distribution (2.54) in the Boltzmann operator (2.34).

2.6 Inelastic Maxwell Models

Inelastic Maxwell Models (IMM) for dilute granular gases (or suspensions) are introduced in this section. Article 6 uses IMM to *exactly* obtain the rheological properties of a sheared granular suspension.

One of the main limitations of the Boltzmann kinetic equation relies on the affordability of the calculations involving the collisional moments. The real difficulty arises

from the form of the collision rate appearing inside the Boltzmann collision operator (2.2). To overcome the difficulty associated to the IHS core, one may assume an interaction model where the collision rate is independent of the relative velocity of the colliding pair. In the case of elastic collisions [206], Maxwell models can be understood by the introduction of a repulsive potential that is proportional to the inverse of the fourth power of distance between particles. Conversely, for inelastic collisions, the collision rules (2.3) should be changed in order to consider the Maxwell potential. Nonetheless, as pointed out by Ernst [198], IMM can be introduced at the level of the cross section, without any special reference to an interaction potential.

To obtain the Boltzmann collision operator for IMM, the scalar product $|\widehat{\boldsymbol{\sigma}}\cdot\mathbf{g}_{12}|$ is replaced by a term proportional to the thermal velocity $v_{\text{th}}=\sqrt{2T/m}$ and independent of the relative velocity $\mathbf{g}_{12}$ [4]. In this case, the Boltzmann collision operator $J_{\text{IMM}}f,f]$ reads [240]

$$J_{\text{IMM}}[\mathbf{v}|f,f]=\frac{\nu_{\text{M}}}{n\Omega_d}\int \mathrm{d}\mathbf{v}_2\int \mathrm{d}\widehat{\boldsymbol{\sigma}}\left[\alpha^{-2}f(\mathbf{v}_1'')f(\mathbf{v}_2'')-f(\mathbf{v}_1)f(\mathbf{v}_2)\right], \tag{2.64}$$

where $\Omega_d=2\pi^{d/2}/\Gamma(d/2)$ is the solid angle in d dimensions and the precollisional velocities $(\mathbf{v}_1'',\mathbf{v}_2'')$ are given by the collision rules (2.3). The collision frequency ν_{M} is independent of velocity but depends on space and time through its dependence on density and temperature. It plays the role of $\upsilon(\alpha)$ in the case of the BGK-type model, i.e., it acts as a free parameter of the model that can be chosen to optimize agreement with some property of interest of the original Boltzmann equation. It can be defined as $\nu_{\text{M}}\propto T^q$, where q can be seen as a generic parameter that is picked upon request to mimic different potentials. The case $q=0$ is closer to the classical Maxwell Models, whereas $q=\frac{1}{2}$ mimics the hard sphere potential [198].

The main advantage of the IMM is that the collisional moments can be expressed in terms of the velocity moments of the distribution function f, without explicit knowledge of the latter [241]. Thus, the collisional moments of degree k can be expressed in terms of the velocity moments of degree less or equal to k. This opens up the possibility to use the IMM for example to get the dependence of higher-degree moments (third and fourth) on the coefficients of restitution α and β [242, 243].

2.7 Direct Simulation Monte Carlo (DMSC) Method

The kinetic equations derived in this Chapter must be solved by successive approximations that concern the form f, both as regards the local value of $f(\mathbf{r}, \mathbf{v}; t)$ and its time and space derivatives. The former affect the form of the zeroth-order solution $f^{(0)}$, which unlike ordinary gases is not a Maxwellian distribution, yielding a slightly different functional form [220]. Throughout this thesis, we will usually consider the leading terms in a Sonine polynomial expansion of $f^{(0)}$ (first-Sonine approximation) [122]. The second kind of approximations involves the normal or hydrodynamic solution (2.47) that has been already discussed in terms of the Knudsen number $\mathrm{K_n}$.

In the case of a rarefied gas dominated by collisions, an alternative but complementary method to solve the Boltzmann and Enskog equations is the Direct Simulation Monte Carlo (DSMC) method. Although the DSMC method still assumes the molecular chaos hypothesis, it is able to provide the "exact" form of f without making any assumption on the existence of a hydrodynamic solution. Thus, it is worth solving the kinetic equations by means of the DSMC method to test the reliability of the (approximate) theoretical predictions.

The classical DSMC simulations originally proposed by Bird [244] were created with the specific goal of solving rarefied gas flows that are not accessible from a computational point of view to MD simulations. It should, however, be noted that if the Knudsen number is very low (continuum approach), the results obtained from the method are still valid as a solution of the Boltzmann equation [245, 246].

In this thesis, we follow similar steps as those proposed by Montanero and Garzó [154] (who performed simulations for freely cooling granular mixtures) to numerically solve the Boltzmann–Enskog equation of a homogeneous bidisperse granular (molecular) suspension in both transient and steady regimes[1] (Chapters 4 and 5).

The simulation is initiated by drawing the particle velocities from a certain distribution at an initial temperature $T_{i,0}$. The discretized distribution function $f_i^{(N)}$ of species i stems from the velocities $\{\mathbf{v}_k\}$ of N_i "virtual particles":

$$f_i^{(N)}(\mathbf{v}; t) \to \frac{n_i}{N_i} \sum_{k=1}^{N} \delta(\mathbf{v} - \mathbf{v}_k(t)). \tag{2.65}$$

[1] The Monte Carlo simulation results for the monocomponent case that are displayed in Article 1 were obtained in Ref. [148, 149], and hence are not part of the present thesis.

For low-density regimes, since the collisions are assumed to be instantaneous, the free flight of particles and the collision stage can be decoupled in time. The DSMC method maintains this assumption and therefore the method can be divided into two steps: the convective and the collision stages. However, since the granular gas is assumed to be spatially homogeneous in our simulations, only the collision stage is described here. The procedure can be summarized as follows:

Granular mixtures:

1. To simulate the collisions between particles of species i with j a required number of $N_{ij}^{\delta t}$ candidate pairs to collide in a time δt is selected. This number is given by [154]
$$N_{ij}^{\delta t} = \frac{2^{d-1} d\Gamma\left(\frac{d}{2}\right)}{\pi^{(d-2)/2}} \frac{N_i N_j \sigma_{12}^2}{\sum_i N_i \sigma_i^d} \phi \chi_{ij} g_{ij}^{\max} \delta t, \tag{2.66}$$
where N_i is the total number of simulated particles of species i and $g_{ij}^{\max}$ is an upper bound of the average relative velocity between two particles. A good estimate is $g_{ij}^{\max} = C v_{ij}^{\text{th}}$, where $v_{ij}^{\text{th}} = \sqrt{2T_g/\overline{m}}$ is the mean thermal velocity, $\overline{m} = (m_i + m_j)/2$, and C is a constant, e.g., $C = 5$ [246]. Note that the number of candidate pairs is enhanced by the presence of the pair correlation function χ_{ij} to solve the Enskog equation [247].

2. A colliding direction $\widehat{\boldsymbol{\sigma}}_{k\ell}$ for a pair of colliding particles labeled as k and ℓ is randomly selected with equal probability.

3. The collision is accepted if
$$|\widehat{\boldsymbol{\sigma}}_{k\ell} \cdot \mathbf{g}_{k\ell}| = |\widehat{\boldsymbol{\sigma}}_{k\ell} \cdot (\mathbf{v}_k - \mathbf{v}_\ell)| > \mathrm{R}(0,1) g_{ij}^{\max}, \tag{2.67}$$
where $\mathrm{R}(0,1)$ is a random number uniformly distributed in $[0,1]$.

4. If the collision is accepted, the velocities of particles are updated according to the scattering rules [4]:
$$\begin{aligned} \mathbf{v}_k &\to \mathbf{v}_k - \mu_{ji} (1 + \alpha_{ij}) (\mathbf{g}_{k\ell} \cdot \widehat{\boldsymbol{\sigma}}_{k\ell}) \widehat{\boldsymbol{\sigma}}_{k\ell}, \\ \mathbf{v}_\ell &\to \mathbf{v}_\ell + \mu_{ij} (1 + \alpha_{ij}) (\mathbf{g}_{k\ell} \cdot \widehat{\boldsymbol{\sigma}}_{k\ell}) \widehat{\boldsymbol{\sigma}}_{k\ell}. \end{aligned} \tag{2.68}$$

5. Repeat the procedure for all the permutations of $i = 1, 2$ and $j = 1, 2$.

Binary suspensions:

For a three-dimensional system ($d = 3$), the influence of the interstitial fluid on grains is taken into account by updating the velocity $\mathbf{v}_k$ of every single grain each time step δt according to [94]:

$$\mathbf{v}_k \to e^{-\gamma_i \delta t}\mathbf{v}_k + \left(\frac{6\gamma_i T_{\mathrm{ex}}\delta t}{m_i}\right)^{1/2}\mathbf{R}[-1,1]. \tag{2.69}$$

Here, $\mathbf{R}$ is a uniformly distributed random vector in $[-1,1]^3$. Equation (2.69) converges to the Fokker–Plank operator (2.26) when the time step δt is much smaller than the mean free time between collisions [94].[1]

[1]Note that $\mathbf{R}$[-1,1] can be replaced by any random vector of zero mean and unit variance. Here, we have chosen a uniformly distributed random vector for the sake of simplicity.

Chapter 3

Transport Coefficients for Granular Suspensions at Moderate Densities

3.1 Summary

An ensemble of solid particles (disks for $d = 2$ or spheres for $d = 3$) of mass m and diameter σ immersed in a viscous fluid at a fixed temperature T_{ex} is considered. Particles are assumed to be completely smooth so the inelasticity of collisions is represented by a constant coefficient of normal restitution $\alpha \leq 1$. In accordance with direct numerical simulations (DNS) at low-Reynolds numbers [137], the influence of the interstitial gas on the dynamics of grains is account for by an effective force composed of two different terms: (i) a drag force proportional to the instantaneous velocity of the particles and (ii) a stochastic Langevin-like term in the form of a Gaussian white noise. The first term models the friction of grains on the viscous fluid, whereas the second tries to mimic the energy gained by the grains when they collide with the particles of the interstitial gas. The amplitude of the white noise is chosen in such a way that the fluctuation-dissipation relation is recovered in the elastic limit ($\alpha = 1$) [see equation (2.15)].

The starting point of the present work is the Enskog kinetic equation at moderate densities. Once the action of the external force on the one-body distribution function f is settled, the balance equations for the hydrodynamic quantities (namely the density

n, flow velocity $\mathbf{U}$, and granular temperature T) can be obtained by multiplying the Enskog equation by $\left\{m, m\mathbf{v}, \frac{1}{2}mv^2\right\}$ and integrating over velocity. Unfortunately, the presence of the momentum and heat fluxes as well as the cooling rate make the balance equations not to be closed equations for the hydrodynamic quantities. Thus, the constitutive equations for these quantities (that measure the response of the system to the gradients of hydrodynamic variables) must be determined. In this work, we use the Chapman–Enskog method [122] conveniently adapted to dissipative dynamics as a reliable procedure to obtain the transport properties of a granular suspension, and hence to achieve a closure relation for the balance equations. Here, we retain our calculations up to the first-order solution; Navier–Stokes hydrodynamic level.

To compute the NS transport coefficients, one needs to characterize first the zeroth-order solution or, in other words, the reference state of the perturbation scheme. The reference or homogeneous state conforms the simplest situation in which we can test the different assumptions taken to compute the distribution function and the collisional moments. More precisely, we assume first that the normal solution (2.47) exists, namely, a special solution of the Enskog equation where all the spatial and time dependence of the distribution function occurs through the hydrodynamic variables. Then, an approximate solution is proposed based on a Sonine expansion of the zeroth-order distribution $f^{(0)}$. The latter slightly perturbs the local equilibrium function (i.e., the reference state in the elastic case) in terms of Laguerre polynomials [220]. Moreover, in the absence of gradients, the loss of energy due to the inelasticity of collisions is compensated for by the action of the bath. Hence, a homogeneous steady state is reached. The steady values for the granular temperature T and the fourth cumulant a_2 —measuring the deviation of $f^{(0)}$ from its Maxwellian form— are confronted against DSMC simulations.

In addition, while in the dry granular case the distribution $f^{(0)}$ is chosen to be the local version of the homogeneous cooling state, there is more flexibility in the choice of $f^{(0)}$ in granular suspensions. Since the response to the action of the bath is not instantaneous, the effect of inelasticity cannot be locally compensated by the presence of the interstitial fluid, and hence the zeroth-order distribution is not in general a stationary distribution. Thus, although the NS transport coefficients are computed under steady-state conditions, one should previously consider the time dependence of $f^{(0)}$. This condition requires the knowledge of the derivatives of a_2 with respect to the

hydrodynamic fields through the dependence on the parameters of the bath. Besides the dependence on the temperature ratio T/T_{ex} and in contrast to previous works [148, 149], we also take into account an additional dependence of a_2 on the density field n since the drag coefficient γ contemplates the effect of density in our suspension model [see Eq. (2.20)].

Once the reference state is characterized, the CE method is implemented. To first order in spatial gradients, the CE solution allows us to identify the NS transport coefficients associated with the momentum and heat fluxes. Explicit forms for the shear and bulk viscosities, the thermal and diffusive heat conductivities, and the first-order contribution to the cooling rate, are obtained in steady-state conditions by retaining the leading terms in a Sonine polynomial expansion. As an application, the stability of the HSS is analyzed showing that it is always linearly stable under small perturbations.

3.2 Article 1

Title: Transport coefficients for granular suspensions at moderate densities

Authors: Rubén Gómez González[1] and Vicente Garzó[2]

Affiliations:

[1] Departamento de Física, Universidad de Extremadura, E-06006 Badajoz, Spain

[2] Departamento de Física and Instituto de Computación Científica Avanzada (ICCAEx), Universidad de Extremadura, E-06006 Badajoz, Spain

Journal: Journal of Statistical Mechanics: Theory and Experiment

Volume: 2019

Pages: 093204

Year: 2019

DOI: 10.1088/1742-5468/ab3786

Copy of the work: "Preprint version (arXiv:1902.05018v2) of Rubén Gómez González and Vicente Garzó, *Transport coefficients for granular suspensions at moderate densities*, Journal of Statistical Mechanics: Theory and Experiment 2019, 093204 (2019) https://doi.org/10.1088/
1742-5468/ab3786"

Transport coefficients for granular suspensions at moderate densities

Rubén Gómez González*
Departamento de Física, Universidad de Extremadura, E-06006 Badajoz, Spain

Vicente Garzó†
Departamento de Física and Instituto de Computación Científica Avanzada (ICCAEx), Universidad de Extremadura, E-06006 Badajoz, Spain
(Dated: July 12, 2019)

The Enskog kinetic theory for moderately dense granular suspensions is considered as a model to determine the Navier-Stokes transport coefficients. The influence of the interstitial gas on solid particles is modeled by a viscous drag force term plus a stochastic Langevin-like term. The suspension model is solved by means of the Chapman–Enskog method conveniently adapted to dissipative dynamics. The momentum and heat fluxes as well as the cooling rate are obtained to first order in the deviations of the hydrodynamic field gradients from their values in the homogeneous steady state. Since the cooling terms (arising from collisional dissipation and viscous friction) cannot be compensated for by the energy gained by grains due to collisions with the interstitial gas, the reference distribution (zeroth-order approximation of the Chapman–Enskog solution) depends on time through its dependence on temperature. On the other hand, to simplify the analysis and given that we are interested in computing transport properties in the first order of deviations from the reference state, the steady-state conditions are considered. This simplification allows us to get explicit expressions for the Navier–Stokes transport coefficients. The present work extends previous results [Garzó *et al.* 2013, Phys Rev. E **87**, 032201] since it incorporates two extra ingredients (an additional density dependence of the zeroth-order solution and the density dependence of the reduced friction coefficient) not accounted for by the previous theoretical attempt. While these two new ingredients do not affect the shear viscosity coefficient, the transport coefficients associated with the heat flux as well as the first-order contribution to the cooling rate are different from those obtained in the previous study. In addition, as expected, the results show that the dependence of the transport coefficients on both inelasticity and density is clearly different from that found in its granular counterpart (no gas phase). Finally, a linear stability analysis of the hydrodynamic equations with respect to the homogeneous steady state is performed. In contrast to the granular case (no gas-phase), no instabilities are found and hence, the homogeneous steady state is (linearly) stable.

I. INTRODUCTION

Although in nature granular matter is surrounded by an interstitial fluid (like the air, for instance), most of theoretical and computational studies have neglected the impact of the gas phase on the dynamics of solid particles. On the other hand, it is known that in many practical applications (like for instance species segregation in granular mixtures [1–6]) the effect of the surrounding fluid on grains cannot be ignored. Needless to say, at a kinetic theory level, the description of granular suspensions (namely, a suspension of solid particles in a viscous gas) is a quite complex problem since a complete microscopic description of the gas-solid system involves the solution of a set of two coupled kinetic equations for each one of the velocity distribution functions of the different phases. Thus, due to the mathematical difficulties embodied in this approach and in order to gain some insight into this problem, an usual model for describing gas-solid flows [7] is to consider a kinetic equation for the solid particles where the influence of the surrounding fluid on them is modeled by means of an effective external force. As usual [8, 9], the external force modeling the effect of the gas phase is constituted by two terms: (i) a viscous drag force (via a term involving a drift or friction coefficient γ) accounting for the friction of grains on the interstitial fluid and (ii) a stochastic Langevin-like term (via a term involving the background or bath temperature T_{ex}) accounting for the energy gained by the grains due to their collisions with particles of the background fluid.

Recently the above suspension model has been employed to study the so-called discontinuous shear thickening in non-Newtonian gas-solid suspensions [9, 10]. The results show the transition from the discontinuous shear thickening (observed for very dilute gases) to the continuous shear thickening as the density of the system increases. These analytical results (approximately obtained by means of Grad's moment method [9] and from an exact solution of the

* Electronic address: ruben@unex.es
† Electronic address: vicenteg@unex.es; URL: http://www.unex.es/eweb/fisteor/vicente/

Boltzmann equation for inelastic Maxwell models [10]) compare quite well with molecular dynamics simulations [9] for conditions of practical interest. This good agreement highlights again the good performance of kinetic theory tools in reproducing the transport properties of gas-solid flows.

On the other hand, to the best of our knowledge, most of the efforts in kinetic theory of granular suspensions has been mainly focused on non-Newtonian transport properties (which are directly related with the pressure tensor). In particular, much less is known about the energy transport in gas-solid flows. The knowledge of the transport coefficients associated with the heat flux is interesting by itself and also for possible practical applications in suspensions where temperature and density gradients are present in the system. In this context, it would be desirable to provide simulators with the appropriate expressions of the Navier–Stokes transport coefficients to work when studying gas-solid flows where collisions among particles are inelastic.

The aim of this paper is to determine the Navier–Stokes transport coefficients of granular suspensions in the framework of the Enskog kinetic equation. Since this equation applies for moderate densities (let's say for instance, solid volume fraction $\phi \lesssim 0.25$ for hard spheres), the comparison between kinetic theory and molecular dynamics simulations becomes practical. Attempts on the evaluation of the Navier–Stokes transport coefficients for granular suspensions modeled by the Enskog equation have been previously published. Thus, in Ref. [8] the authors determined the transport coefficients of gas-solid flows starting from the suspension model constituted by the viscous drag force plus the stochastic Langevin term. Their results show that the effect of the gas phase on both the shear viscosity and the diffusive heat conductivity coefficients is non-negligible for industrially relevant portions of the parameter space. However, for the sake simplicity, the temperature dependence of the scaled friction coefficient $\gamma^* = \gamma/\nu(T)$ (where $\nu \propto T^{1/2}$ is an effective collision frequency for hard spheres and T is the granular temperature) was implicitly neglected in the above calculations [8] to get analytic (explicit) expressions for the transport coefficients. The above temperature dependence of γ^* was accounted for in a subsequent paper [11] *but* for a simplified model where only the drag force term was considered in the Enskog equation.

A more careful study was carried out later in Ref. [12] where the transport coefficients were explicitly computed by considering both the temperature dependence of the reduced friction coefficient as well as the complete form of the suspension model. On the other hand, although computer simulations [13] have clearly shown that the friction coefficient depends on the volume fraction, the calculations performed in Ref. [12] were carried out by assuming that the driven parameters of the model are constant. Needless to say, the impact of the density dependence of γ on transport properties is expected to be more relevant as the gas phase becomes denser. Apart from this simplification, although not explicitly stated, another limitation of the above theory [12] is that it was obtained by neglecting contributions to the transport coefficients coming from an additional density dependence of the zeroth-order distribution $f^{(0)}$ (in fact, although this simplification was noted in a subsequent erratum [14], it has not been implemented so far in the calculations). This extra density dependence of $f^{(0)}$ is expected to be involved in the evaluation of the heat flux transport coefficients.

The question arises then as to whether, and if so to what extent, the conclusions drawn from Ref. [12] may be altered when the above two new ingredients (density dependence of both the distribution $f^{(0)}$ and the friction coefficient γ) are accounted for in the theory. In this paper we address this question by extending the results derived in Ref. [12] to situations not covered by previous studies on granular suspensions. The present theory subsumes all previous analyses [8, 11, 12], which are recovered in the appropriate limits. In particular, a comparison between the results obtained here for the transport coefficients with those derived in [12] shows that while the expression of the shear viscosity coefficient is formally equivalent to the one obtained before, the heat flux transport coefficients and the first-order contribution to the cooling rate differ from those reported in Ref. [12].

As in previous works [8, 15, 16], the transport coefficients are obtained by solving the Enskog equation by means of the application of the Chapman–Enskog method [17]. Since a reference equilibrium state is missing in granular gases, an important point in the Chapman–Enskog expansion is the choice of the zeroth-order solution $f^{(0)}$ (reference base state of the perturbation scheme). While in the dry granular case (no gas phase) the distribution $f^{(0)}$ is chosen to be the local version of the homogeneous cooling state, there is more flexibility in the choice of $f^{(0)}$ in driven granular gases (or, equivalently in gas-solid flows). In the case of gas-solid flows [12], for simplicity one possibility is to take a steady distribution $f^{(0)}$ at any point of the system [18, 19]. However, the presence of the interstitial fluid introduces the possibility of a local energy unbalance and hence, the zeroth-order distribution is not in general a stationary distribution. This fact introduces new contributions to the transport coefficients, which were not considered when a local steady state was assumed at zeroth-order [18, 19]. Thus, for *general* small deviations from the homogeneous steady state the energy gained by grains due to collisions with the background fluid cannot be compensated locally with the cooling terms (viscous friction plus inelastic collisions). Thus, although we are interested in determining the transport coefficients under steady state conditions, we have to start from an *unsteady* zeroth-order solution in order to achieve the integral equation verifying the first-order solution $f^{(1)}$. The solution to this equation under steady state conditions provides the explicit forms of the transport coefficients.

The plan of the paper is as follows. In section II, the Enskog kinetic equation for granular suspensions is introduced

and the corresponding balance equations for the densities of mass, momentum, and energy are derived. Then, section III studies the homogeneous steady state where some theoretical predictions are compared against available computer simulation results. The comparison shows an excellent agreement for conditions of practical interest. Section IV addresses the Chapman–Enskog expansion around the unsteady reference distribution $f^{(0)}(\mathbf{r},\mathbf{v},t)$ up to first-order in spatial gradients. The explicit expressions of the Navier–Stokes transport coefficients and the cooling rate are displayed in section V for steady state conditions. In dimensionless form, these coefficients are given in terms of the coefficient of restitution α, the volume fraction ϕ, and the (reduced) background temperature T_{ex}^*. The dependence of the transport coefficients and the cooling rate on the parameter space is illustrated for several systems showing that the influence of the gas phase on them is in general quite significant. As an application of the results found here, a linear stability analysis of the Navier–Stokes hydrodynamic equations around the homogeneous steady state is carried out in section VI; the analysis shows that the homogeneous state is linearly stable. This finding agrees with the previous stability analysis performed in Ref. [12]. We close the paper in section VII with a brief discussion of the results reported here.

II. ENSKOG KINETIC EQUATION FOR GRANULAR SUSPENSIONS

We consider a set of solid particles of diameter σ and mass m immersed in a viscous gas. Collisions between grains are inelastic and are characterized by a (positive) constant coefficient of normal restitution $\alpha \leq 1$, where $\alpha = 1$ corresponds to elastic collisions (ordinary gases). At moderate densities, the one-particle velocity distribution function of solid particles $f(\mathbf{r},\mathbf{v};t)$ obeys the Enskog kinetic equation

$$\frac{\partial f}{\partial t} + \mathbf{v}\cdot\nabla f + \mathcal{F}f = J_{\text{E}}[\mathbf{r},\mathbf{v}|f,f], \tag{1}$$

where

$$J_{\text{E}}\left[\mathbf{r},\mathbf{v}_1|f,f\right] = \sigma^{d-1}\int d\mathbf{v}_2 \int d\widehat{\boldsymbol{\sigma}}\,\Theta(\widehat{\boldsymbol{\sigma}}\cdot\mathbf{g}_{12})(\widehat{\boldsymbol{\sigma}}\cdot\mathbf{g}_{12})\left[\alpha^{-2}f_2(\mathbf{r},\mathbf{r}-\boldsymbol{\sigma},\mathbf{v}_1'',\mathbf{v}_2'',t) - f_2(\mathbf{r},\mathbf{r}+\boldsymbol{\sigma},\mathbf{v}_1,\mathbf{v}_2,t)\right] \tag{2}$$

is the Enskog collision operator. Here,

$$f_2(\mathbf{r}_1,\mathbf{r}_2,\mathbf{v}_1,\mathbf{v}_2,t) = \chi(\mathbf{r}_1,\mathbf{r}_2)f(\mathbf{r}_1,\mathbf{v}_1,t)f(\mathbf{r}_2,\mathbf{v}_2,t), \tag{3}$$

d is the dimensionality of the system ($d = 2$ for disks and $d = 3$ for spheres), $\boldsymbol{\sigma} = \sigma\widehat{\boldsymbol{\sigma}}$, $\widehat{\boldsymbol{\sigma}}$ being a unit vector, Θ is the Heaviside step function, and $\mathbf{g}_{12} = \mathbf{v}_1 - \mathbf{v}_2$. The double primes on the velocities in Eq. (2) denote the initial values $\{\mathbf{v}_1'',\mathbf{v}_2''\}$ that lead to $\{\mathbf{v}_1,\mathbf{v}_2\}$ following a binary collision:

$$\mathbf{v}_1'' = \mathbf{v}_1 - \frac{1}{2}\left(1+\alpha^{-1}\right)(\widehat{\boldsymbol{\sigma}}\cdot\mathbf{g}_{12})\widehat{\boldsymbol{\sigma}}, \quad \mathbf{v}_2'' = \mathbf{v}_2 + \frac{1}{2}\left(1+\alpha^{-1}\right)(\widehat{\boldsymbol{\sigma}}\cdot\mathbf{g}_{12})\widehat{\boldsymbol{\sigma}}. \tag{4}$$

In addition, $\chi[\mathbf{r},\mathbf{r}\pm\boldsymbol{\sigma}|\{n(t)]$ is the equilibrium pair correlation function at contact as a functional of the nonequilibrium density field $n(\mathbf{r},t)$ defined by

$$n(\mathbf{r},t) = \int d\mathbf{v} f(\mathbf{r},\mathbf{v},t). \tag{5}$$

In Eq. (1), the operator $\mathcal{F}$ represents the fluid-solid interaction force that models the effect of the viscous gas on solid particles. In order to fully account for the influence of the interstitial molecular fluid on the dynamics of grains, a instantaneous fluid force model is employed [8, 9, 11]. For low Reynolds numbers, it is assumed that the external force $\mathbf{F}$ acting on solid particles is composed by two independent terms. One term corresponds to a viscous drag force $\mathbf{F}^{\text{drag}}$ proportional to the (instantaneous) velocity of particle $\mathbf{v}$. This term takes into account the friction of grains on the viscous gas. Since the model attempts to mimic gas-solid flows, the drag force is defined in terms of the relative velocity $\mathbf{v} - \mathbf{U}_g$ where $\mathbf{U}_g$ is the (known) mean flow velocity of the surrounding molecular gas. Thus, the drag force $\mathbf{F}^{\text{drag}} = -m\gamma\left(\mathbf{v}-\mathbf{U}_g\right)$ is represented in the Enskog equation (1) by the term

$$\mathcal{F}^{\text{drag}}f \to -\gamma\frac{\partial}{\partial\mathbf{v}}\cdot\left(\mathbf{v}-\mathbf{U}_g\right)f, \tag{6}$$

where γ is the drag or friction coefficient. The second term in the total force corresponds to a stochastic force that tries to simulate the kinetic energy gain due to eventual collisions with the (more rapid) molecules of the background

fluid. It does this by adding a random velocity to each particle between successive collisions [20]. This stochastic force $\mathbf{F}^{\rm st}$ has the form of a Gaussian white noise with the properties [21]

$$\langle \mathbf{F}_i^{\rm st}(t)\rangle = \mathbf{0}, \quad \langle \mathbf{F}_i^{\rm st}(t)\mathbf{F}_j^{\rm st}(t')\rangle = 2m\gamma T_{\rm ex}\mathsf{I}\delta_{ij}\delta(t-t'), \tag{7}$$

where I is the unit tensor and i and j refer to two different particles. Here, $T_{\rm ex}$ can be interpreted as the temperature of the background (or bath) fluid. In the context of the Enskog kinetic equation, the stochastic external force is represented by a Fokker–Planck operator of the form [21, 22]

$$\mathcal{J}^{\rm st} f \to -\frac{\gamma T_{\rm ex}}{m}\frac{\partial^2 f}{\partial v^2}. \tag{8}$$

Note that the strength of correlation in Eq. (8) has been chosen to be consistent with the fluctuation-dissipation theorem for elastic collisions [21].

Although the drift coefficient γ is in general a tensor, here for simplicity we assume that this coefficient is a scalar proportional to the square root of $T_{\rm ex}$ because the drag coefficient is proportional to the viscosity of the solvent [7]. In addition, as usual in granular suspension models [13, 23], γ is a function of the solid volume fraction

$$\phi = \frac{\pi^{d/2}}{2^{d-1}d\Gamma\left(\frac{d}{2}\right)} n\sigma^d. \tag{9}$$

Thus, the drift coefficient γ can be written as

$$\gamma = \gamma_0 R(\phi), \tag{10}$$

where $\gamma_0 \propto \eta_g \propto \sqrt{T_{\rm ex}}$, η_g being the viscosity of the solvent or gas phase. In the case of hard spheres ($d = 3$), for Stokes flow we can use the existing analytical closure derived by Koch [23] for the function $R(\phi)$ in the case of very dilute suspensions ($\phi \le 0.1$):

$$R(\phi) = 1 + 3\sqrt{\frac{\phi}{2}}. \tag{11}$$

For $\phi > 0.1$, Koch and Sangani [13] used simulations based on multipole expansions to propose the ϕ-dependence of R. It is given by

$$R(\phi) = 1 + \frac{3}{\sqrt{2}}\phi^{1/2} + \frac{135}{64}\phi\ln\phi + 11.26\phi(1 - 5.1\phi + 16.57\phi^2 - 21.77\phi^3) - \phi\chi(\phi)\ln\epsilon_m. \tag{12}$$

Here, $\epsilon_m\sigma$ can be regarded as a length scale characterizing the impact of non-continuum effects on the lubrication forces between two smooth particles at contact. Typical values of ϵ_m are in the range 0.01–0.05. Since this term contributes to $R(\phi)$ through a weak logarithmic factor, the influence of its explicit value is not important in the final results. Here, we take $\epsilon_m = 0.01$ as a typical value.

The suspension model defined by Eqs. (1), (6), and (8) is a simplified version of the model employed in Ref. [12] to get the Navier–Stokes transport coefficients. In this latter model [8], the friction coefficient of the drag force (γ_b in the notation of Ref. [12]) and the strength of the correlation (ξ_b^2 in the notation of Ref. [12]) are considered to be in general different. Here, as mentioned before, both coefficients are related as $\xi_b^2 = 2\gamma_b T_{\rm ex}/m^2$ to be consistent with the fluctuation-dissipation theorem. Thus, some of the results derived in this paper (mainly those regarding homogeneous states) can be directly obtained from those reported in Ref. [12] by making the changes $\gamma_b \to m\gamma$ and $\xi_b^2 \to 2\gamma T_{\rm ex}/m$ with $R(\phi) = 1$. We have preferred in this paper to adopt the notation introduced in Eqs. (6) and (8) because this is the notation used in previous studies of sheared granular suspensions [9, 10].

According to Eqs. (6) and (8), the Enskog equation (1) reads

$$\frac{\partial f}{\partial t} + \mathbf{v}\cdot\nabla f - \gamma\Delta\mathbf{U}\cdot\frac{\partial f}{\partial \mathbf{v}} - \gamma\frac{\partial}{\partial\mathbf{v}}\cdot\mathbf{V}f - \gamma\frac{T_{\rm ex}}{m}\frac{\partial^2 f}{\partial v^2} = J_{\rm E}[\mathbf{r},\mathbf{V}|f,f]. \tag{13}$$

Here, $\Delta\mathbf{U} = \mathbf{U} - \mathbf{U}_g$, $\mathbf{V} = \mathbf{v} - \mathbf{U}$ is the peculiar velocity, and

$$\mathbf{U}(\mathbf{r},t) = \frac{1}{n(\mathbf{r},t)}\int d\mathbf{v}\ \mathbf{v} f(\mathbf{r},\mathbf{v},t) \tag{14}$$

is the mean particle velocity. Another relevant hydrodynamic field is the *granular* temperature $T(\mathbf{r},t)$ defined as

$$T(\mathbf{r},t)=\frac{m}{dn(\mathbf{r},t)}\int d\mathbf{v}\; V^2 f(\mathbf{r},\mathbf{v},t). \tag{15}$$

Note that in the model defined in [12]) the mean flow velocity of the interstitial gas is assumed to be equal to the mean flow velocity of solid particles ($\mathbf{U}_g=\mathbf{U}$) for the sake of simplicity.

The macroscopic balance equations for the granular suspension are obtained when one multiplies the Enskog equation (13) by $\{1,m\mathbf{v},mv^2\}$ and integrates over velocity. After some algebra, one gets the balance equations [8, 12, 15]

$$D_t n+n\nabla\cdot\mathbf{U}=0\;, \tag{16}$$

$$D_t\mathbf{U}=-\rho^{-1}\nabla\cdot\mathsf{P}-\gamma\Delta\mathbf{U}\;, \tag{17}$$

$$D_t T+\frac{2}{dn}\left(\nabla\cdot\mathbf{q}+\mathsf{P}:\nabla\mathbf{U}\right)=2\gamma\left(T_{\rm ex}-T\right)-\zeta T. \tag{18}$$

In the above equations, $D_t=\partial_t+\mathbf{U}\cdot\nabla$ is the material derivative and $\rho=mn$ is the mass density. The cooling rate ζ is proportional to $1-\alpha^2$ and is due to dissipative collisions. The pressure tensor $\mathsf{P}(\mathbf{r},t)$ and the heat flux $\mathbf{q}(\mathbf{r},t)$ have both *kinetic* and *collisional transfer* contributions, i.e., $\mathsf{P}=\mathsf{P}^{\rm k}+\mathsf{P}^{\rm c}$ and $\mathbf{q}=\mathbf{q}^{\rm k}+\mathbf{q}^{\rm c}$. Their kinetic contributions are defined by

$$\mathsf{P}^{\rm k}=\int d\mathbf{v} m\mathbf{V}\mathbf{V}f(\mathbf{r},\mathbf{v},t),\quad \mathbf{q}^{\rm k}=\int d\mathbf{v}\frac{m}{2}V^2\mathbf{V}f(\mathbf{r},\mathbf{v},t), \tag{19}$$

and the collisional transfer contributions are [15]

$$\mathsf{P}^{\rm c}=\frac{1+\alpha}{4}m\sigma^d\int d\mathbf{v}_1\int d\mathbf{v}_2\int d\widehat{\boldsymbol{\sigma}}\,\Theta(\widehat{\boldsymbol{\sigma}}\cdot\mathbf{g}_{12})(\widehat{\boldsymbol{\sigma}}\cdot\mathbf{g}_{12})^2\widehat{\boldsymbol{\sigma}}\widehat{\boldsymbol{\sigma}}\int_0^1 dx\; f_2\left[\mathbf{r}-x\boldsymbol{\sigma},\mathbf{r}+(1-x)\boldsymbol{\sigma},\mathbf{v}_1,\mathbf{v}_2,t\right], \tag{20}$$

$$\mathbf{q}^{\rm c}=\frac{1+\alpha}{4}m\sigma^d\int d\mathbf{v}_1\int d\mathbf{v}_2\int d\widehat{\boldsymbol{\sigma}}\,\Theta(\widehat{\boldsymbol{\sigma}}\cdot\mathbf{g}_{12})(\widehat{\boldsymbol{\sigma}}\cdot\mathbf{g}_{12})^2(\mathbf{G}_{12}\cdot\widehat{\boldsymbol{\sigma}})\widehat{\boldsymbol{\sigma}}\int_0^1 dx\; f_2\left[\mathbf{r}-x\boldsymbol{\sigma},\mathbf{r}+(1-x)\boldsymbol{\sigma},\mathbf{v}_1,\mathbf{v}_2,t\right],$$

where $\mathbf{G}_{12}=\frac{1}{2}(\mathbf{V}_1+\mathbf{V}_2)$ is the velocity of center of mass. Finally, the cooling rate ζ is given by

$$\zeta=\frac{\left(1-\alpha^2\right)}{4dnT}m\sigma^{d-1}\int d\mathbf{v}_1\int d\mathbf{v}_2\int d\widehat{\boldsymbol{\sigma}}\Theta(\widehat{\boldsymbol{\sigma}}\cdot\mathbf{g}_{12})(\widehat{\boldsymbol{\sigma}}\cdot\mathbf{g}_{12})^3 f_2(\mathbf{r},\mathbf{r}+\boldsymbol{\sigma},\mathbf{v}_1,\mathbf{v}_2,t). \tag{21}$$

Before closing this section, it is important to recall the range of validity of the suspension model (13). As already discussed before [8], the assumptions made in the model are relevant to the range of dimensionless physical parameters encountered in a circulating fluidized bed (low Reynolds numbers and moderate densities). A crucial aspect of the model is that the form of the Enskog collision operator $J_{\rm E}[\mathbf{r},\mathbf{v}|f,f]$ is assumed to be the same as for a dry granular gas (i.e., when the influence of the interstitial gas is neglected). This means that the collision dynamics does not contain any parameter of the environmental gas. As it has been noted in several papers [7, 23–26], the above assumption requires that the mean-free time between collisions is assumed to be much less than the time needed by the fluid forces to significantly affect the dynamics of solid particles. Thus, we expect that the suspension model (3) may be reliable in situations where the gas phase has a weak influence on the motion of grains (solid particles immersed in air, for instance). Of course, this assumption fails for instance in the case of liquid flows (high density) where the presence of fluid must be taken into account in the collision process.

III. HOMOGENEOUS STEADY STATE

Before computing the transport coefficients, it is instructive to analyze the homogeneous steady state. This state was widely analyzed in Refs. [12, 27]. For homogeneous situations, the density n and the temperature T are spatially uniform, and with an appropriate selection of the frame of reference, the mean flow velocities vanish ($\mathbf{U}=\mathbf{U}_g=\mathbf{0}$). Consequently, Eq. (13) becomes

$$\frac{\partial f}{\partial t}-\gamma\frac{\partial}{\partial\mathbf{v}}\cdot\mathbf{v}f-\gamma\frac{T_{\rm ex}}{m}\frac{\partial^2 f}{\partial v^2}=J_{\rm E}[\mathbf{V}|f,f], \tag{22}$$

where

$$J_{\mathrm{E}}\left[f,f\right]=\chi\sigma^{d-1}\int d\mathbf{v}_2\int d\widehat{\boldsymbol{\sigma}}\Theta(\widehat{\boldsymbol{\sigma}}\cdot\mathbf{g}_{12})(\widehat{\boldsymbol{\sigma}}\cdot\mathbf{g}_{12})\left[\alpha^{-2}f(v_1'')f(v_2'')-f(v_1)f(v_2)\right]. \tag{23}$$

Here, χ is the pair correlation function evaluated at the (homogeneous) density n. The collision operator (23) can be recognized as the Boltzmann operator for inelastic collisions multiplied by the factor χ. For homogeneous states, the only nontrivial balance equation is that of the temperature (18):

$$\partial_t T=2\gamma\left(T_{\mathrm{ex}}-T\right)-\zeta T. \tag{24}$$

As usual, for times longer than the mean free time, one expects that the system achieves a hydrodynamic regime where the distribution f qualifies as a *normal* distribution [17] in the sense that f depends on time only through its dependence on the temperature T. In this regime, $\partial_t f=(\partial_T f)(\partial_t T)$ and Eq. (22) reads

$$\left[2\gamma\left(\theta^{-1}-1\right)-\zeta\right]T\frac{\partial f}{\partial T}-\gamma\frac{\partial}{\partial\mathbf{v}}\cdot\mathbf{v}f-\frac{\gamma T_{\mathrm{ex}}}{m}\frac{\partial^2 f}{\partial v^2}=J_{\mathrm{E}}[f,f], \tag{25}$$

where $\theta\equiv T/T_{\mathrm{ex}}$ and use has been made of Eq. (24). In addition, for homogeneous states, Eq. (21) gives the following form for the cooling rate ζ:

$$\zeta(t)=\frac{\pi^{(d-1)/2}}{4d\Gamma\left(\frac{d+3}{2}\right)}(1-\alpha^2)\frac{m\sigma^{d-1}}{nT}\chi\int\,d\mathbf{v}_1\int\,d\mathbf{v}_2\,g_{12}^3\,f(\mathbf{v}_1,t)\,f(\mathbf{v}_2,t). \tag{26}$$

For elastic collisions ($\alpha=1$ and so, $\zeta=0$), as expected Eq. (25) admits the solution

$$f_0(v,t)=n\left(\frac{m}{2\pi T(t)}\right)^{d/2}\exp\left(-\frac{mv^2}{2T(t)}\right) \tag{27}$$

where the temperature obeys the time-dependent equation

$$\partial_t T=2\gamma\left(T_{\mathrm{ex}}-T\right). \tag{28}$$

The system therefore is in a time-dependent "equilibrium state" before reaching the asymptotic steady state where $T=T_{\mathrm{ex}}$. For inelastic collisions, $\zeta\neq 0$ and to date the solution to Eq. (25) has not been found.

On the other hand, after a transient stage, the system achieves a *steady* state characterized by the steady temperature T_{s}. According to Eq. (28), T_{s} is given by the condition

$$2\gamma\left(\theta_{\mathrm{s}}^{-1}-1\right)-\zeta_{\mathrm{s}}=0, \tag{29}$$

where the subscript s means that the quantities are evaluated at $T=T_{\mathrm{s}}$. At a given value of the environmental temperature T_{ex} (which acts as a bath temperature in the sense that it is considered as a thermal energy reservoir), Eq. (29) implies that in the steady state the energy gained by grains due to their collisions with the interstitial fluid (γT_{ex}) is exactly compensated by the cooling terms arising from collisional dissipation (ζT) and viscous friction (γT). Moreover, as usual in the granular literature, the effects of the energy balance on the internal degrees of freedom of grains are not considered in the description.

As shown in previous works [12, 27–29], dimensionless analysis requires that f_{s} has the scaled form

$$f_{\mathrm{s}}(\mathbf{v},\gamma,T_{\mathrm{ex}})=nv_0^{-d}\varphi_{\mathrm{s}}(\mathbf{c},\gamma_{\mathrm{s}}^*)\equiv nv_0^{-d}\varphi_{\mathrm{s}}(\mathbf{c},\lambda,\theta_{\mathrm{s}}), \tag{30}$$

where $v_0=\sqrt{2T_{\mathrm{s}}/m}$ is the thermal speed and the unknown scaled distribution φ_{s} is a function of the dimensionless parameters $\mathbf{c}\equiv\mathbf{v}/v_0$ and γ_{s}^* where

$$\gamma_{\mathrm{s}}^*(\lambda,\theta_{\mathrm{s}})=\lambda\theta_{\mathrm{s}}^{-1/2},\quad \lambda(\phi)=\frac{\gamma_0 R(\phi)\ell}{\sqrt{2T_{\mathrm{ex}}/m}}=\frac{\sqrt{2}\pi^{d/2}}{2^d d\Gamma\left(\frac{d}{2}\right)}\frac{R(\phi)}{\phi\sqrt{T_{\mathrm{ex}}^*}}. \tag{31}$$

Here, $T_{\mathrm{ex}}^*\equiv T_{\mathrm{ex}}/(m\sigma^2\gamma_0^2)$ is the (reduced) background gas temperature. In the second relation of Eq. (31), $\ell=1/(n\sigma^{d-1})$ is proportional to the mean free path of hard spheres. The scaling given by Eq. (30) is equivalent to the one proposed in Refs. [12, 27] when one makes the mapping $\xi_{\mathrm{s}}^*\to 2\lambda\theta_{\mathrm{s}}^{-3/2}$ with $R(\phi)=1$. Here, ξ_{s}^* is defined by Eq. (24) of [12]. This means that the results for homogeneous states can be directly obtained from those derived in Refs.

[12, 27] by making the above change. On the other hand, we have preferred here to revisit the homogeneous state in order to check the previous results.

In terms of $\varphi_{\rm s}$, in the steady state, Eq. (22) for $f_{\rm s}$ can be rewritten as

$$-\gamma_{\rm s}^*\frac{\partial}{\partial \mathbf{c}}\cdot \mathbf{c}\varphi_{\rm s}-\frac{\gamma_{\rm s}^*}{2\theta_{\rm s}}\frac{\partial^2\varphi_{\rm s}}{\partial c^2}=J_{\rm E}^*[\varphi_{\rm s},\varphi_{\rm s}], \tag{32}$$

where we have introduced the dimensionless collision operator $J_{\rm E}^*=\ell v_0^{d-1}J_{\rm E}/n$. Although the exact form of $\varphi_{\rm s}$ is not known, an indirect information on it can be obtained from the kurtosis or fourth cumulant

$$a_{2,{\rm s}}=\frac{4}{d(d+2)}\int d\mathbf{c}\, c^4\varphi_s(c)-1. \tag{33}$$

The cumulant $a_{2,{\rm s}}$ measures the deviation of φ_s from its Maxwellian form $\pi^{-d/2}e^{-c^2}$. This coefficient can be obtained by multiplying Eq. (32) by c^4 and integrating over velocity. The result is

$$d(d+2)\left(\gamma_{\rm s}^*a_{2,{\rm s}}-\frac{1}{2}\zeta_{\rm s}^*\right)=\beta_4, \tag{34}$$

where $\zeta_{\rm s}^*\equiv \ell\zeta_{\rm s}/v_0$ and

$$\beta_4=\int d\mathbf{c}\, c^4\, J_{\rm E}^*[\varphi_{\rm s},\varphi_{\rm s}]. \tag{35}$$

Upon deriving Eq. (34) use has been made again of the steady state condition (29).

As expected, Eq. (34) cannot be solved unless one knows the collisional moments $\zeta_{\rm s}^*$ and β_4. As in previous works [12, 22, 27], a good estimate of $\zeta_{\rm s}^*$ and β_4 can be obtained by replacing $\varphi_{\rm s}$ by its leading Sonine approximation [22]:

$$\varphi_{\rm s}\simeq \frac{e^{-c^2}}{\pi^{d/2}}\left\{1+a_{2,{\rm s}}\left[\frac{c^4}{2}-\frac{(d+2)c^2}{2}+\frac{d(d+2)}{8}\right]\right\}. \tag{36}$$

In this case, retaining only linear terms in $a_{2,{\rm s}}$, one has

$$\zeta_{\rm s}^*\to\zeta_0^{(0)}+\zeta_0^{(1)}a_{2,{\rm s}},\quad \beta_4\to\beta_4^{(0)}+\beta_4^{(1)}a_{2,{\rm s}}, \tag{37}$$

where [22]

$$\zeta_0^{(0)}=\frac{2K}{d}\chi(1-\alpha^2),\quad \zeta_0^{(1)}=\frac{3}{16}\zeta_0^{(0)}, \tag{38}$$

$$\beta_4^{(0)}=-K\chi\left(1-\alpha^2\right)\left(d+\frac{3}{2}+\alpha^2\right),\quad \beta_4^{(1)}=-K\chi\left(1-\alpha^2\right)\left[\frac{3}{32}\left(10d+39+10\alpha^2\right)+\frac{d-1}{1-\alpha}\right], \tag{39}$$

and

$$K=\frac{\pi^{(d-1)/2}}{\sqrt{2}\Gamma(d/2)}. \tag{40}$$

With these results, Eq. (34) can be easily solved with the result

$$a_{2,{\rm s}}=\frac{16(1-\alpha)(1-2\alpha^2)}{73+56d-3\alpha(35+8d)+30(1-\alpha)\alpha^2+32d(d+2)\gamma_{\rm s}^*/K\chi(1+\alpha)}. \tag{41}$$

Notice that in Eq. (41), $\gamma_{\rm s}^*$ is consistently obtained from the steady state condition (29) by replacing $\zeta_{\rm s}^*\to\zeta_0^{(0)}$. The expression (41) agrees with the one obtained in Ref. [12] when one takes the steady state condition $\xi_{\rm s}^*=2\gamma_{\rm s}^*+\zeta_0^{(0)}$ in Eq. (31) of [12].

Once $a_{2,{\rm s}}$ is known, the dependence of the cooling rate on both the coefficient of restitution α and the (reduced) external temperature $T_{\rm ex}^*$ can be obtained from the first relation of Eq. (37). Finally, the (reduced) steady temperature θ_s is determined by solving the cubic equation

$$2\lambda\left(\theta_{\rm s}^{-1}-1\right)=\frac{\sqrt{2}}{d}\frac{\pi^{(d-1)/2}}{\Gamma\left(\frac{d}{2}\right)}(1-\alpha^2)\chi(\phi)\left(1+\frac{3}{16}a_{2,{\rm s}}\right)\sqrt{\theta_{\rm s}}. \tag{42}$$

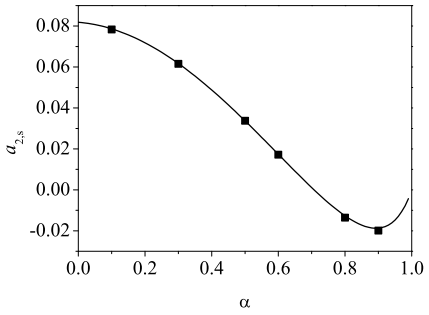

FIG. 1: Plot of the fourth cumulant $a_{2,\mathrm{s}}$ as a function of the coefficient of restitution α for a two-dimensional ($d = 2$) granular suspension with $\phi = 0.25$. The line is the theoretical result given by Eq. (41) (with $R(\phi) = 1$) and the symbols are the Monte Carlo simulation results obtained in Ref. [12]. The parameters of the simulation are $m = 1$, $\sigma = 0.01$, $\gamma_0 = 1$, and $T_{\mathrm{ex}} = 1$.

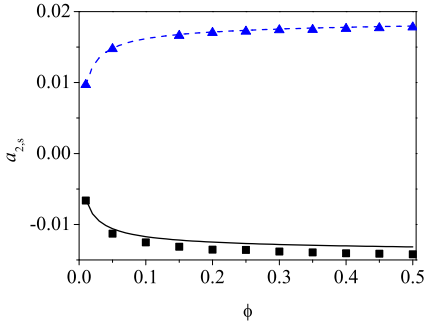

FIG. 2: Plot of the fourth cumulant $a_{2,\mathrm{s}}$ as a function of the volume fraction ϕ for a two-dimensional ($d = 2$) granular suspension. Two different values of the coefficient of restitution are considered: $\alpha = 0.8$ (solid line and squares) and $\alpha = 0.6$ (dashed line and triangles). The lines are the theoretical results given by Eq. (41) (with $R(\phi) = 1$) and the symbols are the Monte Carlo simulation results. The parameters of the simulation are $m = 1$, $\sigma = 0.01$, $\gamma_0 = 1$, and $T_{\mathrm{ex}} = 1$.

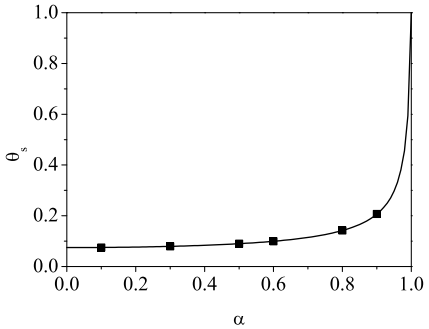

FIG. 3: Plot of the (reduced) temperature $\theta_{\mathrm{s}} \equiv T_{\mathrm{s}}/T_{\mathrm{ex}}$ as a function of the coefficient of restitution α for a two-dimensional ($d = 2$) granular suspension with $\phi = 0.25$. The line is the theoretical result given by Eq. (42) (with $R(\phi) = 1$) and the symbols are the Monte Carlo simulation results obtained in Ref. [12]. The parameters of the simulation are $m = 1$, $\sigma = 0.01$, $\gamma_0 = 1$, and $T_{\mathrm{ex}} = 1$.

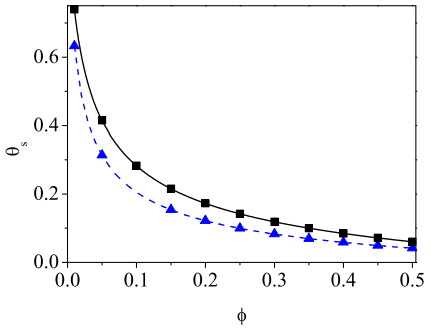

FIG. 4: Plot of the (reduced) temperature $\theta_{\rm s} \equiv T_{\rm s}/T_{\rm ex}$ as a function of the volume fraction ϕ for a two-dimensional ($d = 2$) granular suspension. Two different values of the coefficient of restitution are considered: $\alpha = 0.8$ (solid line and squares) and $\alpha = 0.6$ (dashed line and triangles). The lines are the theoretical results given by Eq. (42) (with $R(\phi) = 1$) and the symbols are the Monte Carlo simulation results. The parameters of the simulation are $m = 1$, $\sigma = 0.01$, $\gamma_0 = 1$, and $T_{\rm ex} = 1$.

As expected, Eq. (42) is consistent with Eq. (33) of Ref. [12] for the steady temperature when one takes $R(\phi) = 1$ and makes the replacement $\xi_{\rm s}^* \to 2\lambda\theta_{\rm s}^{-3/2}$.

Figure 1 shows the α-dependence of the fourth cumulant $a_{2,\rm s}$ for hard disks ($d = 2$) with the solid volume fraction $\phi = 0.25$. In the case of hard disks, we have chosen the following form for $\chi(\phi)$ [30]:

$$\chi(\phi) = \frac{1 - \frac{7}{16}\phi}{(1-\phi)^2}. \tag{43}$$

The theoretical results given by Eq. (41) are compared against the results obtained in Ref. [12] by numerically solving the Enskog equation from the direct simulation Monte Carlo (DSMC) method [31]. The parameters of the simulation are $m = 1$, $\sigma = 0.01$, $\gamma_0 = 1$, and $T_{\rm ex} = 1$. In addition, the function $R(\phi) = 1$ in the simulations. Although this figure was already presented in Ref. [12], we plot it again here to remark the excellent agreement between theory and simulations observed in the complete range of values of α. Since the values of $a_{2,\rm s}$ are very small (in fact their magnitude is smaller than the one found in the dry granular case [22, 32]) then, the Sonine approximation (36) can be considered as a good representation of the scaled distribution $\varphi_s(c)$. As a complement of Fig. 1, Fig. 2 shows $a_{2,\rm s}$ versus ϕ for two values of α. It is quite apparent that the qualitative dependence of the fourth cumulant on the density depends strongly on the inelasticity since while $a_{2,\rm s}$ decreases monotonically with ϕ at $\alpha = 0.8$, the opposite happens at $\alpha = 0.6$. We do not actually have an intuitive explanation for the change of behaviour of $a_{2,\rm s}$ when the coefficient of restitution varies from 0.8 to 0.6. Next, the (reduced) temperature θ_s is considered. Figure 3 shows $\theta_{\rm s}$ versus α for $d = 2$, $\phi = 0.25$, and the same parameters as the one considered in Figs. 1 and 2. First, as expected, $\theta_{\rm s} = 1$ for elastic collisions. Moreover, the steady granular temperature decreases with inelasticity. It is illustrated in Fig. 4 (which was also plotted in Ref. [12]) where $\theta_{\rm s}$ is plotted against the density ϕ for two different values of α. Figures 3 and 4 highlight again the excellent agreement between theory and simulations, even for extreme values of both inelasticity and/or density.

IV. TRANSPORT AROUND THE HOMOGENEOUS STEADY STATE. CHAPMAN–ENSKOG EXPANSION

As in previous studies [12, 15, 33], we assume that we perturb the homogeneous steady state by small spatial gradients. These perturbations give rise to nonzero contributions to the pressure tensor and the heat flux, which are characterized by transport coefficients. The evaluation of the transport coefficients is the main objective of the present contribution. In order to get them, we will solve the Enskog equation (13) by means of the Chapman–Enskog method [17] conveniently adapted to granular fluids. As usual, the Chapman–Enskog method assumes the existence of a normal solution such that all space and time dependence of the velocity distribution function occurs through the hydrodynamic fields, namely,

$$f(\mathbf{r}, \mathbf{v}, t) = f\left[\mathbf{v}|n(t), T(t), \mathbf{U}(t)\right]. \tag{44}$$

The notation on the right hand side indicates a functional dependence on the density, temperature and flow velocity. For small spatial variations (i.e., low Knudsen numbers), this functional dependence can be made local in space through an expansion in the gradients of the hydrodynamic fields. To generate it, f is written as a series expansion in a formal parameter ϵ measuring the non-uniformity of the system,

$$f = f^{(0)} + \epsilon\, f^{(1)} + \epsilon^2\, f^{(2)} + \cdots , \tag{45}$$

where each factor of ϵ means an implicit gradient of a hydrodynamic field. In contrast to the case of dry granular gases [15], in ordering the different level of approximations in the kinetic equation, one has to characterize the magnitude of the drift term γ relative to the gradients as well as the term $\Delta\mathbf{U}$. With respect to the first term, since γ does not induce any flux in the system, it is considered to be of zeroth-order in gradients. Regarding the term $\Delta\mathbf{U}$, since in the absence of gradients $\mathbf{U}$ tends to $\mathbf{U}_g$ after a transient period, then $\Delta\mathbf{U}$ is expected to be at least to first order in the spatial gradients.

According to the expansion (45), the Enskog operator J_{E} and the time derivative ∂_t are also given in the representations

$$J_{\mathrm{E}} = J_{\mathrm{E}}^{(0)} + \epsilon J_{\mathrm{E}}^{(1)} + \cdots , \quad \partial_t = \partial_t^{(0)} + \epsilon\partial_t^{(1)} + \cdots . \tag{46}$$

The coefficients in the time derivative expansion are identified by a representation of the fluxes and the cooling rate in the macroscopic balance equations as a similar series through their definitions as functionals of f. This is the usual Chapman–Enskog method [17, 34] for solving kinetic equations. The expansions (46) yield similar expansions for the heat and momentum fluxes and the cooling rate when substituted into Eqs. (19)–(21):

$$P_{ij} = P_{ij}^{(0)} + \epsilon P_{ij}^{(1)} + \cdots , \quad \mathbf{q} = \mathbf{q}^{(0)} + \epsilon\mathbf{q}^{(1)} + \cdots , \quad \zeta = \zeta^{(0)} + \epsilon\zeta^{(1)} + \cdots . \tag{47}$$

Here, we shall restrict our calculations to the first order in the uniformity parameter ϵ.

A. Zeroth-order approximation

To zeroth order in the expansion, the distribution $f^{(0)}$ obeys the kinetic equation

$$\partial_t^{(0)} f^{(0)} - \gamma\frac{\partial}{\partial\mathbf{v}}\cdot\mathbf{V} f^{(0)} - \gamma\frac{T_{\mathrm{ex}}}{m}\frac{\partial^2 f^{(0)}}{\partial v^2} = J_{\mathrm{E}}^{(0)}[f^{(0)}, f^{(0)}], \tag{48}$$

where $J_{\mathrm{E}}^{(0)}[f^{(0)}, f^{(0)}]$ is given by Eq. (23) with the replacement $f_{\mathrm{s}} \to f^{(0)}(\mathbf{r}, \mathbf{v}, t)$. The conservation laws at this order are given by $\partial_t^{(0)} n = 0$, $\partial_t^{(0)}\mathbf{U} = \mathbf{0}$, and

$$\partial_t^{(0)} T = 2\gamma\left(T_{\mathrm{ex}} - T\right) - \zeta^{(0)} T, \tag{49}$$

where $\zeta^{(0)}$ is determined from Eq. (21) to zeroth order. In particular, as said in section III, a good approximation to $\zeta^{(0)}$ is given by the first relation of Eq. (37), namely,

$$\zeta^{(0)} = \frac{2}{d}\frac{\pi^{(d-1)/2}}{\Gamma\left(\frac{d}{2}\right)}(1-\alpha^2)\chi\left(1 + \frac{3}{16}a_2\right) n\sigma^{d-1}\sqrt{\frac{T}{m}}. \tag{50}$$

The kinetic equation (48) can be rewritten in terms of the derivative $\partial_T f^{(0)}$ when one takes into account the zeroth-order balance equations:

$$\left[2\gamma\left(\theta^{-1} - 1\right) - \zeta^{(0)}\right] T\frac{\partial f^{(0)}}{\partial T} - \gamma\frac{\partial}{\partial\mathbf{v}}\cdot\mathbf{V} f^{(0)} - \frac{\gamma T_{\mathrm{ex}}}{m}\frac{\partial^2 f^{(0)}}{\partial v^2} = J_{\mathrm{E}}^{(0)}[f^{(0)}, f^{(0)}]. \tag{51}$$

Equation (51) has the same form as the corresponding Enskog equation (25) for a strictly homogeneous state. However, in Eq. (51) $f^{(0)}(\mathbf{r}, \mathbf{v}, t)$ is a *local* distribution. Therefore, as in the homogeneous state, the solution to Eq. (51) can be written in the form (30) (with the replacement $T_{\mathrm{s}} \to T$) where the scaled distribution $\varphi(\mathbf{c}, \lambda, \theta)$ obeys the *unsteady* equation

$$\left[2\gamma^*\left(\theta^{-1} - 1\right) - \zeta_0^*\right]\theta\frac{\partial\varphi}{\partial\theta} + \left(\frac{\zeta_0^*}{2} - \gamma^*\theta^{-1}\right)\frac{\partial}{\partial\mathbf{c}}\cdot\mathbf{c}\varphi - \frac{\gamma^*}{2\theta}\frac{\partial^2\varphi}{\partial c^2} = J_{\mathrm{E}}^*[\varphi, \varphi], \tag{52}$$

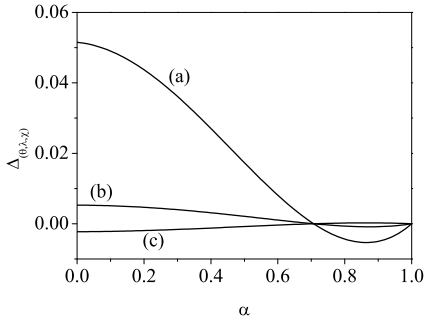

FIG. 5: Plot of the derivatives Δ_θ (a), Δ_λ (b), and Δ_χ (c) for $d = 3$, $\phi = 0.25$, and $T_{\text{ex}}^* = 0.9$.

where $\zeta_0^* \equiv \ell\zeta^{(0)}/v_0(T)$ and $\gamma^* = \lambda\theta^{-1/2}$. Upon deriving Eq. (52) use has been made of the property

$$T\frac{\partial f^{(0)}}{\partial T} = -\frac{1}{2}\frac{\partial}{\partial \mathbf{V}}\cdot\mathbf{V}f^{(0)} + nv_0^{-d}\theta\frac{\partial\varphi}{\partial\theta}, \tag{53}$$

where the derivative $\partial\varphi/\partial\theta$ is taken at constant $\mathbf{c}$.

The velocity distribution function $f^{(0)}$ is isotropic in $\mathbf{V}$ so that, according to Eqs. (19)–(21), the heat flux to zeroth-order vanishes as expected ($\mathbf{q}^{(0)} = \mathbf{0}$) and the pressure tensor $P_{ij}^{(0)} = p\delta_{ij}$, where the hydrostatic pressure is

$$p = nT\left[1 + 2^{d-2}(1+\alpha)\phi\chi\right]. \tag{54}$$

As discussed in section III, although the explicit form of φ is not known, a good approximation is given by the Sonine approximation (36). In particular, the equation for the *unsteady* fourth cumulant a_2 can be easily obtained from Eq. (52) as

$$\frac{d(d+2)}{4}\Lambda^{(0)}\theta\frac{\partial a_2}{\partial\theta} + d\,(d+2)\left(\gamma^*\theta^{-1} - \frac{\zeta_0^*}{2}\right)(1+a_2) - d\,(d+2)\,\gamma^*\theta^{-1} = \beta_4, \tag{55}$$

where $\Lambda^{(0)} \equiv 2\gamma^*\left(\theta^{-1}-1\right) - \zeta_0^*$ and β_4 is defined in Eq. (35). In the steady state, $\Lambda^{(0)} = 0$ and the solution to Eq. (55) is given by Eq. (41) once one expands ζ_0^* and β_4 in powers of a_2. Beyond the steady state, Eq. (55) must be numerically solved to get the dependence of a_2 on the (reduced) temperature. On the other hand, as we will show in section V, in order to get the transport coefficients in the steady state we need to know the derivatives $\Delta_\theta \equiv (\partial a_2/\partial\theta)_{\text{s}}$, $\Delta_\lambda \equiv (\partial a_2/\partial\lambda)_{\text{s}}$, and $\Delta_\chi \equiv (\partial a_2/\partial\chi)_{\text{s}}$. These derivatives provide an indirect information (through the fourth cumulant) on the departure of the time-dependent solution $f^{(0)}$ from its stationary form f_{s}. According to Eq. (55), the former derivative is given by

$$\frac{\partial a_2}{\partial\theta} = \frac{\frac{4}{d(d+2)}\beta_4^{(0)} + 2\zeta_0^{(0)} + 2\left(\frac{2}{d(d+2)}\beta_4^{(1)} - 2\gamma^*\theta^{-1} + \frac{19}{16}\zeta_0^{(0)}\right)a_2}{\theta\left[2\gamma^*(\theta^{-1}-1) - \left(\zeta_0^{(0)} + \zeta_0^{(1)}a_2\right)\right]}, \tag{56}$$

where here the expansions (37) have been considered and as usual nonlinear terms in a_2 have been neglected. In the steady state, the numerator and denominator of Eq. (56) vanish, hence the quantity Δ_θ becomes indeterminate. As in Ref. [12], this problem can be solved by applying l'Hôpital's rule. The final result yields a quadratic equation for Δ_θ. However, given that the magnitude of Δ_θ is quite small, one can neglect the term proportional to Δ_θ^2 in the above quadratic equation and obtain the simple expression

$$\Delta_\theta = \frac{6\gamma_{\text{s}}^*\theta_{\text{s}}^{-2}a_{2,\text{s}}}{2\gamma_{\text{s}}^* - \frac{15}{8}\zeta_0^{(0)} - \frac{4}{d(d+2)}\beta_4^{(1)}}. \tag{57}$$

Equation (57) is consistent with Eq. (A6) of Ref. [12] when one neglects nonlinear terms in $(\partial a_2/\partial\xi^*)_{\text{s}}$ and takes $\beta = \frac{1}{2}$. The derivatives Δ_λ and Δ_χ can be easily derived from Eq. (55) with the results

$$\Delta_\lambda = \frac{4\theta_{\text{s}}^{-3/2}a_{2,\text{s}} + 2\theta_{\text{s}}^{1/2}\left(\theta_{\text{s}}^{-1}-1\right)}{\frac{4}{d(d+2)}\beta_4^{(1)} - 4\gamma_{\text{s}}^* + \frac{3}{8}\zeta_0^{(0)}}, \tag{58}$$

$$\Delta_\chi = \frac{\frac{4}{d(d+2)}\beta_4^{(0)} + 2\zeta_0^{(0)} + \frac{4}{d(d+2)}\beta_4^{(1)} + \frac{19}{8}\zeta_0^{(0)} + \zeta_0^{(0)}\theta_{\rm s}\Delta_\theta}{2\chi\left(2\gamma_{\rm s}^* - \frac{2}{d(d+2)}\beta_4^{(1)} - \frac{3}{16}\zeta_0^{(0)}\right)}. \tag{59}$$

Note that in Eqs. (57)–(59), $\theta_{\rm s}$ is obtained from Eq. (42) by neglecting $a_{2,{\rm s}}$. The dependence of the derivatives Δ_θ, Δ_λ, and Δ_χ on the coefficient of restitution α is plotted in Fig. 5 for $d = 3$ and $\phi = 0.25$. Here, $T_{\rm ex}^* = 0.9$; this is a typical value for the (reduced) background temperature used in previous simulations [9]. It is seen that while the magnitude of Δ_λ, and Δ_χ is much smaller than that of the kurtosis $a_{2,{\rm s}}$, Δ_θ is of the same order of magnitude as $a_{2,{\rm s}}$.

B. First-order approximation

The mathematical steps involved in the derivation of the first-order distribution function $f^{(1)}$ are quite similar to those carried out in Ref. [12]. On the other hand, given that the calculations performed in this paper take into account some additional density dependencies not accounted for in the previous derivation [12], we have preferred here to perform an independent calculation where most of the technical details are provided in the Appendix A for the sake of completeness. To first-order in spatial gradients, $f^{(1)}$ is given by

$$f^{(1)}(\mathbf{V}) = \boldsymbol{\mathcal{A}}(\mathbf{V})\cdot\nabla\ln T + \boldsymbol{\mathcal{B}}(\mathbf{V})\cdot\nabla\ln n + \mathcal{C}_{ij}(\mathbf{V})\frac{1}{2}\left(\frac{\partial U_i}{\partial r_j} + \frac{\partial U_j}{\partial r_i} - \frac{2}{d}\delta_{ij}\nabla\cdot\mathbf{U}\right) + \mathcal{D}(\mathbf{V})\nabla\cdot\mathbf{U}, \tag{60}$$

where, in the steady state ($\Lambda^0 = 0$), the quantities $\boldsymbol{\mathcal{A}}$, $\boldsymbol{\mathcal{B}}$, $\mathcal{C}_{ij}$, and $\mathcal{D}$ verify the following set of coupled linear integral equations:

$$-\left(2\gamma\theta^{-1} + \frac{1}{2}\zeta^{(0)} + \zeta^{(0)}\theta\frac{\partial\ln\zeta_0^*}{\partial\theta}\right)\boldsymbol{\mathcal{A}} - \gamma\frac{\partial}{\partial\mathbf{v}}\cdot\mathbf{V}\boldsymbol{\mathcal{A}} - \frac{\gamma T_{\rm ex}}{m}\frac{\partial^2}{\partial v^2}\boldsymbol{\mathcal{A}} + \mathcal{L}\boldsymbol{\mathcal{A}} = \mathbf{A}, \tag{61}$$

$$\begin{aligned}-\gamma\frac{\partial}{\partial\mathbf{v}}\cdot\mathbf{V}\boldsymbol{\mathcal{B}} - \frac{\gamma T_{\rm ex}}{m}\frac{\partial^2}{\partial v^2}\boldsymbol{\mathcal{B}} + \mathcal{L}\boldsymbol{\mathcal{B}} \;=\; \mathbf{B} + \Bigg[&\zeta^{(0)}\left(1 + \phi\frac{\partial\ln\chi}{\partial\phi}\right) + \chi\phi\frac{\partial\chi}{\partial\phi}\frac{\partial}{\partial\chi}\left(\frac{\zeta^{(0)}}{\chi}\right)\\ &-\lambda\left(1 - \phi\frac{\partial\ln R}{\partial\phi}\right)\frac{\partial\zeta^{(0)}}{\partial\lambda} - 2\gamma\left(\theta^{-1} - 1\right)\phi\frac{\partial\ln R}{\partial\phi}\Bigg]\boldsymbol{\mathcal{A}},\end{aligned} \tag{62}$$

$$-\gamma\frac{\partial}{\partial\mathbf{v}}\cdot\mathbf{V}\mathcal{C}_{ij} - \frac{\gamma T_{\rm ex}}{m}\frac{\partial^2}{\partial v^2}\mathcal{C}_{ij} + \mathcal{L}\mathcal{C}_{ij} = C_{ij}, \tag{63}$$

$$-\gamma\frac{\partial}{\partial\mathbf{v}}\cdot\mathbf{V}\mathcal{D} - \frac{\gamma T_{\rm ex}}{m}\frac{\partial^2}{\partial v^2}\mathcal{D} - \zeta_1^{(1)}T\frac{\partial f^{(0)}}{\partial T} + \mathcal{L}\mathcal{D} = D. \tag{64}$$

In Eq. (64), $\zeta_1^{(1)}$ is a functional of $\mathcal{D}$ defined by Eq. (B16). Moreover, in Eqs. (61)–(64), $\mathcal{L}$ is the linearized collision operator

$$\mathcal{L}f^{(1)} = -\left(J_{\rm E}^{(0)}[f^{(0)}, f^{(1)}] + J_{\rm E}^{(0)}[f^{(1)}, f^{(0)}]\right), \tag{65}$$

R is defined by Eqs. (10)–(12) and the coefficients $\mathbf{A}$, $\mathbf{B}$, C_{ij}, and D are functions of the peculiar velocity $\mathbf{V}$ and the hydrodynamic gradients. They are defined by Eqs. (A9)–(A12). Note that all the quantities appearing in Eqs. (61)–(64) are evaluated in the steady state (the subscript s has been omitted here for the sake of simplicity). Thus, the transport coefficients obtained by solving Eqs. (10)–(12) will be provided in terms of the steady temperature $T_{\rm s}$. It is worthwhile to remark that since we are here interested in obtaining the momentum and heat fluxes in the first order of the deviations from the steady state, we only need to know the transport coefficients to zeroth order in the deviations. This means that the solution to the integral equations (61)–(64) will provide us the forms of the transport coefficients and the cooling rate in steady state conditions.

According to the Chapman–Enskog scheme [17], acceptable solutions to Eqs. (61)–(64) must obey

$$\int d\mathbf{v}\left(1, \mathbf{V}, V^2\right) f^{(1)} = (0, \mathbf{0}, 0)\,. \tag{66}$$

These are necessary conditions for the solution to the integral equations to exist (the so-called Fredholm alternative [35]). Since $\boldsymbol{\mathcal{A}}(\mathbf{V}) \propto \mathbf{A}(\mathbf{V})$, $\boldsymbol{\mathcal{B}}(\mathbf{V}) \propto \mathbf{B}(\mathbf{V})$, $\mathcal{C}_{ij}(\mathbf{V}) \propto C_{ij}(\mathbf{V})$, and $\mathcal{D}(\mathbf{V}) \propto D(\mathbf{V})$, then the solubility conditions (66) can be proved when one takes into account the explicit forms of $\mathbf{A}$, $\mathbf{B}$, C_{ij}, and D.

V. NAVIER–STOKES TRANSPORT COEFFICIENTS

To first order in the spatial gradients, the constitutive equations for the pressure tensor $P_{ij}^{(1)}$ and the heat flux $\mathbf{q}^{(1)}$ are

$$P_{ij}^{(1)} = -\eta\left(\frac{\partial U_i}{\partial r_j} + \frac{\partial U_j}{\partial r_i} - \frac{2}{d}\delta_{ij}\nabla\cdot\mathbf{U}\right) - \eta_{\rm b}\delta_{ij}\nabla\cdot\mathbf{U}, \tag{67}$$

$$\mathbf{q}^{(1)} = -\kappa\nabla T - \mu\nabla n. \tag{68}$$

Here, η is the shear viscosity, $\eta_{\rm b}$ is the bulk viscosity, κ is the thermal conductivity, and μ is the diffusive heat conductivity. This latter coefficient vanishes for ordinary gases ($\alpha = 1$). While the coefficients η, κ, and μ have kinetic and collisional contributions, the bulk viscosity $\eta_{\rm b}$ has only collisional contributions and hence, it vanishes for dilute gases. In addition, as already mentioned in Ref. [8], the forms of the collisional contributions to the transport coefficients are exactly the same as those obtained in the dry granular case (namely, in the absence of the gas phase) [15, 16], except that $a_{2,\rm s}$ depends on γ^*. Thus, we will focus here our attention on the kinetic contributions to the transport coefficients and the cooling rate. Some technical details on this calculation are provided in the Appendix B.

A. Shear and bulk viscosities

The bulk viscosity $\eta_{\rm b}$ is given by

$$\eta_{\rm b} = \frac{2^{2d+1}}{\pi(d+2)}\phi^2\chi(1+\alpha)\left(1-\frac{a_{2,\rm s}}{16}\right)\eta_0, \tag{69}$$

where

$$\eta_0 = \frac{d+2}{8}\frac{\Gamma\left(\frac{d}{2}\right)}{\pi^{(d-1)/2}}\sigma^{1-d}\sqrt{mT_{\rm s}} \tag{70}$$

is the low density value of the shear viscosity for an ordinary gas of hard spheres ($\alpha = 1$). The shear viscosity η can be written as

$$\eta = \frac{\eta_0}{\nu_\eta^* + 2K'\gamma_{\rm s}^*}\left[1 - \frac{2^{d-2}}{d+2}\chi\phi(1+\alpha)(1-3\alpha)\right]\left[1 + \frac{2^{d-1}}{d+2}(1+\alpha)\phi\chi\right] + \frac{d}{d+2}\eta_{\rm b}, \tag{71}$$

where $K' = (d+2)/8K$, K is defined by Eq. (40) and the (reduced) collision frequency ν_η^* is [36]

$$\nu_\eta^* = \frac{3}{4d}\chi\left(1-\alpha+\frac{2}{3}d\right)(1+\alpha)\left(1+\frac{7}{16}a_{2,\rm s}\right), \tag{72}$$

where $a_{2,\rm s}$ is defined by Eq. (41). The expression (71) for the shear viscosity agrees with the one obtained in Ref. [12] when $R(\phi) = 1$. This is because the new contributions to the fluxes coming from the extra density dependencies not accounted for in [12] do not affect the form of the pressure tensor.

B. Thermal conductivity and diffusive heat conductivity

The thermal conductivity is given by

$$\kappa = \kappa_{\rm k}\left[1 + 3\frac{2^{2-d}}{d+2}\phi\chi\,(1+\alpha)\right] + \frac{2^{2d+1}\,(d-1)}{(d+2)^2\,\pi}\phi^2\chi\,(1+\alpha)\left(1+\frac{7}{16}a_{2,\rm s}\right)\kappa_0, \tag{73}$$

where

$$\kappa_0 = \frac{d(d+2)}{2(d-1)}\frac{\eta_0}{m} \tag{74}$$

is the low density value of the thermal conductivity for an ordinary gas of hard spheres ($\alpha = 1$) and $\kappa_{\rm k}$ denotes the kinetic contribution to the thermal conductivity. Its explicit expression is

$$\kappa_{\rm k} = \kappa_0 \frac{d-1}{d} \frac{1 + 2a_{2,{\rm s}} + \theta_{\rm s}\Delta_\theta + 3\frac{2^{d-3}}{d+2}\chi\phi\,(1+\alpha)^2\left[2\alpha - 1 + a_{2,{\rm s}}\,(1+\alpha) + \frac{1}{2}\,(1+\alpha)\,\theta_{\rm s}\Delta_\theta\right]}{\nu_\kappa^* + K'\left(\gamma_{\rm s}^* - \frac{3}{2}\zeta_0^* - \theta_{\rm s}\zeta_0^{(1)}\Delta_\theta\right)}, \tag{75}$$

where $\zeta_0^{(1)}$ is defined by Eq. (38) and the derivative Δ_θ is given by Eq. (57). In addition, the (reduced) collision frequency ν_κ^* is [36]

$$\nu_\kappa^* = \frac{1+\alpha}{d}\chi\left[\frac{d-1}{2} + \frac{3}{16}\,(d+8)\,(1-\alpha) + \frac{296 + 217d - 3\,(160+11d)\,\alpha}{256}a_{2,{\rm s}}\right]. \tag{76}$$

To compare the expression (75) with the one derived in Ref. [12] (see Eq. (65) of this reference), one has to make the mapping $\xi_{\rm s}^*(\partial a_2/\partial\xi^*)_{\rm s} \to -(2/3)\theta_{\rm s}\Delta_\theta$ and takes $R(\phi) = 1$. In this case, we find that the form (75) of the thermal conductivity coefficient is consistent with the one obtained in [12] except for the last term of the numerator (i.e., the term proportional to $\frac{1}{2}\,(1+\alpha)\,\theta_{\rm s}\Delta_\theta$). This term comes from the collision integral (B13). We have checked that Eq. (75) gives the correct result and hence it fixes the slight mistake of Eq. (65) of Ref. [12].

The diffusive heat conductivity μ is

$$\mu = \mu_{\rm k}\left[1 + 3\frac{2^{d-2}}{d+2}\phi\chi\,(1+\alpha)\right], \tag{77}$$

where the kinetic contribution $\mu_{\rm k}$ is given by

$$\begin{aligned}
\mu_{\rm k} \;=\; & \frac{\kappa_0 T_{\rm s}}{n}\left(\nu_\kappa^* - 3K'\gamma_{\rm s}^*\right)^{-1}\left\{\frac{\kappa_{\rm k}}{\kappa_0}\left[K'\zeta_0^*\left(1 + \phi\frac{\partial\ln\chi}{\partial\phi}\right) + K'\zeta_0^{(1)}\left(\phi\frac{\partial\chi}{\partial\phi}\Delta_\chi - \lambda\left(1 - \phi\frac{\partial\ln R}{\partial\phi}\right)\Delta_\lambda\right)\right.\right. \\
& \left. -2\left(\theta_{\rm s}^{-1} - 1\right)\gamma_{\rm s}^*\phi\frac{\partial\ln R}{\partial\phi}\right] + \frac{d-1}{d}\left[a_{2,{\rm s}} - \lambda\left(1 - \phi\frac{\partial\ln R}{\partial\phi}\right)\Delta_\lambda + \phi\frac{\partial\chi}{\partial\phi}\Delta_\chi\right] \\
& + 3\frac{2^{d-4}\,(d-1)}{d\,(d+2)}\chi\phi\,(1+\alpha)^3\left[\phi\frac{\partial\chi}{\partial\phi}\Delta_\chi - \lambda\left(1 - \phi\frac{\partial\ln R}{\partial\phi}\right)\Delta_\lambda\right] \\
& \left. + 3\frac{2^{d-2}\,(d-1)}{d\,(d+2)}\chi\phi\,(1+\alpha)\left(1 + \frac{1}{2}\phi\frac{\partial\ln\chi}{\partial\phi}\right)\left[\alpha\,(\alpha-1) + \frac{a_{2,{\rm s}}}{6}\left(10 + 2d - 3\alpha + 3\alpha^2\right)\right]\right\}.
\end{aligned} \tag{78}$$

Here, the derivatives Δ_λ and Δ_χ are defined by Eqs. (58) and (59), respectively. The expression (78) agrees with Eq. (69) of Ref. [12] when one neglects (i) the density dependence of the function R (i.e., $\partial_\phi R = 0$) and (ii) all the derivatives of a_2 with respect to θ, λ, and χ in the steady state (i.e., $\Delta_\theta = \Delta_\lambda = \Delta_\chi = 0$). In addition, as in the case of a dry granular gas [15, 16, 42], the coefficient μ vanishes for elastic collisions.

C. Cooling rate

The cooling rate is

$$\zeta = \zeta_{\rm s}^{(0)} + \zeta_U \nabla\cdot\mathbf{U}, \tag{79}$$

where $\zeta_{\rm s}^{(0)}$ is given by Eq. (50) with the replacement $T \to T_{\rm s}$. The coefficient ζ_U can be written as

$$\zeta_U = \zeta_1^{(0)} + \zeta_1^{(1)}, \tag{80}$$

where

$$\zeta_1^{(0)} = -3\frac{2^{d-2}}{d}\chi\phi(1-\alpha^2), \tag{81}$$

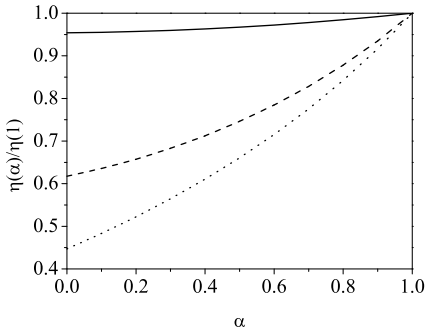

FIG. 6: Dependence of the (scaled) shear viscosity $\eta(\alpha)/\eta(1)$ on the coefficient of restitution α for $d = 3$, $T_{\text{ex}}^* = 0.9$, and three different values of the solid volume fraction: $\phi = 0.01$ (a), $\phi = 0.1$ (b), and $\phi = 0.2$ (c). Here, $\eta(1)$ refers to the shear viscosity coefficient of a suspension with elastic collisions.

$$\zeta_1^{(1)} = \frac{9(d+2)2^{d-8}}{d^2}\chi\left(1-\alpha^2\right)\left(\nu_\gamma^* + 4K'\gamma_{\text{s}}^*\right)^{-1}\left\{\frac{\omega^*\phi\chi}{2(d+2)} - 2^{2-d}\frac{d}{3}\Big[\lambda\left(1-\phi\frac{\partial\ln R}{\partial\phi}\right)\Delta_\lambda - \phi\frac{\partial\chi}{\partial\phi}\Delta_\chi - \frac{2}{d}\theta_{\text{s}}\Delta_\theta\Big] - (1+\alpha)\left(\frac{1}{3}-\alpha\right)\left(2a_{2,\text{s}} + \theta_{\text{s}}\Delta_\theta\right)\phi\chi\right\}. \tag{82}$$

Here, we have introduced the quantities

$$\omega^* = (1+\alpha)\left\{\left(1-\alpha^2\right)(5\alpha-1) - \frac{a_{2,\text{s}}}{6}\left[15\alpha^3 - 3\alpha^2 + 3(4d+15)\alpha - (20d+1)\right]\right\}, \tag{83}$$

$$\nu_\gamma^* = -\frac{1+\alpha}{192}\chi\left[30\alpha^3 - 30\alpha^2 + (105+24d)\alpha - 56d - 73\right]. \tag{84}$$

It is quite apparent that $\zeta_U = 0$ for elastic collisions ($\alpha = 1$). As in the case of the diffusive heat conductivity, to compare Eq. (82) with the expression (73) for $\zeta_1^{(1)}$ obtained in Ref. [12] one has to make the replacement $\theta\Delta_\theta \to -(3/2)\xi_{\text{s}}^*(\partial a_2/\partial\xi^*)_{\text{s}}$, take $R(\phi) = 1$, and neglect the derivatives of a_2 with respect to λ and χ ($\Delta_\lambda = \Delta_\chi = 0$). After these changes, we see that both results agree except for a misprint we have found in Eq. (73) of Ref. [12]. Note also that $\zeta_U \neq 0$ for dilute granular suspensions [29].

D. Some illustrative examples

In summary, the Navier–Stokes transport coefficients η_{b}, η, κ, and μ are given by Eqs. (69), (71), (73), and (77), respectively, while the first-order contribution ζ_U to the cooling rate is given by Eqs. (80)–(82). As expected, all these coefficients present an intricate dependence on the coefficient of restitution α, the density ϕ, and the (reduced) background temperature T_{ex}^*. In addition, their dimensionless forms are defined in terms of the steady temperature θ_{s} and the derivatives Δ_θ, Δ_λ, and Δ_χ. While these derivatives are explicitly given by Eqs. (57)–(59), the granular temperature is given in terms of the physical solution of the cubic equation (42).

As in previous works [8, 12], it is quite apparent that one of the principal new features of the present paper lies on the dependence of the Navier–Stokes transport coefficients of granular suspensions on the coefficient of restitution α. Therefore, to illustrate the differences between granular ($\alpha \neq 1$) and ordinary ($\alpha = 1$) suspensions, the transport coefficients are scaled with respect to their values for elastic collisions. In addition, we consider a three-dimensional system ($d = 3$) with $T_{\text{ex}}^* = 0.9$ and three different values of the volume fraction ϕ: $\phi = 0.01$ (very dilute system), $\phi = 0.1$, and $\phi = 0.2$ (moderately dense system).

In Figs. 6–8, the above Navier–Stokes transport coefficients are plotted as functions of α. While in the case of the shear viscosity and thermal conductivity coefficients we observe that their deviation from their forms for elastic collisions is in general significant, no happens the same in the case of the diffusive heat conductivity since the magnitude of the scaled coefficient $n\mu(\alpha)/T\kappa(1)$ is much smaller than that of the (scaled) coefficient $\kappa(\alpha)/\kappa(1)$. Since

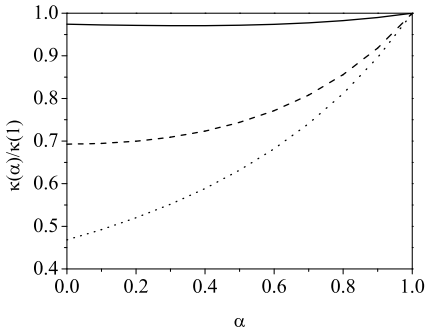

FIG. 7: Dependence of the (scaled) thermal conductivity $\kappa(\alpha)/\kappa(1)$ on the coefficient of restitution α for $d = 3$, $T^*_{\text{ex}} = 0.9$, and three different values of the solid volume fraction: $\phi = 0.01$ (a), $\phi = 0.1$ (b), and $\phi = 0.2$ (c). Here, $\kappa(1)$ refers to the thermal conductivity coefficient of a suspension with elastic collisions.

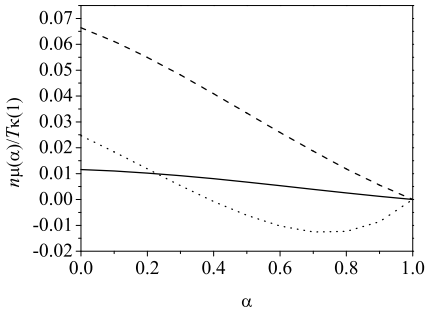

FIG. 8: Dependence of the (scaled) diffusive heat conductivity $n\mu(\alpha)/T\kappa(1)$ on the coefficient of restitution α for $d = 3$, $T^*_{\text{ex}} = 0.9$, and three different values of the solid volume fraction: $\phi = 0.01$ (a), $\phi = 0.1$ (b), and $\phi = 0.2$ (c). Here, $\kappa(1)$ refers to the thermal conductivity coefficient of a suspension with elastic collisions.

both κ and μ characterize the heat flux, one could neglect the term proportional to the density gradient in the heat flux. Thus, for practical purposes and analogously to ordinary (elastic) suspensions, one could assume that the heat flux verifies Fourier's law $\mathbf{q}^{(1)} = -\kappa\nabla T$. With respect to the α-dependence of η and κ, Figures 6 and 7 highlight that both transport coefficients are decreasing functions of the inelasticity regardless of the density of the system. In addition, the influence of collisional dissipation on momentum and heat transport increases with density, being very tiny in the limit of dilute suspensions. A comparison with the results obtained for dry granular fluids (see for instance, Fig. 1 of Ref. [37]) shows significant differences between dry (no gas phase) and granular suspensions. In particular, both theory [15, 16, 38] and simulations [39] show that for relatively dilute dry granular gases ($\phi \lesssim 0.1$) η increases with inelasticity, while the opposite occurs for sufficiently dense dry granular fluids ($\phi \gtrsim 0.1$). The same qualitative behavior is observed for the thermal conductivity coefficient [15, 16, 38]. This non-monotonic behavior contrasts with the predictions found here for granular suspensions where η and κ always decreases with decreasing α. Regarding the coefficient μ, we see that the impact of density on it is significant since while μ is always positive for dilute suspensions, it can be negative for moderately dense suspensions. It is worthwhile to note that the behavior of the shear viscosity and thermal conductivity on both density and coefficient of restitution found here is qualitatively similar to that of a confined quasi-two-dimensional granular fluid [40].

Finally, the dependence of the magnitude of the first-order contribution $|\zeta_U|$ to the cooling rate is plotted in Fig. 9 for the same parameters employed in Figs. 6–8. As the coefficient μ, $\zeta_U = 0$ for elastic collisions. On the other hand, in contrast to the diffusive heat conductivity, we observe that the influence of inelasticity on ζ_U is important, specially at large densities. This means that the contribution of ζ_U to the cooling rate must be considered as the inelasticity increases.

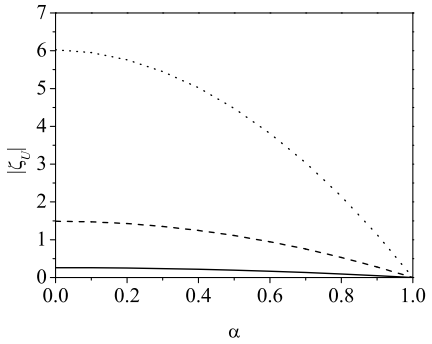

FIG. 9: Dependence of the magnitude of the first-order contribution $|\zeta_U|$ to the cooling rate on the coefficient of restitution α for $d = 3$, $T_{\text{ex}}^* = 0.9$, and three different values of the solid volume fraction: $\phi = 0.1$ (a), $\phi = 0.3$ (b), and $\phi = 0.5$ (c).

VI. STABILITY OF THE HOMOGENEOUS STEADY STATE

The knowledge of the Navier–Stokes transport coefficients and the cooling rate opens up the possibility of solving the hydrodynamic equations for n, $\mathbf{U}$, and T for situations close to the homogeneous steady state. The solution of the linearized hydrodynamic equations allows us to study the stability of the homogeneous steady state. This is likely one of the nicest applications of the Navier–Stokes equations. In order to obtain them, one has to substitute the equation of state (54), the Navier–Stokes constitutive equations (67) and (68) for the pressure tensor and heat flux, respectively, and Eq. (79) for the cooling rate into the exact balance equations (16)–(18). The Navier–Stokes hydrodynamic equations read

$$D_t n + \nabla \cdot \mathbf{U} = 0, \tag{85}$$

$$D_t U_i + \rho^{-1} \partial_i p = \rho^{-1} \partial_j \left[\eta \left(\partial_i U_j + \partial_j U_i - \frac{2}{d} \delta_{ij} \nabla \cdot \mathbf{U} \right) + \eta_b \delta_{ij} \nabla \cdot \mathbf{U} \right] - \gamma \Delta \mathbf{U}, \tag{86}$$

$$\begin{aligned} \left(D_t + 2\gamma \left(1 - \theta^{-1} \right) + \zeta^{(0)} \right) T \;=\; & \frac{2}{dn} \nabla \cdot (\kappa \nabla T + \mu \nabla n) + \frac{2}{dn} \left[\eta \left(\partial_i U_j + \partial_j U_i - \frac{2}{d} \delta_{ij} \nabla \cdot \mathbf{U} \right) \right. \\ & \left. + \eta_b \delta_{ij} \nabla \cdot \mathbf{U} \right] \partial_i U_j - T \zeta_U \nabla \cdot \mathbf{U} - \frac{2}{dn} p \nabla \cdot \mathbf{U}. \end{aligned} \tag{87}$$

As mentioned in several previous papers [37, 41], the general form of the cooling rate ζ should include second-order gradient contributions of the form $\zeta_n \nabla^2 n$ and $\zeta_T \nabla^2 T$ in Eq. (87). Nevertheless, as shown for a dilute (dry) granular gas [42], given that the ratios ζ_n/μ and ζ_T/κ were shown to be very small for not very inelastic particles, the terms $\zeta_n \nabla^2 n$ and $\zeta_T \nabla^2 T$ were neglected in the Navier–Stokes transport equations. We assume that the same happens for dense gases and hence, these second-order contributions can be neglected for practical purposes. Apart from this approximation, Eqs. (85)–(87) are exact to second order in the spatial gradients for a granular suspension at moderate densities.

The stability analysis of the homogeneous steady state was also carried out in Ref. [12]. On the other hand and as mentioned in section I, the present work generalizes the results derived before [12] since it takes into account both an extra density dependence of the zeroth-order distribution $f^{(0)}$ and the dependence of the friction coefficient γ on the volume fraction ϕ ($R(\phi) \neq 1$). Thus, it is worth to assess to what extent the previous theoretical results [12] are indicative of what happens in the stability analysis of the homogeneous state when the above density dependencies for the transport coefficients and the cooling rate are considered. This is the main motivation of this Section.

To analyze the stability of the homogeneous solution, Eqs. (85)–(87) must be linearized around the homogeneous steady state. In this state, the hydrodynamic fields take the homogeneous steady values $n \equiv$ const., $T_s \equiv$ const., and $\mathbf{U}_g = \mathbf{U} \equiv \mathbf{0}$. For small spatial gradients, we assume that the deviations $\delta y_\beta(\mathbf{r}, t) = y_\beta(\mathbf{r}, t) - y_{\beta,s}$ are small, where $\delta y_\beta(\mathbf{r}, t)$ denotes the deviations of the hydrodynamic fields $\{y_\beta; \beta = 1, \cdots, d+2\} = \{n, \mathbf{U}, T\}$ from their values in the

homogeneous *steady* state. Moreover, as usual we also suppose that the interstitial fluid is not perturbed and hence, $\mathbf{U}_g = \mathbf{U} = \mathbf{0}$.

It must be recalled that here, in contrast to the linear stability analysis for dry granular gases [37, 43, 44], the reference state is stationary and so one does not have to eliminate the time dependence of the transport coefficients. On the other hand, in order to compare our results with those obtained for granular fluids [37], the following space and time variables are introduced:

$$\tau = \frac{1}{2} n\sigma^{d-1}\sqrt{\frac{T_s}{m}}t, \quad \mathbf{r}' = \frac{1}{2} n\sigma^{d-1}\mathbf{r}. \tag{88}$$

The dimensionless time scale τ measures the average number of collisions per particle in the time interval between 0 and t. The unit length $\mathbf{r}'$ is proportional to the mean free path of solid particles. As usual, a set of Fourier transformed dimensionless variables are then introduced by

$$\rho_{\mathbf{k}}(\tau) = \frac{\delta n_{\mathbf{k}}(\tau)}{n}, \quad \mathbf{w}_{\mathbf{k}}(\tau) = \frac{\delta \mathbf{U}_{\mathbf{k}}(\tau)}{\sqrt{T_s/m}}, \quad \theta_{\mathbf{k}}(\tau) = \frac{\delta T_{\mathbf{k}}(\tau)}{T_s}, \tag{89}$$

where $\delta y_{\mathbf{k}\beta} \equiv \{\rho_{\mathbf{k}}(\tau), \mathbf{w}_{\mathbf{k}}(\tau), \theta_{\mathbf{k}}(\tau)\}$ is defined as

$$\delta y_{\mathbf{k}\beta}(\tau) = \int d\mathbf{r}' \mathrm{e}^{-i\mathbf{k}\cdot\mathbf{r}'} \delta y_\beta(\mathbf{r}', \tau), \tag{90}$$

where here the wave vector $\mathbf{k}$ is dimensionless.

In terms of the above dimensionless variables, as expected, the $d-1$ transverse velocity components $\mathbf{w}_{\mathbf{k}\perp} = \mathbf{w}_{\mathbf{k}} - \left(\mathbf{w}_{\mathbf{k}}\cdot\widehat{\mathbf{k}}\right)\widehat{\mathbf{k}}$ (orthogonal to the wave vector $\mathbf{k}$) decouple from the other three modes. Their evolution equation is

$$\frac{\partial \mathbf{w}_{\mathbf{k}\perp}}{\partial\tau} + \left(2\sqrt{2}\gamma_s^* + \frac{1}{2}\eta^* k^2\right)\mathbf{w}_{\mathbf{k}\perp} = 0, \tag{91}$$

where $\eta^* = \eta/\sigma^{1-d}\sqrt{mT_s}$. The solution to Eq. (91) is

$$\mathbf{w}_{\mathbf{k}\perp}(\mathbf{k},\tau) = \mathbf{w}_{\mathbf{k}\perp}(0)\exp\left[-\left(\frac{1}{2}\eta^* k^2 + 2\sqrt{2}\gamma_s^*\right)\tau\right]. \tag{92}$$

Since both the (reduced) friction coefficient γ_s^* and the (reduced) shear viscosity coefficient η^* are positive, then the transversal shear modes of the granular suspension are linearly stable.

The remaining (longitudinal) modes correspond to $\rho_{\mathbf{k}}$, $\theta_{\mathbf{k}}$, and the longitudinal velocity component of the velocity field, $w_{\mathbf{k}\parallel} = \mathbf{w}_{\mathbf{k}}\cdot\widehat{\mathbf{k}}$ (parallel to $\mathbf{k}$). These modes are coupled and obey the equation

$$\frac{\partial \delta y_{\mathbf{k}\beta}(\tau)}{\partial\tau} + M_{\beta\mu}\delta y_{\mathbf{k}\mu}(\tau) = 0, \tag{93}$$

where $\delta y_{\mathbf{k}\beta}(\tau)$ denotes now the set $\left\{\rho_{\mathbf{k}}, w_{\mathbf{k}\parallel}, \theta_{\mathbf{k}}\right\}$ and M is the square matrix

$$\mathsf{M} = \begin{pmatrix} 0 & ik & 0 \\ ikp^* C_p & 2\sqrt{2}\gamma_s^* + \nu_\ell^* k^2 & ikp^* \\ 2\sqrt{2}\left(\zeta_0^* C_\chi + \zeta_0^{(1)} C_n + C_\gamma\right) + \mu^* k^2 & \frac{2}{d}ik\left(p^* + \frac{d}{2}\zeta_U\right) & 2\sqrt{2}\left(2\gamma_s^*\theta_s^{-1} + \frac{1}{2}\zeta_0^* + \zeta_0^{(1)}\theta_s\Delta_\theta\right) + D_T^* k^2 \end{pmatrix}. \tag{94}$$

Here, the (reduced) transport coefficient ν_ℓ^*, μ^*, and D_T^* are defined as

$$\nu_\ell^* = \frac{1}{2\sigma^{1-d}\sqrt{mT_s}}\left(2\frac{d-1}{d}\eta + \eta_b\right), \quad D_T^* = \frac{\kappa}{d\sigma^{1-d}\sqrt{T_s/m}}, \quad \mu^* = \frac{\rho}{d\sigma^{1-d}T_s\sqrt{mT_s}}\mu, \tag{95}$$

while $p^* \equiv p_s/nT_s = 1 + 2^{d-2}(1+\alpha)\chi\phi$, $\rho = mn$, and the quantities C_p, C_χ, C_n, and C_γ are given by

$$C_p = 1 + \phi\frac{\partial \ln p^*}{\partial\phi}, \quad C_\chi = 1 + \phi\frac{\partial \ln\chi}{\partial\phi}, \tag{96}$$

$$C_n = \phi\frac{\partial\chi}{\partial\phi}\Delta_\chi + \phi\frac{\partial\lambda}{\partial\phi}\Delta_\lambda, \quad C_\gamma = 2\left(1-\theta_s^{-1}\right)\gamma_s^*\phi\frac{\partial \ln R}{\partial\phi}. \tag{97}$$

In the above equations, it is understood that the transport coefficients η^*, ν_ℓ^*, D_T^*, and μ^* are evaluated in the homogeneous steady state.

The longitudinal three modes have the form $\exp[\Lambda_\ell(k)\tau]$ for $\ell = 1, 2, 3$, where $\Lambda_\ell(k)$ are the eigenvalues of the matrix M, namely, they are the solutions of the cubic equation

$$\Lambda^3 + X(k)\Lambda^2 + Y(k)\Lambda + Z(k) = 0, \tag{98}$$

where

$$X(k) = \sqrt{2}\left(\zeta_0^* + 2\zeta_0^{(1)}\theta_s\Delta_\theta + 4\gamma_s^*\theta_s^{-1}\right) + k^2\left(D_T^* + \nu_\ell^*\right), \tag{99}$$

$$Y(k) = \left(2\sqrt{2}\gamma_s^* + k^2\nu_\ell^*\right)\left[k^2 D_T^* + \sqrt{2}\left(\zeta_0^* + 2\zeta_0^{(1)}\theta_s\Delta_\theta + 4\gamma_s^*\theta_s^{-1}\right)\right] + k^2 p^*\left(C_p + \zeta_U + \frac{2}{d}p^*\right), \tag{100}$$

$$Z(k) = p^* k^2\left[k^2\left(C_p D_T^* - \mu^*\right) + \sqrt{2}C_p\left(\zeta_0^* + 2\zeta_0^{(1)}\theta_s\Delta_\theta + 4\gamma_s^*\theta_s^{-1}\right) - 2\sqrt{2}\left(\zeta_0^* C_\chi + \zeta_0^{(1)} C_n + C_\gamma\right)\right]. \tag{101}$$

In general, one of the longitudinal modes can be unstable for $k < k_h$, where k_h is obtained from Eq. (98) when $\Lambda = 0$, namely, $Z(k_h) = 0$. The result is

$$k_h^2 = \sqrt{2}\frac{2\left(\zeta_0^* C_\chi + \zeta_0^{(1)} C_n + C_\gamma\right) - C_p\left(\zeta_0^* + 2\zeta_0^{(1)}\theta_s\Delta_\theta + 4\gamma_s^*\theta_s^{-1}\right)}{C_p D_T^* - \mu^*}. \tag{102}$$

At a fixed value of the background temperature T_{ex}^*, a careful analysis of the dependence of k_h^2 on both the coefficient of restitution α and the volume fraction ϕ shows that k_h^2 is always negative. This means that there are no physical values of the wave numbers for which the longitudinal modes become unstable. Therefore, as in the case of the transversal shear modes, we can conclude that *all* the eigenvalues of the dynamical matrix M have a *positive* real part and no instabilities are found in the homogeneous steady state of a granular suspension.

In summary, the stability analysis performed here by including the extra density dependencies of the transport coefficients shows no surprises relative to the earlier analysis [12]: the homogenous steady state of a moderately dense granular suspension is linearly stable. On the other hand, the dispersion relations derived here are different from those obtained in Ref. [12] since for instance the functional form of the heat flux transport coefficients differs in both approaches.

VII. CONCLUSIONS

In this paper we have undertaken a rather complete study on the transport properties of granular suspensions in the Navier–Stokes domain (first-order in the spatial gradients). The starting point of our study has been the Enskog kinetic equation where the effect of the gas phase on the solid particles is via the introduction of two additional terms: (i) a viscous drag force term proportional to the velocity of particle and (ii) a stochastic Langevin-like term. While the first term attempts to model the friction of solid particles on the viscous surrounding gas, the second term mimics the kinetic energy gained by grains due to eventual collisions with the more rapid molecules of the interstitial gas. Both terms are characterized by the friction coefficient γ (which is a function of the volume fraction ϕ) and the background temperature T_{ex} (which is a known quantity of the model).

A previous attempt on the derivation of the Navier–Stokes transport coefficients of dense granular suspensions was worked out by Garzó *et al.* [12] by starting from a similar suspension model. However, the above work has two deficiencies: (i) it neglects an additional density dependence of the zeroth-order distribution $f^{(0)}$ through the parameter $\lambda(\phi)$ (defined in Eq. (31)), and (ii) it assumes that the friction coefficient γ is constant. While the former simplification may be relevant in the evaluation of the diffusive heat conductivity coefficient (the transport coefficient associated to the density gradient in the heat flux), the latter simplification may be not reliable as the suspension becomes denser. The present analysis incorporates both extra new ingredients (the density dependence of λ in $f^{(0)}$ and $\gamma = \gamma_0 R(\phi)$, γ_0 being constant) in the Chapman–Enskog solution. The results show that while these two new density dependencies do not formally affect the expression of the shear viscosity coefficient obtained in Ref. [12], the forms of the heat flux transport coefficients and the cooling rate obtained here differ from those derived before. These findings are likely the most significant contributions of the present work. In this context, this paper complements and extends previous papers on transport properties in granular suspensions [8, 11, 12].

Before considering inhomogeneous situations, the homogeneous steady state has been analyzed. As expected, after a transient period, the steady distribution function f_s adopts the form (30) where the temperature dependence of the scaled distribution φ_s is encoded through the dimensionless velocity $\mathbf{c} = \mathbf{v}/v_0$ ($v_0 = \sqrt{2T_s/m}$ being the thermal speed) and the (scaled) friction coefficient $\gamma_s^* = \lambda(\phi)\theta_s^{-1/2}$ ($\theta_s = T_s/T_{ex}$ being the reduced steady temperature). As in previous works on granular fluids driven by thermostats [12, 28], the above scaling differs from the one assumed for undriven granular fluids [22, 43, 44] where φ_s depends on T only through the scaled velocity $\mathbf{c}$. Although the exact form of φ_s is not known, a good approximation of this distribution (at least in the thermal velocity region $c \sim 1$) is provided by the leading Sonine approximation (36). By using this distribution, we have explicitly obtained the fourth cumulant $a_{2,s}$; this coefficient provides an indirect information on the deviation of φ_s from its Maxwellian form $\pi^{-d/2}e^{-c^2}$. Once $a_{2,s}$ is known, the steady temperature θ_s is obtained by solving the cubic equation (42). In spite of the above approximations, the theoretical predictions for θ_s and $a_{2,s}$ show an excellent agreement with Monte Carlo simulation results. As expected, the results obtained for homogeneous systems agree with those derived in Ref. [12] when one makes the mapping $\xi_s^* \to 2\lambda\theta_s^{-3/2}$ with $R(\phi) = 1$.

Once the steady reference state is well characterized, we have considered the transport processes occurring in granular suspensions with small spatial gradients of the hydrodynamic fields. In this situation, the Enskog kinetic equation has been solved by means of the Chapman–Enskog method [17] where only terms up to the first order in the spatial gradients have been retained (Navier–Stokes hydrodynamic order). As in previous papers on the application of the Chapman–Enskog method to granular systems [12, 15, 16, 42], the spatial gradients have been assumed to be independent of the coefficient of restitution α. Thus, although the constitutive equations for the irreversible fluxes are limited to first order in spatial gradients, the corresponding transport coefficients appearing in these equations apply *a priori* to arbitrary degree of collisional dissipation. This type of expansion differs from the ones considered by other authors [45–48] where the Chapman–Enskog solution is given in powers of both the Knudsen number (or spatial gradients as in the conventional scheme) and the degree of collisional dissipation $\delta \equiv 1 - \alpha^2$. The results reported here are consistent with the ones obtained in those papers [45–48] in the limit $\delta \to 0$.

As in the Chapman–Enskog solution obtained in Ref. [12], a subtle but important point is the choice of the zeroth-order approximation $f^{(0)}$ in the perturbation expansion. Although we are interested in obtaining the transport coefficients in steady state conditions, for general small perturbations around the homogeneous steady state, the density and temperature are specified separately in the local reference state $f^{(0)}$ and hence, it is not expected that the temperature is stationary at any point of the system. This means that $\partial_t^{(0)} T \neq 0$ in the reference base state and consequently, the complete determination of the Navier–Stokes transport coefficients requires to know for instance the temperature dependence of the fourth cumulant a_2 of the *unsteady* reference state. This of course involves the numerical integration of the differential equation (56). This is quite an intricate problem that goes beyond the objective of this paper. Since we are essentially motivated by a desire for analytic expressions, the steady state conditions have been considered. On the other hand, given that $\partial_t^{(0)} T \neq 0$ in the Chapman–Enskog scheme, the transport coefficients are defined not only in terms of the hydrodynamic fields in the steady state but also there are contributions to the transport coefficients [such as the derivatives Δ_θ, Δ_λ, and Δ_χ defined by Eqs. (57)–(59), respectively] accounting for the vicinity of the perturbed state to the steady state.

As usual, in order to obtain explicit expressions for the transport coefficients, the leading terms in a Sonine polynomial expansion have been considered. These forms have been displayed along the section V: the bulk η_b and shear η viscosities are given by Eqs. (69) and (71), respectively, the thermal conductivity κ is given by Eqs. (73) and (75), the heat diffusive conductivity μ is given by Eqs. (77) and (78) and the first-order contribution ζ_U to the cooling rate is given by Eqs. (81) and (82). As said before, the expressions of η_b and η agree with those derived in [12] (once one takes $R(\phi) = 1$) while the expressions of κ, μ, and ζ_U reduce to those obtained in [12] when the contributions coming from the derivatives Δ_θ, Δ_λ, and Δ_χ are neglected.

In reduced forms, it is quite apparent that the Navier–Stokes coefficients of the granular suspension exhibit a complex dependence on the (steady) temperature θ_s, the coefficient of restitution α, the solid volume fraction ϕ, and the (reduced) background temperature T_{ex}^*. In addition, Figs. (6)–(8) highlight the significant impact of the gas phase on the Navier–Stokes transport coefficients η, κ, and μ since their α-dependence is clearly different from the one previously found for dry granular gases [15, 42].

As an application of the previous results, the stability of the special homogeneous steady state solution has been analyzed. This has been achieved by solving the linearized Navier–Stokes hydrodynamic equations for small perturbations around the homogeneous steady state. The linear stability analysis performed here shows no new surprises relative to the earlier work [12]: the homogeneous steady state is linearly stable with respect to long enough wavelength excitations (namely, long enough small spatial gradients). On the other hand, it is worthwhile to recall that the conclusion reached here for the reference homogeneous steady state differs from the one found for freely cooling granular fluids where it was shown [37, 42] that the resulting hydrodynamic equations exhibit a long wavelength instability for three of the hydrodynamic modes. This shows again the influence of the interstitial fluid on the dynamics

of solid particles.

It is quite apparent that the theoretical results obtained in this paper under certain approximations should be tested against computer simulations. This would allow us to gauge the degree of accuracy of the theoretical predictions. As happens for dry granular gases [39, 49–57], we expect that the present results stimulate the performance of appropriate simulations where the kinetic theory calculations reported here can be assessed. We also plan to undertake such kind of simulations for the case of the shear viscosity. More specifically, we want to perform simulations of granular suspensions under uniform shear flow where the Navier–Stokes shear viscosity might be measured in the Newtonian regime (very small shear rates). Another possible project for the next future is the extension of the present results to the relevant subject of multicomponent granular suspensions. Work along these lines will be worked out in the near future.

Acknowledgments

We want to thank Moisés García Chamorro for providing us the simulation data included in Figs. 1–4. The present work has been supported by the Spanish Government through Grant No. FIS2016-76359-P and by the Junta de Extremadura (Spain) Grant Nos. IB16013 (V.G.) and GR18079, partially financed by "Fondo Europeo de Desarrollo Regional" funds. The research of Rubén Gómez González has been supported by the predoctoral fellowship BES-2017-079725 from the Spanish Government.

Appendix A: Some technical details on the first-order solution

Up to the first order in the expansion, the velocity distribution function $f^{(1)}$ verifies the Enskog kinetic equation

$$\partial_t^{(0)} f^{(1)} - \gamma \frac{\partial}{\partial \mathbf{v}} \cdot \mathbf{V} f^{(1)} - \frac{\gamma T_{\text{ex}}}{m} \frac{\partial^2 f^{(1)}}{\partial v^2} = -\left(D_t^{(1)} + \mathbf{V}\cdot\nabla\right) f^{(0)} + \gamma \Delta \mathbf{U} \cdot \frac{\partial f^{(0)}}{\partial \mathbf{v}} + J_{\text{E}}^{(1)}[f,f], \tag{A1}$$

where $D_t^{(1)} \equiv \partial_t^{(1)} + \mathbf{U}\cdot\nabla$ and $J_{\text{E}}^{(1)}[f,f]$ denotes the first-order contribution to the expansion of the Enskog collision operator in powers of the spatial gradients. In order to explicitly determine $J_{\text{E}}^{(1)}[f,f]$ we need the results

$$\chi\left(\mathbf{r}, \mathbf{r}\pm\boldsymbol{\sigma}|n\right) \to \chi\left(1 \pm \frac{1}{2} n \frac{\partial \ln \chi}{\partial n} \boldsymbol{\sigma}\cdot\nabla \ln n\right), \tag{A2}$$

$$f^{(0)}(\mathbf{r}\pm\boldsymbol{\sigma}, \mathbf{v}; t) \to f^{(0)}(\mathbf{r}, \mathbf{v}; t) \pm f^{(0)}(\mathbf{r}, \mathbf{v}; t)\left[n\frac{\partial f^{(0)}}{\partial n}\boldsymbol{\sigma}\cdot\nabla \ln n + T\frac{\partial f^{(0)}}{\partial T}\boldsymbol{\sigma}\cdot\nabla \ln T - \frac{\partial f^{(0)}}{\partial V_i}(\boldsymbol{\sigma}\cdot\nabla)U_i\right], \tag{A3}$$

where χ is obtained from the functional $\chi(\mathbf{r}, \mathbf{r}\pm\boldsymbol{\sigma}|n)$ by evaluating all density fields at $n(\mathbf{r}, t)$. Taking into account Eqs. (A2) and (A3), $J_{\text{E}}^{(1)}$ reads [12]

$$\begin{aligned} J_{\text{E}}^{(1)}[f,f] \;=\; & -\boldsymbol{\mathcal{K}}\left[n\frac{\partial f^{(0)}}{\partial n}\right]\cdot\nabla \ln n - \frac{1}{2}\phi\left(\frac{\partial \ln \chi}{\partial \phi}\right)\boldsymbol{\mathcal{K}}\left[f^{(0)}\right]\cdot\nabla \ln n - \boldsymbol{\mathcal{K}}\left[T\frac{\partial f^{(0)}}{\partial T}\right]\cdot\nabla \ln T \\ & + \frac{1}{2}\mathcal{K}_i\left[\frac{\partial f^{(0)}}{\partial V_j}\right]\left(\frac{\partial U_i}{\partial r_j} + \frac{\partial U_j}{\partial r_i} - \frac{2}{d}\delta_{ij}\nabla\cdot\mathbf{U}\right) + \frac{1}{d}\mathcal{K}_i\left[\frac{\partial f^{(0)}}{\partial V_i}\right]\nabla\cdot\mathbf{U} - \mathcal{L}f^{(1)}, \end{aligned} \tag{A4}$$

where $\mathcal{L}$ is defined by Eq. (65) and the operator $\boldsymbol{\mathcal{K}}[X]$ is given by

$$\boldsymbol{\mathcal{K}}[X] = \sigma^d \chi \int d\mathbf{v}_2 \int d\widehat{\boldsymbol{\sigma}}\Theta(\widehat{\boldsymbol{\sigma}}\cdot\mathbf{g}_{12})\left(\widehat{\boldsymbol{\sigma}}\cdot\mathbf{g}_{12}\right)\widehat{\boldsymbol{\sigma}}\left[\alpha^{-2} f^{(0)}(\mathbf{v}_1'')X(\mathbf{v}_2'') + f^{(0)}(\mathbf{v}_1)X(\mathbf{v}_2)\right]. \tag{A5}$$

As already noted in Ref. [12], upon obtaining Eq. (A4) use has been made of the symmetry property $\mathcal{K}_i[\partial_{V_j} f^{(0)}] = \mathcal{K}_j[\partial_{V_i} f^{(0)}]$ that follows from the isotropy of the zeroth-order solution. Thus we are able to separate the contributions from the flow field gradients into independent traceless and diagonal components.

The macroscopic balance equations to first order in the gradients are

$$D_t^{(1)} n = -n\nabla\cdot\mathbf{U}, \quad D_t^{(1)}\mathbf{U} = -\rho^{-1}\nabla p - \gamma\Delta\mathbf{U}, \quad D_t^{(1)} T = -\frac{2p}{dn}\nabla\cdot\mathbf{U} - \zeta^{(1)} T, \tag{A6}$$

where $\zeta^{(1)}$ is the first order contribution to the cooling rate. Since the cooling rate is a scalar, corrections to first-order in the gradients can arise only from $\nabla\cdot\mathbf{U}$ since ∇n and ∇T are vectors and the tensor $\partial_j U_i+\partial_i U_j-\frac{2}{d}\delta_{ij}\nabla\cdot\mathbf{U}$ is a traceless tensor. Thus, $\zeta^{(1)}$ can be written as

$$\zeta^{(1)}=\zeta_U\nabla\cdot\mathbf{U}. \tag{A7}$$

The unknown quantity ζ_U is a functional of the first-order distribution $f^{(1)}$. A more explicit form for ζ_U is obtained by expanding Eq. (21) to first-order in gradients. This yields Eq. (80) where $\zeta_1^{(0)}$ and $\zeta_1^{(1)}$ are defined by Eqs. (81) and (B16), respectively.

The use of the balance equations (A6) allows us to evaluate the right-hand side of Eq. (A1). The combination of these results with the forms (A4) of the Enskog collision operator $J_{\rm E}^{(1)}$ and (80) of ζ_U leads to the expression

$$\left(\partial_t^{(0)}+\mathcal{L}\right)f^{(1)}-\gamma\frac{\partial}{\partial\mathbf{v}}\cdot\mathbf{V}f^{(1)}-\frac{\gamma T_{\rm ex}}{m}\frac{\partial^2 f^{(1)}}{\partial v^2}\;-\;\zeta_1^{(1)}T\frac{\partial f^{(0)}}{\partial T}\nabla\cdot\mathbf{U}=\mathbf{A}\cdot\nabla\ln T+\mathbf{B}\cdot\nabla\ln n$$
$$+C_{ij}\frac{1}{2}\left(\frac{\partial U_i}{\partial r_j}+\frac{\partial U_j}{\partial r_i}-\frac{2}{d}\delta_{ij}\nabla\cdot\mathbf{U}\right)+D\nabla\cdot\mathbf{U}, \tag{A8}$$

where

$$\mathbf{A}(\mathbf{V})=-\mathbf{V}T\frac{\partial f^{(0)}}{\partial T}-\frac{p}{\rho}\frac{\partial f^{(0)}}{\partial\mathbf{V}}-\boldsymbol{\mathcal{K}}\Big[T\frac{\partial f^{(0)}}{\partial T}\Big], \tag{A9}$$

$$\mathbf{B}(\mathbf{V})=-\mathbf{V}n\frac{\partial f^{(0)}}{\partial n}-\frac{p}{\rho}\left(1+\phi\frac{\partial\ln p^*}{\partial\phi}\right)\frac{\partial f^{(0)}}{\partial\mathbf{V}}-\boldsymbol{\mathcal{K}}\Big[n\frac{\partial f^{(0)}}{\partial n}\Big]-\frac{1}{2}\phi\left(\frac{\partial\ln\chi}{\partial\phi}\right)\boldsymbol{\mathcal{K}}\Big[f^{(0)}\Big], \tag{A10}$$

$$C_{ij}(\mathbf{V})=V_i\frac{\partial f^{(0)}}{\partial V_j}+\mathcal{K}_i\Big[\frac{\partial f^{(0)}}{\partial V_j}\Big], \tag{A11}$$

$$D(\mathbf{V})=\frac{1}{d}\frac{\partial}{\partial\mathbf{V}}\cdot\Big(\mathbf{V}f^{(0)}\Big)+\left(\zeta_1^{(0)}+\frac{2}{d}p^*\right)T\frac{\partial f^{(0)}}{\partial T}-f^{(0)}+n\frac{\partial f^{(0)}}{\partial n}+\frac{1}{d}\mathcal{K}_i\Big[\frac{\partial f^{(0)}}{\partial V_i}\Big]. \tag{A12}$$

Here, $p^*\equiv p/(nT)$. The structure of Eqs. (A8)–(A12) is formally equivalent to the ones derived for driven granular gases [12]. The only difference lies on the dependence of the zeroth-order solution $f^{(0)}$ on density and temperature.

As for dry granular gases [15], the solution to the kinetic equation (A8) is given by Eq. (60) where the unknown functions $\boldsymbol{\mathcal{A}}$, $\boldsymbol{\mathcal{B}}$, $\mathcal{C}_{ij}$, and $\mathcal{D}$ are determined by solving Eq. (A8). Since the gradients of the hydrodynamic fields are all independent, substitution of (60) into Eq. (A8) yields a set of linear, inhomogeneous integral equations. In order to obtain them, one needs the result

$$\partial_t^{(0)}\nabla\ln T\;=\;\nabla\partial_t^{(0)}\ln T=\nabla\Big(2\gamma\left(\theta^{-1}-1\right)-\zeta^{(0)}\Big)=-\Bigg[\zeta^{(0)}\left(1+\phi\frac{\partial\ln\chi}{\partial\phi}\right)+\chi\phi\frac{\partial\chi}{\partial\phi}\frac{\partial}{\partial\chi}\left(\frac{\zeta^{(0)}}{\chi}\right)$$
$$-\lambda\left(1-\phi\frac{\partial\ln R}{\partial\phi}\right)\frac{\partial\zeta^{(0)}}{\partial\lambda}-2\left(\theta^{-1}-1\right)\gamma\phi\frac{\partial\ln R}{\partial\phi}\Bigg]\nabla\ln n$$
$$-\left(2\gamma\theta^{-1}+\frac{1}{2}\zeta^{(0)}+\zeta^{(0)}\theta\frac{\partial\ln\zeta_0^*}{\partial\theta}\right)\nabla\ln T. \tag{A13}$$

The integral equations (61)–(64) can be easily obtained after taking into account Eq. (A13) and the steady state condition $\Lambda^{(0)}=0$.

Appendix B: Kinetic contributions to the transport coefficients

In this Appendix we give some details on the determination of the kinetic contributions to the transport coefficients η, κ, and μ as well as the first-order contribution ζ_U to the cooling rate. Since all these quantities are obtained int he steady state, the subscript s appearing along the main text will be omitted here for the sake of brevity.

The kinetic part of the shear viscosity $\eta_{\rm k}$ is defined as

$$\eta_{\rm k}=-\frac{1}{(d-1)(d+2)}\int d\mathbf{v}\; D_{ij}(\mathbf{V})\; C_{ij}(\mathbf{V}), \tag{B1}$$

where

$$D_{ij}=m\left(V_iV_j-\frac{1}{d}V^2\delta_{ij}\right). \tag{B2}$$

As usual, to get $\eta_{\rm k}$ one multiplies both sides of Eq. (61) by D_{ij} and integrates over velocity. The result is

$$(2\gamma+\nu_\eta)\,\eta_{\rm k}=nT-\frac{1}{(d-1)(d+2)}\int d\mathbf{V}D_{ij}(\mathbf{V})\mathcal{K}_i\left[\frac{\partial f^{(0)}}{\partial V_j}\right], \tag{B3}$$

where

$$\nu_\eta=\frac{\int d\mathbf{v}D_{ij}(\mathbf{V})\mathcal{L}\mathcal{C}_{ij}(\mathbf{V})}{\int d\mathbf{v}D_{ij}(\mathbf{V})\mathcal{C}_{ij}(\mathbf{V})}, \tag{B4}$$

and [15, 16, 38]

$$\int d\mathbf{V}D_{ij}(\mathbf{V})\mathcal{K}_i\left[\frac{\partial f^{(0)}}{\partial V_j}\right]=2^{d-2}(d-1)nT\chi\phi(1+\alpha)(1-3\alpha). \tag{B5}$$

The expression of $\eta_{\rm k}$ can be easily obtained when one takes into account Eq. (B5) and the explicit form (72) of ν_η. This latter expression is obtained from Eq. (B4) by considering the leading terms in a Sonine polynomial expansion of the unknown $\mathcal{C}_{ij}(\mathbf{V})$.

The kinetic parts $\kappa_{\rm k}$ and $\mu_{\rm k}$ are defined, respectively, as

$$\kappa_{\rm k}=-\frac{1}{dT}\int d\mathbf{v}\mathbf{S}(\mathbf{V})\cdot\boldsymbol{\mathcal{A}}(\mathbf{V}), \tag{B6}$$

$$\mu_{\rm k}=-\frac{1}{dn}\int d\mathbf{v}\mathbf{S}(\mathbf{V})\cdot\boldsymbol{\mathcal{B}}(\mathbf{V}), \tag{B7}$$

where

$$\mathbf{S}(\mathbf{V})=\left(\frac{m}{2}V^2-\frac{d+2}{2}T\right)\mathbf{V}. \tag{B8}$$

As in the case of $\eta_{\rm k}$, $\kappa_{\rm k}$ is obtained by multiplying both sides of Eq. (61) by $\mathbf{S}(\mathbf{V})$ and integrating over $\mathbf{v}$. The result is

$$\left(\nu_\kappa+\gamma\theta^{-1}-2\zeta^{(0)}-\zeta^{(0)}\theta\frac{\partial\ln\zeta_0^*}{\partial\theta}\right)\kappa_{\rm k}=-\frac{1}{dT}\int d\mathbf{V}\mathbf{S}(\mathbf{V})\cdot\mathbf{A}, \tag{B9}$$

where use has been made of the steady state condition (29) and

$$\nu_\kappa=\frac{\int d\mathbf{v}\mathbf{S}(\mathbf{V})\cdot\mathcal{L}\boldsymbol{\mathcal{A}}(\mathbf{V})}{\int d\mathbf{v}\mathbf{S}(\mathbf{V})\cdot\boldsymbol{\mathcal{A}}(\mathbf{V})}. \tag{B10}$$

The right hand side of Eq. (B9) can be computed when one takes into account Eq. (A9) and the relationship (53). After some algebra, one gets

$$\begin{aligned}-\frac{1}{dT}\int d\mathbf{V}\mathbf{S}\cdot\mathbf{A}\;=\;&\frac{1}{dT}\Bigg\{\frac{d(d+2)}{2m}nT^2\left(1+2a_2+\theta\Delta_\theta\right)-\frac{1}{2}\int d\mathbf{v}\mathbf{S}(\mathbf{V})\cdot\boldsymbol{\mathcal{K}}\left[\frac{\partial}{\partial\mathbf{V}}\cdot\left(\mathbf{V}f^{(0)}\right)\right]\\&+\frac{\theta}{a_2}\Delta_\theta\int d\mathbf{v}\mathbf{S}(\mathbf{V})\cdot\boldsymbol{\mathcal{K}}\left[f^{(0)}-f_{\rm M}\right]\Bigg\},\end{aligned} \tag{B11}$$

where $f_{\rm M}(\mathbf{c}) = n\pi^{-d/2}v_0^{-d}\mathrm{e}^{-c^2}$ and use has been made of the Sonine approximation (36) to $f^{(0)}$ and the property (53). The first collision integral involving the operator $\boldsymbol{\mathcal{K}}$ has been calculated in previous works [15, 16, 38] and the result is

$$\int d\mathbf{V}\mathbf{S}(\mathbf{V})\cdot\boldsymbol{\mathcal{K}}\left[\frac{\partial}{\partial\mathbf{V}}\cdot\left(\mathbf{V}f^{(0)}\right)\right] = -\frac{3}{8}2^d d\frac{nT^2}{m}\chi\phi\,(1+\alpha)^2\left[2\alpha-1+a_2(1+\alpha)\right]. \tag{B12}$$

The second collision integral in (B11) has not been evaluated before. After some algebra, one gets

$$\int d\mathbf{V}\mathbf{S}(\mathbf{V})\cdot\boldsymbol{\mathcal{K}}\left[f^{(0)}-f_{\rm M}\right] = \frac{3}{32}2^d d\frac{nT^2}{m}\chi\phi\,(1+\alpha)^3\,a_2. \tag{B13}$$

With the above results, $\kappa_{\rm k}$ can be finally written in the form (75). As in the case of ν_η, the (reduced) collision frequency ν_κ can be well estimated by considering the leading Sonine approximation to $\boldsymbol{\mathcal{A}}$.

The evaluation of $\mu_{\rm k}$ follows similar mathematical steps to those made for $\kappa_{\rm k}$ since one has to multiply both sides of Eq. (62) by $\mathbf{S}(\mathbf{V})$ and integrate over $\mathbf{v}$. In order to get its explicit form (78), one needs the partial results

$$\begin{aligned}-\frac{1}{dn}\int d\mathbf{V}\mathbf{S}\cdot\mathbf{B} \;=\; & \frac{d+2}{2}\frac{T^2}{m}\left[a_2-\lambda\left(1-\phi\frac{\partial\ln R}{\partial\phi}\right)\Delta_\lambda+\phi\frac{\partial\chi}{\partial\phi}\Delta_\chi\right]\\ & -\frac{a_2^{-1}}{dn}\left[\lambda\left(1-\phi\frac{\partial\ln R}{\partial\phi}\right)\Delta_\lambda-\phi\frac{\partial\chi}{\partial\phi}\Delta_\chi\right]\int d\mathbf{V}\mathbf{S}(\mathbf{V})\cdot\boldsymbol{\mathcal{K}}\left[f^{(0)}-f_{\rm M}\right]\\ & +\frac{1}{dn}\left(1+\frac{1}{2}\phi\frac{\partial\ln\chi}{\partial\phi}\right)\int d\mathbf{V}\mathbf{S}(\mathbf{V})\cdot\boldsymbol{\mathcal{K}}\left[f^{(0)}\right],\end{aligned} \tag{B14}$$

$$\int d\mathbf{V}\mathbf{S}(\mathbf{V})\cdot\boldsymbol{\mathcal{K}}\left[f^{(0)}\right] = \frac{3}{8}2^d d\frac{nT^2}{m}\chi\phi\,(1+\alpha)\left[\alpha\,(\alpha-1)+\frac{a_2}{6}\left(10+2d-3\alpha+3\alpha^2\right)\right]. \tag{B15}$$

The expression (78) can be derived by using Eqs. (B14) and (B15).

Finally, the contribution $\zeta_1^{(1)}$ to the cooling rate ζ_U is defined as

$$\zeta_1^{(1)} = \frac{1}{2nT}\frac{\pi^{(d-1)/2}}{d\Gamma\left(\frac{d+3}{2}\right)}\sigma^{d-1}\chi m\left(1-\alpha^2\right)\int d\mathbf{V}_1\int d\mathbf{V}_2 g^3 f^{(0)}(\mathbf{V}_1)\mathcal{D}(\mathbf{V}_2), \tag{B16}$$

where the unknown function $\mathcal{D}(\mathbf{V})$ is the solution of the linear integral equation (64). As before, an approximate solution to (64) can be obtained by taking the Sonine approximation

$$\mathcal{D}(\mathbf{V}) \to e_D\; f_{\rm M}(\mathbf{V})\; F(\mathbf{V}), \tag{B17}$$

where

$$F(\mathbf{V}) = \left(\frac{m}{2T}\right)^2 V^4 - \frac{d+2}{2}\frac{m}{T}V^2 + \frac{d\,(d+2)}{4}. \tag{B18}$$

The coefficient e_D is given by

$$e_D = \frac{2}{d\,(d+2)}\frac{1}{n}\int d\mathbf{V}\mathcal{D}(\mathbf{V})F(\mathbf{V}). \tag{B19}$$

Substitution of Eq. (B17) into Eq. (B16) gives

$$\zeta_1^{(1)} = \frac{3\,(d+2)}{32d}\chi\left(1-\alpha^2\right)\left(1+\frac{3}{32}a_2\right)\nu_0 e_D, \tag{B20}$$

where $\nu_0 = nT/\eta_0$. The coefficient e_D is obtained by substituting the Sonine solution (B17) into the integral equation (64), multiplying it by the polynomial $F(\mathbf{V})$ and integrating over velocity. After some algebra one gets the expression (82) for $\zeta_1^{(1)}$.

[1] Möbius M E, Lauderdale B E, Nagel S R and Jaeger H M, 2001 Nature **414**, 270

[2] Naylor M A, Swift M R and King P J, 2003 Phys. Rev. E **68**, 012301
[3] Sánchez P, Swift, M R and King, P J, 2004 Phys. Rev. Lett. **93**, 184302
[4] Wylie J J, Zhang Q, Xu H Y and Sun X X, 2008 Europhys. Lett. **81**, 54001
[5] Clement C. P, Pacheco-Martínez H A, Swift M R and King P J, 2010 Europhys. Lett. **91**, 54001
[6] Pastenes J C, Géminard J C and Melo F, 2014 Phy. Rev. E **89**, 062205
[7] Koch D L and Hill R J, 2001 Annu. Rev. Fluid Mech. **33**, 619
[8] Garzó V, Tenneti S, Subramaniam S and Hrenya C M, 2012 J. Fluid Mech. **712**, 129
[9] Hayakawa H, Takada S and Garzó V, 2017 Phys. Rev. E **96**, 042903
[10] Gómez González R and Garzó V, 2019 J. Stat. Mech. **013206**
[11] Garzó V, Fullmer W D, Hrenya C M and Yin X, 2016 Phys. Rev. E **93**, 012905
[12] Garzó V, Chamorro M G and Vega Reyes F, 2013 Phys. Rev. E **87**, 032201
[13] Koch D L and Sangani A S, 1999 J. Fluid Mech. **400**, 229
[14] Garzó V, Chamorro M G and Vega Reyes F, 2013 Phys. Rev. E **87**, 059906 (erratum)
[15] Garzó V and Dufty J W, 1999 Phys. Rev. E **59**, 5895
[16] Lutsko J F, 2005 Phys. Rev. E **72**, 021306
[17] Chapman S and Cowling T G, 1970 *The Mathematical Theory of Nonuniform Gases* (Cambridge University Press, Cambridge)
[18] Garzó V and Montanero J M, 2002 Physica A **313**, 336
[19] Garzó V, 2011 Phys. Rev. E **84**, 012301
[20] Williams D R M and MacKintosh F C, 1996 Phys. Rev. E **54**, R9
[21] van Kampen N G, 1981 *Stochastic Processes in Physics and Chemistry* (North Holland, Amsterdam)
[22] van Noije T P C and Ernst M H, 1998 Granular Matter **1**, 57
[23] Koch D L, 1990 Phys. Fluids A **2**, 1711
[24] Tsao H-K and Koch D L, 1995 J. Fluid Mech. **296**, 211
[25] SanganiA S, Mo G, Tsao H-K and Koch D L, 1996 J. Fluid Mech. **313**, 309
[26] Wylie J J, Koch D L and Ladd J C, 2003 J. Fluid Mech. **480**, 95
[27] Chamorro M G, Vega Reyes F and and Garzó V, 2013 J. Stat. Mech. **P07013**
[28] García de Soria M I, Maynar P and Trizac E, 2012 Phys. Rev. E **85**, 051301
[29] García de Soria M I, Maynar P and Trizac E, 2013 Phys. Rev. E **87**, 022201
[30] Torquato S, 1995 Phys. Rev. E **51**, 3170
[31] Bird G A, 1994 *Molecular Gas Dynamics and the Direct Simulation Monte Carlo of Gas Flows* (Clarendon, Oxford)
[32] Montanero J M and Santos A, 2000 Granular Matter **2**, 53
[33] Khalil N and Garzó V, 2013 Phys. Rev. E **88**, 052201
[34] Garzó V and Santos A, 2003 *Kinetic Theory of Gases in Shear Flows. Nonlinear Transport* (Kluwer Academic Publishers, Dordrecht)
[35] Margeneau H and Murphy G M, 1956 *The Mathematics of Physics and Chemistry* (Krieger, Huntington, New York)
[36] Garzó V, Santos A and Montanero J M, 2007 Physica A **376**, 94
[37] Garzó V, 2005 Phys. Rev. E **72**, 021106
[38] Garzó V, 2013 Phys. Fluids **25**, 043301
[39] Montanero J M, Santos A and Garzó V, 2005 *24th International Symposium on Rarefied Gas Dynamics*, edited by M. Capitelli (AIP Conf. Proc.), vol. 762, pp. 797–802
[40] Garzó V, Brito R and Soto R, 2018 Phys. Rev. E **98**, 052904
[41] Garzó V, Montanero J M and and Dufty J W, 2006 Phys. Fluids **18**, 083305
[42] Brey J J, Dufty J W, Kim C S and Santos A, 1998 Phys. Rev. E **58**, 4638
[43] Brilliantov N and Pöschel T, 2004 *Kinetic Theory of Granular Gases* (Oxford University Press, Oxford)
[44] Garzó V, 2019 *Granular Gaseous Flows* (Springer Nature, Switzerland)
[45] Goldhirsch I and Sela N, 1996 Phys. Rev. E **54**, 4458
[46] Sela N, Goldhirsch I and Noskowicz S H, 1996 Phys. Fluids **8**, 2337
[47] Sela N and Goldhirsch I, 1998 J. Fluid Mech. **361**, 41
[48] Goldhirsch I, Noskowicz S H and Bar-Lev O, 2005 Phys. Rev. Lett. **95**, 068002
[49] Brey J J, Ruiz–Montero M J and and Moreno F, 1998 Phys. Fluids **10**, 2976
[50] Brey J J, Ruiz–Montero M J and Cubero D., 1999 Europhys. Lett. **48**, 359
[51] Brey J J and Ruiz–Montero M J, 2004 Phys. Rev. E **70**, 051301
[52] Brey J J, Ruiz–Montero M J, Maynar P and García de Soria M I, 2005 J. Phys.: Condens. Matter **17**, S2489
[53] Montanero J M, Santos A and Garzó V, 2007 Physica A **376**, 75
[54] Mitrano P P, Dhal S R, Cromer D J, Pacella M S and Hrenya C M, 2011 Phys. Fluids **23**, 093303
[55] Mitrano P P, Garzó V, Hilger A M, Ewasko C J and Hrenya C M, 2012 Phys. Rev. E **85**, 041303
[56] Brey J J and Ruiz–Montero M J, 2013 Phys. Rev. E **87**, 022210
[57] Mitrano P P, Garzó V and Hrenya C M, 2014 Phys. Rev. E **89**, 020201(R)

Chapter 4

Homogeneous States of Bidisperse Suspensions

4.1 Summary

The homogeneous states of a bidisperse granular suspension at moderate densities are analyzed. The suspension is modeled as a set of hard disks ($d = 2$) or spheres ($d = 3$) composed of two different species of masses m_i and diameters σ_i ($i = 1, 2$) immersed in a viscous fluid. Spheres are assumed to be completely smooth so that inelasticity of collisions between particles of the species i with particles of the species j is characterized only by the constant (positive) coefficients of restitution $\alpha_{ij} \leq 1$. As in the monocomponent case, the presence of interstitial gas is represented in the Enskog equations by a Fokker–Planck (drag force plus stochastic term) operator acting on the one-body distribution function f_i of the species i. In accordance with simulations of bidisperse gas-solid flows [172–174], the drag coefficients γ_i of the species $i = 1, 2$ are chosen to be different and functions of density.

The main aims of this chapter are two-fold. On the one hand we want to analyze the transient regime towards the asymptotic steady state. While in the case of molecular mixtures, the final state is that of equilibrium, a non-equilibrium steady state is reached in the case of granular mixtures. As discussed above, the hydrodynamic solution is the key point of the CE method. Thus, it is interesting to ascertain the existence of a hydrodynamic regime in the case of bidisperse granular suspensions. The study of the "aging to hydrodynamics" in a multicomponent granular suspension is the first objective of the

present work. It is found that for times longer than the mean free time and regardless of the initial conditions, the system reaches a universal hydrodynamic solution where the distribution function depends only on the temperature of the mixture T through the dimensionless velocity $\mathbf{c}$ (which is scaled with $v_0 = \sqrt{2T/\overline{m}}$, $\overline{m} = [m_1 + m_2]/2$), and the granular to external temperature ratio T/T_{ex}. To confirm this result, we show that the evolution of the partial (reduced) temperature T_1/T_{ex} collapses in a single time-evolution curve whose shape is only determined through the instantaneous values of T/T_{ex}. Time-dependent DSMC simulations are performed showing an excellent agreement with the theoretical predictions.

At the early stages of the evolution, the system has not yet reached the hydrodynamic stage. However, due to the presence of interstitial gas, the evolution of the total T and partial temperatures T_i are also coupled. This coupling gives rise to the emergence of memory effects. A system possesses memory when the evolution of the hydrodynamic variables depends on the whole microscopic configuration composed by kinetic and macroscopic quantities. Here, we focus our efforts in the study of the so-called Mpemba effect. Namely, when a hotter sample cools down sooner [182]. In this context, we want to study what initial conditions $(T_0, T_{1,0}/T_{2,0})$, if any, lead to a crossover in the temperature evolution of two identical samples. However, the presence of the total and partial cooling rates makes more difficult the derivation of analytical results, and hence we focus first on the study of the Mpemba-like effect in molecular suspensions (elastic collisions). A exhaustive analysis of the Mpemba effect and its inverse counterpart (namely when the two initial temperatures are below the equilibrium one) in situations close and far away from equilibrium is carried out. In this case, f_i is approximated by its Maxwellian form for the sake of simplicity. DSMC and MD data show a good agreement with theoretical results proving not only the accuracy of the hydrodynamic and Maxwellian solution, but also of the molecular chaos hypothesis. An exhaustive analysis of the Mpemba-like effect in granular suspensions is also performed. The inelasticity of collisions enhances the emergence of the effect and we can observe even the existence of non-linear Mpemba effects (non-monotonic and mixed) in far-from-equilibrium situations [248].

The second goal of this chapter is devoted to the study of the homogeneous steady state. In previous studies on homogeneous states of driven granular mixtures [94], the steady values of the temperature ratio T_1/T_2 and the fourth cumulants c_1 and c_2

(measuring the departure of the velocity distributions f_1 and f_2 from their Maxwellian forms) were confronted against MD simulations. Although the comparison shows a good agreement for the temperature ratio between theory and simulations for dilute and moderate densities, some discrepancies were found in the case of the cumulants. Given that molecular dynamics avoids any assumption inherent in the kinetic theory (such as the molecular chaos hypothesis), it is not clear whether the origin of the differences between theory and MD simulations are due to the failure of the Enskog kinetic theory or to the approximations made in solving the Enskog kinetic equation. Thus, it is desirable to provide also Monte Carlo results to find out the origin of the discrepancies encountered in the case of the cumulants. The stationary values of T_1/T_2, c_1, and c_2 are plotted in three different situations: as a function of (i) the mass ratio m_1/m_2, (ii) the size ratio σ_1/σ_2, and (iii) the partial volume fractions ratio ϕ_1/ϕ_2. Finally, a linear stability analysis of the steady state solution is also carried out showing that the steady state is always linearly stable.

4.2 Article 2

Title: Time-dependent homogeneous states of binary granular suspensions
Authors: Rubén Gómez González[1] and Vicente Garzó[2]
Affiliations:
[1] Departamento de Física, Universidad de Extremadura, E-06006 Badajoz, Spain
[2] Departamento de Física and Instituto de Computación Científica Avanzada (ICCAEx), Universidad de Extremadura, E-06006 Badajoz, Spain
Journal: Physics of Fluids
Volume: 33
Pages: 093315
Year: 2021
DOI: 10.1063/5.0062425

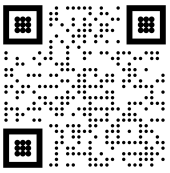

Physics of Fluids ARTICLE scitation.org/journal/phf

Time-dependent homogeneous states of binary granular suspensions

Cite as: Phys. Fluids **33**, 093315 (2021); doi: 10.1063/5.0062425
Submitted: 5 July 2021 · Accepted: 2 September 2021 ·
Published Online: 23 September 2021

Rubén Gómez González[1,a] and Vicente Garzó[2,b]

AFFILIATIONS

[1]Departamento de Física, Universidad de Extremadura, E-06071 Badajoz, Spain
[2]Departamento de Física and Instituto de Computación Científica Avanzada (ICCAEx), Universidad de Extremadura, E-06071 Badajoz, Spain

[a]**Author to whom correspondence should be addressed**: ruben@unex.es
[b]**Electronic mail**: vicenteg@unex.es. **URL:** http://www.unex.es/eweb/fisteor/vicente/

ABSTRACT

The time evolution of a homogeneous bidisperse granular suspension is studied in the context of the Enskog kinetic equation. The influence of the surrounding viscous gas on the solid particles is modeled via a deterministic viscous drag force plus a stochastic Langevin-like term. It is found first that, regardless of the initial conditions, the system reaches (after a transient period lasting a few collisions per particle) a universal unsteady hydrodynamic regime where the distribution function of each species not only depends on the dimensionless velocity (as in the homogeneous cooling state) but also on the instantaneous temperature scaled with respect to the background temperature. To confirm this result, theoretical predictions for the time-dependent partial temperatures are compared against direct simulation Monte Carlo (DSMC) results; the comparison shows an excellent agreement confirming the applicability of hydrodynamics in granular suspensions. Also, in the transient regime, the so-called Mpemba-like effect (namely, when an initially hotter sample cools sooner than the colder one) is analyzed for inelastic collisions. The theoretical analysis of the Mpemba effect is performed for initial states close to and far away from the asymptotic steady state. In both cases, good agreement is found again between theory and DSMC results. As a complement to the previous studies, we determine in this paper the dependence of the steady values of the dynamic properties of the suspension on the parameter space of the system. More specifically, we focus our attention on the temperature ratio T_1/T_2 and the fourth degree cumulants c_1 and c_2 (measuring the departure of the velocity distributions f_1 and f_2 from their Maxwellian forms). While our approximate theoretical expression for T_1/T_2 agrees very well with computer simulations, some discrepancies are found for the cumulants. Finally, a linear stability analysis of the steady state solution is also carried out showing that the steady state is always linearly stable.

I. INTRODUCTION

An effective way of accounting for the influence of the interstitial fluid on the dynamics of solid particles is through a nonconservative external force.[1] Usually, for low Reynolds numbers, this force is composed of two terms: (i) a deterministic drag force proportional to the particle velocity and (ii) a stochastic Langevin-like term. While the first contribution attempts to model background friction (or viscous damping) of grains, the second term mimics the energy gained by solid particles due to their interactions with the particles of the surrounding molecular gas. The friction of grains on the interstitial gas must not be confused with the static solid body friction which has been shown to play an important role in sheared suspensions.[2–4] The suspension model considered here can also be formally derived from the corresponding collision integral by retaining the leading term of the Kramer–Moyal expansion in powers of the mass ratio of the background and solid particles.[5–7]

The Navier–Stokes transport coefficients of a binary granular suspension have been recently determined[8] by solving the above suspension model by means of the Chapman–Enskog method[9] conveniently adapted to dissipative dynamics. The starting point of this study is the set of Enskog kinetic equations for the mixture with the inclusion of drag and stochastic forces for each one of the kinetic equations of the components of the mixture. In addition, it is assumed that the state of the surrounding gas is not affected by the presence of solid particles. It is worth noting that this suspension model is inspired by simulation results reported in the granular literature,[10] where the drift coefficients depend on both the partial and global volume fractions and the mechanical properties of grains (masses and diameters).

Physics of Fluids ARTICLE scitation.org/journal/phf

On the other hand, given the intricacies associated with the computation of transport coefficients in the time-dependent problem, steady state conditions (namely, when the cooling terms arising from viscous and collisional dissipation are exactly balanced by the heat injected in the system by the bath) were considered to get explicit forms of the diffusion coefficients and the shear and bulk viscosities. The results derived in Ref. 8 show that the forms of diffusion coefficients are, in general, very different from those found in the case of dry (no gas phase) granular mixtures.[11] With respect to the shear viscosity, it is found that its form for granular suspensions compares qualitatively well with the one obtained in the dry granular case[11] for not quite high densities. However, significant quantitative discrepancies between both descriptions (with and without the gas phase) appear for strong inelasticity. The suspension model has been recently[12] employed for studying the rheology of a dilute binary mixture of inertial suspension under simple shear flow.

A crucial point on the derivation of the Navier–Stokes hydrodynamic equations is the existence of a *normal* (or hydrodynamic) solution[9] in the homogeneous problem. This state is taken in fact as the reference state (zeroth-order approximation) in the Chapman–Enskog expansion around the *local* version of the homogeneous time-dependent state. As widely discussed in different textbooks,[9,13,14] two separate stages can be clearly identified in the evolution of a *molecular* suspension toward equilibrium. First, for times of the order of the mean free time, a *kinetic* stage is identified where the collisions between particles give rise to a relaxation of the distribution function toward a local equilibrium distribution. This kinetic stage depends on the initial preparation of the system. Then, for times much longer than the mean free time, a *hydrodynamic* stage is identified. The hydrodynamic regime is characterized by a slower evolution of the hydrodynamic fields as they approach toward equilibrium. The main feature of the hydrodynamic regime is that the system has practically *forgotten* the details of the initial conditions, except for an implicit dependence on these conditions through the hydrodynamic fields. In the case of granular suspensions, the above two-stage regimes are also expected to be identified, but with the caveat that in the kinetic regime the inelasticity of collisions causes a relaxation toward a non-equilibrium distribution function instead of the local equilibrium distribution. For the sake of clarification, a schematic representation of the two-regime (kinetic and hydrodynamic) evolution of the distribution functions f_i for homogeneous time-dependent states can be found in Fig. 1.

Although the applicability of a hydrodynamic description to granular fluids has been supported in recent years by theory in both the Navier–Stokes[11] and the non-Newtonian[15,16] regimes,

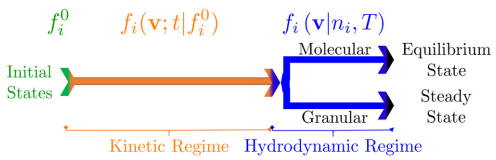

FIG. 1. Schematic representation of the time evolution of the distribution functions f_i for molecular and granular mixtures in homogeneous time-dependent states with vanishing mean flow velocity.

simulations,[17–19] and experiments,[20–22] it is interesting to analyze the existence of a hydrodynamic regime in the case of bidisperse granular suspensions. The study of the "aging to hydrodynamics" in a multicomponent granular suspension is the first objective of the present work.

We find that, before reaching the stationary regime, the system "quickly" forgets its initial preparation and then evolves toward an unsteady universal (hydrodynamic) state where the velocity distribution function $f_i(\mathbf{v};t)$ of species i has the scaling form

$$f_i(\mathbf{v};t) = n_i v_0(t)^{-d}\varphi_i(\mathbf{c}(t), T(t)/T_{\text{ex}}). \tag{1}$$

Here, n_i is the number density of species i; $v_0(t) = \sqrt{2T(t)/\bar{m}}$ [$\bar{m} = (m_1 + m_2)/2$, m_i being the mass of species i] is the thermal speed; T is the global granular temperature; $\mathbf{c} = \mathbf{v}/v_0$; and T_{ex} is the (known) background temperature. As in previous studies on driven granular fluids[23,24] and in contrast to the homogeneous cooling state,[25] the scaling distribution φ_i depends on T not only through the dimensionless velocity $\mathbf{c}$ but also on the instantaneous temperature, suitably scaled with respect to the known bath temperature T_{ex}. A consequence of the scaling solution (1) is that the velocity moments of f_i evolve in time in a similar form. Thus, for arbitrary initial conditions, one expects that the partial temperatures $T_i(t)/T_{\text{ex}}$ achieve a universal function (independent of the initial conditions) that depends on time only through the (scaled) temperature $T(t)/T_{\text{ex}}$. This theoretical result is indeed confirmed here by direct Monte Carlo simulations (DSMC)[26] of the Enskog kinetic equation.

The fact that a multicomponent granular suspension admits a hydrodynamic-like type of description opens up possible applications. Among them, thermal diffusion segregation of an intruder immersed in a granular suspension is a very interesting problem. The determination of a segregation criterion will allow us to assess the impact of the interstitial gas on the dynamics of the intruder by comparing this criterion against the one previously reported[27–29] when the gas phase was neglected.

A surprising and fascinating phenomenon in the transient regime toward the final asymptotic steady state is the so-called Mpemba effect.[30] The Mpemba effect is a counterintuitive phenomenon where two samples of fluids at initially different temperatures can evolve in time in such a way that their temperatures cross each other at a given time t_c; the curve for the initially cooler sample stays below the other one for longer times $t > t_c$. Although this exciting phenomenon was first found in the case of water, similar behaviors to the Mpemba effect have been observed in other systems.[31,32] However, in spite of the extensive number of works devoted to this problem, the origin of this phenomenon is still unknown. For this reason, different studies based on kinetic theory[33–40] have been reported in the granular literature for unveiling in a clean way the origin of the Mpemba-like effect (and its inverse counterpart). In the context of molecular suspensions (elastic collisions), we have recently analyzed the Mpemba effect[38,39] for initial states close to and far away from equilibrium. Theoretical results have been confronted against computer simulations (DSMC and molecular dynamics simulations) showing, in general, excellent agreement. As a complement to the results reported in Refs. 38 and 39, we offer in this paper a quantitative analysis of the Mpemba-like effect for binary granular suspensions, namely, when collisions between solid particles are inelastic. The study of the Mpemba-like effect is the second target of the paper.

Physics of Fluids ARTICLE scitation.org/journal/phf

As expected, for long times, the suspension reaches an asymptotic stationary state. A study of the dependence of the *steady* values of the dynamic properties of the suspension on the parameter space of the system is the third goal of the present paper. More specifically, we are interested in obtaining the ratio of kinetic temperatures T_1/T_2 and the fourth-degree cumulants c_1 and c_2 (which measure non-Gaussian properties of the velocity distributions f_1 and f_2, respectively) as functions of the mass and diameter ratios, concentration, density, coefficients of restitution, and the background temperature. Theory is compared with DSMC simulations for different systems and coefficients of restitution. While the theoretical predictions for the temperature ratio compare very well with computer simulations, some discrepancies are found for the cumulants. These discrepancies are of the same order of magnitude as those previously found in dry (no gas phase) granular mixtures.[41]

The plan of the paper is as follows. Section II deals with the Enskog equation of the binary granular suspension for homogeneous time-dependent states. The corresponding evolution equations for the global temperature $T(t)$ and the partial kinetic temperatures $T_i(t)$ (measuring the mean kinetic energy of each species) are also derived from the set of Enskog kinetic equations. Time evolution toward the unsteady hydrodynamic regime is studied in Sec. III where the existence of a universal hydrodynamic solution (1) is shown at the level of the partial temperatures and the cumulants. Section III addresses the Mpemba-like effect where exact expressions for the crossing time t_c and the critical value of the initial temperature differences (which provides information on the occurrence or not of the Mpemba effect) are obtained for initial states close to the asymptotic steady state. A more qualitative analysis is carried out for the so-called large Mpemba-like effect (namely, for initial situations far from the steady state). In both cases (small and large Mpemba effect), theory shows very good agreement with Monte Carlo simulations. Results for the dynamic properties in the stationary state are studied in Sec. IV while a linear stability analysis of this steady state is also carried out in Sec. V. The analysis shows that the steady state is always linearly stable. The paper is closed in Sec. VI with a discussion of the results reported here.

II. MODEL AND KINETIC DESCRIPTION OF BINARY GRANULAR SUSPENSIONS

Let us consider a granular binary mixture modeled as a gaseous mixture of *inelastic* hard disks ($d=2$) or spheres ($d=3$) of masses m_1 and m_2 and diameters σ_1 and σ_2. For the sake of simplicity, the spheres are assumed to be perfectly smooth and, so, collisions among all pairs are characterized by three (positive) constant coefficients of normal restitution $\alpha_{ij} \leq 1$ $(i,j=1,2)$. The coefficients α_{ij} can be different for the three types of binary collisions.

Grains (solid particles) are immersed in a viscous gas of viscosity $\eta_g \propto \sqrt{T_{\text{ex}}}$. We assume that the granular mixture is sufficiently rarefied so that one can suppose that the state of the interstitial fluid (like air or water) is not disturbed by the presence of the solid particles and it can be treated as a *thermostat*. Thus, we assume that both η_g and T_{ex} are constant quantities. Moreover, as has been widely discussed in previous works,[42–46] we also assume that the stresses exerted by the background gas on solid particles are sufficiently weak so they have a small influence on the motion of grains. Thus, the impact of gas phase on collision dynamics can be neglected and, consequently, the Enskog–Boltzmann collision operators are not affected by the presence of the interstitial gas. This assumption becomes less reliable as the particle-to-fluid density ratio decreases (for instance, glass beads in liquid water) where one should consider the influence of the gas phase on the collision operator. The use of the kinetic-theory analogy to gas–solid systems is appropriate for relatively massive particles (i.e., high Stokes number) engaging in nearly instantaneous collisions.[47] These type of systems occur in a wide range of engineering operations, including the riser section of a circulating fluidized bed, pneumatic conveying systems, or bubbling fluidized beds. Figure 2 shows a schematic diagram of the system considered in this work.

Under the above conditions, for moderate densities, the one-particle velocity distribution function $f_i(\mathbf{v},\mathbf{r};t)$ of species or component i of the mixture $(i=1,2)$ obeys a set of coupled nonlinear Enskog kinetic equations. For homogeneous and isotropic states, this set reads

$$\frac{\partial f_i}{\partial t}+\mathcal{F}_i f_i=\sum_{j=1}^{2} J_{ij}[\mathbf{v}|f_i,f_j], \tag{2}$$

where the Enskog–Boltzmann collision operator $J_{ij}[f_i,f_j]$ is given by

$$J_{ij}[f_i,f_j]=\sigma_{ij}^{d-1}\chi_{ij}\int d\mathbf{v}_2\int d\widehat{\boldsymbol{\sigma}}\,\Theta(\widehat{\boldsymbol{\sigma}}\cdot\mathbf{g}_{12})(\widehat{\boldsymbol{\sigma}}\cdot\mathbf{g}_{12}) \times\left[\alpha_{ij}^{-2}f_i(\mathbf{v}_1'';t)f_j(\mathbf{v}_2'';t)-f_i(\mathbf{v}_1;t)f_j(\mathbf{v}_2;t)\right]. \tag{3}$$

Here, $\boldsymbol{\sigma}_{ij}=\sigma_{ij}\widehat{\boldsymbol{\sigma}}$, $\sigma_{ij}=(\sigma_i+\sigma_j)/2$, $\widehat{\boldsymbol{\sigma}}$ is a unit vector directed along the line of centers from the sphere of component i to that of component j at contact, Θ is the Heaviside step function, $\mathbf{g}_{12}=\mathbf{v}_1-\mathbf{v}_2$ is the relative velocity, and $\chi_{ij}(\sigma_{ij})$ is the equilibrium pair correlation function evaluated at contact. The relationship between the pre- and post-collisional velocities is

$$\begin{aligned}\mathbf{v}_1''&=\mathbf{v}_1-\mu_{ji}\left(1+\alpha_{ij}^{-1}\right)(\widehat{\boldsymbol{\sigma}}\cdot\mathbf{g}_{12})\widehat{\boldsymbol{\sigma}},\\ \mathbf{v}_2'&=\mathbf{v}_2+\mu_{ij}\left(1+\alpha_{ij}^{-1}\right)(\widehat{\boldsymbol{\sigma}}\cdot\mathbf{g}_{12})\widehat{\boldsymbol{\sigma}},\end{aligned} \tag{4}$$

where $\mu_{ij}=m_i/(m_i+m_j)$.

In Eq. (2), the operator $\mathcal{F}_i$ represents the gas–solid interaction force that models in an effective way the effect of the background viscous gas on the solid particles of component i. For low Reynolds numbers (only laminar flows are considered), this force is usually constituted by two terms: (i) a deterministic viscous drag force

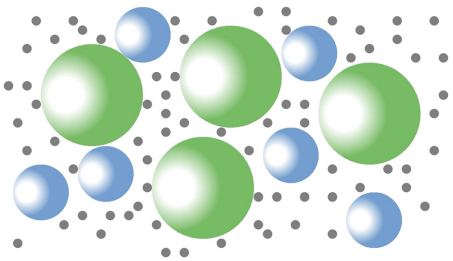

FIG. 2. Schematic diagram of the binary suspension. Two kinds of particles of masses m_1 and m_2 are surrounded by a gas of mass $m_g \ll m_{1,2}$.

Physics of Fluids ARTICLE scitation.org/journal/phf

proportional to the (instantaneous) particle velocity $\mathbf{v}$ and (ii) a stochastic Langevin-like term that takes into account the effects on a particle of species i coming from neighboring particles.[47] While the drag force term attempts to account for the loss of energy of particles due to their friction on the surrounding viscous gas (viscous damping), the stochastic term models the energy gained by grains due to their (random) collisions with gas particles. This latter term is represented by a Fokker–Planck collision operator.[48] Therefore, the Enskog equation (2) can be written as[8]

$$\frac{\partial f_i}{\partial t} - \gamma_i \frac{\partial}{\partial \mathbf{v}} \cdot \mathbf{v} f_i - \frac{\gamma_i T_{\text{ex}}}{m_i} \frac{\partial^2 f_i}{\partial v^2} = \sum_{j=1}^{2} J_{ij}[\mathbf{v}|f_i, f_j], \tag{5}$$

where the coefficients γ_i are the drag or drift coefficients. Upon writing Eq. (5), we have assumed that the mean flow velocity of the gas phase vanishes for homogeneous states. Although the drag coefficients γ_i should be in general tensorial quantities (as a result of the hydrodynamic interactions between solid particles), here we will assume that those coefficients are scalar quantities independent of the configuration of grains. As said in previous works,[49] this simple model is expected to be reliable for describing inertial suspensions where the mean diameter of suspended particles ranges approximately from 1 to 70 μm.

On the other hand, lattice-Boltzmann simulations[10,50,51] for binary granular suspensions have shown that the coefficients γ_i must be functions of the partial volume fractions

$$\phi_i = \frac{\pi^{d/2}}{2^{d-1} d \Gamma\left(\frac{d}{2}\right)} n_i \sigma_i^d \tag{6}$$

and the total volume fraction $\phi = \phi_1 + \phi_2$. Here, the number density of component i is defined as

$$n_i(t) = \int d\mathbf{v} f_i(\mathbf{v}; t). \tag{7}$$

The drag coefficients γ_i can be written as $\gamma_i = \gamma_0 R_i$, where $\gamma_0 \propto \eta_g$ and the dimensionless quantities R_i depend on the mole fraction $x_1 = n_1/(n_1 + n_2)$, the mass ratio m_1/m_2, the diameter ratio σ_1/σ_2, and the total volume fraction ϕ. Although several expressions for the coefficients γ_i can be found in the literature on polydisperse gas–solid flows, in this work we assume the expression provided in Ref. 10 for a three-dimensional system ($d = 3$) as follows:

$$\gamma_i = 18 \frac{\eta_g}{\rho \sigma_{12}^2} R_i, \tag{8}$$

where $\rho = \rho_1 + \rho_2$, $\rho_i = m_i n_i$ is the mass density of species i and the dimensionless function R_i is given by

$$R_i = \frac{\rho \sigma_{12}^2}{\rho_i \sigma_i^2} \frac{(1-\phi)\phi_i \sigma_i}{\phi} \sum_{j=1}^{2} \frac{\phi_j}{\sigma_j} \left[\frac{10\phi}{(1-\phi)^2} + (1-\phi)^2 \left(1 + 1.5\sqrt{\phi}\right) \right], \quad i = 1, 2. \tag{9}$$

In homogeneous states, the properties of primary interest in a binary mixture are the total granular temperature $T(t)$ and the partial temperatures $T_i(t)$ associated with the kinetic energy of each species. They are defined as

$$T(t) = \sum_{i=1}^{2} x_i T_i(t), \quad T_i(t) = \frac{1}{d n_i(t)} \int d\mathbf{v}\, m_i v^2 f_i(\mathbf{v}; t), \tag{10}$$

where $x_2 = 1 - x_1$. The time-dependence of $T(t)$ and $T_i(t)$ follows from the set of Enskog equations (2) that gives[8]

$$\frac{\partial T}{\partial t} = 2 \sum_{i=1}^{2} x_i \gamma_i (T_{\text{ex}} - T_i) - \zeta T, \tag{11}$$

$$\frac{\partial T_i}{\partial t} = 2\gamma_i (T_{\text{ex}} - T_i) - \zeta_i T_i, \tag{12}$$

where ζ_i is the cooling rate associated with T_i and ζ is the total cooling rate. The latter quantity gives the rate of change of the total kinetic energy due to inelastic collisions among all components of the mixture. The cooling rates ζ and ζ_i are defined, respectively, as

$$\zeta = \frac{1}{T} \sum_{i=1}^{2} x_i T_i \zeta_i, \quad \zeta_i = -\frac{m_i}{d n_i T_i} \sum_{j=1}^{2} \int d\mathbf{v}\, v^2 J_{ij}[\mathbf{v}|f_i, f_j]. \tag{13}$$

Equation (11) shows the competing mechanisms appearing in the evolution of the granular temperature toward its steady state $T_s = \lim_{t\to\infty} T(t)$. Thus, the stationary temperature is approached from below [$T(t) < T_s$] when the heat supplied by the external bath ($2\sum_i x_i \gamma_i T_{\text{ex}}$) prevails over the cooling terms arising from viscous friction ($2\sum_i x_i \gamma_i T_i$) and collisional cooling (ζT); this situation will be referred to as the *heating* case. Otherwise, the stationary temperature is achieved from above [$T(t) > T_s$] and this will be referred to as the *cooling* case. The interesting question is if an *unsteady* hydrodynamic regime exists in both situations (heating and/or cooling cases) before the granular binary suspension achieves an asymptotic steady state.

III. TIME EVOLUTION TOWARD THE STATIONARY STATE: THE UNSTEADY HYDRODYNAMIC REGIME

In order to analyze the homogeneous transient regime throughout the evolution of $T(t)$ and $T_i(t)$, it is convenient to introduce dimensionless variables for temperature and time. Let us define the reduced temperatures $\theta(t) = T(t)/T_{\text{ex}}$ and $\theta_i(t) = T_i(t)/T_{\text{ex}}$, the reduced friction coefficients $\gamma_i^*(t) = \gamma_i/\nu(t)$, and the reduced cooling rates $\zeta^*(t) = \zeta(t)/\nu(t)$ and $\zeta_i^*(t) = \zeta_i(t)/\nu(t)$. Here, the effective collision frequency $\nu(t)$ is defined as

$$\nu(t) = n \sigma_{12}^{d-1} v_0(t), \tag{14}$$

where $n = n_1 + n_2$ is the total number density of the mixture and we recall that $v_0(t) = \sqrt{2T(t)/m}$. According to Eqs. (8) and (9), the dimensionless drag coefficients γ_i^* can be expressed more explicitly in terms of the dimensionless functions R_i and the (reduced) temperature θ as

$$\gamma_i^* = \lambda_i \theta^{-1/2}, \quad \lambda_i = \frac{\sqrt{2}\pi^{d/2}}{2^d d \Gamma\left(\frac{d}{2}\right)} \frac{R_i}{\sqrt{T_{\text{ex}}^*} \sum_j (\sigma_{12}/\sigma_j)^d \phi_j}, \tag{15}$$

where

$$T_{\text{ex}}^* \equiv \frac{T_{\text{ex}}}{m \sigma_{12}^2 \gamma_0^2} \tag{16}$$

Physics of Fluids ARTICLE scitation.org/journal/phf

is the reduced background temperature. In terms of the above dimensionless quantities, Eqs. (11) and (12) can be written as

$$\frac{\partial\theta}{\partial t^*} = 2\sum_{i=1}^{2} x_i\lambda_i(1-\theta_i) - \theta^{3/2}\zeta^*, \tag{17}$$

$$\frac{\partial\theta_i}{\partial t^*} = 2\lambda_i(1-\theta_i) - \theta^{1/2}\zeta_i^*\theta_i, \tag{18}$$

where the reduced time $t^* = n\sigma_{12}^{d-1}\sqrt{2T_{\rm ex}/\bar{m}}\,t$ and $\zeta^* = \theta^{-1}(x_1\theta_1\zeta_1^* + x_2\theta_2\zeta_2^*)$.

It is quite apparent that to solve the Enskog kinetic equations (5) one has to provide specific initial conditions $f_i(\mathbf{v};0) \equiv f_i^0(\mathbf{v})$. In this sense, the solution $f_i(\mathbf{v};t)$ can be considered as a functional of the initial distribution, namely, $f_i(\mathbf{v};t) = f_i(\mathbf{v};t|f_i^0)$.[15] Analogously, the velocity moments of f_i (such as the partial temperatures θ_i) are also functionals of the initial distribution. Since the only time-dependent hydrodynamic variable in the homogeneous state is the granular temperature, for times longer than the mean free time, the existence of a hydrodynamic regime necessarily implies that the time-dependence of the distribution function $f_i(\mathbf{v};t)$ is through the temperature $T(t)$. It follows from dimensional analysis that $f_i(\mathbf{v};t)$ has the scaling form (1), i.e.,

$$f_i(\mathbf{v};t|f_i^0) \to n_i v_0(t)^{-d}\varphi_i(\mathbf{c}(t),\theta(t)), \tag{19}$$

where we recall that $\mathbf{c}(t) \equiv \mathbf{v}/v_0(t)$ is the particle velocity expressed in units of the time-dependent thermal speed. Upon writing the right-hand side of Eq. (19), we have accounted for the dependance of $\gamma_i^*(t)$ on time is only through its dependence on $\theta(t)$. For given values of the parameters of the mixture (concentration, masses, sizes, density, and coefficients of restitution), the scaled distribution $\varphi_i(\mathbf{c}(t),\theta(t))$ is a universal function independent of the initial distribution f_i^0; its time-dependence is enclosed not only in the dimensionless velocity $\mathbf{c}$ but also in the scaled temperature θ. The fact that the velocity statistics is envisioned by a two-parameter scaling form (at variance with the homogenous cooling state in undriven granular mixtures[11,25]) is a common feature in driven granular gases.[23,24] Thus, if an unsteady hydrodynamic description exists, the different solutions $f_i(\mathbf{v};t|f_i^0)$ to the set of Enskog equations (5) must *collapse* to the universal form (19). Then, for very long times, the steady state is eventually achieved where $\varphi_i(\mathbf{c},\theta) \to \varphi_i(\mathbf{c},\theta_s)$, θ_s being the stationary value of the (reduced) temperature. A consequence of Eq. (19) is that the velocity moments of the distribution $f_i(\mathbf{v};t)$ will evolve in a similar way. In particular, regardless of the initial state, the partial temperature $\theta_i(t|f_i^0)$ will be *attracted* by the universal function $\theta_i(\theta(t))$.

On the other hand, according to Eqs. (17) and (18), to confirm the existence of the hydrodynamic solution one needs to know the partial cooling rates ζ_i^*, which are defined by Eq. (13) in terms of the velocity distributions $f_i(\mathbf{v};t)$. Here, to estimate ζ_i^* we take the simplest approximation for the distributions $f_i(\mathbf{v};t)$, namely, the Maxwellian distributions $f_{i,\rm M}(\mathbf{v};t)$ defined with the partial temperatures $T_i(t)$ as follows:

$$f_{i,\rm M}(\mathbf{v};t) = n_i\left(\frac{m_i}{2\pi k_B T_i(t)}\right)^{d/2}\exp\left(-\frac{m_i v^2}{2k_B T_i(t)}\right). \tag{20}$$

In this approximation, the (reduced) partial cooling rates ζ_i^* are given by[11]

$$\zeta_i^* = \frac{4\pi^{(d-1)/2}}{d\Gamma\left(\frac{d}{2}\right)}\sum_{j=1}^{2} x_j\chi_{ij}\mu_{ji}\left(\frac{\sigma_{ij}}{\sigma_{12}}\right)^{d-1}\left(\frac{\beta_i+\beta_j}{\beta_i\beta_j}\right)^{1/2} \times (1+\alpha_{ij})\left[1 - \frac{\mu_{ji}}{2}(1+\alpha_{ij})\frac{\beta_i+\beta_j}{\beta_j}\right], \tag{21}$$

where $\beta_i = M_i\theta/\theta_i$ and $M_i = m_i/\bar{m}$. In addition, to make a plot $\theta_i(t)$ vs $\theta(t)$, the form of the pair correlation function is also needed. A good approximation for χ_{ij} for spheres ($d=3$) is[52,53]

$$\chi_{ij} = \frac{1}{1-\phi} + \frac{3}{2}\frac{\phi}{(1-\phi)^2}\frac{\sigma_i\sigma_j M_2}{\sigma_{ij}M_3} + \frac{1}{2}\frac{\phi^2}{(1-\phi)^3}\left(\frac{\sigma_i\sigma_j M_2}{\sigma_{ij}M_3}\right)^2, \tag{22}$$

where $M_\ell = \sum_i x_i\sigma_i^\ell$. A parametric plot $\theta_1(t^*)$ vs $\theta(t^*)$ is a quite useful test to see if actually an unsteady hydrodynamic regime is established, namely, if $\theta_1(t^*) \to \theta_1(\theta(t^*))$, where the function $\theta_1(\theta)$ must be independent of the initial conditions. Such a parametric plot is shown in Fig. 3 for a binary mixture with parameters $\sigma_1/\sigma_2 = 1$, $m_1/m_2 = 10$, $x_1 = \frac{1}{2}$, $\phi = 0.1$, and $T_{\rm ex}^* = 1$. Two different values of the (common) coefficient of restitution $\alpha_{ij} \equiv \alpha$ are considered: $\alpha = 1$ (elastic collisions) and $\alpha = 0.9$ (inelastic collisions). Different cooling [$\theta(t^*)$ decreases in time] and heating [$\theta(t^*)$ increases in time] cases have been considered in Fig. 3. Lines are the theoretical results derived by numerically solving Eqs. (17) and (18) with the Maxwellian approximation (21) for ζ_i^* while symbols refer to the results obtained via DSMC simulations. Figure 3 highlights that, for sufficiently long times, the different curves (corresponding to different initial conditions) are attracted to a common universal curve (time-dependent hydrodynamic regime) where θ_1 depends on time through the granular temperature θ only. Moreover, excellent agreement is found between the theoretical and the DSMC results in both granular and elastic cases. Although not shown here, similar results are found for smaller values of α ($\alpha \lesssim 0.5$).

A. Unsteady hydrodynamic regime. Leading Sonine approximation

In the unsteady hydrodynamic regime, f_i adopts the hydrodynamic form (19) and, so, the Enskog equation (5) for the scaled distributions $\varphi_i(\mathbf{c},\theta)$ reads

$$\left[2\sum_{i=1}^{2} x_i\gamma_i^*(1-\theta_i) - \zeta^*\theta\right]\frac{\partial\varphi_i}{\partial\theta} + \left[\frac{\zeta^*}{2} - \sum_{i=1}^{2} x_i\gamma_i^*\theta^{-1}(1-\theta_i) - \gamma_i^*\right] \times \frac{\partial}{\partial\mathbf{c}}\cdot\mathbf{c}\varphi_i - \frac{\gamma_i^*}{2M_i\theta}\frac{\partial^2\varphi_i}{\partial c^2} = \sum_{j=1}^{2} J_{ij}^*[\mathbf{c}|\varphi_i,\varphi_j], \tag{23}$$

where $J_{ij}^* = \ell J_{ij}/(n_i v_0^{1-d})$ and use has been made of the property[8]

$$T\frac{\partial f_i}{\partial T} = -\frac{1}{2}\frac{\partial}{\partial\mathbf{v}}\cdot\mathbf{v}f_i + n_i v_0^{-d}\theta\frac{\partial\varphi_i}{\partial\theta}. \tag{24}$$

Here, the derivative $\partial\varphi_i/\partial\theta$ is taken at constant $\mathbf{c}$. In addition, in the hydrodynamic regime, the evolution equation (18) can be rewritten as

$$\Lambda\frac{\partial\theta_i}{\partial\theta} = \Lambda_i, \quad \Lambda_i = 2\gamma_i^*(1-\theta_i) - \theta_i\zeta_i^*, \quad \Lambda = x_1\Lambda_1 + x_2\Lambda_2. \tag{25}$$

Physics of Fluids ARTICLE scitation.org/journal/phf

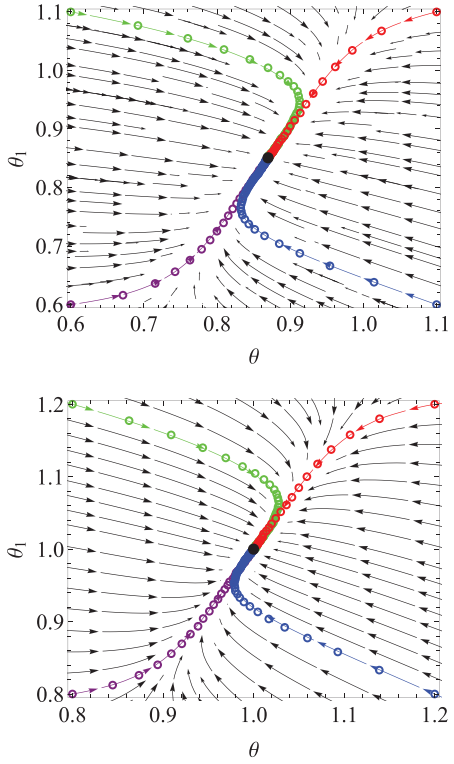

FIG. 3. Evolution of the (reduced) partial temperature $\theta_1(t^*)$ vs the (reduced) temperature $\theta(t^*)$ for $m_1/m_2 = 10$, $\sigma_1/\sigma_2 = 1$, $x_1 = \frac{1}{2}$, and a common coefficient of restitution α ($\alpha \equiv \alpha_{11} = \alpha_{12} = \alpha_{22}$). Solid lines represent the theoretical values and symbols DSMC data. Top panel corresponds to $\alpha = 0.9$ and bottom panel to $\alpha = 1$. Top panel: the initial values $\theta_1(\theta)$ of the colored lines are $\theta_1(0.6) = 0.6$ (purple line and symbols), $\theta_1(0.6) = 1.1$ (green line and symbols), $\theta_1(1.1) = 0.6$ (blue line and symbols), and $\theta_1(1.1) = 1.1$ (red line and symbols). Bottom panel: the initial values $\theta_1(\theta)$ of the colored lines are $\theta_1(0.8) = 0.8$ (purple line and symbols), $\theta_1(0.8) = 1.2$ (green line and symbols), $\theta_1(1.2) = 0.8$ (blue line and symbols), and $\theta_1(1.2) = 1.2$ (red line and symbols). The remaining parameters are $d = 3$, $\phi = 0.1$, and $T_{ex}^* = 1$. The filled circles correspond to the values of θ_1 in the steady state.

The exact solution to the time-dependent Enskog equation (23) is not known to date. Although we have seen before that the Maxwellian distribution (20) yields a good estimate of the partial cooling rates ζ_i^*, the scaled distribution $\varphi_i(\mathbf{c})$ differs from its Maxwellian form

$$\varphi_{i,\mathrm{M}}(\mathbf{c}) = \pi^{-d/2}\beta_i^{d/2}\mathrm{e}^{-\beta_i c^2}. \tag{26}$$

An usual way of assessing the deviations of φ_i from $\varphi_{i,\mathrm{M}}$ in the range of low and intermediate velocities is to expand φ_i in a complete set of Laguerre (or Sonine) polynomials where the coefficients (or cumulants) c_i of such an expansion are the velocity moments of the distribution. Based on the assumption that the cumulants c_i are small, approximate expressions for them can be achieved by truncating the series expansion at a given order. Hence, the leading Sonine approximation to φ_i is given by

$$\varphi_i(\mathbf{c}) = \varphi_{i,\mathrm{M}}(\mathbf{c})\left\{1 + \frac{c_i}{2}\left[\beta_i^2 c^4 - (d+2)\beta_i c^2 + \frac{d(d+2)}{4}\right]\right\}, \tag{27}$$

where the fourth-degree cumulants c_i are defined as

$$c_i = \frac{4}{d(d+2)}\beta_i^2\int \mathrm{d}\mathbf{c}\, c^4\varphi_i(\mathbf{c}) - 1. \tag{28}$$

We want to analyze the time-dependence of the coefficients c_i, or equivalently, the dependence of c_i on θ. To obtain self-consistent results, the partial cooling rates ζ_i^* are now estimated by using the leading Sonine polynomial term (27). Thus, according to the constraint $\theta(t^*) = x_1\theta_1(t^*) + x_2\theta_2(t^*)$, the unknown (independent) quantities are the partial temperature θ_1 and the cumulants c_1 and c_2. The equation governing the time evolution of θ_1 is given by Eq. (25) with $i = 1$. The time evolution equations for the cumulants can be obtained by multiplying the set of Enskog equations (23) by c^4 and integrating over $\mathbf{c}$. After some algebra, one gets

$$\Lambda\frac{\partial c_i}{\partial\theta} + 2\left(\Lambda_i\theta_i^{-1} + 2\gamma_i^*\right)(1 + c_i) - 4\gamma_i^*\theta_i^{-1} = \frac{4\beta_i^2}{d(d+2)}\Sigma_i, \tag{29}$$

where

$$\Sigma_i = \sum_{j=1}^{2}\int \mathrm{d}\mathbf{v}\, c^4 J_{ij}^*[\mathbf{c}|\varphi_i, \varphi_j]. \tag{30}$$

The partial cooling rates ζ_i^* as well as the collisional moments Σ_i are obtained by substituting the leading Sonine approximation (27) into Eqs. (13) and (30), retaining only linear terms in c_i, and integrating over velocity. The final expressions can be written as follows:[54]

$$\zeta_1^* = \zeta_{10} + \zeta_{11}c_1 + \zeta_{12}c_2, \quad \zeta_2^* = \zeta_{20} + \zeta_{22}c_2 + \zeta_{21}c_1, \tag{31}$$

$$\Sigma_1 = \Sigma_{10} + \Sigma_{11}c_1 + \Sigma_{12}c_2, \quad \Sigma_1 = \Sigma_{20} + \Sigma_{22}c_2 + \Sigma_{21}c_1, \tag{32}$$

where the explicit forms of ζ_{ij} and Σ_{ij} are displayed in the Appendix for the sake of completeness.

Figure 4 illustrates the dependence of coefficients c_1 and c_2 on θ for the same initial conditions as in Fig. 3. It is quite apparent that, after a transient period, the cumulants converge toward the universal hydrodynamic regime in the same way as the partial temperatures θ_i do. We also observe that the temporal duration of the unsteady hydrodynamic regime of cumulant c_2 is greater than that of cumulant c_1.

IV. MPEMBA-LIKE EFFECT IN BINARY GRANULAR SUSPENSIONS

As mentioned in Sec. I, before considering steady situations, it is interesting to analyze the so-called Mpemba-like effect in binary granular suspensions. Mpemba-like effect is a counterintuitive phenomenon where an initially hotter sample can cool down sooner than the colder one. This effect was experimentally observed for the first time many years ago by Mpemba and Osborne[30] in the case of water. Although different mechanisms have been proposed in the literature

Physics of Fluids ARTICLE scitation.org/journal/phf

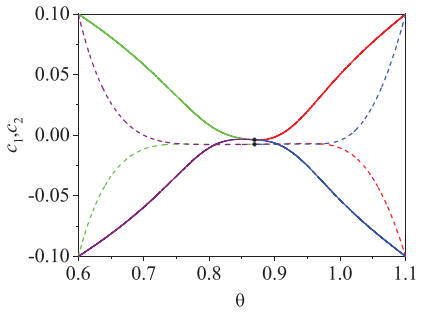

FIG. 4. Evolution of the cumulants c_1 and c_2 vs the (reduced) temperature θ for $m_1/m_2 = 10$, $\sigma_1/\sigma_2 = 1$, $x_1 = \frac{1}{2}$, and a common coefficient of restitution $\alpha = 0.9$ ($\alpha \equiv \alpha_{11} = \alpha_{12} = \alpha_{22}$). Solid and dashed lines represent the time evolution of c_1 and c_2, respectively. The initial values $\{\theta, \theta_1, c_1, c_2\}$ of the colored lines are $\{0.6, 0.6, 0.1, -0.1\}$ (green line and symbols), $\{0.6, 0.6, -0.1, 0.1\}$ (purple line and symbols), $\{1.1, 1.1, 0.1, -0.1\}$ (red line and symbols), and $\{0.6, 0.6, -0.1, 0.1\}$ (blue line and symbols). The remaining parameters are $d = 3$, $\phi = 0.1$, and $T_{ex}^* = 1$. The filled circles correspond to the values of c_1 and c_2 in the steady state.

to explain the Mpemba effect in such a system,[55–61] the problem is still open since there are still doubts about the origin of this exciting phenomenon.[62,63] For this reason, to gain some insight into this complex problem, kinetic theory tools have been widely employed in the last few years to understand the cause of a reduction in the relaxation time as the trigger of the Mpemba-like effect in molecular[36,38] and granular[33–35,37,40] gases. In particular, we have recently analyzed[38,39] this phenomenon (and its inverse and mixed counterparts) in the case of molecular binary mixtures driven by a stochastic bath with friction. Theoretical approximate results have been confronted against computer simulations showing excellent agreement. Although some preliminary results for inelastic collisions were also reported Ref. 38, we complement in this section the results obtained before by offering a more quantitative analysis of the Mpemba-like effect in binary granular suspensions.

Let us assume two identical homogeneous states A and B except for their initial values of the reduced global temperatures $\theta_A^{(0)}$ and $\theta_B^{(0)}$ and their reduced partial temperatures $\theta_{1,A}^{(0)}$ and $\theta_{1,B}^{(0)}$.[64] As discussed in Ref. 38, the fact that the time evolution equations obeying $\theta(t^*)$ and $\theta_1(t^*)$ are coupled [see Eqs. (17) and (18)] opens up the possibility that $\theta_A(t_c^*) = \theta_B(t_c^*)$ at a given crossing time t_c^* (Mpemba-like effect) before reaching the (common) asymptotic steady state value θ_s.

To analyze the time evolution of θ and θ_1, let us rewrite Eqs. (17) and (18) as

$$\frac{\partial \theta}{\partial t^*} = \Phi(\theta, \theta_1), \quad \frac{\partial \theta_1}{\partial t^*} = \Psi(\theta, \theta_1), \tag{33}$$

where

$$\begin{aligned} \Phi(\theta, \theta_1) &= \Phi_1 + \Phi_2(\theta) + \Phi_3(\theta_1) + \Phi_4(\theta, \theta_1), \\ \Psi(\theta, \theta_1) &= \Psi_1 + \Psi_2(\theta) + \Psi_3(\theta, \theta_1). \end{aligned} \tag{34}$$

Here, we have introduced the following quantities:

$$\Phi_1 = 2(x_1\lambda_1 + x_2\lambda_2), \quad \Phi_2(\theta) = -2\lambda_2\theta,$$
$$\Phi_3(\theta_1) = -2x_1(\lambda_1 - \lambda_2)\theta_1,$$
$$\Phi_4(\theta, \theta_1) = -\theta^{1/2}\left[x_1\theta_1\left(\zeta_1^* - \zeta_2^*\right) + \theta\zeta_2^*\right], \tag{35}$$

$$\Psi_1 = 2\lambda_1, \quad \Psi_2(\theta_1) = -2\lambda_1\theta_1, \quad \Psi_3(\theta, \theta_1) = -\theta^{1/2}\theta_1\zeta_1^*. \tag{36}$$

In contrast to other memory effects reported in the case of molecular and granular gases,[33,36,40] here we use the partial temperature as the kinetic variable whose evolution couples with that of the temperature. For this reason, no cumulants are needed in the description of the Mpemba-like effect. Thus, in order to solve Eqs. (35) and (36), since the impact of cumulants c_i on the partial temperatures θ_i is very small, we will neglect them for the sake of simplicity to estimate the partial cooling rates ζ_i^*. In that case, according to Eq. (21), ζ_i^* can be rewritten as

$$\zeta_1^* = \sqrt{\frac{\theta_1}{M_1\theta}}\zeta_1'(\beta), \tag{37}$$

where

$$\zeta_1'(\beta) = \frac{\sqrt{2}\pi^{(d-1)/2}}{d\Gamma\left(\frac{d}{2}\right)}x_1\chi_{11}\left(\frac{\sigma_1}{\sigma_{12}}\right)^{d-1}(1-\alpha_{11}^2) + \frac{4\pi^{(d-1)/2}}{d\Gamma\left(\frac{d}{2}\right)}$$
$$\times x_2\chi_{12}\mu_{21}(1+\beta)^{1/2}(1+\alpha_{12})\left[1 - \frac{\mu_{21}}{2}(1+\alpha_{12})(1+\beta)\right]. \tag{38}$$

Here, $\beta = \beta_1/\beta_2 = m_1\theta_2/m_2\theta_1$. The expression of ζ_2^* can be easily obtained from Eqs. (37) and (38) by interchanging 1 and 2 and setting $\beta \to \beta^{-1}$.

For elastic collisions ($\alpha_{ij} = 1$), $\theta\zeta^* = x_1\theta_1(\zeta_1^* - \zeta_2^*) + \theta\zeta_2^* = 0$ and so, $\Phi_4 = 0$ according to the last identity in Eq. (35). Thus, for molecular mixtures, the study of the Mpemba effect becomes simpler since the time evolution of $\theta(t^*)$ is essentially ruled by the function $\Phi_2(\theta) + \Phi_3(\theta_1)$. On the other hand, for inelastic collisions ($\Phi_4 \neq 0$), the analysis of the Mpemba effect is much more intricate than for molecular mixtures. Thus, in order to offer a quantitative analysis, we consider first initial states which are very close to the final steady state. This will allow us to get an explicit expression for the crossing time t_c^* and, as a consequence, for the initial conditions needed for the crossover in the evolution of the temperatures of the two samples. In this context, the set of coupled differential equations (34) can be linearized around the stationary solutions θ_s and $\theta_{1,s}$, where the subscript s means that the quantity is evaluated in the steady state. An exhaustive study of the dependence of θ_s and $\theta_{1,s}$ on the parameter space will be provided in Sec. V.

We want to solve the set of equations (33) and (34) by assuming small deviations from the steady state solution. Therefore, we write

$$\theta(t^*) = \theta_s + \delta\theta(t^*), \quad \theta_1(t^*) = \theta_{1,s} + \delta\theta_1(t^*). \tag{39}$$

Substituting Eq. (39) into Eq. (34) and retaining only linear terms in $\delta\theta$ and $\delta\theta_1$, one obtains the set of linear differential equations

$$\frac{\partial}{\partial t^*}\begin{pmatrix} \delta\theta \\ \delta\theta_1 \end{pmatrix} = \mathcal{L}\cdot\begin{pmatrix} \delta\theta \\ \delta\theta_1 \end{pmatrix}. \tag{40}$$

The square matrix $\mathcal{L}$ is composed of the following elements:

Physics of Fluids ARTICLE scitation.org/journal/phf

$$\mathcal{L}_{11}=-2\lambda_2-\frac{3}{2}\theta_s^{1/2}\zeta_{2,s}^*-\theta_{1,s}^{1/2}\frac{x_1M_1^{1/2}}{x_2M_2}\left(\frac{\partial\zeta_1'}{\partial\beta}\right)_s+\frac{\theta_{2,s}^{3/2}}{\theta_{1,s}}\frac{M_1}{M_2^{3/2}}\left(\frac{\partial\zeta_2'}{\partial\beta}\right)_s, \tag{41}$$

$$\mathcal{L}_{12}=-2x_1(\lambda_1-\lambda_2)+\frac{3}{2}\theta_s^{1/2}x_1\left(\zeta_{2,s}^*-\zeta_{1,s}^*\right)+\frac{\theta_s}{\theta_{1,s}^{1/2}}\frac{x_1M_1^{1/2}}{x_2M_2}\times\left(\frac{\partial\zeta_1'}{\partial\beta}\right)_s+\frac{\theta_s\theta_{2,s}^{3/2}}{\theta_{1,s}^2}\frac{M_1}{M_2^{3/2}}\left(\frac{\partial\zeta_2'}{\partial\beta}\right)_s, \tag{42}$$

$$\mathcal{L}_{21}=-\theta_{1,s}^{1/2}\frac{M_1^{1/2}}{x_2M_2}\left(\frac{\partial\zeta_1'}{\partial\beta}\right)_s, \tag{43}$$

$$\mathcal{L}_{22}=-2\lambda_1-\frac{3}{2}\theta_s^{1/2}\zeta_{1,s}^*+\theta_s\theta_{1,s}^{-1/2}\frac{M_1^{1/2}}{x_2M_2}\left(\frac{\partial\zeta_1'}{\partial\beta}\right)_s.$$

Here, the derivatives of ζ_1' and ζ_2' on β are evaluated in the steady state. The solution of the matrix equation (40) for $\delta\theta(t^*)$ is

$$\delta\theta(t^*)=\frac{1}{\lambda_+-\lambda_-}\left\{\left[(\mathcal{L}_{11}-\lambda_-)\delta\theta_0+\mathcal{L}_{12}\delta\theta_{1,0}\right]e^{\lambda_+t^*}+\left[(\lambda_+-\mathcal{L}_{11})\delta\theta_0-\mathcal{L}_{12}\delta\theta_{1,0}\right]e^{\lambda_-t^*}\right\}, \tag{44}$$

where $\delta\theta_0$ and $\delta\theta_{1,0}$ are the initial values of $\delta\theta$ and $\delta\theta_1$, respectively. The eigenvalues of the matrix $\mathcal{L}$ are given by

$$\lambda_\pm=\frac{1}{2}\left[\mathcal{L}_{11}+\mathcal{L}_{22}\pm\sqrt{(\mathcal{L}_{11}-\mathcal{L}_{22})^2+4\mathcal{L}_{12}\mathcal{L}_{21}}\right]. \tag{45}$$

Let us assume that the initial temperature of the state A is larger than that of the state B ($\theta_A^{(0)}>\theta_B^{(0)}$). The possible crossing time t_c^* for the occurrence of the Mpemba effect can be obtained from the condition $\delta\theta_A(t_c^*)=\delta\theta_B(t_c^*)$. This leads to the result

$$t_c^*=\frac{1}{\lambda_--\lambda_+}\ln\frac{\mathcal{L}_{12}+(\mathcal{L}_{11}-\lambda_-)\Delta\theta_0/\Delta\theta_{1,0}}{\mathcal{L}_{12}-(\lambda_+-\ell_{11})\Delta\theta_0/\Delta\theta_{1,0}}, \tag{46}$$

where $\Delta\theta_0=\theta_A^{(0)}-\theta_B^{(0)}$ and $\Delta\theta_{1,0}=\theta_{1,A}^{(0)}-\theta_{1,B}^{(0)}$. As expected,[38] in the linear theory, for given values of the parameters of the mixture, t_c^* depends on the initial conditions *only* through the single control parameter $\Delta\theta_0/\Delta\theta_{1,0}$. Moreover, since $\lambda_--\lambda_+<0$ and $t_c^*\in\mathbb{R}^+$, the argument of the logarithm in Eq. (46) belongs to the interval (0, 1). According to this constraint, the initial values must satisfy the following conditions:[38]

$$\begin{aligned}&\frac{\Delta\theta_0}{\Delta\theta_{1,0}}\in\left(0,\frac{\mathcal{L}_{12}}{\lambda_--\mathcal{L}_{11}}\right)\quad\text{if}\quad\frac{\mathcal{L}_{12}}{\lambda_--\mathcal{L}_{11}}>0,\\&\frac{\Delta\theta_0}{\Delta\theta_{1,0}}\in\left(\frac{\mathcal{L}_{12}}{\lambda_--\mathcal{L}_{11}},0\right)\quad\text{if}\quad\frac{\mathcal{L}_{12}}{\lambda_--\mathcal{L}_{11}}<0.\end{aligned} \tag{47}$$

A phase diagram showing the necessary conditions appearing in Eq. (47) as a function of the common coefficient of restitution α is plotted in the top panel of Fig. 5. We consider here an equimolar mixture ($x_1=\frac{1}{2}$) of hard spheres ($d=3$) of equal diameters ($\sigma_1=\sigma_2$) but different masses ($m_1=5m_2$) at moderate densities ($\phi=0.1$). As expected, the inelasticity of collisions enlarges the region where the initial conditions lead to a crossover in temperature relaxations. From a kinetic point of view, as inelasticity grows, particles of the hotter sample A suffer more collisions per time; so, the loss of energy is emphasized when compared with the colder sample B. Thus, the inelasticity brings the relaxation curves of the two samples together and increases the possibility of the occurrence of the Mpemba-like effect. However, the influence of the cooling rate on the time evolution of temperature must be analyzed in conjunction with the action of the interstitial fluid. As already pointed out in Ref. 38, in the case of small inelasticity (values of α close to 1), the influence of the cooling rate on the relative behavior of the two samples can be neglected since it generally represents less than 10% of the external fluid impact. On the contrary, at moderate inelasticities, the origin of the Mpemba-like effect falls on the heterogeneity of the coefficients λ_i. This discrimination in the way of energy transfer from the bath to the components of the mixture causes uneven decay of the partial temperature toward the steady state. Hence, since the global temperature is a sum of partial

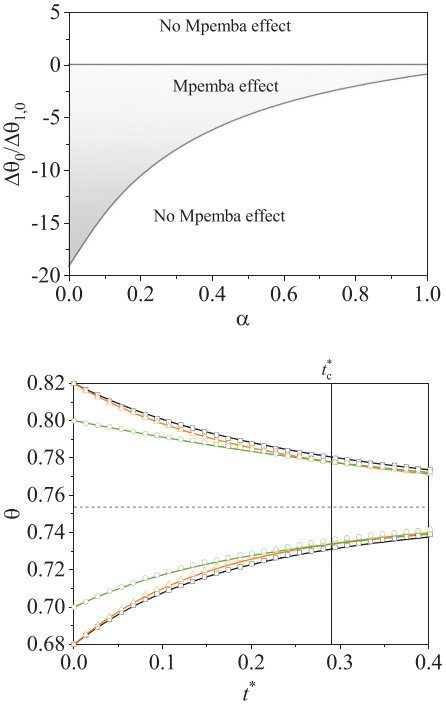

FIG. 5. Top panel: phase diagram of the necessary initial condition $\Delta\theta_0/\Delta\theta_{1,0}$ as a function of the common coefficient of restitution α. Bottom panel: relaxation of the (reduced) temperature θ toward the steady state for $\alpha=0.8$. Solid lines represent theoretical results and symbols the DSMC data. The initial conditions for the temperature difference ratio $\Delta\theta_0/\Delta\theta_{1,0}$ are: –1 (green and orange lines and symbols) and –4 (green and black lines and symbols). The theoretical value of t_c^* is also plotted with a vertical line. The remaining parameters in both panels are $d=3$, $m_1/m_2=5$, $\sigma_1/\sigma_2=1$, $x_1=\frac{1}{2}$, $T_{ex}^*=1$, and $\phi=0.1$. The dashed horizontal line represents the steady value θ_s.

Physics of Fluids ARTICLE scitation.org/journal/phf

temperatures weighted by their respective mole fractions, we select the partial temperature of the component whose interaction with the bath is more effective to be the further one from the steady state. In this way, the relaxation time of the hotter sample can be reduced. In the specific case of Fig. 5, we consider a mixture of two components identical in every way except for their masses ($m_1/m_2 > 1$). Due to inertial effects, the transmission of momentum (and hence the transmission of kinetic energy) between the interstitial fluid and the lighter component is smoother. That is the reason why the necessary initial temperature difference $\theta_A^{(0)} - \theta_B^{(0)} = T_{1,A}^{(0)}/T_{2,A}^{(0)} - T_{1,B}^{(0)}/T_{2,B}^{(0)} < 0$. On the other hand, as inelasticity increases, the action of the cooling rate becomes more relevant and a competition arises between both mechanisms.

Once analyzed the necessary initial conditions for the crossover to happen, we discuss the fulfillment of Eq. (47). For this purpose, a cooling and a heating transition toward the steady state is illustrated in the bottom panel of Fig. 5. Here, we assume the same mechanical conditions as in the phase diagram but we pick up a value for the coefficient of restitution ($\alpha = 0.8$). According to Eq. (47), the initial conditions $\Delta\theta_0/\Delta\theta_{1,0}$ must be in the range comprised between $\ell_{12}/(\lambda_- - \ell_{11}) \simeq -2$ and 0. For this reason, we choose one of the initial conditions to belong to this interval ($\Delta\theta_0/\Delta\theta_{1,0} = -1$) and the other to be outside this interval ($\Delta\theta_0/\Delta\theta_{1,0} = -4$). Specific details of the initial conditions used in the above panels can be found in Table I. The solid lines are the theoretical results as derived from the Enskog equation (33) and symbols refer to the results obtained via DSMC simulations. The reliability of conditions (47) and an excellent agreement between theory and simulations are clearly shown. Moreover, it is also worth noting the accuracy of expression (46) for the crossing time t_c^*.

The linearization of the Enskog equation has allowed us to give a simple explanation of the different mechanisms involved in the occurrence of the Mpemba-like effect. There are, however, situations where small deviations from the steady state cannot be assumed. In this case, no explicit expressions for $\Delta\theta_0/\Delta\theta_{1,0}$ and t_c^* can be achieved. These scenarios include the so-called *large* and *non-monotonic* Mpemba effects. The latter refers to crossovers in temperature relaxation when at least one temperature presents non-monotonic evolution. In the present work, we follow similar steps as those previously made in Ref. 38 to establish the necessary but not sufficient conditions for the emergence of these out-from-equilibrium phenomena.

Let us consider again two identical samples A and B whose initial temperatures $\theta_A^{(0)}$ and $\theta_B^{(0)}$ and/or partial temperatures $\theta_{1,A}^{(0)}$ and $\theta_{1,B}^{(0)}$ are significantly far away from the steady state. At the initial stages of evolution, the condition needed for a crossover in temperature evolution relies on the relative behavior of the initial slopes $\Phi(\theta_A^{(0)}, \theta_{1,A}^{(0)})$ and $\Phi(\theta_B^{(0)}, \theta_{1,B}^{(0)})$. If we assume sample A to be hotter than B, we must choose $\Phi_A < \Phi_B$ at the initial stages of evolution to observe the occurrence of the Mpemba effect. The next step is to analyze the dependence of the function Φ on θ_1. By doing so, we can establish some criterion for the selection of the initial partial temperature $\theta_1^{(0)}$ as a function of $\theta^{(0)}$. For the sake of simplicity, as proven in Ref. 38, we assume first that the influence of inelasticity in collisions on the relative behavior of the evolution of temperatures is negligible as compared with the action of the bath. Thus, we perform the derivative of Φ_3 with respect to θ_1 at fixed θ. The result is

$$\left(\frac{\partial\Phi_3}{\partial\theta_1}\right)_\theta = 2x_1(\lambda_2 - \lambda_1), \tag{48}$$

which is always a positive (negative) function if $\lambda_2 > \lambda_1$ ($\lambda_2 < \lambda_1$). Therefore, keeping in mind that $\theta_A^{(0)} > \theta_B^{(0)}$, then

$$\begin{aligned} \frac{\Delta\theta_0}{\Delta\theta_{1,0}} &> 0 \quad \text{if} \quad \lambda_1 > \lambda_2, \\ \frac{\Delta\theta_0}{\Delta\theta_{1,0}} &< 0 \quad \text{if} \quad \lambda_1 < \lambda_2 \end{aligned} \tag{49}$$

are the required conditions for the presence of the Mpemba effect. Unlike the linear case, the fulfillment of Eq. (49) does not constrain the region that the initial conditions must belong to. So, in order to achieve crossover, the difference between the initial slopes must be selected to be large enough.

Examples of the large and non-monotonic Mpemba effects are plotted in Fig. 6 for the same parameters as in Fig. 5 except for the common coefficient of restitution ($\alpha = 0.7$). Since $\lambda_1 < \lambda_2$, the initial temperature ratio is chosen so that $\Delta\theta_0/\Delta\theta_{1,0} < 0$ (more details can be found in Table II). Solid lines refer to the theoretical results while symbols represent DSMC data. In Fig. 6(a), we observe a large Mpemba effect even when the initial temperature difference is of the same order than the temperatures themselves. In comparison with the elastic case, the inelasticity enables the choice of the partial temperature to be closer for the global temperature. This fact enhances the probability to see the non-monotonic Mpemba effect because a crossover will still be possible when the partial temperature is far away from the global temperature, inducing the appearance of nonlinear effects. This latter effect is shown in Figs. 6(b) and 6(c). On the one hand, the non-monotonic Mpemba and its inverse effect can be observed in Fig. 6(b). In this case, the emergence of this surprising effect is just a matter of the choice of the initial temperature $\theta_{1,0}$. On the other hand, the mixed effect, namely when one initial temperature is above and the other below the steady one (dashed horizontal line), is plotted in Fig. 6(c). A good agreement between the Enskog theory and simulations can be found in all the relaxation cases ensuring the use of Maxwellian approximation to model the distribution functions in highly nonlinear situations.

TABLE I. Initial values of the (reduced) temperatures θ_0 and partial temperatures $\theta_{1,0}$ used to generate the relaxation curves shown in the right panel of Fig. 5.

	θ_0	$\theta_{1,0}$	θ_0	$\theta_{1,0}$
Color	Cooling cases		Heating cases	
Black	0.82	0.815	0.68	0.685
Orange	0.82	0.8	0.68	0.7
Green	0.8	0.82	0.7	0.68

V. STEADY STATE COMPARISON BETWEEN THEORY AND DSMC SIMULATIONS

As discussed in Sec. III, the system achieves a *steady* state for sufficiently long times. The stationary state was widely studied years ago in Ref. 54 where the reliability of the approximate solution to the set of Enskog equations for the temperature ratio T_1/T_2 and the cumulants c_1 and c_2 for a granular mixture driven by a stochastic bath with friction was assessed by molecular dynamics simulations over a wide range of the parameter space. The comparison shows good agreement

Physics of Fluids ARTICLE scitation.org/journal/phf

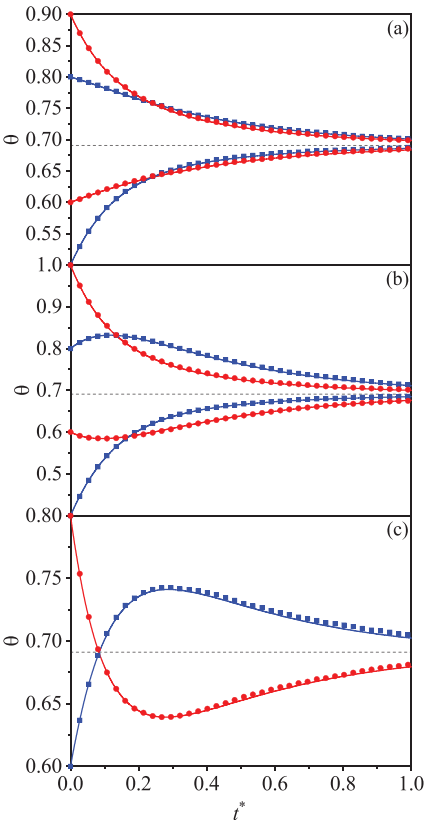

FIG. 6. Relaxation of the (reduced) temperature θ toward the steady state for $\alpha = 0.8$, $d = 3$, $m_1/m_2 = 5$, $\sigma_1/\sigma_2 = 1$, $x_1 = \frac{1}{2}$, $T^*_{\text{ex}} = 1$, and $\phi = 0.1$. Solid lines represent theoretical results and symbols the DSMC data. (a) Large Mpemba effect: the initial conditions for the temperature difference ratio are $\Delta\theta_0/\Delta\theta_{1,0} = -1$ in both the heating and the cooling transitions. (b) Non-monotonic Mpemba effect: the initial conditions for the temperature difference ratio $\Delta\theta_0/\Delta\theta_{1,0}$ are $-2/3$ in the heating process and $-1/2$ in the cooling transition. (c) Mixed Mpemba effect: the initial condition for the temperature difference ratio is $\Delta\theta_0/\Delta\theta_{1,0} = -2/7$. The dashed horizontal lines represent the steady value θ_s.

for the temperature ratio between theory and simulations for dilute and moderate densities, which contrasts with the comparison performed in *dry* (or undriven) granular mixtures[19] where important differences between theory and molecular dynamics simulations for T_1/T_2 were found for moderately dense mixtures. Regarding the comparison carried out in Ref. 54 for the cumulants, the results show good agreement for dilute driven mixtures but significant systematic deviations appear as the density increases. Given that molecular dynamics avoids any assumption inherent in the kinetic theory (such as molecular chaos hypothesis), it is not clear whether the origin of the differences between theory and molecular dynamics simulations is due to the failure of the Enskog kinetic theory at high densities and/or strong inelasticity or the approximations made in solving the Enskog kinetic equation. To clarify this point, we compare in this section the (approximate) Enskog results for T_1/T_2, c_1, and c_2 with those obtained by numerically solving the Boltzmann–Enskog equation by means of the DSMC method.[26] Since the DSMC method (which is also based on the molecular chaos assumption) has been proved to be a powerful tool for numerically solving the Boltzmann–Enskog equation, it is quite apparent that the present comparison allows us to gauge the degree of accuracy of the approximations involved in the determination of the temperature ratio and the cumulants.

TABLE II. Initial values of the (reduced) temperatures θ_0 and partial temperatures $\theta_{1,0}$ used to generate the relaxation curves shown in Fig. 6.

	Figure 4(a)		Figure 4(b)		Figure 4(c)	
Color	θ_0	$\theta_{1,0}$	θ_0	$\theta_{1,0}$	θ_0	$\theta_{1,0}$
Cooling cases						
Red	0.9	0.8	1.0	0.8	0.8	0.3
Blue	0.8	0.9	0.8	1.2	⋯	
Heating cases						
Red	0.6	0.5	0.6	0.3	⋯	
Blue	0.5	0.6	0.4	0.6	0.6	1.0

The steady state is defined by the conditions $\partial_\theta\theta_1 = \partial_\theta\theta_2 = 0$. According to Eq. (25), the above conditions imply that $\Lambda_1 = \Lambda_2 = 0$, which yields the following set of equations for the partial temperatures θ_1 and θ_2:

$$2\gamma_1^*(1-\theta_1) = \theta_1(\zeta_{10} + \zeta_{11}c_1 + \zeta_{12}c_2), \tag{50}$$

$$2\gamma_2^*(1-\theta_2) = \theta_2(\zeta_{20} + \zeta_{21}c_1 + \zeta_{22}c_2). \tag{51}$$

Upon writing Eqs. (50) and (51), use has been made of the expansions (31). In Eqs. (50) and (51) and the remaining part of this section, it is understood that all quantities are evaluated in the steady state. Equations (50) and (51) are coupled to those of the cumulants c_1 and c_2. The equations for cumulants are obtained from Eq. (29) by taking the steady state conditions $\Lambda_1 = \Lambda_2 = 0$. This leads to the following set of algebraic linear equations:

$$d(d+2)\left(\frac{\theta_1}{M_1\theta}\right)^2\gamma_1^*(1-\theta_1^{-1}) - \Sigma_{10} = \left[\Sigma_{11} - d(d+2)\left(\frac{\theta_1}{M_1\theta}\right)^2\gamma_1^*\right]c_1 + \Sigma_{12}c_2, \tag{52}$$

$$d(d+2)\left(\frac{\theta_2}{M_2\theta}\right)^2\gamma_2^*(1-\theta_2^{-1}) - \Sigma_{20} = \left[\Sigma_{22} - d(d+2)\left(\frac{\theta_2}{M_2\theta}\right)^2\gamma_2^*\right]c_2 + \Sigma_{21}c_1, \tag{53}$$

where use has been made of the expansion (32).

Solution to the set of equations (50)–(53) provides the stationary values of the ratio of partial temperatures T_1/T_2 and the cumulants c_1

Physics of Fluids ARTICLE scitation.org/journal/phf

and c_2. These quantities are given as a function of the dimensionality d; the (reduced) background temperature T^*_{ex}; the mass ratio m_1/m_2; the concentration ratio ϕ_1/ϕ_2; the ratio of diameters σ_1/σ_2; the density ϕ; and the coefficients of restitution α_{11}, α_{22}, and α_{12}. Since the parameter space of the problem is large, as usual and to reduce the number of independent parameters, we consider a three-dimensional system ($d=3$), a (reduced) bath temperature $T^*_{ex}=1$, a moderate density $\phi=0.1$, and a common coefficient of restitution $\alpha\equiv\alpha_{11}=\alpha_{22}=\alpha_{12}$. This reduces the parameter space to four dimensionless quantities: $\{m_1/m_2, \phi_1/\phi_2, \sigma_1/\sigma_2, \alpha\}$.

As in Ref. 54, the set of dimensionless quantities $\Xi \equiv \{T_1/T_2, c_1, c_2\}$ have been obtained from the approximate theory and DSMC simulations in three different cases. Two different values of α have been considered in each case: $\alpha=0.9$ (moderate inelasticity) and $\alpha=0.8$ (strong inelasticity). In the first case (case I), the set Ξ is determined as a function of the mass ratio m_1/m_2 for $\phi_1/\phi_2=\sigma_1/\sigma_2=1$, while in the second case (case II) Ξ is obtained as a function of the ratio of diameters σ_1/σ_2 for $m_1/m_2=\phi_1/\phi_2=1$. Finally, in case III, Ξ is given as a function of concentration ϕ_1/ϕ_2 for $m_1/m_2=8$ and $\sigma_1/\sigma_2=1$. Given the disparity of parameters of the mixture analyzed in the three different cases, the test of the approximate kinetic theory can be considered as stringent.

Case I is shown in Fig. 7. While the solid lines correspond to the (approximate) theoretical results, the symbols represent the Monte Carlo simulation data (squares for $\alpha=0.9$ and triangles for $\alpha=0.8$). As expected, the extent of energy nonequipartition increases with the mass disparity of the mixture. On the other hand, the departure form energy equipartition is more noticeable in dry granular mixtures than in binary granular suspensions. Figure 7 highlights the excellent agreement between theory and simulations for the temperature ratio, even for quite disparate masses. With respect to the cumulants, we observe that the magnitude of c_1 and c_2 is much smaller than that of a dry granular mixture.[19,25,41] In addition, while the theoretical results for c_1 compare well with simulations, some discrepancies are found in the case of cumulant c_2 (specially for large values of the mass ratio) since the theory slightly underestimates the value of c_2. In any case, the quantitative discrepancies between theory and simulations are of the same order as those observed in the dry granular limit case[41] since the largest relative error of c_2 is about 9%.

Figure 8 shows the results of case II, Ξ as function of the ratio of diameters σ_1/σ_2. As in Fig. 7, the agreement is again excellent for the temperature ratio; more significant discrepancies are observed for both cumulants in case II than in case I. These discrepancies could be likely mitigated by considering nonlinear terms in c_1 and c_2 in the approximate theory and/or by considering more terms in the Sonine polynomial expansion of $\varphi_i(\mathbf{c})$. However, given that the price to be paid for considering these type of terms is very high (since the involved calculations would be very cumbersome), we think that the approximate theory reported here is still an accurate approach to estimate the cumulants. In fact, as in case I, the largest relative error found in Fig. 8 for c_1 is 9.4% and 8.2% for c_2. Finally, Fig. 9 shows case III, Ξ vs the concentration ϕ_1/ϕ_2. It is quite apparent that Fig. 9 exhibits similar trends as those observed before for Figs. 7 and 8: while T_1/T_2 displays excellent agreement between theory and simulations, there are small differences for the cumulants.

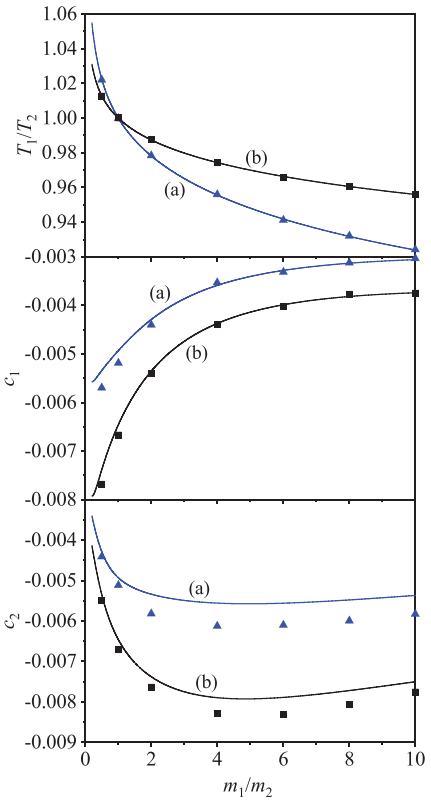

FIG. 7. Case I: Plot of the temperature ratio T_1/T_2 and the cumulants c_1 and c_2 as a function of the mass ratio m_1/m_2 for $\sigma_1/\sigma_2=\phi_1/\phi_2=1$, and two different values of the (common) coefficient of restitution α: $\alpha=0.8$ (a) (blue lines and triangles) and $\alpha=0.9$ (b) (black lines and squares). The lines are the Enskog predictions and the symbols refer to the DSMC simulation results. The remaining parameters are $T^*_{ex}=1$, $\phi=0.1$, and $d=3$.

VI. LINEAR STABILITY ANALYSIS OF THE STEADY SOLUTION

Although the study offered in Sec. V has focused on the determination of the temperature ratio and the cumulants in steady state conditions, it is worthwhile to analyze if the stationary solution is linearly stable. To study the stability of this steady solution, we will take into account the effect of cumulants c_1 and c_2 on the evolution equations of θ and θ_1. Retaining only linear terms in the above cumulants, the evolution equations of θ, θ_1, c_1, and c_2 can be written, respectively, as

Physics of Fluids ARTICLE scitation.org/journal/phf

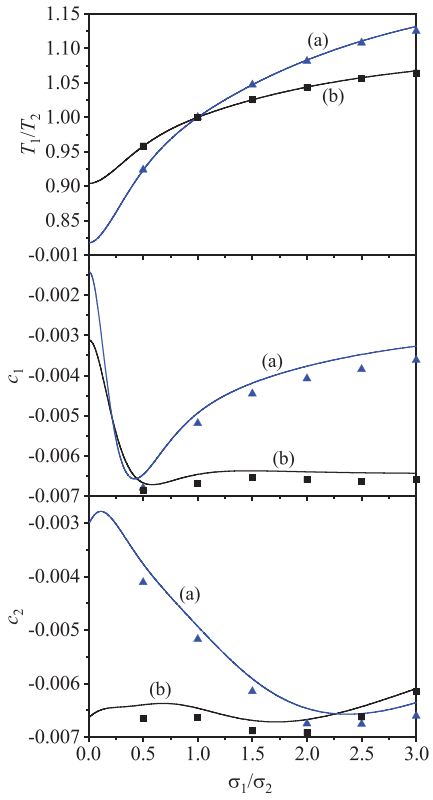

FIG. 8. Case II: Plot of the temperature ratio T_1/T_2 and the cumulants c_1 and c_2 as a function of the size ratio σ_1/σ_2 for $m_1/m_2 = \phi_1/\phi_2 = 1$, and two different values of the (common) coefficient of restitution α: $\alpha = 0.8$ (a) (blue lines and triangles) and $\alpha = 0.9$ (b) (black lines and squares). The lines are the Enskog predictions and the symbols refer to the DSMC simulation results. The remaining parameters are $T_{ex}^* = 1$, $\phi = 0.1$, and $d = 3$.

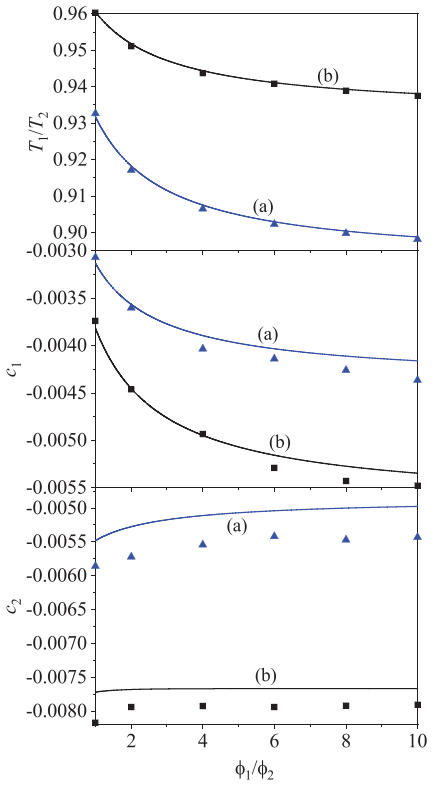

FIG. 9. Case III: Plot of the temperature ratio T_1/T_2 and the cumulants c_1 and c_2 as a function of the partial density ratio ϕ_1/ϕ_2 for $m_1/m_2 = 8$, $\sigma_1/\sigma_2 = 1$, and two different values of the (common) coefficient of restitution α: $\alpha = 0.8$ (a) (blue lines and triangles) and $\alpha = 0.9$ (b) (black lines and squares). The lines are the Enskog predictions and the symbols refer to the DSMC simulation results. The remaining parameters are $T_{ex}^* = 1$, $\phi = 0.1$, and $d = 3$.

$$\frac{\partial\theta}{\partial t^*} = 2[x_1\lambda_1 + x_2\lambda_2 - x_1(\lambda_1 - \lambda_2)\theta_1 - \lambda_2\theta] - \theta^{1/2}\{x_1\theta_1[\zeta_{10} - \zeta_{20} + (\zeta_{11} - \zeta_{21})c_1 + (\zeta_{12} - \zeta_{22})c_2] + \theta(\zeta_{20} + \zeta_{21}c_1 + \zeta_{22}c_2)\}, \tag{54}$$

$$\frac{\partial\theta_1}{\partial t^*} = 2\lambda_1(1 - \theta_1) - \theta^{1/2}\theta_1(\zeta_{10} + \zeta_{11}c_1 + \zeta_{12}c_2), \tag{55}$$

$$\frac{\partial c_1}{\partial t^*} = -4\lambda_1(\theta_1^{-1} - 1)(1 + c_1) + 2\theta^{1/2}[\zeta_{10} + (\zeta_{10} + \zeta_{11})c_1 + \zeta_{12}c_2] + 4\lambda_1\theta_1^{-1} + \frac{4\theta^{5/2}}{d(d+2)}\left(\frac{M_1}{\theta_1}\right)^2(\Sigma_{10} + \Sigma_{11}c_1 + \Sigma_{12}c_2), \tag{56}$$

$$\frac{\partial c_2}{\partial t^*} = -4\lambda_2(\theta_2^{-1} - 1)(1 + c_2) + 2\theta^{1/2}[\zeta_{20} + (\zeta_{20} + \zeta_{22})c_2 + \zeta_{21}c_1] + 4\lambda_2\theta_2^{-1} + \frac{4\theta^{5/2}}{d(d+2)}\left(\frac{M_2}{\theta_2}\right)^2(\Sigma_{20} + \Sigma_{21}c_1 + \Sigma_{22}c_2). \tag{57}$$

Here, we recall that $\theta_2(t^*) = x_2^{-1}[\theta(t^*) - x_1\theta_1(t^*)]$ and use has been made of the expansions (31) and (32) for obtaining Eqs. (54)–(57).

Now, as in Sec. III, one looks for solutions of the form

$$\theta(t^*) = \theta_s + \delta\theta(t^*), \quad \theta_1(t^*) = \theta_{1,s} + \delta\theta_1(t^*), \quad c_1(t^*) = c_{1,s} + \delta c_1(t^*), \quad c_2(t^*) = c_{2,s} + \delta c_2(t^*) \tag{58}$$

Physics of Fluids ARTICLE scitation.org/journal/phf

and neglects nonlinear terms in the perturbations $\{\delta\theta, \delta\theta_1, \delta c_1, \delta c_2\}$. If the real parts of the eigenvalues ℓ_i $(i = 1, 2, 3, 4)$ are negative, the steady solution $\{\theta_s, \theta_{1,s}, c_{1,s}, c_{2,s}\}$ is (linearly) stable. The expressions of the eigenvalues ℓ_i are very large and will be omitted here for the sake of brevity. On the other hand, in the simplest case where the cumulants c_i are neglected in the determination of the cooling rates ζ_i^* and the collisional moments $\mathbf{\Sigma}_i$, the time evolution of $\delta\theta(t^*)$ and $\delta\theta_1(t^*)$ is governed by the eigenvalues ℓ_1 and ℓ_2 defined by Eq. (45). A careful analysis of the eigenvalues shows that $\mathrm{Re}(\ell_i) < 0$ $(i = 1, 2, 3, 4)$, so that the steady state is always stable.

As an illustration, the real parts of the eigenvalues ℓ_i are plotted in Fig. 10 against the common coefficient of restitution $\alpha \equiv \alpha_{12} = \alpha_{12} = \alpha_{22}$ for $d = 3$, $\sigma_1/\sigma_2 = 1$, $x_1 = \frac{1}{2}$, $\phi = 0.1$, and $T_{\mathrm{ex}}^* = 1$. Two values of mass ratio are considered: $m_1/m_2 = 10$ and $m_1/m_2 = \frac{1}{2}$. It is quite apparent that the real part of the eigenvalues ℓ_i is always negative. Moreover, the inset of Fig. 10 shows a comparison of the eigenvalues ℓ_1 and ℓ_2 when the cumulants are neglected vs those obtained by solving the set of coupled equations (54)–(57). No significant discrepancies between both approaches are found in the qualitative behavior of ℓ_i and, hence, the reliability of the Maxwellian approximation is ensured once again.

VII. DISCUSSION

In this paper, we have analyzed the time-dependent homogeneous state of a binary granular suspension. The starting point of the study has been the set of two coupled Enskog kinetic equations for the velocity distribution functions $f_i(\mathbf{v}; t)$ $(i = 1, 2)$ of the solid particles. As usual, the influence of the surrounding viscous gas on the dynamics of grains has been accounted for in an effective way by means of a force constituted by two terms: a deterministic viscous drag force plus a stochastic Langevin-like term. This simple suspension model is mainly based on the assumption that the interstitial fluid is not perturbed by the grains and, so, it can be considered as a thermostat at the (known) temperature T_{ex}. On the other hand, since the model is inspired by numerical and experimental results,[10] the friction coefficients γ_i display a complex dependence on the partial ϕ_i and global $\phi = \phi_1 + \phi_2$ volume fractions, and the masses m_i and diameters σ_i of the mixture [see Eqs. (8) and (9)].

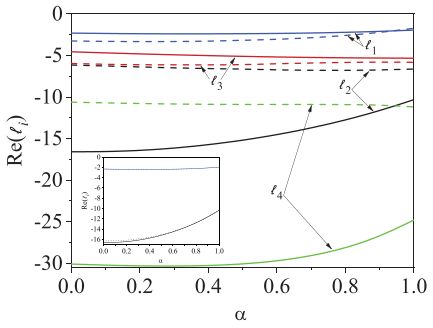

FIG. 10. Plot of the real parts of the eigenvalues ℓ_i $(i = 1, 2, 3, 4)$ of the matrix $\mathcal{L}$ for $\sigma_1/\sigma_2 = 1$, $x_1 = \frac{1}{2}$, $T_{\mathrm{ex}}^* = 1$, $\phi = 0.1$, and $d = 3$. Solid lines correspond to $m_1/m_2 = 10$ and dashed lines to $m_1/m_2 = \frac{1}{2}$. The inset shows a comparison of ℓ_i $(i = 1, 2)$ for $m_1/m_2 = 10$ when cumulants (solid lines) and no cumulants (dashed lines) are considered.

The objective of this paper is twofold. First, we want to characterize the temporal evolution of the system toward the asymptotic steady state. In particular, we have investigated the existence of an unsteady "hydrodynamic" stage [where the velocity distributions f_i depend on time only through the global temperature $T(t)$] before achieving the stationary regime. The existence of the above time-dependent state is crucial for deriving the corresponding Navier–Stokes hydrodynamic equations since this state plays the role of "reference" state in the application of the Chapman–Enskog method[9] to granular suspensions.[8] As a complement to this study, we have also explored the occurrence of the so-called Mpemba-like effect (an initially hotter gas cools sooner than the colder one) in bidisperse granular suspensions. By doing so, we have extended the results obtained for molecular suspensions to the inelastic case.[38,39] Beyond the transient regime and as a second objective, we have also determined the temperature ratio T_1/T_2 and the cumulants c_1 and c_2 (which measure the departure of the distributions f_i from their Maxwellian forms) in the stationary state as functions of the mass and size ratios, the concentration, the volume fraction, the coefficients of restitution, and the background temperature. It is worth remarking that the (approximate) theoretical results obtained in each one of the different issues covered along the paper have been tested against DSMC simulations[26] for different systems and conditions.

Regarding the transient regime, theory and simulations have clearly shown that, after a kinetic stage and before the steady state is reached, the system evolves toward a universal unsteady hydrodynamic stage that no longer depends on the initial conditions. As for driven granular gases,[23,24] the distributions $f_i(\mathbf{v}; t)$ have the form (19) where the time-dependence of the scaled distributions φ_i occurs not only through the dimensionless velocity $\mathbf{c}(t) = \mathbf{v}/v_0(t)$ but also through the scaled temperature $\theta(t) = T(t)/T_{\mathrm{ex}}$. A consequence of this scaling is that the velocity moments $\theta_i(t^*) = T_i(t^*)/T_{\mathrm{ex}}$ and $c_i(t^*)$ tend toward the universal functions $\theta_i(\theta(t^*))$ and $c_i(\theta(t^*))$, respectively, where the functions $\theta_i(\theta)$ and $c_i(\theta)$ are independent of the initial conditions.

With respect to the Mpemba-like effect, as expected this phenomenon is also present when collisions in the binary mixture are inelastic. However, in contrast to the analysis performed in Refs. 38 and 39 for elastic collisions, the presence of the cooling term ζ^* [which gives rise to the granular new term Φ_4 in the evolution equation of the temperature $\theta(t^*)$; see Eq. (33)] makes it more difficult to find clean initial conditions for the occurrence of the Mpemba-like effect. To gain some insight, situations near the final asymptotic steady state have been considered first to get explicit expressions for the crossing time t_c^*. By analyzing the dependence of t_c^* on the initial conditions, we have been able to study the necessary conditions for the effect to occur. Figure 5 illustrates the dependence of the initial temperature ratio $\Delta\theta_0/\Delta\theta_{1,0}$ as a function of the common coefficient of restitution α. As expected, inelasticity of collisions increases the possibilities to observe the Mpemba-like effect. Moreover, the necessary conditions given in Eq. (47) are tested against DSMC simulations in the right panel of Fig. 5 for a cooling and a heating transition. The excellent agreement found between theory and simulations ensure the use of the Maxwellian approximation.

Once we have studied the Mpemba-like effect in situations close to the steady state, we explored the nonlinear situations. The coupling

Physics of Fluids ARTICLE scitation.org/journal/phf

between θ and θ_1 provokes the appearance of large and non-monotonic Mpemba effects. In the former, the large Mpemba effect has been observed even when the initial temperature difference is about 10% of the temperatures themselves. Inelasticity of collisions enlarges the necessary distance between θ_0 and $\theta_{1,0}$ that leads to a crossover in the evolution of temperatures. Thus, nonlinear effects arise and we can observe the non-monotonic and mixed Mpemba effects. Figure 6 illustrates the large, non-monotonic, and mixed effects for a given case and exhibits a good agreement between theory and simulations in the set of parameters considered. However, we have neglected the influence of inelasticity to determine the necessary conditions for the emergence of the Mpemba effect in the nonlinear regime. Therefore, we could consider a *dry* (no gas phase) granular mixture to easily draw conclusions about the effect of inelasticity in the appearance of such effect. We plan to carry out a more exhaustive study on the necessary conditions for the onset of the Mpemba-like effect in dry granular mixtures in the near future.

Finally, the stationary values of the temperature ratio and the fourth cumulants have been determined and compared with DSMC simulations. This study complements a previous comparison made in Ref. 54 between kinetic theory and molecular dynamics simulations. In this context, the comparison carried out here in Sec. IV can be seen as a test of the approximations involved in the computation of T_1/T_2 and c_i but not as a test of the kinetic equation itself since the DSMC method does not avoid the inherent assumptions of kinetic theory (molecular chaos hypothesis). As Figs. 7–9 clearly show, theoretical results for T_1/T_2 agree very well with DSMC results for all the systems considered in the simulations. On the other hand, in the case of cumulants, although theory compares qualitatively well with simulations, more quantitative discrepancies are found between both approaches (especially in the case of c_2). This quantitative disagreement between theory and simulations could be mitigated by the inclusion of cumulants of higher order as well as nonlinear terms in c_1 and c_2. However, based on previous results obtained for monocomponent granular gases[65,66] on the possible lack of convergence of the Sonine polynomial expansion, the absolute value of higher order cumulants could increase with inelasticity. In this case, the Sonine expansion could be not relevant in the sense that one would need to retain a large number of Sonine coefficients to achieve an accurate estimate of the fourth-degree cumulants.

Although the results derived in this paper have been focused on smooth inelastic spheres, the extension to *rough* hard inelastic spheres is a very challenging problem. This study could allow us to assess the impact of solid body friction on the applicability of a hydrodynamic description to granular suspensions and/or the occurrence of the Mpemba effect. Based on previous results,[67] we expect that the effect of roughness on the dynamic properties of grains can play an important role. We will work on this issue in the near future.

In summary, we believe our results provide additional support to the validity of hydrodynamics for studying time-dependent homogeneous states in multicomponent granular suspensions. As said before, this conclusion is relevant since the local version of the time-dependent homogeneous state is considered as the zeroth-order approximation in the Chapman–Enskog expansion. In addition, we have also shown the occurrence of the Mpemba-like effect in bidisperse granular suspensions for situations close to and far away from the asymptotic stationary state. In both cases, approximate theoretical results agree very well with DSMC simulations. As a complement to the previous studies, the temperature ratio T_1/T_2 and the fourth-degree cumulants c_i have been determined in the stationary state also. While theory shows excellent agreement with simulations for T_1/T_2, some differences are found in the case of cumulants. However, these differences are relatively small and, in fact, they are of the same order as those observed in the homogeneous cooling state for undriven granular mixtures.[25,41]

ACKNOWLEDGMENTS

The work has been supported by the Spanish Government through Grant No. PID2020-112936GB-I00 and by the Junta de Extremadura (Spain) Grant Nos. IB20079 and GR18079, partially financed by "Fondo Europeo de Desarrollo Regional" funds. The research of R.G.G. has also been supported by the predoctoral fellowship BES-2017–079725 from the Spanish Government.

The authors have no conflicts to disclose.

APPENDIX: EXPRESSIONS FOR THE PARTIAL COOLING RATES AND THE FOURTH-DEGREE COLLISIONAL MOMENTS

In this appendix, we display the explicit expressions of the (reduced) partial cooling rates ζ_i^* and the fourth-degree collisional moments Σ_i. Their forms are provided by Eqs. (31) and (32) when nonlinear terms in c_i are neglected. The corresponding expressions of ζ_{ij} and Σ_{ij} are given by[54]

$$\zeta_{10} = \frac{\sqrt{2}\pi^{(d-1)/2}}{d\Gamma\left(\frac{d}{2}\right)} x_1\chi_{11}\left(\frac{\sigma_1}{\sigma_{12}}\right)^{d-1}\beta_1^{-1/2}(1-\alpha_{11}^2) + \frac{4\pi^{(d-1)/2}}{d\Gamma\left(\frac{d}{2}\right)} x_2\chi_{12}\mu_{21}\left(\frac{1+\beta}{\beta}\right)^{1/2}(1+\alpha_{12})\beta_2^{-1/2} \times\left[1-\frac{1}{2}\mu_{21}(1+\alpha_{12})(1+\beta)\right], \tag{A1}$$

$$\zeta_{11} = \frac{3\pi^{(d-1)/2}}{8\sqrt{2}d\Gamma\left(\frac{d}{2}\right)} x_1\chi_{11}\left(\frac{\sigma_1}{\sigma_{12}}\right)^{d-1}\beta_1^{-1/2}(1-\alpha_{11}^2) + \frac{\pi^{(d-1)/2}}{2d\Gamma\left(\frac{d}{2}\right)} x_2\chi_{12}\mu_{21}\frac{(1+\beta)^{-3/2}}{\beta^{1/2}}(1+\alpha_{12})\beta_2^{-1/2} \times\left[3+4\beta-\frac{3}{2}\mu_{21}(1+\alpha_{12})(1+\beta)\right], \tag{A2}$$

$$\zeta_{12} = -\frac{\pi^{(d-1)/2}}{2d\Gamma\left(\frac{d}{2}\right)} x_2\chi_{12}\mu_{21}\left(\frac{1+\beta}{\beta}\right)^{-3/2}(1+\alpha_{12})\beta_2^{-1/2} \times\left[1+\frac{3}{2}\mu_{21}(1+\alpha_{12})(1+\beta)\right], \tag{A3}$$

Physics of Fluids ARTICLE scitation.org/journal/phf

$$\Sigma_{10} = -\frac{\pi^{(d-1)/2}}{\sqrt{2}\Gamma\left(\frac{d}{2}\right)}\beta_1^{-5/2}x_1\chi_{11}\left(\frac{\sigma_1}{\sigma_{12}}\right)^{d-1}\frac{3+2d+2\alpha_{11}^2}{2}\left(1-\alpha_{11}^2\right)+\frac{2\pi^{(d-1)/2}}{\Gamma\left(\frac{d}{2}\right)}\beta_1^{-5/2}x_2\chi_{12}(1+\beta)^{-1/2}$$
$$\times\mu_{21}(1+\alpha_{12})\left\{-[d+3+(d+2)\beta]+\frac{\mu_{21}}{2}(1+\alpha_{12})(1+\beta)\left(11+d+\frac{d^2+5d+6}{d+3}\theta\right)\right.$$
$$\left.-4\mu_{21}^2(1+\alpha_{12})^2(1+\beta)^2+\mu_{21}^3(1+\alpha_{12})^3(1+\beta)^3\right\}, \tag{A4}$$

$$\Sigma_{11} = -\frac{\sqrt{2}\pi^{(d-1)/2}}{\Gamma\left(\frac{d}{2}\right)}\beta_1^{-5/2}x_1\chi_{11}\left(\frac{\sigma_1}{\sigma_{12}}\right)^{d-1}\left[\frac{d-1}{2}(1+\alpha_{11})+\frac{3}{64}\left(10d+39+10\alpha_{11}^2\right)\left(1-\alpha_{11}^2\right)\right]$$
$$+\frac{\pi^{(d-1)/2}}{4\Gamma\left(\frac{d}{2}\right)}\beta_1^{-5/2}x_2\chi_{12}(1+\beta)^{-5/2}\mu_{21}(1+\alpha_{12})\left\{-\left[45+15d+(114+39d)\beta+(88+32d)\beta^2+(16+8d)\beta^3\right]\right.$$
$$+\frac{3}{2}\mu_{21}(1+\alpha_{12})(1+\beta)\left[55+5d+9(10+d)\beta+4(8+d)\beta^2\right]$$
$$\left.-12\mu_{21}^2(1+\alpha_{12})^2(1+\beta)^2(5+4\beta)+15\mu_{21}^3(1+\alpha_{12})^3(1+\beta)^3\right\}, \tag{A5}$$

$$\Sigma_{12} = \frac{\pi^{(d-1)/2}}{4\Gamma\left(\frac{d}{2}\right)}\theta_1^{-5/2}x_2\chi_{12}\beta^2(1+\beta)^{-5/2}\mu_{21}(1+\alpha_{12})\left[d-1+(d+2)\beta+\frac{3}{2}\mu_{21}(1+\alpha_{12})(1+\beta)\times[d-1+(d+2)\beta]\right.$$
$$\left.-12\mu_{21}^2(1+\alpha_{12})^2(1+\beta)^2+15\mu_{21}^3(1+\alpha_{12})^3(1+\beta)^3\right]. \tag{A6}$$

The expressions for ζ_{20}, ζ_{21}, ζ_{22}, Σ_{20}, Σ_{22}, and Σ_{21} can easily be obtained from Eqs. (A1)–(A6) by changing $1 \to 2$ and $\beta \to \beta^{-1}$.

DATA AVAILABILITY

The data that support the findings of this study are available from the corresponding author upon reasonable request.

REFERENCES

[1]D. L. Koch and R. J. Hill, "Inertial effects in suspensions and porous-media flows," Annu. Rev. Fluid Mech. **33**, 619–647 (2001).
[2]R. Seto, R. Mari, J. F. Morris, and M. M. Denn, "Discontinuous shear thickening of frictional hard-sphere suspensions," Phys. Rev. Lett. **111**, 218301 (2013).
[3]R. Mari and R. Seto, "Shear thickening, frictionless and frictional rheologies in non-Brownian suspensions," J. Rheol. **58**, 1693–1724 (2014).
[4]A. Singh, C. Ness, R. Seto, J. J. de Pablo, and H. M. Jaeger, "Shear thickening and jamming of dense suspensions: The "roll" of friction," Phys. Rev. Lett. **124**, 248005 (2020).
[5]P. Résibois and M. de Leener, *Classical Kinetic Theory of Fluids* (Wiley, New York, 1977).
[6]N. G. van Kampen, *Stochastic Processes in Physics and Chemistry* (North-Holland, Amsterdam, 2007).
[7]A. Osinsky, A. S. Bodrova, and N. V. Brilliantov, "Size-polydisperse dust in molecular gas: Energy equipartition versus nonequipartition," Phys. Rev. E **101**, 022903 (2020).
[8]R. Gómez González, N. Khalil, and V. Garzó, "Enskog kinetic theory for multicomponent granular suspensions," Phys. Rev. E **101**, 012904 (2020).
[9]S. Chapman and T. G. Cowling, *The Mathematical Theory of Nonuniform Gases* (Cambridge University Press, Cambridge, 1970).
[10]X. Yin and S. Sundaresan, "Fluid-particle drag in low-Reynolds-number polydisperse gas-solid suspensions," AIChE J. **55**, 1352 (2009).
[11]V. Garzó, *Granular Gaseous Flows* (Springer Nature, Cham, 2019).
[12]S. Takada, H. Hayakawa, and V. Garzó, "Rheology of a dilute binary mixture of inertial suspension under simple shear flow," arXiv:2107.10522 (2021).
[13]J. H. Ferziger and G. H. Kaper, *Mathematical Theory of Transport Processes in Gases* (North-Holland, Amsterdam, 1972).
[14]V. Garzó and A. Santos, *Kinetic Theory of Gases in Shear Flows: Nonlinear Transport* (Kluwer Academic Publishers, Dordrecht, 2003).
[15]A. Astillero and A. Santos, "Aging to non-Newtonian hydrodynamics in a granular gas," Europhys. Lett. **78**, 24002 (2007).
[16]A. Astillero and A. Santos, "Unsteady non-Newtonian hydrodynamics in granular gases," Phys. Rev. E **85**, 021302 (2012).
[17]J. J. Brey, M. J. Ruiz-Montero, and F. Moreno, "Hydrodynamics of an open vibrated granular system," Phys. Rev. E **63**, 061305 (2001).
[18]J. J. Brey, M. J. Ruiz-Montero, F. Moreno, and R. García-Rojo, "Transversal inhomogeneities in dilute vibrofluidized granular fluids," Phys. Rev. E **65**, 061302 (2002).
[19]S. R. Dahl, C. M. Hrenya, V. Garzó, and J. W. Dufty, "Kinetic temperatures for a granular mixture," Phys. Rev. E **66**, 041301 (2002).
[20]E. C. Rericha, C. Bizon, M. D. Shattuck, and H. L. Swinney, "Shocks in supersonic sand," Phys. Rev. Lett. **88**, 014302 (2002).
[21]X. Yang, C. Huan, D. Candela, R. W. Mair, and R. L. Walsworth, "Measurements of grain motion in a dense, three-dimensional granular fluid," Phys. Rev. Lett. **88**, 044301 (2002).
[22]C. Huan, X. Yang, D. Candela, R. W. Mair, and R. L. Walsworth, "NMR experiments on a three-dimensional vibrofluidized granular medium," Phys. Rev. E **69**, 041302 (2004).
[23]M. I. García de Soria, P. Maynar, and E. Trizac, "Universal reference state in a driven homogeneous granular gas," Phys. Rev. E **85**, 051301 (2012).
[24]M. G. Chamorro, F. Vega Reyes, and V. Garzó, "Homogeneous steady states in a granular fluid driven by a stochastic bath with friction," J. Stat. Mech. **2013**, P07013.

[25]V. Garzó and J. W. Dufty, "Homogeneous cooling state for a granular mixture," Phys. Rev. E **60**, 5706–5713 (1999).
[26]G. A. Bird, *Molecular Gas Dynamics and the Direct Simulation Monte Carlo of Gas Flows* (Clarendon, Oxford, 1994).
[27]V. Garzó, "Brazil-nut effect versus reverse Brazil-nut effect in a moderately granular dense gas," Phys. Rev. E **78**, 020301 (R (2008).
[28]V. Garzó, "Segregation by thermal diffusion in moderately dense granular mixtures," Eur. Phys. J. E **29**, 261–274 (2009).
[29]V. Garzó, "Thermal diffusion segregation in granular binary mixtures described by the Enskog equation," New J. Phys. **13**, 055020 (2011).
[30]E. B. Mpemba and D. G. Osborne, "Cool?," Phys. Educ. **4**, 172–175 (1969).
[31]A. Kumar and J. Bechhoefer, "Exponentially faster cooling in a colloidal system," Nature **584**, 64 (2020).
[32]N. Vadakkayil and S. K. Das, "Should a hotter paramagnet transform quicker to a ferromagnet? Monte carlo simulation results for Ising model," Phys. Chem. Chem. Phys. **23**, 11186 (2021).
[33]A. Lasanta, F. Vega Reyes, A. Prados, and A. Santos, "When the hotter cools more quickly: Mpemba effect in granular fluids," Phys. Rev. Lett. **119**, 148001 (2017).
[34]A. Torrente, M. A. López-Castaño, A. Lasanta, F. Vega Reyes, A. Prados, and A. Santos, "Large Mpemba-like effect in a gas of inelastic rough hard spheres," Phys. Rev. E **99**, 060901(R) (2019).
[35]A. Biswas, V. V. Prasad, O. Raz, and R. Rajesh, "Mpemba effect in driven granular Maxwell gases," Phys. Rev. E **102**, 012906 (2020).
[36]A. Santos and A. Prados, "Mpemba effect in molecular gases under nonlinear drag," Phys. Fluids **32**, 072010 (2020).
[37]S. Takada, H. Hayakawa, and A. Santos, "Mpemba effect in inertial suspensions," Phys. Rev. E **103**, 032901 (2021).
[38]R. Gómez González, N. Khalil, and V. Garzó, "Mpemba-like effect in driven binary mixtures," Phys. Fluids **33**, 053301 (2021).
[39]R. Gómez González and V. Garzó, "Non-monotonic Mpemba effect in binary molecular suspensions," EPJ Web Conf. **249**, 09005 (2021).
[40]E. Mompó, M. A. López-Castaño, A. Lasanta, F. Vega Reyes, and A. Torrente, "Memory effects in a gas of viscoelastic particles," Phys. Fluids **33**, 062005 (2021).
[41]J. M. Montanero and V. Garzó, "Monte Carlo simulation of the homogeneous cooling state for a granular mixture," Granular Matter **4**, 17–24 (2002).
[42]D. L. Koch, "Kinetic theory for a monodisperse gas-solid suspension," Phys. Fluids A **2**, 1711–1722 (1990).
[43]H.-K. Tsao and D. L. Koch, "Simple shear flows of dilute gas-solid suspensions," J. Fluid Mech. **296**, 211–245 (1995).
[44]A. S. Sangani, G. Mo, H.-K. Tsao, and D. L. Koch, "Simple shear flows of dense gas-solid suspensions at finite Stokes numbers," J. Fluid Mech. **313**, 309–341 (1996).
[45]J. J. Wylie, D. L. Koch, and J. C. Ladd, "Rheology of suspensions with high particle inertia and moderate fluid inertia," J. Fluid Mech. **480**, 95 (2003).
[46]V. Garzó, W. D. Fullmer, C. M. Hrenya, and X. Yin, "Transport coefficients of solid particles immersed in a viscous gas," Phys. Rev. E **93**, 012905 (2016).
[47]V. Garzó, S. Tenneti, S. Subramaniam, and C. M. Hrenya, "Enskog kinetic theory for monodisperse gas-solid flows," J. Fluid Mech. **712**, 129–168 (2012).
[48]D. R. M. Williams and F. C. MacKintosh, "Driven granular media in one dimension: Correlations and equation of state," Phys. Rev. E **54**, R9–R12 (1996).
[49]H. Hayakawa, S. Takada, and V. Garzó, "Kinetic theory of shear thickening for a moderately dense gas-solid suspension: From discontinuous thickening to continuous thickening," Phys. Rev. E **96**, 042903 (2017).
[50]X. Yin and S. Sundaresan, "Drag law for bidisperse gas-solid suspensions containing equally sized spheres," Ind. Eng. Chem. Res. **48**, 227 (2009).
[51]W. Holloway, X. Yin, and S. Sundaresan, "Fluid-particle drag in inertial polydisperse gas-solid suspensions," AIChE J. **56**, 1995 (2010).
[52]E. W. Grundke and D. Henderson, "Distribution functions of multicomponent fluid mixtures of hard spheres," Mol. Phys. **24**, 269–281 (1972).
[53]L. L. Lee and D. Levesque, "Perturbation theory for mixtures of simple liquids," Mol. Phys. **26**, 1351–1370 (1973).
[54]N. Khalil and V. Garzó, "Homogeneous states in driven granular mixtures: Enskog kinetic theory versus molecular dynamics simulations," J. Chem. Phys. **140**, 164901 (2014).
[55]S. Esposito, R. D. Risi, and L. Somma, "Mpemba effect and phase transitions in the adiabatic cooling of water before freezing," Physica A **387**, 757–763 (2008).
[56]J. I. Katz, "When hot water freezes before cold," Am. J. Phys. **77**, 27–29 (2009).
[57]J. Jin and W. A. Goddard, "Mechanisms underlying the Mpemba effect in water from molecular dynamics simulations," J. Phys. Chem. C **119**, 2622–2629 (2015).
[58]R. T. Ibekwe and J. P. Cullerne, "Investigating the Mpemba effect: When hot water freezes faster than cold water," Phys. Educ. **51**, 025011 (2016).
[59]N. C. Keim, J. D. Paulsen, Z. Zeravcic, S. Sastry, and S. R. Nagel, "Memory formation in matter," Rev. Mod. Phys. **91**, 035002 (2019).
[60]I. Klich, O. Raz, O. Hirschberg, and M. Vucelja, "Mpemba index and anomalous relaxation," Phys. Rev. X **9**, 021060 (2019).
[61]A. Gijón, A. Lasanta, and E. R. Hernández, "Path towards equilibrium in molecular systems: The case of water," Phys. Rev. E **100**, 032103 (2019).
[62]H. C. Burridge and P. F. Linden, "Questioning the Mpemba effect: Hot water does not cool more quickly than cold," Sci. Rep. **6**, 37665 (2016).
[63]H. C. Burridge and O. Hallstadius, "Observing the Mpemba effect with minimal bias and the value of the Mpemba effect to scientific outreach and engagement," Proc. R. Soc. A **476**, 20190829 (2020).
[64]Here, in contrast to the analysis made in Ref. 38, the temperature θ_1 is employed instead of the temperature ratio θ_1/θ_2 for studying the Mpemba-like effect. The results are, of course, equivalent in both descriptions.
[65]N. V. Brilliantov and T. Pöschel, "Breakdown of the Sonine expansion for the velocity distribution of granular gases," Europhys. Lett. **74**, 424–430 (2006).
[66]N. V. Brilliantov and T. Pöschel, "Erratum: Breakdown of the Sonine expansion for the velocity distribution of granular gases," Europhys. Lett. **75**, 188 (2006).
[67]R. Gómez González and V. Garzó, "Non-Newtonian rheology in inertial suspensions of inelastic rough hard spheres under simple shear flow," Phys. Fluids **32**, 073315 (2020).

4.3 Article 3

Title: Mpemba-like effect in driven binary mixtures

Authors: Rubén Gómez González[1], Nagi Khalil[2], and Vicente Garzó[3]

Affiliations:

[1] Departamento de Física, Universidad de Extremadura, E-06006 Badajoz, Spain

[2] Escuela Superior de Ciencias Experimentales y Tecnología (ESCET) and GISC, Universidad Rey Juan Carlos, Móstoles, 28933 Madrid, Spain

[3] Departamento de Física and Instituto de Computación Científica Avanzada (ICCAEx), Universidad de Extremadura, E-06006 Badajoz, Spain

Journal: Physics of Fluids

Volume: 33

Pages: 053301

Year: 2021

DOI: 10.1063/5.0050530

Physics of Fluids ARTICLE scitation.org/journal/phf

Mpemba-like effect in driven binary mixtures

Cite as: Phys. Fluids **33**, 053301 (2021); doi: 10.1063/5.0050530
Submitted: 16 March 2021 · Accepted: 8 April 2021 ·
Published Online: 3 May 2021

Rubén Gómez González,[1,a] Nagi Khalil,[2,b] and Vicente Garzó[3,c]

AFFILIATIONS

[1]Departamento de Física, Universidad de Extremadura, E-06071 Badajoz, Spain
[2]Escuela Superior de Ciencias Experimentales y Tecnología (ESCET) and GISC, Universidad Rey Juan Carlos, Móstoles, 28933 Madrid, Spain
[3]Departamento de Física and Instituto de Computación Científica Avanzada (ICCAEx), Universidad de Extremadura, E-06071 Badajoz, Spain

[a]Electronic mail: ruben@unex.es
[b]Electronic mail: nagi.khalil@urjc.es
[c]Author to whom correspondence should be addressed: vicenteg@unex.es. URL: http://www.unex.es/eweb/fisteor/vicente/

ABSTRACT

The Mpemba effect occurs when two samples at different initial temperatures evolve in such a way that the temperatures cross each other during the relaxation toward equilibrium. In this paper, we show the emergence of a Mpemba-like effect in a molecular binary mixture in contact with a thermal reservoir (bath). The interaction between the gaseous particles of the mixture and the thermal reservoir is modeled via a viscous drag force plus a stochastic Langevin-like term. The presence of the external bath couples the time evolution of the total and partial temperatures of each component allowing the appearance of the Mpemba phenomenon, even when the initial temperature differences are of the same order of the temperatures themselves. Analytical results are obtained by considering multitemperature Maxwellian approximations for the velocity distribution functions of each component. The theoretical analysis is carried out for initial states close to and far away (large Mpemba-like effect) from equilibrium. The former situation allows us to develop a simple theory where the time evolution equation for the temperature is linearized around its asymptotic equilibrium solution. This linear theory provides an expression for the crossover time. We also provide a qualitative description of the large Mpemba effect. Our theoretical results agree very well with computer simulations obtained by numerically solving the Enskog kinetic equation by means of the direct simulation Monte Carlo method and by performing molecular dynamics simulations. Finally, preliminary results for driven granular mixtures also show the occurrence of a Mpemba-like effect for inelastic collisions.

I. INTRODUCTION

The Mpemba effect is a counterintuitive phenomenon in which two samples of fluids, A and B, at initially different temperatures ($T_{A,0} > T_{B,0}$) can evolve in time in such a way that their temperatures cross each other at a given time t_c; the curve for T_A (initially hotter sample) stays below the other one T_B for longer times $t > t_c$. Although this anomalous cooling process was first reported in the case of water many years ago by Mpemba,[1] its origin for that liquid is yet unclear.[2–16] In addition, although similar behaviors to the Mpemba effect have been observed in other systems,[17–19] the existence of the Mpemba effect still remains very controversial.[20,21] This is in part due to the arduous task of knowing and monitoring the initial conditions of the two samples that give rise to a crossing of the respective cooling curves.

For the above reason, in order to gain some insight into the understanding of this problem, the kinetic theory approach to granular gases[22–25] has been widely employed in recent years as a reliable tool for unveiling in a clean way the origin of the Mpemba-like effect (and its inverse one, namely, when initially cooler systems equilibrate faster than the hotter ones[26]) from a more fundamental point of view. Granular gases can be considered as a collection of macroscopic particles (typically of the orders of micrometers or larger) whose interactions are dissipative. The inelastic character of the collisions among granular particles gives rise to the coupling of the (granular) temperature with other velocity moments of the velocity distribution function, such as (i) the fourth cumulant or *kurtosis* a_2 (a quantity measuring the departure of the distribution function from its Maxwellian form in driven granular gases),[22] (ii) the rotational-to-translational temperature ratio in a granular gas of inelastic rough hard spheres,[23] (iii) the partial temperatures ratio in a binary granular mixture,[24] and (iv) the shear stress in a sheared inertial suspension.[25] The above couplings are

Physics of Fluids ARTICLE scitation.org/journal/phf

the origin of the emergence of the Mpemba-like effect in granular gases, which now accounts for the evolution of the system toward a final asymptotic nonequilibrium steady state.

Among the above previous studies, to the best of our knowledge and in the context of kinetic theory, the only paper where the Mpemba-like effect has been studied for driven granular mixtures has been carried out by Biswas *et al.*[24] Since the number of parameters involved in multicomponent mixtures is much larger than that of a monocomponent gas, for the sake of simplicity, they consider the inelastic Maxwell model, namely, a simplified model for a granular gas where the collision rate is assumed to be independent of the relative velocity of the colliding particles.[27] The use of this simple model allows them to offer an exact analysis of the conditions under which the Mpemba-like effect is present. In addition, no simulations are performed in this work and only analytical results are reported.[24] Thus, given that inelastic Maxwell gases are an idealized version of the more realistic hard-sphere model, it is quite apparent that a study of the Mpemba-like effect in driven mixtures of hard spheres is still lacking.

Aside from granular gases, a recent paper[28] has shown that the Mpemba effect can also take place in homogeneous and isotropic states of molecular gases (i.e., when collisions are elastic) in contact with a background fluid. The particles of the system are assumed to be hard spheres surrounded by an interstitial fluid at equilibrium. When the particles of the background fluid are much lighter than that of the gas (Brownian particles), the particles of the gas are subjected to a *nonlinear* drag force plus a stochastic force with *nonlinear* variance. After a transient period, the velocity distribution function is ensured to achieve a Maxwellian distribution with temperature given by the background fluid. To characterize the transient toward equilibrium, the first Sonine approximation to the distribution function (which includes the kurtosis a_2) was considered. As in the analysis performed in Ref. 22, the Mpemba effect arises from the coupling of the time evolution of the temperature T with that of the kurtosis a_2. This coupling is due here to the nonlinear form of the drag term. Nonetheless, as happens in the case of granular gases,[27,29] since a_2 is small then the initial temperatures must be very close to each other in order to achieve a crossover in the evolution curves. As a consequence, the Mpemba crossover takes place in the very early stage of the relaxation toward equilibrium.

In this work, we analyze the occurrence of the Mpemba-like effect in a driven binary mixture of hard spheres. The driving of the mixture is due to its interaction with the surrounding molecular fluid. When the density of the gas is sufficiently low, one can assume that the interstitial fluid is not perturbed by the gas particles and so, it may be treated as a thermostat. As noted by Takada *et al.*,[25] the system we consider (inertial suspension) could be close to the original setup of Mpemba and Osborne[1] since they study a system of ice-mix, which is a suspension system.

Under the above conditions, as usual in granular literature,[30] the interaction between gas particles and the surrounding fluid can be modeled by means of an effective external force. This fluid–solid interaction force (which follows the fluctuation–dissipation theorem[31–33]) is composed of two terms: (i) a *linear* drag force proportional to the (instantaneous) velocity of particles and (ii) a stochastic force. While the first contribution mimics the friction exerted by the viscous background fluid to the gas particles, the second term simulates the transmission of energy through random and instantaneous collisions with the external bath. This type of driving mechanism can be also formally obtained from the corresponding collision integral by considering the leading term in the Kramer–Moyal expansion in powers of the mass-ratio of the background and grain particles.[34–38]

In order to provide a simple explanation of the subjacent mechanisms involved in the Mpemba-like effect, we assume first a driven gas mixture of molecular gases (elastic collisions). This allows us to obtain simple conditions for the occurrence of such a phenomenon. An extension of the study to inelastic collisions is briefly analyzed and illustrated in Sec. V. However, given the complexity of the analytical expressions achieved for granular mixtures, it is not easy to provide simple conditions for the existence of the Mpemba-like effect for these systems.

As usual in driven mixtures, we consider the Enskog kinetic theory (which applies to small and moderate densities) in combination with the Fokker–Planck suspension model[39] mentioned above. Starting from the set of Enskog kinetic equations for the mixture, the time evolution of the total temperature $T(t)$ and the partial temperatures $T_1(t)$ and $T_2(t)$ is obtained. As expected, the coupling between $T(t)$, $T_1(t)$, and $T_2(t)$ is behind the emergence of the Mpemba-like memory effect. In addition, to get explicit results, the partial production rates ξ_i (which give the rate of energy change in collisions i-j) appearing in the evolution equation of the partial temperatures are estimated here by assuming Maxwellian distributions at the temperatures T_i. This means that, in contrast to previous works,[22,24,28] neither cumulants nor the presence of a nonlinear drag force is needed for the emergence of the Mpemba effect.

Moreover, in accordance with simulations of bidisperse gas–solid flows,[40–42] the fact that the friction coefficients γ_i accounting for the interaction of the component i with the background fluid are different ($\gamma_1 \neq \gamma_2$) makes different energies transferred from the external bath to each component. As a consequence, the relaxation of T_i toward its common equilibrium value ($T_1 = T_2 = T$) for molecular mixtures can be quite different for both partial temperatures. This makes the Mpemba effect arises even when the systems are initially prepared in Maxwellian velocity distribution functions at different partial temperatures. Moreover, the use of the partial temperatures as the control parameter allows some flexibility in the selection of the initial conditions and so, the magnitude of the Mpemba effect is not limited (namely, the so-called "large" Mpemba effect can be observed).

Nevertheless, given that the theoretical predictions derived here are based on a simple approximation (Maxwellian distributions for evaluating the production rates), a comparison with computer simulations turns out to be crucial to gauge their reliability. In this work, kinetic-theory results are compared against two independent simulation methods: (i) a modified algorithm of the standard direct Monte Carlo simulation (DSMC) method[43] to numerically solve the Enskog equation for a *driven* binary mixture[44,45] and (ii) event-driven molecular dynamics (MD) simulations.[29,46,47] Both simulation methods complement each other since, on the one hand, DSMC offers a way to solve the Enskog equation by means of Monte Carlo-like simulations. It inherently assumes the molecular chaos hypothesis and an approximate form of the pair distribution function at contact; both hypotheses stemming from the kinetic-theory description. At the same time, the DSMC method provides the *exact* form of the time-dependent velocity distribution function, allowing us to assess the reliability of the approximate theory in the transient regime. On the other hand, for the

Physics of Fluids ARTICLE scitation.org/journal/phf

suspension model considered here, given that MD solves numerically Newton's equations of motion with the action of a deterministic drag force plus a stochastic Langevin-like force, the limitations of the Enskog theory itself can be tested.

The paper is organized as follows: Sec. II deals with the Enskog equation for homogeneous states conveniently adapted to the case of driven molecular binary mixtures. Evolution equations for the temperature ratio $T_1(t)/T_2(t)$ and the (total) temperature $T(t)$ are also derived. Next, Sec. III analyzes states close to equilibrium. This allows us to linearize the above set of differential equations around the equilibrium solution and to solve them analytically. Exact expressions for the crossing time and the critical value of the initial temperature difference (which determines Mpemba and no Mpemba effects) are obtained and compared against DSMC simulations showing an excellent agreement. The large Mpemba-like effect is explored in Sec. IV in which we carry out a more qualitative analysis. Some examples regarding the fulfillment of the necessary but no sufficient conditions to achieve the Mpemba effect are tested against both DSMC and MD simulations. Again, the theoretical results compare very well with computer simulations. Some preliminary results obtained for granular gases are presented in Sec. V while the paper ends in Sec. VI with a brief discussion of the results derived in this work.

II. ENSKOG KINETIC THEORY FOR MOLECULAR BINARY MIXTURES IN CONTACT WITH A THERMAL RESERVOIR

Let us consider a binary mixture of hard particles of masses m_1 and m_2 and diameters σ_1 and σ_2. For the sake of simplicity and to provide a simple analysis of the conditions under which the Mpemba-like effect appears, we study first molecular binary mixtures (namely, when collisions between particles are elastic). Granular mixtures will be considered in Sec. V. For moderate densities, the one-particle velocity distribution function $f_i(\mathbf{r},\mathbf{v},t)$ $(i=1,\,2)$ of the component i obeys the Enskog kinetic equation.[48] We assume that the mixture interacts with a thermal reservoir (or equivalently, particles of the gas are surrounded by an interstitial fluid) so that the total temperature of the mixture does not remain constant and changes in time. To model the interaction of the particles of the gas with the surrounding fluid, one possibility would be to describe the molecular suspension in terms of a set of two coupled kinetic equations for each one of the velocity distributions of the different phases. However, the resulting theory would be very difficult to solve, in particular in the case of multicomponent mixtures. For this reason, due to the technical difficulties involved in the above approach, it is more usual in gas–solid flows to model the influence of the interstitial fluid on particles of the gas mixture by means of an effective external force.[30]

For *homogeneous* and isotropic states, the set of Enskog coupled equations reads[48,49]

$$\frac{\partial f_i}{\partial t}=\sum_{j=1}^{2}J_{ij}\left[\mathbf{v}|f_i,f_j\right]+\mathcal{C}_{i,\text{ex}}\quad(i=1,2),\tag{1}$$

where the Boltzmann–Enskog collision operator $J_{ij}[f_i,f_j]$ for homogeneous states is[48,49]

$$J_{ij}\left[\mathbf{v}_1|f_i,f_j\right]=\chi_{ij}\sigma_{ij}^{d-1}\int d\mathbf{v}_2\int d\hat{\boldsymbol{\sigma}}\,\Theta(\hat{\boldsymbol{\sigma}}\cdot\mathbf{g}_{12})(\hat{\boldsymbol{\sigma}}\cdot\mathbf{g}_{12})\times\left[f_i(\mathbf{v}_1')f_j(\mathbf{v}_2')-f_i(\mathbf{v}_1)f_j(\mathbf{v}_2)\right].\tag{2}$$

Here, $\sigma_{ij}=(\sigma_i+\sigma_j)/2$, $\hat{\boldsymbol{\sigma}}$ is an unit vector along the line of centers, Θ is the Heaviside step function, d is the dimensionality of the system ($d=2$ for disks and $d=3$ for spheres), $\mathbf{g}_{12}=\mathbf{v}_1-\mathbf{v}_2$ is the relative velocity, and the relation between the precollisional velocities $(\mathbf{v}_1,\mathbf{v}_2)$ and the postcollisional velocities $(\mathbf{v}_1',\mathbf{v}_2')$ is

$$\mathbf{v}_1'=\mathbf{v}_1-2\mu_{ji}(\hat{\boldsymbol{\sigma}}\cdot\mathbf{g}_{12})\hat{\boldsymbol{\sigma}},\quad\mathbf{v}_2'=\mathbf{v}_1+2\mu_{ij}(\hat{\boldsymbol{\sigma}}\cdot\mathbf{g}_{12})\hat{\boldsymbol{\sigma}},\tag{3}$$

where $\mu_{ij}=m_i/(m_i+m_j)$. Moreover, χ_{ij} is the pair correlation function at thermal equilibrium for particles of types i and j when they are in contact, i.e., separated by σ_{ij}. Except for the presence of the pair correlation functions χ_{ij}, the Enskog equation for homogeneous states is identical to the Boltzmann equation.

The second term $\mathcal{C}_{i,\text{ex}}$ of the right-hand side of Eq. (1) describes the coupling between the thermal reservoir and particles of the component i. As said in the Introduction, if the gaseous mixture is sufficiently dilute, one can neglect the impact of gas particles on the surrounding fluid and so, the latter plays the role of a thermostat. In this case, a reliable model for describing suspensions is the Langevin equation,[25,32,33] so that the influence of the background fluid on gas particles is accounted for by (i) a deterministic viscous (linear) drag force proportional to the particle velocity[30] (ii) a stochastic Langevin force representing Gaussian white noise.[35] This latter term is represented by a Fokker–Planck collision operator.[50–52] While the drag force term models the friction of particles of the component i with the surrounding fluid, the stochastic term attempts to mimic the energy gained by particles of the gas due to their interactions with the more rapid particles of the interstitial fluid. Thus, the term $\mathcal{C}_{i,\text{ex}}$ reads

$$\mathcal{C}_{i,\text{ex}}=\gamma_i\frac{\partial}{\partial\mathbf{v}}\cdot\mathbf{v}f_i+\frac{\gamma_i T_{\text{ex}}}{m_i}\frac{\partial^2 f_i}{\partial v^2},\tag{4}$$

where the coefficients γ_i are the friction or drift coefficients and T_{ex} is the background temperature. Here, we have taken units for the temperature for which the Boltzmann constant $k_B=1$. The structure of Eq. (4) can be also derived from the Boltzmann–Lorentz collision operator (characterizing the effect of collisions on the distribution f_i between the Brownian particle i and fluid particles) by considering the leading term in the Kramers–Moyal expansion in powers of the mass ratio m_f/m_i when the background fluid is at equilibrium.[34–37] Here, m_f denotes the mass of the particles of the background fluid.

It must be noted that in general, the friction coefficients may be tensorial quantities as a result of the hydrodynamic interactions between particles, which strongly depends on the configuration of particles. Here, the isotropic case is considered for the sake of simplicity and so, the coefficients γ_i are scalar quantities. Thus, in the case of granular particles, the suspension model employed here might be applicable to describe inertial suspensions where the diameter of suspended particles ranges approximately from 1 to 70 μm.[30]

Under the above conditions, Enskog–Fokker–Planck kinetic equation (1) is[53]

$$\frac{\partial f_i}{\partial t}-\gamma_i\frac{\partial}{\partial\mathbf{v}}\cdot\mathbf{v}f_i-\frac{\gamma_i T_{\text{ex}}}{m_i}\frac{\partial^2 f_i}{\partial v^2}=\sum_{j=1}^{2}J_{ij}\left[f_i,f_j\right].\tag{5}$$

The coefficients γ_i can be written as $\gamma_i=\gamma_0 R_i$, where $\gamma_0\propto\sqrt{T_{\text{ex}}}$. The dimensionless quantities R_i may depend on the mass ratio m_1/m_2, the diameter ratio σ_1/σ_2, the total volume fraction $\phi=\phi_1+\phi_2$, and the partial volume fractions ϕ_i defined as

Physics of Fluids ARTICLE scitation.org/journal/phf

$$\phi_i = \frac{\pi^{d/2}}{2^{d-1} d\Gamma\left(\frac{d}{2}\right)} n_i \sigma_i^d. \tag{6}$$

Suspension model (5) has been recently employed to determine the Navier–Stokes transport coefficients of bidisperse granular suspensions[53] as well as the rheological properties in inertial suspensions of inelastic rough hard spheres under simple shear flow.[54]

Explicit forms of R_i have been displayed in the literature of polydisperse gas–solid flows.[40–42] In particular, we adopt the expression $\gamma_i = (18\eta_g/\rho\sigma_{12}^2)R_i$ proposed by Yin and Sundaresan.[41] Here, $\rho = \sum_i m_i n_i$ is the total mass density and

$$n_i = \int d\mathbf{v} f_i(\mathbf{v}) \tag{7}$$

is the number density of the component i. For a three-dimensional low-Reynolds-number fluid at moderate densities, the dimensionless function R_i is given by

$$R_i(\phi_i, \phi) = \frac{\rho\sigma_{12}^2}{\rho_i\sigma_i^2}\frac{(1-\phi)\phi_i\sigma_i}{\phi} \times \sum_{j=1}^{2}\frac{\phi_j}{\sigma_j}\left[\frac{10\phi}{(1-\phi)^2} + (1-\phi)^2\left(1+1.5\sqrt{\phi}\right)\right]. \tag{8}$$

At a kinetic level, one of the most relevant quantities for a binary mixture is the partial temperatures $T_i(t)$. They measure the mean kinetic energy of the component i and are defined as

$$T_i = \frac{1}{n_i d}\int d\mathbf{v}\, m_i v^2 f_i(\mathbf{v}). \tag{9}$$

Alternatively, the same information is provided by the temperature ratio $\theta(t) = T_1(t)/T_2(t)$ and the (total) temperature $T(t)$ of the mixture,

$$T(t) = x_1 T_1(t) + x_2 T_2(t), \tag{10}$$

where $x_i = n_i/(n_1+n_2)$ is the mole fraction of the component i. The ratios T_1/T and T_2/T can be easily expressed in terms of θ as

$$\frac{T_1}{T} = \frac{\theta}{1+x_1(\theta-1)}, \quad \frac{T_2}{T} = \frac{1}{1+x_1(\theta-1)}. \tag{11}$$

The evolution equations for both the temperature ratio θ and the (total) temperature T can be obtained by multiplying both sides of the Enskog equation (5) by $m_i v^2$ and integrating over velocity. They are given by

$$\frac{\partial}{\partial t}\ln T = 2x_1\gamma_1\frac{T_{ex}-T_1}{T} + 2x_2\gamma_2\frac{T_{ex}-T_2}{T}, \tag{12}$$

$$\frac{\partial}{\partial t}\ln\theta = 2\gamma_1\left(\frac{T_{ex}}{T_1}-1\right) - 2\gamma_2\left(\frac{T_{ex}}{T_1}\theta - 1\right) + \xi_2 - \xi_1, \tag{13}$$

where

$$\xi_i = -\frac{m_i}{dn_i T_i}\int d\mathbf{v}\, v^2 J_{ij}[f_i, f_j] \quad (i \neq j) \tag{14}$$

are the so-called partial production rates. They measure the rate of change of the kinetic energy of the particles of component i due to collisions with the particles of component j. Since the collisions are elastic, we have $x_1 T_1 \xi_1 + x_2 T_2 \xi_2 = 0$.

In the particular case of mechanically equivalent particles ($m_1 = m_2$, $\sigma_1 = \sigma_2$, and $\phi_1 = \phi_2$), the friction coefficients $\gamma_1 = \gamma_2 = \gamma$ and the solution to Eq. (13) is simply

$$T(t) = T_{ex} + [T(0) - T_{ex}]e^{-2\gamma t}. \tag{15}$$

Thus, since $\gamma > 0$, the temperature decays monotonically in time and the Mpemba effect is not present. However, when both components are different ($\gamma_1 \neq \gamma_2$), the evolution equations of $T(t)$ and $\theta(t)$ are coupled: the curve of the initially hotter (cooler) sample may cross that of the initally cooler (hotter) one and remain below (above) it until the systems reach equilibrium. This is the usual (or *inverse*) Mpemba-like effect.

According to Eq. (14), it is quite apparent that one needs to know the velocity distributions f_1 and f_2 to determine the partial production rates ξ_1 and ξ_2. Here, we estimate both production rates by taking the simplest approximation for the distributions f_1 and f_2, namely, the Maxwellian distributions $f_{i,M}$ defined with partial temperatures T_i,

$$f_{i,M}(\mathbf{v};t) = n_i\left(\frac{m_i}{2\pi T_i(t)}\right)^{d/2}\exp\left(-\frac{m_i v^2}{2T_i(t)}\right). \tag{16}$$

In the Maxwellian approximation, ξ_1 is given by[55–57]

$$\xi_1 = \frac{8\pi^{(d-1)/2}}{d\Gamma\left(\frac{d}{2}\right)} n_2\mu_{12}\mu_{21}\chi_{12}\sigma_{12}^{d-1}\left(\frac{2T_1}{m_1}+\frac{2T_2}{m_2}\right)^{1/2}\left(1-\frac{T_2}{T_1}\right). \tag{17}$$

The expression of ξ_2 can be easily inferred from Eq. (17) by making the change $1 \leftrightarrow 2$ in the subindexes. When energy equipartition holds ($T_1 = T_2$), $\xi_1 = \xi_2 = 0$ as expected. However, if energy equipartition is broken ($T_1 \neq T_2$), then $\xi_i \neq 0$.

In the long-time limit, the mixture achieves an equilibrium state where energy equipartition applies, $T_1^{eq} = T_2^{eq} = T_{eq} = T_{ex}$. However, in the transient regime, it is expected that energy equipartition fails and so, $T_1(t) \neq T_2(t)$. This means that the Mpemba effect in a driven molecular mixture stems from the nonequipartition of energy. Remarkably, this effect can be explained by computing ξ_i by a Maxwellian distribution, and hence, the existence of different partial temperatures is sufficient to explain such a memory effect.

In order to analyze the time dependence of $T(t)$ and $\theta(t)$, it is convenient to introduce dimensionless variables for temperature and time. Thus, we define $T^* = T/T_{ex}$ and $t^* = n\sigma_{12}^{d-1}\sqrt{4T_{ex}/(m_1+m_2)}t$. In the Maxwellian approximation, the evolution equations for T^* and θ can be easily derived from Eqs. (12), (13), and (17). After some algebra, one gets

$$\frac{\partial}{\partial t^*}\ln T^* = \Phi(T^*,\theta), \quad \frac{\partial}{\partial t^*}\ln\theta = \Psi(T^*,\theta), \tag{18}$$

where

$$\Phi(T^*,\theta) = \Phi_1(T^*) + \Phi_2(\theta), \qquad \Psi(T^*,\theta) = \Psi_1 + \Psi_2(T^*,\theta) + \Psi_3(T^*,\theta). \tag{19}$$

Here, we have introduced the quantities

Physics of Fluids ARTICLE scitation.org/journal/phf

$$\Phi_1(T^*) = \frac{2}{T^*}\left(x_1\gamma_1^* + x_2\gamma_2^*\right), \quad \Phi_2(\theta) = -2\frac{x_1\gamma_1^*\theta + x_2\gamma_2^*}{1 + x_1(\theta - 1)}, \tag{20}$$

$$\Psi_1 = -2(\gamma_1^* - \gamma_2^*), \quad \Psi_2(T^*, \theta) = 2\left(\gamma_1^* - \gamma_2^*\theta\right)\frac{1 + x_1(\theta - 1)}{\theta T^*}, \tag{21}$$

$$\Psi_3(T^*, \theta) = \frac{8\pi^{(d-1)/2}}{d\Gamma\left(\frac{d}{2}\right)}\chi_{12}\sqrt{\frac{T^*}{2}\frac{\mu_{12}\mu_{21}(\mu_{12} + \mu_{21}\theta)}{1 + x_1(\theta - 1)}} \times \left(x_1 - x_2 - x_1\theta + x_2\theta^{-1}\right), \tag{22}$$

where

$$\gamma_i^* = \frac{R_i}{\sqrt{2T_{\text{ex}}^*}(n_1 + n_2)\sigma_{12}^d}, \quad T_{\text{ex}}^* = \frac{2T_{\text{ex}}}{(m_1 + m_2)\sigma_{12}^2\gamma_0^2}. \tag{23}$$

As mentioned before, the dependence of Φ on θ is a necessary condition for the existence of the Mpemba-like effect.

III. MPEMBA-LIKE EFFECT FOR INITIAL STATES CLOSE TO EQUILIBRIUM

We consider two homogeneous states A and B characterized by their initial reduced temperatures $T_{I,0}^*$ and temperature ratios $\theta_{I,0}$, where $I = \text{A}, \text{B}$. For the sake of simplicity, we suppose that both states are hotter (cooler) than the equilibrium state, i.e., $T_{A,0}^* > 1$ and $T_{B,0}^* > 1$ ($T_{A,0}^* < 1$ and $T_{B,0}^* < 1$). Furthermore, we also assume that $T_{A,0}^* > T_{B,0}^* > 1$ ($T_{A,0}^* < T_{B,0}^* < 1$ for the cooler case). During the time evolution of the system toward equilibrium, the gas particles exchange energy with the thermal reservoir. This interaction is controlled by the friction coefficients $\gamma_i \propto R_i$, which exhibit a complex dependence on the mass and diameter ratios and the composition [see Eq. (8)]. Thus, the energy transfer (per particle) between each one of the components of the mixture and the background fluid could be more efficient (larger) for some values of m_i, σ_i, and x_i. So, as the energy transmission distinguishes between both components, the decay of the temperature until its equilibrium value will depend separately on the way of releasing energy from each component of the mixture to the bath, and consequently on the initial values of the partial temperatures $\theta_{I,0}$. This coupling between T^* and θ opens up the possibility of a crossroad between the trajectories of both temperatures (Mpemba-like effect), so that $T_A^* = T_B^*$ at some crossing time t_c^* before achieving the equilibrium state.

In order to quantify the constraints in the initial conditions of both trajectories needed for the existence of t_c^*, we consider first in this section initial states that are close to the final equilibrium state. Under these conditions, Eqs. (18) can be linearized around the equilibrium solution $T_{\text{eq}}^* = \theta_{\text{eq}} = 1$. Note that this is a special kind of linearization since *only* the global temperature and the temperature ratio are displaced with respect to their equilibrium values. As we show later, this approach will allow us to solve the corresponding set of linear differential equations and get analytical results.

Let us define $\delta T^* = T^* - 1$ and $\delta\theta = \theta - 1$. Substitution of these definitions into Eqs. (18) and retaining only linear terms in δT^* and $\delta\theta$, one gets

$$\frac{\partial}{\partial t^*}\begin{pmatrix}\delta T^* \\ \delta\theta\end{pmatrix} = \mathcal{L}\begin{pmatrix}\delta T^* \\ \delta\theta\end{pmatrix}, \tag{24}$$

where the matrix $\mathcal{L}$ is composed of the following elements:

$$\mathcal{L}_{11} = -2(x_1\gamma_1^* + x_2\gamma_2^*),$$
$$\mathcal{L}_{12} = 2x_1x_2(\gamma_2^* - \gamma_1^*), \quad \mathcal{L}_{21} = 2(\gamma_2^* - \gamma_1^*),$$
$$\mathcal{L}_{22} = -2(x_2\gamma_1^* + x_1\gamma_2^*) - \frac{4\pi^{(d-1)/2}}{d\Gamma\left(\frac{d}{2}\right)}\chi_{12}\sqrt{2\mu_{21}\mu_{12}}. \tag{25}$$

The solution to matrix equation (24) can be expressed in terms of the initial conditions δT_0^* and $\delta\theta_0$. After some algebra, the time evolution of the temperature $\delta T^*(t^*)$ reads

$$\delta T^*(t^*) = \frac{1}{\lambda_+ - \lambda_-}\left\{\left[(\mathcal{L}_{11} - \lambda_-)\delta T_0^* + \mathcal{L}_{12}\delta\theta_0\right]e^{\lambda_+ t^*} + \left[(\lambda_+ - \mathcal{L}_{11})\delta T_0^* - \mathcal{L}_{12}\delta\theta_0\right]e^{\lambda_- t^*}\right\}, \tag{26}$$

where

$$\lambda_\pm = \frac{1}{2}\left[\mathcal{L}_{11} + \mathcal{L}_{22} \pm \sqrt{(\mathcal{L}_{11} - \mathcal{L}_{22})^2 + 4\mathcal{L}_{12}\mathcal{L}_{21}}\right] \tag{27}$$

are the eigenvalues of the matrix $\mathcal{L}$. Two observations are in order here. On the one hand, $\lambda_\pm \leq 0$ for any choice of the system parameters since $\mathcal{L}_{11} + \mathcal{L}_{22} \leq 0$ and

$$(\mathcal{L}_{11} + \mathcal{L}_{22})^2 - \left[(\mathcal{L}_{11} - \mathcal{L}_{22})^2 + 4\mathcal{L}_{12}\mathcal{L}_{21}\right] = 8\left[2\gamma_1^*\gamma_2^* + \frac{4\pi^{(d-1)/2}}{d\Gamma\left(\frac{d}{2}\right)}\chi_{12}\sqrt{2\mu_{21}\mu_{12}}\left(x_1\gamma_1^* + x_2\gamma_2^*\right)\right] \geq 0. \tag{28}$$

Hence, Eq. (26) always describes an evolution of the system toward thermal equilibrium. On the other hand, from Eq. (26), it is obvious that any cooling process ($\delta T^* \geq 0$) has its associated heating process ($\delta T^* \leq 0$). One process can be obtained from the other one by a change of signs on the initial conditions: $\delta T_0^* \leftrightarrow -\delta T_0^*$ and $\delta\theta_0 \leftrightarrow -\delta\theta_0$. Hence, at the level of the linear theory, the Mpemba effect occurs if and only if the inverse Mpemba effect occurs, provided the initial conditions are related by the previous sign transformation.

In what follows, we will assume that the initial temperature of state A is greater than that of state B ($T_{A,0}^* > T_{B,0}^*$). From Eq. (26), we can now compute the possible crossing time t_c^* of both trajectories. Given that, in the linear case, this time is invariant under the heating or cooling problem, both cases may be considered simultaneously. From the condition $\delta T_A^*(t_c^*) = \delta T_B^*(t_c^*)$, we obtain the expression

$$t_c^* = \frac{1}{\lambda_- - \lambda_+}\ln\frac{\mathcal{L}_{12} + (\mathcal{L}_{11} - \lambda_-)\Delta T_0^*/\Delta\theta_0}{\mathcal{L}_{12} - (\lambda_+ - \mathcal{L}_{11})\Delta T_0^*/\Delta\theta_0}, \tag{29}$$

where $\Delta T_0^* = T_{A,0}^* - T_{B,0}^*$ and $\Delta\theta_0 = \theta_{A,0} - \theta_{B,0}$. In the linear theory, for given values of the parameters of the mixture, the crossover time t_c^* depends on the initial conditions *only* through the single control parameter $\Delta T_0^*/\Delta\theta_0$. Moreover, since $t_c^* \in \mathbb{R}^+$ and being aware of the inequality $\lambda_+ > \lambda_-$, the argument of the logarithm in Eq. (29) shall fall within the interval (0, 1). Due to this restriction, the initial values must satisfy the following conditions:

Physics of Fluids ARTICLE scitation.org/journal/phf

$$\frac{\Delta T_0^*}{\Delta\theta_0} \in \left(0, \frac{\mathcal{L}_{12}}{\lambda_- - \mathcal{L}_{11}}\right) \quad \text{if} \quad \mathcal{L}_{12} < 0 \Longleftrightarrow \gamma_1^* > \gamma_2^*,$$
$$\frac{\Delta T_0^*}{\Delta\theta_0} \in \left(\frac{\mathcal{L}_{12}}{\lambda_- - \mathcal{L}_{11}}, 0\right) \quad \text{if} \quad \mathcal{L}_{12} > 0 \Longleftrightarrow \gamma_1^* < \gamma_2^*. \tag{30}$$

According to Eq. (30), when $\mathcal{L}_{12} < 0$ or equivalently $\gamma_1^* > \gamma_2^*$ ($\mathcal{L}_{12} > 0$ or equivalently $\gamma_1^* < \gamma_2^*$), since $\lambda_- - \mathcal{L}_{11} < 0$, the control parameter is $\Delta T_0^*/\Delta\theta_0 > 0$ ($\Delta T_0^*/\Delta\theta_0 < 0$) and its maximum (minimum) value for which the Mpemba effect can be observed is $\mathcal{L}_{12}/(\lambda_- - \mathcal{L}_{11})$. This quantity provides the phase diagram for the occurrence of the Mpemba effect, as shown in the upper panels of Figs. 1–3. Here, it is important to study the singularity in the control parameter that emerges if $\theta_{A,0} = \theta_{B,0}$. In this case, the kinetic variables (partial temperatures) are not present in the early relative evolution of the macroscopic fields, T_A and T_B, and therefore, the Mpemba-like effect does not occur.

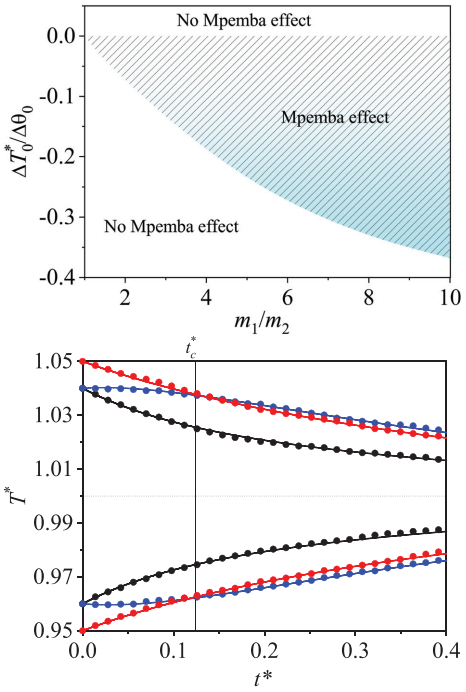

FIG. 1. Upper panel: Phase diagram of the initial condition $\Delta T_0^*/\Delta\theta_0$ as a function of the mass ratio m_1/m_2. Lower panel: Relaxation of the (reduced) temperature T^* over the time t^* for $m_1/m_2 = 10$. The upper and lower curves correspond to the cooling and heating cases, respectively. Solid lines represent theoretical values and symbols DSMC data. The initial values of the control parameter $\Delta T_0^*/\Delta\theta_0 \equiv (T_{A,0}^* - T_{B,0}^*)/(\theta_{A,0} - \theta_{B,0})$ are 0.2 (A: red line and symbols; B: black lines and symbols), and −0.2 (A: red lines and symbols; B: blue lines and symbols). The theoretical value of t_c^* is also plotted with a vertical line. The remaining parameters in both panels are $d = 3$, $T_{ex}^* = 1$, $x_1 = \frac{1}{2}$, $\sigma_1/\sigma_2 = 1$, and $\phi = 0.1$.

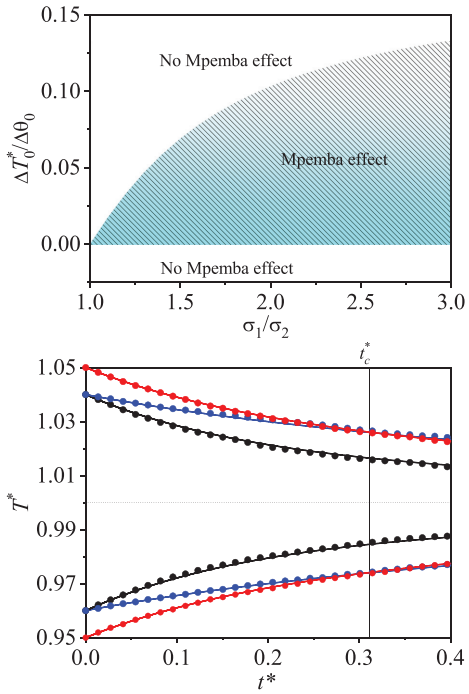

FIG. 2. Upper panel: Phase diagram of the initial condition $\Delta T_0^*/\Delta\theta_0$ as a function of the size ratio σ_1/σ_2. Lower panel: Relaxation of the (reduced) temperature T^* over the time t^* for $\sigma_1/\sigma_2 = 3$. The upper and lower curves correspond to the cooling and heating cases, respectively. Solid lines represent theoretical values and symbols DSMC data. The initial values of the control parameter $\Delta T_0^*/\Delta\theta_0 \equiv (T_{A,0}^* - T_{B,0}^*)/(\theta_{A,0} - \theta_{B,0})$ are 0.1 (A: red lines and symbols; B: blue lines and symbols), and −0.2 (A: red lines and symbols; B: black lines and symbols). The theoretical value of t_c^* is also plotted with a vertical line. The remaining parameters in both panels are $d = 3$, $T_{ex}^* = 1$, $x_1 = \frac{1}{2}$, $m_1/m_2 = 1$, and $\phi = 0.1$.

To illustrate the dependence of the required initial conditions on the parameters of the system, we consider a three-dimensional ($d = 3$) system. In this case, a good approximation for the pair correlation functions χ_{ij} are given by[58–60]

$$\chi_{ij} = \frac{1}{1-\phi} + \frac{3}{2}\frac{\phi}{(1-\phi)^2}\frac{\sigma_i\sigma_j M_2}{\sigma_{ij} M_3} + \frac{1}{2}\frac{\phi^2}{(1-\phi)^3}\left(\frac{\sigma_i\sigma_j M_2}{\sigma_{ij} M_3}\right)^2, \tag{31}$$

where $M_\ell = \sum_i x_i \sigma_i^\ell$.

As said before, the upper panels of Figs. 1–3 show the phase diagram of the initial conditions $\Delta T_0^*/\Delta\theta_0$ as a function of the mass m_1/m_2 and size σ_1/σ_2 ratios and concentration x_1, respectively. We

Physics of Fluids ARTICLE scitation.org/journal/phf

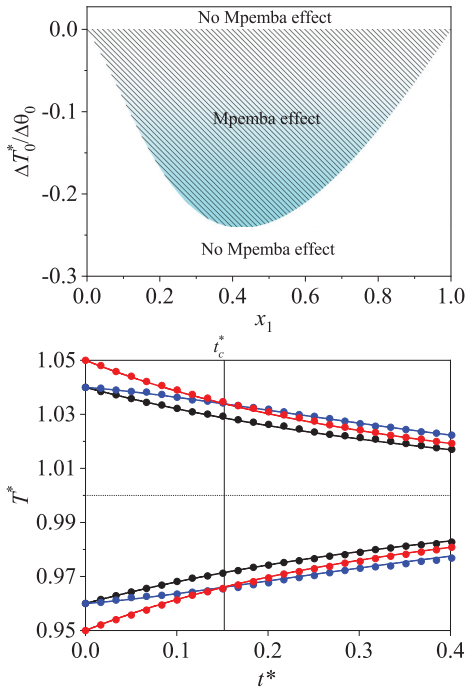

FIG. 3. Upper panel: Phase diagram of the initial condition $\Delta T_0^*/\Delta\theta_0$ as a function of the concentration x_1. Lower panel: Relaxation of the (reduced) temperature T^* over the time t^* for $x_1 = 0.4$. The upper and lower curves correspond to the cooling and heating cases, respectively. Solid lines represent theoretical values and symbols DSMC data. The initial values of the control parameter $\Delta T_0^*/\Delta\theta_0 \equiv (T_{A,0}^* - T_{B,0}^*)/(\theta_{A,0} - \theta_{B,0})$ are -0.1 (A: red lines and symbols; B: blue lines and symbols), and -0.5 (A: red lines and symbols; B: black lines and symbols). The theoretical value of t_c^* is also plotted with a vertical line. The remaining parameters in both panels are $d = 3$, $T_{ex}^* = 1$, $m_1/m_2 = 5$, $\sigma_1/\sigma_2 = 1$, and $\phi = 0.1$.

consider a binary molecular mixture of moderate density ($\phi = 0.1$). If we focus on Fig. 1, we see that $\Delta T_0^*/\Delta\theta_0 < 0$ when $m_1 > m_2$. For a better understanding, let us consider an equimolar binary mixture ($x_1 = \frac{1}{2}$) with two components of identical diameters ($\sigma_1 = \sigma_2$) but different masses ($m_1 \neq m_2$). In these conditions, according to Eq. (6), $\gamma_i^* \propto m_i^{-1}$ and so, $\gamma_1^* < \gamma_2^*$ when $m_1 > m_2$. This means that the lighter component interchanges energy with the bath in a more efficient way than the heavier component. In addition, if we want a reduction in the relaxation time, the component whose partial temperature is further from T_{ex} must be the one whose interaction with the bath is more effective. Since $\Delta T_0^* > 0$ ($T_A^* > T_B^*$), then $\Delta\theta_0 < 0$, namely, the initially hotter system has its kinetic energy more concentrated in the lighter component than in the heavier one. This conclusion agrees with the second condition of Eq. (30). As expected, the boundary between both regions, given by the extreme value $\mathcal{L}_{12}/(\lambda_- - \mathcal{L}_{11})$, decreases with increasing the mass ratio and hence, the discrimination between both species in the exchange of energy with the bath. Similar behavior is found in the upper panel of Fig. 2. Here, we vary the diameters of particles while keeping $m_1 = m_2$. According to Eq. (6), $\gamma_i^* \propto \sigma_i$ and so, $\gamma_1^* > \gamma_2^*$ when $\sigma_1 > \sigma_2$. This implies that $\Delta T_0^*/\Delta\theta_0 > 0$ in agreement with the first condition of Eq. (30). Conversely, the shape of the phase diagram shown in the upper panel of Fig. 3 cannot be qualitatively explained with arguments based on individual properties (such as mass or size) but on collective behavior. As can be noted, the Mpemba effect manifests clearer when there are more particles that interact in a more efficient way with the bath. However, the mixture must also be diversified so there can be more discrepancy between both partial and total temperatures. An example of the competition between both mechanisms is plotted in the phase diagram of Fig. 3 for $m_1 = 5m_2$.

The lower panels of Figs. 1–3 display the relaxation curves of the reduced temperature T^* as a function of the scaled time t^* for some of the mixture parameters considered in the phase diagrams described before. Three different initial conditions are chosen in every figure. Specific details of the initial conditions used in the above panels can be found in Table I. According to these initial values, the control parameter $\Delta T_0^*/\Delta\theta_0$ is greater than or less than 0, and within or without the region limited by $\mathcal{L}_{12}/(\lambda_- - \mathcal{L}_{11})$. In this way, the fulfillment of restrictions (30) is checked in both cooling and heating (inverse Mpemba effect) situations. The solid lines are the theoretical results displayed in Eq. (26) and symbols refer to the results obtained via DSMC simulations. We found an excellent agreement between theory and simulations in all three cases, ensuring the accuracy of Maxwellian approximation (16) to capture the trends of the Mpemba effect. Furthermore, the theoretical prediction for t_c^* exhibits also an excellent agreement with simulations.

DSMC simulations have been carried out following similar steps as those carried out in Ref. 44. At the initial state, one assigns velocities to the particles drawn from Gaussian distributions at the desired partial temperatures. Since the system is assumed to be spatially homogeneous, the velocities of the particles change only due to binary collisions. It includes two physical events: (i) collisions among particles and (ii) collisions of the particles with an external energy source (bath). In the case of event (i), we consider the same algorithm as

TABLE I. Initial values of the (reduced) temperatures T_0^* and temperature ratios θ_0 used to generate the relaxation curves shown in the lower panels of Figs. 1–3.

	Figure 1		Figure 2		Figure 3	
Color of lines and symbols	T_0^*	θ_0	T_0^*	θ_0	T_0^*	θ_0
Cooling cases						
Red	1.05	1.06	1.05	1.11	1.05	1.01
Blue	1.04	1.11	1.04	1.01	1.04	1.11
Black	1.04	1.01	1.04	1.16	1.04	1.03
Heating cases						
Red	0.95	0.94	0.95	0.89	0.95	0.99
Blue	0.96	0.89	0.96	0.99	0.96	0.89
Black	0.96	0.99	0.96	0.84	0.96	0.97

Physics of Fluids ARTICLE scitation.org/journal/phf

proposed by Bird[43] but, in this case, the collision rate is enhanced by a factor that accounts for the spatial correlations.[45] In the case of event (ii), we impose a simultaneous change of all velocities of particles every time step Δt. For a particle of species i and velocity $\mathbf{v}$, the collision with the bath is given by

$$\mathbf{v} \to e^{-\gamma_i \Delta t}\mathbf{v} + \left(\frac{6\gamma_i T_{\text{ex}}}{m_i}\Delta t\right)^{\frac{1}{2}}\mathbf{w}, \tag{32}$$

where $\mathbf{w}$ is a random vector uniformly distributed in $[-1,1]^3$. In Ref. 29, it was shown that these two events (i) and (ii) give rise to the Boltzmann kinetic equation if Δt is taken to be much smaller than the mean free time τ of inter-particle collisions. In our case, we always take $\Delta t/\tau < 10^{-3}$.

As a complement of Figs. 1–3, a density plot of the critical value $\mathcal{L}_{12}/(\lambda_- - \mathcal{L}_{11})$ as a function of the mass and size ratios is plotted in Fig. 4 for an equimolar mixture ($x_1 = \frac{1}{2}$). Although these parameters have similar but opposite influences on the onset of the Mpemba effect, the graphic reveals that discrimination in the diameters of particles (seen as a difference in the surface areas) has a more prominent role in the emergence of the phenomenon than in the masses (seen as a distinction in the inertial forces).

IV. LARGE MPEMBA-LIKE EFFECT IN MOLECULAR MIXTURES

In Sec. III, we have dealt with states which have been initially prepared in conditions close to thermal equilibrium. This has permitted us to linearize Eqs. (18) around the equilibrium solution and provide precise analytical results both for the time evolution of the temperature and for the crossing time. Here, we consider more general conditions, allowing the system to start away from equilibrium. In these cases, we see that the relaxation curves may cross each other in a similar way to that described in Sec. II. Unfortunately, no simple analytical expression for the crossing time t_c^* is found and a more qualitative analysis is required to establish a necessary (but not sufficient) condition for the occurrence of the Mpemba effect.

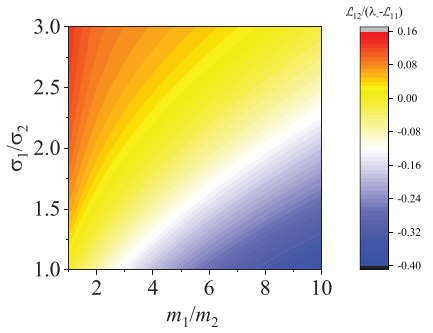

FIG. 4. Density plot of the critical value $\mathcal{L}_{12}/(\lambda_- - \mathcal{L}_{11})$ as a function of the mass m_1/m_2 and size σ_1/σ_2 ratios for an equimolar mixture ($x_1 = \frac{1}{2}$) of hard spheres ($d = 3$). The remaining parameters are $T_{\text{ex}}^* = 1$ and $\phi = 0.1$.

In this section, we analyze crossovers in the temperature transitions from initial situations far away from equilibrium. Thus, the distances between the initial temperatures are assumed to be of the same order as the temperatures themselves. A remarkable fact of this kind of transitions is the asymmetry between the cooling and heating processes produced by the term $\xi_2^* - \xi_1^*$ of Eq. (13). Given two initial temperatures $T_A > T_B$, both at the same distance from equilibrium ($T_A > T_{\text{ex}} > T_B$; $|T_A - T_{\text{ex}}| = |T_B - T_{\text{ex}}|$), one may think that the time to relax is exactly the same in both cases when the temperature ratios $\theta_{A,B}$ are also equally separated from their equilibrium values, in accordance with the linear theory of Sec. III. Nevertheless, on average, particles of system A move more energetically than those of system B and so, the mean free time among collisions of species 1 and 2 of system A is shorter. Hence, the flux of linear momentum is more effective and, as a consequence, relaxation toward the external temperature turns out to be faster. This symmetry breaking results in discrimination between cooling and heating processes in such a way that, for the same initial ratio $\Delta T_0^*/\Delta\theta_0$, the Mpemba effect could only be observed in one of these scenarios.

Let us consider again two homogeneous states A and B arbitrary far away from equilibrium. They are characterized by the initial temperatures $T_{A,0}^*$ and $T_{B,0}^*$ and the temperature ratios $\theta_{A,0}$ and $\theta_{B,0}$. In what follows, for the sake of simplicity, we will suppose that the state A is initially hotter than B ($T_{A,0}^* > T_{B,0}^*$). Under this condition, a physically intuitive necessary condition for a crossover (Mpemba-like effect) in the relaxation curves of both temperatures is that the initially hotter system cools faster than the cooler one. This crossover is expected to happen in the early stage of the evolution where the system still puts away memory of its initial preparation. Following the arguments of Torrente *et al.*,[23] for short enough times, we can assume that the system is exponentially cooling with a characteristic rate roughly equal to the initial value of $-\Phi$ [see Eq. (18)]. Thus, a necessary condition for the presence of the Mpemba effect is $\Phi(T_{B,0}^*, \theta_{B,0}) > \Phi(T_{A,0}^*, \theta_{A,0})$. So, it seems that the function $\Phi(T^*, \theta)$, through its dependence on the variables T^* and θ, is the key quantity for determining when the Mpemba effect can occur.

Let us then analyze Eq. (19) to establish some restrictions to the initial conditions of states A and B. The function $\Phi(T^*, \theta)$ is the sum of two functions $\Phi_1(T^*)$ and $\Phi_2(\theta)$. Thus, all the information about the relative behavior of T_I^* ($I = $A,B) at the initial stages (for fixed T_I^*) falls on the function $\Phi_2(\theta_I)$. The next step is to ensure the functions $\Phi(T^*, \theta)$ behave monotonically with θ; so that, we can establish a criterion for what the temperatures T_A^* and T_B^* will get closer or away from each other. Only the first option will be considered here as a simple way to attain the Mpemba effect (in fact, there are other more complex ways the relaxation curves may cross as occurs for instance in the nonmonotonic Kovacs-like relaxation[61]).

Therefore, to check the occurrence of the Mpemba effect, we perform the derivative of Φ_2 with respect to θ at fixed T^*. The result is

$$\frac{\partial}{\partial\theta}\Phi_2 = \frac{2x_1x_2(\gamma_2^* - \gamma_1^*)}{(x_2 + x_1\theta)^2}, \tag{33}$$

which is always a positive (negative) function if $\gamma_2^* > \gamma_1^*$ ($\gamma_2^* < \gamma_1^*$). Consequently, assuming that the temperature evolves monotonically toward equilibrium, the presence of the Mpemba effect requires that the initial values satisfy the conditions,

Physics of Fluids ARTICLE scitation.org/journal/phf

$$\begin{aligned} \frac{\Delta T_0^*}{\Delta\theta_0} > 0, \quad \gamma_1^* > \gamma_2^*, \\ \frac{\Delta T_0^*}{\Delta\theta_0} < 0, \quad \gamma_1^* < \gamma_2^*. \end{aligned} \tag{34}$$

Equation (34) is in agreement with results (30) derived for initial situations near to equilibrium. However, Eq. (34) does not constraint the regions of initial conditions that turn out in a crossover of temperatures. Namely, the difference between $\Phi(T_{A,0}^*, \theta_{A,0})$ and $\Phi(T_{B,0}^*, \theta_{B,0})$ must be properly chosen to be large enough.

According to Eq. (18), the slope of the curve $T^*(t^*)$ is really the product $T^*\Phi$. Thus, one is tempted to conclude that the necessary condition for the presence of the Mpemba-like effect is $\Phi(T_{B,0}^*, \theta_{B,0})T_{B,0} > \Phi(T_{A,0}^*, \theta_{A,0})T_{A,0}$. On the other hand, since $T_{A,0} > T_{B,0}$, the Mpemba effect cannot occur *unless* $\Phi(T_{B,0}^*, \theta_{B,0}) > \Phi(T_{A,0}^*, \theta_{A,0})$. Therefore, the fulfillment of Eq. (34) is required to observe the Mpemba-like effect.

The large Mpemba-like effect for heating and cooling processes is plotted in Fig. 5 for different initial conditions. Theoretical results are compared against DSMC and MD simulations. The MD simulations have been conducted as follows. The system is initially prepared in a spatially homogeneous state with each of the components of the mixture having Gaussian velocity distributions with different temperatures. The system then evolves using an event-driven algorithm. As in the case of DSMC simulations, two physical events are considered:

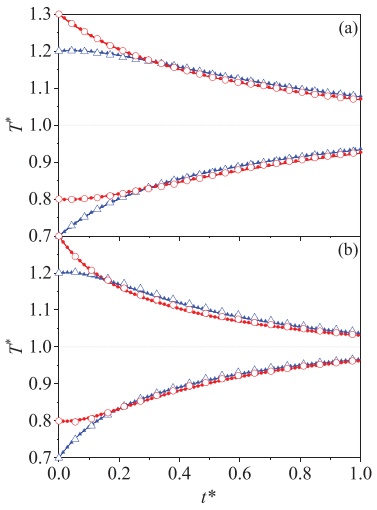

FIG. 5. Evolution of the (reduced) temperature T^* over the time t^* for $m_1/m_2 = 10$, $\sigma_1/\sigma_2 = 1$, $x_1 = \frac{1}{2}$, $d = 3$, and $T_{ex}^* = 1$. Solid lines represent theoretical values, filled symbols DSMC data, and open symbols MD data. The initial values of the control parameter $\Delta T_0^*/\Delta\theta_0 \equiv (T_{A,0}^* - T_{B,0}^*)/(\theta_{A,0} - \theta_{B,0})$ (a: red line and symbols; b: blue line and symbols) are -0.2 (cooling cases), -0.25 [heating case of panel (a)], and $-1/3$ [heating case of panel (b)]. Panel (a) corresponds to $\phi = 0.007\,85$ and panel (b) to $\phi = 0.1$.

TABLE II. Initial values of the (reduced) temperatures T_0^* and temperature ratios θ_0 used to generate the relaxation curves shown in Fig. 5.

	Panel (a)		Panel (b)	
Color of lines and symbols	T_0^*	θ_0	T_0^*	θ_0
Cooling cases				
Red	1.3	1.1	1.3	1.1
Blue	1.2	1.6	1.2	1.6
Heating cases				
Red	0.8	0.5	0.8	0.5
Blue	0.7	0.9	0.7	0.8

(i) collisions among particles and (ii) collisions of the particles with the external bath. For the event (i), we proceeded as usual; see, for instance, Refs. 46 and 47. In the event (ii), we impose a simultaneous change of all velocities of particles every time step Δt. This latter procedure is detailed in Eq. (32).

In Fig. 5, we consider an equimolar ($x_1 = \frac{1}{2}$) binary mixture of hard spheres ($d = 3$) of the same size ($\sigma_1 = \sigma_2$) and different masses ($m_1 = 10m_2$) for two different densities: $\phi = 0.007\,85$ (very dilute system) and $\phi = 0.1$ (moderately dense system). Lines are the theoretical results as derived from the Enskog equation, filled symbols refer to the results obtained via DSMC simulations and open symbols to those obtained by means of MD simulations. When $\phi = 0.007\,85$, $\gamma_1^* = 0.241$, and $\gamma_2^* = 2.411$, while the friction parameters are $\gamma_1^* = 0.445$ and $\gamma_2^* = 4.451$ when $\phi = 0.1$. Therefore, since $\gamma_1^* < \gamma_2^*$ in both cases, initial conditions must be chosen in such a way that $\Delta T_0^*/\Delta\theta_0 < 0$ (see Table II for more details). In addition, the functions $\Phi(T_I^*, \theta_I)$ are separately selected for the cooling and heating cases to enable the intersection of the respective temperature curves. It is quite apparent from the plots of Fig. 5 that the Mpemba-like effect emerges in both (cooling and heating) relaxation problems, even when the relative differences in the initial temperatures are around 10%. Moreover, the panels (a) and (b) of Fig. 5 highlight an excellent agreement between the Enskog theory and both DSMC and MD simulations in both the low-density regime ($\phi = 0.007\,85$) and for moderate densities ($\phi = 0.1$). This good agreement ensures once again the reliability of the Maxwellian approximation (16) as well as the accuracy of the molecular chaos hypothesis for studying this kind of relaxation process. The excellent agreement found in the crossing time t_c^* and in the complete relaxation toward the final equilibrium state makes the Enskog kinetic theory a very reliable theory for modeling molecular fluids at moderate densities.

V. MPEMBA-LIKE EFFECT IN GRANULAR BINARY MIXTURES. PRELIMINARY RESULTS

We assume now that the components of the mixture have macroscopic dimensions (typically of the order of micrometers or larger), and so their collisions are *inelastic*. We also assume that these particles (or grains) are in rapid flow conditions so that, they behave like a gas of activated collisional grains (granular gas).[27,37] It is well-known that in this regime, kinetic theory tools are appropriate to describe the dynamics of the system.

Physics of Fluids ARTICLE scitation.org/journal/phf

For granular mixtures suspended in a background fluid, the Enskog–Fokker–Planck equation (5) still applies, except that the Boltzmann–Enskog collision operator reads[27]

$$J_{ij}^{(\alpha_{ij})}[\mathbf{v}_1|f_i,f_j] = \chi_{ij}\sigma_{ij}^{d-1}\int d\mathbf{v}_2\int d\hat{\boldsymbol{\sigma}}\,\Theta(\hat{\boldsymbol{\sigma}}\cdot\mathbf{g}_{12}) \times(\hat{\boldsymbol{\sigma}}\cdot\mathbf{g}_{12})\left[\alpha_{ij}^{-2}f_i(\mathbf{v}_1'')f_j(\mathbf{v}_2'')-f_i(\mathbf{v}_1)f_j(\mathbf{v}_2)\right], \quad (35)$$

where α_{ij} is the coefficient of normal restitution for collisions between particles of components i and j. Here, the coefficient α_{ij} is assumed to be a positive constant smaller than or equal to 1. The limit case $\alpha_{ij}=1$ corresponds to elastic collisions. In Eq. (35), the double primes denote the precollisional velocities $(\mathbf{v}_1'',\mathbf{v}_2'')$ yielding the postcollisional velocities $(\mathbf{v}_1,\mathbf{v}_2)$. They satisfy the collision rule,

$$\mathbf{v}_1'' = \mathbf{v}_1-\mu_{ji}\frac{1+\alpha_{ij}}{\alpha_{ij}}(\hat{\boldsymbol{\sigma}}\cdot\mathbf{g}_{12})\hat{\boldsymbol{\sigma}}, \quad (36)$$

$$\mathbf{v}_2'' = \mathbf{v}_2+\mu_{ij}\frac{1+\alpha_{ij}}{\alpha_{ij}}(\hat{\boldsymbol{\sigma}}\cdot\mathbf{g}_{12})\hat{\boldsymbol{\sigma}}. \quad (37)$$

The operator $J_{ij}^{(\alpha_{ij})}$ denotes the *inelastic* Enskog–Boltzmann collision operator. When $\alpha_{ij}=1$, its elastic version $J_{ij}^{(1)}$ is given by Eq. (2).

The study of the Mpemba-like effect for driven granular mixtures follows similar mathematical steps as those made in Secs. III and IV for molecular mixtures. Thus, the set of differential equations (18) provides the evolution of the (reduced) temperature T^* and the temperature ratio θ. However, the final forms of the functions Φ and Ψ for inelastic collisions [see Eqs. (A2)–(A7) of the Appendix] appearing in the above set of differential equations are much more intricate than those obtained for molecular gases.

Nonetheless, preliminary straightforward results can be derived if we realize that the dependence of the function $\Phi(T^*,\theta) = \Phi_1(T^*)+\Phi_2(\theta)+\Phi_3(T^*,\theta)$ on inelasticity is fully encoded in the cooling term Φ_3. This cooling term vanishes for elastic collisions ($\Phi_3=0$ when $\alpha_{ij}=1$). Thus, to establish some criterion on the emergence of the Mpemba-like effect, the function Φ is conveniently separated into its entirely molecular part $\Phi_{12}\equiv\Phi_1+\Phi_2$ and the granular term Φ_3.

Let us consider again two different homogeneous samples A and B at different initial granular temperatures $T_{I,0}^*$ and temperature ratios $\theta_{I,0}$, where $I=A,B$. In order to compare the relative behavior between the two slopes Φ_A and Φ_B at the initial stages of the evolution, the steady values of the molecular $\Phi_1(T_s^*)+\Phi_2(\theta_s)$ and the granular $\Phi_3(T_s^*,\theta_s)$ terms are subtracted from their nonsteady slopes $\Phi_1(T^*)+\Phi_2(\theta)$ and $\Phi_3(T^*,\theta)$, respectively. Thus, we can quantify the influence of the granular terms on the relative distance between the relaxation curves and, hence, on the onset of the Mpemba effect.

The set of coupled equations for obtaining the steady forms of both T_s^* and θ_s are given by Eqs. (A9) and (A10). It is quite apparent from Fig. 6 that the granular term Φ_3 has substantially less influence on the relative behavior of the temperature relaxation of two given samples than the molecular counterpart $\Phi_1+\Phi_2$ at moderate values of the coefficients of restitution α_{ij}. In this way, similar conditions to those previously obtained for driven molecular mixtures can be established for granular mixtures to chose the initial values of T^* and θ for the occurrence of the Mpemba-like effect.

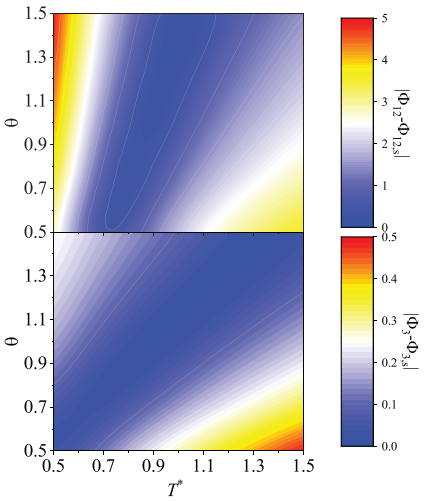

FIG. 6. Density plot of the difference $|\Phi_{12}-\Phi_{12,s}|$ (top panel) and $|\Phi_3-\Phi_{3,s}|$ (bottom panel) as a function of the (reduced) temperature T^* and temperature ratio θ for a granular mixture with a common coefficient of restitution $\alpha_{11}=\alpha_{22}=\alpha_{12}\equiv\alpha=0.9$. The parameters of the mixture are given by $m_1/m_2=10$, $\sigma_1/\sigma_2=1$, $x_1=0.5$, $d=3$, $\phi=0.1$, and $T_{ex}^*=1$. Here, $\Phi_{12}=\Phi_1+\Phi_2$.

Here, as an illustration of the Mpemba-like effect in granular mixtures, the time evolution of T^* is plotted in Fig. 7 for heating and cooling processes. For the sake of comparison, we consider a binary granular suspension with the same mechanical properties as those considered in panel (b) of Fig. 5, except that now the collisions are inelastic. Two different values of the (common) coefficient of restitution $\alpha\equiv\alpha_{11}=\alpha_{22}=\alpha_{12}$ are selected: (a) $\alpha=0.9$ and (b) $\alpha=0.8$. Lines are the theoretical results derived from the Enskog equation conveniently adapted to inelastic collisions (see the Appendix) and symbols refer to the results obtained via DSMC simulations. Since the friction parameters are $\gamma_1^*=0.445$ and $\gamma_2^*=4.451$ in both cases, similar arguments than those derived in the molecular case are set out for the initial conditions to satisfy the relation $\Delta T_0^*/\Delta\theta_0<0$ (more details can be found in Table III). Figure 7 illustrates the emergence of the Mpemba-like effect (and its inverse counterpart) in granular gases when the initial conditions are relatively far away from each other (large Mpemba-like effect). In addition, panels (a) and (b) of Fig. 7 show an excellent agreement between the Enskog theory and DSMC simulations ensuring again the reliability of the Maxwellian approximation used to compute the partial production rates ξ_i given in Eq. (A1).

VI. DISCUSSION

In summary, we have observed a Mpemba-like effect in a molecular binary mixture in contact with a thermal reservoir. As usual,[30,34–36] the bath acts on molecules as they were Brownian

Physics of Fluids ARTICLE scitation.org/journal/phf

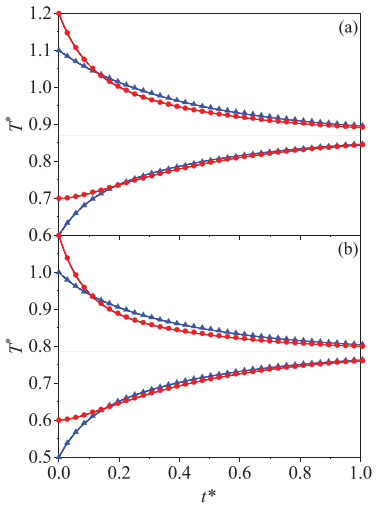

FIG. 7. Evolution of the (reduced) temperature T^* over the time t^* for a granular mixture with a common coefficient of restitution $\alpha_{11} = \alpha_{22} = \alpha_{12} \equiv \alpha$. The parameters of the mixture are given by $m_1/m_2 = 10$, $\sigma_1/\sigma_2 = 1$, $x_1 = \frac{1}{2}$, $d = 3$, $\phi = 0.1$, and $T_{ex}^* = 1$. Solid lines represent theoretical values and symbols DSMC data. The initial values of the control parameter $\Delta T_0^*/\Delta\theta_0 \equiv (T_{A,0}^* - T_{B,0}^*)/(\theta_{A,0} - \theta_{B,0})$ (A: red line and symbols; B: blue line and symbols) are -0.25 (cooling cases), $-1/3$ (heating cases). Panel (a) corresponds to $\alpha = 0.9$ and panel (b) to $\alpha = 0.8$.

particles, i.e., the interaction between gas particles and the thermal reservoir (or background fluid) is accounted for by two forces: a (deterministic) viscous drag force proportional to the velocity of the particles and a stochastic force. Moreover, based on numerical and experimental results carried out in the gas–solid–flows literature,[40–42] the friction coefficients γ_i $(i = 1, 2)$ have been chosen to distinguish between components of the mixture through their dependence on the mechanical properties of particles (masses m_i and diameters σ_i) and on the partial ϕ_i and global $\phi = \phi_1 + \phi_2$ volume fractions. This discrimination

TABLE III. Initial values of the (reduced) temperatures T_0^* and temperature ratios θ_0 used to generate the relaxation curves shown in Fig. 7.

	Panel (a)		Panel (b)	
Color of lines and symbols	T_0^*	θ_0	T_0^*	θ_0
Cooling cases				
Red	1.2	0.9	1.1	0.8
Blue	1.1	1.3	1.0	1.2
Heating cases				
Red	0.7	0.5	0.6	0.4
Blue	0.6	0.8	0.5	0.7

couples the evolution of the total temperature $T(t)$ with the ratio of partial temperatures $\theta(t) = T_1(t)/T_2(t)$ giving rise to the emergence of memory effects. Namely, the time evolution of $T(t)$ is not autonomous but is coupled to $\theta(t)$. One of the most popular problems in which memory effects are notorious is the so-called Mpemba effect,[1] namely, when an initially hotter (cooler) system cools (heats) sooner.

To observe this effect, two identical samples A and B (namely, sharing the same values of masses, diameters, composition, and volume fraction) are initially prepared in isotropic Maxwellian velocity distribution functions at different temperatures ($T_{A,0}$ and $T_{B,0}$) and temperature ratios ($\theta_{A,0}$ and $\theta_{B,0}$). These samples are in contact with a thermal reservoir at temperature T_{ex}. Starting from the above initial conditions, we let the samples evolve until they reach the equilibrium state where energy equipartition holds: $T_i = T_{1,i} = T_{2,i} = T_{ex}$ $(i = A, B)$. During this transient period, particles of the mixture collide among themselves and with the bath exchanging energy in different ways for each component. If we suitable chose the initial values of the total and the partial temperatures, the curves associated with the relaxation of the temperatures $T_A(t)$ and $T_B(t)$ may cross at a given time t_c before reaching the equilibrium state (the so-called crossover time). Contrary to other works on this topic, neither cumulants[22] (measuring the deviations of the distribution functions from their Maxwellian forms) nor the inclusion of a nonlinear drag force[28] is needed to explain the Mpemba effect and hence, the magnitude of the effect may be increased.

The starting point of our theoretical approach has been the Enskog kinetic equation (1) in combination with the Fokker–Planck term accounting for the interaction between gas particles and the thermal reservoir. From this equation, the evolution equations for the total temperature $T(t)$ and the temperature ratio $\theta(t)$ have been derived. To get explicit results, the partial production rates ξ_1 and ξ_2 appearing in the evolution equation (13) of θ have been estimated by replacing the exact distribution functions $f_i(\mathbf{v}; t)$ by their Maxwellian forms (16).

Evolution equations (18) for the reduced quantities $T^* = T/T_{ex}$ and θ have been first analytically solved for situations close to equilibrium. This has allowed us to obtain *explicit* expressions for the (reduced) crossing time t_c^* and the critical value of the initial temperature difference [see Eqs. (29) and (30)]. In addition, the numerical solution of the set of Eqs. (18) provides the dependence of $T^*(t^*)$ and $\theta(t^*)$ on the parameters of the mixture. An illustration of the above results is displayed in Figs. 1–3 where we have varied the mass m_1/m_2 and diameter σ_1/σ_2 ratios and the composition x_1, respectively. The comparison between those theoretical (approximate) predictions with the DSMC results shows an excellent agreement for the whole range of parameters studied.

As a complement of the previous study, we have analyzed the Mpemba effect when the initial states of the samples are far from equilibrium, the so-called large Mpemba effect. In this situation, no analytical solution is admitted and *only* qualitative predictions can be achieved. For the crossover to happen, a necessary criterion for the sign of the initial fraction $\Delta T_0^*/\Delta\theta_0 = (T_{A,0}^* - T_{B,0}^*)/(\theta_{A,0} - \theta_{B,0})$ has been established. This criterion is based on the efficiency or rapidity (measured through the comparison of the two drag coefficients γ_i^*) of each one of the partial temperatures to reach equilibrium. Two examples of cooling and heating relaxation processes for a dilute and a moderately dense system have been plotted in Fig. 5. In particular, the Mpemba-like effect has been shown to take place even when the

Physics of Fluids ARTICLE scitation.org/journal/phf

relative initial temperature difference is around 10%. Moreover, an excellent agreement between theoretical results and both DSMC and MD simulations has been also found.

Finally, we have also considered driven granular mixtures, namely, a collection of discrete macroscopic particles of different sizes. Due to their macroscopic dimensions, in contrast to molecular mixtures, the collisions between the different components of the mixture are inelastic. As expected, the Mpemba-like effect is also present when collisions in the binary mixture are inelastic. However, given that the forms of the functions $\Phi = \Phi_1 + \Phi_2 + \Phi_3$ and Ψ appearing in the evolution equations obeying T^* and θ, respectively, are more complex than those derived for elastic collisions, it is not easy to find clean conditions for the occurrence of the Mpemba effect. On the other hand, since the impact of the granular new term Φ_3 (which vanishes for molecular mixtures) on the relaxation of the temperature is smaller than that of the pure molecular contributions $\Phi_1 + \Phi_2$ for not too strong inelasticities, one can conclude that the conditions for the occurrence of the Mpemba-like effect in granular mixtures are quite similar to those found for driven molecular mixtures. In any case, a more careful analysis is needed to confirm the above conclusion. We plan to carry out a more exhaustive study on the necessary conditions for the onset of the Mpemba-like effect in driven granular mixtures in the near future.

ACKNOWLEDGMENTS

The work of R.G.G. and V.G. has been supported by the Spanish Government through Grant No. FIS2016-76359-P and by the Junta de Extremadura (Spain), Grant No. GR18079, partially financed by "Fondo Europeo de Desarrollo Regional" funds. The research of R.G.G. has also been supported by the Predoctoral Fellowship No. BES-2017-079725 from the Spanish Government.

APPENDIX: EXPRESSIONS FOR DRIVEN GRANULAR MIXTURES

In this appendix, we display the expressions of the functions Φ and Ψ for driven granular mixtures, namely, when collisions between particles of the components i and j are inelastic. For smooth hard spheres, the inelasticity of collisions is characterized by the (constant) coefficients of restitution $\alpha_{ij} \leq 1$. In this case, the expressions of the partial production rates ξ_i in the Maxwellian approximation (16) are given by[27]

$$\xi_1 = \frac{\sqrt{2}\pi^{(d-1)/2}}{d\Gamma\left(\frac{d}{2}\right)} n_1 \chi_{11} \sigma_1^{d-1} \left(\frac{2T_1}{m_1}\right)^{1/2} (1-\alpha_{11}^2) + \frac{4\pi^{(d-1)/2}}{d\Gamma\left(\frac{d}{2}\right)} n_2 \mu_{21} \chi_{12} \sigma_{12}^{d-1} \left(\frac{2T_1}{m_1} + \frac{2T_2}{m_2}\right)^{1/2} (1+\alpha_{12}) \times \left[1 - \frac{\mu_{21}}{2}(1+\alpha_{12})\left(1 + \frac{m_1 T_2}{m_2 T_1}\right)\right]. \tag{A1}$$

The expression for ξ_2 can be easily obtained from Eq. (A1) by making the change $1 \leftrightarrow 2$. In dimensionless variables, the time evolution of T^* and θ can be written in the form (18) where

$$\Phi(T^*, \theta) = \Phi_1(T^*) + \Phi_2(\theta) + \Phi_3(T^*, \theta), \quad \Psi(T^*, \theta) = \Psi_1 + \Psi_2(T^*, \theta) + \Psi_3(T^*, \theta). \tag{A2}$$

Here, we have introduced the quantities

$$\Phi_1(T^*) = \frac{2}{T^*}\left(x_1\gamma_1^* + x_2\gamma_2^*\right), \quad \Phi_2(\theta) = -2\frac{x_1\gamma_1^*\theta + x_2\gamma_2^*}{1 + x_1(\theta - 1)}, \quad \Phi_3(T^*, \theta) = -\xi^*(T^*, \theta), \tag{A3}$$

$$\Psi_1 = -2(\gamma_1^* - \gamma_2^*), \quad \Psi_2(T^*, \theta) = 2\left(\gamma_1^* - \gamma_2^*\theta\right)\frac{1 + x_1(\theta - 1)}{\theta T^*}, \quad \Psi_3(T^*, \theta) = \xi_2^*(T^*, \theta) - \xi_1^*(T^*, \theta), \tag{A4}$$

where

$$\xi^* = \frac{x_1\theta\xi_1^* + x_2\xi_2^*}{1 + x_1(\theta - 1)}, \tag{A5}$$

$$\xi_1^* = \frac{\sqrt{2}\pi^{(d-1)/2}}{d\Gamma\left(\frac{d}{2}\right)} x_1 \chi_{11} \left(\frac{\sigma_1}{\sigma_{12}}\right)^{d-1} \sqrt{\frac{\theta T^*}{2\mu_{12}[1 + x_1(\theta - 1)]}} (1 - \alpha_{11}^2) + \frac{4\pi^{(d-1)/2}}{d\Gamma\left(\frac{d}{2}\right)} x_2 \chi_{12} \sqrt{\frac{\mu_{21}}{\mu_{12}}} \sqrt{\frac{T^*}{2}\frac{\mu_{12} + \mu_{21}\theta}{1 + x_1(\theta - 1)}} (1 + \alpha_{12}) \times \left[1 - \frac{1 + \alpha_{12}}{2}(\mu_{21} + \mu_{12}\theta^{-1})\right], \tag{A6}$$

$$\xi_2^* = \frac{\sqrt{2}\pi^{(d-1)/2}}{d\Gamma\left(\frac{d}{2}\right)} x_2 \chi_{22} \left(\frac{\sigma_2}{\sigma_{12}}\right)^{d-1} \sqrt{\frac{T^*}{2\mu_{21}[\theta + x_2(1 - \theta)]}} (1 - \alpha_{22}^2) + \frac{4\pi^{(d-1)/2}}{d\Gamma\left(\frac{d}{2}\right)} x_1 \chi_{12} \sqrt{\frac{\mu_{12}}{\mu_{21}}} \sqrt{\frac{T^*}{2}\frac{\mu_{12} + \mu_{21}\theta}{1 + x_1(\theta - 1)}} (1 + \alpha_{12}) \times \left[1 - \frac{1 + \alpha_{12}}{2}(\mu_{12} + \mu_{21}\theta)\right]. \tag{A7}$$

For elastic collisions ($\alpha_{11} = \alpha_{22} = \alpha_{12} = 1$), Eqs. (A4)–(A7) reduce to Eqs. (19)–(22) since $\Phi_3 = 0$ and

$$\Psi_3 = \xi_2^* - \xi_1^* = \frac{8\pi^{(d-1)/2}}{d\Gamma\left(\frac{d}{2}\right)} \chi_{12} \sqrt{\frac{T^*}{2}\frac{\mu_{12}\mu_{21}(\mu_{12} + \mu_{21}\theta)}{1 + x_1(\theta - 1)}} \times (x_1 - x_1\theta - x_2 + x_2\theta^{-1}). \tag{A8}$$

In the long-time limit, the steady forms of both T_s^* and θ_s^* can be obtained by solving the set of coupled equations,

$$\frac{2}{T_s^*}\left(x_1\gamma_1^* + x_2\gamma_2^*\right) - 2\frac{x_1\gamma_1^*\theta_s + x_2\gamma_2^*}{1 + x_1(\theta_s - 1)} = \xi_s^*, \tag{A9}$$

$$-2(\gamma_1^* - \gamma_2^*) + 2\left(\gamma_1^* - \gamma_2^*\theta_s\right)\frac{1 + x_1(\theta_s - 1)}{\theta_s T_s^*} = \xi_{1s}^* - \xi_{2s}^*. \tag{A10}$$

For elastic collisions, the solution to Eqs. (A9) and (A10) is simply given by $T_s^* = \theta_s^* = 1$ (energy equipartition). However, for inelastic collisions, energy equipartition does not hold, and T_s^* and θ_s^* have a

Physics of Fluids ARTICLE scitation.org/journal/phf

complex dependence on the parameter space of the problem. A study on this dependence has been carried out in Ref. for a binary mixture and in Ref. 38 for a multicomponent mixture.

DATA AVAILABILITY

The data that support the findings of this study are available from the corresponding author upon reasonable request.

REFERENCES

[1]E. B. Mpemba and D. G. Osborne, "Cool?," Phys. Educ. **4**, 172–175 (1969).
[2]G. S. Kell, "The freezing of hot and cold water," Am. J. Phys. **37**, 564–565 (1969).
[3]E. Deeson, "Cooler-lower down," Phys. Educ. **6**, 42–44 (1971).
[4]I. Firth, "Cooler?," Phys. Educ. **6**, 32–41 (1971).
[5]M. Freeman, "Cooler still—An answer?," Phys. Educ. **14**, 417–421 (1979).
[6]D. Auerbach, "Supercooling and the Mpemba effect: When hot water freezes quicker than cold," Am. J. Phys. **63**, 882–885 (1995).
[7]P. K. Maciejewski, "Evidence of a convective instability allowing warm water to freeze in less time than cold water," J. Heat Transfer **118**, 65–72 (1996).
[8]S. Esposito, R. D. Risi, and L. Somma, "Mpemba effect and phase transitions in the adiabatic cooling of water before freezing," Phys. A **387**, 757–763 (2008).
[9]J. I. Katz, "When hot water freezes before cold," Am. J. Phys. **77**, 27–29 (2009).
[10]M. Vynnycky and S. L. Mitchell, "Evaporative cooling and the Mpemba effect," Heat Mass Transfer **46**, 881–890 (2010).
[11]J. Jin and W. A. Goddard, "Mechanisms underlying the Mpemba effect in water from molecular dynamics simulations," J. Phys. Chem. C **119**, 2622–2629 (2015).
[12]R. T. Ibekwe and J. P. Cullerne, "Investigating the Mpemba effect: When hot water freezes faster than cold water," Phys. Educ. **51**, 025011 (2016).
[13]S. M. Mirabedin and F. Farhadi, "Numerical investigation of solidification of single droplets with and without evaporation mechanism," Int. J. Refrig. **73**, 219–225 (2017).
[14]N. C. Keim, J. D. Paulsen, Z. Zeravcic, S. Sastry, and S. R. Nagel, "Memory formation in matter," Rev. Mod. Phys. **91**, 035002 (2019).
[15]I. Klich, O. Raz, O. Hirschberg, and M. Vucelja, "Mpemba index and anomalous relaxation," Phys. Rev. X **9**, 021060 (2019).
[16]A. Gijón, A. Lasanta, and E. R. Hernández, "Path towards equilibrium in molecular systems: The case of water," Phys. Rev. E **100**, 032103 (2019).
[17]Y. Ahn, H. Kang, D. Koh, and H. Lee, "Experimental verifications of Mpemba-like behaviors of clathrate hydrates," Korean J. Chem. Eng. **33**, 1903–1907 (2016).
[18]C. Hu, J. Li, S. Huang, H. Li, C. Luo, J. Chen, S. Jiang, and L. An, "Conformation directed Mpemba effect on polylactide crystallization," Cryst. Growth Des. **18**, 5757–5762 (2018).
[19]A. Kumar and J. Bechhoefer, "Exponentially faster cooling in a colloidal system," Nature **584**, 64–68 (2020).
[20]H. C. Burridge and P. F. Linden, "Questioning the Mpemba effect: Hot water does not cool more quickly than cold," Sci. Rep. **6**, 37665 (2016).
[21]H. C. Burridge and O. Hallstadius, "Observing the Mpemba effect with minimal bias and the value of the Mpemba effect to scientific outreach and engagement," Proc. R. Soc. A **476**, 20190829 (2020).
[22]A. Lasanta, F. V. Reyes, A. Prados, and A. Santos, "When the hotter cools more quickly: Mpemba effect in granular fluids," Phys. Rev. Lett. **119**, 148001 (2017).
[23]A. Torrente, M. A. López-Castaño, A. Lasanta, F. V. Reyes, A. Prados, and A. Santos, "Large Mpemba-like effect in a gas of inelastic rough hard spheres," Phys. Rev. E **99**, 060901(R) (2019).
[24]A. Biswas, V. V. Prasad, O. Raz, and R. Rajesh, "Mpemba effect in driven granular Maxwell gases," Phys. Rev. E **102**, 012906 (2020).
[25]S. Takada, H. Hayakawa, and A. Santos, "Mpemba effect in inertial suspensions," Phys. Rev. E **103**, 032901 (2021).
[26]Z. Lu and O. Raz, "Nonequilibrium thermodynamics of the Markovian Mpemba effect and its inverse," Proc. Natl. Acad. Sci. U. S. A. **114**, 5083–5088 (2017).
[27]V. Garzó, *Granular Gaseous Flows* (Springer Nature, Cham, 2019).
[28]A. Santos and A. Prados, "Mpemba effect in molecular gases under nonlinear drag," Phys. Fluids **32**, 072010 (2020).
[29]N. Khalil and V. Garzó, "Homogeneous states in driven granular mixtures: Enskog kinetic theory versus molecular dynamics simulations," J. Chem. Phys. **140**, 164901 (2014).
[30]D. L. Koch and R. J. Hill, "Inertial effects in suspension and porous-media flows," Annu. Rev. Fluid Mech. **33**, 619–647 (2001).
[31]T. Kawasaki, A. Ikeda, and L. Berthier, "Thinning or thickening? Multiple rheological regimes in dense suspensions of soft particles," Europhys. Lett. **107**, 28009 (2014).
[32]H. Hayakawa, S. Takada, and V. Garzó, "Kinetic theory of shear thickening for a moderately dense gas–solid suspension: From discontinuous thickening to continuous thickening," Phys. Rev. E **96**, 042903 (2017).
[33]S. Takada, H. Hayakawa, A. Santos, and V. Garzó, "Enskog kinetic theory of rheology for a moderately dense inertial suspension," Phys. Rev. E **102**, 022907 (2020).
[34]P. Résibois and M. de Leener, *Classical Kinetic Theory of Fluids* (Wiley, New York, 1977).
[35]N. van Kampen, *Stochastic Processes in Physics and Chemistry* (Elsevier, Amsterdam, 2007).
[36]R. Zwanzig, *Nonequilibrium Statistical Mechanics* (Oxford University Press, 2001).
[37]N. V. Brilliantov and T. Pöschel, *Kinetic Theory of Granular Gases* (Oxford University Press, 2004).
[38]A. Osinsky, A. S. Bodrova, and N. V. Brilliantov, "Size-polidisperse dust in molecular gas: Energy equipartition versus nonequipartition," Phys. Rev. E **101**, 022903 (2020).
[39]D. L. Koch, "Kinetic theory for a monodisperse gas–solid suspension," Phys. Fluids A **2**, 1711–1723 (1990).
[40]X. Yin and S. Sundaresan, "Drag law for bidisperse gas–solid suspensions containing equally sized spheres," Ind. Eng. Chem. Res. **48**, 227–241 (2009).
[41]X. Yin and S. Sundaresan, "Fluid-particle drag in low-Reynolds-number polydisperse gas–solid suspensions," AIChE **55**, 1352–1368 (2009).
[42]W. Holloway, X. Yin, and S. Sundaresan, "Fluid-particle drag in inertial polydisperse gas–solid suspensions," AIChE **56**, 1995–2004 (2010).
[43]G. A. Bird, *Molecular Gas Dynamics and the Direct Simulation of Gas Flows* (Oxford University Press, Oxford, 1994).
[44]J. M. Montanero and A. Santos, "Simulation of the Enskog equation à la Bird," Phys. Fluids **9**, 2057–2060 (1997).
[45]J. M. Montanero and V. Garzó, "Monte Carlo simulation of the homogeneous cooling state for a granular mixture," Granular Matter **4**, 17–24 (2002).
[46]M. P. Allen and D. J. Tildesley, *Computer Simulation of Liquids* (Oxford University Press, Oxford, 2017).
[47]B. D. Lubachevsky, "How to simulate billiards and similar systems," J. Comput. Phys. **94**, 255–283 (1991).
[48]S. Chapman and T. G. Cowling, *The Mathematical Theory of Non-Uniform Gases* (Cambridge University Press, Cambridge, 1970).
[49]C. Cercignani, *The Boltzmann Equation and Its Applications* (Springer, New York, 1988).
[50]T. van Noije and M. Ernst, "Velocity distributions in homogeneous granular fluids: The free and the heated case," Granular Matter **1**, 57–64 (1998).
[51]C. Henrique, G. Batrouni, and D. Bideau, "Diffusion as a mixing mechanism in granular materials," Phys. Rev. E **63**, 011304 (2000).
[52]S. R. Dahl, C. M. Hrenya, V. Garzó, and J. W. Dufty, "Kinetic temperatures for a granular mixture," Phys. Rev. E **66**, 041301 (2002).
[53]R. Gómez González, N. Khalil, and V. Garzó, "Enskog kinetic theory for multicomponent granular suspensions," Phys. Rev. E **101**, 012904 (2020).
[54]R. Gómez González and V. Garzó, "Non-Newtonian rheology in inertial suspensions of inelastic rough hard spheres under simple shear flow," Phys. Fluids **32**, 073315 (2020).
[55]L. H. Holway, "New statistical models for kinetic theory: Methods of construction," Phys. Fluids **9**, 1658 (1966).
[56]E. Goldman, "Equations for gas mixtures," Phys. Fluids **10**, 1928 (1967).
[57]V. Garzó and A. Santos, *Kinetic Theory of Gases in Shear Flows: Nonlinear Transport* (Kluwer Academic Publishers, Dordrecht, 2003).
[58]T. Boublík, "Hard-sphere equation of state," J. Chem. Phys. **53**, 471–472 (1970).
[59]E. W. Grundke and D. Henderson, "Distribution functions of multicomponent fluid mixtures of hard spheres," Mol. Phys. **24**, 269–281 (1972).
[60]L. L. Lee and D. Levesque, "Perturbation theory for mixtures of simple liquids," Mol. Phys. **26**, 1351–1370 (1973).
[61]A. J. Kovacs, J. J. Aklonis, J. M. Hutchinson, and A. R. Ramos, "Isobaric volume and enthalpy recovery of glasses. II. A transparent multiparameter theory," J. Polym. Sci. Polym. Phys. Ed. **17**, 1097–1162 (1979).

Chapter 5

Enskog Kinetic Theory for Bidisperse Suspensions

5.1 Summary

The transport properties of a bidisperse granular suspension are studied in the context of the Enskog kinetic equation. The granular suspension is composed of two kinds of particles (disks for $d = 2$ or spheres for $d = 3$) of masses m_i and diameters σ_i ($i = 1, 2$) immersed in a viscous fluid. The inelasticity of collisions between species i and j is implemented by means of a constant coefficient of restitution $\alpha_{ij} \leq 1$. The influence of the surrounding viscous gas on each species is modeled via an individual Fokker–Plank term composed by a deterministic viscous drag force plus a stochastic Langevin-like term.

The objective of this chapter is to provide a solution to the set of two-coupled Enskog kinetic equations by means of the Chapman–Enskog method considering up to the Navier–Stokes level of approximation. In the absence of spatial gradients, the system reaches a homogeneous steady state where the energy lost by inelastic collisions and viscous friction is compensated for by the energy injected by the stochastic force. The first step is to characterize this homogeneous state, given that it serves as the reference state of the perturbation scheme. Since to compute the velocity moments we opt for simplicity to take the Maxwellian forms of the one-body distribution functions f_i, simulations are needed to assess the reliability of such approximation. In this sense,

the partial temperature ratio T_1/T_2 are evaluated in the HSS and compared against MD and DSMC simulations.

Once the HSS is characterized, a normal solution to the set of Enskog equations is obtained by means of the CE expansion around the local version of the homogeneous state. This solution states that all the spatial and time dependence of the distribution functions is through the hydrodynamic variables. Therefore, the non-hydrodynamic variables and the cooling rate ζ together with the momentum P, mass $\mathbf{j}_i$, and heat $\mathbf{q}$ fluxes must be therefore expanded in terms of gradients of the hydrodynamic variables. The most relevant non-hydrodynamic or kinetic variables that affect the macroscopic description of a granular mixture are the partial temperatures T_1 and T_2 of species 1 and 2, respectively. Thus, as explained in Section 2.3, they must be also expanded as $T_i = T_i^{(0)} + \epsilon T_i^{(1)} + \cdots$. The existence of a nonzero first-order contribution $T_i^{(1)}$ induces a breakdown of the energy equipartition, additional to the one present in the HSS due to the dissipative character of collisions [197]. The first-order contributions to the partial temperature were already recognized in the pioneering papers in elastic systems [194–196] and recently noticed in an Erratum for driven granular mixtures at low density [197]. Nonetheless, it is worth assessing the impact of these contributions to the partial temperatures on the transport properties in polydisperse dense "dry" granular mixtures. Since $T_i^{(1)}$ is a scalar, it is proportional to the divergence of the flow velocity $\nabla \cdot \mathbf{U}$. Therefore, it will produce *new* contributions to the bulk viscosity η_{b} (proportionality coefficient between the collisional part P^{c} of the pressure tensor and $\nabla \cdot \mathbf{U}$) and to the first-order contribution ζ_U to the cooling rate (proportionality coefficient between ζ and $\nabla \cdot \mathbf{U}$) not considered in previous works [190, 191].

Now that the CE standards are in place, we can extend previous theoretical results for dilute multicomponent granular suspensions [99] to higher densities. To first order in spatial gradients, we obtain the unsteady set of integral equations that we have to solve by considering the leading terms in a Sonine polynomial expansion under steady-state conditions. This procedure allows us to obtain explicit forms of the NS transport coefficients in terms of the mechanical parameters of the mixture (masses and sizes and the coefficients of restitution), the composition, and the density. The evaluation of the complete set of transport coefficients of the binary granular suspension is a quite long task. In this chapter, we will focus our attention in obtaining the four diffusion coefficients associated with the mass flux, the shear and bulk viscosity coefficients, and

the first-order contributions to the partial temperatures and the cooling rate. We plan in the near future to determine the heat flux transport coefficients and to perform a linear stability analysis of the homogeneous steady state.

5.2 Article 4

Title: Influence of the first-order contributions to the partial temperatures on transport properties in polydisperse dense granular mixtures

Authors: Rubén Gómez González[1] and Vicente Garzó[2]

Affiliations:

[1] Departamento de Física, Universidad de Extremadura, E-06006 Badajoz, Spain

[2] Departamento de Física and Instituto de Computación Científica Avanzada (ICCAEx), Universidad de Extremadura, E-06006 Badajoz, Spain

Journal: Physical Review E

Volume: 100

Pages: 032904

Year: 2019

DOI: 10.1103/PhysRevE.100.032904

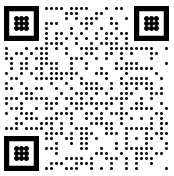

PHYSICAL REVIEW E **100**, 032904 (2019)

Influence of the first-order contributions to the partial temperatures on transport properties in polydisperse dense granular mixtures

Rubén Gómez González*
Departamento de Física, Universidad de Extremadura, E-06006 Badajoz, Spain

Vicente Garzó†
Departamento de Física and Instituto de Computación Científica Avanzada (ICCAEx), Universidad de Extremadura, E-06006 Badajoz, Spain

(Received 18 July 2019; published 19 September 2019)

The Chapman-Enskog solution to the Enskog kinetic equation of polydisperse granular mixtures is revisited to determine the first-order contributions ϖ_i to the partial temperatures. As expected, these quantities (which were neglected in previous attempts) are given in terms of the solution to a set of coupled integrodifferential equations analogous to those for elastic collisions. The solubility condition for this set of equations is confirmed and the coefficients ϖ_i are calculated by using the leading terms in a Sonine polynomial expansion. These coefficients are given as explicit functions of the sizes, masses, composition, density, and coefficients of restitution of the mixture. Within the context of small gradients, the results apply for arbitrary degrees of inelasticity and are not restricted to specific values of the parameters of the mixture. In the case of elastic collisions, previous expressions of ϖ_i for ordinary binary mixtures are recovered. Finally, the impact of the first-order coefficients ϖ_i on the bulk viscosity η_b and on the first-order contribution $\zeta^{(1)}$ to the cooling rate is assessed. It is shown that the effect of ϖ_i on η_b and $\zeta^{(1)}$ is not negligible, specially for disparate mass ratios and strong inelasticity.

DOI: 10.1103/PhysRevE.100.032904

I. INTRODUCTION

The understanding of transport processes occurring in polydisperse granular mixtures (namely, a mixture of smooth hard spheres with inelastic collisions) is still an exciting unsolved problem [1–3]. The reason for this challenging target is twofold: first, there is a large number of relevant parameters involved in the description of the granular mixtures; and second, there is a wide array of intricacies arising in the derivation of kinetic theory models. Thus, to gain some insight into the problem, the two most common simplifications employed in many of the pioneering papers on granular mixtures [4–8] were (i) to consider mixtures constituted by nearly elastic particles and (ii) to assume the equipartition of the total granular kinetic energy in the homogeneous cooling state (namely, they assume that the zeroth-order contributions $T_i^{(0)}$ to the partial temperatures T_i of each species are equal to the granular temperature T). On the other hand, the last assumption can be only justified for quasielastic collisions since the failure of energy equipartition in granular fluids [9,10] has been confirmed by computer simulations [11–18] and observed in real experiments of agitated granular mixtures [19,20]. The above papers have also shown that the departure of energy equipartition depends on the mechanical differences among the particles and the coefficients of restitution of the granular mixture.

The inclusion of energy nonequipartition effects on transport in granular mixtures has been considered in more recent papers of dilute [21–26] and moderate [27–29] densities. In particular, the results derived from the inelastic Enskog equation [27–29] cover some of the aspects not accounted for in previous studies. More specifically, (i) they are expected to be applicable for a wide range of coefficients of restitution (since they take into account the nonlinear dependence of the transport coefficients on the coefficients of restitution); (ii) they consider the impact of nonequipartition of granular energy on the Navier-Stokes transport coefficients; and (iii) they are valid for moderate densities. Thus, these works [27–29] subsume all previous studies for dilute [21–26] and dense quasielastic [4–8] granular mixtures, which are recovered in the appropriate limits.

Nevertheless, the theory developed for dense gases [27–29] is based on a simplifying assumption. Although not explicitly stated, the results derived in Refs. [27–29] were obtained by neglecting the first-order contributions $T_i^{(1)}$ to the partial temperatures T_i. The existence of a nonzero first-order contribution $T_i^{(1)}$ induces a breakdown of the energy equipartition, additional to the one appearing in the homogeneous cooling state (which is only due to the inelastic character of collisions). In fact, $T_i^{(1)} \neq 0$ in the case of ordinary dense mixtures (namely, a dense hard-sphere mixture with elastic collisions). Although the partial temperatures are not hydrodynamic quantities, their determination is interesting in itself. In addition, a careful analysis of the first-order contributions to the collisional part P^c of the pressure tensor and the cooling rate ζ (which

*ruben@unex.es
†vicenteg@unex.es; http://www.unex.es/eweb/fisteor/vicente/

accounts for the rate of kinetic energy dissipation due to inelastic collisions) shows that there are contributions to $\mathsf{P}^{\rm c}$ and ζ coming from the coefficients $T_i^{(1)}$. Since the first-order contributions to the partial temperatures are proportional to the divergence of the flow velocity $\mathbf{U}$, then the coefficients $T_i^{(1)}$ are involved in the evaluation of both the bulk viscosity $\eta_{\rm b}$ (proportionality coefficient between $\mathsf{P}^{\rm c}$ and $\nabla\cdot\mathbf{U}$) and the first-order contribution ζ_U to the cooling rate (proportionality coefficient between ζ and $\nabla\cdot\mathbf{U}$). The coupling between $T_i^{(1)}$ and $\eta_{\rm b}$ was in fact already recognized in the pioneering papers [30–32] of the Enskog theory for multicomponent ordinary mixtures.

The question arises then as to whether, and if so to what extent, the conclusions drawn from Refs. [27–29] for $\eta_{\rm b}$ and ζ may be altered when the above new ingredient (first-order contributions to the partial temperatures) is accounted for in the theory. In this paper we calculate $T_i^{(1)}$ and assess the impact of these coefficients on $\eta_{\rm b}$ and ζ for granular mixtures.

The plan of the paper is as follows. The Enskog kinetic equation for polydisperse granular mixtures is introduced in Sec. II and the corresponding balance equations for the densities of mass, momentum, and energy are recalled. Section III deals with the evaluation of the first-order contributions to the partial temperatures. As expected, the coefficients $T_i^{(1)}$ are given in terms of the solution to a set of linear integral equations. The leading term in a Sonine polynomial expansion is retained in Sec. IV to solve the above set and obtain the partial temperatures in terms of the parameter space of the problem. For the sake of illustration, a binary mixture is considered in Sec. V. The results show that the impact of the coefficients $T_i^{(1)}$ on both the bulk viscosity and the cooling rate is not in general negligible and must be accounted for, specially for disparate mass ratios and strong dissipation. The paper closes in Sec. VI with some concluding remarks.

II. ENSKOG KINETIC EQUATION FOR POLYDISPERSE DENSE GRANULAR MIXTURES

We consider an s-component granular mixture of inelastic hard disks ($d=2$) or spheres ($d=3$) of masses m_i and diameters σ_i. The subscript i labels one of the s mechanically different components and d is the dimension of the system. Spheres are assumed to be completely smooth so that the inelasticity of collisions is only characterized by the constant (positive) coefficients of restitution $\alpha_{ij}\leqslant 1$. The mixture is also assumed to be in the presence of the gravitational field and hence, each particle feels the action of the force $\mathbf{F}_i=m_i\mathbf{g}$, where $\mathbf{g}$ is the gravity acceleration. For moderate densities, the one-particle velocity distribution function $f_i(\mathbf{r},\mathbf{v},t)$ of component i verifies the set of s-coupled nonlinear integrodifferential Enskog equations:

$$\frac{\partial f_i}{\partial t}+\mathbf{v}\cdot\nabla f_i+\mathbf{g}\cdot\frac{\partial f_i}{\partial\mathbf{v}}=\sum_{j=1}^{s}J_{ij}[\mathbf{r},\mathbf{v}|f_i,f_j],\tag{1}$$

where the Enskog collision operator is [3]

$$J_{ij}[\mathbf{r}_1,\mathbf{v}_1|f_i,f_j]=\sigma_{ij}^{d-1}\int d\mathbf{v}_2\int d\widehat{\boldsymbol{\sigma}}\,\Theta(\widehat{\boldsymbol{\sigma}}\cdot\mathbf{g}_{12})(\widehat{\boldsymbol{\sigma}}\cdot\mathbf{g}_{12})\big[\alpha_{ij}^{-2}\chi_{ij}(\mathbf{r}_1,\mathbf{r}_1-\boldsymbol{\sigma}_{ij})f_i(\mathbf{r}_1,\mathbf{v}_1'',t)f_j(\mathbf{r}_1-\boldsymbol{\sigma}_{ij},\mathbf{v}_2'',t)$$
$$-\chi_{ij}(\mathbf{r}_1,\mathbf{r}_1+\boldsymbol{\sigma}_{ij})f_i(\mathbf{r}_1,\mathbf{v}_1,t)f_j(\mathbf{r}_1+\boldsymbol{\sigma}_{ij},\mathbf{v}_2,t)\big].\tag{2}$$

In Eq. (1), $\boldsymbol{\sigma}_{ij}=\sigma_{ij}\widehat{\boldsymbol{\sigma}}$, $\sigma_{ij}=(\sigma_i+\sigma_j)/2$, $\widehat{\boldsymbol{\sigma}}$ is a unit vector directed along the line of centers from the sphere of component i to that of component j at contact, Θ is the Heaviside step function, and $\mathbf{g}_{12}=\mathbf{v}_1-\mathbf{v}_2$ is the relative velocity of the colliding pair. Moreover, $\chi_{ij}(\mathbf{r}_1,\mathbf{r}_1+\boldsymbol{\sigma}_{ij})$ is the equilibrium pair correlation function of two hard spheres, one of component i and the other of component j at contact, i.e., when the distance between their centers is σ_{ij}. The precollisional velocities $(\mathbf{v}_1'',\mathbf{v}_2'')$ are given by

$$\mathbf{v}_1''=\mathbf{v}_1-\mu_{ji}\big(1+\alpha_{ij}^{-1}\big)(\widehat{\boldsymbol{\sigma}}\cdot\mathbf{g}_{12})\widehat{\boldsymbol{\sigma}},\tag{3}$$

$$\mathbf{v}_2''=\mathbf{v}_2+\mu_{ij}\big(1+\alpha_{ij}^{-1}\big)(\widehat{\boldsymbol{\sigma}}\cdot\mathbf{g}_{12})\widehat{\boldsymbol{\sigma}},\tag{4}$$

where $\mu_{ij}=m_i/(m_i+m_j)$.

The first few velocity moments of the distributions f_i define the hydrodynamic fields of the mixture. Thus, the local number density of component i is

$$n_i=\int d\mathbf{v}\,f_i(\mathbf{v}),\tag{5}$$

while the local mean flow velocity of grains is defined as

$$\mathbf{U}=\rho^{-1}\sum_{i=1}^{s}\int d\mathbf{v}\,m_i\mathbf{v}f_i(\mathbf{v}),\tag{6}$$

where $\rho=\sum_i m_i n_i$ is the total mass density. Apart from the partial densities n_i and the flow velocity $\mathbf{U}$, the other important hydrodynamic field is the granular temperature T. It is defined as

$$T=\frac{1}{n}\sum_{i=1}^{s}\int d\mathbf{v}\frac{m_i}{d}V^2f_i(\mathbf{v}),\tag{7}$$

where $n=\sum_i n_i$ is the total number density and $\mathbf{V}=\mathbf{v}-\mathbf{U}$ is the peculiar velocity. At a kinetic level, it is also convenient to introduce the partial kinetic temperatures T_i for each component. These quantities measure the mean kinetic energy of each component. They are defined as

$$T_i=\frac{m_i}{dn_i}\int d\mathbf{v}\,V^2f_i(\mathbf{v}).\tag{8}$$

According to Eq. (7), the granular temperature T of the mixture can be also written as

$$T=\sum_{i=1}^{s}x_iT_i,\tag{9}$$

where $x_i=n_i/n$ is the mole fraction of component i.

An important property of the integrals involving the Enskog collision operator $J_{ij}[\mathbf{r},\mathbf{v}|f_i,f_j]$ is [3,27]

$$
\begin{aligned}
I_{\psi_i} &\equiv \sum_{i,j=1}^{s}\int d\mathbf{v}_1\,\psi_i(\mathbf{v}_1)J_{ij}[\mathbf{r}_1,\mathbf{v}_1|f_i,f_j]\\
&= \frac{1}{2}\sum_{i,j=1}^{s}\sigma_{ij}^{d-1}\int d\mathbf{v}_1\int d\mathbf{v}_2\int d\widehat{\boldsymbol{\sigma}}\,\Theta(\widehat{\boldsymbol{\sigma}}\cdot\mathbf{g}_{12})(\widehat{\boldsymbol{\sigma}}\cdot\mathbf{g}_{12})\Big\{\big[\psi_i(\mathbf{v}_1')+\psi_j(\mathbf{v}_2')-\psi_i(\mathbf{v}_1)-\psi_j(\mathbf{v}_2)\big]f_{ij}(\mathbf{r}_1,\mathbf{v}_1,\mathbf{r}_2,\mathbf{v}_2;t)\\
&\quad+\frac{\partial}{\partial\mathbf{r}_1}\cdot\boldsymbol{\sigma}_{ij}\big[\psi_i(\mathbf{v}_1')-\psi_i(\mathbf{v}_1)\big]\int_0^1 dx\,f_{ij}(\mathbf{r}_1-x\boldsymbol{\sigma}_{ij},\mathbf{v}_1,\mathbf{r}_1+(1-x)\boldsymbol{\sigma}_{ij},\mathbf{v}_2;t)\Big\},
\end{aligned}
\tag{10}
$$

where

$$
f_{ij}(\mathbf{r}_1,\mathbf{v}_1,\mathbf{r}_2,\mathbf{v}_2;t)\equiv\chi_{ij}(\mathbf{r}_1,\mathbf{r}_2)f_i(\mathbf{r}_1,\mathbf{v}_1,t)f_j(\mathbf{r}_2,\mathbf{v}_2,t),
\tag{11}
$$

$\psi_i(\mathbf{v}_1)$ is an arbitrary function of $\mathbf{v}_1$, and

$$
\mathbf{v}_1'=\mathbf{v}_1-\mu_{ji}(1+\alpha_{ij})(\widehat{\boldsymbol{\sigma}}\cdot\mathbf{g}_{12})\widehat{\boldsymbol{\sigma}}.
\tag{12}
$$

The first term on the right-hand side of Eq. (10) represents a collisional effect due to scattering with a change in velocities. The second term provides a pure collisional effect due to the spatial difference of the colliding pair. For elastic collisions, the first term vanishes. The balance equations for the densities of mass, momentum, and energy can be derived by using the property (10). They are given by [3]

$$
D_t n_i+n_i\nabla\cdot\mathbf{U}+\frac{\nabla\cdot\mathbf{j}_i}{m_i}=0,
\tag{13}
$$

$$
D_t\mathbf{U}+\rho^{-1}\nabla\cdot\mathsf{P}=\mathbf{g},
\tag{14}
$$

$$
D_t T-\frac{T}{n}\sum_{i=1}^{s}\frac{\nabla\cdot\mathbf{j}_i}{m_i}+\frac{2}{dn}(\nabla\cdot\mathbf{q}+\mathsf{P}:\nabla\mathbf{U})=-\zeta T.
\tag{15}
$$

In the above equations, $D_t=\partial_t+\mathbf{U}\cdot\nabla$ is the material derivative, $\rho_i=m_i n_i$ is the mass density of component i, and

$$
\mathbf{j}_i=m_i\int d\mathbf{v}\,\mathbf{V}f_i(\mathbf{v})
\tag{16}
$$

is the mass flux for component i relative to the local flow $\mathbf{U}$. A consequence of the definition (16) of the fluxes $\mathbf{j}_i$ is that

$$
\sum_{i=1}^{s}\mathbf{j}_i=\mathbf{0},
\tag{17}
$$

and hence, only $s-1$ mass fluxes are independent. The pressure tensor $\mathsf{P}(\mathbf{r},t)$ and the heat flux $\mathbf{q}(\mathbf{r},t)$ have both kinetic and collisional transfer contributions, i.e.,

$$
\mathsf{P}=\mathsf{P}^{\mathrm{k}}+\mathsf{P}^{\mathrm{c}},\quad \mathbf{q}=\mathbf{q}^{\mathrm{k}}+\mathbf{q}^{\mathrm{c}}.
\tag{18}
$$

The kinetic contributions P^{k} and $\mathbf{q}^{\mathrm{k}}$ are given by

$$
\mathsf{P}^{\mathrm{k}}=\sum_{i=1}^{s}\int d\mathbf{v}\,m_i\mathbf{V}\mathbf{V}f_i(\mathbf{v}),
\tag{19}
$$

$$
\mathbf{q}^{\mathrm{k}}=\sum_{i=1}^{s}\int d\mathbf{v}\,\frac{m_i}{2}V^2\mathbf{V}f_i(\mathbf{v}).
\tag{20}
$$

The collisional transfer contributions are [3,27]

$$
\mathsf{P}^{\mathrm{c}}=\sum_{i,j=1}^{s}\sigma_{ij}^{d}m_{ij}\frac{1+\alpha_{ij}}{2}\int d\mathbf{v}_1\int d\mathbf{v}_2\int d\widehat{\boldsymbol{\sigma}}\Theta(\widehat{\boldsymbol{\sigma}}\cdot\mathbf{g}_{12})(\widehat{\boldsymbol{\sigma}}\cdot\mathbf{g}_{12})^2\widehat{\boldsymbol{\sigma}}\widehat{\boldsymbol{\sigma}}\int_0^1 dx f_{ij}(\mathbf{r}-x\boldsymbol{\sigma}_{ij},\mathbf{r}+(1-x)\boldsymbol{\sigma}_{ij},\mathbf{v}_1,\mathbf{v}_2,t),
\tag{21}
$$

$$
\begin{aligned}
\mathbf{q}^{\mathrm{c}}=\sum_{i,j=1}^{s}\sigma_{ij}^{d}m_{ij}\frac{1+\alpha_{ij}}{8}&\int d\mathbf{v}_1\int d\mathbf{v}_2\int d\widehat{\boldsymbol{\sigma}}\Theta(\widehat{\boldsymbol{\sigma}}\cdot\mathbf{g}_{12})(\widehat{\boldsymbol{\sigma}}\cdot\mathbf{g}_{12})^2\widehat{\boldsymbol{\sigma}}\big[4(\widehat{\boldsymbol{\sigma}}\cdot\mathbf{G}_{ij})\\
&+(\mu_{ji}-\mu_{ij})(1-\alpha_{ij})(\widehat{\boldsymbol{\sigma}}\cdot\mathbf{g}_{12})\big]\int_0^1 dx f_{ij}(\mathbf{r}-x\boldsymbol{\sigma}_{ij},\mathbf{r}+(1-x)\boldsymbol{\sigma}_{ij},\mathbf{v}_1,\mathbf{v}_2;t).
\end{aligned}
\tag{22}
$$

Here, $m_{ij}=m_im_j/(m_i+m_j)$ is the reduced mass and $\mathbf{G}_{ij}=\mu_{ij}\mathbf{V}_1+\mu_{ji}\mathbf{V}_2$ is the velocity of the center of mass. Finally, the (total) cooling rate ζ due to inelastic collisions among all components is given by

$$\zeta=\frac{1}{2dnT}\sum_{i,j=1}^{s}\sigma_{ij}^{d-1}m_{ij}\left(1-\alpha_{ij}^2\right)\int d\mathbf{v}_1\int d\mathbf{v}_2\int d\widehat{\boldsymbol{\sigma}}\Theta(\widehat{\boldsymbol{\sigma}}\cdot\mathbf{g}_{12})(\widehat{\boldsymbol{\sigma}}\cdot\mathbf{g}_{12})^3 f_{ij}(\mathbf{r},\mathbf{r}+\boldsymbol{\sigma}_{ij},\mathbf{v}_1,\mathbf{v}_2;t). \tag{23}$$

As expected, the balance equations (13)–(15) are not a closed set of equations for the fields n_i, $\mathbf{U}$, and T. To transform these equations into a set of closed equations, one has to express the fluxes and the cooling rate in terms of the hydrodynamic fields and their gradients. The corresponding constitutive equations can be obtained by solving the set of Enskog kinetic equations (1) with the Chapman-Enskog method [33] adapted to dissipative dynamics.

III. FIRST-ORDER CONTRIBUTIONS TO THE PARTIAL TEMPERATURES

The inelastic Enskog equation (1) was solved in Refs. [27,28] by means of the Chapman-Enskog method. In particular, the first-order velocity distribution functions $f_i^{(1)}$ are given by [27]

$$f_i^{(1)}=\boldsymbol{\mathcal{A}}_i\cdot\nabla\ln T+\sum_{j=1}^{s}\boldsymbol{\mathcal{B}}_{ij}\cdot\nabla\ln n_j + \mathcal{C}_{i,\lambda\beta}\frac{1}{2}\left(\partial_\lambda U_\beta+\partial_\beta U_\lambda-\frac{2}{d}\delta_{\lambda\beta}\nabla\cdot\mathbf{U}\right) + \mathcal{D}_i\nabla\cdot\mathbf{U}, \tag{24}$$

where $\partial_\lambda\equiv\partial/\partial r_\lambda$. The unknowns $\boldsymbol{\mathcal{A}}_i(\mathbf{V})$, $\boldsymbol{\mathcal{B}}_{ij}(\mathbf{V})$, $\mathcal{C}_{i,\lambda\beta}(\mathbf{V})$, and $\mathcal{D}_i(\mathbf{V})$ are functions of the peculiar velocity $\mathbf{V}$ and they are the solutions of a set of coupled linear integral equations [27]. Approximate solutions to this set of integral equations were obtained in Refs. [28,29] by considering the leading terms in a Sonine polynomial expansion. This procedure allows us to obtain explicit forms of the Navier-Stokes transport coefficients in terms of the mechanical parameters of the mixture (masses and sizes and the coefficients of restitution), the composition, and the density. Within the context of small gradients, the results apply in principle for arbitrary values of the coefficients of restitution and a wide range of densities.

However, as said in Sec. I, the influence of the first-order contribution $T_i^{(1)}$ to T_i on the transport coefficients was neglected in the above papers [27,28]. This was essentially assumed because $T_i^{(1)}$ comes from the second-Sonine approximation and hence it is expected that its impact on transport properties is small. Here, we want to determine $T_i^{(1)}$ to assess its influence on the bulk viscosity and the cooling rate.

According to Eq. (8), the first-order contribution to the partial temperature T_i is defined as

$$T_i^{(1)}=\frac{m_i}{dn_i}\int d\mathbf{v}\,V^2 f_i^{(1)}(\mathbf{V}). \tag{25}$$

Since $T_i^{(1)}$ is a scalar, it can be only coupled to the divergence of the flow velocity $\nabla\cdot\mathbf{U}$ since ∇n and ∇T are vectors and $\partial_\lambda U_\beta+\partial_\beta U_\lambda-(2/d)\delta_{\lambda\beta}\nabla\cdot\mathbf{U}$ is a traceless tensor. Thus, $T_i^{(1)}$ can be written as $T_i^{(1)}=\varpi_i\nabla\cdot\mathbf{U}$, where

$$\varpi_i=\frac{m_i}{dn_i}\int d\mathbf{v}\,V^2\mathcal{D}_i(\mathbf{V}). \tag{26}$$

The fact that the total temperature T is not affected by the gradients implies necessarily the constraint $\sum_{i=1}^s n_iT_i^{(1)}=0$. Thus, only $s-1$ partial temperatures are independent. The above constraint comes directly from the solubility condition

$$\sum_{i=1}^{s}\int d\mathbf{v}m_iV^2f_i^{(1)}=0. \tag{27}$$

As said before, apart from obtaining $T_i^{(1)}$, we are also interested here in revisiting previous calculations [27,28] made for the bulk viscosity η_b and the cooling rate ζ. The first coefficient has only collisional contributions and its form can be identified by expanding the collisional transfer contribution P^c to the pressure tensor to first order in spatial gradients. A careful first-order expansion of the expression (21) to P^c gives the following form for η_b:

$$\eta_\mathrm{b}=\eta_\mathrm{b}'+\eta_\mathrm{b}'', \tag{28}$$

where

$$\eta_\mathrm{b}'=\frac{\pi^{(d-1)/2}}{\Gamma\left(\frac{d+3}{2}\right)}\frac{d+1}{2d^2}\sum_{i=1}^{s}\sum_{j=1}^{s}m_{ij}(1+\alpha_{ij})\chi_{ij}^{(0)}\sigma_{ij}^{d+1}\times\int d\mathbf{v}_1\int d\mathbf{v}_2 f_i^{(0)}(\mathbf{V}_1)f_j^{(0)}(\mathbf{V}_2)g_{12}, \tag{29}$$

and

$$\eta_\mathrm{b}''=-\frac{\pi^{d/2}}{d\Gamma\left(\frac{d}{2}\right)}\sum_{i=1}^{s}\sum_{j=1}^{s}\mu_{ji}(1+\alpha_{ij})\chi_{ij}^{(0)}n_in_j\sigma_{ij}^d\varpi_i. \tag{30}$$

In Eq. (29), $f_i^{(0)}$ is the zeroth-order distribution. In addition, it is understood henceforth that the functional dependence of $\chi_{ij}^{(0)}(\mathbf{r},\mathbf{r}'|\{n_i\})$ on the compositions to zeroth order in the gradients has the same functional dependence on the densities replaced by $\{n_i\}\to\{n_i(\mathbf{r},t)\}$ at the point of interest.

The second contribution η_b'' to η_b in Eq. (28) was neglected in previous works [3,27,28]. On the other hand, as said in Sec. I, the contribution η_b'' was already accounted for in the studies on ordinary (elastic collisions) hard-sphere mixtures [30–32] carried out many years ago. In fact, for elastic collisions, Eq. (30) is consistent with Eq. (18a) of Ref. [31].

In the case of the cooling rate, $\zeta\to\zeta^{(0)}+\zeta_U\nabla\cdot\mathbf{U}$ where

$$\zeta^{(0)}=\frac{1}{2dnT}\sum_{i,j=1}^{s}\sigma_{ij}^{d-1}m_{ij}\left(1-\alpha_{ij}^2\right)\chi_{ij}^{(0)}\int d\mathbf{v}_1\int d\mathbf{v}_2\times\int d\widehat{\boldsymbol{\sigma}}\Theta(\widehat{\boldsymbol{\sigma}}\cdot\mathbf{g}_{12})(\widehat{\boldsymbol{\sigma}}\cdot\mathbf{g}_{12})^3 f_i^{(0)}(\mathbf{r},\mathbf{v}_1,t)f_j^{(0)}(\mathbf{r},\mathbf{v}_2,t), \tag{31}$$

and $\zeta_U = \zeta^{(1,0)} + \zeta^{(1,1)}$. Here,

$$\zeta^{(1,0)} = -\frac{3\pi^{d/2}}{d^2\Gamma\left(\frac{d}{2}\right)} \sum_{i=1}^{s}\sum_{j=1}^{s} x_i n_j \mu_{ji} \sigma_{ij}^d \chi_{ij}^{(0)} \gamma_i \left(1-\alpha_{ij}^2\right), \tag{32}$$

and the coefficient $\zeta^{(1,1)}$ is given in terms of the unknowns $\mathcal{D}_i$ as

$$\zeta^{(1,1)} = \frac{1}{nT} \frac{\pi^{(d-1)/2}}{d\Gamma\left(\frac{d+3}{2}\right)} \sum_{i=1}^{s}\sum_{j=1}^{s} \sigma_{ij}^{d-1} \chi_{ij}^{(0)} m_{ij} \left(1-\alpha_{ij}^2\right) \int d\mathbf{v}_1 \int d\mathbf{v}_2\, g_{12}^3\, f_i^{(0)}(\mathbf{V}_1) \mathcal{D}_j(\mathbf{V}_2). \tag{33}$$

In Eq. (32), $\gamma_i \equiv T_i^{(0)}/T$ is the temperature ratio of component i. The temperature ratios γ_i verify the relation $\sum_i x_i \gamma_i = 1$ and they are determined from the conditions $\zeta^{(0)} = \zeta_1^{(0)} = \zeta_2^{(0)} = \cdots = \zeta_s^{(0)}$, where

$$\zeta_i^{(0)} = -\frac{m_i}{dn_i T_i^{(0)}} \sum_{j=1}^{s} \int d\mathbf{v} V^2 J_{ij}^{(0)}\left[f_i^{(0)}, f_j^{(0)}\right]. \tag{34}$$

According to the results obtained in Ref. [27], the coefficients ϖ_i are the solutions of the set of coupled linear integral equations

$$\frac{1}{2}\zeta^{(0)} \frac{\partial}{\partial \mathbf{V}} \cdot \left(\mathbf{V}\mathcal{D}_i\right) + \frac{1}{2}\zeta^{(0)}\mathcal{D}_i + \frac{1}{2}\zeta^{(1,1)} \frac{\partial}{\partial \mathbf{V}} \cdot \left(\mathbf{V} f_i^{(0)}\right) - \sum_{j=1}^{s} \left(J_{ij}^{(0)}\left[\mathcal{D}_i, f_j^{(0)}\right] + J_{ij}^{(0)}\left[f_i^{(0)}, \mathcal{D}_j\right]\right) = D_i, \tag{35}$$

where

$$J_{ij}^{(0)}\left[f_i^{(0)}, f_j^{(0)}\right] = \chi_{ij}^{(0)} \sigma_{ij}^{d-1} \int d\mathbf{v}_2 \int d\widehat{\boldsymbol{\sigma}}\, \Theta(\widehat{\boldsymbol{\sigma}} \cdot \mathbf{g}_{12})(\widehat{\boldsymbol{\sigma}} \cdot \mathbf{g}_{12}) \left[\alpha_{ij}^{-2} f_i^{(0)}(\mathbf{v}_1'') f_j^{(0)}(\mathbf{v}_2'') - f_i^{(0)}(\mathbf{v}_1) f_j^{(0)}(\mathbf{v}_2)\right] \tag{36}$$

is the Boltzmann collision operator multiplied by the (constant) pair distribution function $\chi_{ij}^{(0)}$, and D_i is given by

$$D_i(\mathbf{V}) = \frac{1}{2}\left[\frac{2}{d}(1-p^*) - \zeta^{(1,0)}\right] \frac{\partial}{\partial \mathbf{V}} \cdot \left(\mathbf{V} f_i^{(0)}\right) - f_i^{(0)} + \sum_{j=1}^{s} \left(n_j \frac{\partial f_i^{(0)}}{\partial n_j} + \frac{1}{d} \mathcal{K}_{i,j,\beta}\left[\frac{\partial f_i^{(0)}}{\partial V_\beta}\right]\right). \tag{37}$$

In addition, $\mathcal{K}_{ij}[X_j]$ is the collision operator

$$\mathcal{K}_{ij}[X_j] = \sigma_{ij}^d \chi_{ij}^{(0)} \int d\mathbf{v}_2 \int d\widehat{\boldsymbol{\sigma}} \Theta(\widehat{\boldsymbol{\sigma}} \cdot \mathbf{g}_{12})(\widehat{\boldsymbol{\sigma}} \cdot \mathbf{g}_{12}) \widehat{\boldsymbol{\sigma}} \left[\alpha_{ij}^{-2} f_i^{(0)}(\mathbf{v}_1'') X_j(\mathbf{v}_2'') + f_i^{(0)}(\mathbf{v}_1) X_j(\mathbf{v}_2)\right], \tag{38}$$

and the (reduced) hydrostatic pressure $p^* \equiv p/(nT)$ is

$$p^* = 1 + \frac{\pi^{d/2}}{d\Gamma\left(\frac{d}{2}\right)} \sum_{i=1}^{s}\sum_{j=1}^{s} \mu_{ji} x_i x_j n \sigma_{ij}^d \chi_{ij}^{(0)} \gamma_i (1+\alpha_{ij}). \tag{39}$$

Since $\mathcal{D}_i(\mathbf{V}) \propto D_i(\mathbf{V})$, the solubility condition (27) requires necessarily that

$$\sum_{i=1}^{s} \int d\mathbf{v} m_i V^2 D_i(\mathbf{V}) = 0. \tag{40}$$

This condition can easily be verified by direct integration of Eq. (37) and using Eqs. (32)–(39), the relation $\sum_i x_i \gamma_i = 1$, and the result

$$\begin{aligned} A_i &\equiv \sum_{j=1}^{s} \int d\mathbf{v} m_i V^2 \mathcal{K}_{ij,\lambda}\left[\frac{\partial f_j^{(0)}}{\partial V_\lambda}\right] \\ &= -\frac{\pi^{d/2}}{\Gamma\left(\frac{d}{2}\right)} T \sum_{j=1}^{s} \chi_{ij}^{(0)} n_i n_j \sigma_{ij}^d (1+\alpha_{ij}) \Big[3\mu_{ji}(1+\alpha_{ij}) \\ &\quad \times \left(\frac{\gamma_i}{m_i} + \frac{\gamma_j}{m_j}\right) - 4\frac{\gamma_i}{m_i}\Big]. \end{aligned} \tag{41}$$

In the low-density regime ($n_i \sigma_{ij}^d \to 0$), $p^* = 1$, $\zeta^{(1,0)} = 0$, the combination $\sum_j n_j \partial f_i^{(0)}/\partial n_j - f_i^{(0)}$ and the operator $\mathcal{K}_{ij}[X_j]$ vanish, and so $D_i = 0$ in the integral equation (35). This means $\mathcal{D}_i = 0$ and hence, the first-order contributions ϖ_i to the partial temperatures vanish for *dilute* granular mixtures. This agrees with the previous results obtained in the low-density regime [21,22,24,25].

IV. LEADING SONINE APPROXIMATION

It is quite apparent that the calculation of ϖ_i requires one to solve the integral equation (35) as well as to know the zeroth-order distributions $f_i^{(0)}$. With respect to the latter, previous results [9,11] derived for homogeneous states have clearly shown that in the region of thermal velocities, $f_i^{(0)}$ is well represented by the Maxwellian velocity distribution defined at the lowest-order partial temperature $T_i^{(0)}$, namely,

$$f_i^{(0)}(\mathbf{V}) \to f_{i,\mathrm{M}}(\mathbf{V}) = n_i \left(\frac{m_i}{2\pi T_i^{(0)}}\right)^{d/2} \exp\left(-\frac{m_i V^2}{2T_i^{(0)}}\right). \tag{42}$$

This means that we neglect here non-Gaussian corrections to the distributions $f_i^{(0)}$ and hence, one expects to get simple but accurate expressions for the transport coefficients. With this approximation, $\zeta_i^{(0)}$ is

$$\zeta_i^{(0)} = \frac{4\pi^{(d-1)/2}}{d\Gamma\left(\frac{d}{2}\right)} v_0 \sum_{j=1}^{s} n_j \chi_{ij}^{(0)} \mu_{ji} \sigma_{ij}^{d-1} (1+\alpha_{ij}) \times \left(\frac{\beta_i+\beta_j}{\beta_i\beta_j}\right)^{1/2} \left[1 - \frac{\mu_{ji}}{2}(1+\alpha_{ij})\frac{\beta_i+\beta_j}{\beta_j}\right], \quad (43)$$

where $v_0(T) = \sqrt{2T/\overline{m}}$ is a thermal speed of the mixture, $\overline{m} = \sum_i m_i/s$, and $\beta_i = m_i T/\overline{m} T_i^{(0)}$. Furthermore, according to Eq. (29) the contribution η_b' to the bulk viscosity can also be computed by using the Maxwellian approximation (42) with the result

$$\eta_b' = \frac{\pi^{(d-1)/2}}{d^2\Gamma\left(\frac{d}{2}\right)} v_0 \sum_{i=1}^{2}\sum_{j=1}^{2} m_{ij}(1+\alpha_{ij}) \chi_{ij}^{(0)} n_i n_j \sigma_{ij}^{d+1} \times \left(\frac{\beta_i+\beta_j}{\beta_i\beta_j}\right)^{1/2}. \quad (44)$$

To solve the integral equation (35), one takes the leading Sonine approximation to $\mathcal{D}_i(\mathbf{V})$

$$\mathcal{D}_i(\mathbf{V}) \to f_{i\mathrm{M}}(\mathbf{V}) W_i(\mathbf{V}) \frac{\varpi_i}{T_i^{(0)}}, \quad (45)$$

where

$$W_i(\mathbf{V}) = \frac{m_i V^2}{2T_i^{(0)}} - \frac{d}{2}. \quad (46)$$

The relation between $\zeta^{(1,1)}$ and ϖ_i can be easily obtained by substitution of Eq. (45) into Eq. (33). The result is

$$\zeta^{(1,1)} = \sum_{i=1}^{s} \xi_i \varpi_i, \quad (47)$$

where

$$\xi_i = \frac{3\pi^{(d-1)/2}}{2d\Gamma\left(\frac{d}{2}\right)} \frac{v_0^3}{nTT_i^{(0)}} \sum_{j=1}^{s} n_i n_j \sigma_{ij}^{d-1} \chi_{ij}^{(0)} m_{ij}\left(1-\alpha_{ij}^2\right) \times (\beta_i+\beta_j)^{1/2} \beta_i^{-3/2} \beta_j^{-1/2}. \quad (48)$$

The coefficients ϖ_i can be finally obtained by substituting Eq. (45) into Eq. (35), multiplying it with $m_i V^2$, and integrating over the velocity. After some algebra, the corresponding set of coupled linear algebraic equations for the coefficients ϖ_i are given by

$$\sum_{j=1}^{s} \left(\omega_{ij} + \frac{1}{2}\zeta^{(0)}\delta_{ij} + T_i^{(0)}\xi_j\right)\varpi_j = B_i, \quad (49)$$

where

$$B_i = \frac{2}{d} T_i^{(0)}(1-p^*) - T_i^{(0)}\zeta^{(1,0)} - T\phi\frac{\partial\gamma_i}{\partial\phi} - \frac{A_i}{d^2 n_i}, \quad (50)$$

and

$$\phi = \frac{\pi^{d/2}}{2^{d-1} d\Gamma\left(\frac{d}{2}\right)} \sum_{i=1}^{s} n_i \sigma_i^d \quad (51)$$

is the solid volume fraction. Upon obtaining Eq. (50) we have taken into account that the dependence of the temperature ratios γ_i on the densities n_i is through their dependence on the mole fractions x_i and the volume fraction ϕ. Furthermore, the collision frequencies ω_{ij} are defined as

$$\omega_{ii} = \frac{1}{dn_i T_i^{(0)}} \left(\sum_{j=1}^{s} \int d\mathbf{v} m_i V^2 J_{ij}^{(0)}\left[f_{i,\mathrm{M}} W_i, f_j^{(0)}\right] + \int d\mathbf{v} m_i V^2 J_{ii}^{(0)}\left[f_i^{(0)}, f_{i,\mathrm{M}} W_i\right]\right), \quad (52)$$

$$\omega_{ij} = \frac{1}{dn_i T_j^{(0)}} \int d\mathbf{v} m_i V^2 J_{ij}^{(0)}\left[f_i^{(0)}, f_{j,\mathrm{M}} W_j\right], \quad (i \neq j). \quad (53)$$

In the Maxwellian approximation (42), ω_{ii} and ω_{ij} are

$$\omega_{ii} = -\frac{\pi^{(d-1)/2}}{2dT_i^{(0)}\Gamma\left(\frac{d}{2}\right)} v_0^3 \left\{\frac{3}{\sqrt{2}} n_i \sigma_i^{d-1} m_i \chi_{ii}^{(0)} \beta_i^{-3/2}\left(1-\alpha_{ii}^2\right) - \sum_{j\neq i}^{s} n_j m_{ij} \sigma_{ij}^{d-1} \chi_{ij}^{(0)}(1+\alpha_{ij})(\beta_i+\beta_j)^{-1/2}\beta_i^{-3/2} \times \beta_j^{-1/2}\left[3\mu_{ji}(1+\alpha_{ij})(\beta_i+\beta_j) - 2(2\beta_i+3\beta_j)\right]\right\}, \quad (54)$$

$$\omega_{ij} = \frac{\pi^{(d-1)/2}}{2dT_j^{(0)}\Gamma\left(\frac{d}{2}\right)} v_0^3 n_j m_{ij} \sigma_{ij}^{d-1} \chi_{ij}^{(0)}(1+\alpha_{ij}) \times (\beta_i+\beta_j)^{-1/2}\beta_i^{-1/2}\beta_j^{-3/2}\left[3\mu_{ji}(1+\alpha_{ij}) \times (\beta_i+\beta_j) - 2\beta_j\right]. \quad (55)$$

In Eqs. (54) and (55), it is understood that $i \neq j$. The set of algebraic equations (52) can be now easily solved. In particular, for a binary mixture ($s = 2$) the solution of Eq. (49) for ϖ_1 can be written as

$$\varpi_1 = \frac{B_1}{\omega_{11} - \frac{x_1}{x_2}\omega_{12} + \frac{1}{2}\zeta^{(0)} + T_1^{(0)}\left(\xi_1 - \frac{x_1}{x_2}\xi_2\right)}, \quad (56)$$

where the relation $\varpi_2 = -(x_1/x_2)\varpi_1$ has been accounted for. The expression for ϖ_2 can be easily obtained from Eq. (56) by making the changes $1 \leftrightarrow 2$. The solution (56) is indeed consistent with the requirement $x_1\varpi_1 + x_2\varpi_2 = 0$. This is because $x_1\gamma_1 + x_2\gamma_2 = 1$, $B_2 = -(x_1/x_2)B_1$, and $\omega_{11} - (x_1/x_2)\omega_{12} + \xi_1/x_1 = \omega_{22} - (x_2/x_1)\omega_{21} + \xi_2/x_2$.

The expression (56) provides ϖ_1 in terms of the parameters of the mixture. Its explicit form is relatively long and is omitted here for the sake of brevity. A simple but interesting case corresponds to ordinary mixtures (elastic collisions) where $\zeta^{(0)} = 0$, $\xi_i = 0$, $\gamma_i = 1$, $\beta_1 = 2\mu_{12}$, $\beta_2 = 2\mu_{21}$, and ϖ_1 is

$$\varpi_1 = \frac{4\pi^{d/2}}{d^2\Gamma\left(\frac{d}{2}\right)} T\left(\omega_{11} - \frac{x_1}{x_2}\omega_{12}\right)^{-1}\left[n_2\sigma_{12}^d \chi_{12}^{(0)}(x_2\mu_{21} - x_1\mu_{12}) + \frac{1}{2}x_2\left(n_1\sigma_1^d\chi_{11}^{(0)} - n_2\sigma_2^d\chi_{22}^{(0)}\right)\right]. \quad (57)$$

Equation (57) differs from the one obtained by Jenkins and Mancini [4] for nearly elastic hard spheres ($d = 3$). This discrepancy is essentially due to the fact that the distribution functions of each species in Ref. [4] are assumed to be Maxwellian distributions even in inhomogeneous situations. This was already noted by the authors of this paper since they conclude that their expression for ϖ_1 could be improved by determining the perturbations to the Maxwellians using the Chapman-Enskog procedure [33]. Expression (57) accounts for not only the different centers $\mathbf{r}$ and $\mathbf{r} \pm \boldsymbol{\sigma}_{ij}$ of the colliding pair in the Enskog collision operator (2) but also for the form of the first-order distribution $f^{(1)}$ given by Eq. (24).

On the other hand, for a three-dimensional system ($d = 3$), the expression (57) for ϖ_1 agrees with the one derived in Ref. [31] [see Eq. (22d) of [31]] for a hard-sphere binary mixture. This confirms the relevant known limiting cases for the granular mixture results derived here for the temperature ratios.

Once the first-order contributions to the partial temperatures are known, the first-order contribution ζ_U to the cooling rate can be explicitly obtained by employing Eqs. (32), (33), (47), and (48). In addition, the second contribution η_b'' to the bulk viscosity η_b can be obtained from Eq. (30). Thus, $\eta_b = \eta_b' + \eta_b''$ is completely determined from Eqs. (30) and (44). For elastic collisions ($\alpha_{ij} = 1$), as expected, the corresponding expression for η_b is consistent with previous works on ordinary mixtures [30–32].

V. BINARY GRANULAR MIXTURES

To illustrate the dependence of the coefficients ϖ_i, ζ_U, and η_b on the parameter space of the system, a binary mixture ($s = 2$ and so, $\varpi_2 = -x_1\varpi_1/x_2$) of inelastic hard spheres ($d = 3$) is considered. The above coefficients depend on many parameters: $\{x_1, T, m_1/m_2, \sigma_1/\sigma_2, \phi, \alpha_{11}, \alpha_{22}, \alpha_{12}\}$. A similar complexity also exists in the elastic limit [32], so the relevant new feature is the dependence of ϖ_1, ζ_U, and η_b on the coefficients of restitution. Moreover, for the sake of simplicity, the case of a common coefficient of restitution ($\alpha_{11} = \alpha_{22} = \alpha_{12} \equiv \alpha$) of an equimolar mixture ($x_1 = \frac{1}{2}$) with $\sigma_1 = \sigma_2$ and solid volume fraction $\phi = 0.2$ (moderately dense gas) is considered. This reduces the parameter space to three quantities: $\{T, m_1/m_2, \alpha\}$. The dependence on temperature can be scaled out by introducing the (dimensionless) quantities $\varpi_1^* = (n\sigma_{12}^2 v_0/T)\varpi_1$ and $\eta_b^* \equiv \eta_b(\alpha)/\eta_b(1)$, where $\eta_b(1)$ is the bulk viscosity for elastic collisions. The coefficient ζ_U is dimensionless.

To display the dependence of the coefficients ϖ_1^*, η_b^*, and ζ_U on α, we have still to provide the form for the pair distribution function $\chi_{ij}^{(0)}$. In the case of spheres ($d = 3$), a good approximation of $\chi_{ij}^{(0)}$ is [34–36]

$$\chi_{ij}^{(0)} = \frac{1}{1-\phi} + \frac{3}{2}\frac{\phi}{(1-\phi)^2}\frac{\sigma_i\sigma_j M_2}{\sigma_{ij} M_3} + \frac{1}{2}\frac{\phi^2}{(1-\phi)^3}\left(\frac{\sigma_i\sigma_j M_2}{\sigma_{ij} M_3}\right)^2, \tag{58}$$

where $M_\ell = \sum_i x_i \sigma_i^\ell$. In Fig. 1, the (reduced) coefficient ϖ_1^* is plotted as a function of the coefficient of restitution α for several values of the mass ratio. It is quite apparent first that the influence of the inelasticity on ϖ_1^* is significant, specially for high mass ratios. With respect to the dependence on the mass ratio, we see that while ϖ_1^* increases with inelasticity when $m_1/m_2 < 1$, the opposite happens when $m_1/m_2 > 1$. Furthermore, Fig. 1 also highlights that the magnitude of the first contribution to the partial temperature is in general quite small in comparison with the values of the remaining transport coefficients of the mixture [28,29]. To assess the impact of ϖ_1^* on the bulk viscosity and the first-order contribution to the cooling rate, Figs. 2 and 3 show the α dependence of the (reduced) coefficients $\eta_b(\alpha)/\eta_b(1)$ and ζ_U, respectively, for two values of the mass ratio. We also plot the corresponding values of these coefficients when ϖ_1^* is neglected. Although both predictions (with and without ϖ_1^*) agree qualitatively, we observe that the effect of ϖ_1^* on both transport coefficients cannot be neglected specially for high mass ratios and moderate inelasticity (for instance, $\alpha \simeq 0.6$). This means that previous results [27,28] derived for both

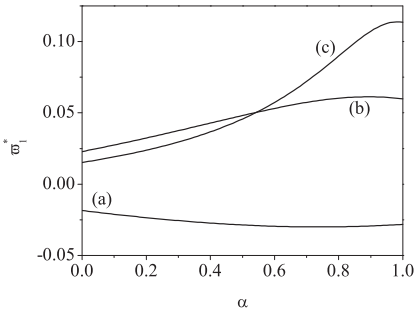

FIG. 1. The (reduced) coefficient ϖ_1^* as a function of the common coefficient of restitution α for a binary mixture of hard spheres ($d = 3$) with $x_1 = \frac{1}{2}$, $\sigma_1 = \sigma_2$, $\phi = 0.2$, and three different values of the mass ratio m_1/m_2: $m_1/m_2 = 0.5$ (a), $m_1/m_2 = 4$ (b), and $m_1/m_2 = 10$ (c).

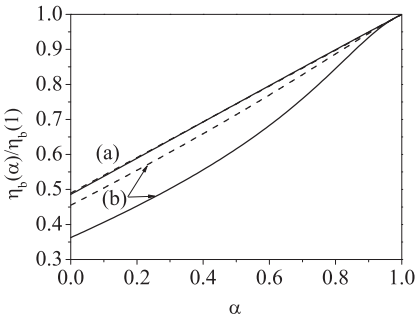

FIG. 2. The (reduced) bulk viscosity $\eta_b(\alpha)/\eta_b(1)$ as a function of the common coefficient of restitution α for a binary mixture of hard spheres ($d = 3$) with $x_1 = \frac{1}{2}$, $\sigma_1 = \sigma_2$, $\phi = 0.2$, and two different values of the mass ratio m_1/m_2: $m_1/m_2 = 0.5$ (a) and $m_1/m_2 = 10$ (b). The dashed lines are the results for the (reduced) bulk viscosity when the contribution η_b'' to η_b is neglected.

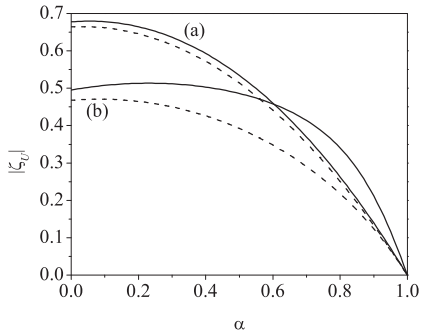

FIG. 3. Magnitude of the (reduced) coefficient ζ_U as a function of the common coefficient of restitution α for a binary mixture of hard spheres ($d = 3$) with $x_1 = \frac{1}{2}$, $\sigma_1 = \sigma_2$, $\phi = 0.2$, and two different values of the mass ratio m_1/m_2: $m_1/m_2 = 0.5$ (a) and $m_1/m_2 = 10$ (b). The dashed lines are the results for the coefficient ζ_U when the contribution $\zeta^{(1,1)}$ to ζ_U is neglected.

the bulk viscosity and the cooling rate of granular mixtures must be slightly changed when the masses of the constituents of the mixture become very disparate and/or the collisional dissipation becomes significant.

VI. CONCLUDING REMARKS

One of the most intriguing differences between ordinary and granular mixtures is the absence of energy equipartition in homogeneous states. This means that the zeroth-order contributions $T_i^{(0)}$ to the *partial* temperatures T_i (measuring the mean kinetic energy of each species) of granular mixtures are different for mechanically different components, reflecting a violation of the equipartition theorem valid for elastic collisions [9]. The origin of this violation is the inelasticity in collisions, and its impact on transport problems such as thermal diffusion segregation [37–39] has been shown to be quite significant, specially for strong dissipation and/or disparate mass ratios.

In addition, as was already noted in some of the pioneering papers of the Enskog theory for multicomponent ordinary mixtures [30–32], a breakdown of energy equipartition is also present in the Navier-Stokes domain (first-order in spatial gradients) for moderately dense mixtures. The origin of this violation is associated with the spatial gradients, and more specifically with the divergence of flow velocity since the first-order contributions $T_i^{(1)}$ to the partial temperatures are proportional to $\nabla \cdot \mathbf{U}$. This additional source of energy nonequipartition is independent of the one appearing in the homogeneous cooling state for granular mixtures.

On the other hand, the coefficients $T_i^{(1)}$ are usually neglected in many of the works devoted to granular mixtures [5,27,28] because only the first terms in the Sonine polynomial expansion are retained. Since $T_i^{(1)} \propto \nabla \cdot \mathbf{U}$, an interesting question is to assess the impact of the first-order coefficients $T_i^{(1)}$ on both the bulk viscosity η_b and the first-order contribution ζ_U to the cooling rate.

The goal of this paper has been to determine the coefficients $T_i^{(1)}$ from the Chapman-Enskog solution to the (inelastic) version of the Enskog kinetic equation [3]. As in previous works [27,28], this task has been achieved in two different steps. First, we have obtained in an *exact* way the set of linear integral equations that the first-order contributions $T_i^{(1)}$ satisfy. This has allowed us to prove the solubility condition for solving this set of integral equations. As a second step, an approximate solution to the above set of equations is required for practical purposes in order to explicitly express the coefficients $T_i^{(1)}$ in terms of the parameter space of the problem (masses, diameters, composition, density, and coefficients of restitution). This task has been achieved by considering the leading terms in the Sonine polynomial expansion. Thus, the results derived here for $T_i^{(1)}$ extend to inelastic collisions the calculations performed many years ago [30–32] for ordinary hard-sphere mixtures. Moreover, the expressions obtained here for η_b [given by Eqs. (28)–(30)] and ζ_U [given by Eqs. (32), (47), and (48)] correct the previous results derived in Refs. [27,28] where the contributions η_b'' and $\zeta^{(1,1)}$ to η_b and ζ_U, respectively, were implicitly neglected.

For the sake of illustration and to assess the impact of $T_i^{(1)}$ on η_b and ζ_U, a binary mixture with a common coefficient of restitution ($\alpha_{ij} \equiv \alpha$) has been considered to analyze the dependence of the above transport coefficients on inelasticity. First, as Fig. 1 shows, we observe that the effect of inelasticity on the first-order contributions to the partial temperatures is in general quite important, specially for large mass ratios. With respect to the influence of $T_1^{(1)}$ on η_b and ζ_U, Figs. 2 and 3 highlight that the impact of the first-order partial temperature on both the bulk viscosity and the cooling rate can be relatively important for moderate inelasticity and/or disparate mass ratios.

An interesting problem is to extend the present results to the case of polydisperse granular mixtures driven by a stochastic bath with friction [40–42]. This kind of thermostat models the effect of the surrounding interstitial viscous gas on the dynamics of grains (granular suspensions). An extensive study on the transport coefficients for driven granular mixtures at low density has been carried out in Refs. [43–45]. In contrast with the findings reported here for *freely* cooling granular dilute gases (where $T_i^{(1)} = 0$ when $\phi = 0$), the results derived for driven systems [45] show that the first-order contributions $T_i^{(1)}$ to the partial temperatures are different from zero even when $\phi = 0$. The extension of the results obtained in Refs. [43–45] to finite density is an interesting project. Work along this line will be initiated in the near future.

In summary, we have revisited previous works on polydisperse granular mixtures [27,28] where the first-order contributions $T_i^{(1)}$ to the partial temperatures were neglected. The present work fixes the above limitation by including not only the calculation of $T_i^{(1)}$ but also their influence on the bulk viscosity η_b and on the first-order contribution ζ_U to the cooling rate. Our results show first that the first-order coefficients $T_i^{(1)}$ exhibit in general a complex dependence on the coefficients of restitution of the mixture. In addition, they also show that the impact of $T_i^{(1)}$ on both η_b and ζ_U cannot be neglected for disparate masses and/or strong dissipation. In this context, the results derived before for polydisperse dense granular mixtures [27,28] must be slightly modified by including the

contributions coming from the partial temperatures $T_i^{(1)}$ to the transport properties and the cooling rate.

ACKNOWLEDGMENTS

We are grateful to Dr. Mariano López de Haro for a critical reading of the manuscript and for calling our attention to the papers [30,31]. The present work has been supported by the Spanish Government through Grant No. FIS2016-76359-P and by the Junta de Extremadura (Spain) Grants No. IB16013 (V.G.) and No. GR18079, partially financed by "Fondo Europeo de Desarrollo Regional" funds. The research of R.G.G. has been supported by the predoctoral fellowship BES-2017-079725 from the Spanish Government.

[1] N. Brilliantov and T. Pöschel, *Kinetic Theory of Granular Gases* (Oxford University, Oxford, 2004).
[2] K. K. Rao and P. R. Nott, *An Introduction to Granular Flow* (Cambridge University, Cambridge, England, 2008).
[3] V. Garzó, *Granular Gaseous Flows* (Springer Nature Switzerland, Basel, 2019).
[4] J. T. Jenkins and F. Mancini, J. Appl. Mech. **54**, 27 (1987).
[5] J. T. Jenkins and F. Mancini, Phys. Fluids A **1**, 2050 (1989).
[6] P. Zamankhan, Phys. Rev. E **52**, 4877 (1995).
[7] B. Arnarson and J. T. Willits, Phys. Fluids **10**, 1324 (1998).
[8] J. T. Willits and B. Arnarson, Phys. Fluids **11**, 3116 (1999).
[9] V. Garzó and J. W. Dufty, Phys. Rev. E **60**, 5706 (1999).
[10] P. A. Martin and J. Piasecki, Europhys. Lett. **46**, 613 (1999).
[11] J. M. Montanero and V. Garzó, Granular Matter **4**, 17 (2002).
[12] A. Barrat and E. Trizac, Granular Matter **4**, 57 (2002).
[13] S. R. Dahl, C. M. Hrenya, V. Garzó, and J. W. Dufty, Phys. Rev. E **66**, 041301 (2002).
[14] R. Pagnani, U. M. Bettolo Marconi, and A. Puglisi, Phys. Rev. E **66**, 051304 (2002).
[15] P. E. Krouskop and J. Talbot, Phys. Rev. E **68**, 021304 (2003).
[16] H. Q. Wang, G. J. Jin, and Y. Q. Ma, Phys. Rev. E **68**, 031301 (2003).
[17] J. J. Brey, M. J. Ruiz-Montero, and F. Moreno, Phys. Rev. Lett. **95**, 098001 (2005).
[18] M. Schröter, S. Ulrich, J. Kreft, J. B. Swift, and H. L. Swinney, Phys. Rev. E **74**, 011307 (2006).
[19] R. D. Wildman and D. J. Parker, Phys. Rev. Lett. **88**, 064301 (2002).
[20] K. Feitosa and N. Menon, Phys. Rev. Lett. **88**, 198301 (2002).
[21] V. Garzó and J. W. Dufty, Phys. Fluids **14**, 1476 (2002).
[22] D. Serero, I. Goldhirsch, S. H. Noskowicz, and M. L. Tan, J. Fluid Mech. **554**, 237 (2006).
[23] V. Garzó, J. M. Montanero, and J. W. Dufty, Phys. Fluids **18**, 083305 (2006).
[24] V. Garzó and J. M. Montanero, J. Stat. Phys. **129**, 27 (2007).
[25] D. Serero, S. H. Noskowicz, M. L. Tan, and I. Goldhirsch, Eur. Phys. J. ST **179**, 221 (2009).
[26] V. Garzó, J. A. Murray, and F. Vega Reyes, Phys. Fluids **25**, 043302 (2013).
[27] V. Garzó, J. W. Dufty, and C. M. Hrenya, Phys. Rev. E **76**, 031303 (2007).
[28] V. Garzó, C. M. Hrenya, and J. W. Dufty, Phys. Rev. E **76**, 031304 (2007).
[29] J. A. Murray, V. Garzó, and C. M. Hrenya, Powder Technol. **220**, 24 (2012).
[30] J. Karkheck and G. Stell, J. Chem. Phys. **71**, 3620 (1979).
[31] J. Karkheck and G. Stell, J. Chem. Phys. **71**, 3636 (1979).
[32] M. López de Haro, E. G. D. Cohen, and J. Kincaid, J. Chem. Phys. **78**, 2746 (1983).
[33] S. Chapman and T. G. Cowling, *The Mathematical Theory of Nonuniform Gases* (Cambridge University, Cambridge, England, 1970).
[34] T. Boublik, J. Chem. Phys. **53**, 471 (1970).
[35] E. W. Grundke and D. Henderson, Mol. Phys. **24**, 269 (1972).
[36] L. L. Lee and D. Levesque, Mol. Phys. **26**, 1351 (1973).
[37] V. Garzó, Phys. Rev. E **78**, 020301(R) (2008).
[38] V. Garzó, Eur. Phys. J. E **29**, 261 (2009).
[39] V. Garzó, New J. Phys. **13**, 055020 (2011).
[40] A. Puglisi, V. Loreto, U. M. B. Marconi, A. Petri, and A. Vulpiani, Phys. Rev. Lett. **81**, 3848 (1998).
[41] A. Sarracino, D. Villamaina, G. Gradenigo, and A. Puglisi, Europhys. Lett. **92**, 34001 (2010).
[42] A. Sarracino, D. Villamaina, G. Costantini, and A. Puglisi, J. Stat. Mech. (2010) P04013.
[43] N. Khalil and V. Garzó, Phys. Rev. E **88**, 052201 (2013).
[44] N. Khalil and V. Garzó, Phys. Rev. E **97**, 022902 (2018).
[45] N. Khalil and V. Garzó, Phys. Rev. E **99**, 059901(E) (2019).

5.3 Article 5

Title: Enskog kinetic theory for multicomponent granular suspensions

Authors: Rubén Gómez González[1], Nagi Khalil[2], and Vicente Garzó[3]

Affiliations:

[1] Departamento de Física, Universidad de Extremadura, E-06006 Badajoz, Spain

[2] Escuela Superior de Ciencias Experimentales y Tecnología (ESCET), Universidad Rey Juan Carlos, Móstoles, 28933 Madrid, Spain

[3] Departamento de Física and Instituto de Computación Científica Avanzada (ICCAEx), Universidad de Extremadura, E-06006 Badajoz, Spain

Journal: Physical Review E

Volume: 101

Pages: 012904

Year: 2020

DOI: 10.1103/PhysRevE.101.012904

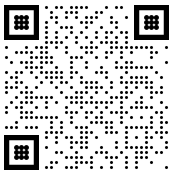

PHYSICAL REVIEW E **101**, 012904 (2020)

Enskog kinetic theory for multicomponent granular suspensions

Rubén Gómez González[*]
Departamento de Física, Universidad de Extremadura, E-06006 Badajoz, Spain

Nagi Khalil[†]
Escuela Superior de Ciencias Experimentales y Tecnología (ESCET), Universidad Rey Juan Carlos, Móstoles 28933, Madrid, Spain

Vicente Garzó[‡]
Departamento de Física and Instituto de Computación Científica Avanzada (ICCAEx), Universidad de Extremadura, E-06006 Badajoz, Spain

(Received 30 October 2019; published 17 January 2020)

The Navier-Stokes transport coefficients of multicomponent granular suspensions at moderate densities are obtained in the context of the (inelastic) Enskog kinetic theory. The suspension is modeled as an ensemble of solid particles where the influence of the interstitial gas on grains is via a viscous drag force plus a stochastic Langevin-like term defined in terms of a background temperature. In the absence of spatial gradients, it is shown first that the system reaches a homogeneous steady state where the energy lost by inelastic collisions and viscous friction is compensated for by the energy injected by the stochastic force. Once the homogeneous steady state is characterized, a *normal* solution to the set of Enskog equations is obtained by means of the Chapman-Enskog expansion around the *local* version of the homogeneous state. To first order in spatial gradients, the Chapman-Enskog solution allows us to identify the Navier-Stokes transport coefficients associated with the mass, momentum, and heat fluxes. In addition, the first-order contributions to the partial temperatures and the cooling rate are also calculated. Explicit forms for the diffusion coefficients, the shear and bulk viscosities, and the first-order contributions to the partial temperatures and the cooling rate are obtained in steady-state conditions by retaining the leading terms in a Sonine polynomial expansion. The results show that the dependence of the transport coefficients on inelasticity is clearly different from that found in its granular counterpart (no gas phase). The present work extends previous theoretical results for *dilute* multicomponent granular suspensions [Khalil and Garzó, Phys. Rev. E **88**, 052201 (2013)] to higher densities.

DOI: 10.1103/PhysRevE.101.012904

I. INTRODUCTION

It is known that granular matter in nature is generally immersed in a fluid, like air or water, and so a granular flow is a multiphase process. However, there are situations where the influence of the interstitial fluid on the granular flow can be ignored. This happens, for instance, when the stress due to the grains is greater than that exerted by the fluid phase. Otherwise, there are many interesting phenomena (such as species segregation in granular mixtures [1–6]) where the effect of the fluid phase cannot be neglected, and hence, in principle, one has to start from a theoretical description that accounts for both phases (fluid and solid phases). In the case of monodisperse gas-solid flows, one possibility would be to describe the granular suspension in terms of a set of two coupled kinetic equations for each one of the velocity distributions of the different phases. However, the resulting theory would be very difficult to solve, since in particular the different phases evolve over quite different spatial and temporal scales. The problem would be even more complex when one considers multicomponent gas-solid flows. Thus, due to the technical difficulties involved in the above approach, it is more frequent in gas-solid flows to consider a suspension model where the effect of the interstitial fluid on the solid particles is via an effective external force [7].

The fluid-solid external force that models the effect of the viscous gas on solid particles is usually constituted by two different terms [8–11]. On the one hand, the first term includes a dissipative force obeying Stokes' law, namely, a viscous drag force proportional to the instantaneous particle velocity. On the other hand, the second term has a stochastic component, modeled as a Gaussian white noise [12]. This stochastic force provides kinetic energy to the solid particles by randomly kicking them [13]. Hence, while the drag force tries to model the friction of grains with the interstitial gas phase, the stochastic Langevin-like term mimics the energy transfer from the surrounding gas particles to the granular particles. The above suspension model has been recently [14] employed to get the Navier-Stokes transport coefficients of

[*]ruben@unex.es
[†]nagi.khalil@urjc.es
[‡]vicenteg@unex.es; http://www.unex.es/eweb/fisteor/vicente/

monocomponent granular suspensions by solving the Enskog equation for inelastic hard spheres by means of the Chapman-Enskog method [15] adapted to dissipative dynamics.

The determination of the Navier-Stokes transport coefficients of multicomponent granular suspensions is challenging. This target is relevant not only from a fundamental point of view but also from a more practical point of view since real gas-solid flows are usually present in nature as an ensemble of particles of different masses, sizes, and coefficients of restitution. In such a case, given that the number of variables and parameters involved in the analysis of multicomponent systems is very large, it is usual to consider first more simple systems, such as multicomponent granular suspensions at low density. This was carried out previously in three papers [10,16,17] where the complete set of Navier-Stokes transport coefficients of a binary mixture were obtained from the Boltzmann kinetic equation.

The objective of this paper is to extend the analysis performed for *dilute* bidisperse suspensions [10,16,17] to the (inelastic) Enskog kinetic theory [18] for a description of hydrodynamics and transport at higher densities. Since this theory applies for moderate densities (let's say, for instance, solid volume fraction $\phi \lesssim 0.25$ for hard spheres), a comparison between kinetic theory and molecular dynamics (MD) simulations becomes practical. This is perhaps one of the main motivations of the present study.

As mentioned before, we want to derive here the Navier-Stokes hydrodynamic equations of multicomponent granular suspensions by solving the Enskog kinetic equation with the Chapman-Enskog method. An important point in the application of this method to the Enskog equation is the reference state to be used in the perturbation scheme. As in the case of *dry* (no gas phase) granular gases [18], the zeroth-order velocity distribution $f_i^{(0)}$ of the component i cannot be chosen *a priori* and must be consistently obtained as a solution of the Enskog equation in the absence of spatial gradients. Since we are interested here in computing the transport coefficients under steady-state conditions, for simplicity one could take a steady distribution $f_i^{(0)}$ at any point of the system [19,20]. However, this steady distribution is not the most general election for $f_i^{(0)}$ since the presence of the interstitial fluid introduces the possibility of a local energy unbalance, and, hence, the zeroth-order distributions $f_i^{(0)}$ of each component in the Chapman-Enskog solution are not in general stationary distributions. This is because for arbitrary small deviations from the homogeneous steady state the energy gained by grains due to collisions with the background fluid cannot be locally compensated with the other cooling terms arising from the viscous friction and the collisional dissipation. Thus, in order to get the transport coefficients, we have to achieve first the *unsteady* set of integral equations verifying the first-order distributions $f_i^{(1)}$, and then we have to solve the above set under steady-state conditions. As a consequence, the transport coefficients depend not only on the steady temperature but also on some quantities (derivatives of the temperature ratio) which provide indirect information on the departure of the time-dependent solution $f_i^{(0)}$ from its stationary form.

The mass, momentum, and heat fluxes are calculated here up to first order in the spatial gradients of the hydrodynamic fields. In addition, there are contributions to the partial temperatures and the cooling rate proportional to the divergence of the flow velocity field. These new contributions have been recently [21] evaluated for dry granular mixtures. As happens for binary systems [22–24], the determination of the 12 relevant Navier-Stokes transport coefficients of a binary mixture (10 transport coefficients and two first-order contributions to the partial temperatures and the cooling rate) requires one to solve 10 coupled integral equations. This is, of course, a very long task. For this reason, in this work we will address the determination of the four diffusion coefficients associated with the mass flux, the shear and bulk viscosities coefficients, and the first-order contributions to the partial temperatures and the cooling rate.

The plan of the paper is as follows. The set of coupled Enskog equations for multicomponent granular suspensions and the corresponding balance equations for the densities of mass, momentum, and energy are derived in Sec. II. Then Sec. III analyzes the steady homogeneous state. As in previous works [10,25,26], scaling solutions are proposed whose dependence on the temperature T occurs through the dimensionless velocity $\mathbf{c} = \mathbf{v}/v_0$ (v_0 being a thermal speed) and the reduced temperature $\theta = T/T_{\text{ex}}$ (T_{ex} being the background temperature). Theoretical predictions for the temperature ratio of both components T_1/T_2 are compared against MD simulations. The comparison shows in general a good agreement for conditions of practical interest. Section IV is focused on the application of the Chapman-Enskog expansion around the unsteady reference distributions $f_i^{(0)}(\mathbf{r}, \mathbf{v}, t)$ up to first order in the spatial gradients. The Navier-Stokes transport coefficients are defined in Sec. V and given in terms of the solutions of a set of linear coupled integral equations. The leading terms in a Sonine polynomial expansion are considered in Sec. VI to solve the integral equations defining the diffusion coefficients, the shear viscosity, and the first-order contributions to the partial temperatures and the cooling rate. All these coefficients are explicitly determined as functions of both the granular and background temperatures, the density, the concentration, and the mechanical parameters of the mixture (masses, diameters, and coefficients of restitution). The dependence of the transport coefficients, the partial temperatures, and the cooling rate on the parameter space is illustrated in Sec. VII for several systems. It is shown that the impact of the gas phase on the transport coefficients is in general quite significant since their dependence on inelasticity is different from the one obtained for dry granular mixtures [18,22–24]. The paper is concluded in Sec. VIII with a brief discussion of the results obtained in this work. Further details of the calculations carried out here are given in three appendices.

II. ENSKOG KINETIC EQUATION FOR POLYDISPERSE GAS-SOLID FLOWS

A. Model for multicomponent granular suspensions

We consider a binary mixture composed of inelastic hard disks ($d = 2$) or spheres ($d = 3$) of masses m_i and diameters σ_i ($i = 1, 2$). The solid particles are immersed in an ordinary gas of viscosity η_g. Spheres are assumed to be completely smooth so that inelasticity of collisions between particles of the component i with particles of the component j is characterized only by the constant (positive) coefficients of

restitution $\alpha_{ij} \leqslant 1$. The mixture is also assumed to be in the presence of the gravitational field, and, hence, each particle feels the action of the force $\mathbf{F}_i = m_i\mathbf{g}$, where $\mathbf{g}$ is the gravity acceleration. For moderate densities, the one-particle velocity distribution function $f_i(\mathbf{r}, \mathbf{v}, t)$ of the component i verifies the set of nonlinear Enskog equations [18]

$$\frac{\partial f_i}{\partial t} + \mathbf{v}\cdot\nabla f_i + \mathbf{g}\cdot\frac{\partial f_i}{\partial \mathbf{v}} + \mathcal{F}_i f_i = \sum_{j=1}^{2} J_{ij}[\mathbf{r}, \mathbf{v}|f_i, f_j], \quad (1)$$

where the Enskog collision operator is

$$\begin{aligned} J_{ij}[\mathbf{r}_1, \mathbf{v}_1|f_i, f_j] &= \sigma_{ij}^{d-1}\int d\mathbf{v}_2 \int d\widehat{\boldsymbol{\sigma}}\,\Theta(\widehat{\boldsymbol{\sigma}}\cdot\mathbf{g}_{12})(\widehat{\boldsymbol{\sigma}}\cdot\mathbf{g}_{12}) \\ &\times\left[\alpha_{ij}^{-2}\chi_{ij}(\mathbf{r}_1, \mathbf{r}_1 - \boldsymbol{\sigma}_{ij})f_i(\mathbf{r}_1, \mathbf{v}_1'', t)f_j(\mathbf{r}_1 - \boldsymbol{\sigma}_{ij}, \mathbf{v}_2'', t)\right. \\ &\left. - \chi_{ij}(\mathbf{r}_1, \mathbf{r}_1 + \boldsymbol{\sigma}_{ij})f_i(\mathbf{r}_1, \mathbf{v}_1, t)f_j(\mathbf{r}_1 + \boldsymbol{\sigma}_{ij}, \mathbf{v}_2, t)\right]. \quad (2) \end{aligned}$$

In Eq. (1) the operator $\mathcal{F}_i$ represents the fluid-solid interaction force that models the effect of the viscous gas on the solid particles of the component i. Its explicit form will be given below. In addition, $\boldsymbol{\sigma}_{ij} = \sigma_{ij}\widehat{\boldsymbol{\sigma}}$, $\sigma_{ij} = (\sigma_i + \sigma_j)/2$, $\widehat{\boldsymbol{\sigma}}$ is a unit vector directed along the line of centers from the sphere of the component i to that of the component j at contact, Θ is the Heaviside step function, $\mathbf{g}_{12} = \mathbf{v}_1 - \mathbf{v}_2$ is the relative velocity of the colliding pair, and $\chi_{ij}(\mathbf{r}_1, \mathbf{r}_1 + \boldsymbol{\sigma}_{ij})$ is the equilibrium pair correlation function of two hard spheres, one for the component i and the other for the component j at contact (namely, when the distance between their centers is σ_{ij}). The precollisional velocities $(\mathbf{v}_1'', \mathbf{v}_2'')$ are given by

$$\mathbf{v}_1'' = \mathbf{v}_1 - \mu_{ji}\left(1 + \alpha_{ij}^{-1}\right)(\widehat{\boldsymbol{\sigma}}\cdot\mathbf{g}_{12})\widehat{\boldsymbol{\sigma}}, \quad (3)$$

$$\mathbf{v}_2' = \mathbf{v}_2 + \mu_{ij}\left(1 + \alpha_{ij}^{-1}\right)(\widehat{\boldsymbol{\sigma}}\cdot\mathbf{g}_{12})\widehat{\boldsymbol{\sigma}}, \quad (4)$$

where $\mu_{ij} = m_i/(m_i + m_j)$.

As in previous works on granular suspensions [9,11,14,27], the influence of the surrounding gas on the dynamics of grains is accounted for via an instantaneous fluid force. For low Reynolds numbers, we assume that the external force is composed of two independent terms. One term is a viscous drag force ($\mathbf{F}_i^{\text{drag}}$) proportional to the particle velocity $\mathbf{v}$. This term takes into account the friction of particles of the component i with the viscous gas. A subtle point in the choice of the explicit form of the drag force $\mathbf{F}_i^{\text{drag}}$ for multicomponent systems is that it can be defined to be the same for both components, or it can be chosen to be different for both components. Here, for consistency with simulations of bidisperse gas-solid flows [28–30], we will assume that

$$\mathbf{F}_i^{\text{drag}} = -m_i\gamma_i(\mathbf{v} - \mathbf{U}_g), \quad (5)$$

where γ_i is the (positive) drift or friction coefficient associated with the component i. In addition, since the model tries to model gas-solid flows, the drag force (5) has been defined in terms of the relative velocity $\mathbf{v} - \mathbf{U}_g$ where $\mathbf{U}_g$ is the mean fluid velocity of the gas phase. This latter quantity is assumed to be a known quantity of the suspension model. Thus, according to Eq. (5), in the Enskog equation (1) the drag force is represented by the operator

$$\mathcal{F}_i^{\text{drag}} f_i \to -\gamma_i\frac{\partial}{\partial \mathbf{v}}\cdot(\mathbf{v} - \mathbf{U}_g)f_i. \quad (6)$$

The second term in the gas-to-solid force corresponds to a stochastic Langevin force ($\mathbf{F}_i^{\text{st}}$) representing Gaussian white noise [12]. This force attempts to simulate the kinetic energy gain of grains due to eventual collisions with the more energetic particles of the surrounding gas [13]. In the context of the Enskog equation (1), the stochastic force is represented by a Fokker-Planck collision operator of the form [31–34]

$$\mathcal{F}_i^{\text{st}} f_i \to -\frac{\gamma_i T_{\text{ex}}}{m_i}\frac{\partial^2 f_i}{\partial v^2}, \quad (7)$$

where T_{ex} can be interpreted as the temperature of the background (or bath) gas.

Although the drift coefficient γ_i is in general a tensor, here for simplicity we assume that this coefficient is a scalar proportional to the viscosity of the gas phase η_g [7]. In addition, according to the results obtained in lattice-Boltzmann simulations of low-Reynolds-number fluid flow in bidisperse suspensions [28–30], the friction coefficients γ_i must be functions of the partial volume fractions ϕ_i and the total volume fraction $\phi = \phi_1 + \phi_2$ where

$$\phi_i = \frac{\pi^{d/2}}{2^{d-1}d\Gamma\left(\frac{d}{2}\right)}n_i\sigma_i^d. \quad (8)$$

Here

$$n_i = \int d\mathbf{v}\, f_i(\mathbf{v}) \quad (9)$$

is the local number density of the component i. The coefficients γ_i can be written as

$$\gamma_i = \gamma_0 R_i(\phi_i, \phi), \quad (10)$$

where $\gamma_0 \propto \eta_g \propto \sqrt{T_{\text{ex}}}$. Explicit forms of $R_i(\phi_i, \phi)$ can be found in the literature for polydisperse gas-solid flows [28–30]. In particular, for hard spheres ($d = 3$), low-Reynolds-number fluid and moderate densities, Yin and Sundaresan [29] have proposed the expression $\gamma_i = (18\eta_g/\rho\sigma_{12}^2)R_i$ where the dimensionless function R_i is

$$\begin{aligned} R_i(\phi_i, \phi) = \frac{\rho\sigma_{12}^2}{\rho_i\sigma_i^2}\frac{(1-\phi)\phi_i\sigma_i}{\phi}\sum_{j=1}^{2}\frac{\phi_j}{\sigma_j}\left[\frac{10\phi}{(1-\phi)^2}\right. \\ \left. + (1-\phi)^2(1 + 1.5\sqrt{\phi})\right]. \quad (11) \end{aligned}$$

Hence, according to Eqs. (6) and (7), the operator $\mathcal{F}_i f_i$ reads

$$\begin{aligned} \mathcal{F}_i f_i &= \mathcal{F}_i^{\text{drag}} f_i + \mathcal{F}_i^{\text{st}} f_i \\ &\to -\gamma_i\Delta\mathbf{U}\cdot\frac{\partial f_i}{\partial \mathbf{v}} - \gamma_i\frac{\partial}{\partial \mathbf{v}}\cdot\mathbf{V}f_i - \frac{\gamma_i T_{\text{ex}}}{m_i}\frac{\partial^2 f_i}{\partial v^2}, \end{aligned} \quad (12)$$

and the Enskog equation for the component i becomes

$$\begin{aligned} \frac{\partial f_i}{\partial t} + \mathbf{v}\cdot\nabla f_i + \mathbf{g}\cdot\frac{\partial f_i}{\partial \mathbf{v}} - \gamma_i\Delta\mathbf{U}\cdot\frac{\partial f_i}{\partial \mathbf{v}} - \gamma_i\frac{\partial}{\partial \mathbf{v}}\cdot\mathbf{V}f_i \\ - \frac{\gamma_i T_{\text{ex}}}{m_i}\frac{\partial^2 f_i}{\partial v^2} = \sum_{j=1}^{2} J_{ij}[f_i, f_j]. \quad (13) \end{aligned}$$

In Eq. (12), $\Delta\mathbf{U} = \mathbf{U} - \mathbf{U}_g$, $\mathbf{V} = \mathbf{v} - \mathbf{U}$ is the peculiar velocity, and

$$\mathbf{U} = \rho^{-1} \sum_{i=1}^{2} \int d\mathbf{v}\, m_i \mathbf{v} f_i(\mathbf{v}) \tag{14}$$

is the local mean flow velocity of the mixture. Here $\rho = \sum_i \rho_i$ is the total mass density, and $\rho_i = m_i n_i$ is the mass density of the component i.

The suspension model (13) is similar to the one proposed in Ref. [10] to obtain the Navier-Stokes transport coefficients of multicomponent granular suspensions at low density. In this latter model [10], the gas phase depends on two parameters: the friction coefficient of the drag force (γ_b in the notation of Ref. [10]) and the strength of the correlation (ξ_b^2 in the notation of Ref. [10]). However, in contrast with the suspension model proposed here, both parameters (γ_b and ξ_b^2) were assumed to be independent and the same for each one of the components. Therefore, in the low-density limit, the results derived here reduce to those obtained previously [10] when one makes the changes $\gamma_1 = \gamma_2 = \gamma_b$ [with $R_i(\phi_i, \phi) = 1$] and $\xi_b^2 = 2\gamma_b T_{ex}$. Here, in the notation of Ref. [10], the other constants of the driven model are chosen to be $\beta = 0$ and $\lambda = 1$; this is one of the possible elections consistent with the fluctuation-dissipation theorem for elastic collisions [12].

B. Balance equations

Apart from the partial densities n_i and the flow velocity $\mathbf{U}$, the other important hydrodynamic field is the granular temperature T. It is defined as

$$T = \frac{1}{n} \sum_{i=1}^{2} \int d\mathbf{v} \frac{m_i}{d} V^2 f_i(\mathbf{v}), \tag{15}$$

where $n = n_1 + n_2$ is the total number density. The granular temperature T can also be defined in terms of the partial kinetic temperatures T_1 and T_2 of the components 1 and 2, respectively. The partial kinetic temperature T_i measures the mean kinetic energy of the component i. They are defined as

$$T_i = \frac{m_i}{d n_i} \int d\mathbf{v}\, V^2 f_i(\mathbf{v}), \quad i = 1, 2. \tag{16}$$

In accordance with Eq. (15), the granular temperature T of the mixture also can be written as

$$T = \sum_{i=1}^{2} x_i T_i, \tag{17}$$

where $x_i = n_i/n$ is the concentration or mole fraction of the component i.

In order to obtain the balance equations for the hydrodynamic fields, an important property of the integrals involving the (inelastic) Enskog collision operator $J_{ij}[\mathbf{r}, \mathbf{v}|f_i, f_j]$ is [18,35]

$$\begin{aligned} I_\psi &\equiv \int d\mathbf{v}_1\, \psi(\mathbf{v}_1) J_{ij}[\mathbf{r}_1, \mathbf{v}_1|f_i, f_j] \\ &= \sigma_{ij}^{d-1} \int d\mathbf{v}_1 \int d\mathbf{v}_2 \int d\widehat{\boldsymbol{\sigma}}\, \Theta(\widehat{\boldsymbol{\sigma}} \cdot \mathbf{g}_{12})(\widehat{\boldsymbol{\sigma}} \cdot \mathbf{g}_{12}) \\ &\quad \times \chi_{ij}(\mathbf{r}_1, \mathbf{r}_1 + \boldsymbol{\sigma}_{ij}) f_i(\mathbf{r}_1, \mathbf{v}_1, t) f_j(\mathbf{r}_1 + \boldsymbol{\sigma}_{ij}, \mathbf{v}_2, t) \\ &\quad \times [\psi(\mathbf{v}_1') - \psi(\mathbf{v}_1)], \end{aligned} \tag{18}$$

where $\psi(\mathbf{v})$ is an arbitrary function of $\mathbf{v}$ and

$$\mathbf{v}_1' = \mathbf{v}_1 - \mu_{ji}(1 + \alpha_{ij})(\widehat{\boldsymbol{\sigma}} \cdot \mathbf{g}_{12})\widehat{\boldsymbol{\sigma}}. \tag{19}$$

The balance equations for the densities of mass, momentum, and energy can be derived by taking velocity moments in the Enskog equation (13) and using the property (18). They read

$$D_t n_i + n_i \nabla \cdot \mathbf{U} + \frac{\nabla \cdot \mathbf{j}_i}{m_i} = 0, \tag{20}$$

$$D_t \mathbf{U} + \rho^{-1} \nabla \cdot \mathsf{P} = \mathbf{g} - \rho^{-1} \Delta\mathbf{U} \sum_{i=1}^{2} \rho_i \gamma_i - \rho^{-1}(\gamma_1 - \gamma_2)\mathbf{j}_1, \tag{21}$$

$$\begin{aligned} D_t T - \frac{T}{n} \sum_{i=1}^{2} \frac{\nabla \cdot \mathbf{j}_i}{m_i} + \frac{2}{dn}(\nabla \cdot \mathbf{q} + \mathsf{P} : \nabla\mathbf{U}) \\ = -\frac{2}{dn} \Delta\mathbf{U} \cdot \sum_{i=1}^{2} \gamma_i \mathbf{j}_i + 2 \sum_{i=1}^{2} x_i \gamma_i (T_{ex} - T_i) - \zeta T. \end{aligned} \tag{22}$$

In the above equations, $D_t = \partial_t + \mathbf{U} \cdot \nabla$ is the material derivative, and

$$\mathbf{j}_i = m_i \int d\mathbf{v}\, \mathbf{V} f_i(\mathbf{v}) \tag{23}$$

is the mass flux for the component i relative to the local flow $\mathbf{U}$. A consequence of the definition (23) of the fluxes $\mathbf{j}_i$ is that $\mathbf{j}_1 = -\mathbf{j}_2$. The pressure tensor $\mathsf{P}(\mathbf{r}, t)$ and the heat flux $\mathbf{q}(\mathbf{r}, t)$ have both kinetic and collisional transfer contributions:

$$\mathsf{P} = \mathsf{P}^{k} + \mathsf{P}^{c}, \quad \mathbf{q} = \mathbf{q}^{k} + \mathbf{q}^{c}. \tag{24}$$

The kinetic contributions P^{k} and $\mathbf{q}^{k}$ are given by

$$\mathsf{P}^{k} = \sum_{i=1}^{2} \int d\mathbf{v}\, m_i \mathbf{V}\mathbf{V} f_i(\mathbf{v}), \tag{25}$$

$$\mathbf{q}^{k} = \sum_{i=1}^{2} \int d\mathbf{v}\, \frac{m_i}{2} V^2 \mathbf{V} f_i(\mathbf{v}). \tag{26}$$

The collisional transfer contributions are [22]

$$\begin{aligned} \mathsf{P}^{c} = \sum_{i=1}^{2} \sum_{j=1}^{2} \sigma_{ij}^{d} m_{ij} \frac{1 + \alpha_{ij}}{2} \int d\mathbf{v}_1 \int d\mathbf{v}_2 \int d\widehat{\boldsymbol{\sigma}} \\ \times \Theta(\widehat{\boldsymbol{\sigma}} \cdot \mathbf{g}_{12})(\widehat{\boldsymbol{\sigma}} \cdot \mathbf{g}_{12})^2 \widehat{\boldsymbol{\sigma}}\widehat{\boldsymbol{\sigma}} \int_0^1 dx \\ \times f_{ij}^{(2)}[\mathbf{r} - x\boldsymbol{\sigma}_{ij}, \mathbf{r} + (1 - x)\boldsymbol{\sigma}_{ij}, \mathbf{v}_1, \mathbf{v}_2, t], \end{aligned} \tag{27}$$

$$\begin{aligned} \mathbf{q}^{c} = \sum_{i=1}^{2} \sum_{j=1}^{2} \sigma_{ij}^{d} m_{ij} \frac{1 + \alpha_{ij}}{8} \int d\mathbf{v}_1 \int d\mathbf{v}_2 \int d\widehat{\boldsymbol{\sigma}} \\ \times \Theta(\widehat{\boldsymbol{\sigma}} \cdot \mathbf{g}_{12})(\widehat{\boldsymbol{\sigma}} \cdot \mathbf{g}_{12})^2 \widehat{\boldsymbol{\sigma}} [4(\widehat{\boldsymbol{\sigma}} \cdot \mathbf{G}_{ij}) \\ + (\mu_{ji} - \mu_{ij})(1 - \alpha_{ij})(\widehat{\boldsymbol{\sigma}} \cdot \mathbf{g}_{12})] \int_0^1 dx \\ \times f_{ij}^{(2)}[\mathbf{r} - x\boldsymbol{\sigma}_{ij}, \mathbf{r} + (1 - x)\boldsymbol{\sigma}_{ij}, \mathbf{v}_1, \mathbf{v}_2; t]. \end{aligned} \tag{28}$$

Here $m_{ij} = m_i m_j/(m_i + m_j)$ is the reduced mass, $\mathbf{G}_{ij} = \mu_{ij}\mathbf{V}_1 + \mu_{ji}\mathbf{V}_2$ is the velocity of the center of mass, and

$$f_{ij}^{(2)}(\mathbf{r}_1, \mathbf{r}_2, \mathbf{v}_1, \mathbf{v}_2, t) \equiv \chi_{ij}(\mathbf{r}_1, \mathbf{r}_2) f_i(\mathbf{r}_1, \mathbf{v}_1, t) f_j(\mathbf{r}_2, \mathbf{v}_2, t). \tag{29}$$

Finally, the (total) cooling rate ζ is due to inelastic collisions among all components. It is given by

$$\zeta = \frac{1}{2dnT}\sum_{i=1}^{2}\sum_{j=1}^{2}\sigma_{ij}^{d-1} m_{ij}\left(1-\alpha_{ij}^2\right)\int d\mathbf{v}_1 \int d\mathbf{v}_2 \int d\widehat{\boldsymbol{\sigma}} \times \Theta(\widehat{\boldsymbol{\sigma}}\cdot\mathbf{g}_{12})(\widehat{\boldsymbol{\sigma}}\cdot\mathbf{g}_{12})^3 f_{ij}^{(2)}[\mathbf{r}, \mathbf{r}+\boldsymbol{\sigma}_{ij}, \mathbf{v}_1, \mathbf{v}_2; t]. \tag{30}$$

As expected, the balance equations (20)–(22) are not a closed set of equations for the fields n_1, n_2, $\mathbf{U}$, and T. To turn these equations into a set of closed equations, one has to express the fluxes and the cooling rate in terms of the hydrodynamic fields and their gradients. The corresponding constitutive equations can be obtained by solving the Enskog kinetic equation (13) from the Chapman-Enskog method [15] adapted to dissipative dynamics. This will be worked out in Sec. IV.

III. HOMOGENEOUS STEADY STATES

A. Time-dependent state

Before considering inhomogeneous states, we will study first the homogeneous problem. This state has been widely analyzed in Ref. [10] for a similar suspension model. In the homogeneous state, the partial densities $n_i(\mathbf{r}, t) \equiv n_i$ are constant, the granular temperature $T(\mathbf{r}, t) \equiv T(t)$ is spatially uniform, the gas velocity $\mathbf{U}_g$ is assumed to be uniform, and, with an appropriate selection of the reference frame, both mean flow velocities vanish ($\mathbf{U} = \mathbf{U}_g = \mathbf{0}$). Under these conditions and in the absence of gravity ($\mathbf{g} = \mathbf{0}$), Eq. (13) reads

$$\partial_t f_i - \gamma_i \frac{\partial}{\partial \mathbf{v}}\cdot\mathbf{v} f_i - \frac{\gamma_i T_{\rm ex}}{m_i}\frac{\partial^2 f_i}{\partial v^2} = \sum_{j=1}^{2} J_{ij}[f_i, f_j], \tag{31}$$

where

$$J_{ij}[f_i, f_j] = \chi_{ij}\sigma_{ij}^{d-1}\int d\mathbf{v}_2 \int d\widehat{\boldsymbol{\sigma}}\,\Theta(\widehat{\boldsymbol{\sigma}}\cdot\mathbf{g}_{12})(\widehat{\boldsymbol{\sigma}}\cdot\mathbf{g}_{12}) \times\left[\alpha_{ij}^{-2} f_i(\mathbf{v}_1'') f_j(\mathbf{v}_2'') - f_i(\mathbf{v}_1) f_j(\mathbf{v}_2)\right] \tag{32}$$

is the Boltzmann collision operator multiplied by the (constant) pair correlation function χ_{ij}. For homogeneous states, the fluxes vanish, and so the only nontrivial balance equation is that of the temperature (22):

$$\partial_t T = 2\sum_{i=1}^{2} x_i\gamma_i(T_{\rm ex} - T_i) - \zeta T, \tag{33}$$

where, according to Eq. (30), the expression of ζ for homogeneous states can be written as

$$\zeta = \frac{\pi^{(d-1)/2}}{2d\Gamma\left(\frac{d+3}{2}\right)}\frac{1}{nT}\sum_{i=1}^{2}\sum_{j=1}^{2}\sigma_{ij}^{d-1} m_{ij}\chi_{ij}\left(1-\alpha_{ij}^2\right) \times\int d\mathbf{v}_1\int d\mathbf{v}_2\, g_{12}^3\, f_i(\mathbf{v}_1) f_j(\mathbf{v}_2). \tag{34}$$

Analogously, the evolution equation for the partial temperatures T_i can be obtained from Eq. (31) as

$$\partial_t T_i = 2\gamma_i(T_{\rm ex} - T_i) - \zeta_i T_i, \tag{35}$$

where we have introduced the partial cooling rates ζ_i for the partial temperatures T_i. They are defined as

$$\zeta_i = -\frac{m_i}{dn_i T_i}\sum_{j=1}^{2}\int d\mathbf{v}\, V^2 J_{ij}[f_i, f_j]. \tag{36}$$

The total cooling rate ζ can be rewritten in terms of the partial cooling rates ζ_i when one takes into account the constraint (17) and the evolution equations (33) and (35). The result is

$$\zeta = \sum_{i=1}^{2} x_i\tau_i\zeta_i, \tag{37}$$

where $\tau_i = T_i/T$ is the temperature ratio of the component i.

As usual, for times longer than the mean-free time, the system is expected to reach a hydrodynamic regime where the distributions f_i depend on time through the only time-dependent hydrodynamic field of the problem: the granular temperature T [36]. In this regime,

$$\partial_t f_i = \frac{\partial f_i}{\partial T}\partial_t T = \left[2\sum_{i=1}^{2} x_i\gamma_i(\theta^{-1} - \tau_i) - \zeta\right] T\frac{\partial f_i}{\partial T}, \tag{38}$$

and the homogeneous Enskog equation (31) becomes

$$\left[2\sum_{i=1}^{2} x_i\gamma_i(\theta^{-1} - \tau_i) - \zeta\right] T\frac{\partial f_i}{\partial T} - \gamma_i\frac{\partial}{\partial \mathbf{v}}\cdot\mathbf{v} f_i - \frac{\gamma_i T_{\rm ex}}{m_i}\frac{\partial^2 f_i}{\partial v^2} = \sum_{j=1}^{2} J_{ij}[f_i, f_j], \tag{39}$$

where $\theta = T/T_{\rm ex}$.

B. Steady state

In the *steady* state ($\partial_t T_i = 0$), Eq. (35) gives the following set of coupled equations for the (asymptotic) partial temperatures $T_{i,s}$:

$$2\gamma_i(T_{\rm ex} - T_{i,s}) - \zeta_{i,s}T_{i,s} = 0, \tag{40}$$

where the subscript s means that all the quantities are evaluated in the steady state. To determine these temperatures one has to get the steady-state solution to Eq. (39). By using the relation

$$2\sum_{i=1}^{2} x_i\gamma_i(\theta^{-1} - \tau_i) - \zeta = 0, \tag{41}$$

Eq. (39) reads

$$-\gamma_i\frac{\partial}{\partial \mathbf{v}}\cdot\mathbf{v} f_{i,s} - \frac{\gamma_i T_{\rm ex}}{m_i}\frac{\partial^2 f_{i,s}}{\partial v^2} = \sum_{j=1}^{2} J_{ij}[f_{i,s}, f_{j,s}]. \tag{42}$$

As shown for dilute driven multicomponent granular gases [10], dimensionless analysis requires that $f_{i,s}$ has the scaled form

$$f_{i,s}(n_i, \mathbf{v}, \gamma_i, T_{\rm ex}) = n_i v_0^{-d}\varphi_{i,s}(\mathbf{c}, x_1, \gamma_{i,s}^*, \theta_s), \tag{43}$$

where the unknown scaled function $\varphi_{i,s}$ depends on the dimensionless parameters

$$\mathbf{c} = \frac{\mathbf{v}}{v_{0s}}, \quad \gamma_{i,s}^* = \frac{\gamma_i}{n\sigma_{12}^{d-1} v_{0s}}. \tag{44}$$

Here $v_{0s} = \sqrt{2T_s/\overline{m}}$ is the thermal speed and $\overline{m} = \sum_i m_i/2$. Note that the time-dependent velocity distribution function $f_i(\mathbf{v}, t)$ also admits the scaling form (43).

The (reduced) drift parameters $\gamma_{i,s}^*$ can be easily expressed in terms of the mole fraction, the volume fractions ϕ_i and ϕ, and the (reduced) temperature θ_s as

$$\gamma_{i,s}^* = \lambda_i \theta_s^{-1/2}, \quad \lambda_i = \frac{\sqrt{2}\pi^{d/2}}{2^d d\Gamma\left(\frac{d}{2}\right)} \frac{R_i(\phi_i, \phi)}{\sqrt{T_{\rm ex}^*} \sum_j (\sigma_{12}/\sigma_j)^d \phi_j}, \tag{45}$$

$T_{\rm ex}^* \equiv T_{\rm ex}/(\overline{m}\sigma_{12}^2\gamma_0^2)$ being the (dimensionless) background gas temperature. Note that $\lambda_1/R_1 = \lambda_2/R_2$. As expected from previous works [10,14,37,38], the dependence of the scaled distribution $\varphi_{i,s}$ on the temperature is not only through the dimensionless velocity $\mathbf{c}$ but also through the dimensionless parameter θ_s. This scaling differs from the one assumed in free cooling systems [31,39] where all the temperature dependence of $\varphi_{i,s}$ is encoded through $\mathbf{c}$.

The scaling given by Eq. (43) is equivalent to the one proposed in Ref. [10] when one makes the mapping $\xi_{\rm s}^* \to 2\lambda\theta_{\rm s}^{-3/2}$, where $\lambda_1 = \lambda_2 = \lambda$ and $R_1 = R_2 = 1$. The dimensionless parameter $\xi_{\rm s}^*$ is defined by Eq. (34) of Ref. [10]. Thus, in the particular case of $\lambda_i = \lambda$ and $R_i = 1$, the results for homogeneous states are consistent with those derived before [10] in the dilute regime ($\phi \to 0$).

In reduced form, Eq. (42) can be rewritten as

$$-\gamma_{i,s}^* \frac{\partial}{\partial \mathbf{c}} \cdot \mathbf{c}\varphi_{i,s} - \frac{\gamma_{i,s}^*}{2M_i\theta_s} \frac{\partial^2 \varphi_{i,s}}{\partial c^2} = \sum_{j=1}^{2} J_{ij}^*[\varphi_{i,s}, \varphi_{j,s}], \tag{46}$$

where $M_i = m_i/\overline{m}$ and $J_{ij}^* = \ell J_{ij}/n_i v_{0s}^{1-d}$, $\ell = 1/n\sigma_{12}^{d-1}$ being proportional to the mean-free path of hard spheres. The knowledge of the distributions φ_i allows us to get the partial temperatures and the partial cooling rates. In the case of elastic collisions ($\alpha_{ij} = 1$), $T_{1,s} = T_{2,s} = T_s = T_{\rm ex}$ and hence, Eq. (46) admits the simple solution $\varphi_{i,s} = \pi^{-d/2} M_i^{d/2} e^{-M_i c^2}$. However, the exact form of the above distributions is not known for inelastic collisions, and, hence, one has to consider approximate forms for $\varphi_{i,s}$. In particular, previous results derived for driven granular mixtures [34,40,41] have shown that the partial temperatures can be well estimated by using Maxwellian distributions at different temperatures for the scaled distributions $\varphi_{i,s}(\mathbf{c})$:

$$\varphi_{i,s}(\mathbf{c}) \to \varphi_{i,\rm M}(\mathbf{c}) = \pi^{-d/2} \beta_i^{d/2} e^{-\beta_i c^2}, \tag{47}$$

where $\beta_i = M_i T_s/T_{i,s}$. The (reduced) cooling rate $\zeta_{i,s}^* = \ell\zeta_{i,s}/v_{0s}$ can be determined by taking the approximation (47) in Eq. (36). The result is

$$\zeta_{i,s}^* = \frac{4\pi^{(d-1)/2}}{d\Gamma\left(\frac{d}{2}\right)} \sum_{j=1}^{2} x_j \chi_{ij} \mu_{ji} \left(\frac{\sigma_{ij}}{\sigma_{12}}\right)^{d-1} \left(\frac{\beta_i + \beta_j}{\beta_i \beta_j}\right)^{1/2} \times (1 + \alpha_{ij}) \left[1 - \frac{\mu_{ji}}{2}(1 + \alpha_{ij}) \frac{\beta_i + \beta_j}{\beta_j}\right]. \tag{48}$$

The (reduced) partial temperatures $\theta_{i,s} = T_{i,s}/T_{\rm ex}$ can be obtained from the steady-state condition (40) for $i = 1, 2$. In reduced form, the equation for $\theta_{i,s}$ can be written as

$$2\lambda_i \theta_s^{-1/2}(1 - \theta_{i,s}) - \zeta_{i,s}^* \theta_{i,s} = 0. \tag{49}$$

Note that Eq. (17) imposes the constraint $x_1\theta_{1,s} + x_2\theta_{2,s} = \theta_s$. Substitution of Eq. (48) into the set of equations (49) allows us to get the partial temperatures in terms of the concentration x_1, the solid volume fraction ϕ, the (reduced) background temperature $T_{\rm ex}^*$, and the mechanical parameters of the mixture (mass and diameter ratios and coefficients of restitution). In the low-density limit, Eq. (49) is consistent with the one obtained in Ref. [10] after making the change $2\lambda_i\theta_s^{-1/2} = \xi_s^*$.

Figure 1 shows the dependence of the temperature ratio $T_{1,s}/T_{2,s}$ on the (common) coefficient of restitution α ($\alpha \equiv \alpha_{11} = \alpha_{22} = \alpha_{12}$) for a binary granular suspension of hard spheres ($d = 3$). The lines are the theoretical results derived from the Enskog equation, and the symbols refer to the results obtained via event-driven MD simulations [42,43]. We have simulated a system constituted by a total number of $N = 20^3$ inelastic, smooth hard spheres. The system is inside a three-dimensional box of size L with periodic boundary conditions. In addition to the interparticle collisions, particles of each component change their velocities due to the interactions with the bath (with $\mathbf{U}_g = \mathbf{0}$), as explained in Ref. [41]. Three different values of the solid volume fractions ϕ have been analyzed: $\phi = 0.00785$, $\phi = 0.1$, and $\phi = 0.2$. The first system corresponds to a very dilute granular suspension, while the two latter can be considered as moderately dense granular suspensions. Two different values of the common coefficient of restitution have been chosen, $\alpha = 0.8$ and $\alpha = 0.9$. Both values of α represent a moderate degree of inelasticity. The symbols are the simulation data where the squares are for $\alpha = 0.8$ and the triangles are for $\alpha = 0.9$. The Enskog theoretical predictions are given by the solid ($\alpha = 0.8$) and dashed ($\alpha = 0.9$) lines.

Figure 1 highlights the excellent agreement found between the Enskog theory and simulations in both the low-density limit ($\phi = 0.00785$) and moderate density ($\phi = 0.1$). This agreement is kept for both values of inelasticity and over the whole range of mass ratios studied. The agreement is also excellent for $\phi = 0.2$ and $\alpha = 0.9$; more quantitative discrepancies appear for $\alpha = 0.8$, especially for large values of the mass ratio. These differences between the Enskog theory and MD simulations for moderate densities and strong inelasticity could be due to the fact that the impact of the cumulants (which have been neglected in our solution) on the temperature ratio could be non-negligible in this region of the parameter space or due to a failure of the Enskog theory (namely, molecular chaos hypothesis fails at high densities and strong inelasticity). In any case, the good performance of the Enskog results found here for the temperature ratio contrasts with the results obtained in freely cooling granular mixtures [33] where significant differences between theory and simulations were found at $\phi = 0.2$ (see, for instance, Fig. 2 of Ref. [33]).

In summary, the comparison performed here for the temperature ratio in homogeneous steady states for granular suspensions shows again that the range of densities for which

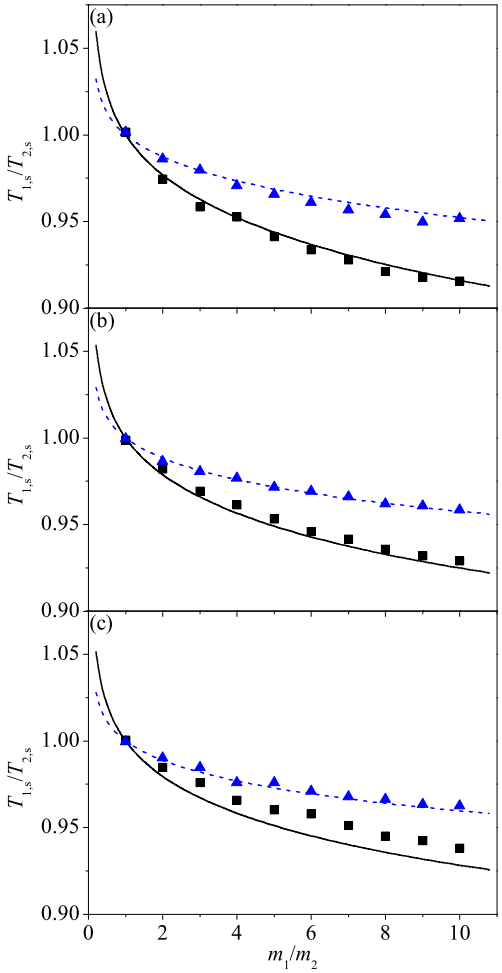

FIG. 1. Plot of the temperature ratio $T_{1,s}/T_{2,s}$ versus the mass ratio m_1/m_2 for a binary mixture of hard spheres ($d = 3$) with $x_1 = \frac{1}{2}$, $\sigma_1/\sigma_2 = 1$ and two different values of the (common) coefficient of restitution α: $\alpha = 0.8$ (solid lines and squares) and $\alpha = 0.9$ (dashed lines and triangles). The lines are the theoretical Enskog results, and the symbols refer to the MD simulation results. From top to bottom, panel (a) corresponds to $\phi = 0.00785$, panel (b) to $\phi = 0.1$, and panel (c) to $\phi = 0.2$. The value of the (reduced) background temperature is $T_{\text{ex}}^* = 1$.

the Enskog kinetic equation becomes reliable likely decreases with increasing inelasticity. This finding has been already achieved in some previous works [41,44–48]. However, despite this limitation, the Enskog theory can be still considered as a remarkable theory for describing transport properties for fluids with elastic and inelastic collisions.

IV. CHAPMAN-ENSKOG SOLUTION OF THE ENSKOG EQUATION

We assume now that the homogeneous steady state is slightly perturbed by the presence of spatial gradients. These gradients induce fluxes of mass, momentum, and energy. The knowledge of these fluxes allows us to identify the relevant transport coefficients of the bidisperse granular suspension. As in previous works on granular mixtures [10,22,23,49], we consider states that deviate from the reference state (homogeneous time-dependent state) by small spatial gradients. In this situation, the set of Enskog equations (13) can be solved by means of the Chapman-Enskog method [15] conveniently adapted to take into account the inelasticity in collisions.

As usual, for times longer than the grain-grain mean-free time and distances larger than the grain-grain mean-free path, we assume that the granular suspension has reached the so-called hydrodynamic regime [15,50]. In this regime, (1) the system has completely "forgotten" the details of the initial conditions and in addition (2) the hydrodynamic description is limited to the bulk domain of the system (namely, a region far away from the boundaries). Under these conditions, the Chapman-Enskog method seeks a special solution to the Enskog kinetic equation: the so-called *normal* or hydrodynamic solution. This type of solution is characterized by the fact that all space and time dependence of the distributions $f_i(\mathbf{r}, \mathbf{v}, t)$ occurs only via a functional dependence on the hydrodynamic fields.

On the other hand, as noted in previous papers of granular mixtures [22,49,51], there is more flexibility in the choice of the hydrodynamic fields for the mass and heat fluxes of multicomponent granular fluids. Here, to compare with the results previously derived for undriven dense granular mixtures [22], we take the partial densities n_1 and n_2, the temperature T, and the d components of the local flow velocity $\mathbf{U}$ as the $d + 3$ independent fields of the binary mixture. Therefore, in the hydrodynamic regime, the distributions $f_i(\mathbf{r}, \mathbf{v}, t)$ adopt the normal form

$$f_i(\mathbf{r}, \mathbf{v}, t) = f_i[\mathbf{v}|n_1(t), n_2(t), T(t), \mathbf{U}(t)]. \tag{50}$$

The notation on the right-hand side of Eq. (50) indicates a functional dependence on the partial densities, temperature, and flow velocity. Note that the functional dependence means that in order to determine f_i at the point $\mathbf{r}$ we need to know the fields not only at $\mathbf{r}$ but also at the remaining points of the system. This is formally equivalent to knowing n_1, n_2, T, and $\mathbf{U}$ and their spatial derivatives at $\mathbf{r}$.

Since we are perturbing the reference state with small spatial gradients, we can simplify the functional dependence (50) by expanding the distributions f_i in powers of the spatial gradients. In practice, in order to generate this expansion, f_i is expressed as a series expansion in a formal or bookkeeping parameter ϵ:

$$f_i = f_i^{(0)} + \epsilon f_i^{(1)} + \epsilon^2 f_i^{(2)} + \cdots, \tag{51}$$

where each factor ϵ means an implicit spatial gradient. Moreover, in ordering the different level of approximations in the Enskog kinetic equation, one has to characterize the magnitude of the friction coefficients γ_i, the gravity field $\mathbf{g}$, and the term $\Delta\mathbf{U}$ relative to the spatial gradients. As in the case of elastic collisions [15], since the gravity field induces a

pressure gradient ∇p (the so-called barometric formula), it is assumed first that the magnitude of $\mathbf{g}$ is at least of first order in the perturbation expansion. In addition, since γ_i does not give rise to any flux in the mixture, it is considered to be to zeroth order in gradients. Finally, with respect to the term $\Delta\mathbf{U}$, it is expected that this term is at least to first order in gradients because $\mathbf{U}$ relaxes to $\mathbf{U}_g$ in the absence of gradients.

As in the conventional Chapman-Enskog method [15], the time derivative ∂_t is also expanded as

$$\partial_t = \partial_t^{(0)} + \epsilon\partial_t^{(1)} + \cdots . \tag{52}$$

These expansions lead to similar expansions for the Enskog operators J_{ij}:

$$J_{ij} = J_{ij}^{(0)} + \epsilon J_{ij}^{(1)} + \cdots , \tag{53}$$

and the fluxes and the cooling rate when substituted into Eqs. (23)–(30):

$$\mathbf{j}_i = \mathbf{j}_i^{(0)} + \epsilon\mathbf{j}_i^{(1)} + \cdots , \quad \mathsf{P} = \mathsf{P}^{(0)} + \epsilon\mathsf{P}^{(1)} + \cdots , \tag{54}$$

$$\mathbf{q} = \mathbf{q}^{(0)} + \epsilon\mathbf{q}^{(1)} + \cdots , \quad \zeta = \zeta^{(0)} + \epsilon\zeta^{(1)} + \cdots . \tag{55}$$

In addition, although the partial temperatures T_i are not hydrodynamic quantities, they must be also expanded in powers of the gradients as [17,21]

$$T_i = T_i^{(0)} + \epsilon T_i^{(1)} + \cdots . \tag{56}$$

As usual, the hydrodynamic fields n_i, $\mathbf{U}$, and T are defined in terms of the zeroth-order approximation:

$$\int d\mathbf{v}\left(f_i - f_i^{(0)}\right) = 0, \tag{57}$$

$$\sum_{i=1}^{2}\int d\mathbf{v}\left\{m_i\mathbf{v}, \frac{m_i}{2}V^2\right\}\left(f_i - f_i^{(0)}\right) = \{\mathbf{0}, 0\}. \tag{58}$$

Since the constraints (57) and (58) must hold at any order in ϵ, one has

$$\int d\mathbf{v} f_i^{(\ell)} = 0 \tag{59}$$

and

$$\sum_{i=1}^{2}\int d\mathbf{v}\left\{m_i\mathbf{v}, \frac{m_i}{2}V^2\right\} f_i^{(\ell)} = \{\mathbf{0}, 0\} \tag{60}$$

for $\ell \geqslant 1$. A consequence of Eq. (60) is that $\mathbf{j}_1^{(\ell)} = -\mathbf{j}_2^{(\ell)}$ and $n_1 T_1^{(\ell)} = -n_2 T_2^{(\ell)}$ for $\ell \geqslant 1$. This is the usual application of the Chapman-Enskog method to solve kinetic equations. Here we will restrict our calculations to first order in ϵ, the so-called Navier-Stokes hydrodynamic order.

A. Zeroth-order approximation

To zeroth order in ϵ, the Enskog kinetic equation (13) for $f_i^{(0)}$ reads

$$\partial_t^{(0)} f_i^{(0)} - \gamma_i\frac{\partial}{\partial\mathbf{v}}\cdot\mathbf{V}f_i^{(0)} - \gamma_i\frac{T_{\text{ex}}}{m_i}\frac{\partial^2 f_i^{(0)}}{\partial v^2} = \sum_{j=1}^{2} J_{ij}^{(0)}\left[f_i^{(0)}, f_j^{(0)}\right], \tag{61}$$

where the collision operator $J_{ij}^{(0)}[f_i^{(0)}, f_j^{(0)}]$ is given by Eq. (32) with the replacement $f_i \to f_i^{(0)}(\mathbf{r}, \mathbf{v}, t)$. The balance equations at this order give

$$\partial_t^{(0)} n_i = 0, \quad \partial_t^{(0)}\mathbf{U} = \mathbf{0} \tag{62}$$

and

$$\partial_t^{(0)} T = 2\sum_{i=1}^{2} x_i\gamma_i\left(T_{\text{ex}} - T_i^{(0)}\right) - \zeta^{(0)}T, \tag{63}$$

where $\zeta^{(0)}$ is determined by Eq. (34) to zeroth order. In terms of $\zeta_i^{(0)}$, $\zeta^{(0)}$ is given by Eq. (37). An accurate estimate of $\zeta_i^{(0)}$ is obtained by considering the Maxwellian approximation (47) to φ_i. In this case, $\zeta_i^{(0)} = v_0\zeta_{i,0}^*/\ell$ where $v_0(T) = \sqrt{2T/m}$ and $\zeta_{i,0}^*$ is given by Eq. (48) with the replacements $x_i \to x_i(\mathbf{r}, t)$, $\chi_{ij} \to \chi_{ij}^{(0)}(\mathbf{r}, t)$, $T_{i,s} \to T_i^{(0)}(\mathbf{r}, t)$, and $T_s \to T(\mathbf{r}, t)$. Here $\chi_{ij}^{(0)}$ is obtained from the functional $\chi_{ij}(\mathbf{r}, \mathbf{r} \pm \boldsymbol{\sigma}_{ij}|\{n_\ell\})$ by evaluating all the densities n_ℓ at the point of interest $\mathbf{r}$. Furthermore, in Eqs. (62) and (63), use has been made of the isotropy in velocity of the zeroth-order distributions $f_i^{(0)}$ which lead to $\mathbf{j}_i^{(0)} = \mathbf{q}^{(0)} = \mathbf{0}$ and $P_{\lambda\beta} = p\delta_{\lambda\beta}$, where the hydrostatic pressure p is [22]

$$p = nT + \frac{\pi^{d/2}}{d\Gamma\left(\frac{d}{2}\right)}\sum_{i=1}^{2}\sum_{j=1}^{2}\mu_{ji}n_i n_j\sigma_{ij}^d\chi_{ij}^{(0)}T_i^{(0)}(1+\alpha_{ij}). \tag{64}$$

Since $f_i^{(0)}$ is a normal solution and the zeroth-order time derivatives of n_i and $\mathbf{U}$ are zero, then $\partial_t^{(0)} f_i^{(0)} = (\partial_T f_i^{(0)})\partial_t^{(0)} T$ where $\partial_t^{(0)} T$ is given by Eq. (63). With this result, Eq. (61) can be rewritten as

$$\Lambda^{(0)} T\frac{\partial f_i^{(0)}}{\partial T} - \gamma_i\frac{\partial}{\partial\mathbf{v}}\cdot\mathbf{V}f_i^{(0)} - \frac{\gamma_i T_{\text{ex}}}{m_i}\frac{\partial^2 f_i^{(0)}}{\partial v^2} = \sum_{j=1}^{2} J_{ij}^{(0)}\left[f_i^{(0)}, f_j^{(0)}\right], \tag{65}$$

where

$$\Lambda^{(0)} \equiv 2\sum_{i=1}^{2} x_i\gamma_i(\theta^{-1} - \tau_i) - \zeta^{(0)}. \tag{66}$$

Although Eq. (65) has the same form as the one corresponding Enskog equation (39) for a strictly homogeneous state, the zeroth-order solution $f_i^{(0)}(\mathbf{r}, \mathbf{v}, t)$ is a local distribution function. In fact, the stationary solution to Eq. (65) corresponds to $\Lambda^{(0)} = 0$ and has been previously studied in Sec. III. However, as noted in previous works [10,14,37,52], since the densities $n_i(\mathbf{r}, t)$ and the granular temperature $T(\mathbf{r}, t)$ are defined separately in the local reference state $f_i^{(0)}$, then the temperature is in general a time-dependent function ($\partial_t^{(0)} T \neq 0$). Thus, the distribution $f_i^{(0)}$ depends on time through its dependence on the temperature.

The solution to Eq. (65) can be expressed in the form (43) (with the replacements $\gamma_{i,s}^* \to \gamma_i^*$ and $\theta_s \to \theta$) where the scaled distribution φ_i verifies the *unsteady* equation

$$\left[2\sum_{i=1}^{2} x_i\gamma_i^*(\theta^{-1} - \tau_i) - \zeta_0^*\right]\theta\frac{\partial\varphi_i}{\partial\theta} + \left[\frac{\zeta_0^*}{2} - \sum_{i=1}^{2} x_i\gamma_i^* \times (\theta^{-1} - \tau_i) - \gamma_i^*\right]\frac{\partial}{\partial\mathbf{c}}\cdot\mathbf{c}\varphi_i - \frac{\gamma_i^*}{2M_i\theta}\frac{\partial^2\varphi_i}{\partial c^2} = \sum_{j=1}^{2} J_{ij}^*[\varphi_i, \varphi_j]. \tag{67}$$

Here the derivative $\partial\varphi_i/\partial\theta$ is taken at constant $\mathbf{c}$, $\zeta_0^* = \ell\zeta^{(0)}/v_0$, $\gamma_i^* = \lambda_i\theta^{-1/2}$, and upon deriving Eq. (67) use has been made of the property

$$T\frac{\partial f_i^{(0)}}{\partial T} = -\frac{1}{2}\frac{\partial}{\partial \mathbf{V}}\cdot\mathbf{V}f_i^{(0)} + n_i v_0^{-d}\theta\frac{\partial\varphi_i}{\partial\theta}. \tag{68}$$

The evolution of the temperature ratios τ_i may be easily obtained by multiplying Eq. (67) by c^2 and integrating over $\mathbf{c}$. In compact form, the result can be written as

$$\Lambda^*\theta\frac{\partial\tau_i}{\partial\theta} = -\tau_i\Lambda^* + \Lambda_i^*, \tag{69}$$

where $\tau_i = T_i^{(0)}/T$,

$$\Lambda^* = \frac{\ell\Lambda^{(0)}}{v_0} = x_1\Lambda_1^* + x_2\Lambda_2^*, \tag{70}$$

and

$$\Lambda_i^* = 2\gamma_i^*(\theta^{-1} - \tau_i) - \tau_i\zeta_{i,0}^*. \tag{71}$$

In the steady state ($\Lambda^* = \Lambda_i^* = 0$), Eqs. (69) are consistent with Eqs. (49) for $i = 1, 2$. Beyond the steady state, Eq. (69) must be numerically solved to obtain the dependence of τ_1 and τ_2 on θ. In addition, as will be shown in Sec. V, to determine the diffusion transport coefficients in the steady state one needs to know the derivatives $\Delta_{\theta,1} \equiv (\partial\tau_1/\partial\theta)_s$, $\Delta_{\lambda_1,1} \equiv (\partial\tau_1/\partial\lambda_1)_s$, $\Delta_{x_1,1} \equiv (\partial\tau_1/\partial x_1)_s$, and $\Delta_{\phi,1} \equiv (\partial\tau_1/\partial\phi)_s$. Here, as before, the subscript s means that all the derivatives are evaluated at the steady state. Since $\lambda_2 = (R_2/R_1)\lambda_1$, then $(\partial\tau_1/\partial\lambda_2)_s = (R_1/R_2)(\partial\tau_1/\partial\lambda_1)_s$. Analytical expressions of these derivatives are provided in Appendix A.

The dependence of the derivatives $\Delta_{\theta,1}$, $\Delta_{\lambda_1,1}$, $\Delta_{x_1,1}$, and $\Delta_{\phi,1}$ on the common coefficient of restitution $\alpha_{ij} \equiv \alpha$ is plotted in Fig. 2. We have considered a three-dimensional system ($d = 3$) with $x_1 = \frac{1}{2}$, $m_1/m_2 = 10$, $\sigma_1/\sigma_2 = 1$, $\phi = 0.2$, and $T_{\rm ex}^* = 0.1$. We observe that in general the magnitude of the derivatives is not negligible, especially the derivatives $\Delta_{\theta,1}$ and $\Delta_{\phi,1}$ at strong inelasticity.

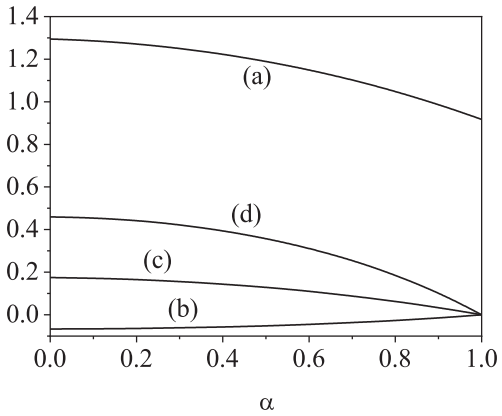

FIG. 2. Plot of the derivatives $\Delta_{\theta,1}$ (a), $\Delta_{\lambda_1,1}$ (b), $\Delta_{x_1,1}$ (c), and $\Delta_{\phi,1}$ (d) for $d = 3$, $x_1 = \frac{1}{2}$, $m_1/m_2 = 10$, $\sigma_1/\sigma_2 = 1$, $\phi = 0.2$, and $T_{\rm ex}^* = 0.1$.

B. First-order approximation

The analysis to first order in spatial gradients is more complex than that of the zeroth order. It follows similar steps as those worked out for undriven dense granular mixtures [22,23] and driven dilute granular mixtures [10]. Some technical details are displayed in Appendix B for the sake of completeness. The first-order velocity distribution functions $f_i^{(1)}$ are given by

$$f_i^{(1)} = \boldsymbol{\mathcal{A}}_i\cdot\boldsymbol{\nabla}\ln T + \sum_{j=1}^{2}\boldsymbol{\mathcal{B}}_{ij}\cdot\boldsymbol{\nabla}\ln n_j + \mathcal{C}_{i,\lambda\beta}\frac{1}{2}\Big(\partial_\lambda U_\beta + \partial_\beta U_\lambda - \frac{2}{d}\delta_{\lambda\beta}\boldsymbol{\nabla}\cdot\mathbf{U}\Big) + \mathcal{D}_i\boldsymbol{\nabla}\cdot\mathbf{U} + \boldsymbol{\mathcal{E}}_i\cdot\Delta\mathbf{U}, \tag{72}$$

where $\partial_\beta \equiv \partial/\partial r_\beta$. The unknowns $\boldsymbol{\mathcal{A}}_i(\mathbf{V})$, $\boldsymbol{\mathcal{B}}_{ij}(\mathbf{V})$, $\mathcal{C}_{i,\lambda\beta}(\mathbf{V})$, $\mathcal{D}_i(\mathbf{V})$, and $\boldsymbol{\mathcal{E}}_i(\mathbf{V})$ are functions of the peculiar velocity, and they are the solutions of the linear integral equations (B19)–(B23).

On the other hand, as already pointed out in previous works [10,14,37], the evaluation of the transport coefficients under *unsteady* conditions requires one to know the complete time dependence of the first-order corrections to the mass, momentum, and heat fluxes. This is quite an intricate problem. A more tractable situation occurs when one is interested in evaluating the transport coefficients in steady-state conditions. In this case, since the fluxes $\mathbf{j}_1^{(1)}$, $P_{\lambda\beta}^{(1)}$, and $\mathbf{q}^{(1)}$ are of first order in gradients, then the transport coefficients must be determined to zeroth order in the deviations from the steady state (namely, when the condition $\Lambda^{(0)} = 0$ applies). In this situation, the set of coupled linear integral equations (B19)–(B23) becomes, respectively,

$$-\left[2\sum_{j=1}^{2}\gamma_j x_j\left(\theta^{-1} + \theta\frac{\partial\tau_j}{\partial\theta}\right) + \frac{1}{2}\zeta^{(0)} + \zeta^{(0)}\theta\frac{\partial\ln\zeta_0^*}{\partial\theta}\right]\boldsymbol{\mathcal{A}}_i - \gamma_i\frac{\partial}{\partial\mathbf{v}}\cdot\mathbf{V}\boldsymbol{\mathcal{A}}_i - \frac{\gamma_i T_{\rm ex}}{m_i}\frac{\partial^2}{\partial v^2}\boldsymbol{\mathcal{A}}_i$$
$$+ (\gamma_2 - \gamma_1)D_1^T\frac{\partial f_i^{(0)}}{\partial\mathbf{V}} - \sum_{j=1}^{2}\left(J_{ij}^{(0)}[\boldsymbol{\mathcal{A}}_i, f_j^{(0)}] + J_{ij}^{(0)}[f_i^{(0)}, \boldsymbol{\mathcal{A}}_j]\right) = \mathbf{A}_i, \tag{73}$$

$$-\gamma_i\frac{\partial}{\partial\mathbf{v}}\cdot\mathbf{V}\boldsymbol{\mathcal{B}}_{ij} - \frac{\gamma_i T_{\rm ex}}{m_i}\frac{\partial^2}{\partial v^2}\boldsymbol{\mathcal{B}}_{ij} + (\gamma_2 - \gamma_1)\frac{m_1\rho_j}{\rho^2}D_{1j}\frac{\partial f_i^{(0)}}{\partial\mathbf{V}} - \sum_{\ell=1}^{2}\left(J_{i\ell}^{(0)}[\boldsymbol{\mathcal{B}}_{ij}, f_\ell^{(0)}] + J_{i\ell}^{(0)}[f_i^{(0)}, \boldsymbol{\mathcal{B}}_{\ell j}]\right) = \mathbf{B}_{ij}$$
$$+\left(n_j\frac{\partial\zeta^{(0)}}{\partial n_j} - 2n_j\sum_{\ell=1}^{2}\left\{\gamma_\ell x_\ell\left[(\theta^{-1} - \tau_\ell)\left(\frac{\partial\ln\gamma_\ell}{\partial n_j} + \frac{\partial\ln x_\ell}{\partial n_j}\right) - \left(\frac{\partial\tau_\ell}{\partial x_1}\frac{\partial x_1}{\partial n_j} + \frac{\partial\tau_\ell}{\partial\lambda_1}\frac{\partial\lambda_1}{\partial n_j} + \frac{\partial\tau_\ell}{\partial\phi}\frac{\partial\phi}{\partial n_j}\right)\right]\right\}\right)\boldsymbol{\mathcal{A}}_i, \tag{74}$$

$$-\gamma_i\frac{\partial}{\partial\mathbf{v}}\cdot\mathbf{V}\mathcal{C}_{i,\lambda\beta}-\frac{\gamma_i T_{\rm ex}}{m_i}\frac{\partial^2}{\partial v^2}\mathcal{C}_{i,\lambda\beta}-\sum_{j=1}^{2}\left(J_{ij}^{(0)}[\mathcal{C}_{i,\lambda\beta},f_j^{(0)}]+J_{ij}^{(0)}[f_i^{(0)},\mathcal{C}_{j,\lambda\beta}]\right)=\mathcal{C}_{i,\lambda\beta},\tag{75}$$

$$-\gamma_i\frac{\partial}{\partial\mathbf{v}}\cdot\mathbf{V}\mathcal{D}_i-\frac{\gamma_i T_{\rm ex}}{m_i}\frac{\partial^2}{\partial v^2}\mathcal{D}_i-\left(\zeta^{(1,1)}T+2\sum_{j=1}^{2}\gamma_j x_j\varpi_j\right)\frac{\partial f_i^{(0)}}{\partial T}-\sum_{j=1}^{2}\left(J_{ij}^{(0)}[\mathcal{D}_i,f_j^{(0)}]+J_{ij}^{(0)}[f_i^{(0)},\mathcal{D}_j]\right)=D_i,\tag{76}$$

$$-\gamma_i\frac{\partial}{\partial\mathbf{v}}\cdot\mathbf{V}\boldsymbol{\mathcal{E}}_i-\frac{\gamma_i T_{\rm ex}}{m_i}\frac{\partial^2}{\partial v^2}\boldsymbol{\mathcal{E}}_i+\rho^{-1}(\gamma_2-\gamma_1)D_1^U\frac{\partial f_i^{(0)}}{\partial\mathbf{V}}-\sum_{j=1}^{2}\left(J_{ij}^{(0)}[\boldsymbol{\mathcal{E}}_i,f_j^{(0)}]+J_{ij}^{(0)}[f_i^{(0)},\boldsymbol{\mathcal{E}}_j]\right)=\mathbf{E}_i.\tag{77}$$

The explicit forms of the coefficients $\mathbf{A}_i$, $\mathbf{B}_{ij}$, $\mathcal{C}_{i,\lambda\beta}$, D_i, and $\mathbf{E}_i$ are given by Eqs. (B11)–(B15), respectively. These coefficients are functions of $\mathbf{V}$ and the hydrodynamic fields.

When writing Eqs. (73), (74), and (77), use has been made of the constitutive equation of the mass flux $\mathbf{j}_1^{(1)}$ to first order in spatial gradients:

$$\mathbf{j}_i^{(1)}=-\sum_{j=1}^{2}\frac{m_i\rho_j}{\rho}D_{ij}\nabla\ln n_j-\rho D_i^T\nabla\ln T-D_i^U\Delta\mathbf{U}.\tag{78}$$

In Eq. (78), D_{ij} are the mutual diffusion coefficients, D_i^T are the thermal diffusion coefficients, and D_i^U are the velocity diffusion coefficients. Since $\mathbf{j}_1^{(1)}=-\mathbf{j}_2^{(1)}$, then $D_{21}=-(m_1/m_2)D_{11}$, $D_{22}=-(m_1/m_2)D_{12}$, $D_2^T=-D_1^T$, and $D_2^U=-D_1^U$. In addition, the form of the first-order contribution $\zeta^{(1)}$ to the cooling rate has been also employed to obtain Eq. (76). This coefficient can be written as

$$\zeta^{(1)}=\zeta_U\nabla\cdot\mathbf{U},\tag{79}$$

where

$$\zeta_U=\zeta^{(1,0)}+\zeta^{(1,1)}.\tag{80}$$

The coefficient $\zeta^{(1,0)}$ is defined by Eq. (B8), while $\zeta^{(1,1)}$ is a functional of the unknowns $\mathcal{D}_i$. Its form is given by Eq. (B25). Also, in Eq. (76), use has been made of the first-order contribution to the partial temperatures $T_1^{(1)}=-n_2T_2^{(1)}/n_1$. Since $T_i^{(1)}$ is a scalar, it is coupled to $\nabla\cdot\mathbf{U}$ and has the form [17,21]

$$T_i^{(1)}=\varpi_i\nabla\cdot\mathbf{U},\tag{81}$$

where

$$\varpi_i=\frac{m_i}{dn_i}\int d\mathbf{v}\,V^2\mathcal{D}_i(\mathbf{V}).\tag{82}$$

The direct integration of Eqs. (B11)–(B15) for the functions $\mathbf{A}_i$, $\mathbf{B}_{ij}$, $\mathcal{C}_{i,\lambda\beta}$, D_i, and $\mathbf{E}_i$ yields the following conditions:

$$\int d\mathbf{v}(\mathbf{A}_i,\mathbf{B}_{ij},\mathcal{C}_{i,\lambda\beta},D_i,\mathbf{E}_i)=(\mathbf{0},\mathbf{0},0,0,\mathbf{0}),\tag{83}$$

$$\sum_{i=1}^{2}\int d\mathbf{v}m_iV_\mu\begin{pmatrix}A_{i,\lambda}\\B_{i,\lambda}\\C_{i,\lambda\beta}\\D_i\\E_{i,\lambda}\end{pmatrix}=\begin{pmatrix}0\\0\\0\\0\\0\end{pmatrix},\tag{84}$$

$$\sum_{i=1}^{2}\int d\mathbf{v}\frac{1}{2}m_iV^2\begin{pmatrix}\mathbf{A}_i\\\mathbf{B}_i\\D_i\\\mathbf{E}_i\end{pmatrix}=\begin{pmatrix}\mathbf{0}\\\mathbf{0}\\0\\\mathbf{0}\end{pmatrix},\tag{85}$$

and

$$\sum_{i=1}^{2}\int d\mathbf{v}\frac{1}{2}m_iV^2\mathcal{C}_{i,\lambda\beta}\left(\partial_\lambda U_\beta+\partial_\beta U_\lambda-\frac{2}{d}\delta_{\lambda\beta}\nabla\cdot\mathbf{U}\right)=0.\tag{86}$$

Since $\boldsymbol{\mathcal{A}}_i\propto\mathbf{A}_i$, $\boldsymbol{\mathcal{B}}_{ij}\propto\mathbf{B}_{ij}$, $\mathcal{C}_{i,\lambda\beta}\propto\mathcal{C}_{i,\lambda\beta}$, $\mathcal{D}_i\propto D_i$, and $\boldsymbol{\mathcal{E}}_i\propto\mathbf{E}_i$, then the solubility conditions (59) and (60) are fulfilled, and, so, there exist solutions to the integral equations (73)–(76); this is the so-called Fredholm alternative [53].

V. NAVIER-STOKES TRANSPORT COEFFICIENTS

The forms of the constitutive equations for the irreversible fluxes to first order in spatial gradients can be written using simple symmetry arguments [18]. While the mass flux $\mathbf{j}_i^{(1)}$ of the component i is given by Eq. (78), the pressure tensor $P_{\lambda\beta}^{(1)}$ has the form

$$P_{\lambda\beta}^{(1)}=-\eta\left(\partial_\lambda U_\beta+\partial_\beta U_\lambda-\frac{2}{d}\delta_{\lambda\beta}\nabla\cdot\mathbf{U}\right)-\delta_{\lambda\beta}\eta_{\rm b}\nabla\cdot\mathbf{U},\tag{87}$$

while the heat flux $\mathbf{q}^{(1)}$ can be written as

$$\mathbf{q}^{(1)}=-\sum_{i=1}^{2}\sum_{j=1}^{2}T^2D_{q,ij}\nabla\ln n_j-T\kappa\nabla\ln T+\kappa_U\Delta\mathbf{U}.\tag{88}$$

In Eqs. (87)–(88), η is the shear viscosity coefficient, $\eta_{\rm b}$ is the bulk viscosity coefficient, κ is the thermal conductivity coefficient, κ_U is the velocity conductivity, and $D_{q,ij}$ are the partial contributions to the Dufour coefficients $D_{q,i}$ defined as [18]

$$D_{q,i}=\sum_{\ell=1}^{2}D_{q,\ell i}.\tag{89}$$

The transport coefficients associated with the mass flux are defined as

$$D_i^T=-\frac{m_i}{d\rho}\int d\mathbf{v}\,\mathbf{V}\cdot\boldsymbol{\mathcal{A}}_i(\mathbf{V}),\tag{90}$$

$$D_{ij}=-\frac{\rho}{d\rho_j}\int d\mathbf{v}\,\mathbf{V}\cdot\boldsymbol{\mathcal{B}}_{ij}(\mathbf{V}),\tag{91}$$

$$D_i^U=-\frac{m_i}{d}\int d\mathbf{v}\,\mathbf{V}\cdot\boldsymbol{\mathcal{E}}_i(\mathbf{V}).\tag{92}$$

As said in Sec. II, in contrast to the mass flux, the pressure tensor and heat flux have kinetic and collisional contributions. To first order, their kinetic contributions are

$$P_{\lambda\beta}^{\mathrm{k}(1)} = \sum_{i=1}^{2} \int d\mathbf{v}\, m_i V_\lambda V_\beta f_i(\mathbf{V}), \tag{93}$$

$$\mathbf{q}^{\mathrm{k}(1)} = \sum_{i=1}^{2} \int d\mathbf{v}\, \frac{m_i}{2} V^2 \mathbf{V} f_i(\mathbf{V}). \tag{94}$$

According to Eqs. (87) and (93), the kinetic contribution η_{k} to the shear viscosity can be written as $\eta_{\mathrm{k}} = \sum_{i=1}^{2} \eta_i^{\mathrm{k}}$, where [18]

$$\eta_i^{\mathrm{k}} = -\frac{1}{(d-1)(d+2)} \int d\mathbf{v}\, m_i V_\lambda V_\beta \mathcal{C}_{i,\lambda\beta}(\mathbf{V}). \tag{95}$$

In the case of the heat flux, according to Eqs. (88) and (94), the kinetic contribution $D_{q,ij}^{\mathrm{k}}$ to the Dufour coefficient is

$$D_{q,ij}^{\mathrm{k}} = -\frac{1}{dT^2} \int d\mathbf{v} \frac{1}{2} m_i V^2 \mathbf{V} \cdot \boldsymbol{\mathcal{B}}_{ij}(\mathbf{V}), \tag{96}$$

while the kinetic contributions κ_{k} and κ_U^{k} to the thermal and velocity conductivity coefficients, respectively, can be written as $\kappa_{\mathrm{k}} = \sum_{i=1}^{2} \kappa_i^{\mathrm{k}}$ and $\kappa_U^{\mathrm{k}} = \sum_{i=1}^{2} \kappa_i^{U\mathrm{k}}$, where

$$\kappa_i^{\mathrm{k}} = -\frac{1}{dT} \int d\mathbf{v} \frac{1}{2} m_i V^2 \mathbf{V} \cdot \boldsymbol{\mathcal{A}}_i(\mathbf{V}). \tag{97}$$

$$\kappa_i^{U\mathrm{k}} = -\frac{1}{d} \int d\mathbf{v} \frac{1}{2} m_i V^2 \mathbf{V} \cdot \boldsymbol{\mathcal{E}}_i(\mathbf{V}). \tag{98}$$

Collisional contributions to the pressure tensor and heat flux can be obtained by expanding Eqs. (27) and (28) to first order in spatial gradients. A careful analysis shows that those collisional contributions are formally the same as those obtained in the dry granular case [18,21–23]. In particular, the bulk viscosity (which has only collisional contributions) can be written as

$$\eta_{\mathrm{b}} = \eta_{\mathrm{b}}' + \eta_{\mathrm{b}}'', \tag{99}$$

where

$$\eta_{\mathrm{b}}' = \frac{\pi^{(d-1)/2}}{\Gamma\left(\frac{d+3}{2}\right)} \frac{d+1}{2d^2} \sum_{i=1}^{2}\sum_{j=1}^{2} m_{ij}(1+\alpha_{ij}) \chi_{ij}^{(0)} \sigma_{ij}^{d+1} \times \int d\mathbf{v}_1 \int d\mathbf{v}_2 f_i^{(0)}(\mathbf{V}_1) f_j^{(0)}(\mathbf{V}_2) g_{12} \tag{100}$$

and

$$\eta_{\mathrm{b}}'' = -\frac{\pi^{d/2}}{d\Gamma\left(\frac{d}{2}\right)} \sum_{i=1}^{2}\sum_{j=1}^{2} \mu_{ji}(1+\alpha_{ij}) \chi_{ij}^{(0)} n_i n_j \sigma_{ij}^{d} \varpi_i. \tag{101}$$

The second contribution η_{b}'' to η_{b} was neglected in the previous works on granular mixtures [18,22,23] because it was implicitly assumed that its contribution to the bulk viscosity was quite small. On the other hand, this influence was already accounted for in the pioneering studies on ordinary (elastic collisions) hard-sphere mixtures [54–56] and has been recently calculated [21] in the case of (dry) polydisperse dense granular mixtures.

The collisional contribution η_{c} to the shear viscosity is

$$\eta^{\mathrm{c}} = \frac{2\pi^{d/2}}{d(d+2)\Gamma\left(\frac{d}{2}\right)} \sum_{i=1}^{2}\sum_{j=1}^{2} \mu_{ij}(1+\alpha_{ij}) \chi_{ij}^{(0)} n_i \sigma_{ij}^{d} \eta_j^{\mathrm{k}} + \frac{d}{d+2} \eta_{\mathrm{b}}'. \tag{102}$$

The expressions of the collisional contributions to the heat flux transport coefficients are more intricate than that of η_{b} and η_{c}. Their explicit forms can be found in Ref. [18].

VI. APPROXIMATE RESULTS: LEADING SONINE APPROXIMATIONS

The evaluation of the complete set of transport coefficients of the binary granular suspension is a quite long task. In this paper, we will focus on our attention in obtaining the transport coefficients associated with the mass flux (D_{ij}, D_i^T, and D_i^U), the shear viscosity coefficient η, and the partial temperatures $T_i^{(1)}$. To determine them, one has to solve the set of coupled linear integral equations (73)–(77) as well as to know the forms of the zeroth-order distributions $f_i^{(0)}$. With respect to the latter, as noted in Sec. III, $f_i^{(0)}$ is well represented by the Maxwellian velocity distribution function

$$f_i^{(0)}(\mathbf{V}) \to f_{i,\mathrm{M}}(\mathbf{V}) = n_i \left(\frac{m_i}{2\pi T_i^{(0)}}\right)^{d/2} \exp\left(-\frac{m_i V^2}{2T_i^{(0)}}\right). \tag{103}$$

This means that we neglect here non-Gaussian corrections to the distributions $f_i^{(0)}$, and, hence, one expects to get simple but accurate expressions for the transport coefficients. By using the Maxwellian approximation (103), the collisional contribution η_{b}' is

$$\eta_{\mathrm{b}}' = \frac{\pi^{(d-1)/2}}{d^2\Gamma\left(\frac{d}{2}\right)} v_0 \sum_{i=1}^{2}\sum_{j=1}^{2} m_{ij}(1+\alpha_{ij}) \chi_{ij}^{(0)} n_i n_j \sigma_{ij}^{d+1} \times \left(\frac{\beta_i+\beta_j}{\beta_i\beta_j}\right)^{1/2}. \tag{104}$$

Regarding the unknowns ($\boldsymbol{\mathcal{A}}_i$, $\boldsymbol{\mathcal{B}}_{ij}$, $\mathcal{C}_{i,\lambda\beta}$, $\mathcal{D}_i$, $\boldsymbol{\mathcal{E}}_i$), as usual we will expand them in a series expansion of orthogonal polynomials (Sonine polynomials) [35], and we will truncate this expansion by considering only the leading term (lowest degree polynomial). In particular, the collisional contribution η_{b}'' will be estimated later when we determine ϖ_i in the first Sonine approximation.

A. Diffusion transport coefficients

In the case of the transport coefficients D_{ij}, D_i^T, and D_i^U, the leading Sonine approximations to $\boldsymbol{\mathcal{A}}_i$, $\boldsymbol{\mathcal{B}}_{ij}$, and $\boldsymbol{\mathcal{E}}_i$ are, respectively,

$$\boldsymbol{\mathcal{A}}_i(\mathbf{V}) \to -\frac{\rho}{n_i T_i} D_i^T f_{i,\mathrm{M}}(\mathbf{V}) \mathbf{V}, \tag{105}$$

$$\boldsymbol{\mathcal{B}}_{ij}(\mathbf{V}) \to -\frac{m_i \rho_j}{\rho n_i T_i} D_{ij} f_{i,\mathrm{M}}(\mathbf{V}) \mathbf{V}, \tag{106}$$

$$\boldsymbol{\mathcal{E}}_i(\mathbf{V}) \to -\frac{D_i^U}{n_i T_i} f_{i,\mathrm{M}}(\mathbf{V}) \mathbf{V}. \tag{107}$$

In order to determine the above diffusion coefficients, we substitute first $\boldsymbol{\mathcal{A}}_i$, $\boldsymbol{\mathcal{B}}_{ij}$, and $\boldsymbol{\mathcal{E}}_i$ by their leading Sonine approximations (105)–(107) in Eqs. (73), (74), and (77), respectively. Then we multiply these equations by $m_i\mathbf{V}$ and integrate over velocity. The final forms of the set of algebraic equations defining the transport coefficients D_i^T, D_{ij}, and D_i^U are given by Eqs. (C1)–(C3) in Appendix C.

The solution to the set of Eqs. (C1)–(C3) provides the dependence of the (relevant) diffusion coefficients D_{11}, D_{12}, D_1^T, and D_1^U on the coefficients of restitution α_{ij}, the concentration x_1, the solid volume fraction ϕ, the masses and diameters of the constituents of the mixture, and the (reduced) background temperature T_{ex}^*. In particular, the expression of D_1^U is

$$D_1^U = \rho_1\rho_2\frac{\gamma_1-\gamma_2}{\rho\nu_D+\rho_1\gamma_2+\rho_2\gamma_1}, \tag{108}$$

where ν_D is defined by Eq. (C11). The explicit form of the thermal diffusion coefficient D_1^T is given by Eq. (C10). The expressions of D_{11} and D_{12} can be obtained by solving the set of Eqs. (C2). Their forms are very large and will be omitted here for the sake of simplicity.

Equations (108) and (C10) show that D_1^U and D_1^T are antisymmetric with respect to the change $1\leftrightarrow 2$ as expected. This can be easily verified since $x_1\tau_1+x_2\tau_2=1$, $\Delta_{\theta,1}=-(x_2/x_1)\Delta_{\theta,2}$ and

$$\frac{\partial p^*}{\partial\theta}=\frac{\pi^{d/2}}{d\Gamma\left(\frac{d}{2}\right)}\sum_{i=1}^{2}\sum_{j=1}^{2}\mu_{ji}x_in_j\sigma_{ij}^d\chi_{ij}^{(0)}\Delta_{\theta,i}(1+\alpha_{ij}), \tag{109}$$

where $p^*\equiv p/(nT)$ is the reduced hydrostatic pressure. Furthermore, in the case of mechanically equivalent particles ($m_1=m_2$, $\sigma_1=\sigma_2$, $\chi_{ij}^{(0)}=\chi^{(0)}$, and $\alpha_{ij}=\alpha$), Eqs. (C2) and (C10) yield $x_1D_{11}^*+x_2D_{12}^*=0$ and $D_1^{T*}=0$, as expected. Here we have introduced the scaled coefficients $D_{ij}^*\equiv D_{ij}(\alpha)/D_{ij}(1)$ and $D_1^{T*}\equiv D_1^T(\alpha)/D_1^T(1)$ where $D_{ij}(1)$ and $D_1^T(1)$ refer to the values of D_{ij} and D_1^T, respectively, for elastic collisions. The above relations confirm the self-consistency of the expressions for the diffusion coefficients reported in this paper.

B. Shear viscosity coefficient

The kinetic contribution to the shear viscosity $\eta_{\text{k}}=\eta_1^{\text{k}}+\eta_2^{\text{k}}$, where the partial contributions η_i^{k} are defined by Eq. (95). To determine the kinetic coefficients η_i^{k}, the function $\mathcal{C}_{i,\lambda\beta}(\mathbf{V})$ is estimated by its leading Sonine approximation

$$\mathcal{C}_{i,\lambda\beta}(\mathbf{V})\to -f_{i,\text{M}}(\mathbf{V})R_{i,\lambda\beta}(\mathbf{V})\frac{\eta_i^{\text{k}}}{n_iT_i^{(0)2}}, \tag{110}$$

where

$$R_{i,\lambda\beta}(\mathbf{V})=m_i\left(V_\lambda V_\beta-\frac{1}{d}\delta_{\lambda\beta}V^2\right). \tag{111}$$

As in the case of the diffusion coefficients, the partial contributions η_i^{k} are obtained by substituting Eq. (110) into the integral equation (75), multiplying it by $R_{i,\lambda\beta}$, and integrating over the velocity. After some algebra, one achieves the set of algebraic equations (C12). The solution to the set (C12) provides the partial contributions η_i^{k}. Their sum then gives the kinetic coefficient η_{k}. Finally, by adding this to the collisional contribution (102) we have the total shear viscosity.

C. First-order contributions to the partial temperatures

Finally, we consider the first-order contribution $T_i^{(1)}$ to the partial temperature T_i. This coefficient is defined by Eqs. (81) and (82). As said before, the coefficients $T_i^{(1)}$ ($i=1,2$) have been recently determined for dry granular mixtures [21]. To determine ϖ_i, we consider the leading Sonine approximation to $\mathcal{D}_i(\mathbf{V})$ given by

$$\mathcal{D}_i(\mathbf{V})\to f_{i\text{M}}(\mathbf{V})W_i(\mathbf{V})\frac{\varpi_i}{T_i^{(0)}},\quad W_i(\mathbf{V})=\frac{m_iV^2}{2T_i^{(0)}}-\frac{d}{2}. \tag{112}$$

The coefficients ϖ_i are coupled with the coefficients $\zeta^{(1,1)}$ through Eq. (B25). The explicit relation between $\zeta^{(1,1)}$ and ϖ_i can be easily obtained by substitution of Eq. (112) into Eq. (B25), with the result

$$\zeta^{(1,1)}=\sum_{i=1}^{2}\xi_i\varpi_i, \tag{113}$$

where

$$\xi_i=\frac{3\pi^{(d-1)/2}}{2d\Gamma\left(\frac{d}{2}\right)}\frac{v_0^3}{nT_i^{(0)}}\sum_{j=1}^{2}n_in_j\sigma_{ij}^{d-1}\chi_{ij}^{(0)}m_{ij}\left(1-\alpha_{ij}^2\right)\times(\beta_i+\beta_j)^{1/2}\beta_i^{-3/2}\beta_j^{-1/2}. \tag{114}$$

As usual, in order to obtain the coefficients ϖ_i, one substitutes first Eq. (112) into Eq. (76) and then multiplies it with m_iV^2 and integrates over the velocity. After some algebra, one gets the set of coupled equations (C18). A careful inspection to the set of Eqs. (C18) shows that $\varpi_1=-(x_2/x_1)\varpi_2$ as the solubility condition (60) requires. This is because $x_1\tau_1+x_2\tau_2=1$, $\Delta_{\theta,2}=-(x_2/x_1)\Delta_{\theta,1}$, and $\omega_{11}-(x_1/x_2)\omega_{12}+T\xi_1/x_1=\omega_{22}-(x_2/x_1)\omega_{21}+T\xi_2/x_2$. The condition $x_1\varpi_1+x_2\varpi_2=0$ guarantees that the temperature T is not affected by the spatial gradients.

The solution to Eq. (C18) gives ϖ_1 in terms of the parameters of the mixture. On the other hand, its explicit form is relatively long and is omitted here for the sake of brevity. A simple but interesting case corresponds to elastic collisions (molecular or ordinary suspensions) where $\xi_i=0$, $\tau_i=1$, $\beta_1=2\mu_{12}$, $\beta_2=2\mu_{21}$, $\Delta_{\theta,i}=\Delta_{x_1,i}=\Delta_{\lambda_1,i}=\Delta_{\phi,i}=0$, and so ϖ_1 is simply given by

$$\varpi_1=\frac{4\pi^{d/2}}{d^2\Gamma\left(\frac{d}{2}\right)}T\frac{n_2\sigma_{12}^d\chi_{12}^{(0)}(x_2\mu_{21}-x_1\mu_{12})+\frac{1}{2}x_2\left(n_1\sigma_1^d\chi_{11}^{(0)}-n_2\sigma_2^d\chi_{22}^{(0)}\right)}{\omega_{11}-\frac{x_1}{x_2}\omega_{12}-2(x_2\gamma_1+x_1\gamma_2)}. \tag{115}$$

Equation (115) is consistent with the one derived many years ago by Karkheck and Stell [55] for ordinary hard-sphere mixtures ($\gamma_1=\gamma_2=0$).

Once the first-order contributions to the partial temperatures are known, the first-order contribution ζ_U to the cooling rate can be explicitly obtained from Eqs. (80), (B8), and (113). In addition, the contribution η_b'' to the bulk viscosity η_b can be obtained from Eq. (101), and, hence, the bulk viscosity is completely determined by Eqs. (101) and (104).

VII. SOME ILLUSTRATIVE SYSTEMS

The results derived in Sec. VI for the diffusion transport coefficients, the shear and bulk viscosities, and the first-order contributions to the partial temperatures and the cooling rate depend on the background temperature T_{ex}, the concentration x_1, the density or volume fraction ϕ, and the mechanical parameters of the binary mixture (masses, diameters, and coefficients of restitution). As in our previous paper [10] on dilute granular suspensions, given that the new relevant feature is the dependence of the transport coefficients on inelasticity, we scale these coefficients with respect to their values for elastic collisions. Thus, the scaled transport coefficients depend on the parameter space: $\{T_{ex}^*, x_1, m_1/m_2, \sigma_1/\sigma_2, \phi, \alpha_{11}, \alpha_{22}, \alpha_{12}\}$. Moreover, for the sake of simplicity, the case of a common coefficient of restitution ($\alpha_{11} = \alpha_{22} = \alpha_{12} \equiv \alpha$) of an equimolar hard-sphere mixture ($x_1 = \frac{1}{2}$ and $d = 3$) with a background temperature $T_{ex}^* = 0.1$ is considered. This reduces the parameter space to four quantities: $\{m_1/m_2, \sigma_1/\sigma_2, \phi, \alpha\}$.

To display the dependence of the transport coefficients on the coefficient of restitution, we have to provide the form for the pair distribution function $\chi_{ij}^{(0)}$. In the case of spheres ($d = 3$), a good approximation of $\chi_{ij}^{(0)}$ is [57–59]

$$\chi_{ij}^{(0)} = \frac{1}{1-\phi} + \frac{3}{2}\frac{\phi}{(1-\phi)^2}\frac{\sigma_i\sigma_j M_2}{\sigma_{ij} M_3} + \frac{1}{2}\frac{\phi^2}{(1-\phi)^3}\left(\frac{\sigma_i\sigma_j M_2}{\sigma_{ij} M_3}\right)^2, \tag{116}$$

where $M_\ell = \sum_i x_i \sigma_i^\ell$. In addition, the functions R_i are defined by Eq. (11).

Figure 3 shows the α dependence of the reduced diffusion coefficients D_{ij}^*, D_1^{T*}, and D_1^{U*} for $m_1/m_2 = 4$, $\sigma_1/\sigma_2 = 1$, and $\phi = 0.1$. We recall that $D_{ij}^* \equiv D_{ij}(\alpha)/D_{ij}(1)$, $D_1^{T*} \equiv D_1^T(\alpha)/D_1^T(1)$, and $D_1^{U*} \equiv D_1^U(\alpha)/D_1^U(1)$, where $D_{ij}(1)$, $D_1^U(1)$, and $D_1^T(1)$ are the values of the diffusion transport coefficients for elastic collisions. It is quite apparent first that the effect of inelasticity on diffusion coefficients is in general significant since the forms of the scaled coefficients D_{ij}^*, D_1^{U*}, and D_1^{T*} differ clearly from their elastic counterparts. This is especially relevant in the case of the thermal diffusion coefficient D_1^{T*}. In addition, a comparison with the results obtained for dry granular mixtures (see, for instance, Figs. 5.5, 5.6, and 5.7 of Ref. [18] for the same mixture parameters) reveals significant differences between dry (no gas phase) and gas-solid flows when grains are mechanically different. Thus, while D_{11}^* and D_{12}^* increase with inelasticity for dry granular mixtures, the opposite happens for granular suspensions since they decrease as increasing inelasticity. The qualitative α dependence of D_1^{T*} is similar in both dry and gas-solid flows, although the influence of inelasticity on D_1^{T*} is much more important in the latter case.

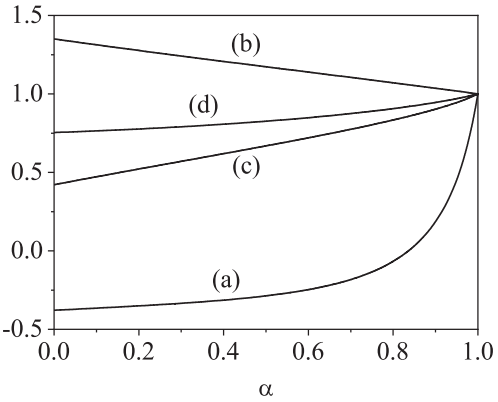

FIG. 3. Plot of the (reduced) diffusion coefficients D_1^{T*} (a), D_1^{U*} (b), D_{11}^* (c), and D_{12}^* (d) as a function of the common coefficient of restitution α for an equimolar mixture ($x_1 = \frac{1}{2}$) of hard spheres ($d = 3$) with $\sigma_1/\sigma_2 = 1$, $m_1/m_2 = 4$, $\phi = 0.2$, and $T_{ex}^* = 0.1$.

We consider now the (reduced) shear viscosity $\eta^* \equiv \eta(\alpha)/\eta(1)$. Figure 4 shows η^* versus α for $\sigma_1/\sigma_2 = 1$, $\phi = 0.2$ and two different values of the mass ratio. As with the diffusion coefficients, the effect of inelasticity on the shear viscosity is again significant since the inelasticity hinders the transport of momentum. Regarding the comparison with dry granular mixtures, we find qualitative differences since both theory [24,39,60,61] and simulations [18,62] have shown that while for relatively dilute dry granular gases η^* increases with inelasticity, the opposite occurs for sufficiently dense granular mixtures. This nonmonotonic behavior with density contrasts with the results obtained here for multicomponent granular

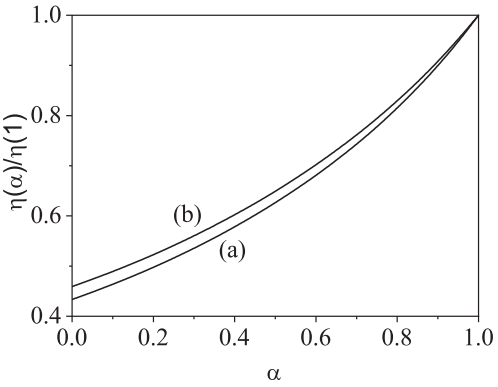

FIG. 4. Plot of the (reduced) shear viscosity coefficient $\eta(\alpha)/\eta(1)$ as a function of the common coefficient of restitution α for an equimolar mixture ($x_1 = \frac{1}{2}$) of hard spheres ($d = 3$) with $\sigma_1/\sigma_2 = 1$, $\phi = 0.2$, and $T_{ex}^* = 0.1$. Two different values of the mass ratio are considered: $m_1/m_2 = 0.5$ (a) and $m_1/m_2 = 4$ (b).

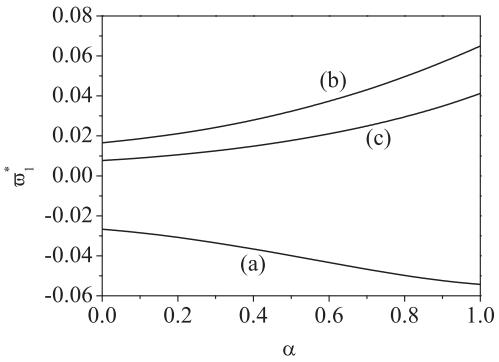

FIG. 5. Plot of the (reduced) coefficient ϖ_1^* as a function of the common coefficient of restitution α for an equimolar mixture ($x_1 = \frac{1}{2}$) of hard spheres ($d = 3$) with $\sigma_1/\sigma_2 = 1$, $\phi = 0.2$, and $T_{ex}^* = 0.1$. Three different values of the mass ratio are considered: $m_1/m_2 = 0.5$ (a), $m_1/m_2 = 4$ (b), and $m_1/m_2 = 10$ (c).

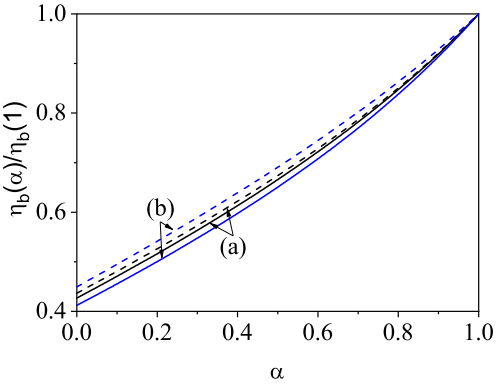

FIG. 6. Plot of the (reduced) bulk viscosity coefficient $\eta_b(\alpha)/\eta_b(1)$ as a function of the common coefficient of restitution α for an equimolar mixture ($x_1 = \frac{1}{2}$) of hard spheres ($d = 3$) with $\sigma_1/\sigma_2 = 1$, $\phi = 0.2$, and $T_{ex}^* = 0.1$. Two different values of the mass ratio are considered: $m_1/m_2 = 0.5$ (a) and $m_1/m_2 = 10$ (b). The dashed lines are the results for the (reduced) bulk viscosity when the contribution η_b'' to η_b is neglected.

suspensions since the scaled coefficient η^* always decreases with increasing inelasticity regardless of the value of the solid volume fraction ϕ. With respect to the influence of the mass ratio on the shear viscosity, we see that its impact on η^* is relatively small. In particular, at a given value of α, η^* decreases with decreasing the mass ratio m_1/m_2.

An interesting quantity is the first-order contribution ϖ_1 to the partial temperature T_1. The reduced coefficient $\varpi_1^* \equiv (n\sigma_{12}^2 v_0/T)\varpi_1$ is plotted in Fig. 5 as a function of α for $\sigma_1/\sigma_2 = 1$, $\phi = 0.2$, and three different values of the mass ratio. We observe that the influence of inelasticity on ϖ_1^* is important, especially for high mass ratios. However, Fig. 5 highlights that the magnitude of ϖ_1^* is much smaller than the other transport coefficients, and, hence, the impact of the first-order contribution $T_1^{(1)}$ on both the bulk viscosity η_b (through the coefficient η_b'') and the first-order contribution ζ_U (through the coefficient $\zeta^{(1,1)}$) to the cooling rate is expected to be small. This is confirmed by Figs. 6 and 7 for the reduced coefficients $\eta_b(\alpha)/\eta_b(1)$ and ζ_U, respectively. It is quite apparent that the theoretical predictions for the above coefficients with and without the contribution of ϖ_1^* are practically identical, especially in the case of the bulk viscosity. As with the shear viscosity coefficient, we also see that the bulk viscosity decreases with increasing inelasticity (independent of the mass ratio considered). Moreover, as for dry granular mixtures [21], the coefficient ζ_U is always negative, and its magnitude increases with inelasticity.

In summary, the mass and momentum transport coefficients for a multicomponent granular suspension differ significantly from those for dry granular mixtures. In most of cases, the differences become greater with increasing inelasticity, and depending on the cases, there is a relevant influence of the mass ratio.

VIII. DISCUSSION

This paper has been focused on the determination of the Navier-Stokes transport coefficients of a binary granular suspension at moderate densities. The starting point of our study has been the set of Enskog kinetic equations for the velocity distribution functions $f_i(\mathbf{r}, \mathbf{v}, t)$ of the solid particles. The effect of the gas phase on the solid particles has been accounted for by an effective force constituted by two terms: a viscous drag force proportional to the velocity of the particles and a stochastic Langevin-like term. Therefore, we have considered a simplified model where the effect of the interstitial gas on grains is explicitly accounted for but the

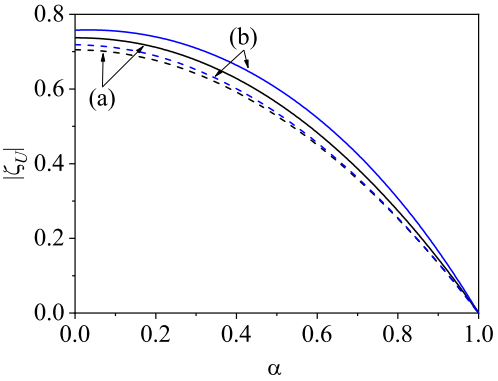

FIG. 7. Plot of the magnitude of the (reduced) coefficient ζ_U as a function of the common coefficient of restitution α for an equimolar mixture ($x_1 = \frac{1}{2}$) of hard spheres ($d = 3$) with $\sigma_1/\sigma_2 = 1$, $\phi = 0.2$, and $T_{ex}^* = 0.1$. Two different values of the mass ratio are considered: $m_1/m_2 = 0.5$ (a) and $m_1/m_2 = 10$ (b). The dashed lines are the results for the coefficient ζ_U when the contribution $\zeta^{(1,1)}$ to ζ_U is neglected.

state of the surrounding gas is assumed to be independent of the solid particles. On the other hand, this model is inspired in numerical and experimental results that can be found in the granular literature [29]. This fact is reflected in the functional dependence of the friction coefficients γ_i on both the partial ϕ_i and global $\phi = \phi_1 + \phi_2$ volume fractions and the mechanical properties of grains (masses m_i and diameters σ_i).

We have derived the Navier-Stokes hydrodynamic equations in two steps. First, the macroscopic balance equations (20)–(22) have been obtained from the Enskog equation (1). Particularly, these equations include terms that account for the impact of the gas phase on grains, and the kinetic and collisional contributions to the fluxes are expressed as functionals of the velocity distribution functions f_i. Second, the mass, momentum, and heat fluxes, together with the cooling rate appearing in the hydrodynamic equations, have been evaluated by solving the Enskog equation by means of the Chapman-Enskog method up to first order in the spatial gradients. The constitutive equation for the mass flux is given by Eq. (78) where the diffusion coefficients D_i^T, D_{ij}, and D_i^U are defined by Eqs. (90)–(92), respectively. The pressure tensor is given by Eq. (87), where the bulk viscosity η_b is defined by Eq. (99) and the shear viscosity η is defined by Eqs. (95) (kinetic contribution) and (102) (collisional contribution). Finally, the constitutive equation for the heat flux is given by Eq. (88) where the kinetic contributions to the Dufour coefficients $D_{q,ij}$, the thermal conductivity κ, and the velocity conductivity κ_U are given by Eqs. (96), (97), and (98), respectively. Within the context of small gradients, all the above results apply in principle to an arbitrary degree of inelasticity and are not restricted to specific values of the parameters of the mixture. The present work extends to moderate densities a previous analysis carried out for dilute bidisperse granular suspensions [10,17].

Before considering inhomogeneous situations, the homogeneous steady state has been studied. In this state, the distributions $f_{i,s}$ adopt the form (43) where the scaled distributions $\varphi_{i,s}$ depend on the steady temperature T_s through the dimensionless velocity $\mathbf{c} = \mathbf{v}/v_0(T_s)$ and the (scaled) temperature $\theta = T_s/T_{ex}$. This scaling differs from the one assumed for dry granular mixtures [36] where the temperature dependence of φ_i is encoded only through the dimensionless velocity $\mathbf{c}$. Although the exact form of the distributions $\varphi_{i,s}$ is not known, in order to estimate the partial temperatures $T_{i,s}/T_{ex}$, the distributions $\varphi_{i,s}$ have been approximated by the Maxwellian distributions (47). This has allowed us to explicitly get the partial temperatures in terms of the parameters of the mixture. In spite of the crudeness of the above approximation, the theoretical predictions for $T_{1,s}/T_{2,s}$ agree well with MD simulations, especially for moderately dense systems. The goodness of the comparison supports the use of the Maxwellian approximation (47) in the evaluation of the transport coefficients. However, we find some discrepancies between theory and simulations that could be mitigated if one would consider the influence of the fourth cumulants on the distributions $\varphi_{i,s}$. We plan to calculate these cumulants in the near future and perform more simulations to assess the reliability of the Enskog theoretical predictions for homogeneous steady states.

Once the steady reference state is well characterized, the diffusion coefficients, the bulk and shear viscosities, and the first-order contributions to the partial temperatures and the cooling rate have been determined. As usual, in order to achieve explicit expressions for the above transport coefficients, the leading terms in a Sonine polynomial expansion have been considered. The explicit forms of the transport coefficients have been displayed in Sec. VI and Appendix C: the coefficients D_{11} and D_{12} are the solutions of the algebraic equations (C2), the coefficients D_1^U and D_1^T are given by Eqs. (108) and (C10), respectively, the shear viscosity η and the first-order coefficients ϖ_i are the solutions of Eqs. (C12) and (C18), respectively, and the first-order contribution $\zeta_U = \zeta^{(1,0)} + \zeta^{(1,1)}$ to the cooling rate is given by Eqs. (B8), (113), and (114). An interesting point is that not only are these coefficients defined in terms of the hydrodynamic fields in the steady state, but, in addition, there are contributions to the transport coefficients coming from the derivatives of the temperature ratio in the vicinity of the steady state. These contributions can be seen as a measure of the departure of the perturbed state from the steady reference state. The inclusion of the above derivatives introduces conceptual and practical difficulties not present in the case of dry granular mixtures [22,23].

In reduced forms, the diffusion transport coefficients and the shear viscosity coefficient of the granular suspension exhibit a complex dependence on the parameter space of the problem. In particular, Fig. 3 highlights the significant impact of the gas phase on the mass transport since the α dependence of the Navier-Stokes transport coefficients D_1^T, D_1^U, and D_{ij} is in general different from the one found in the case of dry granular mixtures [18]. Regarding the shear viscosity coefficient η, a comparison with the dry granular results [18] shows a qualitative agreement between dry and granular suspensions for not quite high densities, although important quantitative differences are found. Apart from these coefficients, the first-order contributions ϖ_i to the partial temperatures T_i have been also computed. The evaluation of these coefficients is interesting by itself and also because they are involved in the calculation of both the bulk viscosity η_b and the first-order contribution ζ_U to the cooling rate. The results obtained here show that the magnitude of ϖ_1 is in general very small (in fact, much smaller than the one recently found [21] in the absence of gas phase), and hence, its impact on η_b and ζ_U is very tiny (see Figs. 6 and 7). This conclusion contrasts with recent findings for dry granular mixtures [21] where the influence of ϖ_1 on both the bulk viscosity and the cooling rate must be taken into account for strong inelasticities and disparate masses.

In a subsequent paper, we plan to determine the heat flux transport coefficients and to perform a linear stability analysis of the homogeneous steady state as a possible application. In particular, given that the homogeneous steady state is stable in the dilute limit, we want to see if the density corrections to the transport coefficients can modify the stability of the above homogeneous state. In addition, it is also quite apparent that the reliability of the theoretical results derived here (which have been obtained under certain approximations) should be assessed against computer simulations. As happens for dry granular mixtures [40,48,63–68], we expect that the present results stimulate the performance of appropriate simulations for bidisperse granular suspensions. In particular, we plan to undertake simulations to obtain the tracer diffusion coefficient

(namely, a binary mixture where the concentration of one of the components is negligible) in a similar way as in the case of granular mixtures [40,63,67]. Moreover, we also plan to carry out simulations to measure the Navier-Stokes shear viscosity η by studying the decay of a small perturbation to the transversal component of the velocity field [69]. Another possible project for the next future is to consider inelastic rough hard spheres in order to assess the impact of friction on the transport properties of the granular suspension. Studies along these lines will be worked out in the near future.

ACKNOWLEDGMENTS

The work of R.G.G. and V.G. has been supported by the Spanish Government through Grant No. FIS2016-76359-P and by the Junta de Extremadura (Spain) Grants No. IB16013 and No. GR18079, partially financed by "Fondo Europeo de Desarrollo Regional" funds. The research of R.G.G. also has been supported by the predoctoral fellowship BES-2017-079725 from the Spanish Government.

APPENDIX A: DERIVATIVES OF THE TEMPERATURE RATIO IN THE VICINITY OF THE STEADY STATE

In this Appendix, the derivatives of the temperature ratio $\tau_1 = T_1^{(0)}/T$ with respect to θ, λ_1, x_1, and ϕ in the vicinity of the steady state are evaluated.

Let us consider first the derivative $(\partial\tau_1/\partial\theta)_{x_1,\lambda_1,\phi}$. To get it, we consider Eq. (69) for $i = 1$:

$$\Lambda^*\theta\frac{\partial\tau_1}{\partial\theta} = -\tau_1\Lambda^* + \Lambda_1^*, \tag{A1}$$

where Λ^* and Λ_1^* are defined by Eqs. (70) and (71), respectively. According to Eq. (48), the (reduced) partial cooling rate $\zeta_{1,0}^*$ can be written as

$$\zeta_{1,0}^* = \tau_1^{1/2}M_1^{-1/2}\zeta_1'(x_1,\beta), \tag{A2}$$

where $\beta = \beta_1/\beta_2 = m_1\tau_2/(m_2\tau_1)$, $\tau_2 = (1 - x_1\tau_1)/x_2$, and

$$\begin{aligned}\zeta_1'(x_1,\beta) = {}& \frac{\sqrt{2}\pi^{(d-1)/2}}{d\Gamma\left(\frac{d}{2}\right)}x_1\chi_{11}^{(0)}\left(\frac{\sigma_1}{\sigma_{12}}\right)^{d-1}\left(1-\alpha_{11}^2\right)\\ &+\frac{4\pi^{(d-1)/2}}{d\Gamma\left(\frac{d}{2}\right)}x_2\chi_{12}^{(0)}\mu_{21}(1+\beta)^{1/2}(1+\alpha_{12})\\ &\times\left[1-\frac{\mu_{21}}{2}(1+\alpha_{12})(1+\beta)\right].\end{aligned} \tag{A3}$$

At the steady state, $\Lambda^* = \Lambda_1^* = \Lambda_2^* = 0$, and hence, according to Eq. (A1), the derivative $\partial\tau_1/\partial\theta$ becomes indeterminate. On the other hand, as for dilute multicomponent granular suspensions [10], the above problem can be fixed by applying l'Hôpital's rule. In this case, we take first the derivative with respect to θ in both sides of Eq. (A1) and then take the steady-state limit. After some algebra, one easily achieves the following quadratic equation for the derivative $\Delta_{\theta,1} = (\partial\tau_1/\partial\theta)_s$:

$$\begin{aligned}&\theta\Lambda_1^{(\theta)}\Delta_{\theta,1}^2 + \left(\theta\Lambda_0^{(\theta)} + \tau_1\Lambda_1^{(\theta)} - \Lambda_{11}^{(\theta)}\right)\Delta_{\theta,1} - \Lambda_{10}^{(\theta)}\\ &+\tau_1\Lambda_0^{(\theta)} = 0,\end{aligned} \tag{A4}$$

where $\Lambda_0^{(\theta)} = x_1\Lambda_{10}^{(\theta)} + x_2\Lambda_{20}^{(\theta)}$ and $\Lambda_1^{(\theta)} = x_1\Lambda_{11}^{(\theta)} + x_2\Lambda_{21}^{(\theta)}$. Here we have introduced the quantities

$$\Lambda_{10}^{(\theta)} = \gamma_1^*\theta^{-1}\tau_1 - 3\gamma_1^*\theta^{-2}, \quad \Lambda_{20}^{(\theta)} = \gamma_2^*\theta^{-1}\tau_2 - 3\gamma_2^*\theta^{-2}, \tag{A5}$$

$$\Lambda_{11}^{(\theta)} = -2\gamma_1^* - \frac{3}{2}\zeta_{10}^* + \tau_1^{-1/2}\frac{M_1^{1/2}}{x_2M_2}\left(\frac{\partial\zeta_1'}{\partial\beta}\right)_{x_1,\phi}, \tag{A6}$$

$$\Lambda_{21}^{(\theta)} = 2\frac{x_1}{x_2}\gamma_2^* + \frac{3}{2}\frac{x_1}{x_2}\zeta_{20}^* + \frac{M_1}{x_2M_2^{3/2}}\frac{\tau_2^{3/2}}{\tau_1^2}\left(\frac{\partial\zeta_2'}{\partial\beta}\right)_{x_1,\phi}. \tag{A7}$$

In Eqs. (A4)–(A7), although the subscript s has been omitted for the sake of simplicity, it is understood that all the quantities are evaluated in the steady state. As for dilute driven granular mixtures [10], an analysis of the solutions to Eq. (A4) shows that in general one of the roots leads to unphysical behavior of the diffusion coefficients. We take the other root as the physical root of the quadratic equation (A4).

Once the derivative $\Delta_{\theta,1}$ is known, we can determine the remaining derivatives in a similar way. In order to get $(\partial\tau_1/\partial\lambda_1)_{\theta,x_1,\phi}$, we take first the derivative of Eq. (A1) with respect to λ_1 and then consider the steady-state conditions. The final result is

$$\Delta_{\lambda_1,1} = -\frac{\tau_1\Lambda_0^{(\lambda_1)} - \Lambda_{10}^{(\lambda_1)} + \theta\Lambda_0^{(\lambda_1)}\Delta_{\theta,1}}{\theta\Lambda_1^{(\theta)}\Delta_{\theta,1} + \tau_1\Lambda_1^{(\theta)} - \Lambda_{11}^{(\theta)}}, \tag{A8}$$

where $\Lambda_0^{(\lambda_1)} = x_1\Lambda_{10}^{(\lambda_1)} + x_2\Lambda_{20}^{(\lambda_1)}$, and

$$\begin{aligned}\Lambda_{10}^{(\lambda_1)} &= 2\theta^{-1/2}(\theta^{-1} - \tau_1),\\ \Lambda_{20}^{(\lambda_1)} &= 2\frac{R_2}{R_1}\theta^{-1/2}(\theta^{-1} - \tau_2).\end{aligned} \tag{A9}$$

Analogously, the derivative $(\partial\tau_1/\partial x_1)_{\theta,\lambda_1,\phi}$ in the steady state is

$$\Delta_{x_1,1} = -\frac{\tau_1\Lambda_0^{(x_1)} - \Lambda_{10}^{(x_1)} + \theta\Lambda_0^{(x_1)}\Delta_{\theta,1}}{\theta\Lambda_1^{(\theta)}\Delta_{\theta,1} + \tau_1\Lambda_1^{(\theta)} - \Lambda_{11}^{(\theta)}}, \tag{A10}$$

where $\Lambda_0^{(x_1)} = x_1\Lambda_{10}^{(x_1)} + x_2\Lambda_{20}^{(x_1)}$, and

$$\Lambda_{10}^{(x_1)} = -\tau_1^{3/2}M_1^{-1/2}\left(\frac{\partial\zeta_1'}{\partial x_1}\right)_{\beta,\phi}, \tag{A11}$$

$$\begin{aligned}\Lambda_{20}^{(x_1)} = {}& 2\frac{\gamma_1^*}{x_2}(\theta^{-1} - \tau_1) - 2\frac{\gamma_2^*}{x_2}(\theta^{-1} - \tau_2)\\ &- \frac{1-\tau_1}{x_2^2}\gamma_2^* + \frac{3}{2}\frac{\tau_1 - \frac{\tau_2}{3}}{x_2}\zeta_{2,0}^* - \frac{\tau_1}{x_2}\zeta_{1,0}^*\\ &-\tau_2^{3/2}M_2^{-1/2}\left(\frac{\partial\zeta_2'}{\partial x_1}\right)_{\beta,\phi}.\end{aligned} \tag{A12}$$

Finally, in the steady state, the derivative $(\partial\tau_1/\partial\phi)_{\theta,x_1,\lambda_1}$ is

$$\Delta_{\phi,1} = -\frac{\tau_1\Lambda_0^{(\phi)} - \Lambda_{10}^{(\phi)} + \theta\Lambda_0^{(\phi)}\Delta_{\theta,1}}{\theta\Lambda_1^{(\theta)}\Delta_{\theta,1} + \tau_1\Lambda_1^{(\theta)} - \Lambda_{11}^{(\theta)}}, \tag{A13}$$

where $\Lambda_0^{(\phi)} = x_1\Lambda_{10}^{(\phi)} + x_2\Lambda_{20}^{(\phi)}$, and

$$\Lambda_{10}^{(\phi)} = -\tau_1^{3/2}M_1^{-1/2}\left(\frac{\partial\zeta_1'}{\partial\phi}\right)_{x_1,\beta}, \tag{A14}$$

$$\Lambda_{20}^{(\phi)} = -\tau_2^{3/2}M_2^{-1/2}\left(\frac{\partial\zeta_2'}{\partial\phi}\right)_{x_1,\beta}. \tag{A15}$$

APPENDIX B: SOME TECHNICAL DETAILS ABOUT THE FIRST-ORDER CHAPMAN-ENSKOG SOLUTION

To first order in the spatial gradients, the distribution function $f_i^{(1)}$ obeys the Enskog kinetic equation

$$\partial_t^{(0)} f_i^{(1)} - \gamma_i \frac{\partial}{\partial \mathbf{v}} \cdot \mathbf{V} f_i^{(1)} - \frac{\gamma_i T_{\text{ex}}}{m_i} \frac{\partial^2 f_i^{(1)}}{\partial v^2} = -\left(D_t^{(1)} + \mathbf{V} \cdot \boldsymbol{\nabla}\right) f_i^{(0)} + \gamma_i \Delta \mathbf{U} \cdot \frac{\partial f_i^{(0)}}{\partial \mathbf{v}} - \mathbf{g} \cdot \frac{\partial f_i^{(0)}}{\partial \mathbf{v}} + \sum_{j=1}^{2} J_{ij}^{(1)}[f_i, f_j], \tag{B1}$$

where $D_t^{(1)} \equiv \partial_t^{(1)} + \mathbf{U} \cdot \boldsymbol{\nabla}$ and $J_{ij}^{(1)}[f_i, f_j]$ denotes the first-order contribution to the expansion of the Enskog collision operator in spatial gradients. To obtain $J_{ij}^{(1)}[f_i, f_j]$ one needs the expansions [18,22]

$$\chi_{ij}(\mathbf{r}, \mathbf{r} \pm \boldsymbol{\sigma}_{ij} | \{n_\ell\}) \to \sum_{\ell=1}^{2} \chi_{ij}^{(0)} \left[1 \pm \frac{1}{2} \left(n_\ell \frac{\partial \ln \chi_{ij}^{(0)}}{\partial n_\ell} + I_{ij\ell} \right) \boldsymbol{\sigma}_{ij} \cdot \boldsymbol{\nabla} \ln n_\ell \right], \tag{B2}$$

$$f_j^{(0)}(\mathbf{r} \pm \boldsymbol{\sigma}_{ij}) \to \sum_{\ell=1}^{2} n_\ell \frac{\partial f_j^{(0)}}{\partial n_\ell} \boldsymbol{\sigma}_{ij} \cdot \boldsymbol{\nabla} \ln n_\ell - \frac{\partial f_j^{(0)}}{\partial V_\beta} (\boldsymbol{\sigma}_{ij} \cdot \boldsymbol{\nabla}) U_\beta + T \frac{\partial f_j^{(0)}}{\partial T} \boldsymbol{\sigma}_{ij} \cdot \boldsymbol{\nabla} \ln T. \tag{B3}$$

In Eq. (B3) the quantities $I_{ij\ell}$ are defined in terms of the functional derivative of the (local) pair distribution function χ_{ij} with respect to the (local) partial densities n_ℓ. These quantities are the origin of the primary difference between the so-called standard and revised Enskog kinetic theories for ordinary mixtures [56,70]. The explicit forms of $I_{ij\ell}$ for a binary mixture of hard disks ($d = 2$) or spheres ($d = 3$) have been provided in Appendix A of Ref. [71]. Taking into account the expansions (B2) and (B3), the operator $J_{ij}^{(1)}[f_i, f_j]$ can be written as

$$\begin{aligned} \sum_{j=1}^{2} J_{ij}^{(1)}[f_i, f_j] \to & -\sum_{j=1}^{2} \sum_{\ell=1}^{2} \left\{ \mathcal{K}_{ij} \left[n_\ell \frac{\partial f_j^{(0)}}{\partial n_\ell} \right] + \frac{1}{2} \left(n_\ell \frac{\partial \ln \chi_{ij}^{(0)}}{\partial n_\ell} + I_{ij\ell} \right) \mathcal{K}_{ij}\left[f_j^{(0)} \right] \right\} \cdot \boldsymbol{\nabla} \ln n_\ell \\ & - \sum_{j=1}^{2} \mathcal{K}_{ij} \left[T \frac{\partial f_j^{(0)}}{\partial T} \right] \cdot \boldsymbol{\nabla} \ln T + \frac{1}{2} \sum_{j=1}^{2} \mathcal{K}_{ij,\lambda} \left[\frac{\partial f_j^{(0)}}{\partial V_\beta} \right] \left(\partial_\lambda U_\beta + \partial_\beta U_\lambda - \frac{2}{d} \delta_{\lambda\beta} \boldsymbol{\nabla} \cdot \mathbf{U} \right) \\ & + \frac{1}{d} \sum_{j=1}^{2} \mathcal{K}_{ij,\lambda} \left[\frac{\partial f_j^{(0)}}{\partial V_\lambda} \right] \boldsymbol{\nabla} \cdot \mathbf{U} + \sum_{j=1}^{2} \left(J_{ij}^{(0)}\left[f_i^{(1)}, f_j^{(0)} \right] + J_{ij}^{(0)}\left[f_i^{(0)}, f_j^{(1)} \right] \right), \end{aligned} \tag{B4}$$

where the operator $\mathcal{K}_{ij}[X_j]$ is given by [18,22]

$$\mathcal{K}_{ij}[X_j] = \sigma_{ij}^d \chi_{ij}^{(0)} \int d\mathbf{v}_2 \int d\widehat{\boldsymbol{\sigma}} \Theta(\widehat{\boldsymbol{\sigma}} \cdot \mathbf{g}_{12}) (\widehat{\boldsymbol{\sigma}} \cdot \mathbf{g}_{12}) \widehat{\boldsymbol{\sigma}} \left[\alpha_{ij}^{-2} f_i^{(0)}(\mathbf{v}_1'') X_j(\mathbf{v}_2'') + f_i^{(0)}(\mathbf{v}_1) X_j(\mathbf{v}_2) \right]. \tag{B5}$$

As for monocomponent granular suspensions [14], upon deriving Eq. (B4) use has been made of the symmetry property $\mathcal{K}_{ij,\lambda}[\partial_{V_\beta} f_j^{(0)}] = \mathcal{K}_{ij,\beta}[\partial_{V_\lambda} f_j^{(0)}]$, which follows from the isotropy in velocity space of the zeroth-order distributions $f_i^{(0)}$.

To first order, the balance equations are

$$D_t^{(1)} n_i = -n_i \boldsymbol{\nabla} \cdot \mathbf{U}, \quad D_t^{(1)} \mathbf{U} = -\rho^{-1} \boldsymbol{\nabla} p - \Delta \mathbf{U} \sum_{i=1}^{2} \frac{\rho_i}{\rho} \gamma_i + \mathbf{g} + \rho^{-1} (\gamma_1 - \gamma_2) \mathbf{j}_1^{(1)}, \tag{B6}$$

$$D_t^{(1)} T = -\frac{2p}{dn} \boldsymbol{\nabla} \cdot \mathbf{U} - \zeta^{(1)} T - 2 \sum_{i=1}^{2} \gamma_i x_i T_i^{(1)}. \tag{B7}$$

Here p is given by Eq. (64), and $\zeta^{(1)}$ is the first-order contribution to the cooling rate. Since $\zeta^{(1)}$ is a scalar, corrections to first order in the gradients can arise only from $\boldsymbol{\nabla} \cdot \mathbf{U}$ since $\boldsymbol{\nabla} n_i$ and $\boldsymbol{\nabla} T$ are vectors and the tensor $\partial_\lambda U_\beta + \partial_\beta U_\lambda - \frac{2}{d} \delta_{\lambda\beta} \boldsymbol{\nabla} \cdot \mathbf{U}$ is a traceless tensor. Thus, $\zeta^{(1)} = \zeta_U \boldsymbol{\nabla} \cdot \mathbf{U}$, where ζ_U can be decomposed as $\zeta_U = \zeta^{(1,0)} + \zeta^{(1,1)}$. The coefficient $\zeta^{(1,0)}$ can be evaluated explicitly with the result [23]

$$\zeta^{(1,0)} = -\frac{3}{nT} \frac{\pi^{d/2}}{d^2 \Gamma\left(\frac{d}{2}\right)} \sum_{i=1}^{2} \sum_{j=1}^{2} n_i n_j \mu_{ji} \sigma_{ij}^d \chi_{ij}^{(0)} T_i^{(0)} \left(1 - \alpha_{ij}^2\right). \tag{B8}$$

On the other hand, the coefficient $\zeta^{(1,1)}$ is given in terms of the first-order distributions $f_i^{(1)}$. Its expression will be displayed later. In addition, according to Eq. (64), ∇p can be written as

$$\nabla p = \sum_{i=1}^{2} n_i \frac{\partial p}{\partial n_i} \nabla \ln n_i + p\left(1 + \theta \frac{\partial \ln p^*}{\partial \theta}\right) \nabla \ln T, \tag{B9}$$

where we recall that $p^* = p/nT$.

The right-hand side of Eq. (B1) can be evaluated by using Eqs. (B6)–(B9) and the expansion (B4) of the Enskog operator. With these results, the corresponding kinetic equation for $f_i^{(1)}$ reads

$$\partial_t^{(0)} f_i^{(1)} - \gamma_i \frac{\partial}{\partial \mathbf{v}} \cdot \mathbf{V} f_i^{(1)} - \frac{\gamma_i T_{\text{ex}}}{m_i} \frac{\partial^2 f_i^{(1)}}{\partial v^2} - \left(T\zeta^{(1,1)} + 2\sum_{j=1}^{2} x_j \gamma_j \varpi_j\right) \frac{\partial f_i^{(0)}}{\partial T} \nabla \cdot \mathbf{U} - \rho^{-1}(\gamma_1 - \gamma_2) \mathbf{j}_1^{(1)} \cdot \frac{\partial f_i^{(0)}}{\partial \mathbf{V}}$$
$$- \sum_{j=1}^{2} \left(J_{ij}^{(0)}\left[f_i^{(1)}, f_j^{(0)}\right] + J_{ij}^{(0)}\left[f_i^{(0)}, f_j^{(1)}\right]\right) = \mathbf{A}_i \cdot \nabla \ln T + \sum_{j=1}^{2} \mathbf{B}_{ij} \cdot \nabla \ln n_j + C_{i,\lambda\beta} \frac{1}{2}\left(\partial_\lambda U_\beta + \partial_\beta U_\lambda - \frac{2}{d}\delta_{\lambda\beta} \nabla \cdot \mathbf{U}\right)$$
$$+ D_i \nabla \cdot \mathbf{U} + \mathbf{E}_i \cdot \Delta \mathbf{U}, \tag{B10}$$

where

$$\mathbf{A}_i(\mathbf{V}) = -\mathbf{V}T \frac{\partial f_i^{(0)}}{\partial T} - \frac{p}{\rho}\left(1 + \theta \frac{\partial \ln p^*}{\partial \theta}\right) \frac{\partial f_i^{(0)}}{\partial \mathbf{V}} - \sum_{j=1}^{2} \mathcal{K}_{ij}\left[T \frac{\partial f_j^{(0)}}{\partial T}\right], \tag{B11}$$

$$\mathbf{B}_{ij}(\mathbf{V}) = -\mathbf{V} n_j \frac{\partial f_i^{(0)}}{\partial n_j} - \frac{n_j}{\rho} \frac{\partial p}{\partial n_j} \frac{\partial f_i^{(0)}}{\partial \mathbf{V}} - \sum_{\ell=1}^{2} \left\{\mathcal{K}_{i\ell}\left[n_j \frac{\partial f_\ell^{(0)}}{\partial n_j}\right] + \frac{1}{2}\left(n_j \frac{\partial \ln \chi_{i\ell}^{(0)}}{\partial n_j} + I_{i\ell j}\right) \mathcal{K}_{i\ell}\left[f_\ell^{(0)}\right]\right\}, \tag{B12}$$

$$C_{i,\beta\lambda}(\mathbf{V}) = V_\lambda \frac{\partial f_i^{(0)}}{\partial V_\beta} + \sum_{j=1}^{2} \mathcal{K}_{ij,\lambda}\left[\frac{\partial f_j^{(0)}}{\partial V_\beta}\right], \tag{B13}$$

$$D_i(\mathbf{V}) = \frac{1}{d} \frac{\partial}{\partial \mathbf{V}} \cdot \left(\mathbf{V} f_i^{(0)}\right) + \left(\zeta^{(1,0)} + \frac{2}{d} p^*\right) T \frac{\partial f_i^{(0)}}{\partial T} - f_i^{(0)} + \sum_{j=1}^{2} \left\{n_j \frac{\partial f_i^{(0)}}{\partial n_j} + \frac{1}{d} \mathcal{K}_{ij,\lambda}\left[\frac{\partial f_j^{(0)}}{\partial V_\lambda}\right]\right\}, \tag{B14}$$

$$\mathbf{E}_i(\mathbf{V}) = \left(\gamma_i - \sum_{j=1}^{2} \frac{\rho_j}{\rho} \gamma_j\right) \frac{\partial f_i^{(0)}}{\partial \mathbf{V}}. \tag{B15}$$

Note that in Eq. (B10), $\zeta_1^{(1)}$ and ϖ_i are functionals of the first-order distributions $f_i^{(1)}$. In Eq. (B12) the derivative $\partial f_i^{(0)}/\partial n_j$ can be more explicitly written when one takes into account the scaling solution (43):

$$n_j \frac{\partial f_i^{(0)}}{\partial n_j} = \delta_{ij} f_j^{(0)} + n_j f_i^{(0)}\left(\frac{\partial \ln \varphi_i}{\partial x_1} \frac{\partial x_1}{\partial n_j} + \frac{\partial \ln \varphi_i}{\partial \lambda_1} \frac{\partial \lambda_1}{\partial n_j} + \frac{\partial \ln \varphi_i}{\partial \phi} \frac{\partial \phi}{\partial n_j}\right), \tag{B16}$$

where

$$n_j \frac{\partial x_1}{\partial n_j} = x_j(x_2\delta_{1j} - x_1\delta_{2j}), \quad n_j \frac{\partial \phi}{\partial n_j} = \phi_j, \tag{B17}$$

$$n_j \frac{\partial \lambda_1}{\partial n_j} = \lambda_1\left(\phi_j \frac{\partial \ln R_1}{\partial \phi} + \frac{\partial \ln R_1}{\partial x_1} n_j \frac{\partial x_1}{\partial n_j}\right) - \lambda_1 x_j - \lambda_1 \frac{\rho_j}{\rho}. \tag{B18}$$

The solution to Eq. (B10) is given by Eq. (72). Because of the gradients ∇n_i, ∇T, and $\nabla \cdot \mathbf{U}$ as well as the traceless tensor $\partial_\lambda U_\beta + \partial_\beta U_\lambda - \frac{2}{d}\delta_{\lambda\beta}\nabla \cdot \mathbf{U}$ are all independents, substitution of the form (72) into Eq. (B10) leads to the following set of linear integral equations for the unknowns $\boldsymbol{\mathcal{A}}_i(\mathbf{V})$, $\boldsymbol{\mathcal{B}}_{ij}(\mathbf{V})$, $\mathcal{C}_{i,\lambda\beta}(\mathbf{V})$, and $\mathcal{D}_i(\mathbf{V})$:

$$\Lambda^{(0)} T \partial_T \boldsymbol{\mathcal{A}}_i - \left[2\sum_{j=1}^{2} \gamma_j x_j\left(\theta^{-1} + \theta \frac{\partial \tau_j}{\partial \theta}\right) + \frac{1}{2}\zeta^{(0)} + \zeta^{(0)} \theta \frac{\partial \ln \zeta_0^*}{\partial \theta}\right] \boldsymbol{\mathcal{A}}_i - \gamma_i \frac{\partial}{\partial \mathbf{v}} \cdot \mathbf{V} \boldsymbol{\mathcal{A}}_i - \frac{\gamma_i T_{\text{ex}}}{m_i} \frac{\partial^2}{\partial v^2} \boldsymbol{\mathcal{A}}_i$$
$$+ (\gamma_2 - \gamma_1) D_1^T \frac{\partial f_i^{(0)}}{\partial \mathbf{V}} - \sum_{j=1}^{2} \left(J_{ij}^{(0)}\left[\boldsymbol{\mathcal{A}}_i, f_j^{(0)}\right] + J_{ij}^{(0)}\left[f_i^{(0)}, \boldsymbol{\mathcal{A}}_j\right]\right) = \mathbf{A}_i, \tag{B19}$$

$$\Lambda^{(0)}T\partial_T\boldsymbol{\mathcal{B}}_{ij}-\gamma_i\frac{\partial}{\partial\mathbf{v}}\cdot\mathbf{V}\boldsymbol{\mathcal{B}}_{ij}-\frac{\gamma_iT_{\rm ex}}{m_i}\frac{\partial^2}{\partial v^2}\boldsymbol{\mathcal{B}}_{ij}+(\gamma_2-\gamma_1)\frac{m_1\rho_j}{\rho^2}D_{1j}\frac{\partial f_i^{(0)}}{\partial\mathbf{V}}-\sum_{\ell=1}^{2}\left(J_{i\ell}^{(0)}[\boldsymbol{\mathcal{B}}_{ij},f_\ell^{(0)}]+J_{i\ell}^{(0)}[f_i^{(0)},\boldsymbol{\mathcal{B}}_{\ell j}]\right)$$

$$=\mathbf{B}_{ij}+\left(n_j\frac{\partial\zeta^{(0)}}{\partial n_j}-2n_j\sum_{\ell=1}^{2}\left\{\gamma_\ell x_\ell\left[(\theta^{-1}-\tau_\ell)\left(\frac{\partial\ln\gamma_\ell}{\partial n_j}+\frac{\partial\ln x_\ell}{\partial n_j}\right)-\left(\frac{\partial\tau_\ell}{\partial x_1}\frac{\partial x_1}{\partial n_j}+\frac{\partial\tau_\ell}{\partial\lambda_1}\frac{\partial\lambda_1}{\partial n_j}+\frac{\partial\tau_\ell}{\partial\phi}\frac{\partial\phi}{\partial n_j}\right)\right]\right\}\right)\boldsymbol{\mathcal{A}}_i, \tag{B20}$$

$$\Lambda^{(0)}T\partial_T\mathcal{C}_{i,\lambda\beta}-\gamma_i\frac{\partial}{\partial\mathbf{v}}\cdot\mathbf{V}\mathcal{C}_{i,\lambda\beta}-\frac{\gamma_iT_{\rm ex}}{m_i}\frac{\partial^2}{\partial v^2}\mathcal{C}_{i,\lambda\beta}-\sum_{j=1}^{2}\left(J_{ij}^{(0)}[\mathcal{C}_{i,\lambda\beta},f_j^{(0)}]+J_{ij}^{(0)}[f_i^{(0)},\mathcal{C}_{j,\lambda\beta}]\right)=C_{i,\lambda\beta}, \tag{B21}$$

$$\Lambda^{(0)}T\partial_T\mathcal{D}_i-\gamma_i\frac{\partial}{\partial\mathbf{v}}\cdot\mathbf{V}\mathcal{D}_i-\frac{\gamma_iT_{\rm ex}}{m_i}\frac{\partial^2}{\partial v^2}\mathcal{D}_i-\left(T\zeta^{(1,1)}+2\sum_{j=1}^{2}\gamma_jx_j\varpi_j\right)\frac{\partial f_i^{(0)}}{\partial T}-\sum_{j=1}^{2}\left(J_{ij}^{(0)}[\mathcal{D}_i,f_j^{(0)}]+J_{ij}^{(0)}[f_i^{(0)},\mathcal{D}_j]\right)=D_i, \tag{B22}$$

$$\Lambda^{(0)}T\partial_T\boldsymbol{\mathcal{E}}_i-\gamma_i\frac{\partial}{\partial\mathbf{v}}\cdot\mathbf{V}\boldsymbol{\mathcal{E}}_i-\frac{\gamma_iT_{\rm ex}}{m_i}\frac{\partial^2}{\partial v^2}\boldsymbol{\mathcal{E}}_i+\rho^{-1}(\gamma_2-\gamma_1)D_1^U\frac{\partial f_i^{(0)}}{\partial\mathbf{V}}-\sum_{j=1}^{2}\left(J_{ij}^{(0)}[\boldsymbol{\mathcal{E}}_i,f_j^{(0)}]+J_{ij}^{(0)}[f_i^{(0)},\boldsymbol{\mathcal{E}}_j]\right)=\mathbf{E}_i, \tag{B23}$$

where $\Lambda^{(0)}$ is defined by Eq. (66). Upon deriving the above integral equations use has been made of the constitutive equation (78) for the mass flux $\mathbf{j}_1^{(1)}$ and the result

$$\partial_t^{(0)}\nabla\ln T=\nabla\partial_t^{(0)}\ln T=\nabla\left(2\sum_{i=1}^{2}\gamma_ix_i(\theta^{-1}-\tau_i)-\zeta^{(0)}\right)$$

$$=-\sum_{j=1}^{2}\left(n_j\frac{\partial\zeta^{(0)}}{\partial n_j}-2n_j\sum_{\ell=1}^{2}\left\{\gamma_\ell x_\ell\left[(\theta^{-1}-\tau_\ell)\left(\frac{\partial\ln\gamma_\ell}{\partial n_j}+\frac{\partial\ln x_\ell}{\partial n_j}\right)-\left(\frac{\partial\tau_\ell}{\partial x_1}\frac{\partial x_1}{\partial n_j}+\frac{\partial\tau_\ell}{\partial\lambda_1}\frac{\partial\lambda_1}{\partial n_j}+\frac{\partial\tau_\ell}{\partial\phi}\frac{\partial\phi}{\partial n_j}\right)\right]\right\}\right)\nabla\ln n_j$$

$$-\left[2\sum_{i=1}^{2}\gamma_ix_i\left(\theta^{-1}+\theta\frac{\partial\tau_i}{\partial\theta}\right)+\frac{1}{2}\zeta^{(0)}+\zeta^{(0)}\theta\frac{\partial\ln\zeta_0^*}{\partial\theta}\right]\nabla\ln T. \tag{B24}$$

Moreover, since $\zeta^{(1,1)}$ is coupled to $\mathcal{D}_i$, its explicit form can be easily identified after expanding the expression (30) of the cooling rate to first order. The result is [23]

$$\zeta^{(1,1)}=\frac{1}{nT}\frac{\pi^{(d-1)/2}}{d\Gamma\left(\frac{d+3}{2}\right)}\sum_{i=1}^{2}\sum_{j=1}^{2}\sigma_{ij}^{d-1}\chi_{ij}^{(0)}m_{ij}\left(1-\alpha_{ij}^2\right)\int d\mathbf{v}_1\int d\mathbf{v}_2\,g_{12}^3\,f_i^{(0)}(\mathbf{V}_1)\mathcal{D}_j(\mathbf{V}_2). \tag{B25}$$

The integral equations (73)–(76) can be obtained from Eqs. (B19)–(B22) when the steady-state condition ($\Lambda^{(0)}=0$) is assumed.

APPENDIX C: ALGEBRAIC EQUATIONS DEFINING THE TRANSPORT COEFFICIENTS

In this Appendix, we display the set of algebraic equations defining the diffusion transport coefficients, the shear viscosity coefficient, and the first-order contributions to the partial temperatures. In the case of the diffusion coefficients D_i^T, D_{ij}, and D_i^U, the set of algebraic equations are, respectively, given by

$$\sum_{j=1}^{2}\left\{\nu_{ij}+(\gamma_2-\gamma_1)\frac{\rho_i}{\rho}\delta_{1j}-\left[2\sum_{\ell=1}^{2}\gamma_\ell x_\ell(\theta^{-1}-\theta\Delta_{\theta,\ell})+\frac{1}{2}\zeta^{(0)}+\zeta^{(0)}\theta\frac{\partial\ln\zeta_0^*}{\partial\theta}-\gamma_i\right]\delta_{ij}\right\}D_j^T$$

$$=-\frac{p\rho_i}{\rho^2}\left(1+\theta\frac{\partial\ln p^*}{\partial\theta}-\frac{\rho n_iT_i^{(0)}}{p\rho_i}\right)+T\frac{n_i}{\rho}\theta\Delta_{\theta,i}+\frac{\pi^{d/2}}{d\Gamma\left(\frac{d}{2}\right)}\frac{n_iT}{\rho}\sum_{j=1}^{2}n_j\mu_{ij}\chi_{ij}^{(0)}\sigma_{ij}^d(1+\alpha_{ij})(\tau_j+\theta\Delta_{\theta,j}), \tag{C1}$$

$$\sum_{\ell=1}^{2}\left[\nu_{i\ell}+(\gamma_2-\gamma_1)\frac{\rho_i}{\rho}\delta_{1\ell}+\gamma_i\delta_{i\ell}\right]m_\ell D_{\ell j}=\frac{\rho T}{\rho_j}\left\{n_j\tau_j\delta_{ij}+n\left[n_j\frac{\partial x_1}{\partial n_j}x_i\Delta_{x_1,i}+n_j\frac{\partial\lambda_1}{\partial n_j}x_i\Delta_{\lambda_1,i}+x_i\phi_j\Delta_{\phi,i}\right]\right\}$$

$$+\frac{\rho^2}{m_j}\left(\frac{\partial\zeta^{(0)}}{\partial n_j}-2\sum_{\ell=1}^{2}\left\{\gamma_\ell x_\ell\left[(\theta^{-1}-\tau_\ell)\left(\frac{\partial\ln\gamma_\ell}{\partial n_j}+\frac{\partial\ln x_\ell}{\partial n_j}\right)-\left(\frac{\partial x_1}{\partial n_j}\Delta_{x_1,\ell}+\frac{\partial\lambda_1}{\partial n_j}\Delta_{\lambda_1,\ell}+\frac{\phi_j}{n_j}\Delta_{\phi,\ell}\right)\right]\right\}\right)D_i^T$$

$$-\frac{\rho_i}{m_j}\frac{\partial p}{\partial n_j}+\frac{\rho T}{\rho_j}\frac{\pi^{d/2}}{d\Gamma\left(\frac{d}{2}\right)}\sum_{\ell=1}^{2}n_i n_\ell\sigma_{i\ell}^d\chi_{i\ell}^{(0)}m_{i\ell}(1+\alpha_{i\ell})\left\{\left[\delta_{j\ell}+\frac{1}{2}\left(n_j\frac{\partial\ln\chi_{i\ell}^{(0)}}{\partial n_j}+I_{i\ell j}\right)\right]\left(\frac{\tau_i}{m_i}+\frac{\tau_\ell}{m_\ell}\right)\right.$$

$$\left.+\frac{n_j}{m_\ell}\frac{\partial x_1}{\partial n_j}\Delta_{x_1,\ell}+\frac{n_j}{m_\ell}\frac{\partial\lambda_1}{\partial n_j}\Delta_{\lambda_1,\ell}+\frac{\phi_j}{m_\ell}\Delta_{\phi,\ell}\right\}, \tag{C2}$$

$$\sum_{j=1}^{2}\left[\nu_{ij}+(\gamma_2-\gamma_1)\frac{\rho_i}{\rho}\delta_{1j}+\gamma_i\delta_{ij}\right]D_j^U=\rho_i\left(\gamma_i-\sum_{j=1}^{2}\frac{\rho_j}{\rho}\gamma_j\right). \tag{C3}$$

Here the derivatives $\partial x_1/\partial n_j$ and $\partial\lambda_1/\partial n_j$ are given by Eqs. (B17) and (B18), respectively, and the collision frequencies ν_{ij} appearing in Eqs. (C1)–(C3) are defined as

$$\nu_{ii}=-\frac{m_i}{dn_iT_i}\int d\mathbf{v}\,\mathbf{V}\cdot J_{ij}^{(0)}[f_{i,\mathrm{M}}\mathbf{V},f_j^{(0)}], \tag{C4}$$

$$\nu_{ij}=-\frac{m_i}{dn_jT_j}\int d\mathbf{v}\,\mathbf{V}\cdot J_{ij}^{(0)}[f_i^{(0)},f_{j,\mathrm{M}}\mathbf{V}], \tag{C5}$$

for $i\neq j$. Note that the self-collision terms of ν_{ii} arising from $J_{ii}^{(0)}[f_{i\mathrm{M}}\mathbf{V},f_i^{(0)}]$ do not occur in Eq. (C4) since they conserve momentum for the component i. In addition, upon deriving Eqs. (C1) and (C2), use has been made of the results

$$\int d\mathbf{v}m_i\mathbf{V}\cdot\mathcal{K}_{ij}\left[T\frac{\partial f_j^{(0)}}{\partial T}\right]=\frac{\pi^{d/2}}{\Gamma\left(\frac{d}{2}\right)}n_in_j\sigma_{ij}^d\chi_{ij}^{(0)}\mu_{ij}(1+\alpha_{ij})T_j^{(0)}\left(1+\frac{\theta}{\tau_j}\Delta_{\theta,j}\right), \tag{C6}$$

$$\int d\mathbf{v}m_i\mathbf{V}\cdot\left\{\mathcal{K}_{i\ell}\left[n_j\frac{\partial f_\ell^{(0)}}{\partial n_j}\right]+\frac{1}{2}\left(n_j\frac{\partial\ln\chi_{i\ell}^{(0)}}{\partial n_j}+I_{i\ell j}\right)\mathcal{K}_{i\ell}\left[f_\ell^{(0)}\right]\right\}=\frac{\pi^{d/2}}{\Gamma\left(\frac{d}{2}\right)}n_iTn_\ell\sigma_{i\ell}^d\chi_{i\ell}^{(0)}m_{i\ell}(1+\alpha_{i\ell})$$

$$\times\left\{\left[\delta_{j\ell}+\frac{1}{2}\left(n_j\frac{\partial\ln\chi_{i\ell}^{(0)}}{\partial n_j}+I_{i\ell j}\right)\right]\left(\frac{\tau_i}{m_i}+\frac{\tau_\ell}{m_\ell}\right)+\frac{n_j}{m_\ell}\frac{\partial x_1}{\partial n_j}\Delta_{x_1,\ell}+\frac{n_j}{m_\ell}\frac{\partial\lambda_1}{\partial n_j}\Delta_{\lambda_1,\ell}+\frac{\phi_j}{m_\ell}\Delta_{\phi,\ell}\right\}, \tag{C7}$$

where $f_i^{(0)}$ has been replaced by $f_{i,\mathrm{M}}$. The explicit forms of the collision frequencies ν_{ii} and ν_{ij} also can be easily obtained by considering the latter replacement. They are given by [72]

$$\nu_{ii}=\frac{2\pi^{(d-1)/2}}{d\Gamma\left(\frac{d}{2}\right)}n_j\sigma_{ij}^{d-1}\chi_{ij}^{(0)}\mu_{ji}v_0(1+\alpha_{ij})\left(\frac{\beta_i+\beta_j}{\beta_i\beta_j}\right)^{1/2}, \tag{C8}$$

$$\nu_{ij}=-\frac{2\pi^{(d-1)/2}}{d\Gamma\left(\frac{d}{2}\right)}n_i\sigma_{ij}^{d-1}\chi_{ij}^{(0)}\mu_{ij}v_0(1+\alpha_{ij})\left(\frac{\beta_i+\beta_j}{\beta_i\beta_j}\right)^{1/2}. \tag{C9}$$

We recall that $i\neq j$ in Eqs. (C8) and (C9). With these results, the explicit form of D_1^T can be written as

$$D_1^T=\left[\nu_D+\frac{\rho_1\gamma_2+\rho_2\gamma_1}{\rho}-2\sum_{j=1}^{2}x_j\gamma_j(\theta^{-1}-\theta\Delta_{\theta,j})-\zeta^{(0)}\left(\frac{1}{2}+\theta\frac{\partial\ln\zeta_0^*}{\partial\theta}\right)\right]^{-1}\left\{\frac{Tn_1}{\rho}\theta\Delta_{\theta,1}\right.$$

$$-\frac{p\rho_1}{\rho^2}\left(1+\theta\frac{\partial\ln p^*}{\partial\theta}-\frac{\rho n_1T_1^{(0)}}{p\rho_1}\right)+\frac{\pi^{d/2}}{d\Gamma\left(\frac{d}{2}\right)}\frac{n_1T}{\rho}\left[\frac{n_1}{2}\chi_{11}^{(0)}\sigma_1^d(1+\alpha_{11})(\tau_1+\theta\Delta_{\theta,1})\right.$$

$$\left.\left.+n_2\mu_{12}\chi_{12}^{(0)}\sigma_{12}^d(1+\alpha_{12})(\tau_2+\theta\Delta_{\theta,2})\right]\right\}, \tag{C10}$$

where ν_D is

$$\nu_D=\nu_{11}-\nu_{12}=\frac{2\pi^{(d-1)/2}}{d\Gamma\left(\frac{d}{2}\right)}n\sigma_{12}^{d-1}\chi_{12}^{(0)}v_0(1+\alpha_{12})\left(\frac{\beta_1+\beta_2}{\beta_1\beta_2}\right)^{1/2}(x_1\mu_{12}+x_2\mu_{21}). \tag{C11}$$

We consider now the kinetic contribution η_{k} to the shear viscosity coefficient η. The kinetic coefficient $\eta_{\mathrm{k}}=\eta_1^{\mathrm{k}}+\eta_2^{\mathrm{k}}$, where the partial contributions η_i^{k} $(i=1,2)$ obey the set of equations

$$\sum_{j=1}^{2}(\tau_{ij}+2\gamma_i\delta_{ij})\eta_j^{\mathrm{k}}=n_iT_i^{(0)}+\frac{\rho_iT\pi^{d/2}}{d(d+2)\Gamma\left(\frac{d}{2}\right)}\sum_{j=1}^{2}n_j\mu_{ji}\sigma_{ij}^d\chi_{ij}^{(0)}(1+\alpha_{ij})\left[\mu_{ji}(3\alpha_{ij}-1)\left(\frac{\tau_i}{m_i}+\frac{\tau_j}{m_j}\right)-4\frac{\tau_i-\tau_j}{m_i+m_j}\right], \tag{C12}$$

where the collision frequencies τ_{ij} are defined as

$$\tau_{ii} = -\frac{1}{(d-1)(d+2)}\frac{1}{n_i T_i^{(0)2}}\left(\int d\mathbf{v} R_{i,\lambda\beta} J_{ii}^{(0)}\left[f_i^{(0)}, f_{i\mathrm{M}} R_{i,\lambda\beta}\right] + \sum_{j=1}^{2}\int d\mathbf{v} R_{i,\lambda\beta} J_{ij}^{(0)}\left[f_{i\mathrm{M}} R_{i,\lambda\beta}, f_j^{(0)}\right]\right), \tag{C13}$$

$$\tau_{ij} = -\frac{1}{(d-1)(d+2)}\frac{1}{n_j T_j^{(0)2}}\int d\mathbf{v} R_{i,\lambda\beta} J_{ij}^{(0)}\left[f_i^{(0)}, f_{j\mathrm{M}} R_{j,\lambda\beta}\right], \quad (i\neq j). \tag{C14}$$

Upon deriving Eq. (C12) use has been made of the result [23]

$$\int d\mathbf{v}\, R_{i,\lambda\beta}\mathcal{K}_{ij,\lambda}\left[\frac{\partial f_j^{(0)}}{\partial V_\beta}\right] = -\frac{\pi^{d/2}(d-1)}{d\Gamma\left(\frac{d}{2}\right)}\rho_i n_j T \mu_{ji}\sigma_{ij}^d \chi_{ij}^{(0)}(1+\alpha_{ij})\left[\mu_{ji}(3\alpha_{ij}-1)\left(\frac{\tau_i}{m_i}+\frac{\tau_j}{m_j}\right) - 4\frac{\tau_i-\tau_j}{m_i+m_j}\right]. \tag{C15}$$

Explicit expressions of the collision frequencies τ_{ii} and τ_{ij} can be obtained by considering the Maxwellian approximation (103) to $f_i^{(0)}$. The results are [23]

$$\tau_{ii} = \frac{2\pi^{(d-1)/2}}{d(d+2)\Gamma\left(\frac{d}{2}\right)} v_0 \Bigg\{ n_i \sigma_i^{d-1}\chi_{ii}^{(0)}(2\beta_i)^{-1/2}(3+2d-3\alpha_{ii})(1+\alpha_{ii}) + 2n_j\chi_{ij}^{(0)}\sigma_{ij}^{d-1}\mu_{ji}(1+\alpha_{ij})\beta_i^{3/2}\beta_j^{-1/2}$$
$$\times\left[(d+3)\beta_{ij}\beta_i^{-2}(\beta_i+\beta_j)^{-1/2} + \frac{3+2d-3\alpha_{ij}}{2}\mu_{ji}\beta_i^{-2}(\beta_i+\beta_j)^{1/2} + \frac{2d(d-1)-4}{2(d-1)}\beta_i^{-1}(\beta_i+\beta_j)^{-1/2}\right]\Bigg\}, \tag{C16}$$

$$\tau_{ij} = \frac{4\pi^{(d-1)/2}}{d(d+2)\Gamma\left(\frac{d}{2}\right)} v_0 n_i \chi_{ij}^{(0)}\sigma_{ij}^{d-1}\mu_{ij}\beta_j^{3/2}\beta_i^{-1/2}(1+\alpha_{ij})\Bigg[(d+3)\beta_{ij}\beta_j^{-2}(\beta_i+\beta_j)^{-1/2} + \frac{3+2d-3\alpha_{ij}}{2}$$
$$\times\mu_{ji}\beta_j^{-2}(\beta_i+\beta_j)^{1/2} - \frac{2d(d+1)-4}{2(d-1)}\beta_j^{-1}(\beta_i+\beta_j)^{-1/2}\Bigg], \tag{C17}$$

where $\beta_{ij} = \mu_{ij}\beta_j - \mu_{ji}\beta_i$ and $i\neq j$.

Finally, the first-order contributions $T_i^{(1)}$ to the partial temperatures are defined as $T_i^{(1)} = \varpi_i \boldsymbol{\nabla}\cdot\mathbf{U}$. The set of algebraic equations defining the coefficients ϖ_i are given by

$$\sum_{j=1}^{2}\left[\omega_{ij} + 2\gamma_j x_j(\tau_i + \theta\Delta_{\theta,i}) - 2\gamma_i\delta_{ij} + \left(T_i^{(0)} + T\theta\Delta_{\theta,i}\right)\xi_j\right]\varpi_j = \frac{2}{d}T_i^{(0)} - \left(\zeta^{(1,0)} + \frac{2}{d}p^*\right)\left(T_i^{(0)} + T\theta\Delta_{\theta,i}\right)$$
$$+ T\sum_{j=1}^{2}\left\{\frac{\pi^{d/2}}{d^2\Gamma\left(\frac{d}{2}\right)} n_j\sigma_{ij}^d\chi_{ij}^{(0)}m_{ij}(1+\alpha_{ij})\left[3\mu_{ji}(1+\alpha_{ij})\left(\frac{\tau_i}{m_i}+\frac{\tau_j}{m_j}\right) - 4\frac{\tau_i}{m_i}\right] - n_j\left(\frac{\partial\lambda_1}{\partial n_j}\Delta_{\lambda_1,i} + \frac{\partial\phi}{\partial n_j}\Delta_{\phi,i}\right)\right\}, \tag{C18}$$

where $\zeta^{(1,0)}$ is defined by Eq. (B8) and the collision frequencies ω_{ij} are

$$\omega_{ii} = \frac{1}{dn_i T_i^{(0)}}\left(\sum_{j=1}^{2}\int d\mathbf{v} m_i V^2 J_{ij}^{(0)}\left[f_{i\mathrm{M}}W_i, f_j^{(0)}\right] + \int d\mathbf{v} m_i V^2 J_{ii}^{(0)}\left[f_i^{(0)}, f_{i\mathrm{M}}W_i\right]\right), \tag{C19}$$

$$\omega_{ij} = \frac{1}{dn_i T_j^{(0)}}\int d\mathbf{v} m_i V^2 J_{ij}^{(0)}\left[f_i^{(0)}, f_{j\mathrm{M}}W_j\right] \quad (i\neq j). \tag{C20}$$

Upon deriving Eq. (C18), we have accounted for that $\sum_j n_j\partial_{n_j}x_1 = 0$, and use has been made of the result [21]

$$\int d\mathbf{v} m_i V^2 \mathcal{K}_{ij,\lambda}\left[\frac{\partial f_j^{(0)}}{\partial V_\lambda}\right] = -\frac{\pi^{d/2}}{\Gamma\left(\frac{d}{2}\right)}\chi_{ij}^{(0)} n_i n_j \sigma_{ij}^d(1+\alpha_{ij})\left[3\mu_{ji}(1+\alpha_{ij})\left(\frac{T_i^{(0)}}{m_i}+\frac{T_j^{(0)}}{m_i}\right) - 4\frac{T_i^{(0)}}{m_i}\right]. \tag{C21}$$

Moreover, in the Maxwellian approximation (103), the collision frequencies ω_{ii} and ω_{ij} read [27]

$$\omega_{ii} = -\frac{\pi^{(d-1)/2}}{2dT_i^{(0)}\Gamma\left(\frac{d}{2}\right)} v_0^3\Bigg\{\frac{3}{\sqrt{2}} n_i\sigma_i^{d-1}m_i\chi_{ii}^{(0)}\beta_i^{-3/2}\left(1-\alpha_{ii}^2\right) - n_j m_{ij}\sigma_{ij}^{d-1}\chi_{ij}^{(0)}(1+\alpha_{ij})$$
$$\times(\beta_i+\beta_j)^{-1/2}\beta_i^{-3/2}\beta_j^{-1/2}[3\mu_{ji}(1+\alpha_{ij})(\beta_i+\beta_j) - 2(2\beta_i+3\beta_j)]\Bigg\}, \tag{C22}$$

$$\omega_{ij} = \frac{\pi^{(d-1)/2}}{2dT_j^{(0)}\Gamma\left(\frac{d}{2}\right)} v_0^3 n_j m_{ij}\sigma_{ij}^{d-1}\chi_{ij}^{(0)}(1+\alpha_{ij})(\beta_i+\beta_j)^{-1/2}\beta_i^{-1/2}\beta_j^{-3/2}[3\mu_{ji}(1+\alpha_{ij})(\beta_i+\beta_j) - 2\beta_j]. \tag{C23}$$

In Eqs. (C22)–(C23) it is understood that $i\neq j$.

[1] M. E. Möbius, B. E. Lauderdale, S. R. Nagel, and H. M. Jaeger, Brazil-nut effect: Size separation of granular particles, Nature (London) **414**, 270 (2001).

[2] M. A. Naylor, M. R. Swift, and P. J. King, Air-driven Brazil nut effect, Phys. Rev. E **68**, 012301 (2003).

[3] P. Sánchez, M. R. Swift, and P. J. King, Stripe Formation in Granular Mixtures Due to the Differential Influence of Drag, Phys. Rev. Lett. **93**, 184302 (2004).

[4] J. J. Wylie, Q. Zhang, H. Y. Xu, and X. X. Sun, Drag-induced particle segregation with vibrating boundaries, Europhys. Lett. **81**, 54001 (2008).

[5] C. P. Clement, H. A. Pacheco-Martínez, M. R. Swift, and P. J. King, The water-enhanced Brazil nut effect, Europhys. Lett. **91**, 54001 (2010).

[6] J. C. Pastenes, J. C. Géminard, and F. Melo, Interstitial gas effect on vibrated granular columns, Phys. Rev. E **89**, 062205 (2014).

[7] D. L. Koch and R. J. Hill, Inertial effects in suspensions and porous-media flows, Annu. Rev. Fluid Mech. **33**, 619 (2001).

[8] G. Gradenigo, A. Sarracino, D. Villamaina, and A. Puglisi, Fluctuating hydrodynamics and correlation lengths in a driven granular fluid, J. Stat. Mech. (2011) P08017.

[9] V. Garzó, S. Tenneti, S. Subramaniam, and C. M. Hrenya, Enskog kinetic theory for monodisperse gas-solid flows, J. Fluid Mech. **712**, 129 (2012).

[10] N. Khalil and V. Garzó, Transport coefficients for driven granular mixtures at low-density, Phys. Rev. E **88**, 052201 (2013).

[11] H. Hayakawa, S. Takada, and V. Garzó, Kinetic theory of shear thickening for a moderately dense gas-solid suspension: From discontinuous thickening to continuous thickening, Phys. Rev. E **96**, 042903 (2017).

[12] N. G. van Kampen, *Stochastic Processes in Physics and Chemistry* (North-Holland, Amsterdam, 1981).

[13] D. R. M. Williams and F. C. MacKintosh, Driven granular media in one dimension: Correlations and equation of state, Phys. Rev. E **54**, R9 (1996).

[14] R. Gómez González and V. Garzó, Transport coefficients for granular suspensions at moderate densities, J. Stat. Mech. (2019) 093204 .

[15] S. Chapman and T. G. Cowling, *The Mathematical Theory of Nonuniform Gases* (Cambridge University Press, Cambridge, 1970).

[16] N. Khalil and V. Garzó, Heat flux of driven granular mixtures at low density: Stability analysis of the homogeneous steady state, Phys. Rev. E **97**, 022902 (2018).

[17] N. Khalil and V. Garzó, Erratum: Transport coefficients for driven granular mixtures at low density [Phys. Rev. E **88**, 052201 (2013)] and Heat flux of driven granular mixtures at low density: Stability analysis of the homogeneous steady state [Phys. Rev. E **97**, 022902 (2018)], Phys. Rev. E **99**, 059901 (2019).

[18] V. Garzó, *Granular Gaseous Flows* (Springer Nature Switzerland, Basel, 2019).

[19] V. Garzó and J. M. Montanero, Transport coefficients of a heated granular gas, Physica A **313**, 336 (2002).

[20] V. Garzó, Transport coefficients of driven granular fluids at moderate volume fractions, Phys. Rev. E **84**, 012301 (2011).

[21] R. Gómez González and V. Garzó, Influence of the first-order contributions to the partial temperatures on transport properties in polydisperse dense granular mixtures, Phys. Rev. E **100**, 032904 (2019).

[22] V. Garzó, J. W. Dufty, and C. M. Hrenya, Enskog theory for polydisperse granular mixtures. I. Navier-Stokes order transport, Phys. Rev. E **76**, 031303 (2007).

[23] V. Garzó, C. M. Hrenya, and J. W. Dufty, Enskog theory for polydisperse granular mixtures. II. Sonine polynomial approximation, Phys. Rev. E **76**, 031304 (2007).

[24] J. A. Murray, V. Garzó, and C. M. Hrenya, Enskog theory for polydisperse granular mixtures. III. Comparison of dense and dilute transport coefficients and equations of state for a binary mixture, Powder Technol. **220**, 24 (2012).

[25] M. I. García de Soria, P. Maynar, and E. Trizac, Universal reference state in a driven homogeneous granular gas, Phys. Rev. E **85**, 051301 (2012).

[26] M. G. Chamorro, F. Vega Reyes, and V. Garzó, Homogeneous steady states in a granular fluid driven by a stochastic bath with friction, J. Stat. Mech. (2013) P07013.

[27] R. Gómez González and V. Garzó, Simple shear flow in granular suspensions: Inelastic Maxwell models and BGK-type kinetic model, J. Stat. Mech. (2019) 013206.

[28] X. Yin and S. Sundaresan, Drag law for bidisperse gas-solid suspensions containing equally sized spheres, Ind. Eng. Chem. Res. **48**, 227 (2009).

[29] X. Yin and S. Sundaresan, Fluid-particle drag in low-Reynolds-number polydisperse gas-solid suspensions, AIChE **55**, 1352 (2009).

[30] W. Holloway, X. Yin, and S. Sundaresan, Fluid-particle drag in inertial polydisperse gas-solid suspensions, AIChE **56**, 1995 (2010).

[31] T. P. C. van Noije and M. H. Ernst, Velocity distributions in homogeneous granular fluids: The free and heated case, Granular Matter **1**, 57 (1998).

[32] C. Henrique, G. Batrouni, and D. Bideau, Diffusion as a mixing mechanism in granular materials, Phys. Rev. E **63**, 011304 (2000).

[33] S. R. Dahl, C. M. Hrenya, V. Garzó, and J. W. Dufty, Kinetic temperatures for a granular mixture, Phys. Rev. E **66**, 041301 (2002).

[34] A. Barrat and E. Trizac, Lack of energy equipartition in homogeneous heated binary granular mixtures, Granular Matter **4**, 57 (2002).

[35] N. Brilliantov and T. Pöschel, *Kinetic Theory of Granular Gases* (Oxford University Press, Oxford, 2004).

[36] V. Garzó and J. W. Dufty, Homogeneous cooling state for a granular mixture, Phys. Rev. E **60**, 5706 (1999).

[37] V. Garzó, M. G. Chamorro, and F. Vega Reyes, Transport properties for driven granular fluids in situations close to homogeneous steady states, Phys. Rev. E **87**, 032201 (2013).

[38] M. I. García de Soria, P. Maynar, and E. Trizac, Linear hydrodynamics for driven granular gases, Phys. Rev. E **87**, 022201 (2013).

[39] V. Garzó and J. W. Dufty, Dense fluid transport for inelastic hard spheres, Phys. Rev. E **59**, 5895 (1999).

[40] V. Garzó and F. V. Reyes, Segregation of an intruder in a heated granular gas, Phys. Rev. E **85**, 021308 (2012).

[41] N. Khalil and V. Garzó, Homogeneous states in driven granular mixtures: Enskog kinetic theory versus molecular

dynamics simulations, J. Chem. Phys. **140**, 164901 (2014).
[42] B. D. Lubachevsky, How to simulate billiards and similar systems, J. Comput. Phys. **94**, 255 (1991).
[43] M. P. Allen and D. J. Tildesley, *Computer Simulation of Liquids* (Clarendon, Oxford, 2005).
[44] J. F. Lutsko, J. J. Brey, and J. W. Dufty, Diffusion in a granular fluid. II. Simulation, Phys. Rev. E **65**, 051304 (2002).
[45] J. F. Lutsko, Rheology of dense polydisperse granular fluids under shear, Phys. Rev. E **70**, 061101 (2004).
[46] J. M. Montanero, V. Garzó, M. Alam, and S. Luding, Rheology of two- and three-dimensional granular mixtures under uniform shear flow: Enskog kinetic theory versus molecular dynamics simulations, Granular Matter **8**, 103 (2006).
[47] G. Lois, A. Lemaître, and J. M. Carlson, Spatial force correlations in granular shear flow. II. Theoretical implications, Phys. Rev. E **76**, 021303 (2007).
[48] P. P. Mitrano, V. Garzó, and C. M. Hrenya, Instabilities in granular binary mixtures at moderate densities, Phys. Rev. E **89**, 020201(R) (2014).
[49] V. Garzó and J. W. Dufty, Hydrodynamics for a granular binary mixture at low density, Phys. Fluids **14**, 1476 (2002).
[50] V. Garzó and A. Santos, *Kinetic Theory of Gases in Shear Flows. Nonlinear Transport* (Kluwer Academic Publishers, Dordrecht, 2003).
[51] V. Garzó, J. M. Montanero, and J. W. Dufty, Mass and heat fluxes for a binary granular mixture at low density, Phys. Fluids **18**, 083305 (2006).
[52] N. Khalil and V. Garzó, Unified hydrodynamic description for driven and undriven inelastic Maxwell mixtures at low density, arXiv:1910.12679.
[53] H. Margeneau and G. M. Murphy, *The Mathematics of Physics and Chemistry* (Krieger, Huntington, NY, 1956).
[54] J. Karkheck and G. Stell, Transport properties of the Widom–Rowlinson hard-sphere mixture model, J. Chem. Phys. **71**, 3620 (1979).
[55] J. Karkheck and G. Stell, Bulk viscosity of fluid mixtures, J. Chem. Phys. **71**, 3636 (1979).
[56] M. López de Haro, E. G. D. Cohen, and J. Kincaid, The Enskog theory for multicomponent mixtures. I. Linear transport theory, J. Chem. Phys. **78**, 2746 (1983).
[57] T. Boublik, Hard-sphere equation of state, J. Chem. Phys. **53**, 471 (1970).
[58] E. W. Grundke and D. Henderson, Distribution functions of multi-component fluid mixtures of hard spheres, Mol. Phys. **24**, 269 (1972).
[59] L. L. Lee and D. Levesque, Perturbation theory for mixtures of simple liquids, Mol. Phys. **26**, 1351 (1973).
[60] J. F. Lutsko, Transport properties of dense dissipative hard-sphere fluids for arbitrary energy loss models, Phys. Rev. E **72**, 021306 (2005).
[61] V. Garzó, Grad's moment method for a granular fluid at moderate densities: Navier–Stokes transport coefficients, Phys. Fluids **25**, 043301 (2013).
[62] J. M. Montanero, A. Santos, and V. Garzó, DSMC evaluation of the Navier–Stokes shear viscosity of a granular fluid, in *24th International Symposium on Rarefied Gas Dynamics, 2004 in Bari, Italy*, edited by M. Capitelli, AIP Conf. Proc., Vol. 762 (AIP, Melville, NY, 2005), pp. 797–802.
[63] J. J. Brey, M. J. Ruiz-Montero, D. Cubero, and R. García-Rojo, Self-diffusion in freely evolving granular gases, Phys. Fluids **12**, 876 (2000).
[64] J. M. Montanero and V. Garzó, Shear viscosity for a heated granular binary mixture at low density, Phys. Rev. E **67**, 021308 (2003).
[65] V. Garzó and J. M. Montanero, Shear viscosity for a moderately dense granular binary mixture, Phys. Rev. E **68**, 041302 (2003).
[66] V. Garzó and J. M. Montanero, Diffusion of impurities in a granular gas, Phys. Rev. E **69**, 021301 (2004).
[67] V. Garzó and F. Vega Reyes, Mass transport of impurities in a moderately dense granular gas, Phys. Rev. E **79**, 041303 (2009).
[68] J. J. Brey and M. J. Ruiz-Montero, Shearing instability of a dilute granular mixture, Phys. Rev. E **87**, 022210 (2013).
[69] J. J. Brey, M. J. Ruiz-Montero, and D. Cubero, On the validity of linear hydrodynamics for low-density granular flows described by the Boltzmann equation, Europhys. Lett. **48**, 359 (1999).
[70] H. van Beijeren and M. H. Ernst, The modified Enskog equation for mixtures, Physica A **70**, 225 (1973).
[71] V. Garzó, Thermal diffusion segregation in granular binary mixtures described by the Enskog equation, New J. Phys. **13**, 055020 (2011).
[72] V. Garzó and J. M. Montanero, Navier–Stokes transport coefficients of d-dimensional granular binary mixtures at low density, J. Stat. Phys. **129**, 27 (2007).

Chapter 6

Non-Newtonian Rheology in Inertial Suspensions Under Simple Shear Flow

6.1 Summary

The non-Newtonian transport properties of a dilute granular suspension under uniform shear flow are determined in the framework of the Boltzmann equation. Particles are modeled as d-dimensional hard particles of mass m and diameter σ. As in previous chapters, the effect of the interstitial fluid on solid particles is accounted for by a drag force proportional to the instantaneous velocity of the particles and a Langevin-like term. In the USF, the system is characterized by a constant density profile n, a uniform granular temperature T , and a flow velocity $U_x = ay$, where a is the shear rate. In addition, as usual in uniform sheared suspensions [127, 128, 133, 249], the mean flow velocity $\mathbf{U}$ follows that of the gas phase $\mathbf{U}_g$. Thus, the viscous heating term due to shear plus the energy gained by grains due to collisions with the interstitial fluid is exactly compensated for by the cooling terms arising from collisional dissipation and the drag term. A steady state is still possible even when the collisions are elastic ($\zeta = 0$). An important feature of the USF is that the one-body distribution function $f(\mathbf{r}, \mathbf{v}; t)$ depends on space only through its dependence on the peculiar velocity $\mathbf{V} = \mathbf{v} - \mathbf{U}$ [250]. As a consequence, the velocity distribution function becomes homogeneous in the reference frame moving with $\mathbf{V}$: $f(\mathbf{r}, \mathbf{v}; t) \to f(\mathbf{V}; t)$. Hence, following symmetry

considerations, the heat flux vanishes $\mathbf{q} = 0$ and the pressure tensor P is the relevant flux. Three alternative but complementary routes are used to study the rheology of inertial suspensions: Grad's moment method [200], BGK-type kinetic model [57] and Inelastic Maxwell Models [240].

The first objective of this chapter is to analyze the USF state of granular suspensions composed of smooth hard spheres. In this case, the inelasticity of collisions is modeled by a constant (positive) coefficient of restitution $\alpha \leq 1$ and only the translational degrees of freedom of grains are involved in the collisional process. As a first step towards achieving this objective, the non-Newtonian transport coefficients measuring the departure from their corresponding Navier–Stokes forms are derived. These properties had been already obtained by solving the Enskog equation by means of Grad's moment method [142, 143]. Given that Grad's method requires a pertinent truncation in the velocity moment hierarchy, it is interesting to revisit the problem and get *exact* expressions of the rheological properties by considering both the Boltzmann equation for IMM and a BGK-type kinetic model for IHS. The determination of the rheological properties can allow us to assess the degree of reliability of IMM and BGK-like kinetic equations to capture the main trends observed for IHS. The (dimensionless) expressions for the steady granular temperature T, the non-Newtonian shear viscosity η, and the viscometric function $\Psi = P_{xx} - P_{yy}$ are displayed as functions of the shear rate (note that $P_{zz} = P_{yy}$ in all the above analytical methods). The analytical expressions of the above quantities obtained from the IMM Boltzmann equation and from the BGK equation match those derived by solving the Boltzmann equation for IHS via Grad's moment method and event-driven Langevin simulations [142, 143]. In particular, both theoretical approaches clearly show that the temperature and non-Newtonian viscosity exhibit an S-shape in a plane of stress–strain rate (DST effect).

Once the reliability of the IMM and BGK models is guaranteed, higher degree velocity moments are also computed. The importance of their knowledge relies on the information that it can provide on the velocity distribution function, especially in the high velocity region. In the USF, the first nontrivial moments beyond the rheological properties (which are related with the second-degree velocity moments) are the fourth-degree moments. We find that while those moments have unphysical values for IMM in a certain region of the parameter space of the system, they are well defined functions of in the case of the BGK kinetic model. The divergence of the fourth-degree moments of the

USF is analyzed in terms of the eigenvalues of the matrix that couples their equations. The results obtained for IMM are compared against the results derived from the BGK equation in the region of the parameter space where all the moments are well defined. Both theoretical predictions are tested with available DSMC simulations [249].

The second part of the chapter extends the previous study to rough spheres. Two coefficients of restitution capture the main trends of dissipative collisions: (i) a coefficient of normal restitution $\alpha \leq 1$ and (ii) another of tangential restitution $-1 \leq \beta \leq 1$. The impact of the roughness is assessed by two complementary routes: Grad's moment method and a BGK-type kinetic model adapted to rough spheres [204]. First, we study the rheological properties. It is worth bearing in mind that the total temperature $T = (T_t + T_r)/2$ is composed of the translational T_t and rotational T_r temperatures. As in the case of smooth spheres, a discontinuous shear thickening emerges for a critical value of the shear rate a. Although the effect of roughness slightly enhances the transition in the viscosity η, the opposite occurs in the case of the rotational temperature T_r. As expected, the fourth-degree velocity moments also exhibit an S-shape which is not qualitatively influenced by the value of β.

As a complement of the previous results, we also analyze the stability of the steady shear flow solution for non-Newtonian rheology. Surprisingly, the analysis shows that there are some regions of the parameter space of the system where the steady solution is linearly unstable.

6.2 Article 6

Title: Simple shear flow in granular suspensions: inelastic Maxwell models and BGK-type kinetic model

Authors: Rubén Gómez González[1] and Vicente Garzó[2]

Affiliations:

[1] Departamento de Física, Universidad de Extremadura, E-06006 Badajoz, Spain

[2] Departamento de Física and Instituto de Computación Científica Avanzada (ICCAEx), Universidad de Extremadura, E-06006 Badajoz, Spain

Journal: Journal of Statistical Mechanics: Theory and Experiment

Volume: 2019

Pages: 013206

Year: 2019

DOI: 10.1088/1742-5468/aaf719

Copy of the work: "Preprint version (arXiv:1811.05859v3) of Rubén Gómez González and Vicente Garzó, *Simple shear flow in granular suspensions: inelastic Maxwell models and BGK-type kinetic model*, Journal of Statistical Mechanics: Theory and Experiment 2019, 013206 (2019) https://doi.org/10.1088/1742-5468/aaf719"

Simple shear flow in granular suspensions: Inelastic Maxwell models and BGK-type kinetic model

Rubén Gómez González*
Departamento de Física, Universidad de Extremadura, E-06071 Badajoz, Spain

Vicente Garzó†
Departamento de Física and Instituto de Computación Científica Avanzada (ICCAEx), Universidad de Extremadura, E-06071 Badajoz, Spain

(Dated: December 10, 2018)

The Boltzmann kinetic equation for low-density granular suspensions under simple shear flow is considered to determine the velocity moments through the fourth degree. The influence of the interstitial gas on solid particles is modeled by a viscous drag force term plus a stochastic Langevin-like term. Two independent but complementary approaches are followed to achieve exact results. First, to keep the structure of the Boltzmann collision operator, the so-called inelastic Maxwell models (IMM) are considered. In this model, since the collision rate is independent of the relative velocity of the two colliding particles, the forms of the collisional moments can be obtained without the knowledge of the velocity distribution function. As a complement of the previous effort, a BGK-type kinetic model adapted to granular gases is solved to get the velocity moments of the velocity distribution function. The analytical predictions of the rheological properties (which are *exactly* obtained in terms of the coefficient of restitution α and the reduced shear rate a^*) show in general an excellent agreement with event-driven simulations performed for inelastic hard spheres. In particular, both theoretical approaches show clearly that the temperature and non-Newtonian viscosity exhibit an S shape in a plane of stress-strain rate (discontinuous shear thickening effect). With respect to the fourth-degree velocity moments, we find that while those moments have unphysical values for IMM in a certain region of the parameter space of the system, they are well defined functions of both α and a^* in the case of the BGK kinetic model. The explicit shear-rate dependence of the fourth-degree moments beyond this critical region is also obtained and compared against available computer simulations.

I. INTRODUCTION

One of the most challenging problems in non-Newtonian gas-solid suspensions is the so-called discontinuous shear thickening, namely, when the non-Newtonian shear viscosity of the suspension drastically increases with increasing the shear rate. This problem (which mainly occurs in concentrated suspensions of particles such as mixtures of cornstarch in water [1]) has attracted the attention of physicists [1–10] in the last few years as a typical nonequilibrium discontinuous transition between a liquid-like phase and a solid-like phase. As pointed out by Brown and Jaeger [4], there are essentially three different possible mechanisms to explain this dramatic version of shear thickening. One mechanism is hydroclustering where the particles tend to move together into clusters under shear and hence, lubrication drag forces between particles are increased due to this type of rearrangement [11, 12]. A second mechanism [13, 14] is related to a transition in the microstructure from ordered layers at small shear rates to disordered layers at higher shear rates (order-disorder transition). Finally, a third mechanism is dilatancy in which the packing volume of particles dilates (expands) with increasing the shear rate [15, 16].

Although most of the studies on shear thickening have been focused on very dense systems, it would be convenient to analyze relatively low-density systems where kinetic theory tools conveniently adapted to account for the dissipative character of collisions can be employed to unveil in a clean way the microscopic mechanisms involved in the discontinuous shear thickening. In particular, some previous papers [17–19] demonstrated the existence of a nonequilibrium discontinuous transition for the granular temperature between a *quenched* state (a low-temperature state) and an *ignited* state (a high-temperature state) in a granular suspension under simple shear flow described by the Boltzmann equation.

A more recent work has been performed by Hayakawa *et al.* [20] in the context of the Enskog kinetic equation for a moderately dense gas-solid suspension under simple shear flow. In contrast to the previous attempts [17–19], the effect of the interstitial gas on solid particles is modeled via a viscous drag force plus a stochastic Langevin-like

* Electronic address: ruben@unex.es
† Electronic address: vicenteg@unex.es; URL: http://www.unex.es/eweb/fisteor/vicente/

term. The Enskog equation is solved by means two complementary routes: (i) Grad's moment method and (ii) event-driven Langevin simulations for inelastic hard spheres (IHS). Both approaches clearly show a transition from the discontinuous shear thickening (observed for very dilute gases) to the continuous shear thickening as the density of the system increases.

On the other hand, as in the case of elastic collisions [21–23], a limitation of the theoretical results obtained in Ref. [20] is that they were *approximately* obtained by means of Grad's moment method (namely, by considering the leading terms in a Sonine polynomial expansion of the velocity distribution function). The source of this limitation comes mainly from the form of the collision rate for hard spheres (which is proportional to the magnitude of the normal component of the relative velocity of the two colliding spheres) appearing inside the Boltzmann collision operator. As for elastic collisions, the lack of exact analytical results of the Boltzmann equation has stimulated the use of the so-called inelastic Maxwell models (IMM), where the collision rate is independent of the relative velocity. IMM have received a lot of attention in the last few years since they allow to assess the influence of inelasticity on the dynamic properties of the system without introducing additional approximations.

Another possible way of overcoming the mathematical difficulties of the Boltzmann collision operator is to consider a kinetic model. The kinetic models retain the relevant physical properties of the Boltzmann kinetic equation and are more tractable than the true kinetic equation. This kind of approach has been widely employed in the case of dilute gases with elastic collisions [24], where several exact solutions in far from equilibrium states have been obtained in the past and shown to be in good agreement with numerical solutions of the Boltzmann equation. Here, we will consider a Bhatnagar–Gross–Krook (BGK) model kinetic equation [25] for granular suspensions to complement the theoretical results derived from the Boltzmann equation for IMM.

The objective of this paper is to determine the dynamic properties of a granular suspension under simple or uniform shear flow (USF). This state is characterized by a constant density, a uniform granular temperature, and a linear velocity profile $U_x = ay$, where a is the constant shear rate. We are interested here in the steady state where the system admits a non-Newtonian hydrodynamic description characterized by shear-rate dependent viscosity and normal stress differences. The evaluation of the rheological properties is one of the most important goals of the present contribution. However, although these transport properties (which are related with the second-degree velocity moments) are physically important, higher degree velocity moments offer also an important piece of information about the velocity distribution function, especially in the high velocity region. By symmetry reasons, the third-degree moments vanish in the steady state in the USF problem. Thus, beyond the rheological properties, the first nontrivial moments are the fourth-degree moments. Their knowledge allows us to gauge partially the joint effect of shearing, interstitial gas, and inelasticity on the velocity distribution function.

The efforts of computing the second- and fourth-degree moments for IMM in the USF problem may be justified at least for three different reasons. First, the determination of the rheological properties can allow us to assess the degree of reliability of IMM to capture the main trends observed previously in sheared granular suspensions of IHS. As a second reason, it is interesting to explore whether or not the divergence of the fourth-degree moments for elastic [26, 27] and inelastic [28] Maxwell gases beyond a certain critical shear rate is also present in granular suspensions and, if so, to what extent. Finally, the knowledge of the fourth-degree moments is needed to evaluate the relevant transport coefficients characterizing states close to the USF state [29]. This knowledge will allow us to analyze the stability of the (steady) USF state in granular suspensions.

The plan of the paper is as follows. In section II, the Boltzmann equation for granular suspensions under USF is introduced and the corresponding balance equations for the densities of mass, momentum, and energy are deduced. Section III deals with the calculations carried out for IMM for the second- and fourth-degree moments. Since the (scaled) granular temperature θ is a multi-evaluated function of the (reduced) shear rate a^*, it is more convenient to analyze the divergence of the fourth-degree moments taking θ as input parameter instead of a^*. Therefore, in a way similar to the case of elastic Maxwell molecules [26, 27] and *dry* granular gases (namely, when the effect of gas phase on solid particles is neglected) [28], we find that, for a given value of α, those moments tend to infinity for certain critical values $\theta_c^{(1)}$ and $\theta_c^{(2)}$ of the granular temperature. More specifically, those moments have unphysical values in the region $\theta_c^{(1)} < \theta < \theta_c^{(2)}$. The results derived from the BGK kinetic model are displayed in section IV where it is shown first that the BGK predictions of the rheological properties coincide with those obtained by solving the Boltzmann equation by means of Grad's moment method [20]. In addition and in contrast with IMM, the BGK moments are well defined functions in the complete parameter space of the system. Comparison between theory and computer simulations at the level of the rheological properties is performed in section V. The excellent agreement found here among the different tools confirms again the reliability of both theoretical approaches (Boltzmann equation for IMM and BGK model for IHS) for studying non-Newtonian transport properties in sheared granular suspensions. Finally, the paper is closed in section VI with some concluding remarks.

II. BOLTZMANN KINETIC EQUATION FOR SHEARED GRANULAR SUSPENSIONS

A. Boltzmann kinetic equation for granular suspensions

Let us consider a set of solid particles of diameter σ and mass m immersed in a viscous gas. Since the grains which make up a granular material are of a macroscopic size, their collisions are inelastic. In the simplest model, the inelasticity of collisions is characterized by a (positive) constant coefficient of normal restitution $\alpha \leq 1$, where $\alpha = 1$ corresponds to elastic collisions (ordinary gases). In the low-density regime, the one-particle velocity distribution function of solid particles $f(\mathbf{r}, \mathbf{v}; t)$ obeys the Boltzmann kinetic equation

$$\frac{\partial f}{\partial t} + \mathbf{v} \cdot \nabla f + \mathcal{F} f = J[\mathbf{v}|f, f], \tag{1}$$

where $J[f, f]$ is the Boltzmann collision operator [30] and $\mathcal{F}$ is an operator representing the fluid-solid interaction force that models the effect of the viscous gas on solid particles. In order to fully account for the influence of the interstitial molecular fluid on the dynamics of grains, a instantaneous fluid force model is employed [20, 31, 32]. For low Reynolds numbers, it is assumed that the external force $\mathbf{F}$ acting on solid particles is composed by two independent terms. One term corresponds to a viscous drag force $\mathbf{F}^{\text{drag}}$ proportional to the (instantaneous) velocity of particle $\mathbf{v}$. This term takes into account the friction of grains on the viscous gas. Since the model attempts to mimic gas-solid flows, the drag force is defined in terms of the relative velocity $\mathbf{v} - \mathbf{U}_g$ where $\mathbf{U}_g$ is the (known) mean flow velocity of the surrounding molecular gas. Thus, the drag force is defined as

$$\mathbf{F}^{\text{drag}} = -m\gamma \left(\mathbf{v} - \mathbf{U}_g\right), \tag{2}$$

where γ is the drag or friction coefficient. The second term in the total force corresponds to a stochastic force that tries to simulate the kinetic energy gain due to eventual collisions with the (more rapid) molecules of the background fluid. It does this by adding a random velocity to each particle between successive collisions [33]. This stochastic force $\mathbf{F}^{\text{st}}$ has the form of a Gaussian white noise with the properties [34]

$$\langle \mathbf{F}_i^{\text{st}}(t) \rangle = \mathbf{0}, \quad \langle \mathbf{F}_i^{\text{st}}(t) \mathbf{F}_j^{\text{st}}(t') \rangle = 2m^2 \gamma T_{\text{ex}} \mathsf{I} \delta_{ij} \delta(t - t'), \tag{3}$$

where I is the unit tensor and i and j refer to two different particles. Here, T_{ex} can be interpreted as the temperature of the background (or bath) fluid. In the context of the Boltzmann equation, the stochastic external force is represented by a Fokker–Planck operator of the form $\mathcal{F}^{\text{st}} f \to -(\gamma T_{\text{ex}}/m)\partial^2 f/\partial v^2$ [34, 35]. Note that the strength of correlation in Eq. (3) has been chosen to be consistent with the fluctuation-dissipation theorem for elastic collisions [34]. In addition, although the drift coefficient γ is in general a tensor, in the case of very dilute suspensions it may be assumed to be an scalar proportional to the square root of T_{ex} because the drag coefficient is proportional to the viscosity of the solvent [36].

Therefore, according to Eqs. (2) and (3), the forcing term $\mathcal{F} f$ can be written as

$$\mathcal{F} f = -\gamma \Delta \mathbf{U} \frac{\partial f}{\partial \mathbf{v}} - \gamma \frac{\partial}{\partial \mathbf{v}} \cdot \mathbf{V} f - \gamma \frac{T_{\text{ex}}}{m} \frac{\partial^2 f}{\partial v^2}, \tag{4}$$

and the Boltzmann equation (1) reads

$$\frac{\partial f}{\partial t} + \mathbf{v} \cdot \nabla f - \gamma \Delta \mathbf{U} \frac{\partial f}{\partial \mathbf{v}} - \gamma \frac{\partial}{\partial \mathbf{v}} \cdot \mathbf{V} f - \gamma \frac{T_{\text{ex}}}{m} \frac{\partial^2 f}{\partial v^2} = J[\mathbf{V}|f, f]. \tag{5}$$

Here, $\Delta \mathbf{U} = \mathbf{U} - \mathbf{U}_g$, $\mathbf{V} = \mathbf{v} - \mathbf{U}$ is the peculiar velocity,

$$\mathbf{U}(\mathbf{r}, t) = \frac{1}{n(\mathbf{r}, t)} \int \mathrm{d}\mathbf{v} \; \mathbf{v} f(\mathbf{r}, \mathbf{v}, t) \tag{6}$$

is the mean particle velocity, and

$$n(\mathbf{r}, t) = \int \mathrm{d}\mathbf{v} \; f(\mathbf{r}, \mathbf{v}, t) \tag{7}$$

is the number density. Another relevant hydrodynamic field is the *granular* temperature $T(\mathbf{r}, t)$ defined as

$$T(\mathbf{r}, t) = \frac{m}{dn(\mathbf{r}, t)} \int \mathrm{d}\mathbf{v} \; V^2 f(\mathbf{r}, \mathbf{v}, t). \tag{8}$$

The suspension model (5) is a simplified version of the model proposed in Ref. [31] for monodisperse gas-solid flows at moderate density. In this latter model, the friction coefficient of the drag force and the strength of the correlation are considered to be different. Here, both coefficients are assumed to be the same for the sake of simplicity. Another relevant point of the model (3) is that the form of the Boltzmann collision operator $J[f,f]$ is assumed to be the same as for a dry granular gas (i.e., when the influence of the interstitial gas is neglected) and hence, the collision dynamics does not contain any parameter of the environmental gas. This means that while the inertia of particles is assumed to be relevant, the inertia of the gas phase is considered to be negligible. As has been previously discussed in several papers [17, 18, 36–38], the above assumption requires that the mean-free time between collisions is assumed to be much less than the time needed by the fluid forces to significantly affect the dynamics of solid particles. Thus, the suspension model (3) is expected to be reliable in situations where the gas phase has a weak impact on the motion of grains. This assumption fails for instance in the case of liquid flows (high density) where the stresses exerted by the background fluid on grains are expected to be important and hence, the presence of fluid should be accounted for in the collision process.

The Boltzmann collision operator conserves the mass and momentum but the energy is not conserved:

$$\int \mathrm{d}\mathbf{v} J[\mathbf{v}|f,f]=0, \quad \int \mathrm{d}\mathbf{v}\, m\mathbf{v} J[\mathbf{v}|f,f]=\mathbf{0}, \tag{9}$$

$$\int \mathrm{d}\mathbf{v}\, \frac{m}{2} V^2 J[\mathbf{v}|f,f]=-\frac{d}{2} nT\zeta, \tag{10}$$

where ζ is the cooling rate due to inelastic collisions between the particles. From Eqs. (5), (9), and (10), the macroscopic balance equations for the granular suspension can be obtained. They are given by

$$D_t n + n\nabla\cdot\mathbf{U}=0, \tag{11}$$

$$\rho D_t \mathbf{U} + \nabla\cdot\mathsf{P}=-\rho\gamma\Delta\mathbf{U}, \tag{12}$$

$$D_t T + \frac{2}{dn}\left(\nabla\cdot\mathbf{q}+\mathsf{P}:\nabla\mathbf{U}\right)=2\gamma\left(T_{\mathrm{ex}}-T\right)-\zeta T. \tag{13}$$

Here, $D_t\equiv\partial_t+\mathbf{U}\cdot\nabla$, $\rho=mn$ is the mass density,

$$\mathsf{P}=\int \mathrm{d}\mathbf{v}\, m\, \mathbf{V}\mathbf{V} f(\mathbf{v}) \tag{14}$$

is the pressure tensor, and

$$\mathbf{q}=\int \mathrm{d}\mathbf{v}\, \frac{m}{2}\, V^2\mathbf{V} f(\mathbf{v}) \tag{15}$$

is the heat flux.

To completely define the suspension model (5), it still remains to explicitly write the form of the Boltzmann collision operator $J[f,f]$. The prototypical model of granular gases consists of a gas of IHS and hence, the collision rate appearing in the Boltzmann operator is proportional to the relative velocity of colliding spheres. Although this is an interaction model widely used in granular literature, it is generally not possible to get *exact* analytical results from the Boltzmann equation for IHS, especially in far from equilibrium states such as the USF. As a consequence, most of the analytical results reported in the literature in the context of the Boltzmann equation for IHS have been obtained by introducing additional, and sometimes uncontrolled, approximations. In particular, the rheological properties of granular suspensions under USF have been recently determined [20] by means of Grad's moment method. Therefore, from a theoretically oriented point of view, if one desires to overcome the mathematical intricacies associated with the Boltzmann operator for IHS and derive exact results, one has at least two fruitful routes. One of them is to retain the mathematical structure of the Boltzmann equation but consider IMM. For this interaction model the collision rate is independent of the relative velocity of the colliding pair. This allows for a number of nice mathematical properties of the Boltzmann collision operator. The second possibility is to consider a kinetic model of the Boltzmann equation, namely, one replaces the operator $J[f,f]$ by a simpler collision model that otherwise retains the most relevant physical properties of the true Boltzmann collision operator. IMM will be considered in Sec. III while the kinetic model will be employed in Sec. IV.

B. Steady uniform shear flow

Let us assume that the granular suspension is under USF. As said in the Introduction, this state is macroscopically defined by a constant density n, a spatially uniform temperature $T(t)$, and a flow velocity $U_i = a_{ij} r_j$, where $a_{ij} = a\delta_{ix}\delta_{jy}$, a being the constant shear rate. In addition, as usual in uniform sheared suspensions [17–19, 39], the average velocity of particles follows the velocity of the fluid phase and so, $\mathbf{U} = \mathbf{U}_g$. One of the main advantages of the USF at a microscopic level is that in this state all the space dependence of the one-particle velocity distribution function $f(\mathbf{r}, \mathbf{v}, t)$ occurs through its dependence on the peculiar velocity $\mathbf{V} = \mathbf{v} - \mathbf{U}(\mathbf{r})$ [40]. Thus, at a more fundamental level, the USF is defined as that which is spatially homogeneous when the velocities of particles are referred to a Lagrangian frame moving with the linear velocity field U_i. In this frame, the distribution function adopts the form

$$f(\mathbf{r}, \mathbf{v}; t) = f(\mathbf{V}; t), \tag{16}$$

and hence, in the steady state, the Boltzmann equation (5) reduces to

$$-aV_y \frac{\partial f}{\partial V_x} - \gamma \frac{\partial}{\partial \mathbf{V}} \cdot \mathbf{V} f - \gamma \frac{T_{\text{ex}}}{m} \frac{\partial^2 f}{\partial V^2} = J[\mathbf{V}|f, f]. \tag{17}$$

Equation (17) is invariant under the transformations $(V_x, V_y) \to (-V_x, -V_y)$ and $V_j \to -V_j$ for $j \neq x, y$.

In the USF problem, the heat flux vanishes ($\mathbf{q} = \mathbf{0}$) and the (uniform) pressure tensor P is the relevant flux. Moreover, the conservation equations (11) and (12) hold trivially and in the steady state the balance equation (13) for the granular temperature becomes

$$-\frac{2}{dn} a P_{xy} - \zeta T + 2\gamma (T_{\text{ex}} - T) = 0. \tag{18}$$

Equation (18) implies that in the steady state the viscous heating term ($-aP_{xy} > 0$) plus the energy gained by grains due to collisions with the interstitial fluid (γT_{ex}) is exactly compensated by the cooling terms arising from collisional dissipation (ζT) and viscous friction (γT). Thus, for a given value of the environmental temperature T_{ex}, the (steady) scaled temperature $\theta \equiv T/T_{\text{ex}}$ is a function of the coefficient of restitution α and the (scaled) shear rate $a^* \equiv a/\gamma$. Of course, in the absence of shear flow ($a = 0$), the solution to Eq. (18) is $T = T_{\text{ex}}$ for elastic collisions ($\alpha = 1$ and so, $\zeta = 0$) as expected. Note that in contrast to *dry* granular gases ($\gamma = 0$), a steady state is still possible for *sheared* suspensions when the collisions between the solid particles are elastic.

The USF state is in general non-Newtonian. This can characterized by generalized transport coefficients measuring their departure from their corresponding Navier–Stokes forms. Thus, a non-Newtonian shear viscosity coefficient $\eta(\alpha, a)$ is defined as

$$\eta = -\frac{P_{xy}}{a}. \tag{19}$$

Moreover, while in the Navier–Stokes domain $P_{xx} = P_{yy} = P_{zz}$, normal stress differences are expected in the USF state ($P_{xx} \neq P_{yy} \neq P_{zz}$). All the above properties may be easily identified from the knowledge of the (reduced) shear stress P_{xy}^* and the (reduced) diagonal elements P_{xx}^*, P_{yy}^*, and P_{zz}^*, where

$$P_{ij}^* \equiv \frac{P_{ij}}{nT_{\text{ex}}}. \tag{20}$$

It is quite apparent that the determination of the rheological properties requires to solve the Boltzmann equation (17). As said before, Grad's moment method [41] has been used to solve Eq. (17) for IHS [20]. Grad's moment method is based on the expansion of the velocity distribution function in a complete set of orthogonal polynomials (generalized Hermite polynomials), the coefficients being the corresponding velocity moments. However, given that the (infinite) hierarchy of moment equations is not a closed set of equations, one has to truncate the above expansion after a certain order. After this truncation, the above hierarchy of moment equations becomes a closed set of coupled equations which can be recursively solved. Thus, given that the results derived in Ref. [20] are approximated, it is interesting to revisit the problem and get exact expressions of the rheological properties by considering both the Boltzmann equation for IMM and a BGK-type kinetic model for IHS. This will be carried out in the next two sections.

III. INELASTIC MAXWELL MODELS

We consider in this section the Boltzmann equation (17) for IMM. In this case, the Boltzmann collision operator $J_{\text{IMM}}[f, f]$ is given by [42]

$$J_{\text{IMM}}[\mathbf{v}_1|f, f] = \frac{\nu_{\text{M}}}{n\Omega_d} \int \mathrm{d}\mathbf{v}_2 \int \mathrm{d}\widehat{\boldsymbol{\sigma}} \left[\alpha^{-1} f(\mathbf{v}_1'') f(\mathbf{v}_2'') - f(\mathbf{v}_1) f(\mathbf{v}_2)\right], \tag{21}$$

where $\Omega_d = 2\pi^{d/2}/\Gamma(d/2)$ is the total solid angle in d dimensions and $\nu_{\rm M}$ is a collision frequency. In addition, the double primes on the velocities denote initial values $\{\mathbf{v}_1'', \mathbf{v}_2''\}$ that lead to $\{\mathbf{v}_1, \mathbf{v}_2\}$ following a binary collision:

$$\mathbf{v}_1'' = \mathbf{v}_1 - \frac{1}{2}\left(1+\alpha^{-1}\right)(\widehat{\boldsymbol{\sigma}}\cdot\mathbf{g})\widehat{\boldsymbol{\sigma}}, \quad \mathbf{v}_2'' = \mathbf{v}_2 + \frac{1}{2}\left(1+\alpha^{-1}\right)(\widehat{\boldsymbol{\sigma}}\cdot\mathbf{g})\widehat{\boldsymbol{\sigma}}, \tag{22}$$

where $\mathbf{g} = \mathbf{v}_1 - \mathbf{v}_2$ is the relative velocity of the colliding pair and $\widehat{\boldsymbol{\sigma}}$ is a unit vector directed along the centers of the two colliding particles. The collision frequency $\nu_{\rm M}(\mathbf{r}, t)$ is independent of velocity but depends on space and time through its dependence on density and temperature. It can be seen as a free parameter of the model that can be chosen to optimize agreement with the properties of interest of the original Boltzmann equation for IHS. For instance, in order to correctly describe the velocity dependence of the original IHS collision rate, we can assume that the IMM collision rate is proportional to $T^{1/2}$.

As noted in previous works on IMM [28, 43], the main advantage of the Boltzmann equation for Maxwell models (both elastic and inelastic) is that the moments of the operator $J[f, f]$ can be *exactly* expressed in terms of the velocity moments of the velocity distribution f, without the knowledge of the latter. This property has been exploited to determine for arbitrary dimensions the explicit forms for all the second, third, and fourth-degree collisional moments as functions of the coefficient of restitution α [43]. In the steady USF problem, the relevant velocity moments are the second- and fourth-degree moments since the third-degree moments vanish by symmetry. In particular, the second-degree collisonal moment (which is needed to get the rheological properties) is given by [43]

$$\int \mathrm{d}\mathbf{V} m V_i V_j J_{\rm IMM}[\mathbf{V}|f, f] = -\nu_{0|2}\Pi_{ij} - p\zeta\delta_{ij}, \tag{23}$$

where $\Pi_{ij} = P_{ij} - p\delta_{ij}$ is the traceless part of the pressure tensor, $p = (P_{xx} + P_{yy} + \cdots)/d = nT$ is the hydrostatic pressure, and

$$\zeta = \frac{1-\alpha^2}{2d}\nu_{\rm M}, \tag{24}$$

$$\nu_{0|2} = \zeta + \frac{(1+\alpha)^2}{2(d+2)}\nu_{\rm M} = \frac{(d+1-\alpha)(1+\alpha)}{d(d+2)}\nu_{\rm M}. \tag{25}$$

The expressions of the fourth-degree collisional moments are displayed in the Appendix A for the sake of completeness. Equation (24) provides the exact form of the cooling rate for IMM. This form can be used to fix the value of the free parameter $\nu_{\rm M}$. This is chosen under the criterion that ζ of IMM is the same as that of IHS of diameter σ. Given that the cooling rate cannot be exactly evaluated for IHS, we take here for $\zeta_{\rm IHS}$ its expression when f is replaced by the Maxwellian distribution. In this approximation, $\zeta_{\rm IHS}$ is given by [35]

$$\zeta_{\rm IHS} \to \frac{d+2}{4d}(1-\alpha^2)\nu_0, \tag{26}$$

where

$$\nu_0 = \frac{8}{d+2}\frac{\pi^{(d-1)/2}}{\Gamma\left(\frac{d}{2}\right)} n\sigma^{d-1}\sqrt{\frac{T}{m}} \tag{27}$$

is the collision frequency of the shear viscosity coefficient of a dilute ordinary gas. Comparing Eqs. (24) and (26), one gets the relationship

$$\nu_{\rm M} = \frac{d+2}{2}\nu_0. \tag{28}$$

A. Rheological properties

The hierarchy of equations defining the elements of the pressure tensor $P_{k\ell}$ can be easily obtained by multiplying both sides of Eq. (17) (replacing J by $J_{\rm IMM}$) by mV_kV_ℓ and integrating over $\mathbf{V}$. The result is

$$a\left(\delta_{kx}P_{\ell j} + \delta_{\ell x}P_{ky}\right) + 2\gamma\left(P_{k\ell} - nT_{\rm ex}\delta_{k\ell}\right) = -\nu_{0|2}P_{k\ell} - p\left(\zeta - \nu_{0|2}\right)\delta_{k\ell}, \tag{29}$$

where use has been made of Eq. (23). From Eq. (29) is easy to prove that the diagonal elements of the pressure tensor orthogonal to the shear plane xy are equal to P_{yy} (i.e., $P_{yy}=P_{zz}=\ldots=P_{dd}$). As a consequence, $P_{xx}=dp-(d-1)P_{yy}$ and the elements P_{yy} and P_{xy} obey the equations

$$\left(\nu_{0|2}+2\gamma\right)P_{yy}=nT_{\text{ex}}\left[2\gamma-\left(\zeta-\nu_{0|2}\right)\theta\right], \tag{30}$$

$$\left(\nu_{0|2}+2\gamma\right)P_{xy}=-aP_{yy}, \tag{31}$$

where we recall that $\theta\equiv T/T_{\text{ex}}$. The solution to Eqs. (30) and (31) is

$$P_{yy}=\frac{2\gamma-\left(\zeta-\nu_{0|2}\right)\theta}{\nu_{0|2}+2\gamma}nT_{\text{ex}}, \tag{32}$$

$$P_{xy}=-\frac{a}{\nu_{0|2}+2\gamma}P_{yy}=-\frac{2\gamma-\left(\zeta-\nu_{0|2}\right)\theta}{\left(\nu_{0|2}+2\gamma\right)^2}anT_{\text{ex}}. \tag{33}$$

The element P_{xx} can be easily obtained from Eq. (32) as

$$P_{xx}=\frac{d\left(\nu_{0|2}+2\gamma\right)\theta-(d-1)\left[2\gamma-\left(\zeta-\nu_{0|2}\right)\theta\right]}{\nu_{0|2}+2\gamma}nT_{\text{ex}}. \tag{34}$$

The (reduced) temperature θ can be finally determined by substituting Eq. (33) into the steady-state condition (18). In order to compare our theoretical results with those obtained in Ref. [20] by computer simulations, it is convenient to scale the shear rate with the friction coefficient γ (i.e., $a^*\equiv a/\gamma$) and introduce the (reduced) background gas temperature $T_{\text{ex}}^*\equiv T_{\text{ex}}/m\sigma^2\gamma^2$. In terms of these quantities, the solution to Eq. (18) can be written as

$$a^*=\sqrt{\frac{d}{2}\frac{\sqrt{\theta}\zeta^*+2(1-\theta^{-1})}{\sqrt{\theta}(\nu_{0|2}^*-\zeta^*)+2\theta^{-1}}(2+\sqrt{\theta}\nu_{0|2}^*)}, \tag{35}$$

where we have introduced the dimensionless quantities

$$\zeta^*\equiv\frac{\zeta}{\sqrt{\theta}\gamma}=\frac{2\pi^{(d-1)/2}}{d\Gamma\left(\frac{d}{2}\right)}(1-\alpha^2)n^*\sqrt{T_{\text{ex}}^*}, \tag{36}$$

$$\nu_{0|2}^*\equiv\frac{\nu_{0|2}}{\sqrt{\theta}\gamma}=\frac{4\pi^{(d-1)/2}}{d(d+2)\Gamma\left(\frac{d}{2}\right)}(d+1-\alpha)(1+\alpha)n^*\sqrt{T_{\text{ex}}^*}. \tag{37}$$

Since $\gamma\propto\sqrt{T_{\text{ex}}}$, then ζ^* and $\nu_{0|2}^*$ are independent of both the granular temperature T and the background temperature T_{ex}. In Eqs. (36) and (37), $n^*=n\sigma^d$ is the reduced density. Note that this explicit dependence on density comes from the scaling of the shear rate a and the bath temperature T_{ex}. If we had reduced the shear rate for instance with the collision frequency $\nu_0(T)$, then the above density dependence had been removed. On the other hand, since we want to make a close comparison with the simulation data reported in Ref. [20], our theory must employ the same input parameters as in the simulation results.

As happens for IHS [20], it is quite apparent that we cannot express the (reduced) temperature θ in Eq. (35) as an explicit function of both the coefficient of restitution α and the (reduced) shear rate a^*. However, the dependence of θ on the latter parameters can implicitly be obtained from the physical solution to Eq. (35) as $a^{*2}(\theta,\alpha)$. Once θ is known, the remaining rheological functions can be determined from Eqs. (32) and (33) in terms of α and a^*. In particular, the (dimensionless) non-Newtonian shear viscosity

$$\eta^*\equiv-\frac{P_{xy}^*}{a^*} \tag{38}$$

can be easily identified from Eq. (33) with the result

$$\eta^*=\frac{2+\left(\nu_{0|2}^*-\zeta^*\right)\sqrt{\theta}\theta}{\left(\sqrt{\theta}\nu_{0|2}^*+2\right)^2}. \tag{39}$$

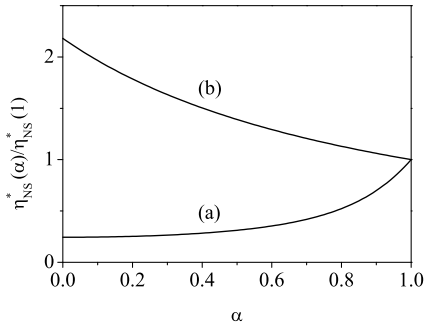

FIG. 1: Plot of the ratios $\eta^*_{\rm NS}(\alpha)/\eta^*_{\rm NS}(1)$ (a) and $\eta^*_{\rm NS,dry}(\alpha)/\eta^*_{\rm NS,dry}(1)$ (b) as functions of the coefficient of restitution α for a three-dimensional system.

Since $P_{yy} = P_{zz}$, the only nonzero (reduced) viscometric function is given by

$$\Psi^* = \frac{P_{xx} - P_{yy}}{nT_{\rm ex}} = d\theta \frac{2\left(1-\theta^{-1}\right) + \sqrt{\theta}\zeta^*}{2 + \sqrt{\theta}\nu^*_{0|2}}, \tag{40}$$

where use has been made of Eqs. (32) and (34). It must be remarked that although the theoretical prediction $P_{yy} = P_{zz}$ disagrees with computer simulations [20], the magnitude of the difference $P_{yy} - P_{zz}$ is in general very small; therefore the expressions (32)–(34) can be still considered as reliable. A careful comparison with the theoretical results obtained for dense granular suspensions of IHS [20] by means of Grad's moment method shows that these expressions differ from those derived here for IMM in the dilute limit. On the other hand, this discrepancy is only due to the different α dependence of the eigenvalue $\nu_{0|2}$ with respect to the one found for IHS.

For illustrative purposes, it is interesting to consider the limits of small and large shear rates. For small shear rates ($a^* \to 0$), $\eta^* \to \eta^*_{\rm NS}$, where the Navier–Stokes shear viscosity of the granular suspension is

$$\eta^*_{\rm NS} = \frac{\theta_{\rm NS}}{2 + \sqrt{\theta_{\rm NS}}\nu^*_{0|2}}. \tag{41}$$

Here, $\theta_{\rm NS}$ is a real solution of the equation

$$\theta_{\rm NS} = \frac{1}{1 + \frac{1}{2}\sqrt{\theta_{\rm NS}}\zeta^*}. \tag{42}$$

For large shear rates ($a^* \to \infty$), the asymptotic forms for $\alpha < 1$ are

$$\theta_\infty \to \frac{2}{d}\frac{\nu^*_{0|2} - \zeta^*}{\nu^{*2}_{0|2}\zeta^*} a^{*2}, \quad \eta^*_\infty \to \sqrt{\frac{d}{2}}\frac{\left(\nu^*_{0|2} - \zeta^*\right)^{3/2}}{\nu^{*3}_{0|2}\sqrt{\zeta^*}} a^*, \tag{43}$$

while for elastic collisions ($\alpha = 1$), one gets

$$\theta_\infty \to \frac{a^{*4}}{d^2\nu^{*2}_{0|2}}, \quad \eta^*_\infty \to \frac{a^{*2}}{d\nu^{*2}_{0|2}}. \tag{44}$$

It is interesting at this point to compare the behaviors of the non-Newtonian shear viscosity obtained here for granular suspensions in the limit of small and high shear rates with those derived before for *dilute* ordinary [24] and dry inelastic [28] Maxwell gases. In both cases, while $\eta^* \equiv$ finite when $a^* \to 0$, $\eta^* \propto a^{*-4/3}$ when $a^* \to \infty$. This means that η^* is a monotonically decreasing function of the shear rate and so, the shearing produces an inhibition of the momentum transport (shear thinning effect) in the sense that the actual value of the shear stress $|P_{xy}|$ is smaller than the one predicted by Newton's law. On the other hand, a completely different behavior is found here for granular suspensions, since while $\eta^* \equiv$ finite when $a^* \to 0$, this coefficient diverges in the limit $a^* \to \infty$ [see Eqs.

(43) and (44)]. Thus, the fact that the ratio $\eta^*(a^*\to\infty)/\eta^*(a^*\to 0)$ becomes very large could explain the existence of discontinuous shear thickening in a structurally simple system due to the connection between the Newtonian and Bagnoldian branches. This behavior changes as the density of the system increases since kinetic theory results predict *continuous* shear thickening for both ordinary gases [44] and granular suspensions [20].

Before considering the shear-rate dependence of the rheological functions, it is worthwhile to compare the α-dependence of the Navier–Stokes shear viscosity (41) with the one obtained in the *dry* granular case. In dimensionless form, the expression of the Navier–Stokes shear viscosity of a granular gas can be written as $\eta_{\text{NS,dry}}=(p/\nu_{\text{M}})\eta^*_{\text{NS,dry}}$, where [45]

$$\eta^*_{\text{NS,dry}}=\frac{4d(d+2)}{(1+\alpha)\left[3d+2-(d-2)\alpha\right]}. \tag{45}$$

Figure 1 shows the ratios $\eta^*_{\text{NS}}(\alpha)/\eta^*_{\text{NS}}(1)$ and $\eta^*_{\text{NS,dry}}(\alpha)/\eta^*_{\text{NS,dry}}(1)$ as functions of the coefficient of restitution α for $d=3$. Here, $\eta^*_{\text{NS}}(1)$ and $\eta^*_{\text{NS,dry}}(1)$ refer to the values of the shear viscosity coefficients for elastic collisions for the suspension and dry granular cases, respectively. It is quite apparent that the α dependence of both viscosities is qualitatively different since while the shear viscosity of a granular suspension decreases (with respect to its value for elastic collisions) with increasing inelasticity, the opposite happens for granular gases. Moreover, the impact of inelasticity on both shear viscosity coefficients is quite significant.

B. Fourth-degree moments

As mentioned in section I, although the rheological properties are the most important transport properties of the granular suspension, the determination of higher degree velocity moments is also an appealing problem. Since the third-degree moments vanish in the steady USF by symmetry reasons, the fourth-degree moments are the first nonzero moments beyond the second-degree moments. Here, we will focus on a three-dimensional system ($d=3$). As for ordinary gases [24, 27], for $d=3$, there are 15 independent fourth-degree moments; 6 are *asymmetric* (in the sense that they vanish in the steady state) and 9 are *symmetric* (they are different from zero in the steady state). The symmetric and asymmetric moments are uncoupled. Since we are not interested in this paper in analyzing the time evolution of the fourth-degree moments, we will address here only the study of the (steady) symmetric moments.

In parallel to the elastic case [24, 27], we choose the following set of 9 symmetric moments:

$$\left\{M_{4|0},M_{2|xx},M_{2|yy},M_{2|xy},M_{0|xxxx},M_{0|yyyy},M_{0|zzzz},M_{0|xxxy},M_{0|xyyy}\right\}. \tag{46}$$

Here, we have introduced the velocity moments

$$\left(M_{4|0},M_{2|ij},M_{0|ijk\ell}\right)=\int \mathrm{d}\mathbf{V}\,\left(Y_{4|0},Y_{2|ij},Y_{0|ijk\ell}\right)f(\mathbf{V}), \tag{47}$$

where the fourth-degree Ikenberry polynomials are defined as [46]

$$Y_{4|0}(\mathbf{V})=V^4,\quad Y_{2|ij}(\mathbf{V})=V^2\left(V_iV_j-\frac{1}{3}V^2\delta_{ij}\right), \tag{48}$$

$$\begin{aligned}Y_{0|ijk\ell}(\mathbf{V}) &= V_iV_jV_kV_\ell-\frac{V^2}{7}\Big(V_iV_j\delta_{k\ell}+V_iV_k\delta_{j\ell}+V_iV_\ell\delta_{jk}+V_jV_jk\delta_{i\ell}+V_jV_\ell\delta_{ik}\\ &\quad +V_kV_\ell\delta_{ij}\Big)+\frac{V^4}{35}\Big(\delta_{ij}\delta_{k\ell}+\delta_{ik}\delta_{j\ell}+\delta_{i\ell}\delta_{jk}\Big).\end{aligned} \tag{49}$$

As for ordinary gases [24, 27], it is easy to prove that the combination

$$3M_{0|xxxx}-4\left(M_{0|yyyy}+M_{0|zzzz}\right)=0 \tag{50}$$

in the steady USF state. This means that we really have 8 independent fourth-degree symmetric moments since for instance $M_{0|xxxx}=\frac{4}{3}\left(M_{0|yyyy}+M_{0|zzzz}\right)$. As expected, the eight independent moments are coupled. The corresponding equations obeying those eight moments can be determined by multiplying both sides of Eq. (17) by the set of velocity polynomials

$$\left\{Y_{4|0},Y_{2|xx},Y_{2|yy},Y_{2|xy},Y_{0|yyyy},Y_{0|zzzz},Y_{0|xxxy},Y_{0|xyyy}\right\} \tag{51}$$

and integrating over velocity. In addition, to explicitly obtain the hierarchy of moment equations, one needs the collisional moments (A3)–(A7) associated with the above fourth-degree polynomials. In dimensionless form, the set of coupled equations for the fourth-degree moments can be written in matrix form as

$$\mathcal{L}_{\mu\nu}\mathcal{M}_\nu = \mathcal{N}_\mu, \quad \mu = 1, 2, \ldots, 8. \tag{52}$$

Here, $\boldsymbol{\mathcal{M}}$ is the column matrix defined by the set

$$\left\{M^*_{4|0}, M^*_{2|xx}, M^*_{2|yy}, M^*_{0|yyyy}, M^*_{0|zzzz}, M^*_{2|xy}, M^*_{0|xxxy}, M^*_{0|xyyy}\right\}, \tag{53}$$

and $\boldsymbol{\mathcal{L}}$ is the square matrix

$$\boldsymbol{\mathcal{L}} = 4\boldsymbol{I} + \boldsymbol{\mathcal{L}}', \tag{54}$$

where $\boldsymbol{I}$ is the 8×8 unit matrix and

$$\boldsymbol{\mathcal{L}}' = \begin{pmatrix}
\sqrt{\theta}\nu^*_{4|0} & 0 & 0 & 0 & 0 & 4a^* & 0 & 0 \\
0 & \sqrt{\theta}\nu^*_{2|2} & 0 & 0 & 0 & \frac{32}{21}a^* & 2a^* & 0 \\
0 & 0 & \sqrt{\theta}\nu^*_{2|2} & 0 & 0 & -\frac{10}{21}a^* & 0 & 2a^* \\
0 & 0 & 0 & \sqrt{\theta}\nu^*_{0|4} & 0 & -\frac{96}{245}a^* & 0 & -\frac{12}{7}a^* \\
0 & 0 & 0 & 0 & \sqrt{\theta}\nu^*_{0|4} & \frac{24}{245}a^* & \frac{12}{7}a^* & \frac{12}{7}a^* \\
\frac{7}{15}a^* & \frac{2}{7}a^* & \frac{9}{7}a^* & -\frac{7}{3}a^* & -\frac{1}{3}a^* & \sqrt{\theta}\nu^*_{2|2} & 0 & 0 \\
0 & \frac{15}{49}a^* & -\frac{6}{49}a^* & -\frac{5}{2}a^* & -\frac{5}{14}a^* & 0 & \sqrt{\theta}\nu^*_{0|4} & 0 \\
0 & -\frac{6}{49}a^* & \frac{15}{49}a^* & 2a^* & \frac{1}{7}a^* & 0 & 0 & \sqrt{\theta}\nu^*_{0|4}
\end{pmatrix}. \tag{55}$$

The scaled moments $M^*_{4|0}$, $M^*_{2|ij}$, and $M^*_{0|ijk\ell}$ are defined as

$$\left\{M^*_{4|0}, M^*_{2|ij}, M^*_{0|ijk\ell}\right\} = n^{-1}\left(\frac{m}{T_{\text{ex}}}\right)^2 \left\{M_{4|0}, M_{2|ij}, M_{0|ijk\ell}\right\}, \tag{56}$$

and in Eq. (55), $\nu^*_{4|0} \equiv \nu_{4|0}/(\sqrt{\theta}\gamma)$, $\nu^*_{2|2} \equiv \nu_{2|2}/(\sqrt{\theta}\gamma)$, and $\nu^*_{0|4} \equiv \nu_{0|4}/(\sqrt{\theta}\gamma)$. The expressions of $\nu_{4|0}$, $\nu_{2|2}$, and $\nu_{0|4}$ are given by Eqs. (A8) and (A9), respectively. In addition, the elements of the column matrix $\boldsymbol{\mathcal{N}}$ are made of second-degree moments:

$$\mathcal{N}_1 = 9\theta^2\sqrt{\theta}\lambda^*_1 - 2\sqrt{\theta}\lambda^*_2\left(3\Pi^{*2}_{yy} + \Pi^{*2}_{xy}\right) + 60\theta, \tag{57}$$

$$\mathcal{N}_2 = -6\theta\sqrt{\theta}\lambda^*_3\Pi^*_{yy} - \frac{\sqrt{\theta}}{3}\lambda^*_4\left(2\Pi^{*2}_{yy} - \Pi^{*2}_{xy}\right) - 28\Pi^*_{yy}, \tag{58}$$

$$\mathcal{N}_3 = 3\theta\sqrt{\theta}\lambda^*_3\Pi^*_{yy} + \frac{\sqrt{\theta}}{3}\lambda^*_4\left(3\Pi^{*2}_{yy} + \Pi^{*2}_{xy}\right) + 14\Pi^*_{yy}, \tag{59}$$

$$\mathcal{N}_4 = \frac{3}{35}\sqrt{\theta}\lambda^*_5\left(27\Pi^{*2}_{yy} - 16\Pi^{*2}_{xy}\right), \tag{60}$$

$$\mathcal{N}_5 = \frac{3}{35}\sqrt{\theta}\lambda^*_5\left(27\Pi^{*2}_{yy} + 4\Pi^{*2}_{xy}\right), \tag{61}$$

$$\mathcal{N}_6 = 3\theta\sqrt{\theta}\lambda^*_3\Pi^*_{xy} + \sqrt{\theta}\lambda^*_4\Pi^*_{yy}\Pi^*_{xy} + 14\Pi^*_{xy}, \tag{62}$$

$$\mathcal{N}_7 = -\frac{36}{7}\sqrt{\theta}\lambda^*_5\Pi^*_{yy}\Pi^*_{xy}, \tag{63}$$

$$\mathcal{N}_8 = \frac{27}{7}\sqrt{\theta}\lambda^*_5\Pi^*_{yy}\Pi^*_{xy}, \tag{64}$$

where $\lambda^*_i \equiv \lambda_i/(\sqrt{\theta}\gamma)$ and $\Pi^*_{ij} \equiv \Pi_{ij}/nT_{\text{ex}}$. The quantities $\lambda_i (i = 1, \cdots, 5)$ are defined by Eqs. (A10) and (A11).

The solution to Eq. (52) is

$$\boldsymbol{\mathcal{M}} = \boldsymbol{\mathcal{L}}^{-1} \cdot \boldsymbol{\mathcal{N}}. \tag{65}$$

Equation (65) provides the dependence of the (symmetric) fourth-degree moments on both the (reduced) shear rate a^* and the coefficient of restitution α. This dependence will be analyzed in section V.

IV. BGK-TYPE KINETIC MODEL OF THE BOLTZMANN EQUATION

We consider now the results derived for the USF from a BGK-type kinetic model of the Boltzmann equation [25]. In the USF problem, the steady kinetic model for the granular suspension described by the Boltzmann equation (17) reads

$$-aV_y\frac{\partial f}{\partial V_x}-\gamma\frac{\partial}{\partial \mathbf{V}}\cdot\mathbf{V}f-\frac{\gamma T_{\text{ex}}}{m}\frac{\partial^2 f}{\partial V^2}=-\chi(\alpha)\nu_0\left(f-f_{\text{L}}\right)+\frac{\zeta}{2}\frac{\partial}{\partial \mathbf{V}}\cdot\mathbf{V}f, \tag{66}$$

where ν_0 is the effective collision frequency defined by Eq. (27), ζ is defined by Eq. (24) [or equivalently, by Eq. (26)] and

$$f_{\text{L}}(\mathbf{V})=n\left(\frac{m}{2\pi T}\right)^{d/2}e^{-mV^2/2T} \tag{67}$$

is the local equilibrium distribution function In addition, $\chi(\alpha)$ is a free parameter of the model chosen to optimize the agreement with the Boltzmann results.

One of the main advantages of using a kinetic model instead of the Boltzmann equation is that it lends itself to determine all the velocity moments of the velocity distribution function. For the sake of convenience, let us define the general velocity moments

$$M_{k_1,k_2,k_3}=\int \mathrm{d}\mathbf{V}\, V_x^{k_1}V_y^{k_2}V_z^{k_3}f(\mathbf{V}). \tag{68}$$

As for IMM, although we are mainly interested in the three-dimensional case, we will perform our results for $d=3$ and $d=2$. Of course, for hard disks ($d=2$), $k_3=0$ since the z-axis is meaningless. To get M_{k_1,k_2,k_3}, we multiply both sides of Eq. (66) by $V_x^{k_1}V_y^{k_2}V_z^{k_3}$ and integrate over velocity to achieve the result

$$ak_1M_{k_1-1,k_2+1,k_3}+\left(\chi\nu_0+k\lambda\right)M_{k_1,k_2,k_3}=N_{k_1,k_2,k_3}, \tag{69}$$

where $\lambda=\gamma+\zeta/2$, $k=k_1+k_2+k_3$, and

$$N_{k_1,k_2,k_3}=\frac{\gamma T_{\text{ex}}}{m}R_{k_1,k_2,k_3}+\chi\nu_0M^{\text{L}}_{k_1,k_2,k_3}. \tag{70}$$

In Eq. (70), we have introduced the quantities

$$\begin{aligned}R_{k_1,k_2,k_3} &= \int \mathrm{d}\mathbf{V}\, f(\mathbf{V})\frac{\partial^2}{\partial V^2}\left(V_x^{k_1}V_y^{k_2}V_z^{k_3}\right)\\ &= k_1(k_1-1)M_{k_1-2,k_2,k_3}+k_2(k_2-1)M_{k_1,k_2-2,k_3}+k_3(k_3-1)M_{k_1,k_2,k_3-2},\end{aligned} \tag{71}$$

and

$$M^{\text{L}}_{k_1,k_2,k_3}=n\left(\frac{2T}{m}\right)^{k/2}\pi^{-d/2}\Gamma\left(\frac{k_1+1}{2}\right)\Gamma\left(\frac{k_2+1}{2}\right)\Gamma\left(\frac{k_3+1}{2}\right) \tag{72}$$

if k_1, k_2, and k_3 are even, being zero otherwise. The solution to Eq. (69) can be cast into the form (see the Appendix B)

$$M_{k_1,k_2,k_3}=\sum_{q=0}^{k_1}\frac{k_1!}{(k_1-q)!}\frac{(-a)^q}{\left(\chi\nu_0+k\lambda\right)^{1+q}}N_{k_1-q,k_2+q,k_3}. \tag{73}$$

The first nontrivial moments are related with the pressure tensor P_{ij}. The expressions of its nonzero elements are

$$P_{yy}=P_{zz}=nT_{\text{ex}}\frac{\theta\chi\nu_0+2\gamma}{\chi\nu_0+2\lambda},\quad P_{xy}=-nT_{\text{ex}}\frac{\theta\chi\nu_0+2\gamma}{\left(\chi\nu_0+2\lambda\right)^2}a, \tag{74}$$

$$P_{xx}=dnT-(d-1)P_{yy}=nT_{\text{ex}}\frac{\theta\chi\nu_0+2\gamma}{\chi\nu_0+2\lambda}\left[1+\frac{2a^2}{\left(\chi\nu_0+2\lambda\right)^2}\right]. \tag{75}$$

The non-Newtonian shear viscosity η^* and the viscometric function Ψ^* defined by Eqs. (38) and (39), respectively, can be easily identified from Eqs. (74) and (75). Their expressions in the BGK model are

$$\eta^* = \frac{2+\chi\nu_0^*\sqrt{\theta}\theta}{\left[\sqrt{\theta}\left(\chi\nu_0^*+\zeta^*\right)+2\right]^2}, \tag{76}$$

$$\Psi^* = d\theta\frac{2\left(1-\theta^{-1}\right)+\sqrt{\theta}\zeta^*}{2+\sqrt{\theta}\left(\chi\nu_0^*+\zeta^*\right)}, \tag{77}$$

where ζ^* is given by Eq. (36) and

$$\nu_0^* \equiv \frac{\nu_0}{\sqrt{\theta}\gamma} = \frac{8}{d+2}\frac{\pi^{(d-1)/2}}{\Gamma\left(\frac{d}{2}\right)}n^*\sqrt{T_{\text{ex}}^*}. \tag{78}$$

Finally, the steady granular temperature $\theta \equiv T/T_{\text{ex}}$ can be obtained from the steady-state condition (18). After some algebra, one gets the implicit equation

$$a^* = \sqrt{\frac{d}{2}\frac{\sqrt{\theta}\zeta^*+2(1-\theta^{-1})}{\sqrt{\theta}\chi\nu_0^*+2\theta^{-1}}}\left[2+\sqrt{\theta}\left(\chi\nu_0^*+\zeta^*\right)\right]. \tag{79}$$

Comparison of Eqs. (76), (77), and (79) with those obtained by solving the Boltzmann equation via Grad's moment method [20] shows that the BGK results for the rheological properties agree with the Boltzmann ones when the parameter $\chi(\alpha)$ is given by

$$\chi(\alpha) = \frac{1+\alpha}{2}\left[1-\frac{d-1}{2d}(1-\alpha)\right]. \tag{80}$$

Furthermore, for elastic collisions, Eqs. (76), (77), and (79) agree with previous results [47] obtained by solving the BGK model for ordinary dilute gases by means of Grad's moment method.

The expressions of the fourth-degree moments can be easily obtained from Eq. (73) with the choice (80). The shear-rate dependence of these moments will be compared with the ones derived before for IMM for $d = 3$ in section V.

A. Transport properties at $T_{\text{ex}} = 0$

Apart from getting the velocity moments, the use of the BGK equation allow us in some cases to obtain explicitly the velocity distribution function f. On the other hand, we have not been able to derive an expression for f for the suspension model (66). An exception corresponds to the simple limit case $T_{\text{ex}} = 0$ but keeping $\gamma \equiv$ const. It corresponds to a situation where the background temperature T_{ex} is much smaller than the granular temperature T and hence, the model ignores the effects of thermal fluctuations on solid particles and the impact of the gas phase is only accounted for by the drag force term. Of course, it is also understood that γ does not depend on the background temperature. This simple model has been employed in several previous works to study simple shear flows in gas-solid flows [17–19, 39], particle clustering due to hydrodynamic interactions [48], steady states of particle systems driven by a vibrating boundary [49] and more recently [8, 9, 50, 51] to analyze the rheology of frictional sheared hard-sphere suspensions.

Note that, in spite of the absence of the Langevin-like term $T_{\text{ex}}\partial^2 f/\partial v^2$ in this suspension model, the Boltzmann equation (5) still admits a simple solution in the homogeneous state (zero shear rate) for elastic collisions ($\alpha = 1$). Thus, if one chooses a convenient selection of frame then $\mathbf{U} = \mathbf{U}_g = \mathbf{0}$, and Eq. (5) admits the time-dependent solution

$$f_{\text{L}}(\mathbf{v},t) = n\left(\frac{m}{2\pi T(t)}\right)^{d/2} e^{-mv^2/2T(t)}, \tag{81}$$

where $T(t)$ verifies the equation

$$\frac{\partial \ln T}{\partial t} = -2\gamma. \tag{82}$$

An H-theorem has been also proved [52] for this time-dependent Maxwellian distribution in the sense that, starting from any initial condition and in the presence of the viscous drag force $\gamma\mathbf{v}$, the velocity distribution function $f(\mathbf{r},\mathbf{v},t)$ reaches in the long time limit the Maxwellian form with a time-dependent temperature.

In this limit case ($T_{\text{ex}}=0$), according to Eqs. (74) and (75), the elements of the pressure tensor can be written in a more compact form as [53]

$$P_{yy}=P_{zz}=\frac{nT}{1+2\xi},\quad P_{xx}=dnT-(d-1)P_{yy},\quad P_{xy}=-\frac{nT}{(1+2\xi)^2}\widetilde{a}, \tag{83}$$

where $\widetilde{a}=a/(\nu_0\chi)$, and ξ is the real root of the cubic equation

$$d\xi(1+2\xi)^2=\widetilde{a}^2, \tag{84}$$

namely,

$$\xi(\widetilde{a})=\frac{2}{3}\sinh^2\left[\frac{1}{6}\cosh^{-1}\left(1+\frac{27}{d}\widetilde{a}^2\right)\right]. \tag{85}$$

The friction coefficient γ obeys the steady-state condition (18):

$$\gamma=\chi\nu_0\xi-\frac{1}{2}\zeta. \tag{86}$$

Since $\gamma\geq 0$, at a given value of α, there is a critical value $\widetilde{a}_c(\alpha)$ of the (reduced) shear rate such that physical solutions to Eq. (80) only exist for $\widetilde{a}\geq\widetilde{a}_c(\alpha)$. The critical value $\widetilde{a}_c$ is obtained from the condition $2\chi\nu_0\xi=\zeta$. Thus, if $\alpha\neq 1$, then $\widetilde{a}_c>0$ and the expression for the Newtonian shear viscosity cannot be recovered when $\widetilde{a}\to 0$. This is a drawback of this suspension model ($T_{\text{ex}}=0$). It must be remarked that Tsao and Koch [17] solved time ago this simple model and showed the existence of a discontinuous transition for the temperature between a "quenched" state (a low temperature state) and an "ignited" state (a high temperature state).

Finally, the velocity distribution function $f(\mathbf{V})$ can be also determined explicitly in this limit case. When $T_{\text{ex}}=0$, the BGK equation (66) becomes

$$-aV_y\frac{\partial f}{\partial V_x}-\lambda\frac{\partial}{\partial\mathbf{V}}\cdot\mathbf{V}f+\chi\nu_0 f=\chi\nu_0 f_{\text{L}}. \tag{87}$$

This equation can be rewritten as

$$\left(1-d\widetilde{\lambda}-\widetilde{a}V_y\frac{\partial}{\partial V_x}-\widetilde{\lambda}\mathbf{V}\cdot\frac{\partial}{\partial\mathbf{V}}\right)f=f_{\text{L}}, \tag{88}$$

where $\widetilde{\lambda}=\lambda/(\chi\nu_0)$. The hydrodynamic solution to Eq. (88) is

$$\begin{aligned} f &= \left(1-d\widetilde{\lambda}-\widetilde{a}V_y\frac{\partial}{\partial V_x}-\widetilde{\lambda}\mathbf{V}\cdot\frac{\partial}{\partial\mathbf{V}}\right)^{-1}f_{\text{L}} \\ &= \int_0^\infty \mathrm{d}s\, e^{-(1-d\widetilde{\lambda})s}\, e^{\widetilde{a}sV_y\frac{\partial}{\partial V_x}}\, e^{\widetilde{\lambda}s\mathbf{V}\cdot\frac{\partial}{\partial\mathbf{V}}}f_{\text{L}}(\mathbf{V}). \end{aligned} \tag{89}$$

The action of the velocity operators $e^{\widetilde{a}sV_y\frac{\partial}{\partial V_x}}$ and $e^{\widetilde{\lambda}t\mathbf{V}\cdot\frac{\partial}{\partial\mathbf{V}}}$ on an arbitrary function $g(\mathbf{V})$ is

$$e^{\widetilde{a}sV_y\frac{\partial}{\partial V_x}}g(V_x,V_y,V_z)=g(V_x+\widetilde{a}sV_y,V_y,V_z), \tag{90}$$

$$e^{\widetilde{\lambda}s\mathbf{V}\cdot\frac{\partial}{\partial\mathbf{V}}}g(V_x,V_y,V_z)=g\left(e^{\widetilde{\lambda}s}V_x,e^{\widetilde{\lambda}s}V_y,e^{\widetilde{\lambda}s}V_z\right). \tag{91}$$

Taking into account these operators, the velocity distribution function f can be finally written as

$$f(\mathbf{V})=n\left(\frac{m}{2T}\right)^{d/2}\varphi(\mathbf{c}), \tag{92}$$

where $\mathbf{c}=(m/2T)^{1/2}\mathbf{V}$ is the reduced peculiar velocity and the reduced velocity distribution function $\varphi(\mathbf{c})$ is

$$\begin{aligned} \varphi(\mathbf{c}) &= \pi^{-d/2}\int_0^\infty \mathrm{d}s\, e^{-(1-d\widetilde{\lambda})s}\, \exp\left[-e^{2\widetilde{\lambda}s}\left(\mathbf{c}+s\,\widetilde{\mathbf{a}}\cdot\mathbf{c}\right)^2\right] \\ &= \pi^{-d/2}\int_0^\infty \mathrm{d}s\, e^{-(1-d\widetilde{\lambda})s}\, \exp\Big\{-e^{2\widetilde{\lambda}s}\left[(c_x+\widetilde{a}sc_y)^2+c_y^2+c_z^2\right]\Big\}. \end{aligned} \tag{93}$$

Here, we have introduced the tensor $\widetilde{a}_{ij}=\widetilde{a}\delta_{ix}\delta_{jy}$.

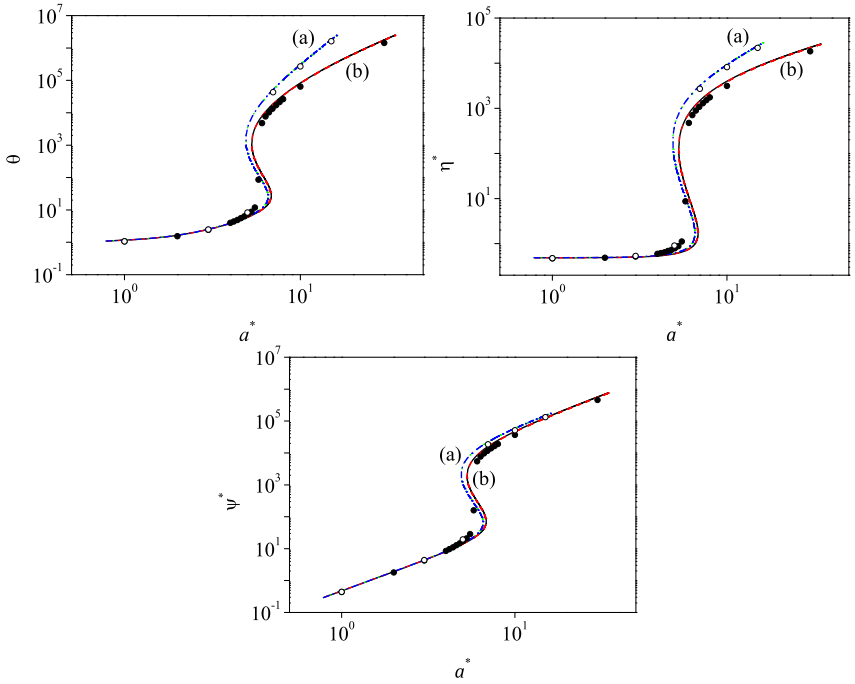

FIG. 2: Plots of the steady granular temperature θ, the non-Newtonian shear viscosity η^*, and the viscometric function Ψ^* versus the (reduced) shear rate a^* for $n^* = 0.01$ and $T_{\text{ex}}^* = 0.9$. Two different values of the coefficient of restitution α have been considered: $\alpha = 1$ (a), and $\alpha = 0.9$ (b). The solid and dotted lines correspond to the results obtained from the Boltzmann equation for IMM. The dashed and dash–dotted lines correspond to the results obtained from the BGK equation for IHS. Symbols refer to computer simulation results: empty circles for $\alpha = 1$ and filled circles for $\alpha = 0.9$.

V. RHEOLOGICAL PROPERTIES AND FOURTH-DEGREE MOMENTS. COMPARISON WITH COMPUTER SIMULATIONS

In sections IV and V we have solved the Boltzmann and BGK kinetic equations to obtain the shear-rate dependence of the second- and fourth-degree moments of a sheared granular suspension. In dimensionless form, those moments are given in terms of the coefficient of restitution α, the reduced density $n^* \equiv n\sigma^d$, the (reduced) background temperature $T_{\text{ex}}^* \equiv T_{\text{ex}}/(m\sigma^2\gamma^2)$, and the (reduced) shear rate $a^* \equiv a/\gamma$. The theoretical results obtained for the steady (scaled) granular temperature θ and the rheological functions η^* and Ψ^* are compared here against recent event-driven simulations [20] performed for a three-dimensional system ($d = 3$). In the simulations, $n^* = 0.01$ and $T_{\text{ex}}^* = 0.9$. Henceforth, we will consider these values for n^* and T_{ex}^* for the remaining plots displayed in this section.

The shear-rate dependence of θ, η^*, and Ψ^* is plotted in Fig. 2 for two different values of the coefficient of restitution α: $\alpha = 1$ (elastic collisions) and $\alpha = 0.9$ (inelastic collisions). The analytical expressions of the above quantities obtained from the Boltzmann equation for IMM are given by Eqs. (35), (39), and (40) while Eqs. (76), (77), and (79) correspond to the results derived from the BGK equation for IHS. Recall that the latter results coincide with those derived by solving the Boltzmann equation for IHS [20] via Grad's moment method [41]. First, it is quite apparent that the agreement of both theoretical results with simulations is excellent in the complete range of (scaled) shear rates analyzed. As in previous works on sheared granular flows [54], the good agreement found here between IMM and simulations of IHS confirms again the reliability of IMM to reproduce the main trends observed for IHS. Moreover, as remarked in previous studies [20, 47], Fig. 2 highlights the existence of a discontinuous shear thickening effect, namely, the non-Newtonian shear viscosity η^* discontinuously increases/decreases (at a certain value of a^*) as the (scaled) shear rate gradually increases/decreases. The origin of this saddle-node bifurcation is a consequence of the connection between the behaviors of the non-Newtonian shear viscosity for small [Newtonian branch, Eq. (41)] and

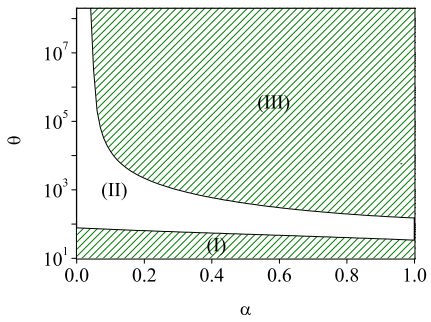

FIG. 3: Phase diagram for the behavior of the (symmetric) fourth-degree moments for IMM. The hatched regions below the curve $\theta_c^{(1)}(\alpha)$ (region I) and above the curve $\theta_c^{(2)}(\alpha)$ (region III) correspond to states with well-defined values of the scaled fourth-degree moments. The region II $[\theta_c^{(1)}(\alpha) < \theta < \theta_c^{(2)}(\alpha)]$ defines the states where the fourth-degree moments have unphysical values. Here, $n^* = 0.01$ and $T_{\text{ex}}^* = 0.9$.

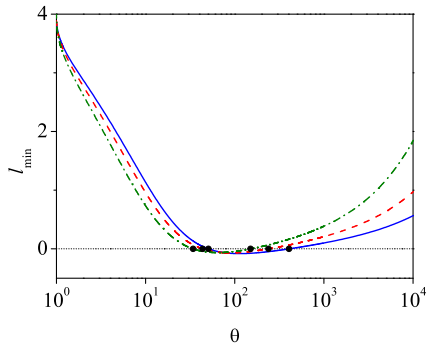

FIG. 4: Plot of the smallest eigenvalue, $\ell_{\min}$, associated with the time evolution of the (symmetric) fourth-degree moments for IMM as a function of the (scaled) temperature θ for $\alpha = 0.5$ (solid line), $\alpha = 0.7$ (dashed line), and $\alpha = 1$ (dash-dotted line). The circles indicate the location of the corresponding values of the critical temperatures $\theta_c^{(1)}(\alpha)$ and $\theta_c^{(2)}(\alpha)$. Here, $n^* = 0.01$ and $T_{\text{ex}}^* = 0.9$.

large [Bagnoldian branch, Eqs. (43) and (44)] shear rates. At a more quantitative level, in the case of the viscosity η^*, we also observe that simulation data suggest a sharper transition than the one obtained from the analytical results. These discrepancies (which are qualitatively small) could be in part due to the limitations of the molecular chaos ansatz of the Boltzmann equation which are of course avoided in the molecular dynamics method.

It must be remarked that the results (both theory and simulations) reported in Ref. [20] have shown that there is a transition from discontinuous shear thickening in dilute suspensions to continuous shear thickening at relatively low density. This finding is consistent with previous works [17, 18] where only the transition between the quenched and the ignited states for the steady temperature θ was analyzed but it contrasts with typical experimental observations in dense suspensions. With respect to the impact of the coefficient of restitution α on rheology, we see that the effect of α on the viscometric function Ψ^* is smaller than the one found for the temperature θ and the shear viscosity η^*.

We consider now the (symmetric) fourth-degree moments. They are given by Eq. (65) for the Boltzmann equation for IMM and Eq. (73) for the BGK kinetic model for IHS. As Fig. 2 shows, the function $\theta(a^*)$ becomes a multi-valued function in a certain interval (in the vicinity of the saddle point) of values of the shear rate, namely, in this region there are two or three different values of θ leading to the same value of a^*. Thus, in order to detect the possible singularities of the fourth-degree moments, it is more convenient to use θ as input parameter instead of the (scaled) shear rate a^*. Once θ is known, $a^*(\theta)$ can be easily determined from Eqs. (35) and (79) for IMM and the BGK model, respectively. An inspection of the (simple) BGK-forms of these moments shows that they are well defined functions of both α and θ for any value of the coefficient of restitution α. However, as occurs in dry granular gases [28], for

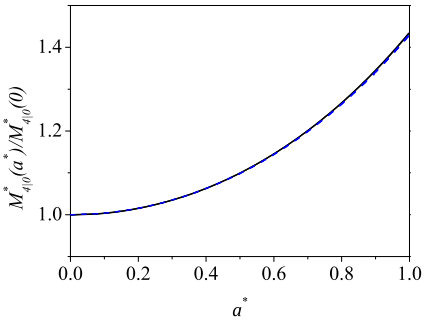

FIG. 5: Plot of the scaled moment $M^*_{4|0}(a^*)/M^*_{4|0}(0)$ as a function of a^* for $\alpha = 0.7$ (solid and dotted lines) and 1 (dashed and dash-dotted lines). The solid and dashed lines correspond to the results obtained from the Boltzmann equation for IMM while the (indistinguishable) dotted and dash-dotted lines refer to the results obtained from the BGK equation for IHS. Here, $n^* = 0.01$ and $T^*_{\rm ex} = 0.9$.

any given value of α, the matrix $\boldsymbol{\mathcal{L}}$ becomes singular ($\det \boldsymbol{\mathcal{L}} = 0$) for two certain "critical" values $\theta_c^{(1)}(\alpha)$ and $\theta_c^{(2)}(\alpha)$, where $\theta_c^{(2)}(\alpha) > \theta_c^{(1)}(\alpha)$. This means that the (symmetric) fourth-degree moments tend to infinity when $\theta \to \theta_c^{(i)}$ ($i = 1, 2$). Moreover, for $\theta_c^{(1)}(\alpha) < \theta < \theta_c^{(2)}(\alpha)$, the solutions to Eq. (65) are unphysical (e.g., $M^*_{4|0} < 0$) and hence, the stationary USF is limited to the regions $0 < \theta < \theta_c^{(1)}(\alpha)$ and $\theta > \theta_c^{(2)}(\alpha)$. The phase diagram associated with the singular behavior of the fourth-degree moments is plotted in Fig. 3 for $n^* = 0.01$ and $T^*_{\rm ex} = 0.9$. The curves $\theta_c^{(1)}(\alpha)$ (bottom curve) and $\theta_c^{(2)}(\alpha)$ (top curve) split the parameter space in three regions: the regions I and III correspond to states (θ, α) with finite values of the fourth-degree moments while the region II defines the states where those moments have no physical values. Figure 3 highlights the fact that the boundaries of the region II are nontrivial since at a given value of α there is a reentrance feature: we first find a transition from the region I (where the moments are well defined) to region II (unphysical values) by increasing the temperature θ, followed by a subsequent transition to a well defined region (the region III). Moreover, while $\theta_c^{(2)}(\alpha) > \theta_c^{(1)}(\alpha)$, $a_c^{(1)*}(\alpha) > a_c^{(2)*}(\alpha)$ where $a_c^{(i)*}$ denotes the critical shear rate associated with $\theta_c^{(i)}$. As said before, $a_c^{(i)*}$ is determined from Eq. (35) by the replacement $\theta \to \theta_c^{(i)}$. As an example, at $\alpha = 0.7$, $\theta_c^{(1)} = 43.573$ and $\theta_c^{(2)} = 238.639$ while $a_c^{(1)*} = 7.437$ and $a_c^{(2)*} = 6.441$. Similar behaviors are found for other values of α.

It is important to recall that the divergence of the fourth-degree moments of the USF is also present for both elastic [24, 26, 27] and inelastic [28] Maxwell models. In both cases, an analysis of the time evolution of the fourth-degree moments shows that the eigenvalue $\ell_{\rm min}$ of the matrix $\boldsymbol{\mathcal{L}}$ with the smallest real part governing the long time behavior of those moments becomes negative for shear rates larger than a critical value. Consequently, those moments exponentially grow in time (and so, they diverge in time) for $a^* > a_c^*$. To check if actually the origin of the singular behavior of the fourth-degree moments found here for granular suspensions is linked to the change of sign of the eigenvalue $\ell_{\rm min}$, Fig. 4 shows the dependence of $\ell_{\rm min}$ on the (scaled) temperature θ for three different values of α. At a given value of α, we observe that $\ell_{\rm min}$ exhibits a non-monotonic dependence on θ since it first decreases with increasing θ, then it becomes negative in the region $\theta_c^{(1)}(\alpha) < \theta < \theta_c^{(2)}(\alpha)$, and eventually becomes positive for $\theta > \theta_c^{(2)}$ where it increases with increasing θ. The corresponding critical values $\theta_c^{(1)}$ and $\theta_c^{(2)}$ are the same as those obtained from the condition $\det \boldsymbol{\mathcal{L}} = 0$, confirming the above expectation.

On the other hand, for states with $\theta < \theta_c^{(1)}(\alpha)$ and $\theta > \theta_c^{(2)}(\alpha)$ the (symmetric) fourth-degree moments have well-defined values and hence, one can study their shear-rate dependence. Here, for the sake of illustration, we consider the region $0 < a^* < 1$ where all the moments are well defined functions of the shear rate and in addition, nonlinear effects are still significant. Figure 5 shows the ratio $M^*_{4|0}(a^*)/M^*_{4|0}(0)$ versus a^* for $\alpha = 1$ and 0.7. The results obtained for IMM from the Boltzmann equation are compared against the results derived for IHS from the BGK equation. This figure highlights that both theories agree perfectly well each other, even for quite relatively high values of the shear rate. Regarding the influence of collisional dissipation, we observe that the effect of α on the the moment $M^*_{4|0}$ is very tiny since all the results collapse in a common curve. It is appealing to remark the good performance of the BGK theoretical predictions for granular suspensions since previous comparisons [55] made for ordinary gases at the level of the fourth-degree moments have shown significant discrepancies between the Boltzmann (obtained for

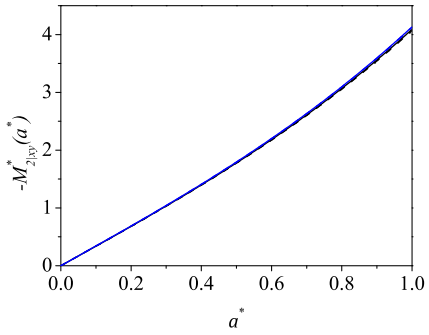

FIG. 6: Plot of the scaled moment $-M^*_{2|xy}(a^*)$ as a function of a^* for $\alpha = 0.7$ (solid and dotted lines) and 1 (dashed and dash-dotted lines). The solid and dashed lines correspond to the results obtained from the Boltzmann equation for IMM while the (indistinguishable) dotted and dash-dotted lines refer to the results obtained from the BGK equation for IHS. Here, $n^* = 0.01$ and $T^*_{\rm ex} = 0.9$.

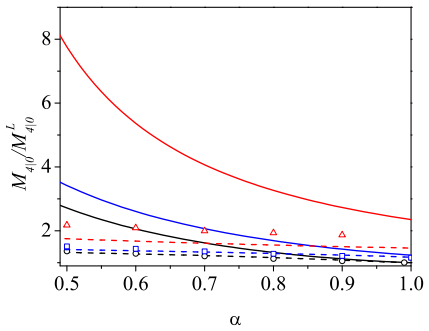

FIG. 7: Plot of the reduced moment $M_{4|0}/M^{\rm L}_{4|0}$ as a function of the coefficient of restitution α for three different values of the (reduced) friction coefficient $\widetilde{\gamma} = \gamma/\nu_0$: $\widetilde{\gamma} = 0$ (black lines and circles), $\widetilde{\gamma} = 0.1$ (blue lines and squares), and $\widetilde{\gamma} = 0.5$ (red lines and triangles). The solid lines correspond to the results obtained from the Boltzmann equation for IMM while the dashed lines refer to the results derived from the BGK equation for IHS. Symbols refer to computer simulation results obtained in Ref. [39].

Maxwell molecules) and BGK results for large shear rates (say, $a^* \geq 0.2$). This disagreement is especially important for moments in which the component V_x is the most relevant one. As a complement of Fig. 5, Fig. 6 shows the shear-rate dependence of the magnitude of the (reduced) moment $M^*_{2|xy}$. This moment vanishes in the absence of shear rate ($a^* = 0$). Similar conclusions to those made for the moment $M^*_{4|0}$ can be done for the moment $M^*_{2|xy}$.

We consider now the special limit case $T_{\rm ex} = 0$ where computer simulations for the moment $M_{4|0}$ are available in the literature [39]. In this limit case, the (reduced) shear rate a^* is a function of the coefficient of restitution α. Moreover, the (reduced) parameter $\widetilde{\gamma} \equiv \gamma/\nu_0$ is employed as input parameter in the DSMC results reported in Ref. [39] instead of the background temperature $T^*_{\rm ex}$. Figure 7 shows the ratio $M_{4|0}/M^{\rm L}_{4|0}$ versus α for three different values of $\widetilde{\gamma}$. Here,

$$M^{\rm L}_{4|0} = \int {\rm d}\mathbf{V} V^4 f_{\rm L}(\mathbf{V}), \tag{94}$$

where $f_{\rm L}$ is defined in Eq. (67). The solid and dashed lines refer to the results obtained from the Boltzmann equation for IMM and from the BGK equation for IHS, respectively. Symbols correspond to the computer simulation results obtained by numerically solving the Boltzmann equation for IHS by means of the DSMC method [56]. In the case of low values of the (reduced) friction coefficient $\widetilde{\gamma}$, we see that while the BGK results agree well with simulations in the full range of values of α represented here, more significant discrepancies between theory and simulations appear

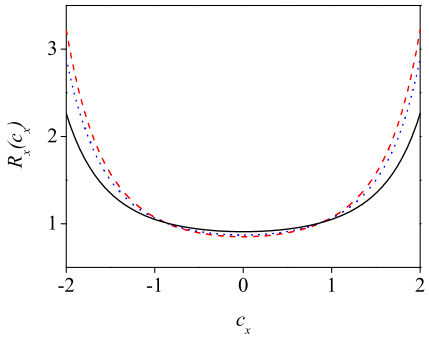

FIG. 8: Plot of the ratio $R_x(c_x) = \varphi_x(c_x)/(\pi^{-1/2}e^{-c_x^2})$ versus the (scaled) velocity c_x for $\widetilde{\gamma} = 0.1$ and three different values of the coefficient of restitution α: $\alpha = 1$ (solid line), $\alpha = 0.7$ (dotted line), and $\alpha = 0.5$ (dashed line).

for IMM. On the other hand, the agreement between the BGK results and simulations is only qualitative for higher values of $\widetilde{\gamma}$ since the BGK predictions clearly underestimate the simulation results. Finally, Fig. 8 plots the ratio $R_x(c_x) = \varphi_x(c_x)/(\pi^{-1/2}e^{-c_x^2})$ for $\widetilde{\gamma} = 0.1$ and three different values of the coefficient of restitution α. Here, the marginal distribution function $\varphi_x(c_x)$ is defined as

$$\begin{aligned}\varphi_x(c_x) &= \int_{-\infty}^{\infty} \mathrm{d}c_y \int_{-\infty}^{\infty} \mathrm{d}c_z\, \varphi(\mathbf{c}) \\ &= \frac{1}{\sqrt{\pi}} \int_0^{\infty} \mathrm{d}s \frac{e^{-(1-\widetilde{\lambda})s}}{\sqrt{1+\widetilde{a}^2 s^2}} \exp\left(-e^{2\widetilde{\lambda}s} \frac{c_x^2}{1+\widetilde{a}^2 s^2}\right),\end{aligned} \tag{95}$$

where the scaled distribution $\varphi(\mathbf{c})$ is given by Eq. (93). It is quite apparent that the distortion from equilibrium ($R_x \neq 1$) is more significant as the inelasticity increases. Although not shown here, comparison between theory and simulations (see Figs. 7 and 8 of Ref. [39]) shows that while the BGK solution agrees very well with simulation data in the region of thermal velocities ($|c_x| \sim 1$), it exhibits quantitative discrepancies with simulations for larger velocities and strong collisional dissipation.

VI. CONCLUDING REMARKS

In spite of the simplicity of the USF, this state has been widely studied to shed light on the non-linear response of the system to strong shear rates. This response is accounted for by non-Newtonian transport properties such as the (scaled) temperature θ, the (reduced) nonlinear shear viscosity η^*, and the (reduced) viscometric function Ψ^*. These properties are related to the second-degree velocity moments (pressure tensor). An interesting feature in *sheared* granular suspensions (not shared by dry granular gases) is the so-called *discontinuous* shear thickening effect, namely, the flow curve $\eta^*(a^*)$ has an S-shape, a^* being the (reduced) shear rate. This means that, at a certain value of the shear rate, η^* discontinuously increases/decreases if a^* is gradually increased/decreased. This phenomena has been usually observed in dense systems and (apart from other factors) it has been recognized that the mutual friction between grains (rough inelastic hard spheres) plays an important role [6–9]. On the other hand, a more recent study [20] based on the Enskog kinetic equation has shown that the discontinuous shear thickening can be also found for smooth IHS in the dilute regime. The theoretical predictions for the rheological properties (which were obtained from Grad's moment method) were shown to compare very well with computer simulations, even for moderate densities. On the other hand, although the momentum transport is the most relevant phenomenon in a sheared suspension, higher degree moments are also important since they provide an indirect information of the velocity distribution function.

Given the intricacies embodied in the hard sphere kernel of the Boltzmann collision operator, to study the above issue one has to consider simplified collision models where velocity moments can be obtained without having to use approximate methods. In the context of the Boltzmann equation, the inelastic Maxwell model (IMM) allows us to determine higher-degree moments in the USF problem. In particular, the fourth-degree moments have been *exactly* determined for dry IMM [28, 43]. An appealing problem is to extend the previous efforts to the case of granular suspensions, namely, when the effect of the interstitial gas phase on solid particles is accounted for. This has likely

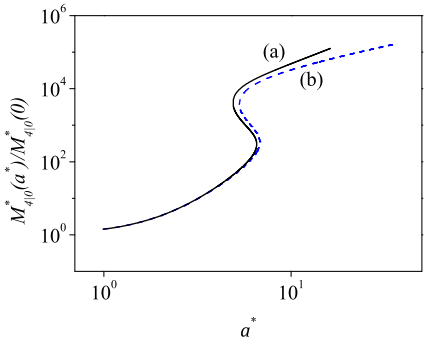

FIG. 9: Shear-rate dependence of the scaled moment $M^*_{4|0}(a^*)/M^*_{4|0}(0)$ for $\alpha = 1$ (solid line, (a)) and 0.9 (dashed line, (b)). The results are obtained from the BGK equation for IHS. Here, $n^* = 0.01$ and $T^*_{\rm ex} = 0.9$.

been one of the main goals of the present contribution. In addition, to complement the results derived from the Boltzmann equation for IMM, a BGK-type kinetic model for granular suspensions [25] has been also solved to get all the velocity moments of the velocity distribution function.

As mentioned in the Introduction section, the motivation of our work is twofold. First, the comparison between the theoretical predictions for θ, η^*, and Ψ^* with computer simulations allow us to assess the accuracy of both approaches (IMM and BGK results) in conditions of practical interest. Thus, the results displayed in Fig. 2 highlight the excellent performance of both theories in reproducing the shear-rate dependence of the rheological properties. In particular, the exact results derived from the Boltzmann equation for IMM shows the existence of the so-called discontinuous shear thickening behavior where several mechanisms [4] have been proposed in the literature to explain the origin of this behavior. What is interesting here is the existence of this shear thickening in a *structurally simple* system. In this case, these non-Newtonian properties are associated with both the behavior of the granular suspension in far from equilibrium situations as well as the impact of the interstitial fluid on the dynamics properties of the granular gas. As a second aspect, the determination of the fourth-degree moments provides information on the combined effect of both the (reduced) shear rate and inelasticity on the high velocity population. In particular, an important result is that, for a given value of the coefficient of restitution α, the (symmetric) fourth-degree moments of IMM have unphysical values in a certain region of the parameter space of the system. This singular behavior contrasts with the BGK results where all velocity moments are regular functions of both a^* and α. Since $\theta(a^*)$ is a multi-valued function (i.e., two or three values of θ correspond to the same value of a^* for a certain range of values of a^*), it is more convenient to carry out the study on the divergence of the fourth-degree moments of IMM taking θ as independent parameter (input) instead of a^*. In this case, our results show that those moments are not well-defined in the region $\theta_c^{(1)}(\alpha) < \theta < \theta_c^{(2)}(\alpha)$ where the critical values $\theta_c^{(i)}(\alpha)$ are obtained from the condition $\det \boldsymbol{\mathcal{L}} = 0$, where the matrix $\boldsymbol{\mathcal{L}}$ is defined by Eqs. (54) and (55). Although this singularity of the fourth-degree moments for IMM is also present in elastic [26, 27] and inelastic [28] systems, the phase diagram showing the regions where those moments are finite in granular suspensions is completely different to the one previously found for the above systems.

On the other hand, for states $\theta < \theta_c^{(1)}$ and $\theta > \theta_c^{(2)}$, the fourth-degree moments of IMM are well-defined functions. In particular, a comparison between the BGK and IMM results for those moments in the region $0 \le a^* \le 1$ (where non-Newtonian effects are still important) surprisingly shows an excellent agreement between both theoretical results (see, for instance, Figs. 5 and 6). This good performance of the BGK model contrasts with a previous comparison made for elastic Maxwell molecules [55] where the BGK predictions differ appreciably from the Boltzmann results for not too large shear rates (say, for instance, $a^* \gtrsim 0.2$). In addition, the shear-rate dependence of the fourth-degree moments is practically independent of inelasticity. It would be interesting to perform computer simulations to assess the accuracy of the above theoretical predictions for the fourth-degree moments.

Although most of the previous works have focused on the study of discontinuous shear thickening effect of the non-Newtonian shear viscosity, a natural question is to see if actually the above behavior is also present in the fourth-degree moments. Since the BGK moments are well defined functions of both the coefficient of restitution and the shear rate, one may analyze the shear-rate dependence of those moments for high values of a^*. As an illustration, Fig. 9 shows the scaled moment $M_{4|0}(a^*)/M_{4|0}(0)$ versus a^* for $\alpha = 1$ and 0.9. It is quite apparent that $M_{4|0}(a^*)/M_{4|0}(0)$ exhibits an S-shape since, at a given value of the shear rate, a small change in the shear rate produces a drastic increase of the fourth-degree moment $M^*_{4|0}$. This behavior has been also observed in the remaining (symmetric) fourth-degree

moments. We expect that this theoretical prediction of the BGK model encourages the development of computer simulations to confirm this interesting result.

As in many previous studies on granular gases, in this paper we have assumed that the coefficient of restitution α is a positive constant. It is well known that experimental observations [57] have shown that α depends on the impact velocity. The simplest model accounting for this velocity dependence of α is the model of viscoelastic particles [58–60]. A possible extension of the results presented here along this direction could be an interesting problem. However, given that the discontinuous shear thickening for elastic suspensions is qualitatively similar to that of inelastic suspensions, we guess that the effect of the velocity dependence of α on the above phenomenon would be irrelevant. Another possible project would be to consider the model of inelastic rough spheres [61, 62] where apart from the coefficient of normal restitution, a *constant* coefficient of tangential restitution is introduced. This is a more realistic model than the model of smooth inelastic hard sphere since the inelasticity of collisions not only affects to the translational degrees of freedom but also to the rotational ones. The extension of the present results to this model would allow us to assess the impact of roughness on the discontinuous shear thickening problem. Finally, it would be also appealing to study the case of multicomponent granular suspensions where problems like segregation can be addressed. Work along these lines are underway.

Acknowledgments

We want to thank Satoshi Takada and Moisés García Chamorro for providing us the simulation data included in Figs. 2 and 7, respectively. The present work has been supported by the Spanish Government through Grant No. FIS2016-76359-P, partially financed by Fondo Europeo de Desarrollo Regional funds. The research of Rubén Gómez González has been supported by the predoctoral fellowship BES-2017-079725 from the Spanish Government.

Appendix A: Fourth-degree collisional moments of IMM

In this Appendix, the expressions of the relevant fourth-degree collisional moments in a three-dimensional system are displayed. The explicit forms of these moments were obtained in Ref. [43]. As mentioned in section III, there are eight independent *symmetric* (or nonvanishing) moments in the geometry of the steady USF state. They are given by the set

$$\left\{M_{4|0}, M_{2|xx}, M_{2|yy}, M_{2|xy}, M_{0|yyyy}, M_{0|zzzz}, M_{0|xxxy}, M_{0|yyyx}\right\}. \tag{A1}$$

where the moments $M_{4|0}$, $M_{2|ij}$, and $M_{0|ijk\ell}$ are defined by Eq. (47). Their corresponding collisional moments are given by

$$\left(J_{4|0}, J_{2|ij}, J_{0|ijk\ell}\right) = \int \mathrm{d}\mathbf{V}\, \left(Y_{4|0}, Y_{2|ij}, Y_{0|ijk\ell}\right) J_{\mathrm{IMM}}[\mathbf{V}|f,f]. \tag{A2}$$

The explicit expressions for the collisional moments are [43]

$$J_{4|0} = -\nu_{4|0} M_{4|0} + 9\frac{p^2}{nm^2}\lambda_1 - \frac{\lambda_2}{nm^2}\Pi_{k\ell}\Pi_{k\ell}, \tag{A3}$$

$$J_{2|xx} = -\nu_{2|2} M_{2|xx} + 3\lambda_3 \frac{p}{nm^2}\Pi_{xx} - \frac{\lambda_4}{nm^2}\left(\Pi_{xk}\Pi_{kx} - \frac{1}{3}\Pi_{k\ell}\Pi_{\ell k}\right), \tag{A4}$$

$$J_{2|xy} = -\nu_{2|2} M_{2|xy} + 3\lambda_3 \frac{p^2}{nm^2}\Pi_{xy} - \frac{\lambda_4}{nm^2}\Pi_{xk}\Pi_{ky}, \tag{A5}$$

$$J_{0|yyyy} = -\nu_{0|4} M_{0|yyyy} + 3\frac{\lambda_5}{nm^2}\left(\Pi_{yy}^2 - \frac{4}{7}\Pi_{yk}\Pi_{ky} + \frac{2}{35}\Pi_{k\ell}\Pi_{\ell k}\right), \tag{A6}$$

$$J_{0|xxxy} = -\nu_{0|4} M_{0|xxxy} + 3\frac{\lambda_5}{nm^2}\left(\Pi_{xx}\Pi_{yy} - \frac{2}{7}\Pi_{xk}\Pi_{ky}\right). \tag{A7}$$

The collisional moments $J_{2|yy}$, $J_{0|zzzz}$, and $J_{0|yyyx}$ can be easily obtained from Eqs. (A4), (A6), and (A7), respectively. In Eqs. (A3)–(A7), the usual Einstein summation convention over repeated indices is assumed. Moreover, we have introduced the effective collision frequencies

$$\nu_{4|0}=2\zeta+\frac{(1+\alpha)^2(5+6\alpha-3\alpha^2)}{120}\nu_{\mathrm{M}},\quad \nu_{2|2}=2\zeta+\frac{(1+\alpha)^2(34+21\alpha-6\alpha^2)}{420}\nu_{\mathrm{M}}, \tag{A8}$$

$$\nu_{0|4}=2\zeta+\frac{(1+\alpha)^2(50+7\alpha-\alpha^2)}{315}\nu_{\mathrm{M}}, \tag{A9}$$

where $\zeta=(1-\alpha^2)\nu_{\mathrm{M}}/6$. Finally, the cross coefficients λ_i in Eqs. (A3)–(A7) are given by

$$\lambda_1=\frac{(1+\alpha)^2(11-6\alpha+3\alpha^2)}{72}\nu_{\mathrm{M}},\quad \lambda_2=\frac{(1+\alpha)^2(1+6\alpha-3\alpha^2)}{60}\nu_{\mathrm{M}},\quad \lambda_3=\frac{(1+\alpha)^2(22-21\alpha+6\alpha^2)}{180}\nu_{\mathrm{M}}, \tag{A10}$$

$$\lambda_4=\frac{(1+\alpha)^2(21\alpha-3\alpha^2-1)}{210}\nu_{\mathrm{M}},\quad \lambda_5=\frac{(1+\alpha)^2(39-21\alpha+3\alpha^2-1)}{945}\nu_{\mathrm{M}}. \tag{A11}$$

Appendix B: Results from the BGK-type kinetic model

The results derived from the BGK kinetic model are displayed in this Appendix. Let us consider first Eq. (69):

$$ak_1M_{k_1-1,k_2+1,k_3}+(\chi\nu_0+k\lambda)\,M_{k_1,k_2,k_3}=N_{k_1,k_2,k_3}, \tag{B1}$$

where N_{k_1,k_2,k_3} is defined by Eq. (70). Given that R_{k_1,k_2,k_3} is a linear combination of velocity moments of degree $k-2$, the quantity N_{k_1,k_2,k_3} is assumed to be known in the equation defining the moments M_{k_1,k_2,k_3} of degree k. To solve the hierarchy of moment equations (B1), we introduce the operators L_1 and L_2 acting on functions $\psi(k_1,k_2,k_3)$ as

$$L_1\psi(k_1,k_2,k_3)=\psi(k_1-1,k_2,k_3),\quad L_2\psi(k_1,k_2,k_3)=\psi(k_1,k_2+1,k_3). \tag{B2}$$

Thus, Eq. (B1) can be written as

$$(ak_1L_1L_2+\chi\nu_0+k\lambda)\,M_{k_1,k_2,k_3}=N_{k_1,k_2,k_3}. \tag{B3}$$

Its formal solution is

$$M_{k_1,k_2,k_3}=(ak_1L_1L_2+\chi\nu_0+k\lambda)^{-1}\,N_{k_1,k_2,k_3}. \tag{B4}$$

Since

$$L_1L_2\left[\chi\nu+(k_1+k_2+k_3)\lambda\right]=\chi\nu_0+(k_1+k_2+k_3)\lambda, \tag{B5}$$

then, the solution (B4) can be written more explicitly as

$$\begin{aligned}M_{k_1,k_2,k_3}&=\frac{1}{\chi\nu_0+k\lambda}\left(1+\frac{ak_1}{\chi\nu_0+k\lambda}L_1L_2\right)^{-1}N_{k_1,k_2,k_3}\\&=\sum_{q=0}^{\infty}\frac{(-a)^q}{(\chi\nu_0+k\lambda)^{1+q}}\,(k_1L_1L_2)^q\,N_{k_1,k_2,k_3}.\end{aligned} \tag{B6}$$

On the other hand, it is straightforward to prove that

$$(k_1L_1L_2)^q\,N_{k_1,k_2,k_3}=\frac{k_1!}{(k_1-q)!}N_{k_1-q,k_2+q,k_3}, \tag{B7}$$

if $q\le k_1$, being zero otherwise. Thus, Eq. (B6) can be finally written in the form

$$M_{k_1,k_2,k_3}=\sum_{q=0}^{k_1}\frac{k_1!}{(k_1-q)!}\frac{(-a)^q}{(\chi\nu_0+k\lambda)^{1+q}}N_{k_1-q,k_2+q,k_3}. \tag{B8}$$

[1] Brown E and H. M. Jeager H M, 2014 Rep. Prog. Phys. **77**, 046602

[2] Barnes H A , 1989 J. Rheol. **33**, 329
[3] Lootens D, van Damme H, Hémar Y and Hébraud P, 2005 Phys. Rev. Lett. **95**, 268302
[4] Brown E and Jaeger H M, 2009 Phys. Rev. Lett. **103**, 086001
[5] Mewis J and Wagner N J, 2011 *Colloidal Suspension Rheology* (Cambridge University Press: New York)
[6] Ciamarra M P, Pastore R, Nicodemi M and Coniglio A, 2011 Phys. Rev. E **84**, 041308
[7] Otsuki M and Hayakawa H, 2011 Phys. Rev. E **83**, 051301
[8] Heussinger C, 2013 Phys. Rev. E **88**, 050201(R)
[9] Seto R, Mari R, Morris J F and Denn M M, 2013 Phys. Rev. Lett. **111**, 218301
[10] Kranz W T, Frahsa F, Zippelius A, Fuchs M and Sperl M, 2018 Phys. Rev. Lett. **121**, 148002
[11] Brady J F and Bossis G, 1985 J. Fluid Mech. **155**, 105
[12] Wagner N J and Brady J F, 2009 Phys. Today **62**, 27
[13] Hoffman R L, 1974 J. Colloid Interface Sci. **46**, 491
[14] Hoffman R L, 1982 Adv. Colloid Interface Sci. **17**, 161
[15] Cates M E, Haw M D and Holmes C B, 2005 J. Phys: Condens. Matter **17** S2517
[16] Brown E and Jaeger H M, 2012 J. Rheol. **39**, 875
[17] Tsao H-K and Koch D, 1995 J. Fluid Mech. **296**, 211
[18] Sangani A S, Mo G, Tsao H-K and Koch D, 1996 J. Fluid Mech. **313**, 309
[19] Saha S and Alam M, 2017 J. Fluid Mech. **833**, 206
[20] Hayakawa H, Takada S and Garzó V, 2017 Phys. Rev. E **96**, 042903
[21] Cercignani C, 1988 *The Boltzmann Equation and Its Applications* (Springer–Verlag: New York)
[22] Chapman S and Cowling T G, 1970 *The Mathematical Theory of Nonuniform Gases* (Cambridge University Press: Cambridge)
[23] Ferziger J H and Kaper G H, 1972 *Mathematical Theory of Transport Processes in Gases* (North–Holland: Amsterdam)
[24] Garzó V and Santos A, *Kinetic Theory of Gases in Shear Flows. Nonlinear Transport* (Kluwer Academic Publishers, Dordrecht, 2003).
[25] Brey J J, Dufty J W and Santos A, 1999 J. Stat. Phys. **97**, 281
[26] Santos A, Garzó V, Brey J J and Dufty J W, 1993 Phys. Rev. Lett. **71**, 3971
Santos A, Garzó V, Brey J J and Dufty J W, 1994 Phys. Rev. Lett. **72**, 1392 (erratum)
[27] Santos A and Garzó V, 1995 Physica A **213**
[28] Santos A and Garzó V, 2007 J. Stat. Mech. **P08021**
[29] Garzó V, 2007 J. Phys. A: Math. Theor. **40**, 10729
[30] Brilliantov N and Pöschel T, 2004 *Kinetic Theory of Granular Gases* (Oxford University Press: Oxford).
[31] Garzó V, Tenneti S, Subramaniam S and Hrenya C M, 2012 J. Fluid Mech. **712**, 129
[32] Garzó V, Fullmer W D, Hrenya C M and Yin X, 2016 Phys. Rev. E **93**, 012905
[33] Williams D R M and MacKintosh F C, 1996 Phys. Rev. E **54**, R9
[34] van Kampen N G, 1981 *Stochastic Processes in Physics and Chemistry* (North–Holland: Amsterdam)
[35] van Noije T P C and Ernst M H, 1998 Granular Matter **1**, 57
[36] Koch D L and Hill R J, 2001 Annu. Rev. Fluid Mech. **33**, 619
[37] Koch D L, 1990 Phys. Fluids A **2**, 1711
[38] Wylie J J, Koch D L and Ladd A J C, 2003 J. Fluid Mech. **480**, 95
[39] Chamorro M G, Vega Reyes F and Garzó V, 2015 Phys. Rev. E **92**, 052205
[40] Dufty J W, Santos A, Brey J J and Rodríguez R F, 1986 Phys. Rev. A **33**, 459
[41] Grad H, 1949 Commun. Pure Appl. Math. **2**, 331
[42] Ben-Naim E and Krapivsky P L, 2003 *Granular Gas Dynamics (Lectures Notes in Physics* vol 624*)*, ed T Pöschel and N Brilliantov (Berlin: Springer) pp 65–93
[43] Garzó V and Santos A, 2007 J. Phys. A: Math. Theor. **40**, 14927
[44] Santos A, Montanero J M, Dufty J W and Brey J J, 1998 Phys. Rev. E **57**, 1644
[45] Santos A, 2003 Physica A **321**, 442
[46] Truesdell C and Muncaster R G, 1980 *Fundamentals of Maxwell's Kinetic Theory of a Simple Monatomic Gas* (Academic Press: New York)
[47] Hayakawa H and Takada S, 2017 Powders&Grains 2017, EPJ Web of Conferences **140**, 09003
[48] Wylie J J and Koch D L, 2000 Phys. Fluids **12**, 964
[49] Wylie J J, Zhang Q, Li Y and Hengyi X, 2009 Phys. Rev. E **79**, 031301
[50] Hilton J E and Tordesillas A, 2013 Phys. Rev. E **88**, 062203
[51] Wang T, Grob M, Zippelius A and Sperl M, 2014 Phys. Rev. E **89**, 042209
[52] Garzó V, Santos A and Brey J J, 1990 Physica A **163**, 651
[53] Garzó V, 2017 Phys. Rev. E **95**, 062906
[54] Goldhirsch I, 2003 Annu. Rev. Fluid Mech. **35**, 267
[55] Garzó V and Santos A, 1995 Physica A **213**, 426
[56] Bird G A, 1994 *Molecular Gas Dynamics and the Direct Simulation Monte Carlo of Gas Flows* (Clarendon: Oxford,
[57] Bridges F G, Hatzes A and Lin D N C, 1984 Nature (London) **309**, 333
[58] Brilliantov N V and Pöschel T, 2000 Phys. Rev. E **61**, 5573
[59] Brilliantov N V and Pöschel T, 2003 Phys. Rev. E **67**, 061304
[60] Dubey A K, Bodrova A, Puri S and Brilliantov N V, 2013 Phys. Rev. E **87**, 062202

[61] Goldshtein A and Shapiro M, 1995 J. Fluid Mech. **282**, 75
[62] Zippelius A, 2006 Physica A **369**, 143

6.3 Article 7

Title: Non-Newtonian rheology in inertial suspensions of inelastic rough hard spheres under simple shear flow

Authors: Rubén Gómez González[1] and Vicente Garzó[2]

Affiliations:

[1] Departamento de Física, Universidad de Extremadura, E-06006 Badajoz, Spain

[2] Departamento de Física and Instituto de Computación Científica Avanzada (ICCAEx), Universidad de Extremadura, E-06006 Badajoz, Spain

Journal: Physics of Fluids

Volume: 33

Pages: 073315

Year: 2020

DOI: 10.1063/5.0015241

Physics of Fluids ARTICLE scitation.org/journal/phf

Non-Newtonian rheology in inertial suspensions of inelastic rough hard spheres under simple shear flow

Cite as: Phys. Fluids **32**, 073315 (2020); doi: 10.1063/5.0015241
Submitted: 28 May 2020 • Accepted: 8 July 2020 •
Published Online: 27 July 2020

Rubén Gómez González[1,a] and Vicente Garzó[2,b]

AFFILIATIONS

[1]Departamento de Física, Universidad de Extremadura, E-06006 Badajoz, Spain
[2]Departamento de Física and Instituto de Computación Científica Avanzada (ICCAEx), Universidad de Extremadura, E-06006 Badajoz, Spain

Note: This paper is part of the Special Topic, Advances in Micro/Nano Fluid Flows: In Memory of Prof. Jason Reese.
[a]Electronic mail: ruben@unex.es
[b]Author to whom correspondence should be addressed: vicenteg@unex.es. URL: http://www.unex.es/eweb/fisteor/vicente/

ABSTRACT

Non-Newtonian transport properties of an inertial suspension of inelastic rough hard spheres under simple shear flow are determined by the Boltzmann kinetic equation. The influence of the interstitial gas on rough hard spheres is modeled via a Fokker–Planck generalized equation for rotating spheres accounting for the coupling of both the translational and rotational degrees of freedom of grains with the background viscous gas. The generalized Fokker–Planck term is the sum of two ordinary Fokker–Planck differential operators in linear $\mathbf{v}$ and angular $\boldsymbol{\omega}$ velocity space. As usual, each Fokker–Planck operator is constituted by a drag force term (proportional to $\mathbf{v}$ and/or $\boldsymbol{\omega}$) plus a stochastic Langevin term defined in terms of the background temperature T_{ex}. The Boltzmann equation is solved by two different but complementary approaches: (i) by means of Grad's moment method and (ii) by using a Bhatnagar–Gross–Krook (BGK)-type kinetic model adapted to inelastic rough hard spheres. As in the case of *smooth* inelastic hard spheres, our results show that both the temperature and the non-Newtonian viscosity increase drastically with an increase in the shear rate (discontinuous shear thickening effect) while the fourth-degree velocity moments also exhibit an *S*-shape. In particular, while high levels of roughness may slightly attenuate the jump of the viscosity in comparison to the smooth case, the opposite happens for the rotational temperature. As an application of these results, a linear stability analysis of the steady simple shear flow solution is also carried out showing that there are regions of the parameter space where the steady solution becomes linearly unstable. The present work extends previous theoretical results (H. Hayakawa and S. Takada, "Kinetic theory of discontinuous rheological phase transition for a dilute inertial suspension," Prog. Theor. Exp. Phys. **2019**, 083J01 and R. G. González and V. Garzó, "Simple shear flow in granular suspensions: Inelastic Maxwell models and BGK-type kinetic model," J. Stat. Mech. **2019**, 013206) to rough spheres.

I. INTRODUCTION

Needless to say, shear thickening (a rheological process in which the viscosity increases with the shear rate) in non-Newtonian gas–solid flows is likely one of the most challenging and open problems in suspensions of particles in gases or liquids. Apart from its practical interest (it has been broadly found in nature[1] and industry[2,3]), its understanding from a more fundamental point of view has attracted the attention of many researchers in the last few years.[4–21] Shear thickening can occur as a smooth increase in the viscosity with an increase in the shear rate; this effect is usually referred to as continuous shear thickening (CST). On the other hand, it can also be observed as a drastic increase in the viscosity at a specific shear rate; this dramatic version of CST is known as discontinuous shear thickening (DST). These two different phenomena can be observed, for instance,

Physics of Fluids ARTICLE scitation.org/journal/phf

in a suspension of cornstarch on water at different cornstarch concentrations.

On the other hand, although the shear-induced solid-like behavior produced in DST has generated significant interest, most of the studies have been focused on densely packed suspensions where extensive simulations have been carried out to disclose the origin of this unexpected phenomenon. As has been widely discussed in the review of Brown and Jaeger,[12] the above-mentioned studies propose three main mechanisms based on particle reorganization to explain the shear thickening phenomena: hydroclustering, order–disorder transition, and/or dilatancy. However, DST has been shown to appear also at relatively low-density regimes[22–30] where specific structural characteristics that influence the stress transmission are not apparently substantial enough to explain such a sharp transition. Thus, in order to unveil in a clean way the microscopic mechanisms involved in DST, it would be also convenient to consider relatively low-density systems where kinetic theory can provide a quantitative theoretical description. In the context of kinetic theory, some previous works[22–26] have shown the existence of a DST-like process for the temperature between a *quenched* state (a low-temperature state) and an *ignited* state (a high-temperature state) in homogeneously sheared gas–solid suspensions.

However, all the above works[22–26] consider a suspension model where the effects of thermal fluctuations on the dynamics of grains were neglected. A more accurate suspension model where the effect of the interstitial gas on solid particles is accounted for via a viscous drag force plus a stochastic Langevin term[31] has been recently considered[27–29] for obtaining the shear-rate dependence of the kinetic temperature and the stress tensor. The theoretical results[27–30] have been compared against event-driven Langevin simulation for hard spheres (EDLSHS),[32] showing very good agreement, especially for low-density systems. Both approaches (kinetic theory and simulations) conclude that there is a transition from DST (found for very dilute systems) to CST as the volume fraction of the granular gas increases.

An important limitation of the above-mentioned theoretical works[22–30] is that the solid particles were modeled as *smooth* inelastic hard spheres. This means that the effects of tangential friction and rotation induced by each binary collision on rheology were ignored in the above attempts. The purpose of the present paper is to extend the previous theoretical efforts of smooth spheres to *rough* spheres in order to assess the impact of roughness on the rheological properties of the suspension. Thus, we want to uncover the whole range values of the normal α and tangential β restitution coefficients and derive explicit expressions for the rotational T_r and translational T_t temperatures as well as for the relevant elements of the pressure tensor $P_{k\ell}$. Given the mathematical difficulties involved in the general problem, as in Refs. 29 and 30, we consider here very dilute systems for which the Boltzmann kinetic equation offers a reliable description. To the best of our knowledge, only three previous papers[5,13,17] have addressed the role of roughness in the rheological phenomena. However, given that these works[5,13,17] consider concentrated colloidal suspensions at the jamming transition, no analytical results were derived since they combine experimental and computer simulation results of spherical colloids. In this sense, the present contribution complements these previous attempts[5,13,17] since our results allows us to unveil the combined effect of both α and β on the shear-rate dependence of the pressure tensor.

As said before, our goal here is to determine the rheological properties of an inertial suspension of inelastic rough hard spheres under simple shear flow. This state is macroscopically characterized by a constant density n, a uniform temperature T, and an homogeneous shear field $U_x = ay$, where a is the constant shear rate. As usual, we are interested here in steady state conditions. In addition, as in previous works,[29,30] the influence of the viscous gas on solid particles is modeled by means of an operator representing the gas–solid interaction force. In the limit case of purely smooth spheres ($\alpha = 1$ and $\beta = -1$), only translational degrees of freedom play a role in the dynamics of grains. In this special case, the fluid-force is composed of a viscous drag force proportional to the (instantaneous) velocity of particles $\mathbf{v}$ (the coefficient of proportionality is the translational drift coefficient γ_t) plus a Langevin-like term defined in terms of the background temperature T_{ex}. On the other hand, beyond the smooth case, one has to take into account the coupling between the rotational degrees of freedom of grains and the interstitial gas. Following a model introduced years ago by Hess[33] for Brownian motion of rotating particles, we assume that the structure of the rotational part of the fluid-force is similar to that of the translational part: a drag force term proportional to the angular velocity $\boldsymbol{\omega}$ (the coefficient of proportionality is the rotational drift coefficient γ_r) plus a stochastic Langevin-like term defined in terms of T_{ex}. The coefficients γ_t and γ_r are proportional to the shear viscosity of the interstitial gas, and hence, both coefficients are proportional to $\sqrt{T_{\text{ex}}}$. This suspension model has been more recently considered to study a segregation problem of microswimmer mixtures.[34]

The suspension model for inelastic rough hard spheres is solved by two different but complementary theoretical tools. First, Grad's moment method[35] is considered to *approximately* get the explicit forms of both the (reduced) translational T_t/T_{ex} and rotational T_r/T_{ex} temperatures and the (reduced) elements $P_{k\ell}/(nT_{\text{ex}})$ of the pressure tensor in terms of the restitution coefficients α and β and the (reduced) shear rate $a^* \equiv a/\gamma_t$. Then, as a second alternative and to overcome the mathematical difficulties of the Boltzmann collision operator, a Bhatnagar–Gross–Krook (BGK) model kinetic equation recently proposed for inelastic rough hard spheres[36] is considered. This kinetic model retains the essential physical properties of the Boltzmann equation and allows one to obtain all the velocity moments of the velocity distribution function. In particular, the results derived for the pressure tensor from the kinetic model coincide with those derived from the Boltzmann equation when one conveniently chooses a free parameter of the model. Apart from the second-degree velocity moments, the shear-rate dependence of the fourth-degree moments is also widely analyzed.

The plan of the paper is as follows. Section II is devoted to the definition of the suspension model for inelastic rough hard spheres in the low-density limit. Starting from the Boltzmann kinetic equation, the exact balance equations for the densities of mass, momentum, and energy are derived with expressions for the momentum and heat fluxes. These expressions are defined in terms of the velocity distribution function. Section III deals with the simple shear flow state where the time evolution of the elements of the pressure tensor $P_{k\ell}$ is exactly obtained. The above set of equations for

Physics of Fluids ARTICLE scitation.org/journal/phf

$P_{k\ell}$ is solved by estimating the collisional moment associated with the transfer of momentum by means of Grad's moment method. This permits to achieve explicit forms for T_r, T_t, and $P_{k\ell}$ under steady state conditions. The results obtained from the BGK-like model are discussed in Sec. IV. Before considering the results for inertial suspensions, Sec. V analyzes the results in the so-called *dry* granular gases, namely, when the influence of the interstitial gas is neglected (i.e., when $\gamma_t = \gamma_r = 0$). Although these results are interesting by themselves, they offer the opportunity to compare the present theory with the results derived many years ago by Lun[37] for nearly elastic collisions ($\alpha \lesssim 1$) and nearly perfectly rough particles ($\beta \lesssim 1$). The results for the rheological properties and the fourth-degree velocity moments of inertial suspensions are illustrated in Sec. VI for several values of the coefficients α and β. It is clearly shown that the roughness does not substantially change the conclusions found in the smooth limit case since DST is also present for inelastic rough spheres. In addition, the BGK results also show that the fourth-degree moments increase dramatically with the shear rate in a certain region of values of the shear rate. A linear stability analysis of the steady simple shear flow solution is carried out in Sec. VII. As expected from the previous analysis performed for smooth spheres,[29] the homogeneous steady sheared solution can be linearly *unstable* in certain regions of the parameter space. The paper is closed in Sec. VIII with a brief discussion on the results reported here.

II. BOLTZMANN KINETIC EQUATION FOR GAS–SOLID FLOWS OF INELASTIC ROUGH HARD SPHERES

A. Boltzmann equation for inertial suspensions

We consider a set of solid particles of diameter σ, mass m, and moment of inertia I immersed in a molecular gas of viscosity η_g. The solid particles are modeled as inelastic rough hard spheres. We assume that the collisions among particles are inelastic and are characterized by constant coefficients of normal restitution (α) and tangential restitution (β). While the coefficient α ranges from 0 (perfectly inelastic collisions) to 1 (perfectly elastic collisions), the coefficient β ranges from -1 (perfectly smooth spheres) to 1 (perfectly rough spheres). Kinetic energy is, in general, dissipated by collisions, except in the cases $\alpha = 1$ and $\beta = \pm 1$. An interesting feature of this model is that inelasticity affects both translational and rotational degrees of freedom of the spheres.

In the low-density regime ($n\sigma^3 \ll 1$, where n is the number density), all the relevant information on the state of the suspension is given through the one-particle velocity distribution function $f(\mathbf{r}, \mathbf{v}, \boldsymbol{\omega}; t)$, where $\mathbf{v}$ and $\boldsymbol{\omega}$ are the (instantaneous) linear (translational) and angular velocities, respectively. Neglecting the effects of the gravity field, the velocity distribution f obeys the Boltzmann kinetic equation,[38–42]

$$\frac{\partial f}{\partial t} + \mathbf{v}\cdot\nabla f + \mathcal{F}f = J[\mathbf{v},\boldsymbol{\omega}|f(t),f(t)], \tag{1}$$

where $\mathcal{F}$ is an operator characterizing the influence of the interstitial gas on grains and $J[f, f]$ is the Boltzmann collision operator given by[41,42]

$$J[\mathbf{v}_1,\boldsymbol{\omega}_1|f,f] = \sigma^2 \int d\mathbf{v}_2 \int d\boldsymbol{\omega}_2 \int d\widehat{\boldsymbol{\sigma}}\,\Theta(\widehat{\boldsymbol{\sigma}}\cdot\mathbf{g})(\widehat{\boldsymbol{\sigma}}\cdot\mathbf{g}) \times\left[\frac{1}{\alpha^2\beta^2} f(\mathbf{r},\mathbf{v}_1'',\boldsymbol{\omega}_1'';t) f(\mathbf{r},\mathbf{v}_2'',\boldsymbol{\omega}_2'';t) - f(\mathbf{r},\mathbf{v}_1,\boldsymbol{\omega}_1;t) f(\mathbf{r},\mathbf{v}_2,\boldsymbol{\omega}_2;t)\right]. \tag{2}$$

Here, $\Theta(x)$ is Heaviside's step function, $\widehat{\boldsymbol{\sigma}}$ is the unit collision vector joining the centers of the two colliding spheres and pointing from the sphere labeled by 1 to the sphere labeled by 2, and $\mathbf{g} = \mathbf{v}_1 - \mathbf{v}_2$ is the relative translational velocity. In Eq. (2), the double primes on the linear and angular velocities denote the initial velocities $\{\mathbf{v}_1'', \boldsymbol{\omega}_1'', \mathbf{v}_2'', \boldsymbol{\omega}_2''\}$ that lead to the final velocities $\{\mathbf{v}_1, \boldsymbol{\omega}_1, \mathbf{v}_2, \boldsymbol{\omega}_2\}$ following a binary restituting collision. The restituting (or *inverse*) collision rules are[37–40,43]

$$\mathbf{v}_1'' = \mathbf{v}_1 - \mathbf{Q}'', \quad \mathbf{v}_2'' = \mathbf{v}_2 + \mathbf{Q}'', \tag{3}$$

$$\boldsymbol{\omega}_1'' = \boldsymbol{\omega}_1 - \frac{2}{\sigma\kappa}\widehat{\boldsymbol{\sigma}}\times\mathbf{Q}'', \quad \boldsymbol{\omega}_2'' = \boldsymbol{\omega}_2 - \frac{2}{\sigma\kappa}\widehat{\boldsymbol{\sigma}}\times\mathbf{Q}'', \tag{4}$$

where $\mathbf{Q}''$ reads

$$\mathbf{Q}'' = \frac{1+\alpha^{-1}}{2}\widehat{\boldsymbol{\sigma}}(\widehat{\boldsymbol{\sigma}}\cdot\mathbf{g}) - \frac{\kappa}{1+\kappa}\frac{1+\beta^{-1}}{2} \times\left[\widehat{\boldsymbol{\sigma}}(\widehat{\boldsymbol{\sigma}}\cdot\mathbf{g}) - \mathbf{g} + \frac{\sigma}{2}\widehat{\boldsymbol{\sigma}}\times(\boldsymbol{\omega}_1+\boldsymbol{\omega}_2)\right]. \tag{5}$$

In Eqs. (4) and (5), $\kappa = 4I/m\sigma^2$ is a dimensionless parameter characterizing the mass distribution within a sphere. It runs from the extreme values $\kappa = 0$ (namely, when the mass is concentrated on the center of the sphere) and $\kappa = \frac{2}{3}$ (namely, when the mass is concentrated on the surface of the sphere). In the case that the mass is uniformly distributed, $\kappa = \frac{2}{5}$.

Similarly, the collisional rules for the *direct* collision $(\mathbf{v}_1, \boldsymbol{\omega}_1, \mathbf{v}_2, \boldsymbol{\omega}_2) \to (\mathbf{v}_1', \boldsymbol{\omega}_1', \mathbf{v}_2', \boldsymbol{\omega}_2')$ are

$$\mathbf{v}_1' = \mathbf{v}_1 - \mathbf{Q}, \quad \mathbf{v}_2' = \mathbf{v}_2 + \mathbf{Q}, \tag{6}$$

$$\boldsymbol{\omega}_1' = \boldsymbol{\omega}_1 - \frac{2}{\sigma\kappa}\widehat{\boldsymbol{\sigma}}\times\mathbf{Q}, \quad \boldsymbol{\omega}_2' = \boldsymbol{\omega}_2 - \frac{2}{\sigma\kappa}\widehat{\boldsymbol{\sigma}}\times\mathbf{Q}, \tag{7}$$

where $\mathbf{Q}$ is given by

$$\mathbf{Q} = \frac{1+\alpha}{2}\widehat{\boldsymbol{\sigma}}(\widehat{\boldsymbol{\sigma}}\cdot\mathbf{g}) - \frac{\kappa}{1+\kappa}\frac{1+\beta}{2} \times\left[\widehat{\boldsymbol{\sigma}}(\widehat{\boldsymbol{\sigma}}\cdot\mathbf{g}) - \mathbf{g} + \frac{\sigma}{2}\widehat{\boldsymbol{\sigma}}\times(\boldsymbol{\omega}_1+\boldsymbol{\omega}_2)\right]. \tag{8}$$

Equations (6) and (8) allow us to evaluate the variation of the total energy (translational plus rotational energy). After some algebra, one gets

$$\Delta E = \frac{m}{2}\left(v_1'^2 + v_2'^2 - v_1^2 - v_2^2\right) + \frac{I}{2}\left(\omega_1'^2 + \omega_2'^2 - \omega_1^2 - \omega_2^2\right) = -m\frac{1-\beta^2}{4}\frac{\kappa}{1+\kappa}\left[\widehat{\boldsymbol{\sigma}}\times\left(\widehat{\boldsymbol{\sigma}}\times\mathbf{g} + \sigma\frac{\boldsymbol{\omega}_1+\boldsymbol{\omega}_2}{2}\right)\right]^2 - m\frac{1-\alpha^2}{4}(\widehat{\boldsymbol{\sigma}}\cdot\mathbf{g})^2. \tag{9}$$

Physics of Fluids ARTICLE scitation.org/journal/phf

The right hand side of Eq. (9) vanishes (and so the total energy is conserved in a collision) when $\alpha = 1$ and $\beta = -1$ (perfectly smooth spheres) and $\alpha = 1$ and $\beta = 1$ (perfectly rough spheres).

As in our previous works on granular suspensions,[27–30,44] the effect of the interstitial gas on the inelastic rough hard spheres is accounted for by the operator $\mathcal{F}$ acting on the velocity distribution function f. In the case that the spheres are perfectly smooth (and so inelasticity only affects the translational degrees of freedom of the spheres), for low Reynolds numbers, the instantaneous fluid force is usually constituted by two terms: (i) a drag force term proportional to the relative velocity $\mathbf{v} - \mathbf{U}_g$ ($\mathbf{U}_g$ being the known mean flow velocity of the background gas) and (ii) a stochastic Langevin-like term modeled as a Gaussian white noise.[45] While the first term (Stokes' law) takes into account the dissipation of energy due to the friction of grains on the viscous gas, the stochastic force gives energy to the solid particles in a random way. This latter term mimics the interaction between the solid particles and the particles of the surrounding (bath) gas. Both terms account for the coupling between the translational degrees of freedom of the spheres and the background gas. Needless to say, one might expect similar effects with the rotational degrees of freedom of grains in the case of inelastic rough spheres.

Therefore, following a generalized Fokker–Planck equation for rotating spheres proposed many years ago by Hess,[33] we write the operator $\mathcal{F}$ acting on f as

$$\mathcal{F}f = \mathcal{F}^{\text{tr}}f + \mathcal{F}^{\text{rot}}f, \tag{10}$$

where $\mathcal{F}^{\text{tr}}$ and $\mathcal{F}^{\text{rot}}$ denote the corresponding Fokker–Planck terms associated with the translational and rotational degrees of freedom of spheres. As usual, the translational part $\mathcal{F}^{\text{tr}}f$ can be written as[27,28,30]

$$\mathcal{F}^{\text{tr}}f = -\gamma_t \frac{\partial}{\partial \mathbf{v}} \cdot (\mathbf{v} - \mathbf{U}_g) f - \gamma_t \frac{T_{\text{ex}}}{m} \frac{\partial^2 f}{\partial v^2}, \tag{11}$$

where γ_t is a drag coefficient associated with the translational degrees of freedom and T_{ex} is the temperature of the interstitial molecular gas. Although γ_t is, in general, a tensor, it may be considered as a scalar proportional to the viscosity of the background fluid $\eta_g \propto \sqrt{T_{\text{ex}}}$ in the case of very dilute suspensions. More specifically, if the diameter of the sphere is very large compared with the mean free path of the viscous gas, then $\gamma_t = 3\pi\sigma\eta_g/m$. It must be noted that the strength of the correlation in the stochastic term of Eq. (11) has been chosen to be consistent with the fluctuation-dissipation theorem when collisions are elastic.[45] Similarly, the rotational part $\mathcal{F}^{\text{rot}}f$ has an analogous structure to Eq. (11), except that the linear velocity $\mathbf{v}$ is replaced by the angular velocity $\boldsymbol{\omega}$. It is given by[33]

$$\mathcal{F}^{\text{rot}}f = -\gamma_r \frac{\partial}{\partial \boldsymbol{\omega}} \cdot \boldsymbol{\omega} f - \gamma_r \frac{T_{\text{ex}}}{m} \frac{\partial^2 f}{\partial \omega^2}, \tag{12}$$

where $\gamma_r = \pi\sigma^3\eta_g/I$. Note that in contrast to $\mathcal{F}^{\text{tr}}$, the "drag" term of $\mathcal{F}^{\text{rot}}$ is proportional to the (instantaneous) angular velocity $\boldsymbol{\omega}$; we are assuming for simplicity that the mean angular velocity of the surrounding gas is zero. Moreover, in Eqs. (11) and (12), we are also neglecting a term which takes into account the coupling of translational and rotational motions. This term stems from the transverse force $\mathbf{v} \times \boldsymbol{\omega}$ and was originally proposed in the Brownian model of rotating particles.[33] A consequence of this decoupling is that the solution to the Boltzmann equation from Grad's method[35] in the uniform shear flow problem is defined in terms of a *two-temperature* Maxwellian distribution [see Eqs. (38) and (40)] where the translational and rotational degrees of freedom are not correlated. By using this simple approach, the corresponding contributions to the stress tensor coming from the above transverse force term vanish by symmetry. A simpler version of the generalized Fokker–Planck model (10) has been recently employed to study the colloidal Brazil nut effect in microswimmer mixtures.[34]

According to Eqs. (11) and (12), the Boltzmann kinetic equation (1) can be written as

$$\frac{\partial f}{\partial t} + \mathbf{v} \cdot \nabla f - \gamma_t \Delta \mathbf{U} \cdot \frac{\partial f}{\partial \mathbf{v}} - \gamma_t \frac{\partial}{\partial \mathbf{v}} \cdot \mathbf{V} f - \gamma_t \frac{T_{\text{ex}}}{m} \frac{\partial^2 f}{\partial v^2} - \gamma_r \frac{\partial}{\partial \boldsymbol{\omega}} \cdot \boldsymbol{\omega} f - \gamma_r \frac{T_{\text{ex}}}{I} \frac{\partial^2 f}{\partial \omega^2} = J[f,f]. \tag{13}$$

Here, $\Delta\mathbf{U} = \mathbf{U} - \mathbf{U}_g$,

$$\mathbf{U}(\mathbf{r};t) = \frac{1}{n(\mathbf{r};t)} \int d\mathbf{v} \int d\boldsymbol{\omega}\, \mathbf{v} f(\mathbf{r},\mathbf{v},\boldsymbol{\omega};t) \tag{14}$$

is the mean flow velocity of spheres, $\mathbf{V} = \mathbf{v} - \mathbf{U}$ is the translational peculiar velocity, and

$$n(\mathbf{r};t) = \int d\mathbf{v} \int d\boldsymbol{\omega}\, f(\mathbf{r},\mathbf{v},\boldsymbol{\omega};t) \tag{15}$$

is the number density.

It is quite apparent that the collision dynamics of the suspension model (13) is not affected by the presence of the background gas (namely, the form of the Boltzmann collision operator is the same as that of a *dry* granular gas), and hence, we neglect the inertia of the gas phase. As has been widely discussed in several papers on suspensions,[22,23,46–48] the above-mentioned approximation requires that the stresses exerted by the molecular gas on the inelastic rough spheres are sufficiently small to assume that they have a mild impact on the motion of grains. As the particle density decreases with respect to the gas/fluid density (for instance, glass beads in liquid water), the inertia of the gas phase is not negligible, and hence, the presence of the background gas must be considered in the Boltzmann collision operator.

B. Balance equations

The transfer equation for an arbitrary dynamic property $\psi(\mathbf{r}, \mathbf{v}, \boldsymbol{\omega}, t)$ can be obtained by multiplying both sides of the Boltzmann equation (13) by ψ and integrating over $\mathbf{v}$ and $\boldsymbol{\omega}$. In order to obtain the transfer equation, an useful property of the Boltzmann collision operator is[42]

$$\mathcal{J}[\psi|f,f] \equiv \int d\mathbf{v}_1 \int d\boldsymbol{\omega}_1 \psi(\mathbf{r},\mathbf{v}_1,\boldsymbol{\omega}_1) J[\mathbf{v}_1,\boldsymbol{\omega}_1|f,f] = \sigma^2 \int d\mathbf{v}_1 \int d\boldsymbol{\omega}_1 \int d\mathbf{v}_2 \int d\boldsymbol{\omega}_2 \int d\widehat{\boldsymbol{\sigma}}\, \Theta(\widehat{\boldsymbol{\sigma}} \cdot \mathbf{g}) \times (\widehat{\boldsymbol{\sigma}} \cdot \mathbf{g}) \left[\psi(\mathbf{r},\mathbf{v}_1',\boldsymbol{\omega}_1') - \psi(\mathbf{r},\mathbf{v}_1,\boldsymbol{\omega}_1)\right], \tag{16}$$

Physics of Fluids ARTICLE scitation.org/journal/phf

where the collisional rules for the direct collision are given by Eqs. (6) and (8).

The evolution equation for the average

$$\langle\psi\rangle = \frac{1}{n(\mathbf{r},t)}\int d\mathbf{v}\int d\boldsymbol{\omega}\,\psi(\mathbf{r},\mathbf{v},\boldsymbol{\omega};t)f(\mathbf{r},\mathbf{v},\boldsymbol{\omega};t) \tag{17}$$

can be now easily obtained with the result

$$\begin{aligned}&\frac{\partial}{\partial t}(n\langle\psi\rangle) - n\left\langle\frac{\partial\psi}{\partial t}\right\rangle + \nabla\cdot(n\langle\mathbf{v}\psi\rangle) - n\langle\mathbf{v}\cdot\nabla\psi\rangle\\ &\quad + n\gamma_t\Delta\mathbf{U}\cdot\left\langle\frac{\partial\psi}{\partial\mathbf{v}}\right\rangle + n\gamma_t\left\langle\mathbf{V}\cdot\frac{\partial\psi}{\partial\mathbf{v}}\right\rangle - n\frac{\gamma_t T_{\rm ex}}{m}\left\langle\frac{\partial^2\psi}{\partial v^2}\right\rangle\\ &\quad + n\gamma_r\left\langle\boldsymbol{\omega}\cdot\frac{\partial\psi}{\partial\boldsymbol{\omega}}\right\rangle - n\frac{\gamma_r T_{\rm ex}}{I}\left\langle\frac{\partial^2\psi}{\partial\omega^2}\right\rangle = \mathcal{J}[\psi|f,f].\end{aligned} \tag{18}$$

The macroscopic balance equations for the densities of mass, momentum, and energy can be obtained from the transfer equation (18) when $\psi \equiv \{1, m\mathbf{v}, mV^2/2 + I\omega^2/2\}$. They are given by

$$D_t n + n\nabla\cdot\mathbf{U} = 0, \tag{19}$$

$$\rho D_t\mathbf{U} = -\rho\gamma_t\Delta\mathbf{U} - \nabla\cdot\mathsf{P}, \tag{20}$$

$$\begin{aligned}&D_t T + \gamma_t(T_t - T_{\rm ex}) + \gamma_r(T_r - T_{\rm ex})\\ &\quad = -\zeta T - \frac{1}{3n}(\nabla\cdot\mathbf{q} + \mathsf{P}:\nabla\mathbf{U}).\end{aligned} \tag{21}$$

In Eqs. (19)–(21), $\rho = mn$ is the mass density, $D_t \equiv \partial_t + \mathbf{U}\cdot\nabla$ is the material time derivative, and the granular temperature $T(\mathbf{r}, t)$ is defined as

$$T = \frac{1}{2}(T_t + T_r), \tag{22}$$

where the (partial) translational T_t and rotational T_r temperatures are defined as

$$T_t = \frac{m}{3}\langle V^2\rangle, \quad T_r = \frac{I}{3}\langle\omega^2\rangle, \tag{23}$$

where the averages $\langle\cdots\rangle$ are defined by Eq. (17). Moreover, the pressure tensor $\mathsf{P}(\mathbf{r}, t)$ is

$$\mathsf{P} = \rho\langle\mathbf{V}\mathbf{V}\rangle, \tag{24}$$

while the heat flux vector $\mathbf{q}(\mathbf{r}, t)$ is given by

$$\mathbf{q} = \mathbf{q}_t + \mathbf{q}_r, \tag{25}$$

where the translational $\mathbf{q}_t$ and rotational $\mathbf{q}_r$ contributions are defined as

$$\mathbf{q}_t = \frac{\rho}{2}\langle V^2\mathbf{V}\rangle, \quad \mathbf{q}_r = \frac{In}{2}\langle\omega^2\mathbf{V}\rangle. \tag{26}$$

Moreover, the cooling rate ζ (which gives the rate of energy dissipation due to inelasticity) is

$$\zeta = \frac{T_t}{2T}\zeta_t + \frac{T_r}{2T}\zeta_r, \tag{27}$$

where the partial energy production rates associated with the translational (ζ_t) and rotational (ζ_r) degrees of freedom are

$$\zeta_t = -\frac{m}{3nT_t}\mathcal{J}[v^2|f,f], \quad \zeta_r = -\frac{I}{3nT_r}\mathcal{J}[\omega^2|f,f]. \tag{28}$$

One third of the trace of the pressure tensor P defines the hydrostatic pressure p as

$$p = nT_t. \tag{29}$$

At a kinetic theory level, it is also convenient to derive the balance equations for the partial temperatures T_t and T_r. They are given by

$$D_t T_t + 2\gamma_t(T_t - T_{\rm ex}) + \zeta_t T_t = -\frac{2}{3n}\left(\nabla\cdot\mathbf{q}_t + \mathsf{P}:\nabla\mathbf{U}\right), \tag{30}$$

$$D_t T_r + 2\gamma_r(T_r - T_{\rm ex}) + \zeta_r T_r = -\frac{2}{3n}\nabla\cdot\mathbf{q}_r. \tag{31}$$

Combination of Eqs. (30) and (31) leads to Eq. (21).

Before finishing this section, it is worth remarking that in the definition of T_r [second relation of Eq. (23)], we have not referred the angular velocities $\boldsymbol{\omega}$ to the mean value $\boldsymbol{\Omega} = \langle\boldsymbol{\omega}\rangle$. This contrasts with the definition of T_t [first relation of Eq. (23)] where the (instantaneous) velocity $\mathbf{v}$ has been referred to $\mathbf{U}$. As noted in previous works,[43] we have not defined T_r in terms of the difference $\boldsymbol{\omega} - \boldsymbol{\Omega}$ because $\boldsymbol{\Omega}$ is not a conserved quantity. In the case that we defined the rotational temperature as $\widetilde{T}_r = \frac{I}{3}\langle(\boldsymbol{\omega} - \boldsymbol{\Omega})^2\rangle$, the granular temperature $\widetilde{T} = (\widetilde{T}_t + \widetilde{T}_r)/2$ would not be a conserved hydrodynamic field in the case of elastic ($\alpha = 1$) and completely rough ($\beta = 1$) spheres, although the total energy is conserved in collisions [see Eq. (9), where $\Delta E = 0$ if $\alpha = \beta = 1$].

III. SIMPLE SHEAR FLOW

We assume that the inertial suspension is under simple (uniform) shear flow. As described in many previous works,[42] this state is macroscopically characterized by a constant number density n, a uniform granular temperature $T(t)$, and a macroscopic velocity field

$$U_i = a_{ij}r_j, \quad a_{ij} = a\delta_{ix}\delta_{jy}, \tag{32}$$

with a being the *constant* shear rate. We also assume that the mean angular velocity $\boldsymbol{\Omega} = \mathbf{0}$ and, as usual in uniform sheared suspensions, the average (linear) velocity of particles follow the velocity of the fluid phase: $\mathbf{U} = \mathbf{U}_g$. At a microscopic level, the main advantage of the simple shear flow is that this state becomes spatially homogeneous when the velocities of the particles $\mathbf{v}$ are referred to the frame moving with the linear velocity field $\mathbf{U}$.[49,50] In this frame, the distribution function has the form $f(\mathbf{r}, \mathbf{v}, \boldsymbol{\omega}; t) = f(\mathbf{V}, \boldsymbol{\omega}; t)$, and hence, the Boltzmann equation (13) becomes

$$\begin{aligned}&\frac{\partial f}{\partial t} - aV_y\frac{\partial f}{\partial V_x} - \gamma_t\frac{\partial}{\partial\mathbf{v}}\cdot\mathbf{V}f - \gamma_t\frac{T_{\rm ex}}{m}\frac{\partial^2 f}{\partial v^2}\\ &\quad - \gamma_r\frac{\partial}{\partial\boldsymbol{\omega}}\cdot\boldsymbol{\omega}f - \gamma_r\frac{T_{\rm ex}}{I}\frac{\partial^2 f}{\partial\omega^2} = J[f,f].\end{aligned} \tag{33}$$

Physics of Fluids ARTICLE scitation.org/journal/phf

Since $\nabla n = \nabla T = 0$, the heat flux vanishes ($\mathbf{q} = \mathbf{0}$) in the simple shear flow and the (uniform) pressure tensor P is the relevant irreversible flux of the problem. The knowledge of P allows us to identify the most significant non-Newtonian transport properties of the suspension.

In the simple shear flow problem, the conservation equations (19) and (20) apply trivially while the balance equations (30) and (31) for the translational T_t and rotational T_r temperatures, respectively, yield

$$\frac{\partial T_t}{\partial t} + 2\gamma_t(T_t - T_{\text{ex}}) + \zeta_t T_t = -\frac{2a}{3n}P_{xy}, \tag{34}$$

$$\frac{\partial T_r}{\partial t} + 2\gamma_r(T_r - T_{\text{ex}}) + \zeta_r T_r = 0. \tag{35}$$

Note that the (partial) energy production rates ζ_t and ζ_r are defined in terms of the velocity distribution function $f(\mathbf{V}, \boldsymbol{\omega})$ [see Eq. (28)]. This means that one has necessarily to get a solution of the Boltzmann equation (33) to determine ζ_t and ζ_r and the stress tensor P_{xy}. Once the above quantities are known, then the partial temperatures T_t and T_r can be obtained by solving Eqs. (34) and (35).

According to Eqs. (34) and (35), there are two competing mechanisms in the time evolution of the temperature. On the one hand, there are cooling terms arising from inelastic cooling and the friction of grains on viscous gas. On the other hand, there are heating terms arising from the viscous heating and the energy provided to the particles by the stochastic driving term. After a transient period, one expects that both mechanisms compensate for each other and a *steady* state is achieved.

In the absence of shear rate ($a = 0$) and in the steady state ($\partial_t f = 0$), for $\alpha = 1$ and $|\beta| = 1$, the total kinetic energy is conserved, and the solution to Eq. (33) is given by the following Maxwellian velocity distribution:

$$f_{\text{M}}(\mathbf{V}, \boldsymbol{\omega}) = n\left(\frac{mI}{4\pi^2 T_{\text{ex}}^2}\right)^{3/2} \exp\left(-\frac{mv^2}{2T_{\text{ex}}}\right)\exp\left(-\frac{I\omega^2}{2T_{\text{ex}}}\right). \tag{36}$$

On the other hand, beyond the above-mentioned two special cases, the solution to Eq. (33) is not known.

The relevant elements of the pressure tensor may be obtained by multiplying both sides of Eq. (33) by mV_kV_ℓ and integrating over $\mathbf{V}$ and $\boldsymbol{\omega}$. The result is

$$\partial_t P_{k\ell} + a_{kj}P_{\ell j} + a_{j\ell}P_{jk} + 2\gamma_t(P_{k\ell} - nT_{\text{ex}}\delta_{k\ell}) = m\mathcal{J}[V_kV_\ell|f,f]. \tag{37}$$

On the other hand, the exact form of $\mathcal{J}[V_kV_\ell|f,f]$ is not known, even in the simplest case $\alpha = 1$ and $\beta = \pm 1$ where the kinetic energy is conserved in collisions. Thus, one has to resort to alternative approaches for computing the pressure tensor P_{ij}. As mentioned in the Introduction, we will determine the elements of the pressure tensor by using two different but complementary routes: (i) by solving the Boltzmann equation by means of Grad's moment method and (ii) by considering a BGK-like kinetic model recently proposed[36] for inelastic rough hard spheres.

IV. GRAD'S MOMENT METHOD

As has been clearly shown in several previous works,[24,27,28,51] Grad's moment method can be considered an accurate tool to estimate the collisional moment $\mathcal{J}[V_kV_\ell|f,f]$. In the same way as in molecular fluids,[35] the idea of Grad's method is to expand the velocity distribution function in powers of generalized Hermite polynomials, the coefficients of the expansion being the corresponding velocity moments. This expansion is truncated at a given order k; therefore, the moments of degree higher than k are neglected in the corresponding solution. In the case of a three-dimensional gas, the usual thirteen-moment approximation includes the density n, the three components of the mean flow velocity $\mathbf{U}$, the six elements of the pressure tensor P [recall that $T_t = (1/3n)(P_{xx} + P_{yy} + P_{zz})$], and the three components of the heat flux vector $\mathbf{q}$.[35,52] Since the heat flux vanishes in the simple shear flow problem, Grad's solution is given by[37,53]

$$f(\mathbf{V}, \boldsymbol{\omega}) \to f_0(\mathbf{V}, \boldsymbol{\omega})\left[1 + \frac{m}{2nT_t^2}\left(V_iV_j - \frac{1}{3}V^2\delta_{ij}\right)\Pi_{ij}\right], \tag{38}$$

where

$$\Pi_{ij} = P_{ij} - p\delta_{ij} \tag{39}$$

is the traceless part of the pressure tensor and f_0 is the *two-temperature* Maxwellian velocity distribution,

$$f_0(\mathbf{V}, \boldsymbol{\omega}) = n\left(\frac{mI}{4\pi^2 T_t T_r}\right)^{3/2} \exp\left(-\frac{mV^2}{2T_t}\right)\exp\left(-\frac{I\omega^2}{2T_r}\right). \tag{40}$$

Upon writing the distribution (38), we have ignored the possible contributions to f coming from the combination of traceless dyadic products of the three vectors $\mathbf{V}$, $(\mathbf{V}\cdot\boldsymbol{\omega})$, and $\mathbf{V}\times\boldsymbol{\omega}$ with unknown scalar coefficients.[54] These contributions are absent because we have neglected the orientational correlations between $\mathbf{V}$ and $\boldsymbol{\omega}$ in the Fokker–Planck operator $\mathcal{F}$ [see Eqs. (10)–(12)]. Thanks to this simplification, we resort to the weight distribution f_0, which is isotropic in velocity space. In addition, we have also neglected in Grad's solution (40) the contribution of the fourth-degree velocity moments (cumulants) to the distribution f. These cumulants have been determined in homogeneous situations,[55–57] showing that, in general, these quantities are small, especially when the system is driven by a white-noise stochastic thermostat.[55,57] On the other hand, despite the above-mentioned approximations, it is worth noting that the theoretical predictions for the temperature ratio T_r/T_t obtained by replacing f by f_0 in homogeneous states have been shown to compare very well with Monte Carlo and molecular dynamics simulations.[56] We expect that this fair agreement is also kept in the simple shear flow state.

The collisional moment $\mathcal{J}[V_kV_\ell|f,f]$ can be computed when the trial distribution (38) is inserted into the definition of this moment. The calculations are long but standard and are based on the relationship (16). After some algebra, one gets[37,54]

$$m\mathcal{J}[V_kV_\ell|f,f] = -\nu_\eta\Pi_{k\ell} - p\zeta_t\delta_{k\ell}, \tag{41}$$

where we recall that $p = nT_t$, and

Physics of Fluids ARTICLE scitation.org/journal/phf

$$\nu_\eta = \left[\left(\widetilde{\alpha}+\widetilde{\beta}\right)\left(2-\widetilde{\alpha}-\widetilde{\beta}\right)+\frac{\widetilde{\beta}^2}{6\kappa}\frac{T_r}{T_t}\right]\nu_t, \tag{42}$$

$$\zeta_t = \frac{5}{3}\left[\widetilde{\alpha}(1-\widetilde{\alpha})+\widetilde{\beta}(1-\widetilde{\beta})-\frac{\widetilde{\beta}^2}{\kappa}\frac{T_r}{T_t}\right]\nu_t. \tag{43}$$

In Eqs. (42) and (43),

$$\widetilde{\alpha} = \frac{1+\alpha}{2}, \quad \widetilde{\beta} = \frac{\kappa}{1+\kappa}\frac{1+\beta}{2}, \tag{44}$$

and ν_t is the effective collision frequency

$$\nu_t = \frac{16}{5}n\sigma^2\sqrt{\frac{\pi T_t}{m}}. \tag{45}$$

In addition, the cooling rate ζ_r associated with the rotational degrees of freedom [defined by the second relation of Eq. (28)] can be also determined from Grad's distribution (38) with the result[37,54]

$$\zeta_r = \frac{5}{6}\frac{\widetilde{\beta}}{\kappa}\left[1-\beta+2\widetilde{\beta}\left(1-\frac{T_t}{T_r}\right)\right]\nu_t. \tag{46}$$

Upon deriving Eq. (41), nonlinear terms in the tensor $\Pi_{k\ell}$ have been neglected. Equation (37) can be more explicitly written when the expression (41) is accounted for. The result is

$$\begin{aligned}&\partial_t P_{k\ell} + a_{kj}P_{j\ell} + a_{\ell j}P_{jk} + 2\gamma_t\left(P_{k\ell} - nT_{\rm ex}\delta_{k\ell}\right)\\ &\quad = -\nu_\eta P_{k\ell} - p(\zeta_t - \nu_\eta)\delta_{k\ell}.\end{aligned} \tag{47}$$

Equation (47) clearly shows that $P_{yy} = P_{zz}$, and hence, the constraint (29) yields $P_{xx} = 3p - 2P_{yy}$. The equality $P_{yy} = P_{zz}$ does not agree with computer simulation results obtained for smooth granular suspensions.[22,24] The above-mentioned drawback could be fixed if one would retain nonlinear terms in $\Pi_{k\ell}$ in the evaluation of $\mathcal{J}[V_kV_\ell|f,f]$. The inclusion of these nonlinear corrections provides nonzero contributions to the normal stress differences in the plane orthogonal to the shear flow (namely, $P_{yy} - P_{zz} \neq 0$).[24] However, the difference $P_{yy} - P_{zz}$ is, in general, very small; therefore the expression (41) can be still considered as a good approximation.

It is convenient now to introduce dimensionless quantities. Among the different possibilities, as in previous works on sheared granular suspensions,[27,28,30] we scale the quantities associated with the solid particles with those referring to the gas phase, namely, γ_t, γ_r, and $T_{\rm ex}$. Since the pressure tensor (which is the most relevant flux in the simple shear flow state) is mainly related to the translational degrees of freedom, we reduce here the shear rate and the external temperature with respect to the (translational) friction coefficient γ_t, namely,

$$a^* \equiv \frac{a}{\gamma_t}, \quad T_{\rm ex}^* \equiv \frac{T_{\rm ex}}{m\sigma^2\gamma_t^2}. \tag{48}$$

In addition, the translational and rotational temperatures are scaled with respect to $T_{\rm ex}$ ($\theta_t \equiv T_t/T_{\rm ex}$ and $\theta_r \equiv T_r/T_{\rm ex}$), and we introduce the dimensionless quantities

$$\zeta_t^* \equiv \frac{\zeta_t}{\sqrt{\theta_t}\gamma_t} = \frac{16}{3}\sqrt{\pi}\left[\widetilde{\alpha}(1-\widetilde{\alpha})+\widetilde{\beta}(1-\widetilde{\beta})-\frac{\widetilde{\beta}^2}{\kappa}\frac{\theta_r}{\theta_t}\right]n^*\sqrt{T_{\rm ex}^*}, \tag{49}$$

$$\nu_\eta^* \equiv \frac{\nu_\eta}{\sqrt{\theta_t}\gamma_t} = \frac{16}{5}\sqrt{\pi}\left[\left(\widetilde{\alpha}+\widetilde{\beta}\right)\left(2-\widetilde{\alpha}-\widetilde{\beta}\right)+\frac{\widetilde{\beta}^2}{6\kappa}\frac{\theta_r}{\theta_t}\right]n^*\sqrt{T_{\rm ex}^*}. \tag{50}$$

Here, $n^* \equiv n\sigma^3$ is the reduced density. As already noted in previous studies,[30] the explicit dependence of ζ_t^* and ν_η^* on density comes from the dimensionless quantities a^* and $T_{\rm ex}^*$. This way of reducing the above-mentioned quantities is closer to the one made in computer simulations for smooth inelastic hard spheres.[27,28] Needless to say, if you had reduced a and $T_{\rm ex}$ with the collision frequency ν_t (this sort of scaling is usual in sheared molecular gases[58]), the above-mentioned density dependence had been removed. Note that ζ_t^* and ν_η^* are independent of both the (translational) temperature T_t and the background temperature $T_{\rm ex}$ because $\gamma_t \propto \sqrt{T_{\rm ex}}$.

In terms of the above-mentioned dimensionless variables, Eq. (47) becomes

$$\begin{aligned}&\partial_\tau P_{k\ell}^* + a_{kj}^*P_{j\ell}^* + a_{\ell j}^*P_{jk}^* + 2\left(P_{k\ell}^* - \delta_{k\ell}\right)\\ &\quad = -\nu_\eta^*\sqrt{\theta_t}P_{k\ell}^* - \theta_t\sqrt{\theta_t}\left(\zeta_t^* - \nu_\eta^*\right)\delta_{k\ell},\end{aligned} \tag{51}$$

where we have introduced the (scaled) time variable τ defined as $d\tau = \gamma_t dt$.

A. Steady state solution

As said before, after a transient regime, one expects that the suspension reaches a *steady* state. The interesting point is that this steady sheared state is inherently non-Newtonian.[59] The main goal of this paper is to determine the rheological properties of the inertial suspension in the steady uniform shear flow.

An inspection of the results derived in the smooth case[30] shows that Eq. (51) (with $\partial_\tau P_{k\ell}^* = 0$) is formally equivalent to that of this limit case when one makes the changes $\theta \to \theta_t$, $\zeta^* \to \zeta_t^*$, and $\nu_{0|2}^* \to \nu_\eta^*$, where the quantities θ, ζ^*, and $\nu_{0|2}^*$ are defined in Ref. 30. Consequently, the expressions of P_{yy}^*, P_{xy}^*, and a^* can be obtained from comparison with those obtained in the smooth case [see Eqs. (32), (33), and (35) of Ref. 30]. They are given by

$$P_{yy}^* = P_{zz}^* = \frac{2+\left(\nu_\eta^* - \zeta_t^*\right)\theta_t\sqrt{\theta_t}}{2+\sqrt{\theta_t}\nu_\eta^*}, \quad P_{xx}^* = 3\theta_t - 2P_{yy}^*, \tag{52}$$

$$P_{xy}^* = -\frac{2+\left(\nu_\eta^* - \zeta_t^*\right)\theta_t\sqrt{\theta_t}}{\left(2+\sqrt{\theta_t}\nu_\eta^*\right)^2}a^*, \tag{53}$$

$$a^* = \sqrt{\frac{3}{2}\frac{\sqrt{\theta_t}\zeta_t^* + 2\left(1-\theta_t^{-1}\right)}{\sqrt{\theta_t}\left(\nu_\eta^* - \zeta_t^*\right) + 2\theta_t^{-1}}}\left(2+\sqrt{\theta_t}\nu_\eta^*\right). \tag{54}$$

The steady (reduced) temperatures θ_t and θ_r can be determined from Eqs. (34) and (35) (with $\partial_t\theta_t = \partial_t\theta_r = 0$) as

Physics of Fluids ARTICLE scitation.org/journal/phf

$$2(\theta_t - 1) + \sqrt{\theta_t}\theta_t\zeta_t^* = -\frac{2}{3}a^* P_{xy}^*, \tag{55}$$

$$2\frac{\gamma_r}{\gamma_t}(\theta_r - 1) + \sqrt{\theta_t}\theta_r\zeta_r^* = 0, \tag{56}$$

where $\gamma_r/\gamma_t = 4/(3\kappa)$ and

$$\zeta_r^* \equiv \frac{\zeta_r}{\sqrt{\theta_t}\gamma_t} = \frac{8}{3}\sqrt{\pi}\frac{\widetilde{\beta}}{\kappa}\left[1 - \beta + 2\widetilde{\beta}\left(1 - \frac{\theta_t}{\theta_r}\right)\right]n^*\sqrt{T_{\text{ex}}^*}. \tag{57}$$

On the other hand, as already happens in smooth granular suspensions,[27,28,30] it is not possible to express in Eq. (54) θ_t in terms of a^* and the remaining parameters of the suspension. Thus, for given values of α, β, κ, n^*, and T_{ex}^*, one can consider θ_t, for instance, as an input parameter and determine a^* and θ_r as the solutions to Eqs. (54) and (56).

Once the (scaled) translational temperature θ_t is known, the rheological properties of the suspension are obtained from Eqs. (52), (53), and (56). In particular, the (dimensionless) non-Newtonian shear viscosity

$$\eta^* = \frac{P_{xy}^*}{a^*} \tag{58}$$

is given by

$$\eta^* = \frac{2 + \left(\nu_\eta^* - \zeta_t^*\right)\sqrt{\theta_t}\theta_t}{\left(2 + \sqrt{\theta_t}\nu_\eta^*\right)^2}. \tag{59}$$

Since (linear) Grad's solution (51) yields $P_{yy}^* = P_{xx}^*$, the only nonvanishing viscometric function is the one associated with the difference $P_{xx}^* - P_{yy}^*$. In the dimensionless form, the first viscometric function is defined as

$$\Psi^* = P_{xx}^* - P_{yy}^* = 3\theta_t\frac{2\left(1 - \theta_t^{-1}\right) + \sqrt{\theta_t}\zeta_t^*}{2 + \sqrt{\theta_t}\nu_\eta^*}. \tag{60}$$

As expected, the expressions (54), (59), and (60) agree with the ones derived for inelastic Maxwell models[30] [see Eqs. (35), (39), and (40) of Ref. 30] when one makes the replacements $\theta_t \to \theta$, $\zeta_t^* \to \zeta^*$, and $\nu_\eta^* \to \nu_{\eta|2}^*$, where the quantities θ, ζ^*, and $\nu_{\eta|2}^*$ are defined in Ref. 30.

B. Navier–Stokes results

In order to get analytical results, it is illustrative to consider the limits of small and large shear rates. First, when $a^* \to 0$, Eq. (54) yields the following relation for determining the (translational) temperature $\theta_t^{(0)}$:

$$\theta_t^{(0)}\left(1 + \frac{1}{2}\zeta_t^*\sqrt{\theta_t^{(0)}}\right) - 1 = 0. \tag{61}$$

The rotational temperature $\theta_r^{(0)}$ is easily obtained from Eq. (56) as

$$\theta_r^{(0)} = \left(1 + \frac{1}{2}\frac{\gamma_t}{\gamma_r}\zeta_r^*\sqrt{\theta_t^{(0)}}\right)^{-1}. \tag{62}$$

Substitution of Eq. (61) into Eq. (59) gives the following form of the Navier–Stokes shear viscosity η_{NS}^*:

$$\eta_{\text{NS}}^* = \frac{\theta_t^{(0)}}{2 + \sqrt{\theta_t^{(0)}}\nu_\eta^*}. \tag{63}$$

In the opposite limit ($a^* \to \infty$), the asymptotic expressions for $\zeta_t^* \neq 0$, $\alpha < 1$, and $|\beta| \neq 1$ are

$$\theta_t^{(\infty)} = \frac{2}{3}\frac{\nu_\eta^* - \zeta_t^*}{\nu_\eta^{*2}\zeta_t^*}a^{*2}, \quad \eta_\infty^* = \sqrt{\frac{3}{2}}\frac{\left(\nu_\eta^* - \zeta_t^*\right)^{3/2}}{\nu_\eta^{*3/2}\sqrt{\zeta_t^*}}a^*. \tag{64}$$

When $\zeta_t^* = 0$, one has $\theta_t^{(\infty)} = a^{*4}/(9\nu_\eta^{*2})$ and $\eta_\infty^* = a^{*2}/(3\nu_\eta^{*2})$. The corresponding expressions for η_∞^* can be obtained from (63) by replacing $\theta_t^{(0)}$ by $\theta_t^{(\infty)}$.

Similarly to suspensions of smooth inelastic hard spheres,[27,28,30] Eqs. (63) and (64) clearly show that while η^* is finite in the Navier–Stokes domain, it diverges for very large shear rates. In fact, the ratio $\eta^*(a^* \to \infty)/\eta^*(a^* \to 0)$ becomes very large as the shear rate increases; this could explain the existence of DST of the shear viscosity coefficient. As mentioned in Sec. I, this behavior gradually changes as the density increases since the theoretical results derived from the Enskog kinetic theory (and confirmed by molecular dynamics simulations) show CST for finite densities.[27,28]

Although we are mainly in this paper interested in non-Newtonian transport properties, Eq. (63) gives the expression of the Navier–Stokes shear viscosity coefficient of a suspension of inelastic rough hard spheres. We are not aware of any previous derivation of this relevant transport coefficient. On the other hand, in the absence of the interstitial gas (*dry* granular gas), the Navier–Stokes shear viscosity coefficient was obtained in Ref. 54. Its explicit form is

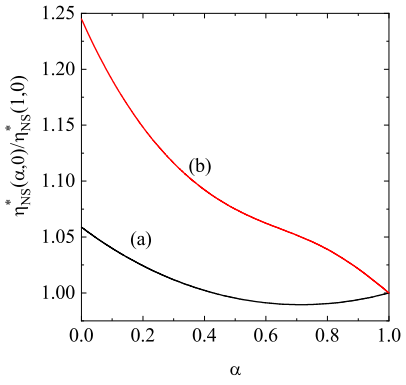

FIG. 1. Plot of the ratio $\eta_{\text{NS}}^*(\alpha)/\eta_{\text{NS}}^*(1)$ vs the coefficient of normal restitution α for granular suspensions (a) and dry granular gases (b). Here, we have assumed spheres with a uniform mass distribution ($\kappa = \frac{2}{5}$) and a coefficient of tangential restitution $\beta = 0$.

Physics of Fluids ARTICLE scitation.org/journal/phf

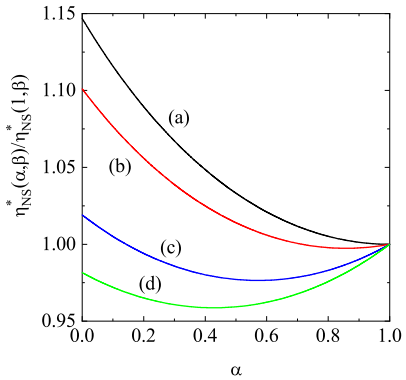

FIG. 2. Plot of the ratio $\eta^*_{NS}(\alpha,\beta)/\eta^*_{NS}(1,\beta)$ vs the coefficient of normal restitution α for $\kappa = \frac{2}{5}$ and four different values of the coefficient of tangential restitution β: $\beta = -1$ (a), $\beta = -0.5$ (b), $\beta = 0.5$ (c), and $\beta = 1$ (d). Here, $\eta^*_{NS}(1,\beta)$ is given by Eq. (63) with $\alpha = 1$.

provided in the Appendix for the sake of completeness. It is quite apparent that the form of the Navier–Stokes shear viscosity of a dry gas of inelastic rough hard spheres [see Eq. (A1)] differs from the one derived here [see Eq. (63)], as expected. To illustrate these differences with and without interstitial gas, Fig. 1 shows the α-dependence of the ratios $\eta^*_{NS}(\alpha)/\eta^*_{NS}(1)$ for granular suspensions [line (a)] and dry granular gases [line (b)]. In the dry case, $\eta^*_{NS} = \eta_{NS}\nu_t/(nT_t)$. In Fig. 1, $\kappa = \frac{2}{5}$, $\beta = 0$, and $\eta^*_{NS}(1)$ refers to the value of the shear viscosity at $\alpha = 1$. We observe that the dependence of the ratio $\eta^*_{NS}(\alpha)/\eta^*_{NS}(1)$ on α is very different in both systems, even at a qualitative level since, while this ratio exhibits a non-monotonic dependence on the coefficient of normal restitution in the case of granular suspensions, it increases with decreasing α in the dry granular case. Regarding granular suspensions and to show the combined effect of α and β on η^*_{NS}, Fig. 2 plots the ratio $\eta^*_{NS}(\alpha,\beta)/\eta^*_{NS}(1,\beta)$ as a function of α for different values of β. We observe that, at fixed α, the above ratios present a monotonic β-dependence since those coefficients decrease from $\beta = -1$ to $\beta = 1$. In addition, at fixed β, we see that while those coefficients increase with decreasing α when β is negative, they exhibit a non-monotonic dependence on α when β is positive. In any case, Fig. 2 highlights the intricate interplay between the coefficients of restitution α and β on the behavior of the Navier–Stokes shear viscosity coefficient.

V. BGK-LIKE KINETIC MODEL OF THE BOLTZMANN EQUATION

To complement the results derived from the Boltzmann equation from Grad's moment method, we consider now a BGK-like kinetic model for a granular gas of inelastic rough hard spheres.[36] As usual in kinetic models, the intricate mathematical structure of the Boltzmann collision operator $J[\mathbf{v},\boldsymbol{\omega}|f,f]$ is replaced by a simpler term $K[\mathbf{v},\boldsymbol{\omega}|f]$ that retains the basic physical properties of the true Boltzmann operator. More specifically, $J[f,f]$ is substituted by the sum of three terms:[36] (i) a relaxation term toward a two-temperature local equilibrium distribution, (ii) a nonconservative drag force proportional to $\mathbf{V}$, and (iii) a nonconservative torque equal to a linear combination of $\boldsymbol{\omega}$ and $\boldsymbol{\Omega}$. In the context of the simple shear flow problem, the operator $K[\mathbf{v},\boldsymbol{\omega}|f]$ becomes

$$K[\mathbf{v},\boldsymbol{\omega}|f] = -\chi(\alpha,\beta)\nu_t(f - f_0) + \frac{\zeta_t}{2}\frac{\partial}{\partial\mathbf{V}}\cdot(\mathbf{V}f) + \frac{\zeta_r}{2}\frac{\partial}{\partial\boldsymbol{\omega}}\cdot(\boldsymbol{\omega}f), \tag{65}$$

where ν_t is the collision frequency defined by Eq. (45), f_0 is given by Eq. (40), and the forms of ζ_t and ζ_r are provided by Eqs. (43) and (46), respectively. Moreover, the quantity $\chi(\alpha,\beta)$ can be seen as a free parameter of the model to be adjusted to agree with some property of interest of the Boltzmann equation. With the replacement (65), the BGK-like model for the granular suspension in the steady state reads

$$-aV_y\frac{\partial f}{\partial V_x} - \lambda_t\frac{\partial}{\partial\mathbf{v}}\cdot\mathbf{V}f - \gamma_t\frac{T_{ex}}{m}\frac{\partial^2 f}{\partial v^2} - \lambda_r\frac{\partial}{\partial\boldsymbol{\omega}}\cdot\boldsymbol{\omega}f - \gamma_r\frac{T_{ex}}{I}\frac{\partial^2 f}{\partial\omega^2} = -\chi\nu_t(f - f_0), \tag{66}$$

where

$$\lambda_t \equiv \gamma_t + \frac{\zeta_t}{2}, \quad \lambda_r \equiv \gamma_r + \frac{\zeta_r}{2}. \tag{67}$$

The use of the BGK-like model allows us to determine not only the rheological properties (which are connected with the elements of the pressure tensor) but also all the velocity moments of the velocity distribution function. For a three-dimensional system, it is convenient in the simple shear flow problem to define the general velocity moments

$$M_{k_1,k_2,k_3} = \int d\boldsymbol{\omega}\int d\mathbf{V}\, V_x^{k_1}V_y^{k_2}V_z^{k_3}f(\mathbf{V},\boldsymbol{\omega}). \tag{68}$$

Note that here we are essentially interested in computing the velocity moments of f involving the translational (peculiar) velocities $\mathbf{V}$. To obtain these moments, we multiply both sides of Eq. (37) by $V_x^{k_1}V_y^{k_2}V_z^{k_3}$ and integrate over $\mathbf{V}$ and $\boldsymbol{\omega}$. The result is

$$ak_1M_{k_1-1,k_2+1,k_3} + (\chi\nu_t + k\lambda_t)M_{k_1,k_2,k_3} = N_{k_1,k_2,k_3}, \tag{69}$$

where $k = k_1 + k_2 + k_3$, and

$$N_{k_1,k_2,k_3} = \frac{\gamma_t T_{ex}}{m}R_{k_1,k_2,k_3} + \chi\nu_t M^{L}_{k_1,k_2,k_3}. \tag{70}$$

The quantities R_{k_1,k_2,k_3} and $M^{L}_{k_1,k_2,k_3}$ are defined, respectively, as

$$R_{k_1,k_2,k_3} = \int d\boldsymbol{\omega}\int d\mathbf{V}\, f(\mathbf{V},\boldsymbol{\omega})\frac{\partial^2}{\partial V^2}\left(V_x^{k_1}V_y^{k_2}V_z^{k_3}\right) = k_1(k_1-1)M_{k_1-2,k_2,k_3} + k_2(k_2-1)M_{k_1,k_2-2,k_3} + k_3(k_3-1)M_{k_1,k_2,k_3-2}, \tag{71}$$

Physics of Fluids ARTICLE scitation.org/journal/phf

and

$$M^{\mathrm{L}}_{k_1,k_2,k_3} = n\left(\frac{2T_t}{m}\right)^{k/2}\pi^{-3/2}\Gamma\left(\frac{k_1+1}{2}\right)\Gamma\left(\frac{k_2+1}{2}\right)\Gamma\left(\frac{k_3+1}{2}\right) \tag{72}$$

if k_1, k_2, and k_3 are even, being zero otherwise. As expected, the structure of Eq. (69) is the same as in the smooth case,[30] and hence, the solution to Eq. (69) can be written as

$$M_{k_1,k_2,k_3} = \sum_{q=0}^{k_1}\frac{k_1!}{(k_1-q)!}\frac{(-a)^q}{(\chi\nu_t+k\lambda_t)^{1+q}}N_{k_1-q,k_2+q,k_3}. \tag{73}$$

The (reduced) nonzero elements of the pressure tensor $P^*_{k\ell}$ and the (reduced) shear rate a^* can be easily obtained from Eqs. (70)–(73). Their expressions are

$$P^*_{yy} = \frac{2+\chi\nu_t^*\sqrt{\theta_t}\theta_t}{2+(\chi\nu_t^*+\zeta_t^*)\sqrt{\theta_t}}, \tag{74}$$

$$P^*_{xy} = -\frac{2+\chi\nu_t^*\sqrt{\theta_t}\theta_t}{\left[2+(\chi\nu_t^*+\zeta_t^*)\sqrt{\theta_t}\right]^2}a^*, \tag{75}$$

$$P^*_{xx} = \frac{2+\chi\nu_t^*\sqrt{\theta_t}\theta_t}{2+(\chi\nu_t^*+\zeta_t^*)\sqrt{\theta_t}}\left[1+\frac{2a^{*2}}{\left[2+(\chi\nu_t^*+\zeta_t^*)\sqrt{\theta_t}\right]^2}\right], \tag{76}$$

$$a^* = \sqrt{\frac{d}{2}\frac{\sqrt{\theta_t}\zeta_t^*+2(1-\theta_t^{-1})}{\sqrt{\theta_t}\chi\nu_t^*+2\theta_t^{-1}}}\left[2+\sqrt{\theta_t}\left(\chi\nu_t^*+\zeta_t^*\right)\right], \tag{77}$$

where ζ_t^* is defined by Eq. (49) and

$$\nu_t^* \equiv \frac{\nu_t}{\sqrt{\theta_t}\gamma_t} = \frac{16}{5}\sqrt{\pi}n^*\sqrt{T^*_{\mathrm{ex}}}. \tag{78}$$

Upon deriving Eqs. (74)–(77), use has been made of the first identity of Eq. (67).

Comparison between Eqs. (43)–(54) (derived from Grad's solution to the Boltzmann equation) and Eqs. (74)–(77) shows that the BGK results for the non-Newtonian transport properties coincide with the Boltzmann ones when $\chi(\kappa,\alpha,\beta)$ is chosen as

$$\chi = \frac{\nu_\eta^*-\zeta_t^*}{\nu_t^*} = \frac{1}{3}\widetilde{\alpha}(1+2\widetilde{\alpha})+\frac{1}{3}\widetilde{\beta}(1+2\widetilde{\beta})-2\widetilde{\alpha}\widetilde{\beta}+\frac{7}{6}\frac{\widetilde{\beta}^2}{\kappa}\frac{\theta_r}{\theta_t}. \tag{79}$$

We will take this choice for computing the remaining moments of the distribution f.

A. Suspension model at $T_{\mathrm{ex}} = 0$ and $\gamma_r = 0$

As happens in the smooth case,[30] despite the apparent simplicity of the BGK-like model (66), it is still intricate to get the explicit form of the velocity distribution function $f(\mathbf{V},\boldsymbol{\omega})$. In order to obtain f and following the arguments of Ref. 36, we focus our attention in the *marginal* distribution function

$$f^{\mathrm{tr}} = \int \mathrm{d}\boldsymbol{\omega}\, f(\mathbf{V},\boldsymbol{\omega}). \tag{80}$$

Given that the rheological properties are essentially linked to the translational part of the distribution f, one expects that f^{tr} captures the main properties of the global distribution f. Moreover, as in Ref. 30, we also assume the simple limit case $T_{\mathrm{ex}} = 0$, $\gamma_r = 0$, but keeping $\gamma_t \equiv$ const. In other words, we are neglecting first the coupling between the rotational degrees of freedom of spheres with the background gas ($\gamma_r = 0$). In addition, we are also supposing that T_{ex} is much smaller than the translational temperature T_t in such a way that the only relevant effect of the surrounding interstitial gas on grains is through the viscous drag force. In the case of smooth inelastic hard spheres, this simple model has been employed to analyze rheology in sheared granular suspensions,[22–26,60] particle clustering due to hydrodynamic interactions,[61] and driven steady states[62] and to assess the impact of friction in sheared hard-spheres suspensions.[10,11,63,64]

The BGK kinetic equation for $f^{\mathrm{tr}}(\mathbf{V})$ can be easily obtained from Eq. (66) by integrating over $\boldsymbol{\omega}$,

$$-aV_y\frac{\partial}{\partial V_x}f^{\mathrm{tr}}-\lambda_t\frac{\partial}{\partial\mathbf{v}}\cdot\mathbf{V}f^{\mathrm{tr}}+\chi\nu_t f^{\mathrm{tr}} = \chi\nu_t f_0^{\mathrm{tr}}, \tag{81}$$

where

$$f_0^{\mathrm{tr}}(\mathbf{V}) = \int \mathrm{d}\boldsymbol{\omega} f_0(\mathbf{V},\boldsymbol{\omega}) = n\left(\frac{m}{2\pi T_t}\right)^{3/2}e^{-mV^2/2T_t}. \tag{82}$$

Exploiting the analogy with the smooth case,[30] the hydrodynamic solution to Eq. (81) is

$$f^{\mathrm{tr}}(\mathbf{V}) = \int_0^\infty \mathrm{d}s\, e^{-(1-3\widetilde{\lambda}_t)s}\, e^{\widetilde{a}sV_y\frac{\partial}{\partial V_x}}\, e^{\widetilde{\lambda}_t s\mathbf{V}\cdot\frac{\partial}{\partial\mathbf{V}}}f_0^{\mathrm{tr}}(\mathbf{V}), \tag{83}$$

where $\widetilde{\lambda}_t \equiv \lambda_t/(\chi\nu_t)$ and $\widetilde{a} \equiv a/(\chi\nu_t)$. In Eq. (83), the action of the velocity operators $e^{\widetilde{a}sV_y\frac{\partial}{\partial V_x}}$ and $e^{\widetilde{\lambda}_t s\mathbf{V}\cdot\frac{\partial}{\partial\mathbf{V}}}$ on an arbitrary function $g(\mathbf{V})$ is

$$e^{\widetilde{a}sV_y\frac{\partial}{\partial V_x}}g(V_x,V_y,V_z) = g(V_x+\widetilde{a}sV_y,V_y,V_z), \tag{84}$$

$$e^{\widetilde{\lambda}_t s\mathbf{V}\cdot\frac{\partial}{\partial\mathbf{V}}}g(V_x,V_y,V_z) = g\left(e^{\widetilde{\lambda}_t s}V_x,e^{\widetilde{\lambda}_t s}V_y,e^{\widetilde{\lambda}_t s}V_z\right). \tag{85}$$

The elements of the pressure tensor can be computed from the marginal distribution function (83). They are[60]

$$P_{yy} = P_{zz} = \frac{nT_t}{1+2\xi}, \quad P_{xy} = -\frac{nT_t}{(1+2\xi)^2}\widetilde{a}, \tag{86}$$

and $P_{xx} = 3p - 2P_{yy}$. Here, ξ is the real root of the cubic equation $3\xi(1+2\xi)^2 = \widetilde{a}^2$. More explicitly, it is given by

$$\xi(\widetilde{a}) = \frac{2}{3}\sinh\left[\frac{1}{6}\cosh^{-1}\left(1+\frac{27}{3}\widetilde{a}^2\right)\right]. \tag{87}$$

Here, the steady balance equation (34) for T_t becomes $2\gamma_t T_t + \zeta_t T_t = -(2/3n)aP_{xy}$. This equation can be more explicitly written when one takes into account Eqs. (86) and (87) with the result

$$\gamma_t = \chi\nu_t\xi - \frac{1}{2}\zeta_t. \tag{88}$$

Thus, as noted in previous works,[30,60] at given values of α, β, and κ, the right hand side of Eq. (88) vanishes for a certain value $\widetilde{a}_0(\alpha,\beta,\kappa)$

Physics of Fluids ARTICLE scitation.org/journal/phf

of the (reduced) shear rate. Since γ_t is strictly positive (except for $a = 0$ and $\zeta_t = 0$), physical solutions to (88) are only possible for values of the shear rate $\widetilde{a}$ larger than or equal to $\widetilde{a}_0$. Thus, in particular, when $\alpha \neq 1$ or $|\beta| \neq 1|$, the constraint (88) prevents the possibility of obtaining the Navier–Stokes shear viscosity (i.e., when $\widetilde{a} \to 0$) of the granular suspension. This is, in fact, a drawback of this simple model not shared by the generalized Fokker–Planck suspension model introduced in Sec. II. In the case of smooth inelastic hard spheres, this drag model has been widely used for many authors[22,25,26] to study the discontinuous transition for the temperature between the *quenched* and the *ignited* state.

VI. RHEOLOGY OF SHEARED DRY GRANULAR GASES

Although the main goal of this paper is to assess the influence of the interstitial gas on the rheological properties of inelastic rough hard spheres, it is interesting first to analyze the results obtained in the dry limit case (namely, when the effect of the background gas is neglected). To the best of our knowledge, this problem was independently studied many years ago for moderately dense gases by Jenkins and Richman[38] for hard disks and by Lun[37] for hard spheres. In both works, the calculations were in principle restricted to nearly elastic collisions ($\alpha \lesssim 1$) and either nearly smooth particles ($\beta \lesssim 1$) or nearly perfectly rough spheres ($\beta \gtrsim -1$). A more recent study has been performed by Santos[36] by using the BGK-like kinetic model defined in Eq. (65). Given that the BGK results for rheology agree with those derived by solving the Boltzmann equation from Grad's moment method, only a comparison with the theoretical predictions reported by Lun[37] for a three-dimensional gas will be offered in this section.

A way of obtaining the results for the dry case consists in formally setting $\gamma_t = \gamma_r = 0$. However, one has to take care in extracting the results for the dry case from those derived in Sec. V since practically all of them have been expressed in terms of dimensionless quantities that diverge when $\gamma_t \to 0$. Thus, one has to solve first the set (47) for the nonzero elements P_{yy}^{dry} and P_{xy}^{dry} (recall that $P_{xx}^{\text{dry}} = 3p - 2P_{yy}^{\text{dry}}$) and then substitute these forms into the balance equation (34). After some simple algebra, one simply gets

$$P_{yy}^{\text{dry}} = P_{zz}^{\text{dry}} = 1 - \frac{\zeta_t}{\nu_\eta}, \quad P_{xy}^{\text{dry}} = -\frac{P_{yy}^{\text{dry}}}{\nu_\eta} a, \tag{89}$$

$$a^2 = \frac{3}{2}\frac{\zeta_t \nu_\eta}{P_{yy}^{\text{dry}}}, \tag{90}$$

where ν_η and ζ_t are given by Eqs. (42) and (43), respectively. Finally, the ratio of the rotational to translational temperature can be easily obtained from the balance equation (35) by taking $\gamma_r = 0$. It leads to the condition $\zeta_r = 0$, which according to Eq. (46) yields

$$\left(\frac{T_r}{T_t}\right)^{\text{dry}} = \kappa \frac{1+\beta}{1-\beta+2\kappa}. \tag{91}$$

Equation (91) was already obtained by Lun.[37] As happens in the homogeneous steady state driven by a white-noise thermostat,[57] the temperature ratio of the steady shear flow problem is independent of the coefficient of restitution α. This conclusion contrasts with the results derived in the homogeneous cooling case,[40,66–68] where T_r/T_t depends on both α and β [see Eq. (A3) of the Appendix.]

Contrary to the case of granular suspensions, the balance equation (34) establishes an intrinsic relation between the (reduced) shear rate a/ν_t and the mechanical parameters of the system (the coefficients of normal restitution α and tangential restitution β and the dimensionless moment of inertia κ). This means that a/ν_t is not an independent parameter and is a function of α, β, and κ.

Since the results derived by Lun[37] apply in principle to slightly inelastic, slightly rough spheres, the normal stress differences vanish: $P_{xx}^{\text{dry}} = P_{yy}^{\text{dry}} = P_{zz}^{\text{dry}} = p$. On the other hand, his expressions for P_{xy}^{dry} and a/ν_t are formally equivalent to our results when one takes $P_{yy}^{\text{dry}} = 1$ in Eqs. (89) and (90). Figure 3 shows the α-dependence of the (reduced) yy-element P_{yy}^{dry}/nT_t for $\kappa = \frac{2}{5}$ and four different values of β: $\beta = -1$ (perfectly smooth spheres), $\beta = -0.5$ (moderate roughness), $\beta = 0.5$ (medium roughness), and $\beta = 1$ (strong roughness). Results obtained Direct Simulation Monte Carlo (DSMC) method simulations[65] for perfectly smooth spheres are also included. It is quite apparent first that the combined effect of α and β gives rise to anisotropic effects in the yy-element of the pressure tensor; these effects are measured by the departure of the ratio P_{yy}^{dry}/nT_t from 1. We also see that, for a given value of β, these non-Newtonian effects increase monotonically with decreasing α. In addition, for a given value of α, P_{yy}^{dry}/nT_t presents a non-monotonic dependence on β; the impact of roughness is higher for central values of β (let us say $|\beta| \simeq 0.5$). Comparison with Monte Carlo simulations for $\beta = -1$ shows good agreement; we hope that this agreement is also extended for the remaining values of β. As a complement of Fig. 3, Fig. 4 plots

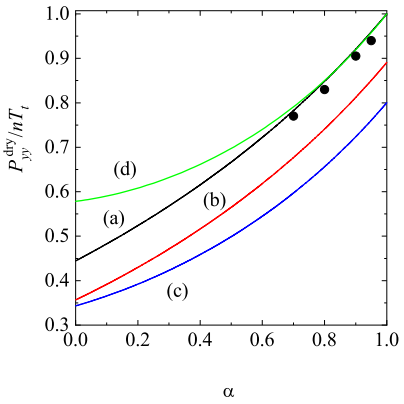

FIG. 3. Plot of the (reduced) element P_{yy}^{dry}/nT_t as a function of the coefficient of normal restitution α for $\kappa = \frac{2}{5}$ and four different values of the coefficient of tangential restitution β: $\beta = -1$ (a), $\beta = -0.5$ (b), $\beta = 0.5$ (c), and $\beta = 1$ (d). Symbols refer to DSMC results obtained for spheres perfectly smooth ($\beta = -1$).[65] Reproduced with permission from J. M. Montanero and V. Garzó, "Rheological properties in a low-density granular mixture," Physica A **310**, 17 (2002). Copyright 2002 Elsevier.

Physics of Fluids ARTICLE scitation.org/journal/phf

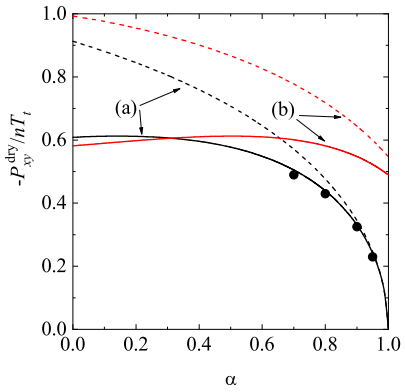

FIG. 4. Plot of the (reduced) element $-P_{xy}^{\rm dry}/nT_t$ as a function of the coefficient of normal restitution α for $\kappa = \frac{2}{5}$ and two different values of the coefficient of tangential restitution β: $\beta = -1$ (a) and $\beta = 0.5$ (b). The solid lines correspond to the results obtained here while the dashed lines refer to the results derived by Lun.[37] Symbols refer to DSMC results obtained for spheres perfectly smooth ($\beta = -1$).[65] Reproduced with permission from J. M. Montanero and V. Garzó, "Rheological properties in a low-density granular mixture," Physica A **310**, 17 (2002). Copyright 2002 Elsevier.

$-P_{xy}^{\rm dry}/nT_t$ vs α for $\beta = -1$ and $\beta = 0.5$. The theoretical predictions of Lun[37] are also represented. As expected, we observe that the agreement between Lun's predictions and our results is excellent for $\alpha \lesssim 1$ and $|\beta| \lesssim 1$. On the other hand, the discrepancies between both theories increase as inelasticity increases (at a given value of roughness) or as roughness increases (at a given value of inelasticity). As in the case of Fig. 3, Fig. 4 highlights again the good performance of Grad's solution when $\alpha = 1$ and $\beta = -1$ since the aforementioned solution compares very well with simulations.

VII. RHEOLOGY AND FOURTH-DEGREE MOMENTS OF SHEARED INERTIAL SUSPENSIONS

We consider now sheared inertial suspensions ($\gamma_t \neq 0$ and $\gamma_r \neq 0$). In Sec. IV, we have determined the elements of the (reduced) pressure tensor $P_{k\ell}^*$ by solving the Boltzmann equation (33) by means of Grad's moment method. Then, in Sec. V, we have replaced the Boltzmann collision operator $J[f, f]$ by the BGK-like collision term (65) and have explicitly obtained all the velocity moments of the velocity distribution function. In dimensionless form, all the aforementioned quantities (pressure tensor and higher degree velocity moments) have been expressed in terms of the restitution coefficients α and β, the (reduced) moment of inertia κ, the reduced density n^*, the (reduced) bath temperature $T_{\rm ex}^*$, and the (reduced) shear rate a^*.

We want essentially to assess the shear-rate dependence of η^*, Ψ^*, θ_t, θ_r, and the fourth-degree moments for fixed values of α, β, κ, n^*, and $T_{\rm ex}$. Since the theoretical results for θ_t, η^*, and Ψ^* will be compared against event-driven simulations[27] carried out for the case $\alpha = 0.9$ and $\beta = -1$, the values of n^* and $T_{\rm ex}$ employed in those simulations ($n^* = 0.01$ and $T_{\rm ex} = 1$) and the value $\kappa = \frac{2}{5}$ will be used in the remaining plots of this section.

A. Rheology

The dependence of the (steady) translational temperature θ_t, the non-Newtonian shear viscosity η^*, and the viscometric function Ψ^* on the (reduced) shear rate a^* is shown in Fig. 5. The analytical forms of the above quantities are given by Eqs. (54), (59), and (60), respectively. We recall that the corresponding expressions of the BGK equation agree with those derived from Grad's solution when one makes the choice (79) for the free parameter χ of the kinetic model. In addition, as will be discussed in Sec. VIII, depending on the values of α and β, the steady solution can be linearly unstable. The thick lines in Fig. 5 denote the linearly unstable regions.

The main conclusion of Fig. 5 is that the roughness does not change the trends observed in previous works[27,28,30] for perfectly smooth inelastic spheres: there is a drastic increase in all the rheological properties with an increase in the shear rate. In particular, panel (c) of Fig. 5 highlights the existence of DST for the shear viscosity η^*, regardless of the value of the coefficient of restitution β. On the other hand, at a more quantitative level, we observe that, for a given value of a^*, high levels of roughness can slightly attenuate the jump of η^* relative to the frictionless case. This is a quite unexpected result since most of the results obtained for concentrated suspensions have shown that friction enhances DST. However, this trend is not monotonic since there is a change in the aforementioned behavior for very high shear rates; in fact, the line corresponding to strong roughness ($\beta = 1$) intersects the curves of $\beta = 0.5$, $\beta = 0$, and $\beta = -0.5$ for $a^* \gtrsim 10$. In addition, the agreement between theory and simulations for perfectly smooth spheres ($\alpha = 0.9$ and $\beta = -1$) is relatively good, except in a small region close to the transition point where simulation data suggest a sharper transition than the Boltzmann one. We think that this small discrepancy is mainly due to the limitations of the Boltzmann equation for accounting small density corrections to η^* around this transition point. As a matter of fact, the Enskog predictions for this quite small density ($n^* = 0.01$) compare slightly better with simulation data than the ones obtained from the Boltzmann equation; see, for instance, Fig. 2 of Ref. 27.

Although similar trends are observed for θ_t and Ψ^*, it is worth noting that the combined effect of α and β on the viscometric function Ψ^* is quite important since, while this quantity is tiny for small shear rates, it suddenly increases for not quite large values of the shear rate (let us say $a^* \approx 1$). It must be recalled that the results obtained in the context of the Enskog equation for moderately dense gases have shown a transition from DST for very dilute suspensions to CST at relatively moderate densities.[27,28]

More influence of roughness on rheology can be found in the case of the (steady) rotational granular temperature $\theta_r = T_r/T_{\rm ex}$. This quantity does not play any role in the perfectly smooth case. Panel (b) of Fig. 5 shows the shear-rate dependence of θ_r. It is quite apparent that, for large shear rates, roughness clearly enhances the value of θ_r in contrast to what happens for θ_t. It must be remarked that similar features of the rheological properties have been observed for other values of the coefficient of restitution.

Physics of Fluids ARTICLE scitation.org/journal/phf

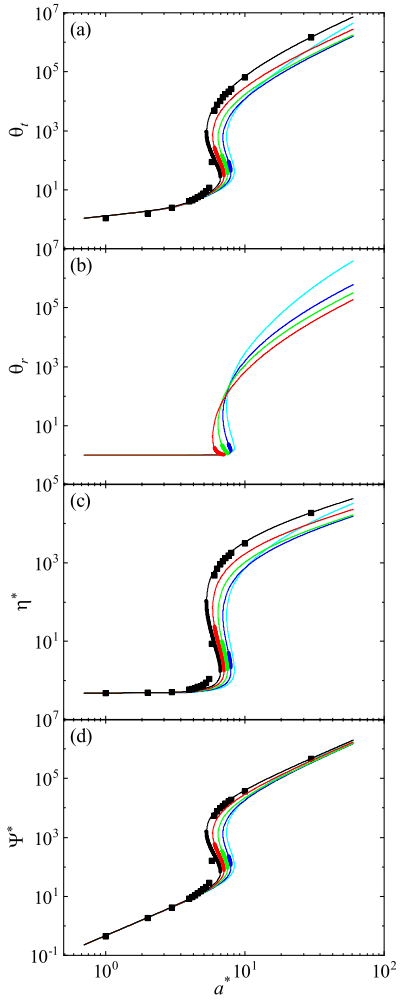

FIG. 5. Plots of the (steady) translational granular temperature θ_t [panel (a)], the (steady) rotational granular temperature θ_r [panel (b)], the non-Newtonian shear viscosity η^* [panel (c)], and the viscometric function Ψ^* [panel (d)] as a function of the (reduced) shear rate a^* for $\alpha = 0.9$ and different values of the coefficient of tangential restitution β: $\beta = -1$ (black line), $\beta = -0.5$ (red line), $\beta = 0$ (green line), $\beta = 0.5$ (blue line), and $\beta = 1$ (cyan line). Here, $\kappa = \frac{2}{5}$, $n^* = 0.01$, and $T_{ex}^* = 1$. The thick lines represent the linearly unstable regions. Symbols refer to computer simulation results obtained for spheres perfectly smooth ($\beta = -1$).[27] Reproduced with permission from H. Hayakawa, S. Takada, and V. Garzó, "Kinetic theory of shear thickening for a moderately dense gas-solid suspension: From discontinuous thickening to continuous thickening," Phys. Rev. E **96**, 042903 (2017). Copyright 2017 American Physical Society.

B. Fourth-degree velocity moments

We consider now the relevant fourth-degree velocity moments obtained in the context of the BGK model. They can be easily determined from Eq. (73). As discussed in Ref. 30, there are eight independent fourth-degree (symmetric) moments: five of them are even functions of the (reduced) shear rate a^* while the remaining three are odd functions of a^*. To illustrate the shear-rate dependence of those moments, we chose the representative moments

$$M_{4|0} = \int d\mathbf{v} \int d\boldsymbol{\omega}\, V^4 f(\boldsymbol{\omega}, \mathbf{V}) = M_{400} + 2(M_{040} + M_{220} + M_{202} + M_{022}), \tag{92}$$

and

$$M_{2|xy} = \int d\mathbf{v} \int d\boldsymbol{\omega}\, V^2 V_x V_y f(\boldsymbol{\omega}, \mathbf{V}) = M_{310} + M_{130} + M_{112}, \tag{93}$$

where the canonical moments M_{k_1,k_2,k_3} are given by Eq. (73). Upon writing Eq. (92), use has been made of the identity $M_{040} = M_{004}$. While the moment $M_{4|0}$ is an even function of a^* (and so $M_{4|0} \neq 0$ when $a^* = 0$), the moment $M_{2|xy}$ is an odd function of a^* (and so $M_{2|xy} = 0$ when $a^* = 0$). To see more clearly the influence of both α and β on $M_{4|0}$ and $M_{2|xy}$, we consider first the region $0 \leqslant a^* \leqslant 1$ where non-Newtonian effects are expected to be still important.

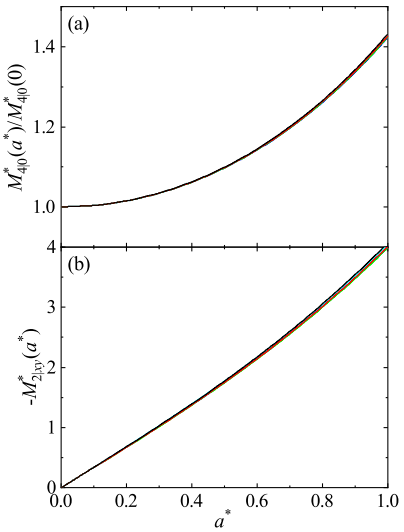

FIG. 6. Shear-rate dependence of the (scaled) fourth-degree moments $M_{4|0}^*(a^*)/M_{4|0}^*(0)$ [panel (a)] and $-M_{2|xy}^*(a^*)$ [panel (b)] for $\alpha = 0.9$ and different values of the coefficient of tangential restitution β: $\beta = -1$ (black line), $\beta = -0.5$ (red line), $\beta = 0$ (green line), $\beta = 0.5$ (blue line), and $\beta = 1$ (cyan line). Here, $\kappa = \frac{2}{5}$, $n^* = 0.01$, and $T_{ex}^* = 1$.

Physics of Fluids ARTICLE scitation.org/journal/phf

Figure 6 shows the shear-rate dependence of $M_{4|0}^*(a^*)/M_{4|0}^*(0)$ and $-M_{2|xy}^*(a^*)$ for $\alpha = 0.9$ and several values of β. Here, we have introduced the dimensionless moments

$$\{M_{4|0}^*, M_{2|xy}^*\} = n^{-1}\left(\frac{m}{T_{\text{ex}}}\right)^2 \{M_{4|0}, M_{2|xy}\}. \tag{94}$$

In Fig. 6, $M_{4|0}^*(0)$ refers to the value of $M_{4|0}^*$ when $a^* = 0$, namely,

$$M_{4|0}^*(0) = \frac{9}{4+\sqrt{\theta_t^{(0)}}(\chi\nu_t^* + 2\zeta_t^*)} \times \left[\chi\nu_t^*\sqrt{\theta_t^{(0)}}\theta_t^{(0)} + 4\frac{2+\chi\nu_t^*\sqrt{\theta_t^{(0)}}\theta_t^{(0)}}{2+\sqrt{\theta_t^{(0)}}(\chi\nu_t^* + \zeta_t^*)}\right], \tag{95}$$

where $\theta_t^{(0)}$ is a real solution of Eq. (61). As expected, we observe first in Fig. 6 that these fourth-degree moments clearly depart from their equilibrium values (in the absence of shear rate). Surprisingly, at a given value of α, the impact of β on those moments is very small since all the curves collapse in a common one. This feature contrasts with the results obtained for the rheological properties since the effect of β on both η^* and Ψ^* is remarkable in this range of values of the shear rate ($a^* \leq 1$). It must be recalled that a similar property appears in the smooth limit case[30] since the effect of α on $M_{4|0}^*(a^*)$ and $-M_{2|xy}^*(a^*)$ was also found very tiny at a given value of the shear rate.

For very large values of the shear rate, it is interesting to see whether the fourth-degree moments increase also dramatically with the shear rate in a similar way as the non-Newtonian shear viscosity η^*. This is illustrated in Fig. 7, where it is clearly shown that both scaled moments exhibit an S-shape for any value of β. In addition, we also see that the effect of β on these moments is really significant for large values of a^*.

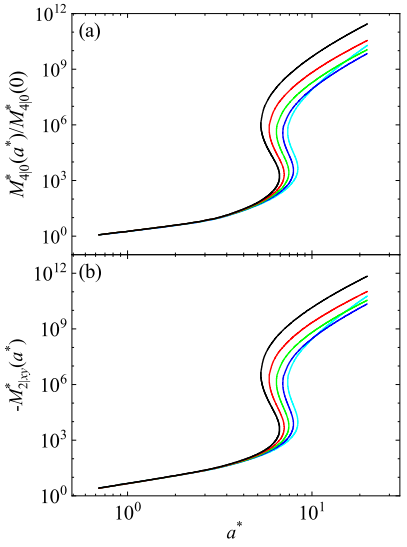

FIG. 7. Shear-rate dependence of the (scaled) fourth-degree moments $M_{4|0}^*(a^*)/M_{4|0}^*(0)$ [panel (a)] and $-M_{2|xy}^*(a^*)$ [panel (b)] for $\alpha = 0.9$ and different values of the coefficient of tangential restitution β: $\beta = -1$ (black line), $\beta = -0.5$ (red line), $\beta = 0$ (green line), $\beta = 0.5$ (blue line), and $\beta = 1$ (cyan line). Here, $\kappa = \frac{2}{5}$, $n^* = 0.01$, and $T_{\text{ex}}^* = 1$.

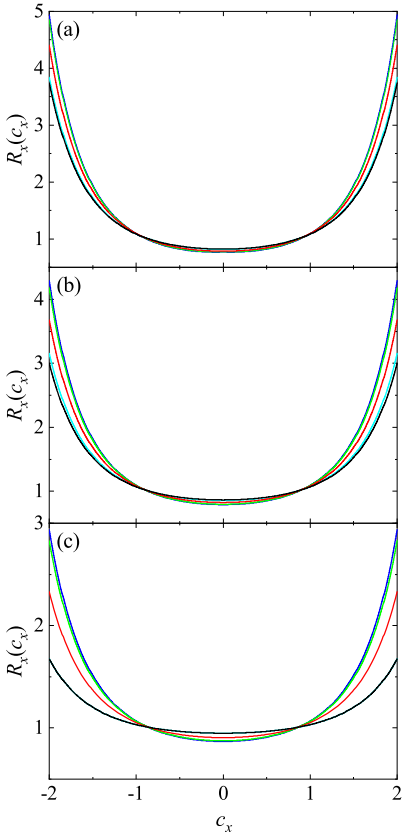

FIG. 8. Plot of the ratio $R_x(c_x) = \varphi(c_x)/(\pi^{-1/2}e^{-c_x^2})$ vs the scaled velocity $c_x = \sqrt{m/2T_t}V_x$ for $\widetilde{\gamma}_t = 0.1$ and five different values of the coefficient of tangential restitution β: $\beta = -1$ (black line), $\beta = -0.5$ (red line), $\beta = 0$ (green line), $\beta = 0.5$ (blue line), and $\beta = 1$ (cyan line). Three different values of the coefficient of normal restitution α are considered: $\alpha = 1$ [panel (a)], $\alpha = 0.7$ [panel (b)], and $\alpha = 0.5$ [panel (c)]. Here, $\kappa = \frac{2}{5}$, $n^* = 0.01$, and $T_{\text{ex}}^* = 1$.

Physics of Fluids ARTICLE scitation.org/journal/phf

C. Velocity distribution function

As mentioned in Sec. V, one of the main practical advantages of kinetic models is the possibility of obtaining the explicit form of the velocity distribution function. Here, we have obtained it in the special case $T_{\text{ex}} = \gamma_r = 0$ and is given by Eq. (83). To illustrate the dependence of $f^{\text{tr}}(\mathbf{V})$ on the parameter space of the problem, let us rewrite this distribution as

$$f^{\text{tr}}(\mathbf{V}) = n\left(\frac{m}{2T_t}\right)^{3/2}\varphi(\mathbf{c}), \tag{96}$$

where $\mathbf{c} = \sqrt{m/2T_t}\mathbf{V}$ is the reduced peculiar velocity and the reduced velocity distributions function $\varphi(\mathbf{c})$ is given by

$$\varphi(\mathbf{c}) = \pi^{-d/2}\int_0^\infty \mathrm{d}s\, e^{-(1-3\widetilde{\lambda}_t)s} \times \exp\left\{-e^{2\widetilde{\lambda}_t s}\left[(c_x + \widetilde{a}sc_y)^2 + c_y^2 + c_z^2\right)\right]\right\}. \tag{97}$$

Upon writing Eq. (97), use has been made of Eqs. (84) and (85). Figure 8 shows the ratio $R_x(c_x) = \varphi_x(c_x)/\left(\pi^{-1/2}e^{-c_x^2}\right)$ for $\widetilde{\gamma}_t = 0.1$ and different values of the restitution coefficients α and β. Here, $\varphi_x(c_x)$ is the marginal distribution,

$$\varphi_x(c_x) = \int_{-\infty}^\infty \mathrm{d}c_y \int_{-\infty}^\infty \mathrm{d}c_z\, \varphi(\mathbf{c}) = \frac{1}{\sqrt{\pi}}\int_0^\infty \mathrm{d}s \frac{e^{-(1-\widetilde{\lambda}_t)s}}{\sqrt{1+\widetilde{a}^2s^2}}\exp\left(-e^{2\widetilde{\lambda}_t s}\frac{c_x^2}{1+\widetilde{a}^2s^2}\right). \tag{98}$$

Figure 8 shows that, in general, $R_x(c_x)$ is clearly different from 1, namely, the distribution $\varphi_x(c_x)$ is highly distorted from its local equilibrium value ($\pi^{-1/2}e^{-c_x^2}$). At a given value of the coefficient of tangential restitution β, the distortion is more significant as the coefficient of normal restitution α decreases (increasing inelasticity). The impact of roughness on $R_x(c_x)$ increases with decreasing α.

VIII. LINEAR STABILITY ANALYSIS OF THE STEADY SOLUTION

Although our study has been mainly focused on the determination of the rheological properties under steady state conditions, an interesting question is to see if actually the steady state solution provided by Eqs. (52)–(56) is indeed a (linearly) stable solution. In order to perform this analysis, we write first the four relevant equations for P_{yy}^*, P_{xy}^*, θ_t, and θ_r from Eq. (51) as follows:

$$\partial_\tau P_{yy}^* + 2\left(P_{yy}^* - 1\right) = -\nu_\eta^*\sqrt{\theta_t}\left(P_{yy}^* - \theta_t\right) - \sqrt{\theta_t}\theta_t\zeta_t^*, \tag{99}$$

$$\partial_\tau P_{xy}^* + a^* P_{yy}^* + 2P_{xy}^* = -\nu_\eta^*\sqrt{\theta_t}P_{xy}^*, \tag{100}$$

$$\partial_\tau \theta_t + 2(\theta_t - 1) + \sqrt{\theta_t}\theta_t\zeta_t^* = -\frac{2}{3}a^* P_{xy}^*, \tag{101}$$

$$\partial_\tau \theta_r + 2\frac{\gamma_r}{\gamma_t}(\theta_r - 1) + \sqrt{\theta_t}\theta_r\zeta_r^* = 0. \tag{102}$$

We want to solve the set of Eqs. (99)–(102) by assuming small deviations from the steady state solution. Thus, we write

$$P_{yy}^*(\tau) = P_{yy,s}^* + \delta P_{yy}^*(\tau), \quad P_{xy}^*(\tau) = P_{xy,s}^* + \delta P_{xy}^*(\tau), \tag{103}$$

$$\theta_t(\tau) = \theta_{t,s} + \delta\theta_t(\tau), \quad \theta_r(\tau) = \theta_{r,s} + \delta\theta_r(\tau), \tag{104}$$

where the subscript s means that the quantity is evaluated in the steady state. Here, for the sake of simplicity, we have assumed that the interstitial fluid is not perturbed, and hence, the parameters γ_t, γ_r, and T_{ex} are constant in the time-dependent shear flow problem. This means that the reduced shear rate $a^* = a/\gamma_t$ is also constant. Substituting Eqs. (103) and (104) into Eqs. (99)–(103) and neglecting nonlinear terms in the perturbations, after some algebra, one gets the set of linear differential equations,

$$\partial_\tau\begin{pmatrix}\widetilde{P}_{yy}\\ \widetilde{P}_{xy}\\ \widetilde{\theta}_t\\ \widetilde{\theta}_r\end{pmatrix} = -\mathsf{L}\cdot\begin{pmatrix}\widetilde{P}_{yy}\\ \widetilde{P}_{xy}\\ \widetilde{\theta}_t\\ \widetilde{\theta}_r\end{pmatrix}, \tag{105}$$

where

$$\widetilde{P}_{yy}(\tau) = \frac{\delta P_{yy}^*(\tau)}{P_{yy,s}^*}, \quad \widetilde{P}_{xy}(\tau) = \frac{\delta P_{xy}^*(\tau)}{P_{xy,s}^*}, \quad \widetilde{\theta}_t(\tau) = \frac{\delta\theta_t(\tau)}{\theta_{t,s}}, \quad \widetilde{\theta}_r(\tau) = \frac{\delta\theta_r(\tau)}{\theta_{r,s}}. \tag{106}$$

The square matrix L is

$$\mathsf{L} = \begin{pmatrix} 2+\sqrt{\theta_t}\nu_\eta^* & 0 & \sqrt{\theta_t}\theta_t\left(\frac{\nu_\eta^* - 2\bar{\nu}_\eta}{2\theta_t} - \frac{\frac{3}{2}\nu_\eta^* - \bar{\nu}_\eta}{P_{yy}^*} + \frac{\frac{3}{2}\zeta_t^* - \bar{\zeta}_t}{P_{yy}^*}\right) & \sqrt{\theta_t}\left(\bar{\nu}_\eta - \frac{11\bar{\nu}_\eta}{P_{yy}^*}\theta_t\right) \\ a^*\frac{P_{yy}^*}{P_{xy}^*} & 2+\sqrt{\theta_t}\nu_\eta^* & \sqrt{\theta_t}\left(\frac{1}{2}\nu_\eta^* - \bar{\nu}_\eta\right) & \sqrt{\theta_t}\bar{\nu}_\eta \\ 0 & \frac{2}{3}\frac{P_{xy}^* a^*}{\theta_t} & \sqrt{\theta_t}\left(\frac{3}{2}\zeta_t^* - \bar{\zeta}_t\right) + 2 & \sqrt{\theta_t}\bar{\zeta}_t \\ 0 & 0 & \sqrt{\theta_t}\left(\frac{1}{2}\zeta_r^* + \bar{\zeta}_r\right) & 2\frac{\gamma_r}{\gamma_t} + \sqrt{\theta_t}\left(\zeta_r^* - \bar{\zeta}_r\right) \end{pmatrix}, \tag{107}$$

Physics of Fluids ARTICLE scitation.org/journal/phf

where the subscript s has been omitted for the sake of brevity. This means that it is understood that all the quantities appearing in the matrix L are evaluated at the steady state. In Eq. (107), we have introduced the quantities

$$\bar{\nu}_\eta = \frac{8}{15}\sqrt{\pi}\frac{\widetilde{\beta}^2}{\kappa}\frac{\theta_r}{\theta_t}n^*\sqrt{T_{\text{ex}}^*}, \quad \bar{\zeta}_t = -10\bar{\nu}_\eta, \quad \bar{\zeta}_r = \frac{\theta_t}{\theta_r}\bar{\zeta}_t. \tag{108}$$

In the purely smooth case ($\beta = -1$), $\widetilde{\beta} = \bar{\nu}_\eta = \bar{\zeta}_t = \bar{\zeta}_r = 0$, and hence, the matrix L is consistent with the one obtained in Ref. 29 for a linear stability analysis for smooth hard spheres.[69]

The eigenvalues ℓ of the square matrix L govern the time evolution of the deviations $\{\widetilde{P}_{yy}, \widetilde{P}_{xy}, \widetilde{\theta}_t, \widetilde{\theta}_r\}$ from the steady solution given by the set $\{P_{yy,s}^*, P_{xy}^*, \theta_{t,s}, \theta_{r,s}\}$. If the real parts of those eigenvalues are positive, the steady solution is linearly stable, while it is unstable otherwise.

On the other hand, as already occurs for smooth spheres,[30] the (steady) translational temperature $\theta_t(a^*)$ turns out to be a multivalued function of the (reduced) shear rate in a certain interval of values of a^* (see the vicinity of the saddle point in Fig. 5). Thus, as already did in Refs. 29 and 30, in order to analyze the stability of the steady solution we take θ_t as an independent parameter instead of a^* for the sake of convenience. Of course, once $\theta_t(a^*)$ is known, a^* can be determined from Eq. (54). As expected from the previous stability analysis performed for smooth spheres,[29] a careful analysis of the eigenvalues ℓ shows that, for given values of α and β, the real part of one of the eigenvalues (the one associated with the rotational temperature θ_r) can become negative for values of θ_t belonging to the range $\theta_t^{(1)} < \theta_t < \theta_t^{(2)}$. The critical values $\theta_t^{(i)}$ depend on n^*, T_{ex}^*, α, β, and κ. This means that the steady simple shear flow solution is linearly *unstable* in the region $\theta_t^{(1)} < \theta_t < \theta_t^{(2)}$.

As an illustration, Fig. 9 shows the real part of the eigenvalues ℓ_i ($i = 1, 2, 3, 4$) of the matrix L as a function of the translational temperature θ_t for $n^* = 0.01$, $T_{\text{ex}}^* = 1$, $\kappa = \frac{2}{5}$, $\alpha = 1$, and $\beta = -0.5$. We find that two of the eigenvalues (let us denote them, for instance, by ℓ_2 and ℓ_3) are complex conjugate while the other two (ℓ_1 and ℓ_4) become a complex conjugate pair for high values of θ_t. It is quite apparent that while the real part of ℓ_2 (or ℓ_3 since $\text{Re}\,\ell_2 = \text{Re}\,\ell_3$) is always positive, the real parts of ℓ_1 and ℓ_4 become negative for certain critical values of θ_t (see the inset where the position of these critical values is more clearly shown). This means that there are two different unstable regions for this system.

The aforementioned feature is clearly confirmed in Fig. 10, where we plot a phase diagram delineating the regions between stable and unstable solutions in the $\{\alpha, \theta_t\}$ plane for smooth inelastic hard spheres ($\beta = -1$) with $n^* = 0.01$, $T_{\text{ex}}^* = 1$, and $\kappa = \frac{2}{5}$. While the hatched regions refer to values of (α, θ_t) where the steady shear flow solution is *stable*, the unfilled regions correspond to combined values of α and θ_t for which the steady solution is *unstable*. It is worth noting that the dependence of the boundary line separating both stable and unstable regions on α is not quite trivial since, at a given value of α, there is a re-entrance feature as the translational temperature θ_t increases: we first find a transition from the stable to unstable region, followed by a subsequent transition to the stable region. Surprisingly, the size of the unstable region decreases with inelasticity. As a complement of Fig. 10, Fig. 11 shows two different phase diagrams in the $\{\beta, \theta_t\}$ plane for two values of the coefficient of normal restitution α: $\alpha = 0.9$ [panel (a)] and $\alpha = 1$ [panel (b)]. We observe first that there are two separate unstable regions around $\beta = -0.5$ in the case of $\alpha = 1$. This is consistent with the findings of Fig. 9. The second unstable region corresponding to higher θ_t's is more squeezed than the first one. In addition, we see that the size of the unstable region decreases with increasing roughness (β increases). This is more apparent in the case of panel (a) of Fig. 11 where only a single unstable region is found. This means that roughness attenuates the instability of the time-dependent sheared problem. In fact, at a given value of α, there exists a critical value $\beta_c(\alpha)$ for which the unstable region is destroyed, and hence, the steady solution is always linearly stable for $\beta > \beta_c$. In particular, $\beta_c \simeq 0.75$ for $\alpha = 0.9$ and $\beta_c \simeq 0.94$ for $\alpha = 1$. Figure 11 also highlights the complex

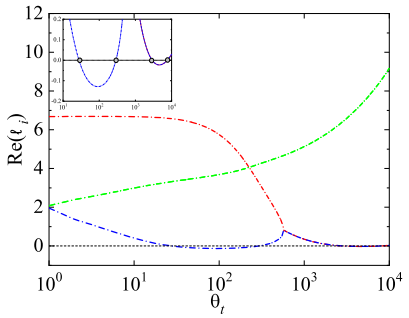

FIG. 9. Plot of the real part of the eigenvalues ℓ_i ($i = 1, 2, 3, 4$) of the matrix L for $n^* = 0.01$, $T_{\text{ex}}^* = 1$, $\kappa = \frac{2}{5}$, $\alpha = 1$, and $\beta = -0.5$. The green line corresponds to the real part of the complex conjugate pair (ℓ_2, ℓ_3). The red and blue lines refer to the other two eigenvalues (ℓ_1, ℓ_4), which become a complex conjugate pair for high values of θ_t. The region where the real parts of ℓ_1 and ℓ_4 vanish is shown more clearly in the inset.

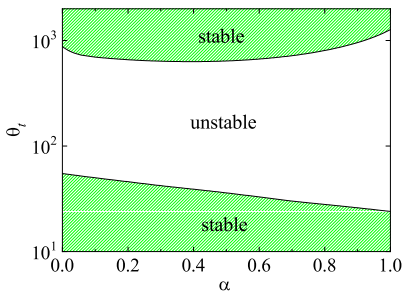

FIG. 10. Phase diagram for the behavior of the eigenvalues of the matrix L in the case of purely smooth granular gases ($\beta = -1$) for $n^* = 0.01$, $T_{\text{ex}}^* = 1$, and $\kappa = \frac{2}{5}$. The hatched regions correspond to states where the steady simple shear flow solution is linearly stable, while the unfilled region refers to states where the steady solution is linearly unstable.

Physics of Fluids ARTICLE scitation.org/journal/phf

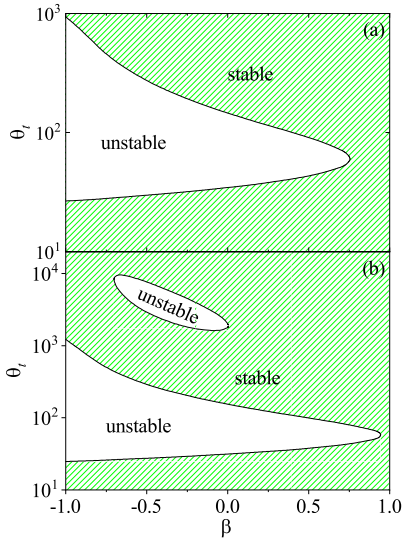

FIG. 11. Phase diagram for the behavior of the eigenvalues of the matrix L for $n^* = 0.01$, $T_{\text{ex}}^* = 1$, $\kappa = \frac{2}{5}$, and two different values of α: $\alpha = 0.9$ [panel (a)] and $\alpha = 1$ [panel (b)]. The hatched regions correspond to states where the steady simple shear flow solution is linearly stable, while the unfilled regions refer to states where the steady solution is linearly unstable.

dependence of the boundary lines for $\alpha = 1$ around $\beta = -0.5$ since the following series stable → unstable → stable → unstable → stable occurs when θ_t increases at fixed β.

In summary, our stability analysis shows that there are regions of the parameter space of the problem where the steady simple shear flow state can be linearly unstable. This restricts, of course, the analysis performed here for rheology to specific regions of the parameter space where the steady solution is stable. Hopefully, the size of the stable regions is, in general, larger than that of unstable regions.

IX. SUMMARY AND DISCUSSION

The determination of the non-Newtonian transport properties in inertial suspensions under simple shear flow has stimulated in the past few years the use of kinetic theory tools. Starting from the Boltzmann kinetic equation (which holds for very dilute systems) and/or the Enskog kinetic equation (which applies for moderately dense systems), several works[22–30] have obtained explicit expressions of the shear-rate dependence of the kinetic temperature, the non-Newtonian viscosity, and the viscometric functions. In most of the cases, the analytical results have been validated against computer simulations showing, in general, good agreement for conditions of practical interest. An interesting conclusion is that the viscosity exhibits DST for very dilute systems;[29,30] this means that there is a sudden relative increase in viscosity with an increase in the shear rate. On the other hand, it has been also shown that DST gradually becomes CST as the density increases.

However, all previous theoretical works[22–30] have considered inertial suspensions of *smooth* inelastic hard spheres, and hence, the effects of tangential friction in particle collisions on non-Newtonian rheology have been neglected. In the context of kinetic theory, we are not aware of any previous attempt on addressing the impact of roughness on the non-Newtonian transport properties. In this paper, we have addressed this problem; more specifically and due to the complexity of the problem, we have considered a granular suspension of inelastic rough hard spheres at low density. In this case, the Boltzmann kinetic equation conveniently adapted for accounting the effect of the interstitial gas on grains is a reliable equation for obtaining the kinetic contributions to the temperature and the relevant elements of the pressure tensor.

In the case of smooth spheres,[27–30] the influence of the gas phase on solid particles has been usually accounted for by a gas–solid force constituted by two terms: (i) a drag force term proportional to the (instantaneous) velocity $\mathbf{v}$ plus (ii) a stochastic term represented by a Fokker–Planck operator of the form $-(\gamma_t T_{\text{ex}}/m)\partial^2 f/\partial v^2$. While the first term models the friction of grains on the continuous gas phase, the second one takes into account thermal fluctuations. On the other hand, when the spheres are not completely smooth and there is a certain friction between both spheres, one has also to take into account the coupling between the rotational degrees of freedom of grains and the gas phase. Here, we have assumed that this coupling has a similar structure to the one assumed in the smooth case; therefore, one has to add two new terms in the corresponding suspension model: a term proportional to the angular velocity $\boldsymbol{\omega}$ plus a Fokker–Planck operator of the form $-(\gamma_r T_{\text{ex}}/m)\partial^2 f/\partial w^2$. The coefficients γ_t and γ_r are proportional to the square root of the background temperature T_{ex}.

Once the suspension model is defined, as a first goal we have approximately solved it by Grad's moment method.[35] More specifically, we have evaluated the collisional moment $\mathcal{J}[V_k, V_\ell|f,f]$ [defined by Eq. (16)] by using Grad's distribution (38). The knowledge of this collisional moment allows us to obtain the explicit forms of the (reduced) rotational θ_r and translational θ_t temperatures as well as the (reduced) relevant elements of the pressure tensor $P_{k,\ell}^*$ in terms of the parameter space of the problem (the restitution coefficients α and β, the reduced moment of inertia κ, the reduced shear rate a^*, the reduced background temperature T_{ex}^*, and the reduced density n^*). Although the determination of non-Newtonian rheological properties (which are directly related with the second-degree velocity moments) is the most important objective of the present contribution, higher degree velocity moments are also relevant since they provide some indirect information on the velocity distribution function, especially in the high velocity region. Given that their evaluation from the true Boltzmann equation is quite intricate, as a second goal we have obtained them by considering a BGK-like kinetic model[36] recently proposed for inelastic rough hard spheres. Beyond non-Newtonian rheology, the fourth-degree moments are the first nontrivial moments in the steady simple shear flow problem. Their knowledge allows us to disclose partially the combined effect of the different physical mechanisms (shearing, gas phase, and inelasticity) involved in the problem on the distribution function.

Physics of Fluids ARTICLE scitation.org/journal/phf

Regarding non-Newtonian rheology, the results derived here for inelastic rough hard spheres show no new surprises relative to the earlier works for smooth inelastic hard spheres:[27–30] the flow curve for the non-Newtonian viscosity $\eta^*(a^*)$ exhibits an S-shape, and hence, DST is present. This means that η^* discontinuously increases/decreases if a^* is gradually increased/decreased [see panel (c) of Fig. 5]. We have also observed that, at a given value of α, the dramatic increase in viscosity is slightly mitigated by roughness (namely, as β increases). The influence of roughness on rheology is more significant in the case of the (reduced) rotational temperature θ_r. Panel (b) of Fig. 5 highlights that, for large shear rates, θ_r increases with increasing β.

With respect to the fourth-degree moments, at a given value of the coefficient of normal restitution α, surprisingly the BGK results show that the shear-rate dependence of those moments is practically independent of roughness in the range $a^* \leq 1$, where nonlinear effects are already important. This feature contrasts with the behavior of $\eta^*(a^*)$ since the value of η^* clearly differs from its Navier–Stokes form in this range of values of the shear rate. For larger shear rates, we find that the fourth-degree moments also display an S-shape in a similar way to the viscosity η^* (see Fig. 7).

As a complement of the previous results, we have also analyzed the stability of the steady simple shear flow solution for non-Newtonian rheology. To perform this analysis, since $\theta_t(a^*)$ is a multi-valued function of a^*, it is more convenient to take θ_t as an independent input parameter instead of the (reduced) shear rate. In this case, as happens for smooth spheres,[29] the linear stability analysis shows regions of the parameter space of the system where the steady solution is linearly *unstable*. More specifically, for given values of the set (n^*, T_{ex}^*, κ, and α), the steady solution becomes unstable in the region $\theta^{(1)} < \theta_t < \theta_t^{(2)}$, where the critical values $\theta_t^{(i)}$ depend on the coefficient of tangential restitution β. In addition, as panel (b) of Fig. 11 clearly illustrates, the dependence of the boundary lines delimitating stable/unstable regimes on β is quite complex, and in fact, there may be two or more separate unstable regions. It is worth noting that the unstable region usually belongs to the range of (reduced) shear rates where DST appears [see the thick lines of panel (c) of Fig. 5]. Thus, it would be tentative to speculate on the possible relation between DST and instability although this connection requires a more rigorous analysis. We plan to elucidate this point in the near future by considering a time-dependent inhomogeneous solution.

As mentioned in Sec. I, the origin of DST has received a lot of attention in the past few years. Several mechanisms[12] have been proposed, most of them directly related to the complex structure of dense suspensions. On the other hand, as already discussed in Ref. 30, what is surprising here is the existence of DST in a structurally simple system. In this case, the origin of DST in dilute suspensions of inelastic hard spheres could be associated with both non-Newtonian rheology in far from equilibrium states as well as the effect of the interstitial gas on the dynamics of inelastic rough hard spheres.

The fact that the roughness of spheres does not have a significant impact on DST (in the sense that the trends observed here are qualitatively similar to those observed for smooth spheres) could be in part due to the Fokker–Planck suspension model considered in this paper. As widely discussed in Sec. II, the above-mentioned suspension model neglects the coupling between translational and rotational degrees of freedom of grains in the form of the operator $\mathcal{F}^{\text{rot}} f$. A way of accounting for this coupling in our theory would be to retain a term proportional to the vectorial product $\mathbf{v} \times \boldsymbol{\omega}$ in the form of $\mathcal{F}^{\text{rot}}$. This would necessarily give rise to new contributions in Grad's solution coming from the combination of traceless dyadic products of $\mathbf{V}$, $(\mathbf{V} \cdot \boldsymbol{\omega})$, and $\mathbf{V} \times \boldsymbol{\omega}$. The extension of the present theoretical results by considering the aforementioned terms in Grad's solution is a very challenging problem to be carried out in the future.

It is apparent that the theoretical results presented here are relevant to make a comparison with computer simulations. Previous simulations[27–29] carried out for perfect smooth inelastic spheres ($\beta = -1$) have shown good agreement with kinetic theory results, as is clearly illustrated in most of the plots presented along the paper. We expect that this agreement is also extended to the case of inelastic rough hard spheres. We plan to carry on those simulations in the near future. Another possible future project is the extension of the present results to finite densities by considering the Enskog kinetic equation. In this context, an interesting question is to see if actually there is a transition from DST to CST as the density increases in a similar way as in the limit case of perfectly smooth spheres. Work on this line will be performed in the future.

ACKNOWLEDGMENTS

This paper is dedicated to the memory of Professor Jason Reese who made significant contributions to gas and liquid flows at the micro/nanoscale. The present work has been supported by the Spanish government through Grant No. FIS2016-76359-P and by the Junta de Extremadura (Spain) through Grant Nos. IB16013 and GR18079, partially financed by "Fondo Europeo de Desarrollo Regional" funds. The research of Rubén Gómez González was supported by the predoctoral fellowship of the Spanish government, Grant No. BES-2017-079725.

APPENDIX: NAVIER–STOKES SHEAR VISCOSITY COEFFICIENT OF DRY GRANULAR GASES

The explicit expression of the Navier–Stokes shear viscosity of a *dry* gas of inelastic rough hard spheres is displayed in this Appendix.[54] It is given by

$$\eta_{\text{NS}} = \frac{nT_t}{\nu_t} \frac{1}{\nu_\eta^* - \frac{1}{2}\zeta^*}, \tag{A1}$$

where ν_t and ν_η^* are defined by Eqs. (45) and (50), respectively, and the (reduced) cooling rate ζ^* is

$$\zeta^* = \frac{5}{12} \frac{1}{1+\theta} \left[1 - \alpha^2 + (1-\beta^2) \frac{\kappa + \theta}{1+\kappa} \right]. \tag{A2}$$

Here, the temperature ratio $\theta \equiv T_r/T_t$ is

$$\theta = h + \sqrt{1+h^2}, \tag{A3}$$

where h is defined by

$$h = \frac{(1+\kappa)^2}{2\kappa(1+\beta)^2} \left[1 - \alpha^2 - (1-\beta^2) \frac{1+\kappa}{1+\kappa} \right]. \tag{A4}$$

Physics of Fluids ARTICLE scitation.org/journal/phf

DATA AVAILABILITY

The data that support the findings of this study are available from the corresponding author upon reasonable request.

REFERENCES

[1] P. Coussot, *Mudflow Rheology and Dynamics* (Balkema, Rotterdam, 1997).
[2] J. Chun, T. Oh, M. Luna, and M. Schweiger, "Effect of particle size distribution on slurry rheology: Nuclear waste simulant slurries," Colloids Surf., A **384**, 304–310 (2011).
[3] R. A. Peterson, E. C. Buck, J. Chun, R. C. Daniel, D. L. Herting, E. S. Ilton, G. J. Lumetta, and S. B. Clark, "Review of the scientific understanding of radioactive waste at the U.S. DOE Hanford site," Environ. Sci. Technol. **52**, 381–396 (2018).
[4] H. A. Barnes, "Shear-tickening ("dilatancy") in suspensions of nonaggregating solid particles dispersed in Newtonian liquids," J. Rheol. **33**, 329 (1989).
[5] D. Lootens, H. van Damme, Y. Hémar, and P. Hébraud, "Dilatant flow of concentrated suspensions of rough particles," Phys. Rev. Lett. **95**, 268302 (2005).
[6] E. Brown and H. M. Jaeger, "Dynamic jamming point for shear thickening suspensions," Phys. Rev. Lett. **103**, 086001 (2009).
[7] J. Mewis and N. J. Wagner, *Colloidal Suspension Rheology* (Cambridge University Press, New York, 2011).
[8] M. P. Ciamarra, R. Pastore, M. Nicodemi, and A. Coniglio, "Jamming phase diagram for frictional particles," Phys. Rev. E **84**, 041308 (2011).
[9] M. Otsuki and H. Hayakawa, "Critical scaling near jamming transition for frictional granular particles," Phys. Rev. E **83**, 051301 (2011).
[10] C. Heussinger, "Shear thickening in granular suspensions: Interparticle friction and dynamically correlated clusters," Phys. Rev. E **88**, 050201(R) (2013).
[11] R. Seto, R. Mari, J. F. Morris, and M. M. Denn, "Discontinuous shear thickening of frictional hard-sphere suspensions," Phys. Rev. Lett. **111**, 218301 (2013).
[12] E. Brown and H. M. Jaeger, "Shear thickening in concentrated suspensions: Phenomenology, mechanisms and relations to jamming," Rep. Prog. Phys. **77**, 046602 (2014).
[13] L. C. Hsiao, S. Jamali, E. Glynos, P. F. Green, R. G. Larson, and M. J. Solomon, "Rheological state diagrams for rough colloids in shear flow," Phys. Rev. Lett. **119**, 158001 (2017).
[14] W. T. Kranz, F. Frahsa, A. Zippelius, M. Fuchs, and M. Sperl, "Rheology of inelastic hard spheres at finite density and shear rate," Phys. Rev. Lett. **121**, 148002 (2018).
[15] Y. Madraki, G. Ovarlez, and S. Hormozi, "Transition from continuous to discontinuous shear thickening: An excluded-volume effect," Phys. Rev. Lett. **121**, 108001 (2018).
[16] R. N. Chacko, R. Mari, M. E. Cates, and S. M. Fielding, "Dynamic vorticity banding in discontinuously shear thickening suspensions," Phys. Rev. Lett. **121**, 108003 (2018).
[17] C.-P. Hsu, S. N. Ramakrishna, M. Zanini, N. D. Spencer, and L. Isa, "Roughness-dependent tribology effects on discontinuous shear thickening," Proc. Natl. Acad. Sci. U. S. A. **115**, 5117–5122 (2018).
[18] A. Singh, S. Pednekar, J. Chun, M. M. Denn, and J. F. Morris, "From yielding to shear jamming in a cohesive fricitional suspension," Phys. Rev. Lett. **122**, 098004 (2019).
[19] S. Jamali and J. F. Brady, "Alternative frictional model for discontinuous shear thickening of dense suspensions: Hydrodynamics," Phys. Rev. Lett. **123**, 138002 (2019).
[20] V. Rathee, D. L. Blair, and J. S. Urbach, "Localized transient jamming in discontinuous shear thickening," J. Rheol. **64**, 299–308 (2020).
[21] A. Singh, C. Ness, R. Seto, J. J. de Pablo, and H. M. Jaeger, "Shear thickening and jamming of dense suspensions: The "roll" of friction," Phys. Rev. Lett. **124**, 248005 (2020).
[22] H.-K. Tsao and D. L. Koch, "Simple shear flows of dilute gas-solid suspensions," J. Fluid Mech. **296**, 211–245 (1995).
[23] A. S. Sangani, G. Mo, H.-K. Tsao, and D. L. Koch, "Simple shear flows of dense gas-solid suspensions at finite Stokes numbers," J. Fluid Mech. **313**, 309–341 (1996).
[24] M. G. Chamorro, F. Vega Reyes, and V. Garzó, "Non-Newtonian hydrodynamics for a dilute granular suspension under uniform shear flow," Phys. Rev. E **92**, 052205 (2015).
[25] S. Saha and M. Alam, "Revisiting ignited-quenched transition and the non-Newtonian rheology of a sheared dilute gas-solid suspension," J. Fluid Mech. **833**, 206–246 (2017).
[26] S. Saha and M. Alam, "Burnett-order constitutive relations, second moment anisotropy and co-existing states in sheared dense gas-solid suspensions," J. Fluid Mech. **887**, A9 (2020).
[27] H. Hayakawa, S. Takada, and V. Garzó, "Kinetic theory of shear thickening for a moderately dense gas-solid suspension: From discontinuous thickening to continuous thickening," Phys. Rev. E **96**, 042903 (2017).
[28] H. Hayakawa, S. Takada, and V. Garzó, "Erratum: Kinetic theory of shear thickening for a moderately dense gas-solid suspension: From discontinuous thickening to continuous thickening," Phys. Rev. E **101**, 069904(E) (2020).
[29] H. Hayakawa and S. Takada, "Kinetic theory of discontinuous rheological phase transition for a dilute inertial suspension," Prog. Theor. Exp. Phys. **2019**, 083J01.
[30] R. Gómez González and V. Garzó, "Simple shear flow in granular suspensions: Inelastic Maxwell models and BGK-type kinetic model," J. Stat. Mech. **2019**, 013206.
[31] V. Garzó, S. Tenneti, S. Subramaniam, and C. M. Hrenya, "Enskog kinetic theory for monodisperse gas-solid flows," J. Fluid Mech. **712**, 129–168 (2012).
[32] A. Scala, "Event-driven Langevin simulations of hard spheres," Phys. Rev. E **86**, 026709 (2012).
[33] S. Hess, "Brownian motion of rotating particles," Z. Naturforsch. **23**, 597–609 (1968).
[34] S. Jahanshahi, C. Lozano, B. ten Hagen, C. Bechinger, and H. Löwen, "Colloidal Brazil nut effect in microswimmer mixtures induced by motility contrast," J. Chem. Phys. **150**, 114902 (2019).
[35] H. Grad, "On the kinetic theory of rarefied gases," Commun. Pure Appl. Math. **2**, 331–407 (1949).
[36] A. Santos, "A Bhatnagar–Gross–Krook-like kinetic equation for a granular gas of inelastic rough hard spheres," AIP Conf. Proc. **1333**, 41–48 (2011).
[37] C. K. K. Lun, "Kinetic theory for granular flow of dense, slightly inelastic, slightly rough spheres," J. Fluid Mech. **233**, 539–559 (1991).
[38] J. T. Jenkins and M. W. Richman, "Kinetic theory for plane flows of a dense gas of identical, rough, inelastic, circular disks," Phys. Fluids **28**, 3485–3493 (1985).
[39] A. Goldshtein and M. Shapiro, "Mechanics of collisional motion of granular materials. Part 1. General hydrodynamic equations," J. Fluid Mech. **282**, 75–114 (1995).
[40] A. Zippelius, "Granular gases," Physica A **369**, 143–158 (2006).
[41] N. Brilliantov and T. Pöschel, *Kinetic Theory of Granular Gases* (Oxford University Press, Oxford, 2004).
[42] V. Garzó, *Granular Gaseous Flows* (Springer Nature Switzerland, Basel, 2019).
[43] A. Santos, G. M. Kremer, and V. Garzó, "Energy production rates in fluid mixtures of inelastic rough hard spheres," Prog. Theor. Phys. Suppl. **184**, 31–48 (2010).
[44] R. Gómez González, N. Khalil, and V. Garzó, "Enskog kinetic theory for multicomponent granular suspensions," Phys. Rev. E **101**, 012904 (2020).
[45] N. G. van Kampen, *Stochastic Processes in Physics and Chemistry* (North Holland, Amsterdam, 1981).
[46] D. L. Koch, "Kinetic theory for a monodisperse gas-solid suspension," Phys. Fluids A **2**, 1711–1722 (1990).
[47] D. L. Koch and R. J. Hill, "Inertial effects in suspensions and porous-media flows," Annu. Rev. Fluid Mech. **33**, 619–647 (2001).
[48] J. J. Wylie, D. L. Koch, and A. J. C. Ladd, "Rheology of suspensions with high particle inertia and moderate fluid inertia," J. Fluid Mech. **480**, 95 (2003).
[49] J. W. Dufty, A. Santos, J. J. Brey, and R. F. Rodríguez, "Model for nonequilibrium computer simulation methods," Phys. Rev. A **33**, 459–466 (1986).
[50] V. Garzó and A. Santos, Kinetic theory of gases in shear flows, in *Nonlinear Transport* (Kluwer Academic Publishers, Dordrecht, 2003).
[51] V. Garzó, "Grad's moment method for a granular fluid at moderate densities: Navier–Stokes transport coefficients," Phys. Fluids **25**, 043301 (2013).

Physics of Fluids ARTICLE scitation.org/journal/phf

[52]H. Struchtrup, *Macroscopic Transport Equations for Rarefied Gas Flows* (Springer, Berlin, 2005).
[53]J. S. Dahler and M. Theodosopulu, "The kinetic theory of dense polyatomic fluids," Adv. Chem. Phys. **31**, 155–229 (1975).
[54]G. Kremer, A. Santos, and V. Garzó, "Transport coefficients of a granular gas of inelastic rough hard spheres," Phys. Rev. E **90**, 022205 (2014).
[55]A. Santos, G. M. Kremer, and M. dos Santos, "Sonine approximation for collisional moments of granular gases of inelastic rough spheres," Phys. Fluids **23**, 030604 (2011).
[56]F. Vega Reyes, G. Kremer, and A. Santos, "Role of roughness on the hydrodynamic homogeneous base state of inelastic hard spheres," Phys. Rev. E **89**, 020202(R) (2014).
[57]F. Vega Reyes and A. Santos, "Steady state in a gas of inelastic rough spheres heated by a uniform stochastic force," Phys. Fluids **27**, 113301 (2015).
[58]D. J. Evans and G. P. Morriss, *Statistical Mechanics of Nonequilibrium Liquids* (Academic Press, London, 1990).
[59]A. Santos, V. Garzó, and J. W. Dufty, "Inherent rheology of a granular fluid in uniform shear flow," Phys. Rev. E **69**, 061303 (2004).
[60]V. Garzó, "Shear-rate-dependent transport coefficients in granular suspensions," Phys. Rev. E **95**, 062906 (2017).
[61]J. J. Wylie and D. L. Koch, "Particle clustering due to hydrodynamic interactions," Phys. Fluids **12**, 964 (2000).
[62]J. J. Wylie, Q. Zhang, Y. Li, and X. Hengyi, "Driven inelastic-particle systems with drag," Phys. Rev. E **79**, 031301 (2009).
[63]J. E. Hilton and A. Tordesillas, "Drag force on a spherical intruder in a granular bed at low Froude number," Phys. Rev. E **88**, 062203 (2013).
[64]T. Wang, M. Grob, A. Zippelius, and M. Sperl, "Active microrhelogy of driven granular particles," Phys. Rev. E **89**, 042209 (2014).
[65]J. M. Montanero and V. Garzó, "Rheological properties in a low-density granular mixture," Physica A **310**, 17–38 (2002).
[66]M. Huthmann and A. Zippelius, "Dynamics of inelastically colliding rough spheres: Relaxation of translational and rotational energy," Phys. Rev. E **56**, R6275–R6278 (1997).
[67]S. Luding, M. Huthmann, S. McNamara, and A. Zippelius, "Homogeneous cooling of rough, dissipative particles: Theory and simulations," Phys. Rev. E **58**, 3416–3425 (1998).
[68]O. Herbst, M. Huthmann, and A. Zippelius, "Dynamics of inelastically colliding spheres with Coulomb friction: Relaxation of translational and rotational energy," Granular Matter **2**, 211–219 (2000).
[69]The only difference between both results is the existence of some contributions proportional to $(\partial a^*/\partial\theta_t)_s$ in Ref. 29 that are absent in our results. However, since $a^* \propto T_{ex}^{-1/2} \equiv$ const. in the time-dependent problem, these type of contributions are not present when one slightly perturbs the steady state by small homogeneous time-dependent perturbations.

Chapter 7

Results and Discussion

7.1 Homogeneous States of Granular Suspensions

At a first step, we have analyzed the time-dependent homogeneous states of granular suspensions. The dynamic properties of grains in homogeneous states have been described in the framework of the Enskog–Boltzmann equation. As usual, the influence of the surrounding viscous gas on the dynamics of grains has been accounted for by an effective force constituted by two terms: a viscous drag force plus a Langevin-like term. This suspension model is based on the assumption that, if the gas phase is dilute enough, the presence of interstitial fluid does not significantly affect the grain-grain collisions and therefore the collision operator can be approximated to that of the dry (without gas phase) granular gas. Moreover, when the number density of the gas phase is greater than that of the granular gas, the state of the interstitial fluid is not affected by the presence of grains and so, the surrounding fluid can be considered as a thermostat at a given temperature T_{ex}. On the other hand, following the results for gas-solid simulations [171, 173], the drag coefficients exhibit a complex dependence on density and have been chosen to be different in the case of bidisperse suspensions [see Eqs. (2.20) and (2.32)].

The objective of this thesis with regard to the study of homogeneous states is twofold. First, we want to characterize the time evolution of the system towards the asymptotic steady state. In particular, we have investigated the existence of a *universal* hydrodynamic stage where the evolution of bidisperse granular mixtures only occurs through its dependence on the global temperature $T(t)$. The existence of the

hydrodynamic or normal solution is the main hypothesis in the application of the Chapman–Enskog method [122] to obtain the Navier–Stokes transport coefficients of granular suspensions [4]. Also in the transient regime, we have explored the so-called Mpemba effect [182, 183] (an initially hotter sample can cool down sooner than a colder one) in bidisperse molecular and granular suspensions. For times much longer than the mean free time, the system is expected to reach a steady state. The steady homogeneous properties of granular suspensions have been derived as a second objective. In the case of monocomponent granular suspensions, the steady values for the granular temperature T and the *kurtosis* or fourth cumulant a_2 have been displayed as functions of the coefficient of restitution, the volume fraction, and the parameters of the bath. On the other hand, the extension to bidisperse mixtures has allowed us to assess also the dependence of the partial temperature ratio T_1/T_2, the fourth cumulants c_1 and c_2 on the mass and size ratios, the concentration, the coefficients of restitution, and the influence of the bath. The theoretical results obtained in each one of the different issues covered in the homogeneous state have been confronted against available and self-made DSMC simulations as well as MD simulations in the case of the temperature ratio T_1/T_2.

Concerning the temporal evolution of the distribution functions f_i, theory and simulations have clearly shown that after a kinetic stage, an *unsteady* hydrodynamic stage is identified. At this stage of evolution, the response of the system to any deviation from the local steady distribution is characterized by the evolution of the only relevant homogeneous hydrodynamic field in the homogeneous time-dependent problem, i.e., the granular temperature T. As for driven granular gases [97, 140], the "hydrodynamic" distribution $f_i(\mathbf{v};t|f_i^{(0)})$ has the scaling form

$$f_i(\mathbf{v};t|f_{i,0}) = n_i v_0^{-d} \varphi_i \left[\mathbf{c}(t), T(t)/T_{\text{ex}}\right], \tag{7.1}$$

where $f_{i,0}$ denotes the initial distribution function. Therefore, the time dependence of φ_i on the temperature occurs through the dimensionless velocity $\mathbf{c}(t) = \mathbf{v}/v_0(t)$, and the granular to external temperature ratio $\theta(t) = T(t)/T_{\text{ex}}$. For the sake of illustration, Figs. 3 and 4 of Article 2 show that the kinetic velocity moments $\theta_i(t) = T_i(t)/T_{\text{ex}}$ and $c_i(t)$ evolve towards a universal hydrodynamic curve characterized by the functions $\theta_i\left[\theta(t)\right]$ and $c_i\left[\theta(t)\right]$ regardless of the initial conditions.

The complex dependence of γ_i on the partial ϕ_i and total $\phi = \phi_1 + \phi_2$ volume fractions, the masses m_i, and diameters σ_i of the mixture gives rise to the emergence of a broad range of complex phenomena. For example, we have observed the Mpemba-like effect in a binary mixture in contact with a thermal reservoir. The bath parameters couple the evolution of the partial temperature ratio $T_1(t)/T_2(t)$ to that of the global temperature $T(t)$ giving rise to the presence of memory effects.

To study this effect, two identical samples A and B characterized by their initial temperatures ($T_{A,0}$ and $T_{B,0}$) and temperature ratios [$(T_{1,0}/T_{2,0})_A$ and $(T_{1,0}/T_{2,0})_B$] have been considered. These samples are in contact with a thermal reservoir at a temperature T_{ex}. We let the systems evolve towards equilibrium where equipartition holds $T_i = T_{i,1} = T_{i,2} = T_{\text{ex}}$ ($i = A, B$). The evolution of temperature is determined by the way of yielding heat from the bath to each one of the species. Since this energy transmission is completely established by the dependence of γ_i on the parameters of the mixture, we can study the energy transmission rate of each species to suitably chose the initial values of the total and the partial temperatures. An appropriate choice may lead the evolution of the temperatures T_A and T_B to cross before reaching the equilibrium state. In contrast to previous works [183], no cumulants are needed for the crossover to happen; in fact we have approximated f_i by their Maxwellian forms.

To gain some insight, situations near the final asymptotic equilibrium state have been first considered. This has allowed us to obtain explicit expressions for the (reduced) crossing time t_c^* and the critical value of the initial temperature difference [see Eqs. (29) and (30) of Article 3]. An illustration of the above results is displayed in Figs. 1–3 of Article 3 as functions of the mass m_1/m_2 and diameter σ_1/σ_2 ratios and the composition x_1, respectively. The comparison between those theoretical predictions with the DSMC results shows an excellent agreement for both the crossing times t_c^* and the phase diagrams regarding the regions of the parameter space where the Mpemba-like effect is observed.

For the sake of completeness, we have explored the Mpemba-like effect for situations far away from equilibrium. The distance to equilibrium of the total and partial temperatures allow the emergence of a large Mpemba effect. Namely, when the initial difference between the temperatures of two samples is of the same order than the temperatures themselves. In this case, no analytical expressions can be obtained and a more qualitative description has been addressed. The necessary but not sufficient

conditions for the existence of the crossover have been given in terms of the sign of the difference $\gamma_1 - \gamma_2$ [see Eq. (34) of Article 3]. These theoretical conditions have been compared with MD and DSMC simulations for two different densities: $\phi = 0.00785$ and $\phi = 0.1$. Fig. 5 of Article 3 shows that the Mpemba effect and its inverse counterpart emerge when the conditions (34) are fulfilled. Moreover, the good agreement with the simulation data ensures the Maxwellian approximation and the validity of the kinetic equations to model out-of-equilibrium systems.

The Mpemba-like effect has also been investigated in the case of driven granular mixtures where the inelasticity of collisions increases the possibility to observe such effect. However, the presence of the cooling term ζ in the evolution equation of T [see Eq. (11) of Article 2] makes more difficult to find initial conditions for the onset of the Mpemba effect. In analogy with the molecular case, both close and far from the steady state situations have been explored. The analytical expression for the crossing time t_c^* and the necessary conditions for the effect to occur have been plotted in Fig. 5 of Article 2 for situations close to the steady state. These conditions [given in Eq. (47) of Article 2] have been compared with DSMC simulations with an excellent agreement. Then, we have explored non-linear situations. The inelasticity of collisions enlarges the region of parameter where we can observe the effect. Therefore, non-linear effects arise and non-Monotonic and mixed Mpemba effects can be detected. Fig. 6 of Article 2 illustrates the large, non-monotonic, and mixed Mpemba effects for a given case and exhibits a good agreement between theory and DSMC simulations.

Finally, the stationary values of the temperatures and fourth cumulants have been determined and compared with computer simulations. On the one hand, as in previous works on granular fluids driven by thermostats [97, 148, 149], the way of scaling the distribution function f_{s} differs from previous works [4, 60, 220] where φ_{s} depends on T only through the scaled velocity $\mathbf{c}$ [see Eq. (30) of Article 1]. Thus, the analysis of the HSS in monocomponent granular gases has allowed us to assess this complex dependence of the reference distribution function, but also to analyze the additional effect of density on the stationary velocity moments. Although the exact form of φ_{s} is not known, a good approximation of this distribution is provided by the leading Sonine approximation [220]. By using this distribution, we have explicitly obtained the fourth cumulant $a_{2,\mathrm{s}}$, which gives information about the departure of φ_{s} from its Maxwellian form. Once obtained, an expression for the (reduced) steady temperature $(T_{\mathrm{s}}/T_{\mathrm{ex}})$ has

been derived. In spite of the approximations involved in such derivations, the theoretical predictions for both quantities agree very well with DSMC simulations performed in Ref. [148, 149] when setting $R(\phi) \to 1$ (see Figs. 1-4 of Article 1). With regard to binary suspensions, the study carried out in this thesis complements a previous comparison made in Ref. [99] between theoretical results and MD simulations. Since the DSMC method does not avoid the inherent assumptions of kinetic theory, it was worth to revisit the problem to analyze whether the origin of the discrepancies found in [99] is related with the existence of velocity correlations or of the Sonine approximation employed to get T_1/T_2, c_1, and c_2. These results have been displayed in Figs. 7–9 of Article 2 where we have varied the mass m_1/m_2, diameter σ_1/σ_2, and partial volume fractions ϕ_1/ϕ_2 ratios. The theoretical results for the temperature ratio T_1/T_2 agree very well with DSMC simulation in all the cases considered. Conversely, some discrepancies have been found in the case of the cumulants c_1 and c_2, specially in c_2. Based on previous results obtained for monocomponent granular gases [251, 252], a straightforward explanation could be given in terms of a possible lack of convergence of the Sonine expansion: the effect of inelasticity could increase the value of higher order cumulants and therefore the truncation in the leading terms of the expansion would not be longer accurate. Finally, as an application, a linear stability analysis of the steady state solution for binary suspensions was also carried out showing that the steady state is always linearly stable.

7.2 Transport Coefficients of Granular Suspensions

Once the reference state is well characterized, we have perturbed the HSS by small spatial gradients of the hydrodynamic fields. The Chapman–Enskog method [122] has been applied to solve the Enskog equations for monocomponent and bidisperse granular suspensions. We have retained in both situations terms up to the first-order contributions in the perturbation scheme (Navier–Stokes hydrodynamic order). The main difference between the monocomponent and binary cases has relied on the different approaches taken to address the reference distribution functions. While the fourth cumulant a_2 of the Sonine polynomial expansion of $f^{(0)}$ has been retained in all the calculations involving the transport coefficients of monocomponent suspensions, the added difficulty of having two coupled equations in the case of binary mixtures causes

that non-Gaussian corrections to the distribution functions $f_i^{(0)}$ have been neglected. This assumption is based on the fact that the values of the cumulants c_1 and c_2 were shown in general to be small enough. This means that $f_i^{(0)}$ has been approximated by its Maxwellian form [see Eq. (47) of Article 5].

Moreover, as noted in previous works [99, 148, 149], since the densities n_i and the granular temperature T fields are defined separately in the local reference state, then the temperature is in general a time-dependent function $\left(\partial_t^{(0)} T \neq 0\right)$. Thus, the distribution functions depend on time through its dependence on the temperature. Although we were interested in obtaining analytical expressions of the transport coefficients under steady state conditions, the fact that $\partial_t^{(0)} T \neq 0$ gives rise to contributions to them that depend not only on the steady hydrodynamic fields, but also on the values of the fields in the vicinity of the perturbed state to the steady state. These new contributions are given in terms of the derivatives of the relevant kinetic variables with respect to the parameters of the suspensions. For example, $(\partial a_2/\partial\theta)_{\rm s}$; $(\partial a_2/\partial\lambda)_{\rm s}$; and $(\partial a_2/\partial\chi)_{\rm s}$ for the monocomponent case, and $(\partial\tau_1/\partial\theta)_{\rm s}$; $(\partial\tau_1/\partial\lambda_1)_{\theta,x_1,\phi}$; $(\partial\tau_1/\partial x_1)_{\theta,\lambda_1,\phi}$; and $(\partial\tau_1/\partial\phi)_{\theta,\lambda_1,x_1}$ for binary suspensions. The inclusion of the above derivatives introduces conceptual and practical difficulties not present in the case of dry granular mixtures [190, 191].

The procedure to obtain the NS transport coefficients has been implemented in two steps. First, we have computed the balance equations [Eqs. (16)–(18) of Article 1 and Eq. (20)–(22) of Article 5] from the Enskog equation. These equation include terms that account for the influence of the bath and the kinetic and collisional contributions to the cooling rate and the mass, momentum, and heat fluxes. Then, the constitutive equation for the fluxes and the cooling rate have been derived and the transport coefficients have been displayed in terms of arbitrary values of the inelasticity and the parameters of the suspension. As usual, in order to obtain analytical expressions, the leading terms in a Sonine polynomial expansion have been considered.

With regard to monocomponent granular suspensions, the explicit forms for the NS transport coefficients have been provided along section 5 of Article 1. In particular, the bulk $\eta_{\rm b}$ and shear η viscosities are given by equations (69) and (71), respectively, the thermal conductivity κ is given by equations (73) and (75), the heat diffusive conductivity μ is given by equations (77) and (78), and the first-order contribution ζ_U to the cooling rate is given by equations (81) and (82). It is quite apparent that the

(reduced) transport coefficients exhibit a complex dependence on both the coefficients of restitution and the density. In addition, Figs. 6–8 of the same paper highlight the impact of the gas phase on the granular properties since the α-dependence is clearly different from that found in dry granular gases (see for instance Figs. 3.1–3.4 of Ref. [4]). Moreover, the *new* density dependence of the drag coefficient γ significantly affects the form of the heat flux transport coefficients and the cooling rate as can be noticed when comparing with the results obtained in Refs. [148, 149].

As an application of the previous results, a stability analysis of the HSS has been carried out. For small spatial gradients, we have perturbed the hydrodynamic fields from their values in the HSS. Moreover, as usual in this sort of stability analysis, we have assumed that the interstitial gas is not perturbed. Equations (92) and (102) of Article 1 show that the eigenvalues for the transversal shear and longitudinal modes have always a positive real part. This means that there are no regions of the parameter space for which the system becomes linearly unstable. These results are consistent with those obtained in Refs. [148, 149] indicating that the density dependence of γ does not affect the stability of the HSS. Nevertheless, it is well worth remembering that the conclusions drawn for the stability of dry granular gases [66, 69] differs from those obtained here because it was found that the time-dependent homogeneous reference state in dry granular gases can turn out to be unstable. This points out again the relevance of the interstitial fluid on the physical properties of granular gases.

The extension to binary mixtures has allowed us to compute the influence of the action of the gas phase not only on the transport properties computed above, but also on those associated to the mass flux. The explicit forms of the transport coefficients have been displayed in Sec. VI and Appendix C of Article 5: the mutual diffusion coefficients D_{11} and D_{12} are the solutions of the algebraic equations (C2), the velocity D_1^U and thermal D_1^T diffusion coefficients are given by Eqs. (108) and (C10), respectively, the shear viscosity η and the first-order coefficients ϖ_i to the partial temperatures are the solutions of Eqs. (C12) and (C18), respectively, and the first-order contribution $\zeta_U = \zeta^{(1,0)} + \zeta^{(1,1)}$ to the cooling rate is given by Eqs. (B8), (113), and (114). In reduced forms, the expressions for the transport coefficients are quite complex and hence, here we only have payed attention to the influence of the inelasticity and the gas phase on the dynamics of grains. In general, the impact of the interstice is important since the α-dependence is quite different from that found when the gas phase is neglected

[4]. For example, comparison of Fig. 3 with Figs. 5.5–5.7 of Ref. [4] clearly shows that in the dry case the (reduced) mutual diffusion coefficients D_{11}^* and D_{12}^* exhibit non-monotonic behaviors whereas the influence of the bath makes their values strictly decrease with inelasticity. In addition, the behavior of D_1^{T*} is completely different when the influence of the interstitial gas is taken into account. In the special case of the shear coefficient η^*, Fig. 4 demonstrates more qualitative similarities between binary suspensions and granular mixtures (see Fig. 5.8 of Ref. [4]). However, there are still significant quantitative differences in both approaches.

On the other hand, the coefficients $T_i^{(1)}$ are usually neglected in many of the previous works devoted to granular mixtures [186, 190, 191]. Since $T_i^{(1)} = \varpi_i \nabla \cdot \mathbf{U}$, an interesting question is to assess the impact of the first-order coefficients ϖ_i on both the bulk viscosity η_b and the first-order contribution ζ_U to the cooling rate. This influence has been evaluated in dry binary mixtures and suspensions. The results obtained in the case of granular mixtures show that the magnitude of ϖ_i is in general quite important, specially for large mass ratios and strong inelasticities (see Fig. 1 of Article 4). Hence, its impact on η_b and ζ_U cannot be neglected for disparate masses and/or strong dissipation (see Figs. 2 and 3 of Article 4). In contrast with the findings reported in Article 4 for freely cooling granular dilute mixtures ($\phi = 0$), the results derived for granular suspensions (Article 5) show that the first-order contributions ϖ_1 are different from zero even when $\phi = 0$. A more complete analysis of the influence of the first-order contributions in dilute regimes can be found in Ref. [253]. However, the gas phase considerably reduces the magnitude of ϖ_1 and hence, its influence on η_b and ζ_U is very tiny (see Figs. 6 and 7 of Article 5).

7.3 Non-Newtonian Properties of Granular Suspensions Under Simple Shear Flow

A widely studied problem in kinetic theory [127, 128, 135, 142–144, 249, 254] is the determination of the non-Newtonian transport properties in inertial suspensions under simple (or uniform) shear flow. Starting from the Boltzmann equation, we have characterized the non-linear response of the system by means of the shear-rate dependence of several properties such as the (scaled) temperature θ, the (reduced) nonlinear shear viscosity η^*, and the (reduced) viscometric function Ψ^* for both smooth and rough

spheres. An interesting conclusion is that the viscosity presents a *discontinuous* shear thickening transition for very dilute systems, namely, the shear viscosity exhibits an abrupt growth at a certain critical shear rate. The same applies to the remaining rheological properties whose flow curves with respect to the shear rate show an S-shape. On the other hand, although the rheological properties are the most relevant quantities in a sheared suspension, higher degree moments are also important since they provide indirect information on the velocity distribution function.

As usual, the influence of the background gas on smooth spheres has been accounted for by an effective force constituted by two terms: (i) a drag force proportional to the instantaneous velocity $\mathbf{v}$ of particles and (ii) a Langevin-like operator in the form $-(\gamma_t T_{\text{ex}})\,\partial^2 f/\partial v^2$. For consistency and according to a generalized Fokker–Planck equation for rotating spheres proposed many years ago by Hess [203], the extension to rough spheres accounting for the coupling between the rotational degrees of freedom of grains and the gas phase has been also modeled by two terms: a drag term proportional to the angular velocity $\boldsymbol{\omega}$ plus a Langevin-like operator $-(\gamma_r T_{\text{ex}})\,\partial^2 f/\partial \omega^2$. Here, γ_t and γ_r are the translational and rotational friction coefficients, respectively.

One of the main mathematical intricacies in solving the Boltzmann equation comes from the form of the Boltzmann collision operator (2.2). Thus, to accomplish the determination of higher-degree moments in the USF problem, one has to consider simplified collision models where velocity moments can be obtained without having to use approximate methods. In particular, we have obtained the rheological properties using the IMM [242, 255] and BGK-like [199] kinetic equations for smooth spheres in Article 6. In particular, the comparison between the *exact* results for θ, η^*, and Ψ^* with approximate Grad's results and computer simulations displayed in Refs. [142, 143] has allowed us to assess the accuracy of both approaches (IMM and BGK results) in conditions of practical interest. The results plotted in Fig. 2 highlight the good performance of IMM and BGK-type models to reproduce the shear-rate dependence of the rheological properties. Whereas we have found a perfect match between IMM, BGK, and IHS results, some discrepancies have been detected in a small region close to the transition point where the simulation data suggest a sharper transition than the Boltzmann results. We think that this small discrepancy is mainly due to the limitations of the Boltzmann equation for accounting small density corrections to η^* around this transition point. Although the origin of the DST has been attributed to structural properties and mutual friction

between grains [256], we have been able to reproduce the DST effect by means of an extremely simple interaction model, such as the IMM.

However, as well as all previous theoretical works [127, 128, 135, 142–144, 249, 254], we had originally considered inertial suspensions of smooth inelastic hard spheres, and hence, the effects of tangential friction in particle collisions on non-Newtonian rheology had been neglect. To address that question, we have derived the rheological properties considering also the rotational velocity of particles. To do so, two different but complementary routes have been used: Grad's moment expansion of the distribution function [223] and a BGK-like kinetic model suitably adapted to rough spheres [204]. Both approximations agree when we make the choice given in the Eq. (79) of Article 7 for the free parameter $\chi(\kappa, \alpha, \beta)$ of the kinetic model. Moreover, Fig. 5 shows the dependence of the (reduced) rheological properties on the shear rate in terms of the parameter space of the problem (the restitution coefficients α and β, the reduced moment of inertia κ, and the reduced background temperature T_{ex}^*). Note that we also have a remaining dependence on the reduced density $n^* = n\sigma^d$ that is neccessary since we want to compare the results for $\beta = -1$ with the simulation data reported in Refs. [142, 143]. Hence, the scaling of the shear rate a and the bath temperature T_{ex} must be the same as in the simulations. The main conclusion reported here is that the roughness does not significantly affect the main trends observed in the smooth case; a sharp transition of the shear viscosity η^* also emerges at a given value of the shear rate a^*. At a more quantitative level, we have also observed that while the roughness slightly smoothes the increase of viscosity η^* at a given value of α, the transition of the (reduced) rotational temperature θ_r is enhanced as β increases. This is a quite unexpected discovery since most of the results obtained for concentrated suspensions have shown that friction enhances DST.

Beyond non-Newtonian rheology, the fourth-degree moments are the first nontrivial moments in the steady simple shear flow problem. As in elastic [257, 258] and inelastic [255] systems, the symmetric (non-vanishing in the steady state) fourth-degree moments of IMM have unphysical values in a certain region of the parameter space of the system. This singularity contrasts with the BGK results where all the moments are well-defined functions. The phase diagram regarding the regions where the IMM moments are not physical values has been obtained from the condition $\det \mathcal{L} = 0$, where $\mathcal{L}$ is the matrix that couples the equations for the fourth-degree moments. In this case, since the

(scaled) temperature θ is a multi-valued function of the (reduced) shear rate a^*, we have taken θ instead of a^* as the input parameter to find out the different regions of divergence of the IMM moments. Our results show that those moments diverge in the region $\theta_c^{(1)}(\alpha) < \theta < \theta_c^{(2)}(\alpha)$, where the critical values $\theta_c^{(i)}(\alpha)$ are completely different from those previously derived for ordinary gases [258] and dry granular gases [255]. At a given value of the coefficient of normal restitution α, surprisingly the BGK and IMM results show an excellent agreement in the region $\theta < \theta_c^{(1)}$ and $\theta > \theta_c^{(2)}$ for values of $a^* \leq 1$, where nonlinear effects are already important (see, for instance, Figs. 5 and 6 of Article 6). In addition, the shear-rate dependence of the fourth-degree moments is practically independent of inelasticity and roughness in this range of values of the shear rate (see Fig. 6 of Article 7). This feature contrasts with the behavior of the Navier–Stokes form of the viscosity $\eta_{\text{NS}}^*(\alpha)$ since its value clearly differs from its elastic and smooth counterparts (see Fig. 2 of Article 7). Moreover, the ratio $\eta_{\text{NS}}^*(\alpha)/\eta_{\text{NS}}^*(1)$ is very different from that found in free cooling granular gases (see Figs. 1 of Article 6 and 7). Namely, while this ratio exhibits a non-monotonic dependence on the coefficient of normal restitution in the case of granular suspensions, it increases with decreasing α in the dry granular case. That underscores the crucial importance of the effect of dissipative dynamics and the role of the interstitial fluid on the transport properties of granular gases.

Since the BGK moments are well defined functions of both α and a^*, we have explored the shear-rate dependence of the fourth degree moments beyond the region $a^* \leq 1$. Figures 9 of Article 6 and 7 of Article 7 show that the scaled moment $M_{4|0}(a^*)/M_{4|0}(0)$ and $M_{2|xy}^*(a^*)$ also display an S-shape in a similar way to the viscosity η^*. This behavior has been also observed in the remaining (symmetric) fourth-degree moments. We plan to assess the reliability of these striking results with computer simulations in the near future.

As a complement of the previous results, we have also analyzed the stability of the steady simple shear flow solution for non-Newtonian rheology. It is worth noting that these instabilities have nothing to do with the divergences of the IMM moments which stem from inaccuracies inherent in the model and model parameters. In this case, the linear stability analysis shows the region of the parameter space where the steady solution is linearly unstable. Figure 11 of Article 7 displays the boundary lines delimiting the stable/unstable regime $\theta_t^{(1)}(\beta) < \theta < \theta_t^{(2)}(\beta)$ as a function of β for fixed

α, κ, n^*, and $T_{\rm ex}^*$. We should underline that the unstable region usually belongs to the range of (reduced) shear rates a^* where DST appears [see the thick lines of Fig. 5 of Article 7]. So it is likely that the emergence of a discontinuous transition in the shear viscosity arises from or in connection with the former instabilities.

Conclusions and Outlooks

In this work transport properties of granular suspensions have been studied. Within the context of the kinetic theory, the Boltzmann and Enskog equations have been conveniently adapted to account for the inelasticity of collisions. While the Boltzmann equation applies to low-density gases, the Enskog equation holds for moderately dense gases. As usual, the influence of the gas phase on grains has been introduced in the Boltzmann and Enskog equations by means of a Fokker–Planck term (drag friction plus stochastic Langevin-like term). Such forces compensate for the inelastic cooling due to binary collisions and so, the system reaches a non-equilibrium steady state. The monocomponent case has been considered as the starting point. Then, the results have been extended to the case of bidisperse suspensions. As far as possible, theoretical results have been compared against computer simulations available in the relevant literature and DSMC data obtained in this thesis.

Firstly, the homogeneous states of monocomponent and binary suspensions have been investigated. The velocity distribution functions have been approximated in most of the situations as a truncated expansion in Sonine polynomials. Namely, the scaled distribution functions have been explicitly written in terms of their fourth velocity moments (or fourth cumulants). In the transient regime, we have assessed that the time evolutions of the partial (reduced) temperatures θ_i and cumulants c_1 and c_2 of a binary granular suspension occur over universal hydrodynamic curves where all their time-dependence is through the scaled temperature θ. This result supports the hydrodynamic or normal solution on which the Chapman–Enskog procedure is built. Also for time-dependent homogeneous situations, we have studied the emergence of the so-called Mpemba-like effect (a hotter sample can cool down sooner) for granular binary suspensions. First, we have derived analytical results for the crossing time t_c^* and the necessary initial conditions for the Mpemba effect to happen in situations close to the

non-equilibrium steady state where the non-linear effects are neglected. Moreover, we also have explored situations far from the asymptotic final steady state where the non-linear large, non-monotonic, and mixed Mpemba effects have been shown to arise. The main conclusion is that the Mpemba-like effect arises even in molecular (elastic) suspensions. In this case, neglecting the influence of the cumulants on the distribution functions, a straightforward explanation in terms of the relative difference of friction coefficients γ_1 and γ_2 has been provided. For times longer than the mean free time, the system reaches a steady state. The steady value of the temperature T, temperature ratio T_1/T_2, and mono a_2 and bidisperse c_1 and c_2 cumulants have been compared against DSMC simulations displaying in general good agreement. Hence, the Sonine approximation is well-justified.

The Navier–Stokes transport coefficients have been determined by solving the Enskog equation by means of the Chapman–Enskog expansion. Heat and momentum fluxes have been determined up to first-order deviations of the hydrodynamic fields from the homogeneous steady state. In reduced forms, the shear η^* and bulk η_{b}^* viscosities, the thermal κ^* and diffusive heat μ^* conductivities, as well as the first-order contribution ζ_U to the cooling rate have been demonstrated to exhibit a complex dependence on the parameters of the granular suspension. In the binary counterpart, we have also computed the shear η^* and bulk η_{b}^* viscosities, the diffusion coefficients D_{ij}^*, D_i^{T*}, and D_i^{U*}, and the first-order contributions to the partial temperatures ϖ_i and the cooling rate ζ_U. These latter coefficients clearly differ from previous works where neither the density dependence of the reference state nor the additional contribution to the non-equipartition of energy coming from the expansion in gradients of the partial temperatures were considered. In addition, we have shown that the influence of the bath can be relevant in conditions of practical interest. For instance, the α-dependence in the special case of the shear viscosity η^* shows qualitative differences with respect to the dry case. While η^* decreases as α increases for very dilute freely cooling granular gases ($\phi = 0$), the opposite behavior have been found in the suspension counterpart. For finite values of the solid volume fraction ($\phi = 0.1$), η^* exhibits a non-monotonic dependence on the inelasticity in the dry case whereas it has been shown that η^* always decreases as the inelasticity increases when the interstitial gas is accounted for. More qualitative similarities between the shear viscosity coefficient of binary suspensions and granular mixtures have been detected. However, there are still significant

relative differences of up to 50% between the shear viscosity of both systems. Another important result obtained for granular suspensions has to do with the stability of the HSS; whereas some instabilities are found in free cooling granular gases, the action of the bath causes that any small perturbation of the HSS is quickly dissipated.

Finally, a complete theoretical description of the non-Newtonian transport properties of a dilute granular suspension under uniform shear flow has been presented. Three different but complementary routes have been used to model the rheology of suspensions composed of smooth and rough spheres: Grad's moment method, BGK-type kinetic model, and Inelastic Maxwell Models. The rheological properties of *smooth* suspensions (associated with the second-order velocity moments) have been computed using the IMM and BGK-like model with good agreement with previous Grad's and EDLSHS results. A surprising finding is that the discontinuous shear thickening effect on the viscosity is also present in *structurally* simple models such as the IMM. Beyond the second-order regime, we have explored the divergence of the IMM fourth-order moments. As in previous elastic and inelastic cases, some unphysical regions have been found and studied in terms of the parameter space of the suspension. Conversely, the BGK results are always well-defined and have shown to display an S-shape transition in the (symmetric) fourth-degree moments in the same way as in the case of the shear viscosity η^*. We have also evaluated the impact of roughness in the above non-Newtonian results. The principal conclusion is that the main trends observed for the smooth case do not substantially change when the friction is accounted for. Nonetheless, more quantitative discrepancies have been found: while the roughness slightly smoothes the increase of viscosity η^* at a given value of the normal coefficient of restitution α, the transition of the (reduced) rotational temperature θ_r is enhanced as the tangential restitution β increases. As an application of the previous results, the stability of the steady simple shear flow solution for non-Newtonian rheology has been analyzed. An unstable region appears in the same range of values of the shear rate a^* where the DST transition occurs. Hence, there might be a relation between the emergence of a discontinuous transition in the shear viscosity and the instabilities of the steady solution.

Outlooks

One of the objectives of the present work has been the determination of the Navier–Stokes transport coefficients of a binary suspension associated to the mass and momentum fluxes. In a subsequent paper, we plan to determine the heat flux transport coefficients and perform a linear stability analysis of the homogeneous steady state as a possible application. Since no instabilities are found in the dilute case, we want to assess if the density corrections to the transport coefficients can modify the stability of the above homogeneous state. Moreover, since the expressions for the transport coefficients are based on several approximations, it is worth to perform computer simulations to test the reliability of the theoretical predictions. As happens for dry granular mixtures [259–266], we expect that the present results stimulate the performance of appropriate simulations for bidisperse granular suspensions. In particular, we plan to undertake simulations to obtain the tracer diffusion coefficient (namely, a binary mixture where the concentration of one of the species is negligible) in a similar way as in the case of granular mixtures [259, 263, 265]. Moreover, we also plan to carry out simulations to measure the Navier–Stokes shear viscosity η by studying the decay of a small perturbation to the transversal component of the velocity field [267]. Work along this line will be done in the near future.

Although the results derived in this thesis have been mainly focused on smooth inelastic spheres, the extension to inelastic rough hard spheres is a very challenging problem. This study could allow us to assess the impact of the solid body friction on the applicability of a hydrodynamic description to granular suspensions and/or the occurrence of the Mpemba effect. Based on the results of Article 7, we expect that the effect of roughness on the dynamic properties of grains can play an important role.

Another aim of the present work has been to determine the non-Newtonian transport properties of a granular suspension under simple shear flow. However, the results derived for the shear viscosity η^* have shown that the effect of the roughness slightly mitigates the discontinuous shear thickening effect. This result could be in part due to the Fokker–Planck suspension model considered in this thesis. As discussed in Section 2.2.3, the above-mentioned suspension model neglects the coupling between translational and rotational degrees of freedom of grains in the form of the operator $\mathcal{F}^{\text{rot}} f$. A way of accounting for this coupling in our theory would be to retain a term proportional

to the vector product $\mathbf{v} \times \boldsymbol{\omega}$ in $\mathcal{F}^{\text{rot}}$. This would necessarily give rise to new contributions in Grad's solution coming from the combination of traceless dyadic products of $\mathbf{V}$, $(\mathbf{V} \cdot \boldsymbol{\omega})$, and $\mathbf{V} \times \boldsymbol{\omega}$. Nonetheless, these new contributions are constituted by non-linear terms in the velocity fields and so, the resulting equation would not maintain the hypothesis of working with low-Reynolds numbers. Thus, they could not probably be introduced without considering also non-linear terms in the drag force. Anyway, it would be interesting to revisit the problem to assess the effect of these couplings on the rheological properties of grains. The above results can be also examined by means of computer simulations. Previous simulations [142, 143, 254] carried out for perfect smooth inelastic spheres ($\beta = -1$) have shown good agreement with kinetic theory results, as is clearly illustrated in most of the plots presented along Article 6. We expect that this agreement is also extended to the case of inelastic rough hard spheres. Another possible future project is the extension of the present results to finite densities by considering the Enskog kinetic equation. In this context, an interesting question is to see if actually there is a transition from DST to CST as the density increases in a similar way as in the limit case of perfectly smooth spheres.

Outside of the context of the present thesis, it would be interesting to apply the Chapman–Enskog method to compute the transport coefficients of active matter. In particular, Marconi *et al* have investigated in a recent paper [268] how the Fokker–Planck equation for interacting spherical active particles can be used to predict the fluctuations of the hydrodynamic fields by employing the methods of linear fluctuating hydrodynamics. Given that the corresponding forms of the transport coefficients were not known, the authors used expressions according to the Enskog theory of elastic hard disks. Thus, it would be desirable to revisit the problem with the appropriate expressions of the transport coefficients.

Conclusiones y Líneas Futuras

En este último Capítulo presentamos algunas de las conclusiones principales que pueden extraerse del trabajo realizado en la presente tesis.

Se han estudiado las propiedades de transporte de suspensiones granulares. En el contexto de la teoría cinética, las ecuaciones de Boltzmann y Enskog se han modificado para tener en cuenta la inelasticidad de las colisiones. Mientras que la ecuación de Boltzmann describe gases diluidos, la ecuación de Enskog contempla gases a densidades moderadas. Como es habitual, la influencia de la fase gaseosa se ha introducido en las ecuaciones de Boltzmann y Enskog mediante un termino de Fokker–Planck (fuerza de arrastre más término tipo Langevin). Estas fuerzas compensan el enfriamiento inelástico debido a colisiones binarias provocando que el sistema alcance un estado estacionario de no equilibrio. El caso monocomponente se ha considerado como punto de partida para después extender los resultados a suspensiones bidispersas. En la medida de los posible, los resultados teóricos se han comparado con resultados de simulación disponibles en la literatura y con simulaciones numéricas de Monte Carlo realizadas en la propia tesis.

En primer lugar, hemos investigado los estados homogéneos dependientes del tiempo correspondientes a suspensiones monocomponentes y binarias. Las funciones de distribución se han aproximado en la mayoría de las situaciones conforme a una expansión en polinomios de Sonine. Es decir, las funciones de distribución escaladas se han escrito explícitamente en términos de sus momentos de cuarto orden (o cuartos cumulantes). En el transitorio, nos hemos asegurado de que la evolución temporal de las temperaturas parciales reducidas θ_i y de los cumulantes c_1 y c_2 de una suspensión granular binaria se produce a través de curvas hidrodinámicas universales cuya dependencia temporal se produce únicamente a través de los valores instantáneos de la temperatura adimensional θ. Este resultado sustenta el uso de la solución hidrodinámica o normal como base

en la aplicación del método de Chapman–Enskog. Asimismo, hemos estudiado el origen del llamado efecto Mpemba (una muestra inicialmente a una temperatura superior puede enfriarse antes que otra muestra idéntica a menos temperatura) en suspensiones binarias granulares. Para ello, hemos calculado analíticamente el tiempo de corte t_c^* y las condiciones iniciales necesarias para que se produzca el efecto en situaciones cercanas al estado final estacionario de no equilibrio. De esta forma, las contribuciones no lineales se pueden despreciar y el análisis es mucho más sencillo. Posteriormente, hemos ampliado el estudio a situaciones alejadas del estado estacionario donde aparecen fenómenos no lineales como es el caso de los efectos Mpemba ampliados, no monótonos o mixtos. La principal conclusión obtenida es que los efectos de tipo Mpemba aparecen incluso en suspensiones moleculares (elásticas) sin necesidad de cumulantes. Esto ha posibilitado la descripción del efecto en términos únicamente de la diferencia relativa entre los coeficientes de fricción γ_1 y γ_2. Cuando el tiempo de evolución del sistema es claramente superior a tiempo promedio entre colisiones, el sistema alcanza un estado estacionario. La sencillez de las ecuaciones en este estado facilita la comparación entre la temperatura total T; el cociente de temperaturas parciales T_1/T_2; y los cumulantes para suspensiones mono a_2 y bidispersas c_1 y c_2, con resultados de simulación de Monte Carlo. Dado que el acuerdo entre los resultados teóricos y de simulación es óptimo, podemos concluir que la aproximación de Sonine es adecuada para describir la función de distribución en situaciones fuera del equilibrio.

Se han obtenido los coeficientes de transporte de Navier–Stokes resolviendo la ecuación de Enskog por el procedimiento de Chapman–Enskog. Los flujos de calor y momento han sido calculados a primer orden en términos de las desviaciones de los campos hidrodinámicos de sus estados estacionarios y homogéneos. En forma adimensional, se ha demostrado que los coeficientes asociados a la viscosidad tangencial η^* y de volumen η_b^*, aquellos correspondientes a la conductividad térmica κ^* y difusiva μ^*, así como la contribución de primer order ζ_U a la frecuencia de enfriamiento muestran una dependencia compleja con los parámetros de la suspensión granular. Asimismo, se han calculado los coeficientes de viscosidad tangencial η^* y de volumen η_b^*, los coeficientes de difusión D_{ij}^*, D_i^{T*} y D_i^{U*}, además de las contribuciones a primer orden de la frecuencia de enfriamiento ζ_U y de las temperaturas parciales ϖ_1. Estos coeficientes difieren claramente de los obtenidos anteriormente despreciando los efectos de densidad en la función de distribución de referencia y la contribución a la ruptura de la equipartición

de la energía procedente de la expansión en gradientes de las temperaturas parciales. Por otra parte, se ha demostrado que la influencia del baño en las propiedades de los granos puede ser relevante en situaciones de interés práctico. Por ejemplo, hemos detectado que la dependencia en la inelasticidad en el caso de la viscosidad tangencial η^* es cualitativamente diferente al caso seco. Mientras que η^* decrece con α para gases granulares muy diluidos ($\phi = 0$), lo opuesto ocurre cuando se considera el fluido intersticial. Además, para densidades más altas ($\phi = 0{,}1$), η^* se comporta de forma no monótona con α en el caso seco, mientras que para suspensiones hemos visto que η^* siempre decrece con la inelasticidad. En el caso de mezclas se han encontrado mayores similitudes en la dependencia de η^* con α al considerar la influencia del baño. Sin embargo, las diferencias relativas entre la viscosidad para los sistemas con y sin intersticio siguen siendo importantes al encontrarse discrepancias de hasta un 50 %. Otro resultado interesante tiene que ver con la estabilidad del estado estacionario y homogéneo; pudiendo ser este estado inestable en gases granulares secos, la acción del baño hace que cualquier pequeña perturbación de dicho estado sea rápidamente atenuada.

Finalmente, se han estudiado teóricamente las propiedades de transporte no newtonianas de una suspensión granular diluida sometida a la acción de un flujo tangencial uniforme. Para ello, se ha estudiado la reología de suspensiones compuestas por esferas lisas y rugosas a través del método de los momentos de Grad, un modelo cinético tipo BGK y modelos de Maxwell inelásticos. En primer lugar, se ha comprobado que los resultados obtenidos mediante los modelos de Maxwell y la ecuación BGK muestran un buen acuerdo con resultados de Grad y de simulaciones EDLSHS que habían sido publicados anteriormente. Un resultado sorprendente es que la transición de espesamiento tangencial de carácter discontinuo se ha observado incluso para modelos que asumen una gran sencillez estructural como son los modelos de Maxwell. Más allá de los momentos de segundo orden, se ha analizado la divergencia de los momentos de cuarto orden obtenidos mediante los modelos de Maxwell. En concordancia con estudios previos de sistemas elásticos e inelásticos, se han descubierto regiones del espacio de parámetros donde estos momentos dan lugar a soluciones no físicas. Por el contrario, dado que los resultados obtenidos con el modelo BGK son siempre finitos, se han aprovechado para estudiar la dependencia de los momentos simétricos de cuarto orden con respecto a la de cizalladura (o gradiente constante de velocidad) a^*. En concreto, se ha demostrado que, al igual que en el caso de la viscosidad tangencial η^*, los momentos

de cuarto orden presentan una transición abrupta en forma de "S". Para completar el estudio, se ha evaluado el impacto de la rugosidad en las propiedades no newtonianas. La principal conclusión extraída es que la rugosidad respeta de manera general el comportamiento observado para esferas lisas. Sin embargo, a escala más cuantitativa, se ha demostrado que la rugosidad afecta a la reología del sistema. Por ejemplo, suaviza la transición para la viscosidad η^* para un valor de α dado y produce el efecto contrario en el caso de la temperatura rotacional θ_r. Como aplicación de los resultados obtenidos, se ha realizado un análisis de estabilidad de la solución estacionaria de las propiedades reológicas sometidas a un flujo tangencial uniforme. Sorprendentemente, se ha detectado una región inestable que coincide en valores de la tasa de cizalladura a^* con la zona donde se produce la transición discontinua de espesamiento tangencial. Es probable, por tanto, que ambos fenómenos estén relacionados.

Líneas futuras

Uno de los objetivos de la presente tesis ha sido calcular los coeficientes de transporte de Navier–Stokes de una suspensión binaria asociados a los flujos de masa y momento. En un futuro próximo, esperamos calcular también los asociados al flujo de calor para así poder analizar la estabilidad del estado homogéneo y estacionario. Dado que en el caso diluido el estado homogéneo es linealmente estable, queremos investigar si los efectos de densidad pueden provocar la aparición de inestabilidades. Además, como los resultados teóricos se sustentan en numerosas aproximaciones, conviene comprobar la veracidad de las expresiones obtenidas para los coeficientes de transporte con resultados de simulación. Al igual que ocurre para mezclas granulares [259–266], esperamos que el acuerdo sea favorable. En concreto, se pueden realizar simulaciones para el caso del coeficiente de difusión en el límite trazador (obtenido cuando uno de los componentes de la suspensión binaria presenta una concentración despreciable) siguiendo pasos análogos al caso de mezclas [259, 263, 265]. Del mismo modo, se puede medir la magnitud de la viscosidad tangencial de Navier–Stokes η mediante el estudio del decaimiento de una pequeña perturbación en la componente transversal de la velocidad [267].

Al igual que en el estudio de la reología de las suspensiones, planeamos extender los resultados del presente trabajo al caso de esferas rugosas. De esta forma, podremos evaluar el efecto de la rugosidad en las propiedades hidrodinámicas o incluso en el origen

del efecto Mpemba. Nuestras expectativas son que este grado de libertad adicional juegue un papel relevante en las propiedades dinámicas de los granos.

Con respecto a las propiedades no newtonianas de las suspensiones, hemos observado que la rugosidad atenúa ligeramente la transición de espesamiento tangencial con respecto al caso liso. Esto puede deberse a la forma del operador de Fokker–Planck presentado en la Sección 2.2.3. Como ya se ha discutido, este operador desprecia las contribuciones asociadas con los acoplamientos entre los campos de velocidades lineal y angular. Una forma de subsanar este problema procedería mediante la inclusión de un término proporcional al producto vectorial $\mathbf{v} \times \boldsymbol{\omega}$ en la forma del operador $\mathcal{F}^{\text{rot}}$. Esto dificultaría enormemente el problema ya que habría que añadir en la solución de Grad nuevas contribuciones provenientes de la combinación de siguientes productos diádicos de traza nula: $\mathbf{V}$, $(\mathbf{V} \cdot \boldsymbol{\omega})$ y $\mathbf{V} \times \boldsymbol{\omega}$. Sin embargo, estas contribuciones contienen términos no lineales en los campos de velocidad. Este hecho rompería la hipótesis de trabajar a bajos números de Reynolds y, por tanto, posiblemente no puedan incluirse sin considerar términos cuadráticos en la fuerza de arrastre. De todos modos, sería interesante analizar el impacto de estas nuevas contribuciones sobre las propiedades reológicas de los granos. Los resultados que se obtengan pueden examinarse mediante distintas simulaciones. Al igual que ocurre en el caso de esferas perfectamente lisas ($\beta = -1$) [142, 143, 254], esperamos que se mantenga el buen acuerdo al considerar esferas inelásticas y rugosas. Otro proyecto futuro relacionado con los fluidos no newtonianos podría ser la extensión de los resultados presentados en esta tesis considerando la ecuación de Enskog. En este contexto, sería interesante analizar si realmente hay una transición por la que el efecto de espesamiento tangencial discontinuo para a ser continuo al aumentar la densidad; exactamente como ocurre en el caso liso.

Por último y menos relacionado con el marco principal de la tesis, sería interesante aplicar el método de Chapman–Enskog para determinar los coeficientes de transporte de un sistema de materia activa. En particular, Marconi *et al.* han analizado recientemente [268] cómo usar la ecuación de Fokker–Planck para esferas activas interaccionantes con el objetivo de predecir las fluctuaciones de los campos hidrodinámicos. Dado que la forma de los coeficientes de transporte que han empleado se corresponde con aquellos obtenidos para discos elásticos mediante la ecuación de Enskog, conviene revisitar el problema usando los coeficientes de transporte apropiados.

Bibliography

[1] J. Duran, *Sands, Powders, and Grains: An Introduction to the Physics of Granular Materials*. Springer, New York, 2012.

[2] B. Andreotti, Y. Forterre, and O. Pouliquen, *Granular Media. Between Fluid and Solid*. Cambridge University Press, Cambridge, 2013.

[3] J. W. Dufty, "Granular flows," in *Encyclopedia of Complexity and Systems Science* (R. A. Meyers, ed.), p. 00038, Springer, 2009.

[4] V. Garzó, *Granular Gaseous Flows*. Springer Nature, Cham, 2019.

[5] C. S. Campbell, "Rapid granular flows," *Annu. Rev. Fluid Mech.*, vol. 22, pp. 57–92, 1990.

[6] H. M. Jaeger, S. R. Nagel, and R. P. Behringer, "Granular solids, liquids, and gases," *Rev. Mod. Phys.*, vol. 68, pp. 1259–1273, 1996.

[7] L. Bates, "Bulk solids characterisation-the need for industrial education in bulk technology," *Bulk Solids Handl.*, vol. 26, pp. 464–475, 2006.

[8] A. Levy and H. Kalman, *Handbook of Conveying and Handling of Particulate Solids*. Elsevier, Amsterdam, 2001.

[9] A. Grucelski, "Effective thermal conductivity in granular media with devolatilization: the Lattice Boltzmann modelling," *Int. J. Coal Sci. Technol.*, vol. 8, pp. 590–604, 2021.

[10] K. M. Hill, A. Caprihan, and J. Kakalios, "Axial segregation of granular media rotated in a drum mixer: Pattern evolution," *Phys. Rev. E*, vol. 56, pp. 4386–4393, 1997.

[11] B. C. Hancock, "The wall friction properties of pharmaceutical powders, blends, and granulations," *J. Pharm. Sci.*, vol. 108, pp. 457–463, 2019.

[12] I. S. Aranson and L. S. Tsimring, "Patterns and collective behavior in granular media: Theoretical concepts," *Rev. Mod. Phys.*, vol. 78, pp. 641–692, 2006.

[13] A. Pascot, J. Morel, S. Antonyuk, M. Jenny, Y. Cheny, and S. K. De Richter, "Discharge of vibrated granular silo: A grain scale approach," *Powder Technol.*, vol. 397, p. 116998, 2022.

[14] I. Einav, "Breakage mechanics—part I: Theory," *J. Mech. Phys. Solids*, vol. 55, pp. 1274–1297, 2007.

[15] S. Parez, T. Travnickova, M. Svoboda, and E. Aharonov, "Strain localization in planar shear of granular media: the role of porosity and boundary conditions," *Eur. Phys. J. E*, vol. 44, pp. 1–17, 2021.

[16] H. Kocharyan and N. Karanjgaokar, "Wave propagation through submerged granular media over a wide range of fluid viscosities," *Powder Technol.*, vol. 380, pp. 126–133, 2021.

[17] P. C. Thomas and M. S. Robinson, "Seismic resurfacing by a single impact on the asteroid 433 Eros," *Nature*, vol. 436, pp. 366–369, 2005.

[18] G. David, P.-Y. Meslin, E. Dehouck, O. Gasnault, A. Cousin, O. Forni, G. Berger, J. Lasue, P. Pinet, R. Wiens, S. Maurice, J.-F. Fronton, and W. Rapin, "Laser-induced breakdown spectroscopy (LIBS) characterization of granular soils: Implications for ChemCam analyses at Gale crater, Mars," *Icarus*, vol. 365, p. 114481, 2021.

[19] J. Capecelatro, "Modeling high-speed gas–particle flows relevant to spacecraft landings," *Int. J. Multiph. Flow*, vol. 150, p. 104008, 2022.

[20] N. Brilliantov, P. L. Krapivsky, A. Bodrova, F. Spahn, H. Hayakawa, V. Stadnichuk, and J. Schmidt, "Size distribution of particles in Saturn's rings from aggregation and fragmentation," *Proc. Natl. Acad. Sci. U.S.A.*, vol. 112, pp. 9536–9541, 2015.

[21] D. Bischoff, B. Gundlach, and J. Blum, "A method to distinguish between micro- and macro-granular surfaces of small solar system bodies," *Mon. Notices Royal Astron. Soc. Society*, vol. 508, pp. 4705–4721, 2021.

[22] J. R. Dorfman, H. van Beijeren, and T. R. Kirkpatrick, *Contemporary Kinetic Theory of Matter*. Cambridge University Press, Cambridge, 2021.

[23] D. Hestroffer, P. Sánchez, L. Staron, A. C. Bagatin, S. Eggl, W. Losert, N. Murdoch, E. Opsomer, F. Radjai, D. C. Richardson, *et al.*, "Small solar system bodies as granular media," *Astron. Astrophys. Rev.*, vol. 27, pp. 1–64, 2019.

[24] A. Brahic, "Dynamical evolution of viscous discs. astrophysical applications to the formation of planetary systems and to the confinement of planetary rings and arcs," in *Granular Gases* (T. Pöschel and S. Luding, eds.), vol. 564 of *Lectures Notes in Physics*, pp. 281–329, Springer, 2001.

[25] J. C. Maxwell, "On the stability of the motion of Saturn's rings; an Essay which obtained the Adams' Prize for the Year 1856, in the University of Cambridge," *Mon. Notices Royal Astron. Soc.*, vol. 19, pp. 297–304, 1859.

[26] N. Mitarai and F. Nori, "Wet granular materials," *Adv. Phys.*, vol. 55, pp. 1–45, 2006.

[27] M. Pilvar, M. J. Pouraghniaei, and A. Shakibaeinia, "Two-dimensional sub-aerial, submerged, and transitional granular slides," *Phys. Fluids*, vol. 31, p. 113303, 2019.

[28] M. Robbe-Saule, C. Morize, R. Henaff, Y. Bertho, A. Sauret, and P. Gondret, "Experimental investigation of tsunami waves generated by granular collapse into water," *J. Fluid Mech.*, vol. 907, p. A11, 2021.

[29] M. M. Denn and J. F. Morris, "Rheology of non-Brownian suspensions," *Annu. Rev. Chem. Biomol.*, vol. 5, pp. 203–228, 2014.

[30] J. M. Martel and M. Toner, "Inertial focusing in microfluidics," *Annu. Rev. Biomed. Eng.*, vol. 16, pp. 371–396, 2014.

[31] J. F. Morris, "Toward a fluid mechanics of suspensions," *Phys. Rev. Fluids*, vol. 5, p. 110519, 2020.

[32] A. Fall, A. Lemaître, F. Bertrand, D. Bonn, and G. Ovarlez, "Shear thickening and migration in granular suspensions," *Phys. Rev. Lett.*, vol. 105, p. 268303, 2010.

[33] C. Gamonpilas, J. F. Morris, and D. M. Denn, "Shear and normal stress measurements in non-Brownian monodisperse and bidisperse suspensions," *J. Rheol.*, vol. 60, pp. 289–296, 2016.

[34] R. A. Bagnold, "Experiments on a gravity-free dispersion of large solid spheres in a Newtonian fluid under shear," *Proc. R. Soc. A*, vol. 225, pp. 49–63, 1954.

[35] I. Goldhirsch, "Introduction to granular temperature," *Powder Technol.*, vol. 182, pp. 130–136, 2008.

[36] M. P. Ciamarra, P. Richard, M. Schröter, and B. P. Tighe, "Statistical mechanics for static granular media: open questions," *Soft Matter*, vol. 8, pp. 9731–9737, 2012.

[37] H. M. Jaeger, T. Shinbrot, and P. B. Umbanhowar, "Does the granular matter?," *Proc. Natl. Acad. Sci. U.S.A.*, vol. 97, pp. 12959–12960, 2000.

[38] A. Lemaître, C. Mondal, I. Procaccia, S. Roy, Y. Wang, and J. Zhang, "Frictional granular matter: Protocol dependence of mechanical properties," *Phys. Rev. Lett.*, vol. 126, p. 075501, 2021.

[39] A. Puglisi, *Transport and Fluctuations in Granular Fluids. From Boltzmann Equation to Hydrodynamics, Diffusion and Motor Effects.* Springer, Heidelberg, 2015.

[40] I. Goldhirsch, "Granular Gases: Probing the Boundaries of Hydrodynamics," in *Granular Gases* (T. Pöschel and S. Luding, eds.), vol. 564 of *Lecture Notes in Physics*, pp. 79–99, Springer, 2001.

[41] T. Guo and C. S. Campbell, "An experimental study of the elastic theory for granular flows," *Phys. Fluids*, vol. 28, p. 083303, 2016.

[42] P. Yu, M. Schröter, and M. Sperl, "Velocity distribution of a homogeneously cooling granular gas," *Phys. Rev. Lett.*, vol. 124, p. 208007, 2020.

[43] D. Bi, S. Henkes, K. E. Daniels, and B. Chakraborty, "The statistical physics of athermal materials," *Annu. Rev. Condens. Matter Phys.*, vol. 6, pp. 63–83, 2015.

[44] Y. Bertho, F. Giorgiutti-Dauphiné, and J. Hulin, "Dynamical Janssen effect on granular packing with moving walls," *Phys. Rev. Lett.*, vol. 90, p. 144301, 2003.

[45] R. L. Stoop and P. Tierno, "Clogging and jamming of colloidal monolayers driven across disordered landscapes," *Commun. Phys.*, vol. 1, p. 68, 2018.

[46] O. Reynolds, "Lvii. on the dilatancy of media composed of rigid particles in contact. With experimental illustrations," *London Edinburgh Philos. Mag. J. Sci*, vol. 20, pp. 469–481, 1885.

[47] I. Zuriguel, A. Janda, A. Garcimartín, C. Lozano, R. Arévalo, and D. Maza, "Silo clogging reduction by the presence of an obstacle," *Phys. Rev. Lett.*, vol. 107, p. 278001, 2011.

[48] D. Houdoux, A. Amon, D. Marsan, J. Weiss, and J. Crassous, "Micro-slips in an experimental granular shear band replicate the spatiotemporal characteristics of natural earthquakes," *Commun. Earth Environ.*, vol. 2, p. 90, 2021.

[49] D. Fenistein and M. van Hecke, "Wide shear zones in granular bulk flow," *Nature*, vol. 425, pp. 256–256, 2003.

[50] I. S. Aranson and L. S. Tsimring, "Continuum theory of partially fluidized granular flows," *Phys. Rev. E*, vol. 65, p. 061303, 2002.

[51] I. Goldhirsch, "Rapid granular flows," *Annu. Rev. Fluid Mech.*, vol. 35, pp. 267–293, 2003.

[52] S. B. Savage, "The mechanics of rapid granular flows," in *Advances in Applied Mechanics* (J. W. Hutchinson and T. Y. Wu, eds.), vol. 24, pp. 289–366, Elsevier, 1984.

[53] I. Goldhirsch and G. Zanetti, "Clustering instability in dissipative gases," *Phys. Rev. Lett.*, vol. 70, pp. 1619–1622, 1993.

[54] I. S. Aranson and L. V. Tsimring, "Patterns and collective behaviour in granular media: Theoretical concepts," *Rev. Mod. Phys.*, vol. 78, pp. 641–692, 2006.

[55] S. Luding, "Structure and cluster formation in granular media," *Pramana*, vol. 64, pp. 893–902, 2005.

[56] J. P. Hansen and I. R. McDonald, *Theory of Simple Liquids: with Applications to Soft Matter*. Academic Press, Oxford, 2013.

[57] J. J. Brey, J. W. Dufty, and A. Santos, "Dissipative dynamics for hard spheres," *J. Stat. Phys.*, vol. 87, pp. 1051–1066, 1997.

[58] J. W. Dufty, "Statistical mechanics, kinetic theory, and hydrodynamics for rapid granular flow," *J. Phys: Condens. Matter*, vol. 12, pp. A47–A56, 2000.

[59] T. P. C. van Noije and M. H. Ernst, "Kinetic Theory of Granular Gases," in *Granular Gases* (T. Pöschel and S. Luding, eds.), vol. 564 of *Lecture Notes in Physics*, pp. 3–30, Springer, 2001.

[60] N. Brilliantov and T. Pöschel, *Kinetic Theory of Granular Gases*. Oxford University Press, Oxford, 2004.

[61] P. Das, S. Puri, and M. Schwartz, "Clustering and velocity distributions in granular gases cooling by solid friction," *Phys. Rev. E*, vol. 94, p. 032907, 2016.

[62] A. Kudrolli, M. Wolpert, and J. P. Gollub, "Cluster formation due to collisions in granular material," *Phys. Rev. Lett.*, vol. 78, pp. 1383–1386, 1997.

[63] H. J. Herrmann, S. Luding, and R. Cafiero, "Dynamics of granular systems," *Physica A*, vol. 295, pp. 93–100, 2001.

[64] S. Luding and Herrmann, "Cluster-growth in freely cooling granular media," *Chaos*, vol. 9, pp. 673–680, 1999.

[65] S. McNamara and W. R. Young, "Inelastic collapse in two dimensions," *Phys. Rev. E*, vol. 50, pp. R28–R31, 1994.

[66] J. J. Brey, J. W. Dufty, C. S. Kim, and A. Santos, "Hydrodynamics for granular flows at low density," *Phys. Rev. E*, vol. 58, pp. 4638–4653, 1998.

[67] J. J. Brey, M. J. Ruiz-Montero, and D. Cubero, "Origin of density clustering in a freely evolving granular gas," *Phys. Rev. E*, vol. 60, pp. 3150–3157, 1999.

[68] R. Soto, M. Mareschal, and M. Malek Mansour, "Nonlinear analysis of the shearing instability in granular gases," *Phys. Rev. E*, vol. 62, pp. 3836–3842, 2000.

[69] V. Garzó, "Instabilities in a free granular fluid described by the Enskog equation," *Phys. Rev. E*, vol. 72, p. 021106, 2005.

[70] P. P. Mitrano, S. R. Dhal, D. J. Cromer, M. S. Pacella, and C. M. Hrenya, "Instabilities in the homogeneous cooling of a granular gas: a quantitative assessment of kinetic-theory predictions," *Phys. Fluids*, vol. 23, p. 093303, 2011.

[71] P. P. Mitrano, V. Garzó, A. M. Hilger, C. J. Ewasko, and C. M. Hrenya, "Assessing a hydrodynamic description for instabilities in highly dissipative, freely cooling granular gases," *Phys. Rev. E*, vol. 85, p. 041303, 2012.

[72] P. P. Mitrano, S. R. Dhal, A. M. Hilger, C. J. Ewasko, and C. M. Hrenya, "Dual role of friction in granular flows: attenuation versus enhancement of instabilities," *J. Fluid Mech.*, vol. 729, pp. 484–495, 2013.

[73] P. P. Mitrano, J. R. Zenk, S. Benyahia, J. E. Galvin, S. R. Dhal, and C. M. Hrenya, "Kinetic-theory predictions of clustering instabilities in granular flows: beyond the small-Knudsen-number regime," *J. Fluid Mech.*, vol. 738, p. R2, 2014.

[74] W. D. Fullmer and C. M. Hrenya, "The clustering instability in rapid granular and gas-solid flows," *Annu. Rev. Fluid Mech.*, vol. 49, pp. 485–510, 2017.

[75] V. Garzó, A. Santos, and G. M. Kremer, "Impact of roughness on the instability of a free-cooling granular gas," *Phys. Rev. E*, vol. 97, p. 052901, 2018.

[76] A. Megías and A. Santos, "Hydrodynamics of granular gases of inelastic and rough hard disks or spheres. II. Stability analysis," *Phys. Rev. E*, vol. 104, p. 034902, 2021.

[77] X. Yang, C. Huan, D. Candela, R. W. Mair, and R. L. Walsworth, "Measurements of grain motion in a dense, three-dimensional granular fluid," *Phys. Rev. Lett.*, vol. 88, p. 044301, 2002.

[78] M. J. Biggs, D. Glass, L. Xie, V. Zivkovic, A. Buts, and M. A. Curt Kounders, "Granular temperature in a gas fluidized bed," *Granular Matter*, vol. 10, pp. 63–73, 2008.

[79] A. Sack, M. Heckel, J. E. Kollmer, F. Zimber, and T. Pöschel, "Energy dissipation in driven granular matter in the absence of gravity," *Phys. Rev. Lett.*, vol. 111, p. 018001, 2013.

[80] K. Harth, T. Trittel, K. May, S. Wegner, and R. Stannarius, "Three-dimensional (3D) experimental realization and observation of a granular gas in microgravity," *Adv. Space Res.*, vol. 55, pp. 1901–1912, 2015.

[81] K. Harth, T. Trittel, S. Wegner, and R. Stannarius, "Free cooling of a granular gas of rodlike particles in microgravity," *Phys. Rev. Lett.*, vol. 120, p. 213301, 2018.

[82] M. Adachi, M. Balter, X. Cheng, J. Drescher, X. Li, M. Sperl, S. Zhao, and P. Yu, "Characteristics of a magnetic bulk thermostat for granular gas investigations in microgravity," *Microgravity Sci. Technol.*, vol. 33, p. 11, 2021.

[83] E. Falcon, R. Wunenburger, P. Èvesque, S. Fauve, C. Chabot, Y. Garrabos, and D. Beysens, "Cluster formation in a granular medium fluidized by vibrations in low gravity," *Phys. Rev. Lett.*, vol. 83, pp. 440–443, 1999.

[84] J. J. Brey, M. J. Ruiz-Montero, F. Moreno, and R. García-Rojo, "Transversal inhomogeneities in dilute vibrofluidized granular fluids," *Phys. Rev. E*, vol. 65, p. 061302, 2002.

[85] B. Meerson, T. Pöschel, P. V. Sasorov, and T. Schwager, "Giant fluctuations at a granular phase separation threshold," *Phys. Rev. E*, vol. 69, p. 021302, 2004.

[86] M. Noirhomme, A. Cazaubiel, E. Falcon, D. Fischer, Y. Garrabos, C. Lecoutre-Chabot, S. Mawet, E. Opsomer, F. Palencia, S. Pillitteri, and N. Vandewalle, "Particle dynamics at the onset of the granular gas-liquid transition," *Phys. Rev. Lett.*, vol. 126, p. 128002, 2021.

[87] A. Puglisi, V. Loreto, U. M. B. Marconi, and A. Vulpiani, "Kinetic approach to granular gases," *Phys. Rev. E*, vol. 59, pp. 5582–5595, 1999.

[88] R. Cafiero, S. Luding, and H. J. Herrmann, "Two-dimensional granular gas of inelastic spheres with multiplicative driving," *Phys. Rev. Lett.*, vol. 84, pp. 6014–6017, 2000.

[89] R. Cafiero and S. Luding, "Mean field theory for a driven granular gas of frictional particles," *Physica A*, vol. 280, pp. 142–147, 2000.

[90] V. Garzó and J. M. Montanero, "Transport coefficients of a heated granular gas," *Physica A*, vol. 313, pp. 336–356, 2002.

[91] A. Fiege, T. Aspelmeier, and A. Zippelius, "Long-time tails and cage effect in driven granular fluids," *Phys. Rev. Lett.*, vol. 102, p. 098001, 2009.

[92] W. T. Kranz, M. Sperl, and A. Zippelius, "Glass transition for driven granular fluids," *Phys. Rev. Lett.*, vol. 104, p. 225701, 2010.

[93] G. Gradenigo, A. Sarracino, D. Villamaina, and A. Puglisi, "Fluctuating hydrodynamics and correlation lengths in a driven granular fluid," *J. Stat. Mech.*, vol. P08017, 2011.

[94] N. Khalil and V. Garzó, "Homogeneous states in driven granular mixtures: Enskog kinetic theory versus molecular dynamics simulations," *J. Chem. Phys.*, vol. 140, p. 164901, 2014.

[95] J. M. Montanero and A. Santos, "Computer simulation of uniformly heated granular fluids," *Granular Matter*, vol. 2, pp. 53–64, 2000.

[96] U. M. B. Marconi and A. Puglisi, "Steady-state properties of a mean-field model of driven inelastic mixtures," *Phys. Rev. E*, vol. 66, p. 011301, 2002.

[97] M. I. García de Soria, P. Maynar, and E. Trizac, "Universal reference state in a driven homogeneous granular gas," *Phys. Rev. E*, vol. 85, p. 051301, 2012.

[98] M. G. Chamorro, F. Vega Reyes, and V. Garzó, "Homogeneous steady states in a granular fluid driven by a stochastic bath with friction," *J. Stat. Mech.*, vol. P07013, 2013.

[99] N. Khalil and V. Garzó, "Transport coefficients for driven granular mixtures at low-density," *Phys. Rev. E*, vol. 88, p. 052201, 2013.

[100] A. Biswas, V. V. Prasad, O. Raz, and R. Rajesh, "Mpemba effect in driven granular Maxwell gases," *Phys. Rev. E*, vol. 102, p. 012906, 2020.

[101] D. Serero, I. Goldhirsch, S. H. Noskowicz, and M. L. Tan, "Hydrodynamics of granular gases and granular gas mixtures," *J. Fluid Mech.*, vol. 554, pp. 237–258, 2006.

[102] M. E. Möbius, B. E. Lauderdale, S. R. Nagel, and H. M. Jaeger, "Brazil-nut effect: Size separation of granular particles," *Nature*, vol. 414, p. 270, 2001.

[103] M. A. Naylor, M. R. Swift, and P. J. King, "Air-driven Brazil nut effect," *Phys. Rev. E*, vol. 68, p. 012301, 2003.

[104] P. Sánchez, M. R. Swift, and P. J. King, "Stripe formation in granular mixtures due to the differential influence of drag," *Phys. Rev. Lett.*, vol. 93, p. 184302, 2004.

[105] J. J. Wylie, Q. Zhang, H. Y. Xu, and X. X. Sun, "Drag-induced particle segregation with vibrating boundaries," *Europhys. Lett.*, vol. 81, p. 54001, 2008.

[106] K. E. Daniels and M. Schröter, "Focus on granular segregation," *New J. Phys.*, vol. 15, p. 035017, 2013.

[107] J. C. Pastenes, J. C. Géminard, and F. Melo, "Interstitial gas effect on vibrated granular columns," *Phy. Rev. E*, vol. 89, p. 062205, 2014.

[108] M. A. Haustein, G. Zhang, and R. Schwarze, "Segregation of granular materials in a pulsating pumping regime," *Granular Matter*, vol. 21, p. 111, 2019.

[109] É. Guazzelli and O. Pouliquen, "Rheology of dense granular suspensions," *J. Fluid Mech.*, vol. 852, p. P1, 2018.

[110] Y. T. Makkawi, P. C. Wright, and R. Ocone, "The effect of friction and inter-particle cohesive forces on the hydrodynamics of gas–solid flow: A comparative analysis of theoretical predictions and experiments," *Powder Technol.*, vol. 163, pp. 69–79, 2006.

[111] N. Y. C. Lin, B. M. Guy, M. Hermes, C. Ness, J. Sun, W. C. K. Poon, and I. Cohen, "Hydrodynamic and contact contributions to continuous shear thickening in colloidal suspensions," *Phys. Rev. Lett.*, vol. 115, p. 228304, 2015.

[112] A. Boromand, S. Jamali, B. Grove, and J. M. Maia, "A generalized frictional and hydrodynamic model of the dynamics and structure of dense colloidal suspensions," *J. Rheol.*, vol. 62, pp. 905–918, 2018.

[113] J. F. Brady and G. Bossis, "Stokesian dynamics," *Ann. Rev. Fluid Mech.*, vol. 20, pp. 111–157, 1988.

[114] D. Gidaspow, *Multiphase Flow and Fluidization.* Academic Press, 1994.

[115] R. Jackson, *The Dynamics of Fluidized Particles.* Cambridge University Press, New York, 2000.

[116] D. L. Koch and R. J. Hill, "Inertial effects in suspensions and porous-media flows," *Annu. Rev. Fluid Mech.*, vol. 33, pp. 619–647, 2001.

[117] S. Tenneti and S. Subramaniam, "Particle-resolved direct numerical simulation fo gas-solid flow model development," *Annu. Rev. Fluid Mech.*, vol. 46, pp. 199–230, 2014.

[118] J. Wang, "Continuum theory for dense gas-solid flow: A state-of-the-art review," *Chem. Eng. Sci.*, vol. 215, p. 115428, 2020.

[119] X. Liu, W. Ge, and L. Wang, "Scale and structure dependent drag in gas–solid flows," *AIChE*, vol. 66, no. 4, p. e16883, 2020.

[120] G. K. Batchelor, "Sedimentation in a dilute dispersion of spheres," *J. Fluid Mech.*, vol. 52, pp. 245–268, 1972.

[121] S. Subramaniam, "Multiphase flows: Rich physics, challenging theory, and big simualtions," *Phys. Rev. Fluids*, vol. 5, p. 110520, 2020.

[122] S. Chapman and T. G. Cowling, *The Mathematical Theory of Nonuniform Gases.* Cambridge University Press, Cambridge, 1970.

[123] J. H. Ferziger and G. H. Kaper, *Mathematical Theory of Transport Processes in Gases*. North-Holland, Amsterdam, 1972.

[124] P. Résibois and M. de Leener, *Classical Kinetic Theory of Fluids*. Wiley, New York, 1977.

[125] D. L. Koch, "Kinetic theory for a monodisperse gas-solid suspension," *Phys. Fluids A*, vol. 2, pp. 1711–1722, 1990.

[126] M. Louge, E. Mastorakos, and J. T. Jenkins, "The role of particle collisions in pneumatic transport," *J. Fluid Mech.*, vol. 231, pp. 345–359, 1991.

[127] H.-K. Tsao and D. L. Koch, "Simple shear flows of dilute gas-solid suspensions," *J. Fluid Mech.*, vol. 296, pp. 211–245, 1995.

[128] A. S. Sangani, G. Mo, H.-K. Tsao, and D. L. Koch, "Simple shear flows of dense gas-solid suspensions at finite Stokes numbers," *J. Fluid Mech.*, vol. 313, pp. 309–341, 1996.

[129] J. J. Wylie, Q. Zhang, Y. Li, and X. Hengyi, "Driven inelastic-particle systems with drag," *Phys. Rev. E*, vol. 79, p. 031301, 2009.

[130] J.-F. Parmentier and O. Simonin, "Transition models from the quenched to ignited states for flows of inertial particles suspended in a simple sheared viscous fluid," *J. Fluid Mech.*, vol. 711, pp. 147–160, 2012.

[131] C. Heussinger, "Shear thickening in granular suspensions: Interparticle friction and dynamically correlated clusters," *Phys. Rev. E*, vol. 88, p. 050201 (R), 2013.

[132] T. Wang, M. Grob, A. Zippelius, and M. Sperl, "Active microrhelogy of driven granular particles," *Phys. Rev. E*, vol. 89, p. 042209, 2014.

[133] S. Saha and M. Alam, "Revisiting ignited-quenched transition and the non-Newtonian rheology of a sheared dilute gas-solid suspension," *J. Fluid Mech.*, vol. 833, pp. 206–246, 2017.

[134] M. Alam, S. Saha, and R. Gupta, "Unified theory for a sheared gas-solid suspension: from rapid granular suspension to its small-Stokes-number limit," *J. Fluid Mech.*, vol. 870, pp. 1175–1193, 2019.

[135] S. Saha and M. Alam, "Burnett-order constitutive relations, second moment anisotropy and co-existing states in sheared dense gas-solid suspensions," *J. Fluid Mech.*, vol. 887, p. A9, 2020.

[136] A. Puglisi, V. Loreto, U. M. B. Marconi, A. Petri, and A. Vulpiani, "Clustering and non-Gaussian behavior in granular matter," *Phys. Rev. Lett.*, vol. 81, pp. 3848–3851, 1998.

[137] V. Garzó, S. Tenneti, S. Subramaniam, and C. M. Hrenya, "Enskog kinetic theory for monodisperse gas-solid flows," *J. Fluid Mech.*, vol. 712, pp. 129–168, 2012.

[138] S. Ogawa, "Multitemperature theory of granular materials," in *Proc. of the US-Japan Seminar on Continuum Mechanical and Statistical Approaches in the Mechanics of Granular Materials, 1978*, pp. 208–217, Gakajutsu Bunken Fukyu-Kai, 1978.

[139] A. Puglisi, A. Baldassarri, and V. Loreto, "Fluctuation-dissipation relations in driven granular gases," *Phys. Rev. E*, vol. 66, p. 061305, 2002.

[140] M. G. Chamorro, F. Vega Reyes, and V. Garzó, "Homogeneous steady states in a granular fluid driven by a stochastic bath with friction," *J. Stat. Mech.*, vol. P07013, 2013.

[141] V. Garzó, W. D. Fullmer, C. M. Hrenya, and X. Yin, "Transport coefficients of solid particles immersed in a viscous gas," *Phys. Rev. E*, vol. 93, p. 012905, 2016.

[142] H. Hayakawa, S. Takada, and V. Garzó, "Kinetic theory of shear thickening for a moderately dense gas-solid suspension: From discontinuous thickening to continuous thickening," *Phys. Rev. E*, vol. 96, p. 042903, 2017.

[143] H. Hayakawa, S. Takada, and V. Garzó, "Erratum: Kinetic theory of shear thickening for a moderately dense gas-solid suspension: From discontinuous thickening to continuous thickening [Phys. Rev. E 96, 042903 (2017)]," *Phys. Rev. E*, vol. 101, p. 069904, 2020.

[144] S. Takada, H. Hayakawa, A. Santos, and V. Garzó, "Enskog kinetic theory of rheology for a moderately dense inertial suspension," *Phys. Rev. E*, vol. 102, p. 022907, 2020.

[145] W. D. Fullmer and C. M. Hrenya, "Quantitative assessment of fine-grid kinetic-theory-based predictions," *AIChE*, vol. 62, pp. 11–17, 2016.

[146] W. D. Fullmer, G. Liu, X. Yin, and C. M. Hrenya, "Clustering instabilities in sedimenting fluid-solid systems: critical assessment of kinetic-theory-based predictions using the direct numerical simulation data," *J. Fluid Mech.*, vol. 823, p. 433, 2017.

[147] A. Sarracino, D. Villamaina, G. Costantini, and A. Puglisi, "Granular Brownian motion," *J. Stat. Mech.*, vol. 2010, p. P04013, 2010.

[148] V. Garzó, M. G. Chamorro, and F. Vega Reyes, "Transport properties for driven granular fluids in situations close to homogeneous steady states," *Phys. Rev. E*, vol. 87, p. 032201, 2013.

[149] V. Garzó, M. G. Chamorro, and F. Vega Reyes, "Erratum: Transport properties for driven granular fluids in situations close to homogeneous steady states [Phys. Rev. E 87, 032201 (2013)]," *Phys. Rev. E*, vol. 87, p. 059906, 2013.

[150] J. M. Ottino and D. V. Khakhar, "Mixing and segregation of granular fluids," *Ann. Rev. Fluid Mech.*, vol. 32, pp. 55–91, 2000.

[151] A. Kudrolli, "Size separation in vibrated granular matter," *Rep. Prog. Phys.*, vol. 67, pp. 209–247, 2004.

[152] V. Garzó and J. W. Dufty, "Homogeneous cooling state for a granular mixture," *Phys. Rev. E*, vol. 60, pp. 5706–5713, 1999.

[153] P. A. Martin and J. Piasecki, "Thermalization of a particle by dissipative collisions," *Europhys. Lett.*, vol. 46, pp. 613–616, 1999.

[154] J. M. Montanero and V. Garzó, "Monte Carlo simulation of the homogeneous cooling state for a granular mixture," *Granular Matter*, vol. 4, pp. 17–24, 2002.

[155] A. Barrat and E. Trizac, "Lack of energy equipartition in homogeneous heated binary granular mixtures," *Granular Matter*, vol. 4, pp. 57–63, 2002.

[156] S. R. Dahl, C. M. Hrenya, V. Garzó, and J. W. Dufty, "Kinetic temperatures for a granular mixture," *Phys. Rev. E*, vol. 66, p. 041301, 2002.

[157] R. Pagnani, U. M. B. Marconi, and A. Puglisi, "Driven low density granular mixtures," *Phys. Rev. E*, vol. 66, p. 051304, 2002.

[158] R. Clelland and C. M. Hrenya, "Simulations of a binary-sized mixture of inelastic grains in rapid shear flow," *Phys. Rev. E*, vol. 65, p. 031301, 2002.

[159] A. Barrat and E. Trizac, "Molecular dynamics simulations of vibrated granular gases," *Phys. Rev. E*, vol. 66, p. 051303, 2002.

[160] P. Krouskop and J. Talbot, "Mass and size effects in three-dimensional vibrofluidized granular mixtures," *Phys. Rev. E*, vol. 68, p. 021304, 2003.

[161] H. Wang, G. Jin, and Y. Ma, "Simulation study on kinetic temperatures of vibrated binary granular mixtures," *Phys. Rev. E*, vol. 68, p. 031301, 2003.

[162] J. J. Brey, M. J. Ruiz-Montero, and F. Moreno, "Energy partition and segregation for an intruder in a vibrated granular system under gravity," *Phys. Rev. Lett.*, vol. 95, p. 098001, 2005.

[163] M. Alam and S. Luding, "Energy nonequipartition, rheology, and microstructure in sheared bidisperse granular mixtures," *Phys. Fluids*, vol. 17, p. 063303, 2005.

[164] M. Schröter, S. Ulrich, J. Kreft, J. B. Swift, and H. L. Swinney, "Mechanisms in the size segregation of a binary granular mixture," *Phys. Rev. E*, vol. 74, p. 011307, 2006.

[165] F. Vega Reyes, A. Lasanta, A. Santos, and V. Garzó, "Energy nonequipartition in gas mixtures of inelastic rough hard spheres: The tracer limit," *Phys. Rev. E*, vol. 96, p. 052901, 2017.

[166] A. Lasanta, F. Vega Reyes, V. Garzó, and A. Santos, "Intruders in disguise: Mimicry effect in granular gases," *Phys. Fluids*, vol. 31, p. 063306, 2019.

[167] R. Brito, R. Soto, and V. Garzó, "Energy nonequipartition in a collisional model of a confined quasi-two-dimensional granular mixture," *Phys. Rev. E*, vol. 102, p. 052904, 2020.

[168] R. D. Wildman and D. J. Parker, "Coexistence of two granular temperatures in binary vibrofluidized beds," *Phys. Rev. Lett.*, vol. 88, p. 064301, 2002.

[169] K. Feitosa and N. Menon, "Breakdown of energy equipartition in a 2D binary vibrated granular gas," *Phys. Rev. Lett.*, vol. 88, p. 198301, 2002.

[170] V. Garzó, "Transport coefficients of driven granular fluids at moderate volume fractions," *Phys. Rev. E*, vol. 84, p. 012301, 2011.

[171] D. L. Koch and A. S. Sangani, "Particle pressure and marginal stability limits for a homogeneous monodiperse gas-fluidized bed: Kinetic theory and numerical simulations," *J. Fluid Mech.*, vol. 400, p. 229, 1999.

[172] X. Yin and S. Sundaresan, "Drag law for bidisperse gas-solid suspensions containing equally sized spheres," *Ind. Eng. Chem. Res.*, vol. 48, p. 227, 2009.

[173] X. Yin and S. Sundaresan, "Fluid-particle drag in low-Reynolds-number polydisperse gas-solid suspensions," *AIChE*, vol. 55, p. 1352, 2009.

[174] W. Holloway, X. Yin, and S. Sundaresan, "Fluid-particle drag in inertial polydisperse gas-solid suspensions," *AIChE*, vol. 56, p. 1995, 2010.

[175] I. Goldhirsch and N. Sela, "Origin of normal stress differences in rapid granular flows," *Phys. Rev. E*, vol. 54, pp. 4458–4461, 1996.

[176] N. Sela, I. Goldhirsch, and S. H. Noskowicz, "Kinetic theoretical study of a simply sheared two-dimensional granular gas to Burnett order," *Phys. Fluids*, vol. 8, pp. 2337–2353, 1996.

[177] N. Sela and I. Goldhirsch, "Hydrodynamic equations for rapid flows of smooth inelastic spheres to Burnett order," *J. Fluid Mech.*, vol. 361, pp. 41–74, 1998.

[178] C. Josserand, A. V. Tkachenko, D. M. Mueth, and H. M. Jaeger, "Memory effects in granular materials," *Phys. Rev. Lett.*, vol. 85, pp. 3632–3635, 2000.

[179] N. C. Keim, J. D. Paulsen, Z. Zeravcic, S. Sastry, and S. R. Nagel, "Memory formation in matter," *Rev. Mod. Phys.*, vol. 91, p. 035002, 2019.

[180] R. Zwanzig, "Memory effects in irreversible thermodynamics," *Phys. Rev.*, vol. 124, pp. 983–992, 1961.

[181] N. Kumar and S. Luding, "Memory of jamming-multiscale models for soft and granular matter," *Granular Matter*, vol. 18, p. 58, 2016.

[182] E. B. Mpemba and D. G. Osborne, "Cool?," *Phys. Educ.*, vol. 4, pp. 172–175, 1969.

[183] A. Lasanta, F. Vega Reyes, A. Prados, and A. Santos, "When the hotter cools more quickly: Mpemba effect in granular fluids," *Phys. Rev. Lett.*, vol. 119, p. 148001, 2017.

[184] A. Santos and A. Prados, "Mpemba effect in molecular gases under nonlinear drag," *Phys. Fluids*, vol. 32, p. 072010, 2020.

[185] S. Takada, H. Hayakawa, and A. Santos, "Mpemba effect in inertial suspensions," *Phys. Rev. E*, vol. 103, p. 032901, 2021.

[186] J. T. Jenkins and F. Mancini, "Kinetic theory for binary mixtures of smooth, nearly elastic spheres," *Phys. Fluids A*, vol. 1, pp. 2050–2057, 1989.

[187] Z. Zamankhan, "Kinetic theory for multicomponent dense mixtures of slightly inelastic spherical particles," *Phys. Rev. E*, vol. 52, pp. 4877–4891, 1995.

[188] B. Arnarson and J. T. Willits, "Thermal diffusion in binary mixtures of smooth, nearly elastic spheres with and without gravity," *Phys. Fluids*, vol. 10, pp. 1324–1328, 1998.

[189] V. Garzó and J. W. Dufty, "Hydrodynamics for a granular binary mixture at low density," *Phys. Fluids.*, vol. 14, pp. 1476–1490, 2002.

[190] V. Garzó, J. W. Dufty, and C. M. Hrenya, "Enskog theory for polydisperse granular mixtures. I. Navier–Stokes order transport," *Phys. Rev. E*, vol. 76, p. 031303, 2007.

[191] V. Garzó, C. M. Hrenya, and J. W. Dufty, "Enskog theory for polydisperse granular mixtures. II. Sonine polynomial approximation," *Phys. Rev. E*, vol. 76, p. 031304, 2007.

[192] D. Serero, S. H. Noskowicz, M. L. Tan, and I. Goldhirsch, "Binary granular gas mixtures: Theory, layering effects and some open questions," *Eur. Phys. J. Special Topics*, vol. 179, pp. 221–247, 2009.

[193] J. A. Murray, V. Garzó, and C. M. Hrenya, "Enskog theory for polydisperse granular mixtures. III. Comparison of dense and dilute transport coefficients and equations of state for a binary mixture," *Powder Technol.*, vol. 220, pp. 24–36, 2012.

[194] J. Karkheck and G. Stell, "Transport properties of the Widom–Rowlinson hard-sphere mixture model," *J. Chem. Phys.*, vol. 71, pp. 3620–3635, 1979.

[195] J. Karkheck and G. Stell, "Bulk viscosity of fluid mixtures," *J. Chem. Phys.*, vol. 71, pp. 3636–3639, 1979.

[196] M. López de Haro, E. G. D. Cohen, and J. Kincaid, "The Enskog theory for multicomponent mixtures. I. Linear transport theory," *J. Chem. Phys.*, vol. 78, pp. 2746–2759, 1983.

[197] N. Khalil and V. Garzó, "Erratum: Transport coefficients for driven granular mixtures at low density [Phys. Rev. E 88, 052201 (2013)] and heat flux of driven granular mixtures at low density: Stability analysis of the homogeneous steady state [Phys. Rev. E 97, 022902 (2018)]," *Phys. Rev. E*, vol. 99, p. 059901 (E), 2019.

[198] M. H. Ernst, "Nonlinear model-Boltzmann equations and exact solutions," *Phys. Rep.*, vol. 78, pp. 1–171, 1981.

[199] J. J. Brey, J. W. Dufty, and A. Santos, "Kinetic models for granular flow," *J. Stat. Phys.*, vol. 97, pp. 281–322, 1999.

[200] H. Grad, "On the kinetic theory of rarefied gases," *Commun. Pure Appl. Math.*, vol. 2, pp. 331–407, 1949.

[201] V. Garzó, "Shear-rate dependent transport coefficients for inelastic Maxwell models," *J. Phys. A: Math. Theor.*, vol. 40, pp. 10729–10757, 2007.

[202] A. Goldshtein and M. Shapiro, "Mechanics of collisional motion of granular materials. Part 1. General hydrodynamic equations," *J. Fluid Mech.*, vol. 282, pp. 75–114, 1995.

[203] S. Hess, "Brownian motion of rotating particles," *Z. Naturforsch.*, vol. 23, no. 4, pp. 597–609, 1968.

[204] A. Santos, "A Bhatnagar–Gross–Krook-like model kinetic equation for a granular gas of inelastic rough hard spheres," *AIP Conf. Proc.*, vol. 1333, pp. 41–48, 2011.

[205] V. Garzó and A. Santos, *Kinetic Theory of Gases in Shear Flows. Nonlinear Transport.* Kluwer Academic Publishers, Dordrecht, 2003.

[206] C. Cercignani, *The Boltzmann Equation and Its Applications.* Springer–Verlag, New York, 1988.

[207] C. Cercignani, R. Illner, and M. Pulvirenti, *The Mathematical Theory of Dilute Gases*, vol. 106. Springer, New York, 2013.

[208] T. P. C. van Noije, M. H. Ernst, and R. Brito, "Ring kinetic theory for an idealized granular gas," *Physica A*, vol. 251, pp. 266–283, 1998.

[209] I. Gallagher, L. Saint-Raymond, and B. Texier, *From Newton to Boltzmann: hard spheres and short-range potentials.* European Mathematical Society, 2013.

[210] M. Pulvirenti and S. Simonella, "The Boltzmann–Grad limit of a hard sphere system: analysis of the correlation error," *Invent. Math.*, vol. 207, no. 3, pp. 1135–1237, 2017.

[211] H. van Beijeren and M. H. Ernst, "The non-linear Enskog–Boltzmann equation," *Phys. Lett. A*, vol. 43, pp. 367–368, 1973.

[212] H. van Beijeren and M. H. Ernst, "The modified Enskog equation," *Physica A*, vol. 68, pp. 437–456, 1973.

[213] H. van Beijeren and M. H. Ernst, "The modified Enskog equation for mixtures," *Physica A*, vol. 70, pp. 225–242, 1973.

[214] H. van Beijeren and M. H. Ernst, "Kinetic theory of hard spheres," *J. Stat. Phys.*, vol. 21, pp. 125–167, 1979.

[215] V. Garzó and J. W. Dufty, "Dense fluid transport for inelastic hard spheres," *Phys. Rev. E*, vol. 59, pp. 5895–5911, 1999.

[216] T. P. C. van Noije, M. H. Ernst, E. Trizac, and I. Pagonabarraga, "Randomly driven granular fluids: Large-scale structure," *Phys. Rev. E*, vol. 59, pp. 4326–4341, 1999.

[217] A. Puglisi, A. Gnoli, G. Gradenigo, A. Sarracino, and D. Villamaina, "Structure factors in granular experiments with homogeneous fluidization," *J. Chem. Phys.*, vol. 136, p. 014704, 2012.

[218] T. Kawasaki, A. Ikeda, and L. Berthier, "Thinning or thickening? Multiple rheological regimes in dense suspensions of soft particles," *EPL*, vol. 107, p. 28009, 2014.

[219] N. G. van Kampen, *Stochastic Processes in Physics and Chemistry.* North Holland, Amsterdam, 1981.

[220] T. P. C. van Noije and M. H. Ernst, "Velocity distributions in homogeneous granular fluids: the free and heated case," *Granular Matter*, vol. 1, pp. 57–64, 1998.

[221] J. T. Jenkins and M. W. Richman, "Kinetic theory for plane flows of a dense gas of identical, rough, inelastic, circular disks," *Phys. Fluids*, vol. 28, pp. 3485–3493, 1985.

[222] A. Zippelius, "Granular gases," *Physica A*, vol. 369, pp. 143–158, 2006.

[223] C. K. K. Lun, "Kinetic theory for granular flow of dense, slightly inelastic, slightly rough spheres," *J. Fluid Mech.*, vol. 233, pp. 539–559, 1991.

[224] A. Santos, G. Kremer, and V. Garzó, "Energy production rates in fluid mixtures of inelastic rough hard spheres," *Prog. Theor. Phys. Suppl.*, vol. 184, pp. 31–48, 2010.

[225] S. Jahanshahi, C. Lozano, B. ten Hagen, C. Bechinger, and H. Löwen, "Colloidal Brazil nut effect in microswimmer mixtures induced by motility contrast," *J. Chem. Phys.*, vol. 150, p. 114902, 2019.

[226] M.-L. Tan and I. Goldhirsch, "Rapid granular flows as mesoscopic systems," *Phys. Rev. Lett.*, vol. 81, pp. 3022–3025, 1998.

[227] J. W. Dufty and J. J. Brey, "Comment on "Rapid granular flows as mesoscopic systems"," *Phys. Rev. Lett.*, vol. 82, p. 4566, 1999.

[228] J. W. Dufty and J. J. Brey, "Hydrodynamic modes for granular gases," *Phys. Rev. E*, vol. 68, p. 030302(R), 2003.

[229] J. J. Brey and J. W. Dufty, "Hydrodynamic modes for a granular gas from kinetic theory," *Phys. Rev. E*, vol. 72, p. 011303, 2005.

[230] N. Khalil and V. Garzó, "Unified hydrodynamic description for driven and undriven inelastic Maxwell mixtures at low density," *J. Phys. A: Math. Theor.*, vol. 53, p. 355002, 2020.

[231] A. Santos, "Does the Chapman–Enskog expansion for sheared granular gases converge?," *Phys. Rev. Lett.*, vol. 100, p. 078003, 2008.

[232] C. Cercignani, *Mathematical Methods in Kinetic Theory.* Plenum Press, New York, 1990.

[233] H. Struchtrup, *Macroscopic Transport Equations for Rarefied Gas Flows.* Berlin: Springer, 2005.

[234] J. S. Dahler and M. Theodosopulu, *The Kinetic Theory of Dense Polyatomic Fluids*, ch. 31, pp. 155–229. John Wiley & Sons, Ltd, 1975.

[235] D. W. Condiff, W. Lu, and J. S. Dahler, "Transport properties of polyatomic fluids, a dilute gas of perfectly rough spheres," *J. Chem Phys.*, vol. 42, pp. 3445–3475, 1965.

[236] G. Kremer, A. Santos, and V. Garzó, "Transport coefficients of a granular gas of inelastic rough hard spheres," *Phys. Rev. E*, vol. 90, p. 022205, 2014.

[237] F. Vega Reyes, G. Kremer, and A. Santos, "Role of roughness on the hydrodynamic homogeneous base state of inelastic hard spheres," *Phys. Rev. E*, vol. 89, p. 020202 (R), 2014.

[238] P. L. Bhatnagar, E. P. Gross, and M. Krook, "A model for collision processes in gases. I. Small amplitude processes in charged and neutral one-component system," *Phys. Rev.*, vol. 94, pp. 511–525, 1954.

[239] P. Welander, "On the temperature jump in a rarefied gas," *Arkiv. Fysik.*, vol. 7, pp. 507–553, 1954.

[240] E. Ben-Naim and P. L. Krapivsky, "The Inelastic Maxwell Model," in *Granular Gas Dynamics* (T. Pöschel and S. Luding, eds.), vol. 624 of *Lectures Notes in Physics*, pp. 65–94, Springer, 2003.

[241] C. Truesdell and R. G. Muncaster, *Fundamentals of Maxwell's Kinetic Theory of a Simple Monatomic Gas*. Academic Press, New York, 1980.

[242] V. Garzó and A. Santos, "Third and fourth degree collisional moments for inelastic Maxwell models," *J. Phys. A: Math. Theor.*, vol. 40, pp. 14927–14943, 2007.

[243] G. M. Kremer and A. Santos, "Granular gas of inelastic and rough Maxwell particles," *arXiv:2203.10119*, 2022.

[244] G. A. Bird, "Approach to translational equilibrium in a rigid sphere gas," *Phys. Fluids*, vol. 6, pp. 1518–1519, 1963.

[245] G. A. Bird, "Direct simulation and the Boltzmann equation," *Phys. Fluids*, vol. 13, pp. 2676–2681, 1970.

[246] G. A. Bird, *Molecular Gas Dynamics and the Direct Simulation Monte Carlo of Gas Flows*. Clarendon, Oxford, 1994.

[247] J. M. Montanero and A. Santos, "Simulation of the Enskog equation *à la* Bird," *Phys. Fluids*, vol. 9, pp. 2057–2060, 1997.

[248] R. Gómez González and V. Garzó, "Non-monotonic Mpemba effect in binary molecular suspensions," *EPJ Web Conf.*, vol. 249, p. 09005, 2021.

[249] M. G. Chamorro, F. Vega Reyes, and V. Garzó, "Non-Newtonian hydrodynamics for a dilute granular suspension under uniform shear flow," *Phys. Rev. E*, vol. 92, p. 052205, 2015.

[250] J. W. Dufty, A. Santos, J. J. Brey, and R. F. Rodríguez, "Model for nonequilibrium computer simulation methods," *Phys. Rev. A*, vol. 33, pp. 459–466, 1986.

[251] N. V. Brilliantov and T. Pöschel, "Breakdown of the Sonine expansion for the velocity distribution of granular gases," *Europhys. Lett.*, vol. 74, pp. 424–430, 2006.

[252] N. V. Brilliantov and T. Pöschel, "Erratum: Breakdown of the Sonine expansion for the velocity distribution of granular gases [Europhys. Lett. 74, 424–430 (2006)]," *Europhys. Lett.*, vol. 75, p. 188, 2006.

[253] R. Gómez González and V. Garzó, "First-order contributions to the partial temperatures in dilute binary granular suspensions," in *Traffic and Granular Flow 2019* (I. Zuriguel, A. Garcimartin, and R. Cruz, eds.), pp. 341–347, Springer, Cham, 2020.

[254] H. Hayakawa and S. Takada, "Kinetic theory of discontinuous rheological phase transition for a dilute inertial suspension," *Prog. Theor. Exp. Phys*, vol. 2019, p. 083J01, 2019.

[255] A. Santos and V. Garzó, "Simple shear flow in inelastic Maxwell models," *J. Stat. Mech.*, vol. P08021, 2007.

[256] E. Brown and H. M. Jeager, "Shear thickening in concentrated suspensions: phenomenology, mechanisms and relations to jamming," *Rep. Prog. Phys.*, vol. 77, p. 046602, 2014.

[257] A. Santos, V. Garzó, J. J. Brey, and J. W. Dufty, "Singular behavior of shear flow far from equilibrium," *Phys. Rev. Lett.*, vol. 71, pp. 3971–3974, 1993.

[258] A. Santos and V. Garzó, "Exact moment solution of the Boltzmann equation for uniform shear flow," *Physica A*, vol. 213, pp. 409–425, 1995.

[259] J. J. Brey, M. J. Ruiz-Montero, D. Cubero, and R. García-Rojo, "Self-diffusion in freely evolving granular gases," *Phys. Fluids.*, vol. 12, pp. 876–883, 2000.

[260] J. M. Montanero and V. Garzó, "Shear viscosity for a heated granular binary mixture at low density," *Phys. Rev. E*, vol. 67, p. 021308, 2003.

[261] V. Garzó and J. M. Montanero, "Shear viscosity for a moderately dense granular binary mixture," *Phys. Rev. E*, vol. 68, p. 041302, 2003.

[262] V. Garzó and J. M. Montanero, "Diffusion of impurities in a granular gas," *Phys. Rev. E*, vol. 69, p. 021301, 2004.

[263] V. Garzó and F. Vega Reyes, "Mass transport of impurities in a moderately dense granular gas," *Phys. Rev. E*, vol. 79, p. 041303, 2009.

[264] J. J. Brey and M. J. Ruiz-Montero, "Shearing instability of a dilute granular mixture," *Phys. Rev. E*, vol. 87, p. 022210, 2013.

[265] V. Garzó and F. Vega Reyes, "Segregation of an intruder in a heated granular gas," *Phys. Rev. E*, vol. 85, p. 021308, 2012.

[266] P. P. Mitrano, V. Garzó, and C. M. Hrenya, "Instabilities in granular binary mixtures at moderate densities," *Phys. Rev. E*, vol. 89, p. 020201(R), 2014.

[267] J. J. Brey, M. J. Ruiz-Montero, and D. Cubero, "On the validity of linear hydrodynamics for low-density granular flows described by the Boltzmann equation," *Europhys. Lett.*, vol. 48, pp. 359–364, 1999.

[268] U. M. B. Marconi, L. Caprini, and A. Puglisi, "Hydrodynamics of simple active liquids: the emergence of velocity correlations," *New J. Phys.*, vol. 23, p. 103024, 2021.